



HAL
open science

Importance des propriétés mécaniques des cellules tumorales circulantes au cours du développement métastatique

Valentin Gensbittel

► **To cite this version:**

Valentin Gensbittel. Importance des propriétés mécaniques des cellules tumorales circulantes au cours du développement métastatique. Cancer. Université de Strasbourg, 2023. Français. NNT : 2023STRAJ082 . tel-04860572

HAL Id: tel-04860572

<https://theses.hal.science/tel-04860572v1>

Submitted on 1 Jan 2025

HAL is a multi-disciplinary open access archive for the deposit and dissemination of scientific research documents, whether they are published or not. The documents may come from teaching and research institutions in France or abroad, or from public or private research centers.

L'archive ouverte pluridisciplinaire **HAL**, est destinée au dépôt et à la diffusion de documents scientifiques de niveau recherche, publiés ou non, émanant des établissements d'enseignement et de recherche français ou étrangers, des laboratoires publics ou privés.

ÉCOLE DOCTORALE DES SCIENCES DE LA VIE ET DE LA SANTÉ
INSERM UMRS_1109

THÈSE présentée par :
Valentin GENSBITTEL
soutenue le : 4 décembre 2023

pour obtenir le grade de : **Docteur de l'université de Strasbourg**
Discipline/ Spécialité : Aspects moléculaires et cellulaires de la biologie

**Importance des propriétés mécaniques des cellules
tumoraux circulantes au cours du développement
métastatique**

THÈSE dirigée par :
Dr. GOETZ Jacky

DR, Université de Strasbourg

RAPPORTEURS :

Dr. MANNEVILLE Jean-Baptiste
Dr. PANNEQUIN Julie

DR, Université Paris Cité
DR, Institut de Génétique Fonctionnelle

AUTRES MEMBRES DU JURY :

Dr. REYMANN Anne-Cécile
Dr. ETIENNE-MANNEVILLE Sandrine

CR, Université de Strasbourg
DR, Institut Pasteur

Remerciements

Tout d'abord, je souhaite remercier la région Grand Est et l'INSERM qui ont co-financé mes trois premières années de thèse, et la Ligue contre le Cancer qui a financé ma quatrième année.

Merci à **Jacky** de m'avoir donné l'opportunité de rejoindre son équipe quand je n'étais encore qu'un étudiant de Master, et de m'avoir supervisé comme il l'a fait tout au long des cinq belles années durant lesquelles j'ai eu la chance de travailler sur ce sujet fascinant.

Merci à **Gautier, Sébastien et Naël** qui m'ont tous supervisé et appris les ficelles du métier à différents moments de ce périple.

Une mention spéciale pour les personnes du laboratoire que j'ai le plus côtoyé au quotidien, à savoir mes voisins de bureau **Amandine**, « petit » **Vincent** et **Nacho**. **Amandine** et **Vincent** auront souvent causé des baisses de productivité dramatiques dans le bureau, mais l'ambiance fût toujours bonne et ce fût souvent un plaisir d'être au bureau pour travailler en leur présence... donc ça compense ? **Nacho** fut un voisin de très bonne compagnie aussi, quand il s'abstenait de partager ses opinions football catastrophiques.

Merci à **Florent**, le prototype du collègue parfait : sympathie inégalable, bonne humeur permanente et toujours le premier à se proposer pour aider, rendre service et faciliter le quotidien des collègues. J'espère encore avoir des occasions, à l'avenir, de te terrasser sur l'échiquier.

Merci à **Olivier** et **Annabel** qui font tourner le laboratoire comme une horloge suisse.

Merci à tous mes collègues co-utilisateurs du poisson-zèbre : **Amandine, Marina, Ben, Nandini** et surtout « grand » **Vincent**. Notre entre-aide et l'entretien de l'animalerie a été un facteur essentiel à la bonne conduite de mes expériences.

Merci à **Louis**, le crack des manip' *ex vivo* grâce à qui un beau chapitre devrait s'ajouter à la fin de mes travaux.

Merci à tous les autres membres du Goetzlab, avec qui je n'aurais pas forcément eu l'opportunité de travailler directement mais qui auront contribué à faire de cette équipe le super environnement de travail qu'il est : **Katka, Cristina, KJ, Lucas, Shima**.

Merci aux nombreux collaborateurs qui auront contribué à mes travaux et aux gars de la plateforme PIC-STRA : **Klemens Uhlmann, Ruchi Goswami, Salvatore Girardo, Martin Kräter, Daniel Balzani, Jochen Guck, Nacho** et **Pascal**.

En dehors du labo maintenant, merci tout d'abord à mes amis **Aurore** et **Nicolas** pour leur soutien et leur amitié indéfectibles qui durent depuis plus de six ans.

Merci à toute **ma famille** pour son soutien et pour m'avoir toujours fait sentir sa fierté. Mention spéciale à **mes parents** et à **mon frère** auprès desquels j'ai souvent rechargé les batteries le week-end.

Merci à ma chère **Marine**, qui aura accepté sans broncher que je la délaisse honteusement pour travailler matins, midis, soirs et week-ends dans la dernière ligne droite de ce périple. J'ai hâte que l'on profite ensemble de ma disponibilité retrouvée : à nous les vacances et les week-ends SPA !

Enfin, merci à mon chat **Blanco** pour les nombreuses heures de ronronthérapie.

Table des matières

I) INTRODUCTION	11
A) CANCER ET METASTASES	12
1) <i>Prévalence du cancer</i>	12
2) <i>La cascade métastatique</i>	13
3) <i>Organotropisme</i>	14
B) ASPECTS BIOMECHANIQUES DE LA PROGRESSION TUMORALE	17
1) <i>Tumeur primaire</i>	17
2) <i>Environnement intravasculaire</i>	23
C) L'ADAPTABILITE MECANIQUE DES CELLULES TUMORALES	35
1) <i>Résumé en français</i>	35
2) <i>"Mechanical Adaptability of Tumor Cells in Metastasis"</i>	36
3) <i>Références complémentaires</i>	52
D) OBJECTIFS DE MES TRAVAUX.....	54
II) APPROCHE EXPÉRIMENTALE	57
A) LE MODELE EMBRYON DE POISSON-ZEBRE	58
1) <i>Injection intravasculaire</i>	59
2) <i>Imagerie des événements de circulation et d'arrêt des CTCs</i>	59
3) <i>Imagerie de l'extravasation des cellules tumorales</i>	61
B) BILLES ELASTIQUES DE POLYACRYLAMIDE.....	63
1) <i>Étude de la contribution du mécanisme d'occlusion dans l'arrêt intravasculaire</i>	63
2) <i>Mesure des forces exercées par l'architecture vasculaire</i>	63
C) GENERATION DE POPULATIONS DE CELLULES TUMORALES MECANIQUEMENT ALTEREES	65
1) <i>Déplétion de protéines liées à la mécanique cellulaire</i>	65
2) <i>Mesure des propriétés viscoélastiques des cellules tumorales</i>	66
III) RÉSULTATS	68
CELL VISCOELASTICITY ORCHESTRATES INTRAVASCULAR AND EARLY STEPS OF METASTASIS	70
<i>Résumé en français</i>	70
<i>Introduction</i>	71
<i>Mechanical occlusion drives intravascular arrest of circulating objects</i>	73
<i>CTCs tap into their viscosity property to navigate the intravascular environment</i>	79
<i>CTC circulation routes and arrest sites are determined by their viscosity levels</i>	85
<i>Tumor cell viscosity plays an impactful role in the extravasation process</i>	91
<i>Discussion</i>	99
<i>Materials and methods</i>	103
IV) PERSPECTIVES & DISCUSSION ÉLARGIE	112
A) TRAVAUX EN COURS.....	113
1) <i>Récapitulation de l'étape d'extravasation</i>	113
2) <i>Analyse des foyers métastatiques</i>	114
3) <i>Suivi de la croissance métastatique</i>	115
B) PROPRIETES MECANIQUES DES CELLULES TUMORALES DANS LA PROGRESSION TUMORALE	116
1) <i>Zones d'ombre subsistantes</i>	116
2) <i>Transition épithélio-mésenchymateuse et mécanique cellulaire</i>	119
3) <i>Métastases collectives et mécanique cellulaire</i>	121
C) IMPLICATIONS EN « MECANO-IMMUNOLOGIE »	125
<i>Evidence and therapeutic implications of biomechanically regulated immunosurveillance in cancer and other diseases</i>	125
RÉFÉRENCES	144
ANNEXES	158

Table des figures

<i>Figure 1 : Projection du nombre de cas estimés, tous cancers confondus, pour 2020 à 2040 en France métropolitaine.....</i>	<i>12</i>
<i>Figure 2 : La cascade métastatique.....</i>	<i>14</i>
<i>Figure 3 : Opposition historique de deux hypothèses expliquant le phénomène d'organotropisme dans les pathologies cancéreuses.</i>	<i>15</i>
<i>Figure 4 : Stress mécanique solide.</i>	<i>17</i>
<i>Figure 5 : Pression hydrostatique interstitielle.</i>	<i>19</i>
<i>Figure 6 : Résumé des forces biomécaniques opérant au site de tumeur primaire.....</i>	<i>22</i>
<i>Figure 7 : Forces de cisaillement.</i>	<i>23</i>
<i>Figure 8 : Extravasation de cellules tumorales par remodelage endothélial.....</i>	<i>26</i>
<i>Figure 9 : Mécanisme de « rolling » des leucocytes.</i>	<i>27</i>
<i>Figure 10 : Processus en deux temps de l'adhésion de cellules tumorales circulantes.....</i>	<i>28</i>
<i>Figure 11 : Flux permissifs pour l'arrêt, l'adhésion et l'extravasation de CTCs.....</i>	<i>29</i>
<i>Figure 12 : Arrêt intravasculaire de CTCs dans les capillaires du cerveau de souris.....</i>	<i>31</i>
<i>Figure 13 : Déformations de CTCs et de leur noyau dans l'environnement intravasculaire.</i>	<i>32</i>
<i>Figure 14 : Résumé des principales forces biomécaniques rencontrées par les cellules tumorales lors de la succession des étapes de la cascade métastatique.....</i>	<i>33</i>
<i>Figure 15 : Fenêtres temporelles pour l'étude des étapes intravasculaires du développement métastatique dans l'embryon de poisson-zèbre.</i>	<i>58</i>
<i>Figure 16 : Injection intravasculaire dans le canal de cuvier.</i>	<i>59</i>
<i>Figure 17 : Imagerie et analyse des événements de circulation et d'arrêt des CTCs.</i>	<i>60</i>
<i>Figure 18 : Les sous-régions vasculaires constituant le plexus caudal de l'embryon de poisson-zèbre.....</i>	<i>61</i>
<i>Figure 19 : Imagerie et analyse des événements de remodelage endothélial et d'extravasation de cellules tumorales.</i>	<i>62</i>
<i>Figure 20 : Injection intravasculaire de billes de polyacrylamide dans l'embryon de poisson-zèbre.....</i>	<i>63</i>
<i>Figure 21 : Analyse numérique de la déformation des billes.</i>	<i>64</i>
<i>Figure 22 : Protéines ciblées pour l'altération des propriétés mécaniques de cellules tumorales D2A1.....</i>	<i>65</i>
<i>Figure 23 : Déroulé de l'expérience d'aspiration par micropipette.</i>	<i>66</i>
<i>Figure 24 : Modèle rhéologique utilisé pour l'ajustement de courbe.....</i>	<i>67</i>
<i>Figure 25 : Approche expérimentale ex vivo pour la visualisation et quantification d'événements d'extravasation dans le poumon de souris.....</i>	<i>114</i>
<i>Figure 26 : Approche expérimentale ex vivo pour l'imagerie et analyse de foyers métastatiques dans le poumon de souris.</i>	<i>114</i>
<i>Figure 27 : Approche expérimentale in vivo pour la quantification de la croissance métastatique dans le modèle souris.</i>	<i>115</i>
<i>Figure 28 : Intravasation en microscopie intravitale.....</i>	<i>117</i>
<i>Figure 29 : Plasticité épithélio-mésenchymateuse.</i>	<i>119</i>
<i>Figure 30 : Mécanismes collectifs vs mécanismes cellule unique.....</i>	<i>122</i>

Liste des abréviations

5-FU	5-Fluorouracile
AFM	Microscopie à force atomique
AVJ	Jonction artério-veineuse
CAF	Fibroblaste associé au cancer
COMPAX	Computational analysis-based cell-scale stress sensing
CPCs	Capillaires du plexus caudal
CTC	Cellule tumorale circulante
CV	Veine caudale
DA	Artère dorsale
dpf	jours post-fertilisation
ECM / MEC	Matrice extracellulaire
GFP	Protéine fluorescente verte
hpi	heures post-injection
ISVs	Vaisseaux intersegmentaires
MEF	Méthode des éléments finis
MPA	Aspiration par micropipette
mpi	minutes post-injection
MRTF	Myocardin-related transcription factor
PBS	Tampon phosphate salin
PEM	Plasticité épithélio-mésenchymateuse
PHI	Pression hydrostatique interstitielle
RT-DC	Cytométrie de déformabilité en temps réel
TEM	Transition épithélio-mésenchymateuse
TGF	Facteur de croissance transformant
VEGF	Facteur de croissance de l'endothélium vasculaire
YAP	yes-associated protein

I) INTRODUCTION

A) Cancer et Métastases

1) Prévalence du cancer

Les pathologies cancéreuses représentent un enjeu de santé publique majeur, avec une augmentation continue du nombre de cas au fil des années. Bien que les chiffres soient encourageants pour certains types de cancers dans certaines régions du monde (l'incidence du cancer du poumon est par exemple en baisse dans les pays développés (Leiter et al., 2023), on dénote une augmentation globale de l'incidence du cancer chez les adultes de moins de 50 ans (Ugai et al., 2022) et les projections, estimant que le nombre de cas de cancer dans le monde doublera au cours des 50 prochaines années, sont extrêmement alarmantes (Soerjomataram & Bray, 2021). La France ne fait pas exception à ces tendances préoccupantes :

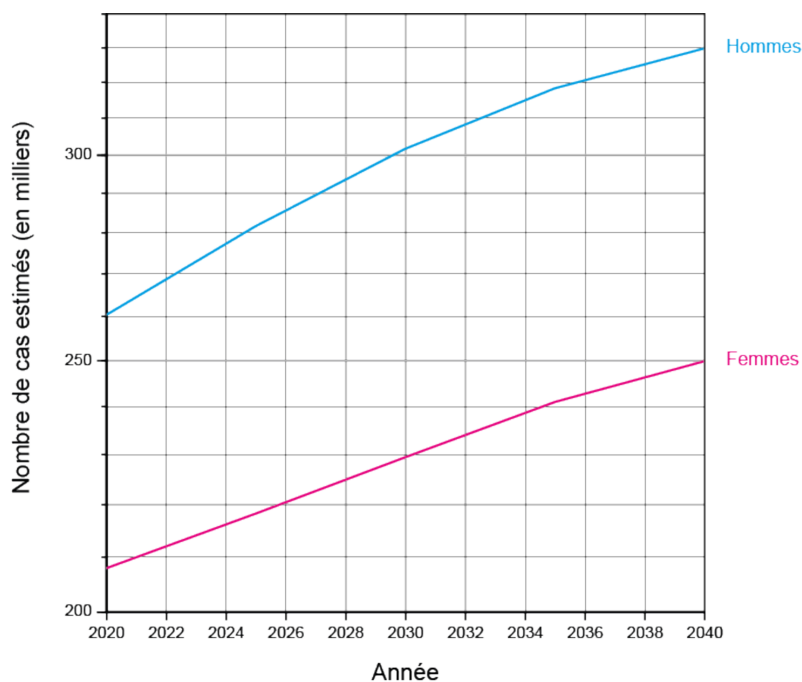


Figure 1 : Projection du nombre de cas estimés, tous cancers confondus, pour 2020 à 2040 en France métropolitaine. Source : Cancer Tomorrow – IARC. Tous droits réservés – 2023.

2) La cascade métastatique

Le développement métastatique étant responsable de la majorité des décès dans les pathologies cancéreuses (Dillekås et al., 2019), d'importants efforts de recherche lui ont été consacrés pour en comprendre les rouages. Si ces derniers n'ont que rarement abouti à l'émergence de thérapies efficaces pour lutter contre ces tumeurs secondaires (Steege, 2016 ; Weiss et al., 2022), ils ont néanmoins permis de caractériser précisément la succession d'étapes conduisant au développement de métastases : la cascade métastatique.

Le processus débute lorsque des cellules saines acquièrent des mutations conduisant à leur prolifération incontrôlée dans un milieu permissif où les voies de signalisation antitumorales sont inhibées. La croissance de la tumeur primaire, les transformations du micro-environnement tumoral et l'acquisition de certaines caractéristiques par les cellules cancéreuses permettent ensuite à un certain nombre d'entre elles d'envahir les tissus environnants. Vient alors une étape de migration dans la matrice extracellulaire permettant aux cellules tumorales d'accéder aux vaisseaux lymphatiques ou aux vaisseaux sanguins dans lesquels elles pourront s'intravaser pour accéder au système circulatoire. Les cellules cancéreuses deviennent alors des cellules tumorales circulantes (CTCs) profitant des fluides pour se disséminer dans l'organisme. L'arrêt peut survenir par occlusion lorsque les CTCs rencontrent un site de rétrécissement vasculaire, ou par adhésion active aux parois des cellules endothéliales constituant les vaisseaux. L'étape d'extravasation, pouvant s'effectuer par différents mécanismes tels que la diapédèse ou le remodelage endothélial, permet ensuite aux cellules tumorales de s'extirper de la circulation et d'atteindre un site distant. Elles pourront alors, si elles survivent et en fonction des caractéristiques du micro-environnement, proliférer et donner naissance à des métastases ou entrer en phase de dormance et attendre un moment plus opportun pour se multiplier (Nguyen et al., 2009 ; Fares et al., 2020).

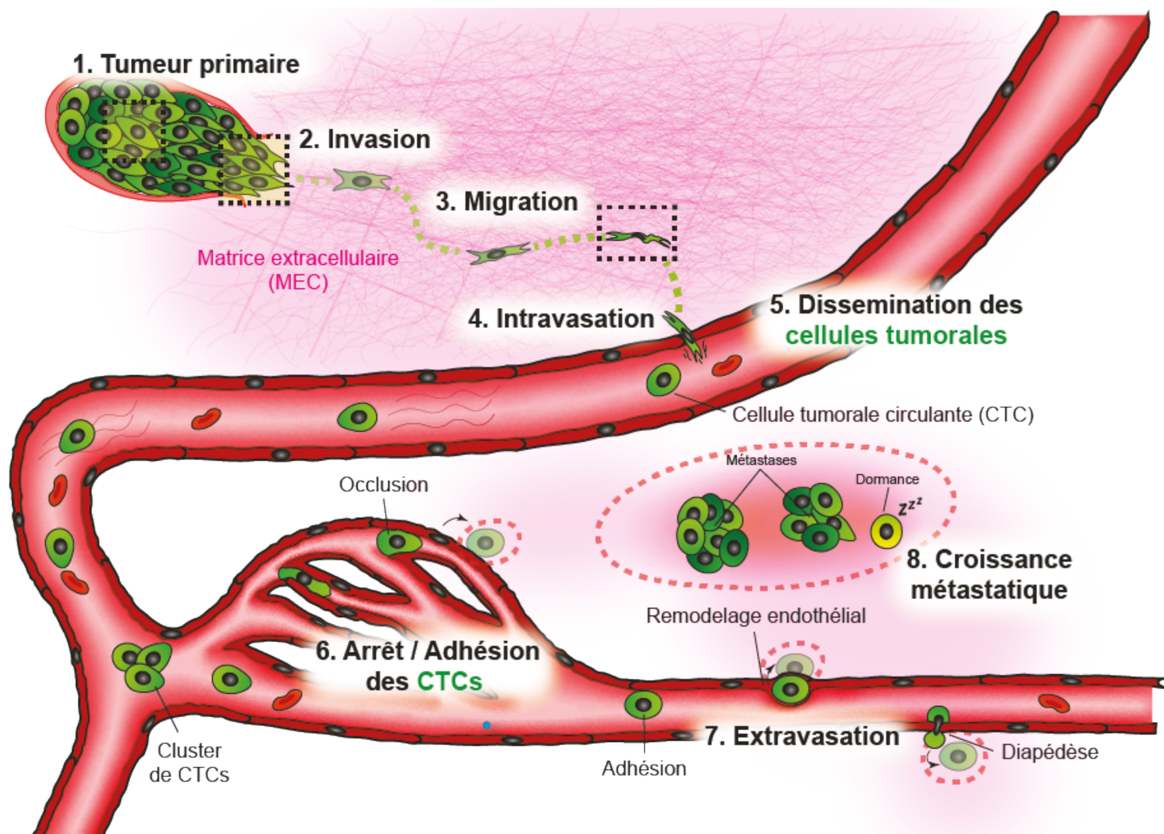


Figure 2 : La cascade métastatique. Les métastases apparaissent à l'issue d'un processus complexe composé de plusieurs étapes. (Adapté de Collin*, Gensbittel* et al., Comptes Rendus Biologies, 2021)

3) Organotropisme

Il est important de noter que ce processus de cascade métastatique ne conduit pas à des apparitions de tumeurs secondaires aléatoires et réparties de manière égale en différents sites de l'organisme. Les données cliniques montrent en effet que tous les sites de tumeurs primaires sont bien spécifiquement associés à des listes restreintes d'organes distants où apparaissent les métastases (Gao et al., 2019). Ce phénomène d'organotropisme s'explique par deux modèles, qui furent un temps opposés, mais dont on sait aujourd'hui qu'ils coexistent tous deux en synergie. D'un côté l'hypothèse du "seed-and-soil" émise en 1889 par le chirurgien Stephen Paget, qui proposa que les cellules tumorales, disséminées de manière égales dans l'ensemble de l'organisme, ne donnent naissance à des tumeurs secondaires que dans les sites où l'environnement leur est favorable (Paget, 1889 ; Langley & Fidler, 2013). De l'autre,

l'hypothèse du pathologiste James Ewing qui soutiendra, en 1928, que les schémas spécifiques d'apparitions de tumeurs secondaires pouvaient intégralement être attribués aux caractéristiques architecturales et hémodynamiques du système circulatoire (Ewing, 1928).

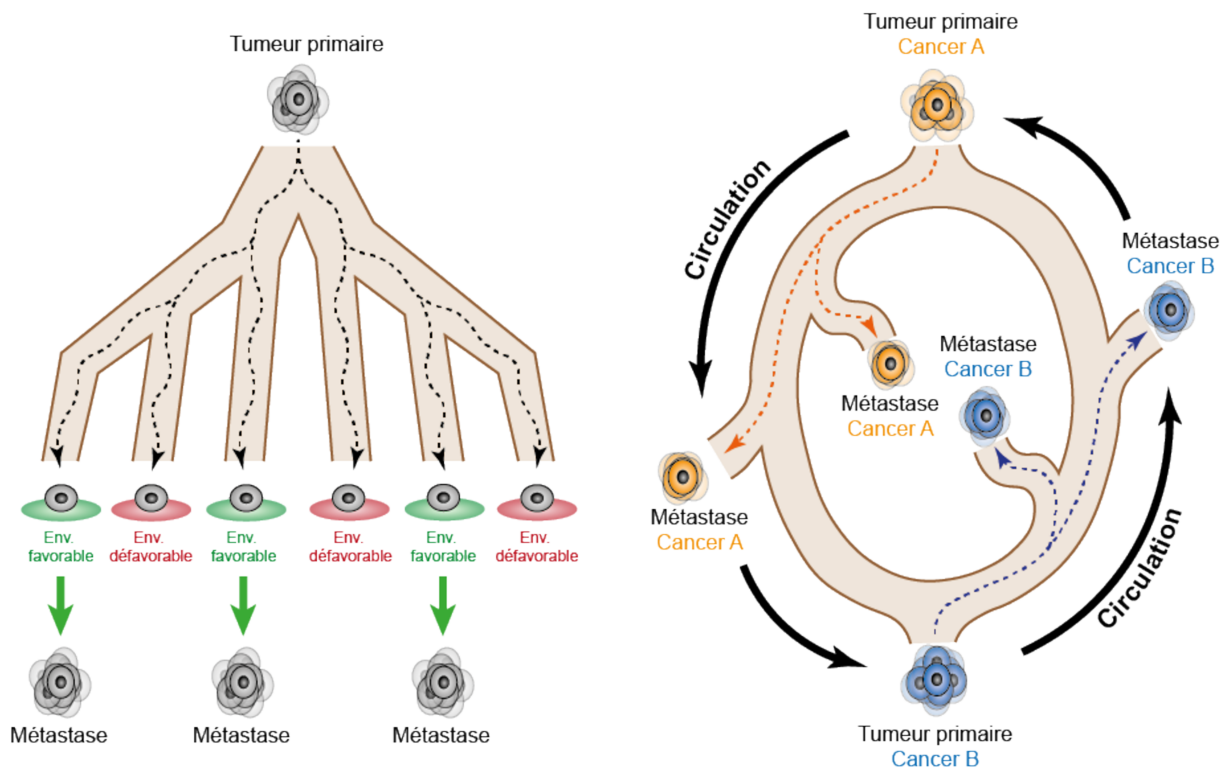


Figure 3 : Opposition historique de deux hypothèses expliquant le phénomène d'organotropisme dans les pathologies cancéreuses. Dans l'hypothèse du « seed-and-soil » (gauche), les cellules tumorales se disséminent dans l'ensemble de l'organisme et le niveau de compatibilité entre la cellule tumorale (« la graine ») et le microenvironnement au site distant atteint (« le terrain ») dicte si croissance métastatique peut s'en suivre. L'hypothèse « biomécanique » (droite) s'y oppose en stipulant que les caractéristiques hémodynamiques du système circulatoire dictant les itinéraires de circulation et les probabilités d'arrêt sont responsables d'une spécificité de dissémination à l'origine du phénomène d'organotropisme.

L'hypothèse du seed-and-soil a depuis très largement été validée par d'innombrables données accumulées au cours de plus d'un siècle de recherche. On citera comme exemples les métastases cérébrales dont l'établissement dépend de la coopération d'astrocytes localement activés par les cellules cancéreuses disséminées (Xing et al., 2013) ou encore les métastases osseuses dont l'agressivité peut dépendre de l'activité

locale d'ostéoclastes (Lu et al., 2011). L'émergence du concept de niche pré-métastatique a par ailleurs entériné l'importance de cette hypothèse, puisqu'il est désormais connu que la tumeur primaire, par le biais de sécrétions de vésicules et de facteurs, prépare à distance le microenvironnement pour l'arrivée future de cellules tumorales disséminées (Peinado et al., 2017).

L'hypothèse biomécanique a elle aussi gagné en crédibilité, notamment grâce à des travaux démontrant très directement que les caractéristiques du système circulatoire et les itinéraires de circulations impactent la dissémination métastatique au même titre que les effets associés à l'hypothèse du "seed-and-soil". En effet, des expériences in vivo dans les modèles souris et poisson-zèbre ont montré que ce sont bien logiquement les caractéristiques du système circulatoire qui déterminent dans un premier temps où les cellules tumorales sont acheminées et où elles s'arrêtent, avant que la compatibilité entre les cellules tumorales et leur environnement n'entre en jeu en impactant la qualité de l'adhésion, la probabilité de réaliser l'extravasation et l'agressivité de la croissance métastatique (Follain et al., 2018 ; Lu et al., 2019 ; Paul et al., 2019).

L'influence de la biomécanique dans les pathologies cancéreuses va bien au-delà de cette contribution au phénomène d'organotropisme. Un vaste domaine de recherche s'est établi pour démontrer la contribution de paramètres biophysiques dans toutes les étapes de la progression tumorale.

B) Aspects biomécaniques de la progression tumorale

Plusieurs forces et facteurs biomécaniques entrent en jeu au cours de la progression tumorale. On peut distinguer les paramètres opérant dans les étapes les plus précoces du processus métastatique au site de tumeur primaire, et ceux entrant en jeu au cours de la dissémination hématogène où l'environnement est drastiquement différent.

1) Tumeur primaire

Les changements de propriétés mécaniques dans les tissus constituent une caractéristique clé des tumeurs. On dénombre trois paramètres particulièrement importants qui sont altérés dans les tumeurs primaires : le stress compressif, la pression hydrostatique interstitielle et la rigidité de la matrice extracellulaire (Nia et al., 2020).

i) Stress compressif

On définit le stress compressif comme l'ensemble des forces de compression et de tension émanant des éléments solides et élastiques constituant l'environnement tumoral, comme les cellules cancéreuses, les cellules stromales ou encore la matrice extracellulaire. La source la plus directe de stress compressif provient de la simple croissance de la tumeur primaire. En effet, alors que les cellules cancéreuses prolifèrent, le volume tumoral augmente et occupe de plus en plus d'espace dans l'environnement, compressant les éléments autour de la tumeur mais également les cellules cancéreuses la constituant (Nia et al., 2016 ; Stylianopoulos et al., 2012).

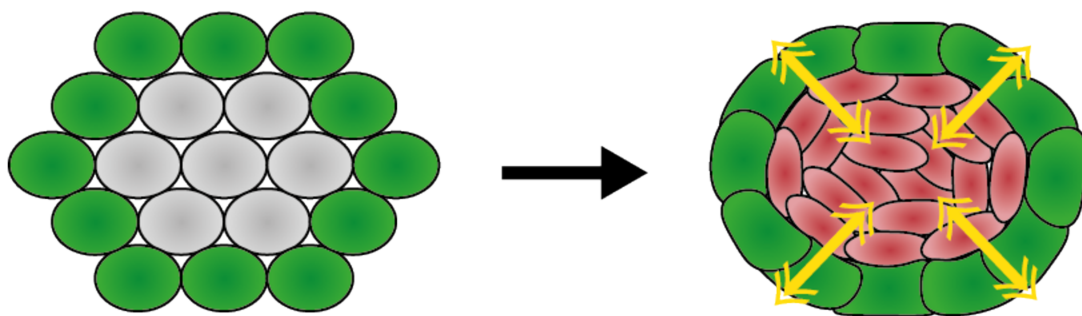


Figure 4 : Stress compressif. Des forces de compression (flèches jaunes) apparaissent lorsque les cellules tumorales (grises initialement, puis rouges quand

compressées) prolifèrent, entraînant la croissance du volume de la tumeur et la compression mutuelle entre la tumeur et les éléments de son microenvironnement (verts).

L'apparition du stress compressif a de multiples conséquences : bien que les cellules tumorales y répondent en ralentissant leur prolifération (Cheng et al., 2009 ; Delarue et al., 2014), il semblerait que ces forces puissent significativement contribuer aux étapes précoces de la cascade métastatique en induisant des changements d'expression de gènes associés à un phénotype invasif (Demou et al., 2010), en induisant la transition épithélio-mésenchymateuse (Zulueta-Coarasa et al., 2022) et en stimulant les capacités de migration de cellules leaders orchestrant des échappées de groupes de cellules tumorales du site de tumeur primaire (Tse et al., 2012). De plus, la croissance de la tumeur peut conduire à l'application de stress compressif sur les vaisseaux sanguins et lymphatiques (Padera et al., 2004 ; Stylianopoulos et al., 2012). La désorganisation de ces vaisseaux contribue à rendre l'environnement tumoral hypoxique, ce qui constitue une caractéristique clé et aggravante dans la progression tumorale (Muz et al., 2015). Outre la favorisation de l'hypoxie, la perturbation des vaisseaux sanguins et lymphatiques contribue également à l'altération d'un autre paramètre biomécanique dans l'environnement tumoral : la pression hydrostatique interstitielle (Griffon-Etienne et al., 1999 ; Stylianopoulos et al., 2012).

ii) Pression hydrostatique interstitielle

Dans des conditions physiologiques normales, la quantité de liquide présent dans l'interstitium est régulée par les apports des vaisseaux sanguins et le drainage des vaisseaux lymphatiques, résultant en une pression hydrostatique interstitielle quasi nulle (Nia et al., 2020). Dans un contexte pathologique tumoral, cet équilibre est rompu et la pression hydrostatique dérégulée dans un grand nombre de cancers (Less et al., 1992). Certaines mesures ont en effet permis de suggérer que la pression hydrostatique interstitielle augmente avec le volume tumoral (Gutmann et al., 1992) et d'autres ont pu établir que sa valeur peut être indicative du statut de la tumeur, en permettant de distinguer tissus sains, tumeurs bénignes et carcinomes invasifs (Nathanson et al., 1994).

L'élévation de la pression hydrostatique interstitielle s'explique d'une part par l'organisation désordonnée des vaisseaux sanguins pénétrant la tumeur. En effet, l'environnement hypoxique et pro-angiogénique conduit à l'apparition de nombreux vaisseaux immatures et extrêmement perméables présentant de nombreux pores et espaces inter-cellulaires (Hashizume et al., 2000 ; Muz et al., 2015). D'autre part, le système lymphatique supposé drainer les excès de liquide dans l'interstitium est lui aussi défectueux dans l'environnement tumoral (Leu et al., 2000 ; Padera et al., 2002). Les conséquences de la dérégulation de la pression hydrostatique interstitielle concernent principalement le sens de déplacements des flux et des molécules dans l'environnement tumoral. La pression étant à son maximum au centre de la tumeur et à son minimum à la périphérie, les flux se déplacent du centre de la tumeur vers l'extérieur (Baxter and Jain, 1989). Ces flux s'opposent donc à toutes éventuelles arrivées de molécules thérapeutiques administrées pour atteindre la tumeur (Heldin et al., 2004).

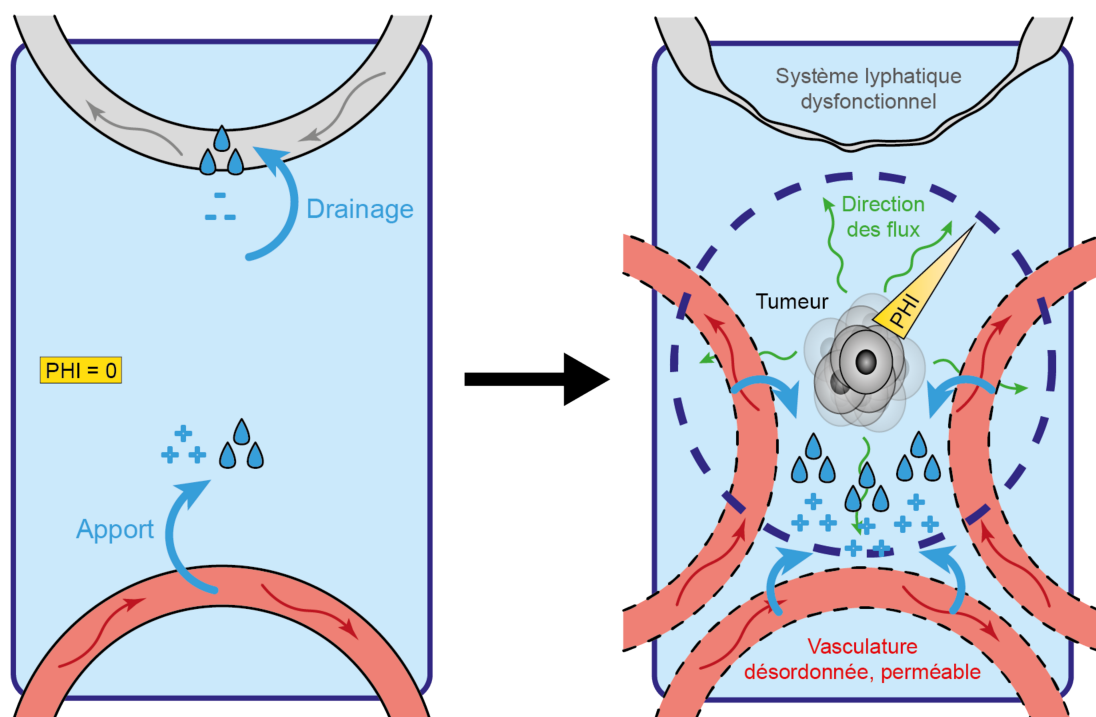


Figure 5 : Pression hydrostatique interstitielle. En conditions physiologiques normales (gauche), la pression hydrostatique interstitielle (PHI) est convenablement régulée et proche de 0. Dans l'environnement tumoral (droite), les dysfonctionnements des systèmes vasculaires et lymphatiques conduisent à une accumulation de liquide et à un dérèglement de la PHI. Elle devient alors plus élevée au centre de la tumeur, générant ainsi des flux allant du centre vers la périphérie de la tumeur.

C'est donc logiquement que des stratégies visant à normaliser la vasculature dans l'environnement tumoral ont été testées dans le but de réduire la pression hydrostatique interstitielle et potentialiser la diffusion de molécules thérapeutiques à la tumeur. Les utilisations d'anti-VEGF (Tong et al., 2004) ou très récemment, de nanoparticules comportant à la fois de la doxorubicine pour cibler les cellules tumorales et du Sunitinib pour normaliser la vasculature (Zeng et al., 2023), ont permis d'obtenir de bons résultats.

Outre la pression hydrostatique interstitielle dont le rôle est bien décrit, d'autres paramètres biomécaniques liés au liquide interstitiel peuvent entrer en jeu au site de tumeur primaire. Des travaux récents ont par exemple suggéré que l'élévation du niveau de viscosité de ce liquide pourrait favoriser la migration des cellules tumorales (Bera et al., 2022).

iii) Rigidité de la matrice extracellulaire

La rigidification des tissus est une caractéristique clé des pathologies cancéreuses qui a historiquement pu être exploitée pour diagnostiquer la maladie. Diverses techniques de mesure de rigidité par élastographie permettent de distinguer les tissus sains des tissus cancéreux dans la prostate (Cochlin et al., 2002), le pancréas (Carrara et al., 2018) ou encore le sein (Boyd et al., 2014). Dans certains cas, la sensibilité de ces mesures peut également permettre de distinguer tumeurs bénignes et malignes. Cela s'est notamment vérifié dans la prostate (Rouvière et al., 2017), le foie (Shahyari et al., 2019) et le sein (Evans et al., 2012).

La rigidification des tissus s'explique principalement par le remodelage de la matrice extracellulaire lorsque l'équilibre entre sécrétion et dégradation de protéines de matrice est rompu. On citera le collagène, la fibronectine ou encore la ténascine-C comme principales protéines de matrice extracellulaire sur-sécrétées (Mohammadi and Sahai, 2018). Dans le cas du collagène, c'est aussi particulièrement sa réticulation et le réalignement de ses fibres qui contribue à la rigidification de l'environnement (Provenzano et al., 2006 ; Levental et al., 2009). Ces mécanismes de remodelage sont principalement orchestrés par un sous-type de fibroblastes appelés "fibroblastes associés au cancer" (CAFs). La forte signalisation TGF- β trouvée dans

l'environnement tumoral pousse en effet les fibroblastes à adopter un phénotype de myofibroblaste associé à une forte sécrétion de protéines de matrice (collagène, acide hyaluronique notamment) (Massagué, 2008).

De plus, ces fibroblastes répondent à la rigidification de leur environnement en augmentant leur activité contractile (Choquet et al, 1997), notamment via le mécano-transducteur YAP (Dupont et al., 2011 ; Calvo et al., 2013). Il en résulte l'application de forces de contraction sur les fibres de matrice extracellulaire, générant ainsi du stress mécanique solide (Han et al., 2018) en plus de contribuer au remodelage et à la rigidification de l'environnement (Goetz et al., 2011). Certains effets du stress mécanique solide tels que la compression des vaisseaux sanguins peuvent ainsi être inversés en inhibant la production de protéines de matrice (Chauhan et al., 2013).

Les conséquences de la rigidification de la matrice extracellulaire sont multiples. Comparablement aux effets du stress compressif discutés précédemment, des expériences *in vitro* montrent que la rigidification de l'environnement peut réguler la croissance des sphéroïdes en ralentissant la prolifération des cellules tumorales (Taubenberger et al., 2019), mais améliore leurs capacités d'invasion et migration (Pathak and Kumar, 2012 ; Lang et al., 2015). L'analyse d'échantillons dérivés de patients humains confirme le lien entre rigidité et invasion/migration améliorées (Acerbi et al., 2015). Outre la rigidité, c'est également l'organisation de la matrice qui facilite l'invasion des cellules tumorales. En effet, ces dernières peuvent utiliser les fibres de collagène alignées comme autoroutes de migration pour envahir les tissus environnants (Provenzano et al., 2006). Des données suggèrent également que la rigidité de la matrice pourrait également promouvoir la migration des cellules tumorales en induisant leur transition épithélio-mésenchymateuse (Yang et al., 2022). En plus d'affecter les cellules tumorales et stromales, la rigidification de la matrice contribue à la mise en place d'une vasculature perméable et défectueuse dans l'environnement tumoral (Bordeleau et al., 2017).

Par ses liens avec le stress compressif et la perturbation des vaisseaux, la rigidité de la matrice et les fibroblastes qui orchestrent son remodelage peuvent être ciblées dans le but d'améliorer la diffusion de molécules thérapeutiques. Les CAFs peuvent par exemple être ciblés via des inhibiteurs de la voie de signalisation hedgehog, résultant en une meilleure diffusion de molécules thérapeutiques (Olive et al., 2009) et en une réponse immunitaire améliorée (Steele et al., 2021). Les mêmes effets positifs peuvent être obtenus avec l'utilisation d'inhibiteurs de lysyl oxydase (LOX), une enzyme qui

contribue fortement à la réticulation des protéines de la matrice et à sa rigidification (Levental et al., 2009 ; Miller et al., 2015).

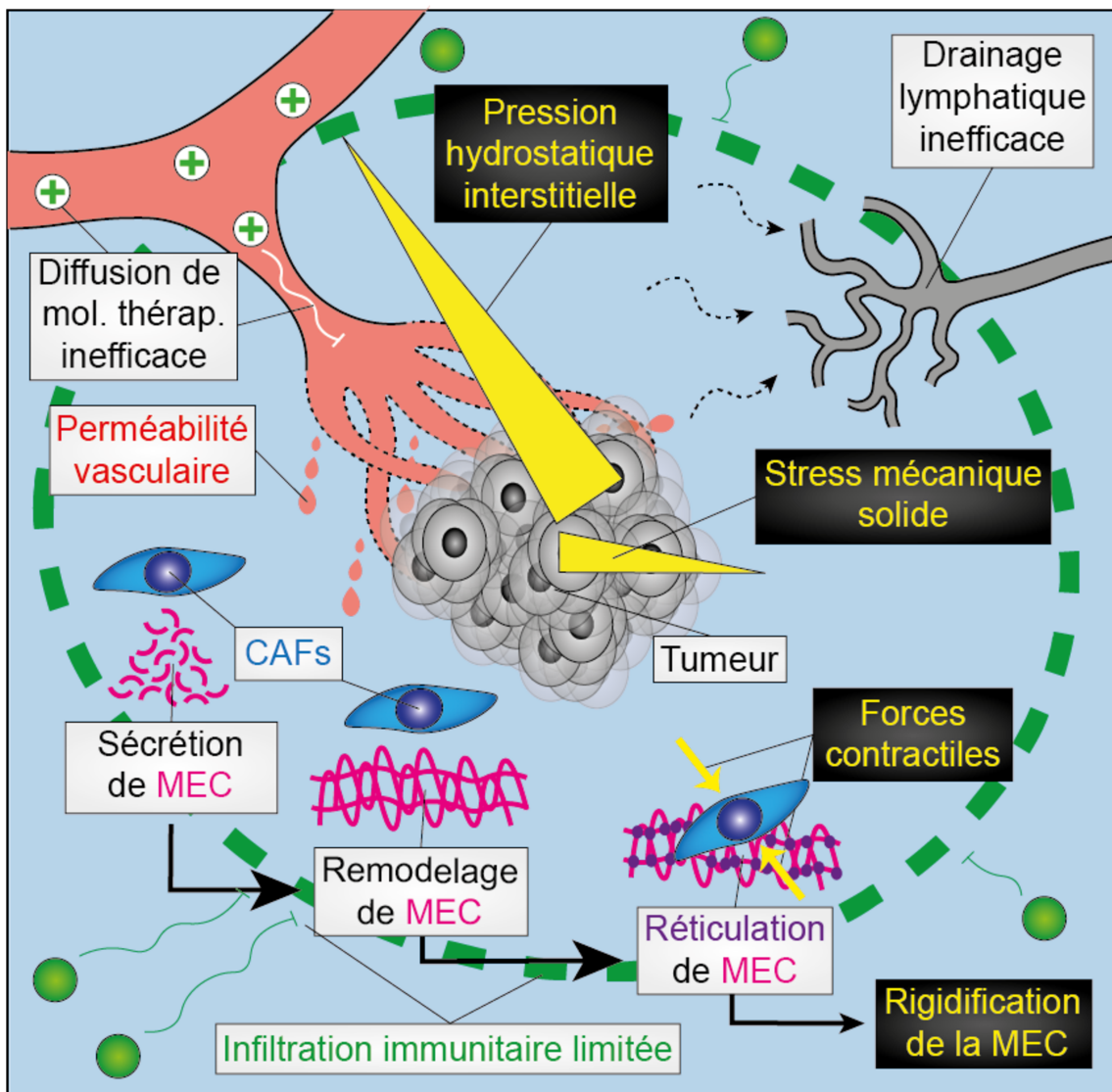


Figure 6 : Résumé des forces biomécaniques opérant au site de tumeur primaire. La croissance du volume tumoral et l'activité contractile des fibroblastes génèrent du stress mécanique solide dans l'environnement. La perméabilité de la vasculature et l'inefficacité du système lymphatique conduisent à l'élévation de la pression hydrostatique interstitielle. La sécrétion de protéines de matrice extracellulaire (MEC), leur remodelage et leur réticulation induisent la rigidification de la matrice. L'ensemble de ces modifications limite la diffusion de molécules thérapeutiques et l'infiltration de cellules immunitaires. (Adapté de Mittelheisser*, Gensbittel* et al., Nature Nanotechnology, in press).

2) Environnement intravasculaire

Après les étapes d'invasion, de migration et d'intravasation, les cellules tumorales deviennent des cellules tumorales circulantes (CTCs) et sont soumises à un environnement drastiquement différent dans lequel de nouveaux paramètres biomécaniques interviennent et jouent un rôle critique dans la suite de la progression tumorale.

i) Forces de cisaillement

Les forces de cisaillement se définissent par la conjonction de deux forces inégales s'appliquant parallèlement à la surface d'un élément et causant ainsi sa déformation. Dans le contexte de la circulation de cellules tumorales, des forces de cisaillement s'appliquent sur les CTCs en raison du différentiel de vitesse d'écoulement du flux, qui est maximale au centre du vaisseau et minimale à son extrémité (Loi de Poiseuille).

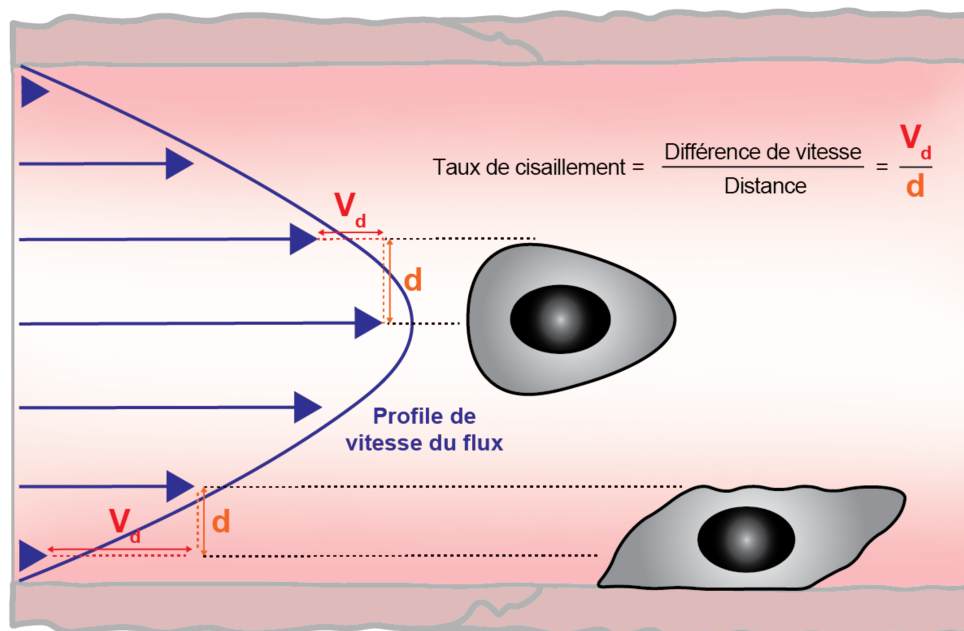


Figure 7 : Forces de cisaillement. Les cellules tumorales circulantes sont déformées par les forces de cisaillement dans l'environnement intravasculaire. La déformation est d'autant plus importante pour les cellules adhérentes à la paroi, où les forces de cisaillement sont les plus élevées. (Adapté de [Gensbittel et al., Developmental Cell, 2021](#))

La grandeur de ces forces peut varier drastiquement d'un type de vaisseau à un autre. On trouve des contraintes de cisaillement allant de 0,64 à 12 Dyn.cm⁻² dans le système lymphatique, de 1 à 4 Dyn.cm⁻² dans les veines, de 10 à 20 Dyn.cm⁻² dans les capillaires et de 4 à 30 Dyn.cm⁻² dans les artères (Coffman & Lempert, 1975 ; Ashikawa et al., 1986 ; Dixon et al., 2006 ; Follain et al., 2020). Les grandeurs de forces de cisaillement peuvent également significativement varier entre différents organes, ce qui peut être particulièrement pertinent pour la discussion de la dimension biophysique du phénomène d'organotropisme évoqué précédemment. Elles peuvent par exemple être 6 à 7 fois plus grandes dans le cerveau comparé aux poumons (Follain et al., 2020). Les forces de cisaillement peuvent significativement affecter les CTCs qui y sont exposées. Une exposition prolongée à des niveaux de forces de cisaillement élevés, tels qu'on en trouve par exemple dans les artères au cours d'un exercice physique (60 Dyn.cm⁻²), peut détruire jusqu'à 90% des CTCs en 4H d'exposition, et induire l'apoptose dans les 10% de cellules survivantes dans les 16 à 24 heures suivant l'exposition, neutralisant donc virtuellement toutes les CTCs (Regmi et al., 2017). Par ailleurs, les forces de cisaillement ne s'appliquent pas qu'au moment où les cellules tumorales circulent, mais également lorsqu'elles sont adhérentes à la paroi de l'endothélium. Dans cette configuration, des données montrent que des expositions à des forces de cisaillement tout à fait pertinentes en termes de grandeurs (0,5 à 12 Dyn.cm⁻²) et de durées (12 à 48 heures) peuvent induire l'arrêt du cycle cellulaire et l'apoptose dans divers modèles de cellules tumorales (Chang et al., 2008 ; Lien et al., 2013).

Il est intéressant de resituer ces effets délétères de l'exposition aux forces de cisaillement dans le contexte de l'inefficacité notoire du processus métastatique. Les cellules tumorales sont très efficaces dans leur utilisation du système circulatoire pour se disséminer. Des cellules tumorales circulantes peuvent en effet être générées à des stades encore très précoces du développement de la tumeur primaire, et ces CTCs précoces pourraient être à l'origine de la grande majorité des métastases (Hosseini et al., 2016). Des travaux ont également montré que le transit dans la circulation se déroule sans accroc pour la majorité des CTCs. Des expériences de métastases expérimentales dans le modèle souris (foie et poumon) ont en effet permis de montrer que 70 à 80% des cellules tumorales injectées dans la circulation s'arrêtent et s'extravasent efficacement dans les organes ciblés, mais que seule une infime partie

d'entre elles prolifère ensuite pour donner naissance à des métastases (Luzzi et al., 1998 ; Cameron et al., 2000). Les effets délétères de l'exposition prolongée aux forces de cisaillement pourraient être à l'origine de ce phénomène. Ces effets se font même ressentir encore plus tôt dans des expériences de métastases expérimentales cérébrales, puisque seule la moitié des cellules tumorales arrêtées dans le cerveau résistent aux forces de cisaillement et parviennent à s'extravaser (Kienast et al., 2010). Ainsi, il n'est probablement pas aberrant d'avancer que les forces de cisaillement sont certainement un des freins les plus importants à la progression métastatique.

Néanmoins, l'exposition à des forces de cisaillement peut également avoir des effets bénéfiques aux cellules tumorales. Il a en effet été démontré qu'une exposition à des forces de cisaillement faibles (0,05 à 5 Dyn.cm⁻²), telles qu'on peut en trouver dans le système lymphatique, améliore les capacités de migration des cellules tumorales via l'expression de YAP1 (Lee et al., 2017). Des forces de cisaillement de niveaux similaires (4,5 Dyn.cm⁻²) pourraient également induire une transition épithélio-mésenchymateuse et conférer aux cellules tumorales des capacités d'auto-renouvellement, augmentant ainsi leur potentiel métastatique (Choi et al., 2019). Ces données sont pertinentes compte-tenu du fait que les cellules tumorales s'intravasent fréquemment dans le système lymphatique dans un premier temps avant de rejoindre la circulation sanguine dans un deuxième temps (Brown et al., 2018 ; Pereira et al., 2018), et que les cellules tumorales transitant par le système lymphatique peuvent être à l'origine d'une proportion assez importante des métastases (un tiers dans le cancer colorectal humain par exemple) (Naxerova et al., 2017). Des travaux récents montrent qu'en plus d'octroyer des capacités d'auto-renouvellement, les forces de cisaillement pourraient également conférer aux cellules tumorales le don d'échapper à la surveillance immunitaire (Huang et al., 2023). Enfin, les forces de cisaillement pourraient également faciliter l'extravasation des cellules tumorales puisqu'elles sont impliquées dans le déclenchement d'un mécanisme de remodelage endothélial, qui extirpe les cellules tumorales arrêtées de la circulation, très bien décrit dans le modèle poisson-zèbre (Stoletov et al., 2010 ; Allen et al., 2016 ; Follain et al., 2018 ; Follain et al., 2021) (Annexe 1) et dans les capillaires du cerveau dans le modèle souris (Karreman et al., 2023).

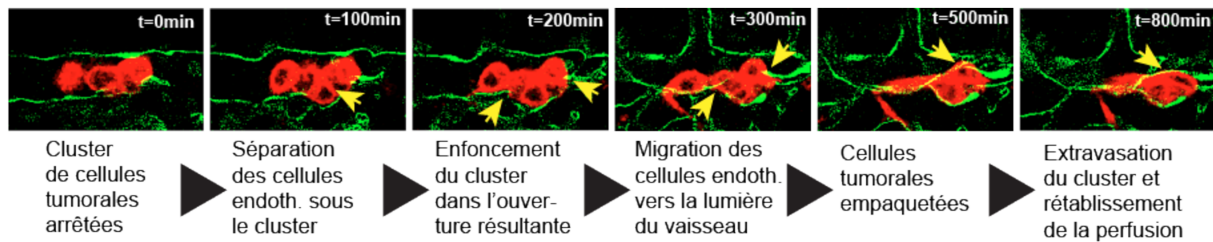


Figure 8 : Extravasation de cellules tumorales par remodelage endothélial. Time lapse de microscopie confocale montrant l'extravasation d'un cluster de cellules tumorales par remodelage endothélial. (Extrait de [Follain et al., Developmental Cell, 2018](#)).

L'ensemble de ces données montrent ainsi que les forces de cisaillement représentent un aspect biomécanique déterminant auquel les cellules tumorales sont particulièrement exposées au cours des étapes intravasculaires du développement métastatique.

ii) Forces d'adhésion

Les forces d'adhésion jouent un rôle critique dans l'étape d'arrêt intravasculaire des CTCs. Des travaux ont en effet suggéré qu'à lui seul, le phénomène d'occlusion qui survient lorsqu'une cellule tumorale s'arrête dans un vaisseau en le bouchant ne permet pas, dans la plupart des cas, aux CTCs de s'arrêter de manière suffisamment stable ([Gassmann et al., 2009](#)).

Le modèle de Bell décrit les multiples paramètres entrant en jeu dans l'adhésion et comment ils s'affectent les uns les autres. Sont particulièrement importants la taille de la surface d'interaction entre les cellules, la fréquence à laquelle des interactions ligand-récepteur se forment, la fréquence à laquelle ces mêmes interactions se rompent, la force de ces interactions et les forces extérieures qui s'y opposent ([Bell et al., 1978](#) ; [Bell et al., 1984](#)).

Différents comportements d'arrêt, d'adhésion et d'extravasation ont été décrits pour les cellules tumorales, avec l'intervention de différentes molécules d'adhésion. Des travaux ont montré que certaines cellules tumorales imitent les leucocytes en ayant recours au même enchaînement de 1) Rolling (roulement contre la paroi endothéliale), 2) adhésion stable et 3) extravasation par diapédèse ([Vestweber et al., 2015](#)). La première étape de rolling fait intervenir un ligand (CD24, CD44, DR3, N-Cadhérine, ...)

à la surface des CTCs qui se lie aux récepteurs sélectine (types P ou E principalement) des cellules endothéliales, assez faiblement pour permettre le rolling (Aigner et al., 1998 ; Strell and Entschladen, 2008). Dans un second temps, des molécules d'adhésion différentes interviennent pour mettre un terme au rolling et stabiliser l'arrêt et l'adhésion. Il s'agit souvent d'intégrines, de VCAM-1 ou de galéctines (Strell and Entschladen, 2008). Bien que moins bien décrite que pour les leucocytes, l'étape d'extravasation des cellules tumorales par diapédèse peut par exemple faire intervenir la N-cadhérine (Qi et al., 2005) ou CD44 (Offeddu et al., 2021).

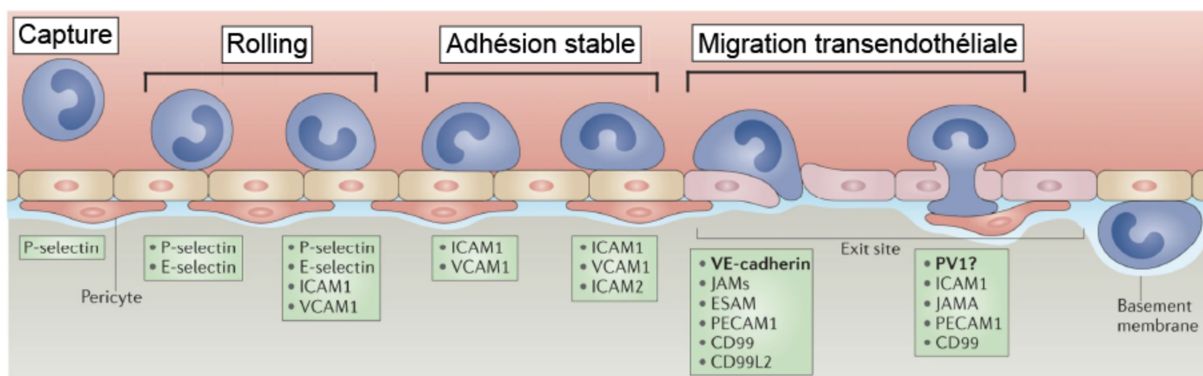


Figure 9 : Mécanisme de « rolling » des leucocytes. Une fois entrés en contact avec la paroi endothéliale, des forces d'adhésion faibles sont engagées dans un premier temps et permettent aux leucocytes de rouler le long de la paroi jusqu'à l'engagement de forces d'adhésion fortes, permettant l'arrêt stable et l'extravasation par diapédèse. (Adapté de Vestweber et al., *Nature Reviews Immunology*, 2015).

Alternativement, les cellules tumorales peuvent également s'arrêter et s'adhérer sans étape de rolling. Dans ce cas, le processus menant à l'extravasation des cellules tumorales se compose toujours de 3 étapes comme pour les leucocytes, sans roulement le long de la paroi endothéliale entre les établissements des adhésions faibles et fortes. CD44 et les intégrines $\beta 3$ ont notamment été identifiés comme responsables des adhésions faibles (80 pN), tandis que les intégrines $\beta 1$ stabiliseraient l'adhésion avec des forces plus élevées (> 200 pN) (Follain et al., 2018 ; Osmani et al., 2019).

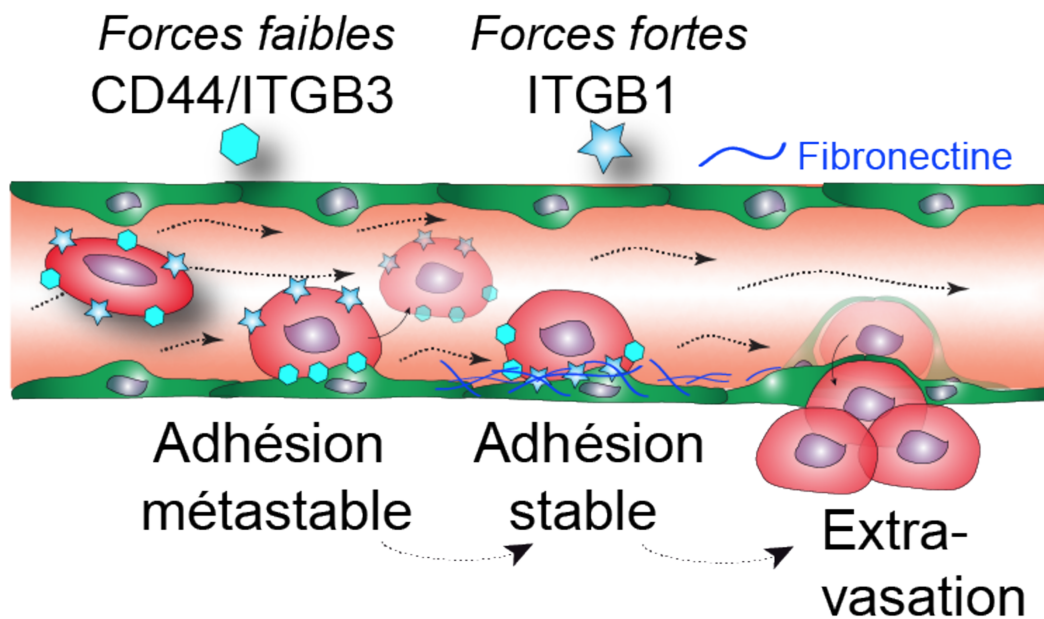


Figure 10 : Processus en deux temps de l’adhésion de cellules tumorales circulantes. Adapté de [Osmani et al., Cell Reports, 2019](#)).

Des travaux ont montré que la combinaison et la compatibilité des ligands et récepteurs exprimés à la surface des cellules tumorales et endothéliales sont des paramètres essentiels dictant les possibilités d’établissement de métastases en des organes spécifiques ([Hiratsuka et al., 2011](#) ; [Paul et al., 2019](#)). Outre cette contribution moléculaire, la dimension biophysique et les forces d’adhésion de ces interactions ligands/récepteurs sont également étroitement liées au phénomène d’organotropisme au travers de leur “collaboration” avec les forces hémodynamiques.

i) et ii) Forces de cisaillement vs Forces d’adhésion

Les forces d’adhésion et les forces de cisaillement se livrant une bataille dont l’issue dicte la possibilité de l’arrêt et de l’adhésion stable des CTCs, elles impactent donc aussi fortement les lieux d’extravasation et de croissance métastatique des cellules tumorales. Il a en effet été démontré in vivo que les CTCs s’arrêtent et s’extravasent dans des régions vasculaires présentant des flux dits “permissifs”, où les forces de cisaillement sont assez modérées pour permettre aux CTCs de s’arrêter et s’adhérer stablement, mais dans le même temps, suffisamment élevées pour contribuer au déclenchement de l’extravasation par remodelage endothélial ([Follain et al., 2018](#) ;

Follain et al., 2021) (Annexe 1). Cela semble également être le cas dans le contexte de métastases cérébrales chez l'humain, où l'analyse cartographique des sites de foyers métastatiques révèle que les foyers métastatiques apparaissent dans les régions vasculaires du cerveau présentant des flux permissifs (Follain et al., 2018).

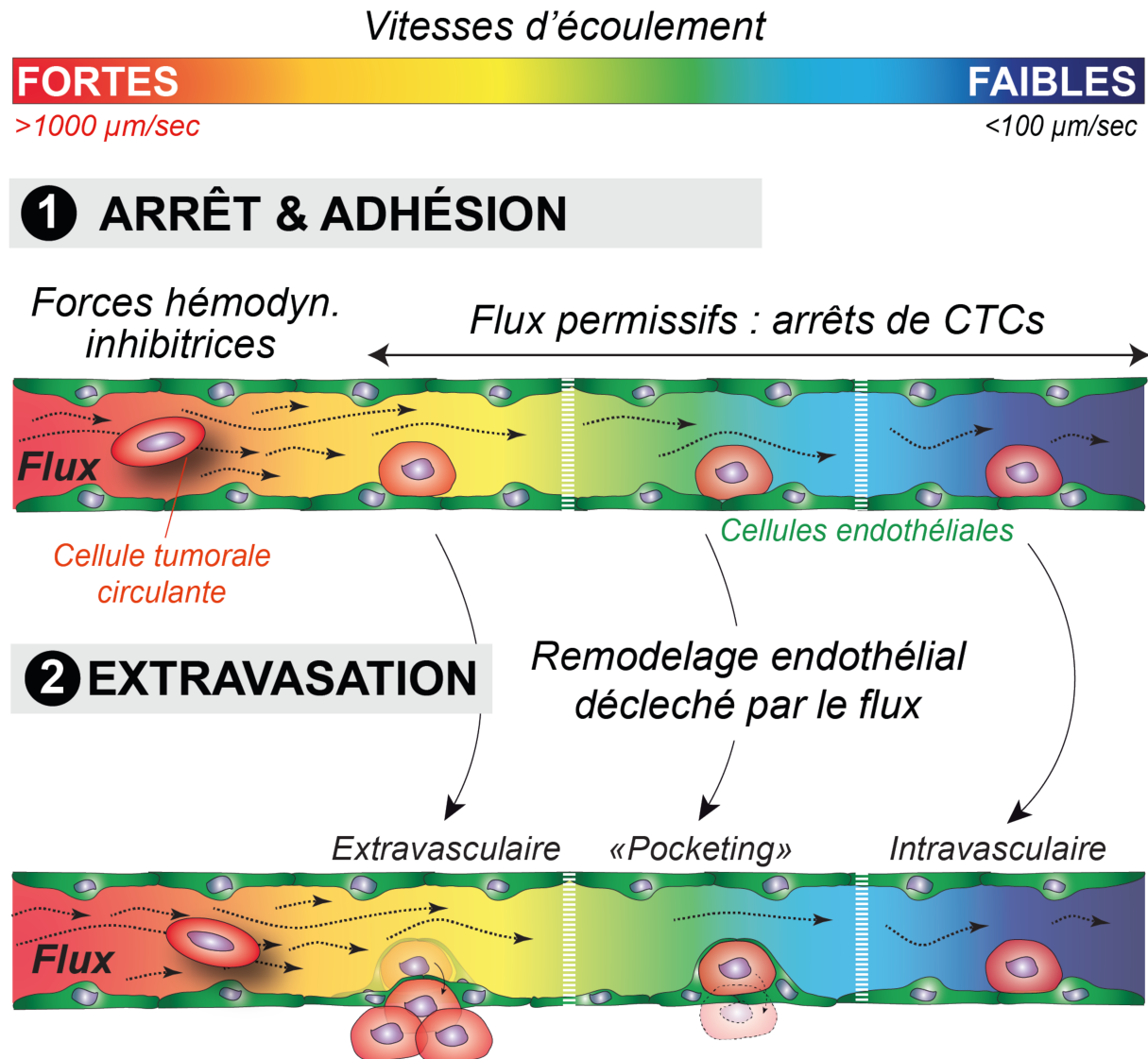


Figure 11 : Flux permissifs pour l'arrêt, l'adhésion et l'extravasation de CTCs. Les forces du flux sanguin ne doivent pas excéder les forces d'adhésion entre les CTCs et les cellules endothéliales sous peine de les arracher avant qu'elles n'aient pu stabiliser leur arrêt. Des forces hémodynamiques trop faibles ne sont cependant pas bénéfiques aux CTCs puisqu'un seuil minimum est requis pour le déclenchement de l'extravasation via remodelage endothélial. (Adapté de Follain et al., *Developmental Cell*, 2018).

Outre les forces hémodynamiques, un autre paramètre de l'environnement intravasculaire exerce des forces mécaniques et coopère avec les forces d'adhésion pour favoriser l'arrêt des CTCs : l'architecture vasculaire.

iii) Architecture vasculaire

Les caractéristiques géométriques du système vasculaire jouent elles aussi un rôle biomécanique important dans l'arrêt des CTCs. Des vaisseaux présentant beaucoup de courbures seraient par exemple des sites d'arrêt plus probables de CTCs (Paul et al., 2019). Des analyses numériques ont suggéré que de tels vaisseaux tortueux offrent une surface d'interaction plus importante aux CTCs, favorisant ainsi leur adhésion en leur permettant de former un plus grand nombre d'interactions ligands/récepteurs (Cui et al., 2020). Plus déterminant encore que leur forme, leur diamètre est un moteur majeur de l'arrêt intravasculaire de CTCs. Le modèle qui veut qu'une CTC s'arrête logiquement lorsqu'elle rencontre un vaisseau dont le diamètre est inférieur à son propre diamètre (Wirtz et al., 2011) est appuyé par de nombreuses données. Des expériences d'injection de cellules tumorales dans des rats de tailles différentes ont révélé qu'une réduction du diamètre moyen des vaisseaux sinusoides du foie de 2 μm entraîne une multiplication par 4 du nombre de cellules arrêtées par occlusion dans ces vaisseaux 5 minutes après injection (Gassmann et al., 2009). Une technique poussée de microscopie intravitale a permis de constater que des cellules tumorales s'arrêtent en se logeant dans de petits capillaires du poumon de souris dans la minute suivant l'injection intravasculaire (Headley et al., 2016). Une technologie similaire utilisée pour visualiser le même type d'événements dans le cerveau a révélé que la grande majorité des CTCs s'arrêtent dans le système vasculaire du cerveau le font après ralentissement en des sites de bifurcations vasculaires où le ratio diamètre CTC / diamètre vaisseau est égal à 1 (Kienast et al., 2010). De récentes analyses numériques sont en accord avec ces observations et établissent-elles aussi un lien entre diamètre relatif CTC/vaisseau et vitesse de circulation (Milosevic et al., 2023)

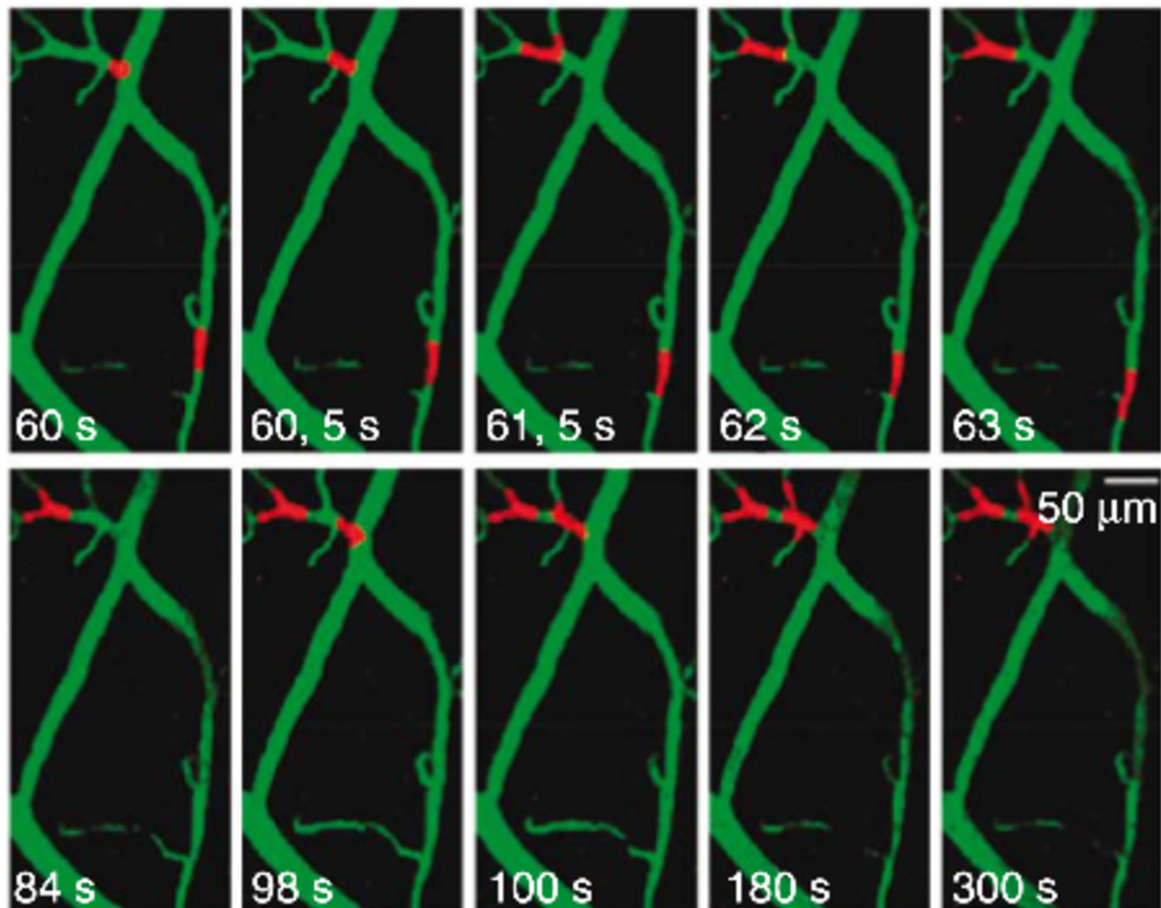


Figure 12 : Arrêt intravasculaire de CTCs dans les capillaires du cerveau de souris. Des cellules de carcinome de poumon (PC14-PE6) s'arrêtent en des sites de bifurcations vasculaires du cerveau de souris lors de leurs premiers instants de circulation après injection dans l'artère carotidienne. (Extrait de [Kienast et al., Nature Medicine, 2010](#)).

Pour une CTC, la rencontre d'un vaisseau étroit constitue une véritable contrainte mécanique qui n'est pas sans conséquences. Un passage d'une forme sphérique à une forme cylindrique a pu être observé dans toutes les études citées ci-dessus s'intéressant à l'arrêt de CTCs dans des capillaires ([Gassmann et al., 2009](#) ; [Headley et al., 2016](#) ; [Kienast et al., 2010](#)). De tels changements drastiques de formes s'accompagnent de fortes augmentations d'aires de surface qui, dans un premier temps, ne causent pas de dégâts grâce à l'accessibilité des CTCs à leurs excès de membrane, mais qui entraînent ensuite la destruction d'une proportion significative de CTCs passant un certain seuil de déformation ([Weiss et al., 1992](#)). En accord avec ces observations, il a été observé qu'une mutation encodant une forme tronquée de Pannexine-1 et résultant en une activité mécano-sensible et anti-apoptotique de

canaux PANX1, permet à des cellules métastatiques de survivre à leurs changements drastiques de formes qui devraient normalement causer leur mort dans la microvasculature (Furlow et al., 2015). Ce mécanisme n'est pas sans rappeler des observations faites dans des cellules tumorales migrants au travers de pores contraignants dans la matrice extracellulaire. Un mécanisme de réparation de dommages à l'enveloppe nucléaire permet en effet à certaines cellules tumorales de survivre aux dégâts de déformation et rupture de leur enveloppe nucléaire tout en bénéficiant des changements pro-métastatiques qui en résultent (Denais et al., 2016). Les preuves de l'existence de bénéfices pro-métastatique similaires résultant de la déformation intravasculaire de CTCs commencent également à apparaître. S'il était déjà connu que le noyau est lui aussi significativement déformé au moment de l'importante déformation cylindrique d'une CTC passant dans un capillaire contraignant (Yamauchi et al., 2005), des données toutes récentes indiquent que la déformation drastique dans les capillaires sélectionne des CTCs mécano-résistantes, avec des voies de prolifération et de réparation des dommages à l'ADN suractivées (Jiang et al., 2023).

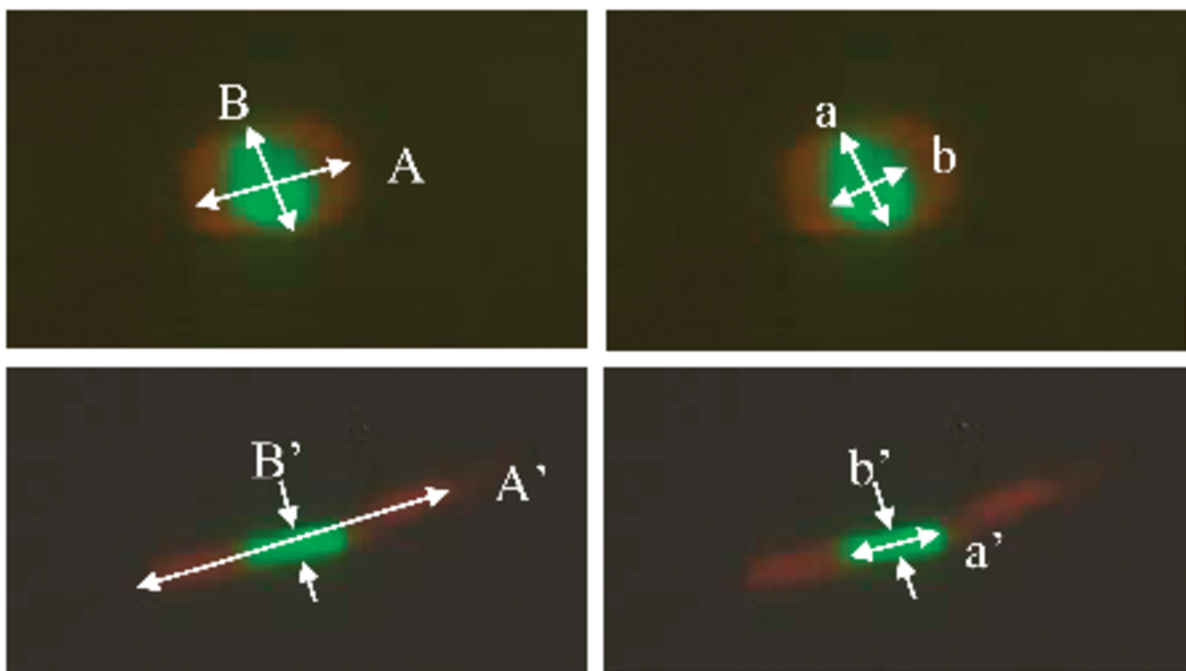


Figure 13 : Déformations de CTCs et de leur noyau dans l'environnement intravasculaire. Un marquage du cytoplasme (rouge) et du noyau (vert) permet de visualiser les formes cylindriques adoptées par des cellules de fibrosarcome (HT-1080) et leurs noyaux dans les capillaires sanguins (images du bas) (Extrait de Yamauchi et al., Cancer Research, 2005).

L'environnement intravasculaire, avec ses forces hémodynamiques, les molécules d'adhésion disponibles à la surface de ses cellules endothéliales et l'architecture de ses vaisseaux présente donc plusieurs défis mécaniques aux cellules tumorales circulantes. Combinés aux nombreuses contributions biophysiques discutées précédemment lors des étapes les plus précoces de la progression tumorale, nous avons ainsi vu que les facteurs biomécaniques sont omniprésents à tous les stades de la cascade métastatique, de la croissance de la tumeur primaire à l'extravasation des cellules tumorales circulantes qui précède l'étape finale de croissance métastatique.

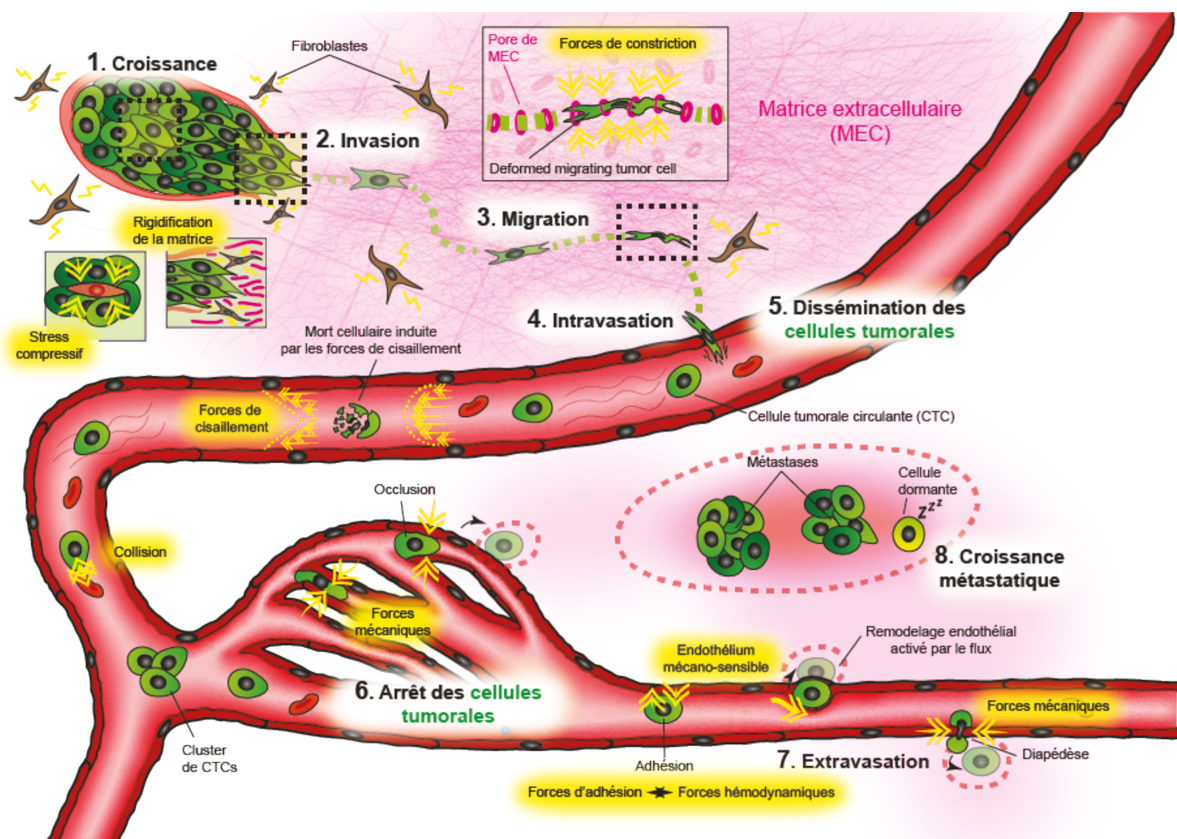


Figure 14 : Résumé des principales forces biomécaniques rencontrées par les cellules tumorales lors de la succession des étapes de la cascade métastatique. (Adapté de Collin*, Gensbittel* et al., Comptes Rendus Biologies, 2021)

Les contributions de ces nombreux facteurs biomécaniques au cours du développement métastatique ont par ailleurs fait l'objet de trois articles auxquels j'ai contribué : un article de recherche dans lequel nous démontrons qu'inhiber la signalisation flux-dépendante VEGFR permet d'enrayer l'extravasation via remodelage endothélial des cellules tumorales, et deux reviews dans lesquelles ces nombreuses contributions biomécaniques sont résumées :

Impairing flow-mediated endothelial remodeling reduces extravasation of tumor cells

Gautier Follain*, Naël Osmani*, Valentin Gensbittel, Nandini Asokan, Annabel Larnicol, Luc Mercier, Maria Jesus Garcia-Leon, Ignacio Busnelli, Angélique Pichot, Nicodème Paul, Raphaël Carapito, Seiamak Bahram, Olivier Lefèbvre, Jacky G. Goetz
Scientific Reports, Jun 23;11(1):13144., 2021

ANNEXE 1

Influence de la mécanique des fluides sur la formation de métastases

Gautier Follain*, Valentin Gensbittel*, Benjamin Mary*, Olivier Lefèbvre, Sébastien Harlepp, Vincent Hyenne, Jacky G. Goetz
Médecine/Science (Paris), Oct;36(10):872-878, 2019

ANNEXE 2

Biomechanics: a driving force behind metastatic progression

Florent Collin*, Valentin Gensbittel*, Jacky G. Goetz
Comptes Rendus. Biologies, Tome 344 no. 3, pp. 249-262., 2021

ANNEXE 3

C) L'adaptabilité mécanique des cellules tumorales

L'accumulation des contraintes mécaniques rencontrées par les cellules tumorales au cours des étapes successives de la cascade métastatique doit forcément menacer leur intégrité mécanique. En ajustant précisément leurs propriétés mécaniques, les cellules tumorales pourraient s'adapter aux nombreuses forces mécaniques qui menacent leur progression métastatique. En particulier, leur degré de rigidité et leur capacité à se déformer pourraient être essentiels pour faire face aux défis biomécaniques dont il est ici question. Les preuves de tels mécanismes d'adaptation ont récemment commencé à émerger. Nous en avons profité pour écrire un article de type "Perspective" résumant ces données et présentant, pour la première fois, l'hypothèse que l'adaptabilité mécanique des cellules tumorales joue un rôle majeur au cours de la progression tumorale.

1) Résumé en français

L'aspect le plus dangereux des pathologies cancéreuses réside dans le développement de métastases. Les cellules tumorales parviennent à former des métastases potentiellement mortelles lorsqu'elles franchissent des étapes séquentielles au cours de leur acheminement de la tumeur primaire vers des organes distants. D'un point de vue biomécanique, la croissance, l'invasion, l'intravasation, la circulation, l'arrêt/adhésion et l'extravasation des cellules tumorales exigent des propriétés mécaniques cellulaires particulières pour survivre et compléter la cascade métastatique. Les cellules métastatiques étant généralement plus molles que leurs homologues non malignes, il est supposé qu'une grande déformabilité de la cellule et de son noyau augmente le potentiel métastatique. Cependant, on ne sait toujours pas s'il existe un état mécanique finement réglé mais fixe qui intègre toutes les caractéristiques mécaniques nécessaires à la survie tout au long de la cascade ou si les cellules tumorales doivent affiner dynamiquement leurs propriétés et leurs composants intracellulaires à chaque nouvelle étape rencontrée. Dans cet article, nous passons en revue les différentes exigences mécaniques auxquelles les cellules cancéreuses doivent répondre tout au long de leur parcours et nous spéculons sur la possibilité qu'elles adaptent dynamiquement leurs propriétés en conséquence. La signature mécanique d'une cellule cancéreuse performante pourrait en fait être sa capacité à s'adapter aux contraintes micro-environnementales successives tout au long des différentes étapes du développement métastatique.

Perspective

Mechanical Adaptability of Tumor Cells in Metastasis

Valentin Gensbittel,^{1,2,3} Martin Kräter,⁴ Sébastien Harlepp,^{1,2,3} Ignacio Busnelli,^{1,2,3} Jochen Guck,^{4,*} and Jacky G. Goetz^{1,2,3,*}

¹INSERM UMR_S1109, Tumor Biomechanics, Strasbourg, France

²Université de Strasbourg, Strasbourg, France

³Fédération de Médecine Translationnelle de Strasbourg (FMTS), Strasbourg, France

⁴Max Planck Institute for the Science of Light & Max-Planck-Zentrum für Physik und Medizin, Erlangen, Germany

*Correspondence: jochen.guck@mpl.mpg.de (J.G.), jacky.goetz@inserm.fr (J.G.G.)

<https://doi.org/10.1016/j.devcel.2020.10.011>

SUMMARY

The most dangerous aspect of cancer lies in metastatic progression. Tumor cells will successfully form life-threatening metastases when they undergo sequential steps along a journey from the primary tumor to distant organs. From a biomechanics standpoint, growth, invasion, intravasation, circulation, arrest/adhesion, and extravasation of tumor cells demand particular cell-mechanical properties in order to survive and complete the metastatic cascade. With metastatic cells usually being softer than their non-malignant counterparts, high deformability for both the cell and its nucleus is thought to offer a significant advantage for metastatic potential. However, it is still unclear whether there is a finely tuned but fixed mechanical state that accommodates all mechanical features required for survival throughout the cascade or whether tumor cells need to dynamically refine their properties and intracellular components at each new step encountered. Here, we review the various mechanical requirements successful cancer cells might need to fulfill along their journey and speculate on the possibility that they dynamically adapt their properties accordingly. The mechanical signature of a successful cancer cell might actually be its ability to adapt to the successive micro-environmental constraints along the different steps of the journey.

THE METASTATIC JOURNEY: COPING WITH STRESS AND EXTERNAL FORCES

Metastatic progression is by far the most lethal aspect of cancer, with the development of secondary tumors being responsible for 90% of the overall cancer-related deaths (Steege, 2016). The process leading to the development of these lethal secondary foci follows a “metastatic cascade” and comprises distinct sequential steps. It starts with a healthy cell acquiring mutations and epigenetic modifications leading to uncontrolled proliferation and tumor growth of an original primary solid tumor in a healthy tissue (Grandér, 1998; Vicente-Dueñas et al., 2018). This initial growth is accompanied by the development of a favorable microenvironment (Werb and Lu, 2015), notably through angiogenesis/lymphangiogenesis in the surroundings of the tumor by newly formed blood/lymphatic vessels (Stacker et al., 2014; Watnick, 2012), inflammatory-like immune response (Whiteside, 2006), and remodeling of the surrounding extracellular matrix (ECM) (Alexander and Cukierman, 2016). At the same time, some tumor cells from the primary tumor acquire new properties that allow them to exit the primary tumor and invade the surrounding stroma or move along nearby blood vessels (Gritsenko et al., 2017). Invasion into the local parenchyma can either be active (cell autonomous) and/or driven by interstitial fluid pressure occurring in the primary tumor (caused by the intra-tumoral growing cells and differences in pressure between the leaky blood vessels and the lymphatic vessels) (Piotrowski-Daspit

et al., 2016; Stuelten et al., 2018). Development of intra-tumoral lymphatic vessels favors lymph node metastasis (Karaman and Detmar, 2014) that, although not lethal, often accompanies the metastatic process. Distant metastasis that is life threatening, however, occurs upon dissemination within the bloodstream, achieved through intravasation directly into blood vessels. Interestingly, recent work has demonstrated that lymph node metastasis can act as platform for blood colonization (Brown et al., 2018; Pereira et al., 2018). Intravasation into blood vessels can be assisted by immune cells (Harney et al., 2015; Linde et al., 2018) and can occur as single cells or collective clusters of invasive cells (Cheung et al., 2016). Tumor cells are then referred to as circulating tumor cells (CTCs) as they transit in the blood flow. If CTCs manage to escape the immune system and survive the tug of war between the blood flow forces and the adhesion forces (Fan et al., 2016), they will eventually arrest and adhere to vessel walls (Osmani et al., 2019). Alternatively, they can also arrest independently from adhesion forces if they get trapped in small-sized capillaries (Kienast et al., 2010). In rare instances (notably in lung metastasis), tumor cells attached to the endothelium can proliferate and form intravascular metastases (Al-Mehdi et al., 2000). In most cases, however, tumor cells need to undergo extravasation, which is the process where arrested tumor cells exit blood circulation. Multiple mechanisms of extravasation have been described such as diapedesis (Strell and Entschladen, 2008) and endothelial remodeling (Lapis et al., 1988). This exiting of the circulation finally allows tumor cells to



reach the stroma/parenchyma of nearby organs, where they can either proliferate and form metastases if the microenvironment at the newly reached organ suits them (Peinado et al., 2017) or remain in a dormant state until their environment evolves and allows them to thrive (Aguirre-Ghiso, 2018; Nguyen et al., 2009).

As the tumor cells progress through all these steps, they are faced with various and changing external mechanical stresses challenging their survival and their progression, requiring specific mechanical properties. At the early steps of tumor growth, cells are exposed to increasing levels of compressive stress (Figure 1), respectively due to imbalances in entry and exit of fluids into the interstitial space (Mohammadi and Sahai, 2018) and the microenvironment pushing back on the expanding tumor volume (Jain et al., 2014; Stylianopoulos et al., 2012). Compressive stress increase is due to the combination of the tumor volume expanding and its microenvironment undergoing stiffening upon stroma remodeling, which occurs in several tumor types such as breast or pancreas cancer. Orchestrated mostly by stromal cells such as tumor-associated fibroblasts, stroma remodeling mainly consists of topographical perturbations and stiffening of the ECM and is known to favor invasion and metastasis (Clark and Vignjevic, 2015; Goetz et al., 2011; Pickup et al., 2014), notably through collagen crosslinking, integrin clustering (Levental et al., 2009; Paszek et al., 2005) and more importantly through induction of paths formed by radially aligned fibers (Provenzano et al., 2006). These tracks can then be used for collective tumor cell migration with help from leading fibroblasts (Gaggioli et al., 2007). Nonetheless, effects of the increasing compressive stress resulting from stroma remodeling include tumor cell-size reduction, proliferation defect and cell-cycle blocking, overall impairing tumor growth when studied *in vitro* (Delarue et al., 2014; Taubenberger et al., 2019). As a result of tumor volume expansion, increased compressive stress and ECM stiffening, cancer tissues are generally found to be stiffer than healthy tissues. At the clinical level, malignant tumors have indeed been shown to be significantly stiffer than their benign counterparts (Lorenzen et al., 2002; Venkatesh et al., 2008). In addition to contributing to compressive stress, a confining primary tumor environment also favors collective cancer cell invasion over single-cell invasion (Haeger et al., 2014). Such effects could drive the intravasation of invasive, soon-to-be CTC clusters, whose metastatic potential is increased 50-fold when compared with single CTCs (Aceto et al., 2014). Interestingly, tumor cell clusters have been found to express keratin-14 in some models (Cheung et al., 2016), which could be associated with increased stiffness (Seltmann et al., 2013) compared with tumor cells that underwent epithelial-to-mesenchymal transition (EMT) and instead display high expression of vimentin for example. The implications of tumor cell clustering for the mechanical properties and mechanical fitness of tumor cells currently remain a black box and will also briefly be speculated upon in this review.

Cancer cells are not only exposed to mechanical stress in the primary tumor environment but also very notably after intravasation, as they travel in the bloodstream and make their way through the intravascular steps of the metastatic cascade (Follain et al., 2020). Once they are circulating in the bloodstream (or within lymphatics), tumor cells are exposed to completely

different mechanical stresses (Figure 1) coming from hemodynamic forces and constricting blood vessels. CTCs have to cope with these stresses if they are to successfully complete the metastatic cascade (Follain et al., 2020). For example, high levels of fluid shear stress (> 1 Pa) have been shown to induce cell-cycle arrest (Chang et al., 2008) or even destroy tumor cells as they circulate (Regmi et al., 2017). In the end, only few CTCs might be able to escape the effects of the fluid shear stress and get the opportunity to arrest and adhere to the endothelium. Of note, also clusters of CTCs have been shown to traverse capillary-sized vessels, which might offer added protection (Au et al., 2016).

Two models prevail for CTC arrest in the blood circulation: they could either arrest by active adhesion to the vessel walls (Follain et al., 2018; Osmani et al., 2019), or by occlusion if the vessel is topographically disordered and/or of small diameter (Entenberg et al., 2018; Headley et al., 2016; Kienast et al., 2010; Paul et al., 2019; Wirtz et al., 2011) (Figure 1). The latter case often occurs in microcapillaries where CTCs are squeezed as they need to be advected through tight constrictions to reach extravasation sites near their target organs. Finally, successful macrometastatic outgrowth is initiated upon extravasation of arrested CTCs in perivascular areas. During this step, metastatic cells need to cross constraining obstacles such as the vascular wall or the blood-brain barrier (in the context of brain metastasis) to either enter dormancy or undergo expansion as the basis of life-threatening metastases.

All of the mechanical stresses that tumor cells encounter in these sequential phases of the metastatic cascade are unequivocally impacting their inner mechanical state. By fine-tuning their mechanical properties, tumor cells could adapt to the various mechanical stresses that threaten metastatic progression at each step of the way. In particular, their own tunable mechanical phenotype could be key in coping with the stresses discussed here. Although this is likely to happen, there is, to our knowledge, only limited demonstration that tumor cells change their mechanical profiles upon receiving specific mechanical or other cues during their progression through the metastatic cascade. We would like to take this opportunity to discuss these concepts and speculate on how mechanical properties of tumor cells could evolve along the cascade. Although they will not be the focus here, chemical and biochemical signals such as pH, temperature, cytokines, adhesive receptors, or oxidative stress are potentially also involved in cell mechanical adaptation (Scholz, 2018; Sun et al., 2014; Sunyer et al., 2009). In this review, we briefly discuss the mechanical profiles of tumor cells along their metastatic journey, complementing, updating, and extending existing reviews on this topic (Kumar and Weaver, 2009; Suresh, 2007; Wirtz et al., 2011). We also discuss how these mechanical profiles are initiated, controlled, and perturbed. We further speculate on how their deformation abilities might contribute to tumor metastasis and highlight why these aspects will be important avenues of research in the future. We finally promote the idea that the picture of a well-defined static mechanical phenotype of a cancer cell is incompatible with the varying mechanical properties required to successfully navigate the metastatic journey. Instead, it might be the ability to dynamically adjust to these requirements that is the mechanical signature of a successful metastatic cancer cell.

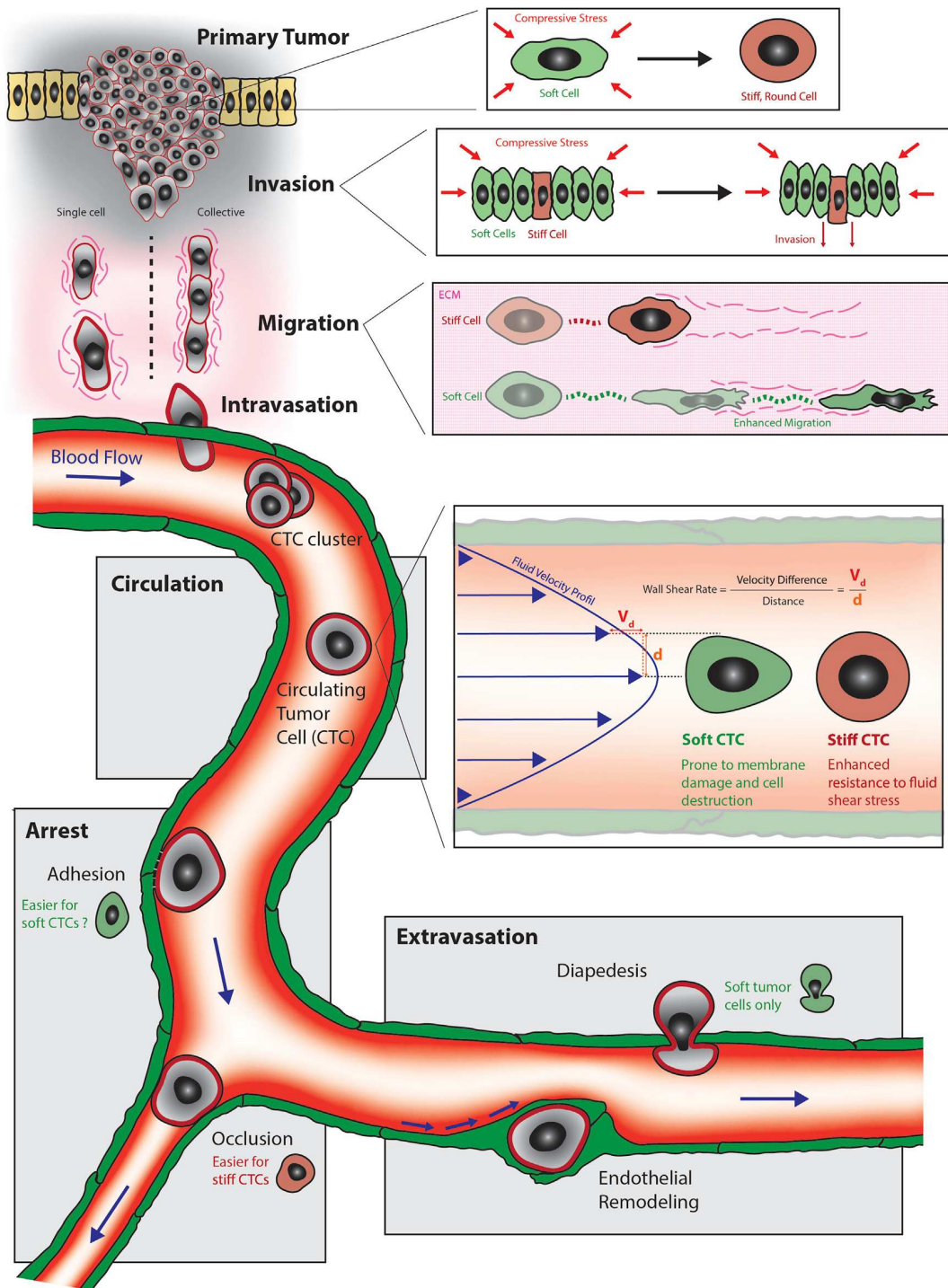


Figure 1. Speculative Look at the Role of Tumor Cell Stiffness throughout the Metastatic Cascade

Invasion, migration, intravasation, circulation, arrest, adhesion, and extravasation all challenge tumor cells' mechanical properties in different ways and favor different mechanical phenotypes.



Table 1. Overview of Select Techniques that Have Been Used to Measure Cancer Cell Mechanical Properties

Technique	Pros	Cons	References
Micropipette aspiration (MPA)	<ol style="list-style-type: none"> (1) Very versatile and robust (2) Can measure both adherent and suspended cells (3) Can quantify mechanical response to substrate stiffness (4) Models exist to extract viscoelastic properties 	<ol style="list-style-type: none"> (1) Low throughput (10 cells/hour) 	González-Bermúdez et al., 2019 ; Hochmuth, 2000 ; Ward et al., 1991
AFM	<ol style="list-style-type: none"> (1) Very sensitive (2) High spatial resolution possible to map distribution of mechanical properties across cell surface (3) Can quantify mechanical response to substrate stiffness (4) Models exist to extract viscoelastic properties 	<ol style="list-style-type: none"> (1) Low throughput (10 cells/hour) (2) Can only measure cells in contact with a surface 	Cross et al., 2007, 2008 ; Darling et al., 2007 ; Dong et al., 2016 ; Lekka et al., 1999 ; Li et al., 2008 ; Liu et al., 2020 ; Physical Sciences - Oncology Centers Network, 2013 ; Plodinec et al., 2012 ; Radmacher et al., 1996 ; Tavares et al., 2017 ; Thomas et al., 2013 ; Xu et al., 2012
Optical traps (e.g., OS)	<ol style="list-style-type: none"> (1) Can measure whole-cell mechanics without contact (2) Models exist to extract viscoelastic properties (3) Can be combined with microfluidic delivery for automation and sorting (4) Can measure circulating cells in native state 	<ol style="list-style-type: none"> (1) Low throughput (100 cells/hour) (2) Cannot measure cells while in contact with substrate 	Faigle et al., 2015 ; Guck et al., 2001, 2005 ; Gullekson et al., 2017 ; Lincoln et al., 2007 ; Remmerbach et al., 2009
Microfluidic techniques (e.g., RT-DC)	<ol style="list-style-type: none"> (1) High throughput (10–10,000 cells/s) (2) Can measure circulating cells in native state (3) Robust and easy to use 	<ol style="list-style-type: none"> (1) Most techniques have no models to extract elasticity (or even viscosity) (2) Only probe very short time-scale mechanics (ms – μs) (3) Cannot measure cells while in contact with substrate 	Ahmed et al., 2018 ; Ciucci et al., 2017 ; Deng et al., 2017 ; Guillou et al., 2016 ; Holenstein et al., 2019 ; Otto et al., 2015 ; Rosendahl et al., 2018 ; Tse et al., 2013 ; Wullkopf et al., 2018 ; Zhang et al., 2012

MEASURING CELLULAR MECHANICS: METHODS, RESULTS, AND LIMITATIONS

There is an urgent need to consider single-cell mechanics independently from tumor mechanics. Up to now, mechanics of tumors has been mostly studied by looking at the whole tumor or its associated stroma. Tissues of most solid tumors are well known to be stiffer than healthy tissues, which is actually exploited in manual palpation ([Levental et al., 2009](#)). However, stiffness of a tumor as a whole cannot be derived from the stiffness of the individual tumor cells that constitute it. First, it is composed of many additional stromal components (ECM, [Eble and Niland, 2019](#); stromal cells, [Denton et al., 2018](#)) that are likely to impact tumor stiffness. Second, many independent studies report that tumor cells are actually softer than healthy cells ([Albert et al., 2017](#)) even when measured in acute tumor slices ([Plodinec et al., 2012](#)). This consensus was reached through the use of a variety of different tools and methods that are available for studying single-cell mechanics across many studies. Although these methods will not be the focus of this review as other reviews have thoroughly covered them ([Darling and Di Carlo, 2015](#); [Urbanska et al., 2020](#); [Van Vliet et al., 2003](#); [Wu et al., 2018](#)), we briefly discuss the pioneer ones as well as the most

recent state-of-the-art tools (see [Table 1](#)) to provide some insight into the way the field is evolving. We will then report on the findings that these methods have enabled regarding tumor cell stiffness before discussing the limitations of these results.

Questions about cell mechanics and ways to probe them or to witness their importance were raised shortly after it first became possible to visualize cells thanks to the invention of the microscope ([Pelling and Horton, 2008](#)). Many steps have since been taken toward the invention of the many modern devices that are now available. Micropipette aspiration (MPA) was first used in the 1950s ([Mitchison and Swann, 1954](#)) and represents the first widely used tool for probing single-cell mechanical properties that is still in use today. Its principle consists in applying a negative pressure at the tip of the micropipette, thus, aspirating part of a cell inside a glass capillary and monitoring the length of cell that is aspirated over time. A variety of different continuum models exist for extracting the rheological parameters of the cells ([González-Bermúdez et al., 2019](#); [Hochmuth, 2000](#)). MPA can be used to study mechanics of both adherent and suspended cells. It was eventually replaced by atomic force microscopy (AFM) as the gold standard in single-cell mechanical analysis ([Dong et al., 2016](#); [Radmacher et al., 1996](#); [Thomas et al., 2013](#)). AFM probes the cells' mechanical properties in an

opposite way, by performing indentation into the cell instead of aspirating it. While generally limited to measuring cells adhered to a surface, its wide acceptance derives from the fact that it is robust yet sensitive. A distinct advantage is the use of differently sized probes, which allows the recording of both whole-cell stiffness and subcellular stiffness maps across the cell's surface. This range constitutes very different mechanical measurements, e.g., ranging from membrane bending stiffness and local cytoskeletal structures underlying the plasma membrane, to bulk cytoskeletal or nuclear measurements. It is also well suited for studying the role of substrate stiffness on cell mechanics (although the presence of the compliant substrate has to be properly accounted for its analysis; Rheinlaender et al., 2020). In contrast to measuring cells adhered to a surface, tools exploiting optical forces, such as the optical stretcher (OS), can trap and deform cells in suspension (Guck et al., 2001). The key feature that sets this technique apart from MPA or AFM is that measurements are completely contact free. This method was also the first that was combined with microfluidic delivery (Lincoln et al., 2007) and sorting (Faigle et al., 2015) to start overcoming the low-throughput flaw that previous methods presented. However, only with very recent developments in microfluidic approaches has cell mechanical analysis really become high throughput—now approaching the speed of conventional fluorescence-based flow cytometers. Real-time deformability cytometry (RT-DC) is one variant of a whole family of such microfluidic techniques developed in recent years (Otto et al., 2015; Urbanska et al., 2020). Cells are flowed at high speed (10 cm/s) through a microfluidic channel, in which they are deformed without any contact by shear stress and pressure gradients. This technique allows mechanical phenotyping at rates of >100 cells/s, opening entirely new applications in the fields of biotechnology and medicine (Toepfner et al., 2018). In summary, the methods for measuring single-cell mechanics come in all shapes and forms, allowing characterization of cells in suspension or on substrates, at the scale of a full cell or a precise region of interest on the cell's surface. Both elasticity and viscosity metrics can be extracted via methods that have varying throughput levels. The main limitation of all of these is that they fail in providing information about the mechanical states of tumor cells *in situ* (see also next sections).

Many studies have used these measurement tools in an effort to investigate the link between the mechanical properties of single-tumor cells and their metastatic potential (Suresh, 2007). Already in the 1990s, MPA experiments found tumorigenic rat fibroblasts having altered viscoelastic properties granting them enhanced deformability compared with their non-tumorigenic counterparts (Ward et al., 1991). AFM studies have consistently reported the same trend. Lekka and colleagues were first in the late 1990s to compare two normal human bladder epithelial cell lines against three cancerous ones with AFM and found that the cancerous cells were considerably more compliant than the normal ones (Lekka et al., 1999). Essentially the same findings were reported for breast epithelial cell lines (Li et al., 2008; Liu et al., 2020), chondrosarcoma cell lines (Darling et al., 2007), gastrointestinal tumor cells (Suresh et al., 2005), and ovarian epithelial cancer cells (Xu et al., 2012). When used to probe the stiffness profiles of human breast biopsies, AFM revealed cancer cells to constitute the very softest spots in malignant tissues

(Plodinec et al., 2012). In addition, nanomechanical AFM analysis of cancer cells and healthy cells collected from patients suffering from lung, breast, or pancreatic cancer revealed cancer cells to be 70% softer (Cross et al., 2007). This number was increased to 80% in a follow-up investigation (Cross et al., 2008). Concomitantly, investigating various cell shape parameters unsurprisingly demonstrated multiple significant geometrical differences between metastatic and non-metastatic human osteosarcoma cells, most importantly cell volume, cell area, cell roundness, and cell elongation (Lyons et al., 2016). A recent study that compared deformability of an isogenic panel of tumor cells further reported that cells that had successfully metastasized to the lung were significantly softer than both circulating and primary tumor cells (Liu et al., 2020). Apparently, deformability confers a selective advantage to metastasizing cells and could be used for prediction (Swaminathan et al., 2011).

While all these studies were done on cells attached to substrates, detaching and measuring cells in suspension also maintained the mechanical difference between normal and cancerous cells. Using an OS to measure multiple breast cancer cell lines (MCF-7, MCF-10, and MDA-MB-231) after detachment in suspension confirmed the close correlation between cell elasticity and metastatic potential (Guck et al., 2005). The finding was supported in further studies on Ras-transformed epithelial cells (Gullekson et al., 2017) and even in primary squamous cell carcinoma cells obtained from the oral mucosa of cancer patients, using the same OS device (Remmerbach et al., 2009). This bodes well for the latest generation of microfluidic high-throughput techniques, which also measure cells in suspension. Indeed, the large majority of publications using high-throughput techniques did again confirm the increased deformability of cancer cells (Ahmed et al., 2018; Ciucci et al., 2017; Deng et al., 2017; Guillou et al., 2016; Holenstein et al., 2019; Wullkopf et al., 2018; Zhang et al., 2012). As a specific example, different osteosarcoma cells measured using RT-DC were found to scale in deformability according to increasing metastatic aggressivity (Holenstein et al., 2019). Another variant of deformability cytometry was already even used to demonstrate that malignant cells can be identified in pleural effusions from patients based on their deformability (Tse et al., 2013), bringing mechanical phenotyping close to clinical application (Guck and Chilvers, 2013).

While all these studies show a strong correlation between single-tumor cell deformability and metastatic potential, few studies have found the opposite. A case in point is a study reporting that highly metastatic human breast tumor cells became more invasive upon stiffening through β -adrenergic signaling (Kim et al., 2016). More recently, invasiveness potential of glioblastoma cells was also shown to scale with cell stiffness, which is conferred through the formin FMN1 (Monzo et al., 2020). This discrepancy suggests that the overwhelmingly demonstrated correlation between cell compliance and metastasis could be more intricate than it might seem, could depend on the method used (Holenstein et al., 2019; Wu et al., 2018), and be possibly context dependent. The latter point seems well established for blood tumors (leukemias), which also show the opposite trend of cancer cells being stiffer (Ekpenyong et al., 2012; Toepfner et al., 2018). This phenomenon is probably due to the fact that in the hematopoietic system mature cells need to be deformable

to circulate, but cancer cells are not fully differentiated blood cells and, thus, still stiffer than healthy blood cells.

Lack of representative context constitutes the major drawback of most of the aforementioned studies. While the studies on blood cancers were close to achieving the goal of performing measurements in a context close to their natural *in vivo* environment with microfluidic techniques, the situation is different for solid tumors: measurements were mostly performed on tumor cell lines that were kept in culture and are therefore only representative of a particular mechanical state that is reached after culture on 2D substrates, which has very little to do with the context in which a tumor cell finds itself *in vivo* during its metastatic journey. Until novel tools that allow non-destructive *in vivo* probing of cell mechanics are established, the findings on metastatic tumor cell biomechanical properties cannot soundly be correlated with successful metastatic journey. Three-dimensional cell culture represents a tool that can be used to start bridging this gap and study tumor cells *in vitro* in more relevant conditions (Lv et al., 2017). Finally, although the variety of tools and methods available to researchers for probing cell mechanics have allowed to tackle the subject from various different angles, it has come with the unfortunate drawback of making it nearly impossible to compare results across different studies, as each method comes with its very specific set of parameters, rules, and rheological metrics (Wu et al., 2018). In particular, measuring the elastic and viscous modulus of cells heavily depends on the frequency or strain rate at which samples are probed and on the nature and size of the probe (Urbanska et al., 2020), which further complicates the drawing of firm conclusions across different studies. Finally, the possibility that mechanical changes observed in tumor cells are simply an epiphenomenon and a side effect of other processes that contribute to metastatic progression, and not leading contributors, cannot be excluded as the studies discussed above have so far been only correlative. It is one of the important next steps in this field to demonstrate causal relations (Guck, 2019).

TUMOR CELL MECHANICS: PASSIVE PROPERTIES AND ACTIVE REGULATORY ELEMENTS

So far, we have discussed the passive mechanical properties of cells that can be measured by application of outside forces and quantification of the resulting deformation. However, there is also an active component to cell's response to mechanical forces. The mechanical characteristics of tumor cells fall into two distinctive categories: active and passive. Any intrinsic property that is responsible for the way a tumor cell or its organelles will change shape due to the applied external forces would fall in the passive category. Active properties on the other hand are constituted of behaviors in which mechano-sensing intervenes to tailor the cells' mechanical parameters/behavior in response to cues from its environment. Another way of putting it is that intrinsic mechanical properties have an impact on the way cells behave in their environment, but at the same time, the environment can trigger active responses in the cells that affect their mechanical properties. It is this aspect of dynamic relationship between mechanical properties and environment that is most notably missing from the studies we have discussed in the previous section. There is thus an urgent need to provide an accu-

rate picture of the role of cell mechanics during the complete metastatic progression, from primary to secondary tumors. In this section, we go through the structural elements of tumor cells that are involved in cell mechanics and that are critical for the cells ability to undergo deformation. We attribute their involvement either to the passive or active aspects of cell mechanics. However, mechanosensing mechanisms will not be discussed in detail as they are well-reviewed elsewhere (Broders-Bondon et al., 2018; Cheng et al., 2017; Chin et al., 2016; Hoffman and Crocker, 2009; Janmey and Miller, 2011).

The cell membrane is the interface between the cell and its environment and as such is the first cell component affected by external forces (Le Roux et al., 2019). The cell membrane has elastic properties that can notably be described by a bending modulus, which constitutes a passive mechanical parameter that determines the membrane's ability to resist bending deformation. The bending modulus is an inherent cellular parameter that varies between cell types (Pontes et al., 2013). In addition, recent work has shown that cells actively respond to, and buffer, mechanical constraints via small and organized plasma membrane invaginations known as caveolae (Nassey and Lamaze, 2012). These affect the surface tension, contribute to the mechanical properties of the membrane and offer some protection against membrane rupture (Echarri et al., 2019; Sinha et al., 2011). Moreover, the membrane is known to actively react to various mechanical stresses such as tensile, compressive, or shear stress and topographical cues in the form of various responses including flattening, folding, or fluidization of the membrane for example (Le Roux et al., 2019). In summary, the cell membrane is involved on both the passive and active fronts of cell mechanics, respectively with its elastic properties that allow deformation and its role as force-sensing and response-triggering interface between the cell and its environment.

The cell membrane interacts with the cytoskeleton and most notably the actomyosin cortex lying just underneath. This part of the cytoskeleton has long been known to impact membrane deformation (Farsad and De Camilli, 2003). Most importantly, the actomyosin cortex is responsible for the cell's cortical tension. In addition to participating to cell stiffness, tension levels or breakages in the cortex, cortical tension limits cell deformation (Chugh and Paluch, 2018) and is involved in membrane bulges (Paluch et al., 2005) and cell-scale contractions (Koenenink and Paluch, 2018), making it an active player in cell mechanics that provides the main resistance to cell deformation at small strains.

The actomyosin cortex is only one of the many components of the cytoskeleton, which in summary can be said to comprise microfilaments, microtubules, and intermediate filaments. These different components are biopolymers that all come with different mechanical properties and are capable of dynamically assembling and disassembling (Janmey, 1991). Complementary to the resistance to small strain deformation that the actomyosin cortex offers, intermediate filaments are responsible for resistance to cell deformation at large strains and act as a security belt against excessive deformation that would destroy the cells (Charrier and Janmey, 2016). As a result, the cytoskeleton as the sum of its parts is directly responsible for the compliance of the cells as it governs their general viscoelastic properties

Table 2. Overview of Intracellular Organelles and Their Role in Cancer Metastasis

Organelle	Phenotype in Metastasis	References
Golgi apparatus	Fragmented	Cheng et al., 2004; Lee et al., 2008; May et al., 1998; Park et al., 2012; Petrosyan, 2015; Petrosyan et al., 2014; Petrosyan and Cheng, 2013; Schultz et al., 2012; Tan et al., 2017; Turner and Tartakoff, 1989
Lysosomes	Located at the periphery of the cells	Caviston et al., 2011; Cordonnier et al., 2001; Dozynkiewicz et al., 2012; Encarnação et al., 2016; Fennelly and Amaravadi, 2017; Macpherson et al., 2014; Mohamed and Sloane, 2006; Pu et al., 2016; Soppina et al., 2009
Centrosome(s)	Structural aberrations and clustering	Godinho and Pellman, 2014; Harrison et al., 2018; LoMastro and Holland, 2019
Mitochondria	Fission	Denisenko et al., 2019

(Wottawah et al., 2005). Its dynamic nature involves it in cellular functions such as cell cycle, migration, and adhesion (Hall, 2009), in which cells actively deform through actin reorganization. Consequently, not only does the cytoskeleton account for the cell's stiffness and its ability to undergo passive deformation but also for the general cell shape that they actively adopt during various processes (Bhadriraju and Hansen, 2002). In addition, the cytoskeleton positions the cell's organelles within its network of filaments, making it a direct link between cell shape/deformation and key organelle repositioning during metastasis. To a much bigger extent than the cell membrane, the cytoskeleton is involved in both active and passive mechanical processes and can be considered the key player of cell mechanics (Fletcher and Mullins, 2010).

The nucleus is one of the many organelles that the cytoskeleton is connected to (Starr and Fridolfsson, 2010) and currently an important topic of interest in the field of cancer research (Denais and Lammerding, 2014). The nuclear envelope is known to be much more than a simple protective barrier. It is involved in various functions critical for cancer progression such as protection from genome alterations, cell-cycle regulation, cytoskeleton organization and cell migration (de Las Heras et al., 2013). Invasion of tumor cells in particular is heavily dependent on the nucleus' passive mechanical properties and ability to squeeze through constraining pores (Harada et al., 2014), as it was demonstrated both in *in vitro* microfluidic systems (Fu et al., 2012) and *in vivo* (Denais et al., 2016) that the nucleus is drastically deformed in tumor cells undergoing transmigration. While the cytoskeleton is capable of dynamic remodeling to allow cells to flow through constraining pores, mechanical constraints are transmitted to organelles, such as the nucleus, which is a comparatively static and stiff elastic object. This sets a hard limit for vital migration through very tight constrictions (Harada et al., 2014). External forces are directly sensed by the nucleus, which behaves as a mechanosensor (Shivashankar, 2011; Kirby and Lammerding, 2018) and impacts key cellular functions such as chromatin organization and gene expression. Cells also use their nucleus as a ruler to measure their degree of spatial confinement and adapt their behavior accordingly (Lomakin et al., 2020). One key mechanism available to cells to increase forces exerted on the nucleus and favor its deformation as they attempt to pass through tight constrictions is the rapid perinuclear actin polymerization driven by the Arp2/3 protein (Thiam et al., 2016). In this process, actin filaments accumulated around the nucleus exert lateral forces on the nuclear envelope, in turn causing transient nuclear lamina rupture to allow stronger nuclear deformation

and passage of the tumor cell. This mechanism is dependent on the presence of lamin A/C, which is one type of intermediate filament and the main structural protein of the nuclear envelope. Lamins are involved in protecting the genome, are mechanosensitive, and can influence important transcriptional regulators for metastasis such as SRF and YAP/TAZ (Irianto et al., 2016). The levels of lamin A/C are critical for the viscoelastic properties of the nucleus (Lammerding et al., 2006; Swift and Discher, 2014) and, by extension, regulate its ability to passively squeeze when subjected to forces to allow passage of the cell through confining spaces (Cao et al., 2016). Chromatin was also found to contribute to nuclear deformability alongside lamin A/C (Hobson et al., 2020; Stephens et al., 2017). The distribution of lipids that constitute the nuclear membrane has recently been established and was found to play a role in deformation as well (Dazzoni et al., 2020). While nuclear deformation is only related to cell deformation at large strains, it is a highly limiting parameter in migration. Not only does nuclear deformation favor metastasis by allowing tumor cells to perform transmigration, but it also triggers DNA damage. DNA damage can in turn increase metastatic aggressivity of tumor cells by driving genome instability (Lim et al., 2016), as long as nuclear envelope and DNA repair systems kick in afterward to prevent cell death (Denais et al., 2016). For example, DNA damage caused by repeated loss of nuclear envelope integrity is now being identified as an important driver of the invasive phenotype in tumor cells (Nader et al., 2020).

Aside from the nucleus, other organelles have recently been found to have altered shapes and/or positions in the context of metastasis as well (Table 2). While the relationships between these alterations and the tumor cells' environment and their role in active/passive mechanical events remain unclear at this point, they will likely constitute an important research avenue in the future, by taking advantage of the recent developments in *in vivo* correlative light and electron microscopy (Karreman et al., 2016) to track organelle shape/positioning throughout the steps of the metastatic cascade (Figure 2).

CELL MECHANICS AND METASTASIS

The role of tumor cell mechanics during metastasis, at each step of the process, is likely overlooked and more intricate than it seems at first glance. In this section, we propose to go through the steps of the metastatic cascade sequentially and speculate on how tumor cell mechanics plays a role in each one of them, addressing the numerous changes of environment that tumor

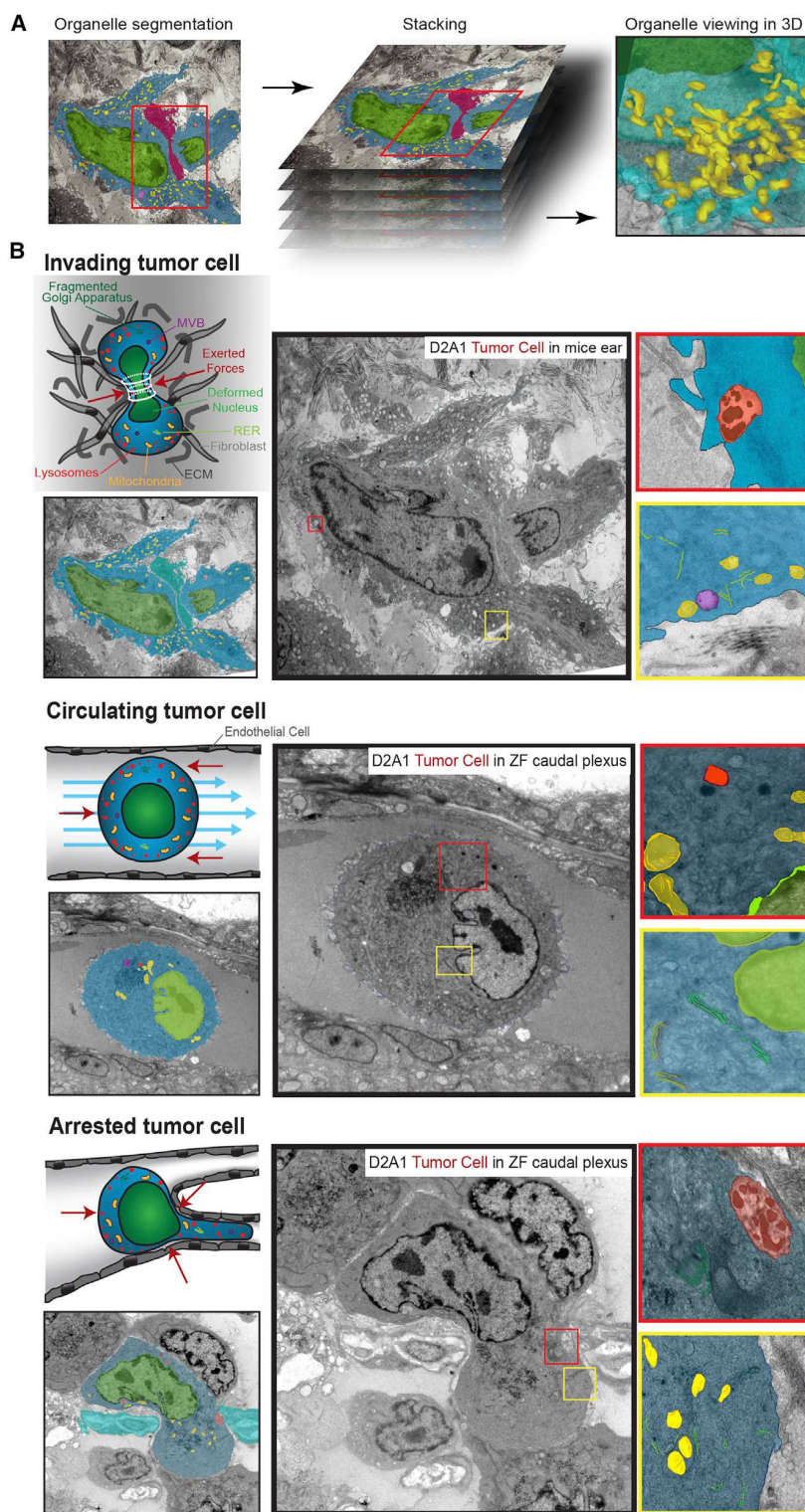


Figure 2. Intravital Correlative Light and Electronic Microscopy as a Tool for Studying Cell Deformation and Organelle Shape/Positioning during Metastasis

(A) EM images obtained upon correlative light and electronic microscopy (CLEM) can be stacked to reconstruct tumor cell volume in its environment in 3 dimensions. Browsing in the resulting reconstructed volume allows clear visualization of the locations and shapes of key organelles. Nucleus appears in green, mitochondria in yellow, lysosomes in orange, and MVBs in dark purple.

(B) Using CLEM, one can dissect cells at different steps of the metastasis cascade (invading, circulating, and arrested) at nanoscale resolution. In the closeups, nucleus and RER are highlighted in light green, Golgi apparatus in dark green, mitochondria in yellow, lysosomes in orange, and MVBs in purple.

cells go through during their metastatic journey. In doing so, we challenge the oversimplified view that an aggressive metastatic cell is necessarily a soft tumor cell.

Starting with the early invasion step, one could hypothesize that in an epithelium subjected to increasing compressive stress levels in the primary tumor environment, stiffer, less deformable tumor cells would be the first to be squeezed out of the epithelium, passively benefiting from a selective advantage over softer cells. In a study mentioned earlier, invasive potential of glioblastoma cells was found to correlate with cell stiffness. This was due to increased expression of the formin FMN1, which stabilizes microtubules (rendering the cells seemingly stiffer) while at the same time modulating assembly of actin-rich protrusive structures and enhancing motility (Monzo et al., 2020). However, the idea that invading tumor cells are softer seem to currently be more widespread. A recent study showed that invasive tumor cells located at the periphery of primary tumors were more likely to get softer and form invasive tips because of water being squeezed from the core to the periphery of the primary tumor (Han et al., 2020). More importantly, besides this passive selection mechanisms of softer tumor cells, the EMT program will result in softer tumor cells of altered cell shape exiting the site of the primary tumor (Chen et al., 2018). Most signs point toward deformability being key in the invasion step, but whether this mechanical phenotype is more of a prerequisite for or a consequence of invasion is not entirely clear. Interestingly, recent work shows, for example, that tumor cells soften during confined migration (Rianna et al., 2020) further suggesting that tumor cells can adaptively tune their mechanical phenotype.

The next task tumor cells need to complete after exiting the primary tumor is 3D migration through tissues. As previously mentioned, it is most likely accurate to state that tumor cells would benefit from a softer nucleus for migration through constraining pores as the nucleus is a passive entity that limits passage (Friedl et al., 2011). A softer nucleus could also be more likely to be mechanically challenged and damaged (Harada et al., 2014), which could in turn enhance the tumor cell's aggressiveness. However, the process of migration through the ECM is complex and depends on a multitude of mechanical and non-mechanical parameters. The mechanism of proteolysis can favor migration and help overcome the shortcomings of a stiff nucleus (Wolf et al., 2013), and fiber realignment during ECM remodeling (Provenzano et al., 2006) as well as tumor cell interactions with stromal cells are other mechanisms that likely reduce mechanical trauma. Moreover, tumor cells migrating collectively are known to express keratin-14 (Cheung et al., 2013), which hints at collective migration mitigating the need for mechanical properties associate with deformability (Seltmann et al., 2013). However, this is speculative and remains unclear at this stage. To conclude on the mechanical angle of this step of the cascade, saying that tumor cells need to be "adaptable" is likely more accurate than "soft" as the process of amoeboid migration is well known to be an active process, in which repeated active adaptation of cell shape is required (Guck et al., 2010). Concomitantly, tumor cells' invasive potential was shown to correlate with the ability to mechanically adapt to the stiffness of the ECM in which they migrate (Wullkopf et al., 2018). Therefore, a high activity/adaptivity of the cytoskeleton (perhaps resulting in an apparent low viscosity)

and probably a soft nucleus, appear to be best suited for this migration step of the cascade.

Next comes a first step of trans-endothelial migration in intravasation. Intravasation and extravasation can, from a very abstract cell mechanical point of view, be discussed together as both processes involve similar mechanical challenges: an object has to deform to get through a small hole in a thin layer. Of course, there are also many differences in the biological specifics of how this happens. Under normal circumstances both are supposedly two-step processes, in which interactions (adhesion) between tumor cells and the endothelial cells are required before tumor cells are able to squeeze in between endothelial cells to enter/exit circulation, in addition to crossing basement membranes. These processes could either be active or passive and seem to involve drastic cell deformations (Chen et al., 2016). However, the contribution of cell deformation during these processes has become uncertain as multiple mechanisms of endothelial transmigration have been described (Strilic and Offermanns, 2017). For example, intravasation of tumor cells can be vastly different from nontumor cells intravasation as tumor cells can be highly disruptive to the structure and integrity of blood vessels, causing high leakiness and sometimes replacing endothelial cells within the endothelium (Chiang et al., 2016). It is also important to note that tumor cells can be intravasated as clusters, which is notably favored by hypoxia (Donato et al., 2020). However, whether this has an impact on mechanical requirements of tumor cells is unknown. Furthermore, extravasation of tumor cells can be assisted by endothelial wall reorganization (Allen et al., 2017; Follain et al., 2018; Lapis et al., 1988). During this process, the remodeling of the endothelium allows tumor cells to enter and exit blood circulation, bypassing the tumor cells' need to undergo any deformation for successfully transmigrating. Such processes render the identification of tumor cell mechanical properties required for intra/extravasation cumbersome, as it is yet unclear what these are as cells enter and exit circulation.

Accordingly, we end this speculative discussion on the circulation step of the metastatic cascade, for which both high and low stiffness seem to offer significant advantages to CTCs. CTCs are exposed to fluid shear stress (FSS) and as such would benefit from arresting, adhering, and extravasating quickly in order to limit their risk of being destroyed. Interestingly, the mechanical properties thought to favor resistance to shear flow stress and quick arrest are still unclear. Regarding FSS survival, two studies have found the actomyosin cytoskeleton to play key and yet completely opposite roles. The first, conducted fully *in vitro*, found FSS-surviving CTCs to have reduced actomyosin activity, exhibiting lower cell stiffness and enhanced chemoresistance (Xin et al., 2019). The second and more recent one found on the contrary that actomyosin activity and cell stiffening increased FSS survival of tumor cells, which was verified *in vivo*. In addition, this study found RhoA and non-muscle myosin II to be part of a mechano-adapting mechanism, by which CTCs increase their stiffness through actomyosin in response to FSS (Moose et al., 2020). Here again, it is important to note that although it remains undemonstrated, clustering of CTCs could have an impact on the mechanical requirements of tumor cells during these intravascular steps of the cascade, as clustering could provide mechanical protection against shear stress. Shear stress survival is not the only aspect

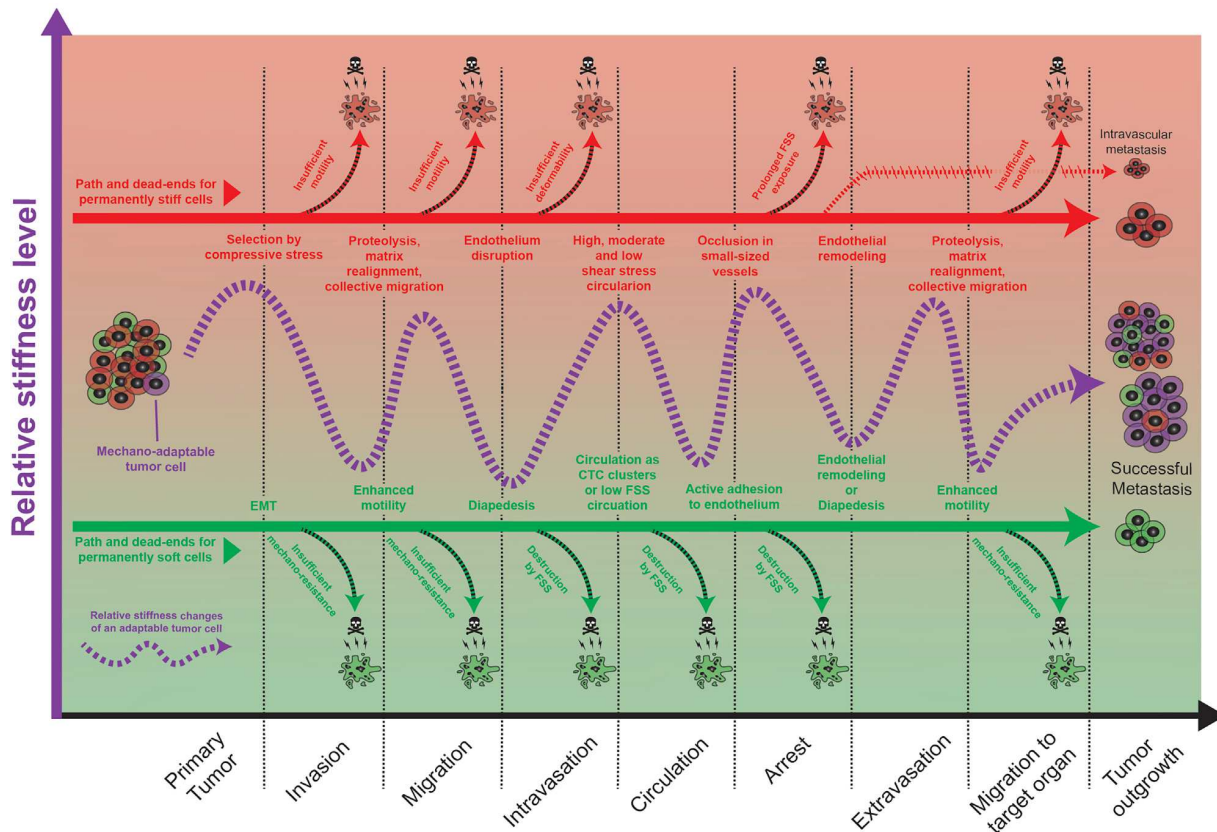


Figure 3. Speculative Look at the Role of Tumor Cell Stiffness in Paths of Successful or Unsuccessful Metastasis

Tumor cells are most likely capable of tuning their mechanical properties according to the mechanical stresses successively subjected to in the environments that they encounter.

of CTC transit in which the intrinsic mechanical properties of tumor cells come into play as their final destination of arrest could also depend on their stiffness level. Softer tumor cells were found to take significantly longer to adhere *in vitro* (Xin et al., 2019). This seems counterintuitive, as deformability should logically increase the contact surface between tumor cells and endothelial cells and have the opposite effect by allowing more adhesion bonds to form and favor cell arrest (Osmani et al., 2019), but such an effect remains undemonstrated. With occlusion being the alternative to adhesion for CTC arrest, one could also speculate that CTC softness would reduce chances of them becoming trapped in small-sized capillaries, in turn contributing to them remaining exposed to the hostile blood flow for longer. Such ability to escape occlusion in small capillaries for softer cells has been observed in mesenchymal stromal cells (MSCs) (Tietze et al., 2019) and in blood cells (Ekpenyong et al., 2012). Conversely, blood cell stiffness in response to chemotherapy has been implicated with vaso-occlusion (Lam et al., 2008). In summary, the ideal mechanical properties for CTCs are still difficult to identify and probe *in vivo*. The reports regarding FSS survival have been conflicting and both stiffness and softness seem to offer advantages for survival and quick arrest.

In conclusion, it is becoming apparent that the role of tumor cell mechanics in metastasis cannot simply be reduced to metastatic

aggressiveness scaling with increasing deformability. Ideal mechanical properties for successfully completing all the steps of the metastatic cascade could either have an extremely delicate range or could considerably vary between the different steps, the latter option being the more likely. Some paths to successful metastatic outgrowth are easier than others (e.g., shear stress is lower in veins compared to arteries, and collective migration/dissemination offers advantages compared with single-cell progression through the cascade), and as a result, tumor cells of different mechanical fitness could make it to the end of the metastatic journey. However, tumor cells do not get to choose these easier paths and might consequently need to sense their environment and dynamically fine-tune their mechanical properties (Figure 3). In any case, it would seem that achieving the right level of tumor cell stiffness would be very challenging and as such contribute to metastatic development being the highly inefficient process that it is known to be (Weiss, 1990).

PERSPECTIVES

Given the lethal nature of cancer metastasis, it is critical to concentrate research efforts not only on classical molecular biology, but on all fronts, including seemingly simpler aspects of biology such as the mechanical properties of cancer cells. Not

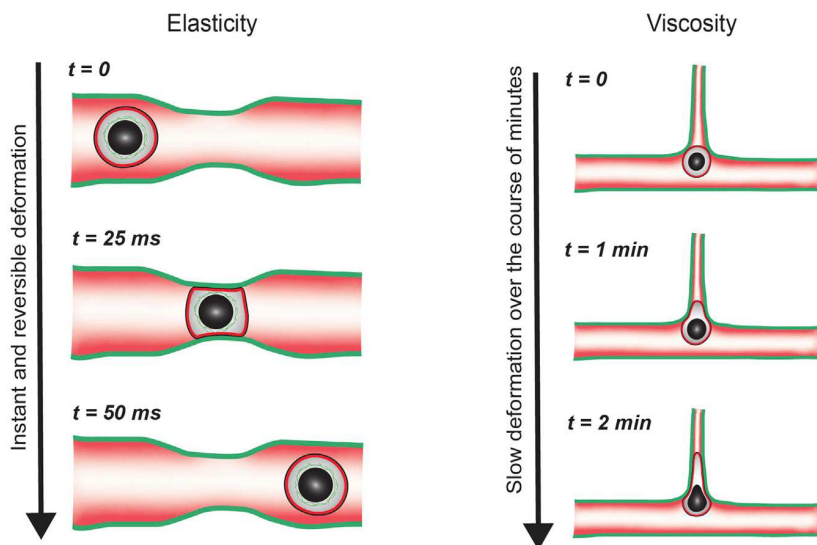


Figure 4. Elasticity and Viscosity Affect Tumor Cell Mechanics at Different Timescales

Elasticity comes into play at very short timescales, while viscosity has an effect when the cell is challenged over longer periods of times.

only is the biophysical aspect of the question essential for fully understanding the process by which metastases appear, but it could also lead to the identification of novel therapeutic targets.

While it is currently admitted that tumor cells (almost exclusively measured after culture *ex vivo*) can generally be considered softer, many parameters need to be taken into account to fully understand how tumor cell stiffness may impact the metastatic journey. For instance, the intricacies of the different timescales at which the tumor cells' mechanical properties can come into play are too rarely addressed (Ekpenyong et al., 2012). An elastic cell capable of instantaneously and reversibly deforming when it collides with an object has very different mechanical properties from a cell progressively making its way through a constricting blood vessel across longer periods of time (Figure 4). Therefore, the respective contributions of elasticity and viscosity need to be better dissected across the steps of the metastatic cascade. Another aspect still poorly understood is the dynamics of tumor cell stiffness changes. While it is becoming more and more apparent that tumor cells are capable of sensing their environment and adapting their stiffness accordingly, the ideal mechanical properties for each step of the metastatic cascade, alongside the means tumor cells have to reach those ideal states, remain to be identified for many steps of the metastatic journey. Intriguingly, metastatic cancer cells seem to change their mechanical properties much more than normal cells in response to passive and active mechanical stimuli (Baker et al., 2010; Wullkopf et al., 2018).

Future challenges will consist in fully characterizing the role of tumor cell deformability at every step of the metastatic progression, using the increasingly advanced tools available and combining them. Optical tweezers were already successfully used *in vivo* (Paul et al., 2019), and a recent technical report also offered some hope along this line by probing mechanical states of tumor cells, or healthy counterparts, *in vivo* (Wu et al., 2020). Using particle tracking microrheology combined with intravital imaging, the study reported that tumor cells displayed

properties (Eldridge et al., 2019)—maybe someday even *in vivo*. The endgame would be the identification of the mechanisms by which tumor cells sense not only mechanical stress, but also chemical and biochemical cues (cytokines, pH, temperature, etc.) in their environment and the pathways that allow them to fine-tune their mechanical properties accordingly.

In the future, our field should emphasize on measuring and tuning mechanical phenotypes of tumor cells along the entire metastasis cascade, in both relevant animal models and patient-derived samples. A careful quantification of mechanical stress imposed on tumor cells during these various steps, using innovative and resolute biophysical and imaging tools, will be instrumental in reaching this goal. In conclusion, the key mechanical signature of a successful metastatic cell might in the end turn out to be the ability to dynamically acquire the mechanical properties required to navigate each step of the metastatic journey, whatever those properties turn out to be. Once we have clearly identified the molecular mechanisms at work, novel therapies to target them may prove to be finally effective in the battle against metastasis.

ACKNOWLEDGMENTS

We thank all members of the Goetz and Guck Labs for helpful discussions. We thank Luc Mercier, Matthia Karreman and Yannick Schwab for their work on one of the EM sample used in Figure 2. This work has been funded by Plan Cancer (Programme Fédérateur Aviesan [PFA] NanoTumor; www.nanotumor.fr; @nanotumor) to J.G.G. and by institutional funds from INSERM and University of Strasbourg to J.G.G.; V.G. is supported by INSERM and Région Grand Est.

REFERENCES

- Aceto, N., Bardia, A., Miyamoto, D.T., Donaldson, M.C., Wittner, B.S., Spencer, J.A., Yu, M., Pely, A., Engstrom, A., Zhu, H., et al. (2014). Circulating tumor cell clusters are oligoclonal precursors of breast cancer metastasis. *Cell* 158, 1110–1122.
- Aguirre-Ghiso, J.A. (2018). How dormant cancer persists and reawakens. *Science* 361, 1314–1315.

- Ahmed, S.M., Bithi, S.S., Pore, A.A., Mubtasim, N., Schuster, C., Gollahon, L.S., and Vanapalli, S.A. (2018). Multi-sample deformability cytometry of cancer cells. *APL Bioeng.* 2, 032002.
- Alexander, J., and Cukierman, E. (2016). Stromal dynamic reciprocity in cancer: intricacies of fibroblastic-ECM interactions. *Curr. Opin. Cell Biol.* 42, 80–93.
- Alibert, C., Goud, B., and Manneville, J.-B. (2017). Are cancer cells really softer than normal cells? *Biol. Cell* 109, 167–189.
- Allen, T.A., Gracieux, D., Talib, M., Tokarz, D.A., Hensley, M.T., Cores, J., Vandergriff, A., Tang, J., de Andrade, J.B.M., Dinh, P.-U., et al. (2017). Angiopoiesis as an alternative mechanism of cell extravasation. *Stem Cells* 35, 170–180.
- Al-Mehdi, A.B., Tozawa, K., Fisher, A.B., Shientag, L., Lee, A., and Muschel, R.J. (2000). Intravascular origin of metastasis from the proliferation of endothelium-attached tumor cells: a new model for metastasis. *Nat. Med.* 6, 100–102.
- Au, S.H., Storey, B.D., Moore, J.C., Tang, Q., Chen, Y.-L., Javaid, S., Sarioglu, A.F., Sullivan, R., Madden, M.W., O’Keefe, R., et al. (2016). Clusters of circulating tumor cells traverse capillary-sized vessels. *Proc. Natl. Acad. Sci. USA* 113, 4947–4952.
- Baker, E.L., Lu, J., Yu, D., Bonnecaze, R.T., and Zaman, M.H. (2010). Cancer cell stiffness: integrated roles of three-dimensional matrix stiffness and transforming potential. *Biophys. J.* 99, 2048–2057.
- Bhadiraju, K., and Hansen, L.K. (2002). Extracellular matrix- and cytoskeleton-dependent changes in cell shape and stiffness. *Exp. Cell Res.* 278, 92–100.
- Broders-Bondon, F., Nguyen Ho-Boulidoires, T.H., Fernandez-Sanchez, M.E., and Farge, E. (2018). Mechanotransduction in tumor progression: the dark side of the force. *J. Cell Biol.* 217, 1571–1587.
- Brown, M., Assen, F.P., Leithner, A., Abe, J., Schachner, H., Asfour, G., Bago-Horvath, Z., Stein, J.V., Uhrin, P., Sixt, M., and Kerjaschki, D. (2018). Lymph node blood vessels provide exit routes for metastatic tumor cell dissemination in mice. *Science* 359, 1408–1411.
- Cao, X., Moeendarbary, E., Isermann, P., Davidson, P.M., Wang, X., Chen, M.B., Burkart, A.K., Lammerding, J., Kamm, R.D., and Shenoy, V.B. (2016). A chemomechanical model for nuclear morphology and stresses during cell transendothelial migration. *Biophys. J.* 111, 1541–1552.
- Caviston, J.P., Zajac, A.L., Tokito, M., and Holzbaur, E.L.F. (2011). Huntingtin coordinates the dynein-mediated dynamic positioning of endosomes and lysosomes. *Mol. Biol. Cell* 22, 478–492.
- Chang, S.F., Chang, C.A., Lee, D.-Y., Lee, P.-L., Yeh, Y.-M., Yeh, C.-R., Cheng, C.-K., Chien, S., and Chiu, J.-J. (2008). Tumor cell cycle arrest induced by shear stress: roles of integrins and Smad. *Proc. Natl. Acad. Sci. USA* 105, 3927–3932.
- Charrier, E.E., and Janmey, P.A. (2016). Mechanical properties of intermediate filament proteins. *Methods Enzymol.* 568, 35–57.
- Chen, J., Zhou, W., Jia, Q., Chen, J., Zhang, S., Yao, W., Wei, F., Zhang, Y., Yang, F., Huang, W., et al. (2016). Efficient extravasation of tumor-repopulating cells depends on cell deformability. *Sci. Rep.* 6, 19304.
- Chen, Y.Q., Lan, H.Y., Wu, Y.C., Yang, W.H., Chiou, A., and Yang, M.H. (2018). Epithelial-mesenchymal transition softens head and neck cancer cells to facilitate migration in 3D environments. *J. Cell. Mol. Med.* 22, 3837–3846.
- Cheng, B., Lin, M., Huang, G., Li, Y., Ji, B., Genin, G.M., Deshpande, V.S., Lu, T.J., and Xu, F. (2017). Cellular mechanosensing of the biophysical microenvironment: a review of mathematical models of biophysical regulation of cell responses. *Phys. Life Rev.* 22–23, 88–119.
- Cheng, K.W., Lahad, J.P., Kuo, W.-L., Lapuk, A., Yamada, K., Auersperg, N., Liu, J., Smith-McCune, K., Lu, K.H., Fishman, D., et al. (2004). The RAB25 small GTPase determines aggressiveness of ovarian and breast cancers. *Nat. Med.* 10, 1251–1256.
- Cheung, K.J., Gabrielson, E., Werb, Z., and Ewald, A.J. (2013). Collective invasion in breast cancer requires a conserved basal epithelial program. *Cell* 155, 1639–1651.
- Cheung, K.J., Padmanaban, V., Silvestri, V., Schipper, K., Cohen, J.D., Fairchild, A.N., Gorin, M.A., Verdone, J.E., Pienta, K.J., Bader, J.S., and Ewald, A.J. (2016). Polyclonal breast cancer metastases arise from collective dissemination of keratin 14-expressing tumor cell clusters. *Proc. Natl. Acad. Sci. USA* 113, E854–E863.
- Chiang, S.P.H., Cabrera, R.M., and Segall, J.E. (2016). Tumor cell intravasation. *Am. J. Physiol. Cell Physiol.* 311, C1–C14.
- Chin, L., Xia, Y., Discher, D.E., and Janmey, P.A. (2016). Mechanotransduction in cancer. *Curr. Opin. Chem. Eng.* 11, 77–84.
- Chugh, P., and Paluch, E.K. (2018). The actin cortex at a glance. *J. Cell Sci.* 131, jcs186254.
- Ciucci, S., Ge, Y., Durán, C., Palladini, A., Jiménez-Jiménez, V., Martínez-Sánchez, L.M., Wang, Y., Sales, S., Shevchenko, A., Poser, S.W., et al. (2017). Enlightening discriminative network functional modules behind principal component analysis separation in differential-omic science studies. *Sci. Rep.* 7, 43946.
- Clark, A.G., and Vignjevic, D.M. (2015). Modes of cancer cell invasion and the role of the microenvironment. *Curr. Opin. Cell Biol.* 36, 13–22.
- Conrad, C., Gray, K.M., Stroka, K.M., Rizvi, I., and Scarcelli, G. (2019). Mechanical characterization of 3D ovarian cancer nodules using Brillouin confocal microscopy. *Cell. Mol. Bioeng.* 12, 215–226.
- Cordonnier, M.N., Dauzonne, D., Louvard, D., and Coudrier, E. (2001). Actin filaments and myosin I alpha cooperate with microtubules for the movement of lysosomes. *Mol. Biol. Cell* 12, 4013–4029.
- Cross, S.E., Jin, Y.-S., Rao, J., and Gimzewski, J.K. (2007). Nanomechanical analysis of cells from cancer patients. *Nat. Nanotechnol.* 2, 780–783.
- Cross, S.E., Jin, Y.S., Tondre, J., Wong, R., Rao, J., and Gimzewski, J.K. (2008). AFM-based analysis of human metastatic cancer cells. *Nanotechnology* 19, 384003.
- Darling, E.M., and Di Carlo, D. (2015). High-throughput assessment of cellular mechanical properties. *Annu. Rev. Biomed. Eng.* 17, 35–62.
- Darling, E.M., Zauscher, S., Block, J.A., and Guilak, F. (2007). A thin-layer model for viscoelastic, stress-relaxation testing of cells using atomic force microscopy: do cell properties reflect metastatic potential? *Biophys. J.* 92, 1784–1791.
- Dazzoni, R., Grélaud, A., Morvan, E., Bouter, A., Applebee, C.J., Loquet, A., Larjani, B., and Dufourc, E.J. (2020). The unprecedented membrane deformation of the human nuclear envelope, in a magnetic field, indicates formation of nuclear membrane invaginations. *Sci. Rep.* 10, 5147.
- de Las Heras, J.I., Batrakou, D.G., and Schirmer, E.C. (2013). Cancer biology and the nuclear envelope: a convoluted relationship. *Semin. Cancer Biol.* 23, 125–137.
- Delarue, M., Montel, F., Vignjevic, D., Prost, J., Joanny, J.-F., and Cappello, G. (2014). Compressive stress inhibits proliferation in tumor spheroids through a volume limitation. *Biophys. J.* 107, 1821–1828.
- Denais, C., and Lammerding, J. (2014). Nuclear mechanics in cancer. *Adv. Exp. Med. Biol.* 773, 435–470.
- Denais, C.M., Gilbert, R.M., Isermann, P., McGregor, A.L., te Lindert, M., Weigel, B., Davidson, P.M., Friedl, P., Wolf, K., and Lammerding, J. (2016). Nuclear envelope rupture and repair during cancer cell migration. *Science* 352, 353–358.
- Deng, Y., Davis, S.P., Yang, F., Paulsen, K.S., Kumar, M., Sinnott DeVaux, R., Wang, X., Conklin, D.S., Oberai, A., Herschkowitz, J.I., and Chung, A.J. (2017). Inertial microfluidic cell stretcher (iMCS): fully automated, high-throughput, and near real-time cell mechanotyping. *Small* 13, 1700705.
- Denisenko, T.V., Gorbunova, A.S., and Zhivotovsky, B. (2019). Mitochondrial involvement in migration, invasion and metastasis. *Front. Cell Dev. Biol.* 7, 355.
- Denton, A.E., Roberts, E.W., and Fearon, D.T. (2018). Stromal cells in the tumor microenvironment. *Adv. Exp. Med. Biol.* 1060, 99–114.
- Donato, C., Kunz, L., Castro-Giner, F., Paasinen-Sohns, A., Strittmatter, K., Szczerba, B.M., Scherrer, R., Di Maggio, N., Heusermann, W., Biehlmaier, O., et al. (2020). Hypoxia triggers the intravasation of clustered circulating tumor cells. *Cell Rep.* 32, 108105.

- Dong, C., Hu, X., and Dinu, C.Z. (2016). Current status and perspectives in atomic force microscopy-based identification of cellular transformation. *Int. J. Nanomedicine* *11*, 2107–2118.
- Dozynkiewicz, M.A., Jamieson, N.B., Macpherson, I., Grindlay, J., van den Berghe, P.V.E., von Thun, A., Morton, J.P., Gourley, C., Timpson, P., Nixon, C., et al. (2012). Rab25 and CLIC3 collaborate to promote integrin recycling from late endosomes/lysosomes and drive cancer progression. *Dev. Cell* *22*, 131–145.
- Eble, J.A., and Niland, S. (2019). The extracellular matrix in tumor progression and metastasis. *Clin. Exp. Metastasis* *36*, 171–198.
- Echarri, A., Pavón, D.M., Sánchez, S., García-García, M., Calvo, E., Huerta-López, C., Velázquez-Carreras, D., Viaris de Lesegno, C., Ariotti, N., Lázaro-Carrillo, A., et al. (2019). An Abl-FBP17 mechanosensing system couples local plasma membrane curvature and stress fiber remodeling during mechanoadaptation. *Nat. Commun.* *10*, 5828.
- Ekpenyong, A.E., Whyte, G., Chalut, K., Pagliara, S., Lautenschläger, F., Fiddler, C., Paschke, S., Keyser, U.F., Chilvers, E.R., and Guck, J. (2012). Viscoelastic properties of differentiating blood cells are fate- and function-dependent. *PLoS One* *7*, e45237.
- Eldridge, W.J., Ceballos, S., Shah, T., Park, H.S., Steelman, Z.A., Zauscher, S., and Wax, A. (2019). Shear modulus measurement by quantitative phase imaging and correlation with atomic force microscopy. *Biophys. J.* *117*, 696–705.
- Elsayad, K., Polakova, S., and Gregan, J. (2019). Probing mechanical properties in biology using Brillouin microscopy. *Trends Cell Biol.* *29*, 608–611.
- Encarnação, M., Espada, L., Escrevente, C., Mateus, D., Ramalho, J., Michelet, X., Santarino, I., Hsu, V.W., Brenner, M.B., Barral, D.C., and Vieira, O.V. (2016). A Rab3a-dependent complex essential for lysosome positioning and plasma membrane repair. *J. Cell Biol.* *213*, 631–640.
- Entenberg, D., Voiculescu, S., Guo, P., Borriello, L., Wang, Y., Karagiannis, G.S., Jones, J., Baccay, F., Oktay, M., and Condeelis, J. (2018). A permanent window for the murine lung enables high-resolution imaging of cancer metastasis. *Nat. Methods* *15*, 73–80.
- Faigle, C., Lautenschläger, F., Whyte, G., Homewood, P., Martín-Badosa, E., and Guck, J. (2015). A monolithic glass chip for active single-cell sorting based on mechanical phenotyping. *Lab Chip* *15*, 1267–1275.
- Fan, R., Emery, T., Zhang, Y., Xia, Y., Sun, J., and Wan, J. (2016). Circulatory shear flow alters the viability and proliferation of circulating colon cancer cells. *Sci. Rep.* *6*, 27073.
- Farsad, K., and De Camilli, P. (2003). Mechanisms of membrane deformation. *Curr. Opin. Cell Biol.* *15*, 372–381.
- Fennelly, C., and Amaravadi, R.K. (2017). Lysosomal biology in cancer. *Methods Mol Biol* *1594*, 293–308.
- Fletcher, D.A., and Mullins, R.D. (2010). Cell mechanics and the cytoskeleton. *Nature* *463*, 485–492.
- Follain, G., Herrmann, D., Harlepp, S., Hyenne, V., Osmani, N., Warren, S.C., Timpson, P., and Goetz, J.G. (2020). Fluids and their mechanics in tumour transit: shaping metastasis. *Nat. Rev. Cancer* *20*, 107–124.
- Follain, G., Osmani, N., Azevedo, A.S., Allio, G., Mercier, L., Karreman, M.A., Solecki, G., Garcia León, M.J., Lefebvre, O., Fekonja, N., et al. (2018). Hemodynamic forces tune the arrest, adhesion, and extravasation of circulating tumor cells. *Dev. Cell* *45*, 33–52.e12.
- Friedl, P., Wolf, K., and Lammerding, J. (2011). Nuclear mechanics during cell migration. *Curr. Opin. Cell Biol.* *23*, 55–64.
- Fu, Y., Chin, L.K., Bourouina, T., Liu, A.Q., and VanDongen, A.M.J. (2012). Nuclear deformation during breast cancer cell transmigration. *Lab Chip* *12*, 3774–3778.
- Gaggioli, C., Hooper, S., Hidalgo-Carcedo, C., Grosse, R., Marshall, J.F., Harrington, K., and Sahai, E. (2007). Fibroblast-led collective invasion of carcinoma cells with differing roles for RhoGTPases in leading and following cells. *Nat. Cell Biol.* *9*, 1392–1400.
- Godinho, S.A., and Pellman, D. (2014). Causes and consequences of centrosome abnormalities in cancer. *Philos. Trans. R. Soc. Lond. B Biol. Sci.* *369*, 20130467.
- Goetz, J.G., Minguet, S., Navarro-Lérida, I., Lazcano, J.J., Samaniego, R., Calvo, E., Tello, M., Osteso-Ibáñez, T., Pellinen, T., Echarri, A., et al. (2011). Biomechanical remodeling of the microenvironment by stromal caveolin-1 favors tumor invasion and metastasis. *Cell* *146*, 148–163.
- González-Bermúdez, B., Guinea, G.V., and Plaza, G.R. (2019). Advances in micropipette aspiration: applications in cell biomechanics, models, and extended studies. *Biophys. J.* *116*, 587–594.
- Grandér, D. (1998). How do mutated oncogenes and tumor suppressor genes cause cancer? *Med. Oncol.* *15*, 20–26.
- Gritsenko, P., Leenders, W., and Friedl, P. (2017). Recapitulating in vivo-like plasticity of glioma cell invasion along blood vessels and in astrocyte-rich stroma. *Histochem. Cell Biol.* *148*, 395–406.
- Guck, J. (2019). Some thoughts on the future of cell mechanics. *Biophys. Rev.* *11*, 667–670.
- Guck, J., Ananthkrishnan, R., Mahmood, H., Moon, T.J., Cunningham, C.C., and Käs, J. (2001). The optical stretcher: a novel laser tool to micromanipulate cells. *Biophys. J.* *81*, 767–784.
- Guck, J., and Chilvers, E.R. (2013). Mechanics meets medicine. *Sci. Transl. Med.* *5*, 212fs41.
- Guck, J., Lautenschläger, F., Paschke, S., and Beil, M. (2010). Critical review: cellular mechanobiology and amoeboid migration. *Integr. Biol. (Camb.)* *2*, 575–583.
- Guck, J., Schinkinger, S., Lincoln, B., Wottawah, F., Ebert, S., Romeyke, M., Lenz, D., Erickson, H.M., Ananthkrishnan, R., Mitchell, D., et al. (2005). Optical deformability as an inherent cell marker for testing malignant transformation and metastatic competence. *Biophys. J.* *88*, 3689–3698.
- Guillou, L., Dahl, J.B., Lin, J.-M.G., Barakat, A.I., Husson, J., Muller, S.J., and Kumar, S. (2016). Measuring cell viscoelastic properties using a microfluidic extensional flow device. *Biophys. J.* *111*, 2039–2050.
- Gullekson, C., Cojoc, G., Schürmann, M., Guck, J., and Pelling, A. (2017). Mechanical mismatch between Ras transformed and untransformed epithelial cells. *Soft Matter* *13*, 8483–8491.
- Haeger, A., Krause, M., Wolf, K., and Friedl, P. (2014). Cell jamming: collective invasion of mesenchymal tumor cells imposed by tissue confinement. *Biochim. Biophys. Acta* *1840*, 2386–2395.
- Hall, A. (2009). The cytoskeleton and cancer. *Cancer Metastasis Rev.* *28*, 5–14.
- Han, Y.L., Pegoraro, A.F., Li, H., Li, K., Yuan, Y., Xu, G., Gu, Z., Sun, J., Hao, Y., Gupta, S.K., et al. (2020). Cell swelling, softening and invasion in a three-dimensional breast cancer model. *Nat. Phys.* *16*, 101–108.
- Harada, T., Swift, J., Irianto, J., Shin, J.-W., Spinler, K.R., Athirasala, A., Diegmiller, R., Dingal, P.C.D.P., Ivanovska, I.L., and Discher, D.E. (2014). Nuclear lamin stiffness is a barrier to 3D migration, but softness can limit survival. *J. Cell Biol.* *204*, 669–682.
- Harney, A.S., Arwert, E.N., Entenberg, D., Wang, Y., Guo, P., Qian, B.-Z., Oktay, M.H., Pollard, J.W., Jones, J.G., and Condeelis, J.S. (2015). Real-time imaging reveals local, transient vascular permeability, and tumor cell intravasation stimulated by TIE2hi macrophage-derived VEGFA. *Cancer Discov.* *5*, 932–943.
- Harrison, L.E., Bleiler, M., and Giardina, C. (2018). A look into centrosome abnormalities in colon cancer cells, how they arise and how they might be targeted therapeutically. *Biochem. Pharmacol.* *147*, 1–8.
- Headley, M.B., Bins, A., Nip, A., Roberts, E.W., Looney, M.R., Gerard, A., and Krummel, M.F. (2016). Visualization of immediate immune responses to pioneer metastatic cells in the lung. *Nature* *531*, 513–517.
- Hobson, C.M., Kern, M., O'Brien, E.T., Stephens, A.D., Falvo, M.R., and Superfine, R. (2020). Correlating nuclear morphology and external force with combined atomic force microscopy and light sheet imaging separates roles of chromatin and lamin A/C in nuclear mechanics. *Mol. Biol. Cell* *31*, 1788–1801.
- Hochmuth, R.M. (2000). Micropipette aspiration of living cells. *J. Biomech.* *33*, 15–22.
- Hoffman, B.D., and Crocker, J.C. (2009). Cell mechanics: dissecting the physical responses of cells to force. *Annu. Rev. Biomed. Eng.* *11*, 259–288.

- Holenstein, C.N., Horvath, A., Schär, B., Schoenenberger, A.D., Bollhalder, M., Goedecke, N., Bartalena, G., Otto, O., Herbig, M., Guck, J., et al. (2019). The relationship between metastatic potential and in vitro mechanical properties of osteosarcoma cells. *Mol. Biol. Cell* **30**, 887–898.
- Irianto, J., Pfeifer, C.R., Ivanovska, I.L., Swift, J., and Discher, D.E. (2016). Nuclear lamins in cancer. *Cell. Mol. Bioeng.* **9**, 258–267.
- Jain, R.K., Martin, J.D., and Stylianopoulos, T. (2014). The role of mechanical forces in tumor growth and therapy. *Annu. Rev. Biomed. Eng.* **16**, 321–346.
- Janmey, P.A. (1991). Mechanical properties of cytoskeletal polymers. *Curr. Opin. Cell Biol.* **3**, 4–11.
- Janmey, P.A., and Miller, R.T. (2011). Mechanisms of mechanical signaling in development and disease. *J. Cell Sci.* **124**, 9–18.
- Karaman, S., and Detmar, M. (2014). Mechanisms of lymphatic metastasis. *J. Clin. Invest.* **124**, 922–928.
- Karremans, M.A., Hyenne, V., Schwab, Y., and Goetz, J.G. (2016). Intravital correlative microscopy: imaging life at the nanoscale. *Trends Cell Biol.* **26**, 848–863.
- Kienast, Y., von Baumgarten, L., Fuhrmann, M., Klinkert, W.E.F., Goldbrunner, R., Herms, J., and Winkler, F. (2010). Real-time imaging reveals the single steps of brain metastasis formation. *Nat. Med.* **16**, 116–122.
- Kim, T.-H., Gill, N.K., Nyberg, K.D., Nguyen, A.V., Hohlbauch, S.V., Geisse, N.A., Nowell, C.J., Sloan, E.K., and Rowat, A.C. (2016). Cancer cells become less deformable and more invasive with activation of β -adrenergic signaling. *J. Cell Sci.* **129**, 4563–4575.
- Kirby, T.J., and Lammerding, J. (2018). Emerging views of the nucleus as a cellular mechanosensor. *Nat. Cell Biol.* **20**, 373–381.
- Koenderink, G.H., and Paluch, E.K. (2018). Architecture shapes contractility in actomyosin networks. *Curr. Opin. Cell Biol.* **50**, 79–85.
- Kumar, S., and Weaver, V.M. (2009). Mechanics, malignancy, and metastasis: the force journey of a tumor cell. *Cancer Metastasis Rev.* **28**, 113–127.
- Lam, W.A., Rosenbluth, M.J., and Fletcher, D.A. (2008). Increased leukaemia cell stiffness is associated with symptoms of leucostasis in paediatric acute lymphoblastic leukaemia. *Br. J. Haematol.* **142**, 497–501.
- Lammerding, J., Fong, L.G., Ji, J.Y., Reue, K., Stewart, C.L., Young, S.G., and Lee, R.T. (2006). Lamins A and C but not lamin B1 regulate nuclear mechanics. *J. Biol. Chem.* **281**, 25768–25780.
- Lapis, K., Paku, S., and Liotta, L.A. (1988). Endothelialization of embolized tumor cells during metastasis formation. *Clin. Exp. Metastasis* **6**, 73–89.
- Le Roux, A.L., Quiroga, X., Walani, N., Arroyo, M., and Roca-Cusachs, P. (2019). The plasma membrane as a mechanochemical transducer. *Philos. Trans. R. Soc. Lond. B Biol. Sci.* **374**, 20180221.
- Lee, M., Lee, H.J., Bae, S., and Lee, Y.S. (2008). Protein sialylation by sialyltransferase involves radiation resistance. *Mol. Cancer Res.* **6**, 1316–1325.
- Lekka, M., Laidler, P., Gil, D., Lekki, J., Stachura, Z., and Hryniewicz, A.Z. (1999). Elasticity of normal and cancerous human bladder cells studied by scanning force microscopy. *Eur. Biophys. J.* **28**, 312–316.
- Levental, K.R., Yu, H., Kass, L., Lakins, J.N., Egeblad, M., Erler, J.T., Fong, S.F.T., Csiszar, K., Giaccia, A., Weninger, W., et al. (2009). Matrix crosslinking forces tumor progression by enhancing integrin signaling. *Cell* **139**, 891–906.
- Li, Q.S., Lee, G.Y.H., Ong, C.N., and Lim, C.T. (2008). AFM indentation study of breast cancer cells. *Biochem. Biophys. Res. Commun.* **374**, 609–613.
- Lim, S., Quinton, R.J., and Ganem, N.J. (2016). Nuclear envelope rupture drives genome instability in cancer. *Mol. Biol. Cell* **27**, 3210–3213.
- Lincoln, B., Wottawah, F., Schinkinger, S., Ebert, S., and Guck, J. (2007). High-throughput rheological measurements with an optical stretcher. *Methods Cell Biol.* **83**, 397–423.
- Linde, N., Casanova-Acebes, M., Sosa, M.S., Mortha, A., Rahman, A., Farias, E., Harper, K., Tardio, E., Reyes Torres, I., Jones, J., et al. (2018). Macrophages orchestrate breast cancer early dissemination and metastasis. *Nat. Commun.* **9**, 21.
- Liu, Z., Lee, S.J., Park, S., Konstantopoulos, K., Glunde, K., Chen, Y., and Barman, I. (2020). Cancer cells display increased migration and deformability in pace with metastatic progression. *FASEB J.* **34**, 9307–9315.
- Lomakin, A., Cattin, C., Cuvelier, D., Alraies, Z., Molina, M., Nader, G., Srivastava, N., Arcos, J.-M.G., Zhitnyak, I., Bhargava, A., et al. (2020). The nucleus acts as a ruler tailoring cell responses to spatial constraints. *Science* **370**, eaba2894.
- LoMastro, G.M., and Holland, A.J. (2019). The emerging link between centrosome aberrations and metastasis. *Dev. Cell* **49**, 325–331.
- Lorenzen, J., Sinkus, R., Lorenzen, M., Dargatz, M., Leussler, C., Röschmann, P., and Adam, G. (2002). MR elastography of the breast: preliminary clinical results. *Rofo* **174**, 830–834.
- Lv, D., Hu, Z., Lu, L., Lu, H., and Xu, X. (2017). Three-dimensional cell culture: a powerful tool in tumor research and drug discovery. *Oncol. Lett.* **14**, 6999–7010.
- Lyons, S.M., Alizadeh, E., Mannheimer, J., Schuamberg, K., Castle, J., Schroder, B., Turk, P., Thamm, D., and Prasad, A. (2016). Changes in cell shape are correlated with metastatic potential in murine and human osteosarcomas. *Biol. Open* **5**, 289–299.
- Macpherson, I.R., Rainero, E., Mitchell, L.E., van den Berghe, P.V.E., Speirs, C., Dozynkiewicz, M.A., Chaudhary, S., Kalna, G., Edwards, J., Timpson, P., and Norman, J.C. (2014). CLIC3 controls recycling of late endosomal MT1-MMP and dictates invasion and metastasis in breast cancer. *J. Cell Sci.* **127**, 3893–3901.
- May, J.A., Ratan, H., Glenn, J.R., Lösche, W., Spangenberg, P., and Heptinstall, S. (1998). GPIIb-IIIa antagonists cause rapid disaggregation of platelets pre-treated with cytochalasin D. Evidence that the stability of platelet aggregates depends on normal cytoskeletal assembly. *Platelets* **9**, 227–232.
- Mitchison, J.M., and Swann, M.M. (1954). The mechanical properties of the cell surface: I. The cell Elastimeter. *J. Exp. Biol.* **31**, 443–460.
- Mohamed, M.M., and Sloane, B.F. (2006). Cysteine cathepsins: multifunctional enzymes in cancer. *Nat. Rev. Cancer* **6**, 764–775.
- Mohammadi, H., and Sahai, E. (2018). Mechanisms and impact of altered tumor mechanics. *Nat. Cell Biol.* **20**, 766–774.
- Monzo, P., Crestani, M., Chong, Y.K., Hennig, K., Ghisleni, A., Li, Q., Richichi, C., Maiuri, P., Bolland, M., Sheetz, M.P., et al. (2020). Adaptive mechanoproperties characterize glioblastoma fitness for invasion. [bioRxiv biorxiv.org/content/10.1101/2020.06.17.156406v1](https://doi.org/10.1101/2020.06.17.156406v1).
- Moose, D.L., Krog, B.L., Kim, T.H., Zhao, L., Williams-Perez, S., Burke, G., Rhodes, L., Vanneste, M., Breheny, P., Milhem, M., et al. (2020). Cancer cells resist mechanical destruction in circulation via RhoA/actomyosin-dependent Mechano-adaptation. *Cell Rep.* **30**, 3864–3874.e6.
- Nader, G., Agüera-Gonzalez, S., Routet, F., Gratia, M., Maurin, M., Cancila, V., Cadart, C., Gentili, M., Yamada, A., Lodillinsky, C., et al. (2020). Compromised nuclear envelope integrity drives tumor cell invasion. [bioRxiv biorxiv.org/content/10.1101/2020.05.22.110122v1](https://doi.org/10.1101/2020.05.22.110122v1).
- Nassoy, P., and Lamaze, C. (2012). Stressing caveolae new role in cell mechanics. *Trends Cell Biol.* **22**, 381–389.
- Nguyen, D.X., Bos, P.D., and Massagué, J. (2009). Metastasis: from dissemination to organ-specific colonization. *Nat. Rev. Cancer* **9**, 274–284.
- Osmani, N., Follain, G., García León, M.J., Lefebvre, O., Busnelli, I., Lamicol, A., Harlepp, S., and Goetz, J.G. (2019). Metastatic tumor cells exploit their adhesion repertoire to counteract shear forces during intravascular arrest. *Cell Rep.* **28**, 2491–2500.e5.
- Otto, O., Rosendahl, P., Mietke, A., Golfier, S., Herold, C., Klaue, D., Girardo, S., Pagliara, S., Ekpenyong, A., Jacobi, A., et al. (2015). Real-time deformability cytometry: on-the-fly cell mechanical phenotyping. *Nat. Methods* **12**, 199–202.
- Paluch, E., Piel, M., Prost, J., Bornens, M., and Sykes, C. (2005). Cortical actomyosin breakage triggers shape oscillations in cells and cell fragments. *Biophys. J.* **89**, 724–733.
- Park, J.J., Yi, J.Y., Jin, Y.B., Lee, Y.J., Lee, J.S., Lee, Y.S., Ko, Y.G., and Lee, M. (2012). Sialylation of epidermal growth factor receptor regulates receptor

- activity and chemosensitivity to gefitinib in colon cancer cells. *Biochem. Pharmacol.* **83**, 849–857.
- Paszek, M.J., Zahir, N., Johnson, K.R., Lakins, J.N., Rozenberg, G.I., Gefen, A., Reinhart-King, C.A., Margulies, S.S., Dembo, M., Boettiger, D., et al. (2005). Tensional homeostasis and the malignant phenotype. *Cancer Cell* **8**, 241–254.
- Paul, C.D., Bishop, K., Devine, A., Paine, E.L., Staunton, J.R., Thomas, S.M., Thomas, J.R., Doyle, A.D., Miller Jenkins, L.M., Morgan, N.Y., et al. (2019). Tissue architectural cues drive organ targeting of tumor cells in zebrafish. *Cell Syst.* **9**, 187–206.e16.
- Peinado, H., Zhang, H., Matei, I.R., Costa-Silva, B., Hoshino, A., Rodrigues, G., Psaila, B., Kaplan, R.N., Bromberg, J.F., Kang, Y., et al. (2017). Pre-metastatic niches: organ-specific homes for metastases. *Nat. Rev. Cancer* **17**, 302–317.
- Pelling, A.E., and Horton, M.A. (2008). An historical perspective on cell mechanics. *Pflug. Arch.* **456**, 3–12.
- Pereira, E.R., Kedrin, D., Seano, G., Gautier, O., Meijer, E.F.J., Jones, D., Chin, S.-M., Kitahara, S., Bouta, E.M., Chang, J., et al. (2018). Lymph node metastases can invade local blood vessels, exit the node, and colonize distant organs in mice. *Science* **359**, 1403–1407.
- Petrosyan, A. (2015). Onco-Golgi: is fragmentation a gate to cancer progression? *Biochem. Mol. Biol. J.* **1**, 16.
- Petrosyan, A., and Cheng, P.-W. (2013). A non-enzymatic function of Golgi glycosyltransferases: mediation of Golgi fragmentation by interaction with non-muscle myosin IIA. *Glycobiology* **23**, 690–708.
- Petrosyan, A., Holzapfel, M.S., Muirhead, D.E., and Cheng, P.W. (2014). Restoration of compact Golgi morphology in advanced prostate cancer enhances susceptibility to galectin-1-induced apoptosis by modifying mucin O-glycan synthesis. *Mol. Cancer Res.* **12**, 1704–1716.
- Physical Sciences - Oncology Centers Network (2013). A physical sciences network characterization of non-tumorigenic and metastatic cells. *Sci. Rep.* **3**, 1449.
- Pickup, M.W., Mouw, J.K., and Weaver, V.M. (2014). The extracellular matrix modulates the hallmarks of cancer. *EMBO Rep.* **15**, 1243–1253.
- Piotrowski-Daspiet, A.S., Tien, J., and Nelson, C.M. (2016). Interstitial fluid pressure regulates collective invasion in engineered human breast tumors via Snail, vimentin, and E-cadherin. *Integr. Biol. (Camb.)* **8**, 319–331.
- Plodinec, M., Loparic, M., Monnier, C.A., Obermann, E.C., Zanetti-Dallenbach, R., Oertle, P., Hyotyla, J.T., Aebi, U., Bentires-Alj, M., Lim, R.Y.H., and Schoenberger, C.-A. (2012). The nanomechanical signature of breast cancer. *Nat. Nanotechnol.* **7**, 757–765.
- Pontes, B., Ayala, Y., Fonseca, A.C.C., Romão, L.F., Amaral, R.F., Salgado, L.T., Lima, F.R., Farina, M., Viana, N.B., Moura-Neto, V., and Nussenzeig, H.M. (2013). Membrane elastic properties and cell function. *PLoS One* **8**, e67708.
- Provenzano, P.P., Eliceiri, K.W., Campbell, J.M., Inman, D.R., White, J.G., and Keely, P.J. (2006). Collagen reorganization at the tumor-stromal interface facilitates local invasion. *BMC Med.* **4**, 38.
- Pu, J., Guardia, C.M., Keren-Kaplan, T., and Bonifacino, J.S. (2016). Mechanisms and functions of lysosome positioning. *J. Cell Sci.* **129**, 4329–4339.
- Radmacher, M., Fritz, M., Kacher, C.M., Cleveland, J.P., and Hansma, P.K. (1996). Measuring the viscoelastic properties of human platelets with the atomic force microscope. *Biophys. J.* **70**, 556–567.
- Regmi, S., Fu, A., and Luo, K.Q. (2017). High shear stresses under exercise condition destroy circulating tumor cells in a microfluidic system. *Sci. Rep.* **7**, 39975.
- Remmerbach, T.W., Wottawah, F., Dietrich, J., Lincoln, B., Wittekind, C., and Guck, J. (2009). Oral cancer diagnosis by mechanical phenotyping. *Cancer Res.* **69**, 1728–1732.
- Rheinlaender, J., Dimitracopoulos, A., Wallmeyer, B., Kronenberg, N.M., Chalut, K.J., Gather, M.C., Betz, T., Charas, G., and Franze, K. (2020). Cortical cell stiffness is independent of substrate mechanics. *Nat. Mater.* **19**, 1019–1025.
- Rianna, C., Radmacher, M., and Kumar, S. (2020). Direct evidence that tumor cells soften when navigating confined spaces. *Mol. Biol. Cell* **31**, 1726–1734.
- Rosendahl, P., Plak, K., Jacobi, A., Kraeter, M., Toepfner, N., Otto, O., Herold, C., Winzi, M., Herbig, M., Ge, Y., et al. (2018). Real-time fluorescence and deformability cytometry. *Nat. Methods* **15**, 355–358.
- Scholz, N. (2018). Cancer cell mechanics: adhesion G protein-coupled receptors in action? *Front. Oncol.* **8**, 59.
- Schultz, M.J., Swindall, A.F., and Bellis, S.L. (2012). Regulation of the metastatic cell phenotype by sialylated glycans. *Cancer Metastasis Rev.* **31**, 501–518.
- Seltmann, K., Fritsch, A.W., Käs, J.A., and Magin, T.M. (2013). Keratins significantly contribute to cell stiffness and impact invasive behavior. *Proc. Natl. Acad. Sci. USA* **110**, 18507–18512.
- Shivashankar, G.V. (2011). Mechanosignaling to the cell nucleus and gene regulation. *Annu. Rev. Biophys.* **40**, 361–378.
- Sinha, B., Köster, D., Ruez, R., Gonnord, P., Bastiani, M., Abankwa, D., Stan, R.V., Butler-Browne, G., Vedie, B., Johannes, L., et al. (2011). Cells respond to mechanical stress by rapid disassembly of caveolae. *Cell* **144**, 402–413.
- Soppina, V., Rai, A.K., Ramaiya, A.J., Barak, P., and Mallik, R. (2009). Tug-of-war between dissimilar teams of microtubule motors regulates transport and fission of endosomes. *Proc. Natl. Acad. Sci. USA* **106**, 19381–19386.
- Stacker, S.A., Williams, S.P., Karnezis, T., Shayan, R., Fox, S.B., and Achen, M.G. (2014). Lymphangiogenesis and lymphatic vessel remodelling in cancer. *Nat. Rev. Cancer* **14**, 159–172.
- Starr, D.A., and Fridolfsson, H.N. (2010). Interactions between nuclei and the cytoskeleton are mediated by SUN-KASH nuclear-envelope bridges. *Annu. Rev. Cell Dev. Biol.* **26**, 421–444.
- Steeg, P.S. (2016). Targeting metastasis. *Nat. Rev. Cancer* **16**, 201–218.
- Stephens, A.D., Banigan, E.J., Adam, S.A., Goldman, R.D., and Marko, J.F. (2017). Chromatin and lamin A determine two different mechanical response regimes of the cell nucleus. *Mol. Biol. Cell* **28**, 1984–1996.
- Strell, C., and Entschladen, F. (2008). Extravasation of leukocytes in comparison to tumor cells. *Cell Commun. Signal.* **6**, 10.
- Strlic, B., and Offermanns, S. (2017). Intravascular survival and extravasation of tumor cells. *Cancer Cell* **32**, 282–293.
- Stuelten, C.H., Parent, C.A., and Montell, D.J. (2018). Cell motility in cancer invasion and metastasis: insights from simple model organisms. *Nat. Rev. Cancer* **18**, 296–312.
- Stylianopoulos, T., Martin, J.D., Chauhan, V.P., Jain, S.R., Diop-Frimpong, B., Bardeesy, N., Smith, B.L., Ferrone, C.R., Hornicek, F.J., Boucher, Y., et al. (2012). Causes, consequences, and remedies for growth-induced solid stress in murine and human tumors. *Proc. Natl. Acad. Sci. USA* **109**, 15101–15108.
- Sun, S., Wong, S., Mak, A., and Cho, M. (2014). Impact of oxidative stress on cellular biomechanics and rho signaling in C2C12 myoblasts. *J. Biomech.* **47**, 3650–3656.
- Sunyer, R., Trepal, X., Fredberg, J.J., Farré, R., and Navajas, D. (2009). The temperature dependence of cell mechanics measured by atomic force microscopy. *Phys. Biol.* **6**, 025009.
- Suresh, S. (2007). Biomechanics and biophysics of cancer cells. *Acta Biomater.* **3**, 413–438.
- Suresh, S., Spatz, J., Mills, J.P., Micoulet, A., Dao, M., Lim, C.T., Beil, M., and Seufferlein, T. (2005). Connections between single-cell biomechanics and human disease states: gastrointestinal cancer and malaria. *Acta Biomater.* **1**, 15–30.
- Swaminathan, V., Myhre, K., O'Brien, E.T., Berchuck, A., Blobe, G.C., and Superfine, R. (2011). Mechanical stiffness grades metastatic potential in patient tumor cells and in cancer cell lines. *Cancer Res.* **71**, 5075–5080.
- Swift, J., and Discher, D.E. (2014). The nuclear lamina is mechano-responsive to ECM elasticity in mature tissue. *J. Cell Sci.* **127**, 3005–3015.
- Tan, X., Banerjee, P., Guo, H.F., Ireland, S., Pankova, D., Ahn, Y.H., Nikolaidis, I.M., Liu, X., Zhao, Y., Xue, Y., et al. (2017). Epithelial-to-mesenchymal transition drives a pro-metastatic Golgi compaction process through scaffolding protein PAQR11. *J. Clin. Invest.* **127**, 117–131.

- Taubenberger, A.V., Girardo, S., Träber, N., Fischer-Friedrich, E., Kräter, M., Wagner, K., Kurth, T., Richter, I., Haller, B., Binner, M., et al. (2019). 3D micro-environment stiffness regulates tumor spheroid growth and mechanics via p21 and ROCK. *Adv. Biosyst.* **3**, e1900128.
- Tavares, S., Vieira, A.F., Taubenberger, A.V., Araújo, M., Martins, N.P., Brás-Pereira, C., Polónia, A., Herbig, M., Barreto, C., Otto, O., et al. (2017). Actin stress fiber organization promotes cell stiffening and proliferation of pre-invasive breast cancer cells. *Nat. Commun.* **8**, 15237.
- Thiam, H.-R., Vargas, P., Carpi, N., Crespo, C.L., Raab, M., Terriac, E., King, M.C., Jacobelli, J., Alberts, A.S., Stradal, T., et al. (2016). Perinuclear Arp2/3-driven actin polymerization enables nuclear deformation to facilitate cell migration through complex environments. *Nat. Commun.* **7**, 10997.
- Thomas, G., Burnham, N.A., Camesano, T.A., and Wen, Q. (2013). Measuring the mechanical properties of living cells using atomic force microscopy. *J. Vis. Exp.* **76**, 50497.
- Tietze, S., Kräter, M., Jacobi, A., Taubenberger, A., Herbig, M., Wehner, R., Schmitz, M., Otto, O., List, C., Kaya, B., et al. (2019). Spheroid culture of mesenchymal stromal cells results in Morphorheological properties appropriate for improved microcirculation. *Adv. Sci. (Weinh.)* **6**, 1802104.
- Toepfner, N., Herold, C., Otto, O., Rosendahl, P., Jacobi, A., Kräter, M., Stächele, J., Menschner, L., Herbig, M., Ciuffreda, L., et al. (2018). Detection of human disease conditions by single-cell morpho-rheological phenotyping of blood. *eLife* **7**, e29213.
- Tse, H.T.K., Gossett, D.R., Moon, Y.S., Masaeli, M., Sohsman, M., Ying, Y., Mislick, K., Adams, R.P., Rao, J., and Di Carlo, D. (2013). Quantitative diagnosis of malignant pleural effusions by single-cell mechanophenotyping. *Sci. Transl. Med.* **5**, 212ra163.
- Turner, J.R., and Tartakoff, A.M. (1989). The response of the Golgi complex to microtubule alterations: the roles of metabolic energy and membrane traffic in Golgi complex organization. *J. Cell Biol.* **109**, 2081–2088.
- Urbanska, M., Muñoz, H.E., Shaw Bagnall, J., Otto, O., Manalis, S.R., Di Carlo, D., and Guck, J. (2020). A comparison of microfluidic methods for high-throughput cell deformability measurements. *Nat. Methods* **17**, 587–593.
- Van Vliet, K.J., Bao, G., and Suresh, S. (2003). The biomechanics toolbox: experimental approaches for living cells and biomolecules. *Acta Mater.* **51**, 5881–5905.
- Venkatesh, S.K., Yin, M., Glockner, J.F., Takahashi, N., Araoz, P.A., Talwalkar, J.A., and Ehman, R.L. (2008). MR elastography of liver tumors: preliminary results. *AJR Am. J. Roentgenol.* **190**, 1534–1540.
- Vicente-Dueñas, C., Hauer, J., Cobaleda, C., Borkhardt, A., and Sánchez-García, I. (2018). Epigenetic priming in cancer initiation. *Trends Cancer* **4**, 408–417.
- Ward, K.A., Li, W.I., Zimmer, S., and Davis, T. (1991). Viscoelastic properties of transformed cells: role in tumor cell progression and metastasis formation. *Biorheology* **28**, 301–313.
- Watanick, R.S. (2012). The role of the tumor microenvironment in regulating angiogenesis. *Cold Spring Harb. Perspect. Med.* **2**, a006676.
- Weiss, L. (1990). Metastatic inefficiency. *Adv. Cancer Res.* **54**, 159–211.
- Werb, Z., and Lu, P. (2015). The role of stroma in tumor development. *Cancer J.* **21**, 250–253.
- Whiteside, T.L. (2006). The role of immune cells in the tumor microenvironment. *Cancer Treat. Res.* **130**, 103–124.
- Wirtz, D., Konstantopoulos, K., and Searson, P.C. (2011). The physics of cancer: the role of physical interactions and mechanical forces in metastasis. *Nat. Rev. Cancer* **11**, 512–522.
- Wolf, K., Te Lindert, M., Krause, M., Alexander, S., Te Riet, J., Willis, A.L., Hoffman, R.M., Figdor, C.G., Weiss, S.J., and Friedl, P. (2013). Physical limits of cell migration: control by ECM space and nuclear deformation and tuning by proteolysis and traction force. *J. Cell Biol.* **201**, 1069–1084.
- Wottawah, F., Schinkinger, S., Lincoln, B., Ananthakrishnan, R., Romeyke, M., Guck, J., and Käs, J. (2005). Optical rheology of biological cells. *Phys. Rev. Lett.* **94**, 098103.
- Wu, P.-H., Aroush, D.R.-B., Asnacios, A., Chen, W.-C., Dokukin, M.-E., Doss, B.L., Durand-Smet, P., Ekpenyong, A., Guck, J., Guz, N.V., et al. (2018). A comparison of methods to assess cell mechanical properties. *Nat. Methods* **15**, 491–498.
- Wu, P.-H., Gambhir, S.S., Hale, C.M., Chen, W.-C., Wirtz, D., and Smith, B.R. (2020). Particle tracking microrheology of cancer cells in living subjects. *Mater. Today*.
- Wullkopf, L., West, A.-K.V., Leijnse, N., Cox, T.R., Madsen, C.D., Oddershede, L.B., and Erler, J.T. (2018). Cancer cells' ability to mechanically adjust to extracellular matrix stiffness correlates with their invasive potential. *Mol. Biol. Cell* **29**, 2378–2385.
- Xin, Y., Chen, X., Tang, X., Li, K., Yang, M., Tai, W.C.-S., Liu, Y., and Tan, Y. (2019). Mechanics and actomyosin-dependent survival/chemoresistance of suspended tumor cells in shear flow. *Biophys. J.* **116**, 1803–1814.
- Xu, W., Mezencev, R., Kim, B., Wang, L., McDonald, J., and Sulchek, T. (2012). Cell stiffness is a biomarker of the metastatic potential of ovarian cancer cells. *PLoS One* **7**, e46609.
- Zhang, W., Kai, K., Choi, D.S., Iwamoto, T., Nguyen, Y.H., Wong, H., Landis, M.D., Ueno, N.T., Chang, J., and Qin, L. (2012). Microfluidics separation reveals the stem-cell-like deformability of tumor-initiating cells. *Proc. Natl. Acad. Sci. USA* **109**, 18707–18712.

3) Références complémentaires

Au chapitre “**Measuring cellular mechanics: methods, results, and limitations**”, on ajoutera qu’une évolution de la technique de cytométrie de déformabilité en temps réel (RT-DC) permet désormais de mesurer à très haut débit à la fois les propriétés d’élasticité et de viscosité de cellules (Gerum et al., 2022).

Au chapitre “**Tumor cell mechanics: passive properties and active regulatory elements**”, il nous faut ajouter que les microtubules peuvent activement participer à la réponse mécanique de cellules soumises à du stress compressif en se stabilisant une fois torsionnés, favorisant au passage la migration des cellules (Li et al., 2023).

À propos du chapitre “**Cell mechanics and metastasis**”, on mentionnera qu’une étude récente a établi un lien entre souplesse mécanique et résistance à la molécule chimiothérapeutique 5-FU (Han et al., 2023).

Concernant les étapes d’invasion et migration, deux études additionnelles méritent d’être mentionnées. L’une apporte un nouvel élément de réponse à la question de la contribution du glucose dans la progression tumorale. En effet, il est démontré que des niveaux de glucose élevés dans la matrice extracellulaire activent la voie cAMP/RhoA/ROCK dans les cellules tumorales, résultant en une activité accrue de myosine non-musculaire II, un réarrangement de l’actine et une rigidification des cellules tumorales qui améliore leurs capacités de migration (Oh et al., 2023). L’autre étude additionnelle à mentionner complémente parfaitement les travaux rapportant qu’une rigidité accrue conférée par les microtubules favorise l’invasion/migration de cellules de glioblastome, en démontrant cette fois-ci que la rigidité conférée par les filaments intermédiaires est également un moteur important de l’invasion pour ces cellules (Van Bodegraven et al., 2023).

Concernant les étapes intravasculaires de la dissémination métastatique, des travaux récents se sont intéressés aux contributions respectives des propriétés d’élasticité et de viscosité au cours de la microcirculation de globules rouges. Des analyses numériques suggèrent que la composante de viscosité joue un rôle déterminant dans le comportement de déformation de la membrane de globules rouges circulants (Gürbüz et al., 2023). Il y a fort à parier que la situation est similaire pour des CTCs,

qui pourront elles aussi exhiber des comportements typiques d'objets viscoélastiques non-récapitulables avec des modèles purement élastiques. Concernant l'étape d'arrêt, l'étude citée qui démontre élégamment que les CTCs se rigidifient en réponse aux forces de cisaillement via la voie de signalisation RhoA/ROCK pour améliorer leurs capacités de survie dans l'environnement intravasculaire (Moose et al., 2020) complémente très bien des travaux antérieurs. En effet, la même voie RhoA/ROCK a été identifiée comme composante permettant aux CTCs de se rigidifier, d'adopter une forme sphérique et ainsi de grandement augmenter leurs chances de s'arrêter dans les vaisseaux capillaires (Huang et al., 2018).

Au sujet de l'adhésion des CTCs à la paroi endothéliale, des études récentes utilisant des modèles numériques prédisent la façon dont la forme des cellules change avec l'établissement de forces d'adhésion (Stotski and Ohtmer., 2022) et avancent qu'une déformabilité accrue permet aux CTCs d'augmenter leur surface de contact avec la paroi endothéliale et ainsi de former plus d'interactions ligand/récepteur et de s'adhérer plus facilement (Cui et al., 2020). De manière très similaires, des travaux employant également une approche numérique se sont intéressés à la contribution de la viscosité dans le mécanisme de rolling des leucocytes que l'on retrouve parfois chez certaines cellules tumorales. Leurs analyses prédisent qu'une viscosité réduite, associée à une déformabilité accrue, devrait résulter en un rolling plus lent et plus stable le long de la paroi endothéliale (Khismatullin et al., 2012).

Enfin, on mentionnera une dernière étude qui a récemment démontré que plusieurs lignées de cellules tumorales s'assouplissent dans leur ensemble et à l'échelle de leur noyau pendant le processus d'extravasation par diapédèse, ce qui constitue encore un bel exemple d'adaptation dynamique des propriétés mécaniques de cellules tumorales confrontées à un défi mécanique (Roberts et al., 2021).

D) Objectifs de mes travaux

La contribution de la mécanique cellulaire est de mieux en mieux comprise dans la quasi-totalité des étapes constituant la cascade métastatique. L'hypothèse de l'adaptabilité mécanique des cellules tumorales au cours de la progression tumorale, forte de l'accumulation récente de données allant en son sens, suggère que la capacité que certaines cellules tumorales pourraient avoir à ajuster dynamiquement leur phénotype mécanique pourrait orchestrer le franchissement de l'ensemble des étapes aboutissant au développement métastatique. Cependant, des zones d'ombre subsistent et nous empêchent encore, pour le moment, d'avoir une compréhension globale et totale du rôle de fil conducteur que pourrait jouer l'adaptabilité mécanique des cellules tumorales. C'est notamment le cas pour les étapes intravasculaires de la cascade métastatique. Bien que le rôle de la rigidité des CTCs soit très bien décrit dans leur capacité à résister aux forces de cisaillement, bien trop peu de données sont disponibles pour caractériser son impact sur les itinéraires de circulation, l'arrêt par occlusion mécanique ou encore la capacité à former des interactions d'adhésion des cellules tumorales circulantes. Concernant l'étape d'extravasation, si des données suggèrent de manière convaincante qu'une déformabilité accrue favoriserait l'extravasation par diapédèse, l'importance que la rigidité cellulaire pourrait avoir dans le mécanisme d'extravasation par remodelage endothélial, dont nous avons déjà vu qu'il pouvait être sensible à des paramètres biomécaniques, reste à ce jour totalement indéterminée. Forts de l'expérience du laboratoire dans l'étude de paramètres biomécaniques orchestrant les étapes intravasculaires du développement métastatique, mes travaux, en s'inscrivant dans la continuité de nos études caractérisant les importances conjointes des forces hémodynamiques et des forces d'adhésion dans l'arrêt, l'adhésion et l'extravasation des cellules tumorales, ont les objectifs suivants :

(i) Démontrer et quantifier la contribution du mécanisme d'occlusion dans l'arrêt des CTCs.

Si quelques rares études ont très élégamment permis de visualiser des événements d'arrêt par occlusion, aucune n'a permis de disséquer les contributions parallèles de l'occlusion mécanique et de l'adhésion active des CTCs dans l'étape d'arrêt. Des outils de modélisation de CTCs permettent de nos jours de quantifier l'importance du

mécanisme d'occlusion par l'expérimentation *in vivo* en s'affranchissant de tout effet d'adhésion.

(ii) Mesurer les forces exercées par l'architecture vasculaire sur les cellules tumorales piégées dans l'environnement intravasculaire.

Pression hydrostatique interstitielle (en mmHg), stress compressif (en Pa), débit sanguin (en $\mu\text{L/s}$), contraintes de cisaillement (en Dynes/cm²) : la grande majorité des forces mécaniques opérant au cours de la progression tumorale sont mesurables. Des senseurs de forces sont maintenant disponibles pour également réaliser des mesures intravasculaires de la pression mécanique exercée par l'architecture vasculaire sur des objets piégés en son sein.

(iii) Générer des populations de cellules tumorales avec des propriétés mécaniques altérées pour tester leur importance à l'aide d'expériences *in vivo*.

L'étude de l'impact de la déformabilité cellulaire au cours des étapes intravasculaires du développement métastatique passe forcément par l'établissement de modèles fiables de cellules tumorales présentant des propriétés mécaniques différentes et pouvant être injectées dans le cadre d'expériences quantitatives *in vivo*.

(iv) Démontrer l'impact de la déformabilité des CTCs sur leur comportement de circulation et leur capacité à accéder à des régions vasculaires présentant des paramètres de taille/topographie différents.

La combinaison de modèles de CTCs mécaniquement altérées avec de la microscopie intravitale doit permettre de quantifier l'importance de la rigidité de cellules tumorales tout juste devenues circulantes au cours des tous premiers instants de leur dissémination hématogène.

(v) Identifier les propriétés mécaniques conférant un avantage aux cellules tumorales pour la réalisation de l'étape d'extravasation.

De même, l'existence de puissants modèles *in vivo* permettant de récapituler et visualiser l'extravasation métastatique doit permettre de jauger le potentiel d'extravasation de cellules tumorales mécaniquement altérées et ainsi d'identifier les propriétés mécaniques avantageuses.

(vi) Resituer, dans le contexte de l'hypothèse de l'adaptabilité mécanique des cellules tumorales, les phénotypes mécaniques identifiés comme importants pour le franchissement des étapes intravasculaires dont il est ici question.

Comparer les propriétés mécaniques avantageuses pour la résistance aux forces de cisaillement, pour la réalisation de l'arrêt intravasculaire, pour l'extravasation ou encore pour la croissance métastatique post-extravasation.

II) APPROCHE EXPÉRIMENTALE

Sont décrits dans cette section les grands piliers sur lesquels repose notre approche expérimentale. Pour les détails de l'ensemble des lignées et protocoles utilisés, se référer à la section "material and methods" incluse dans l'ébauche de l'article en préparation « Cell Viscoelasticity Orchestrates Intravascular and Early Steps of Metastasis » qui constitue la section « [RÉSULTATS](#) ».

A) Le modèle embryon de poisson-zèbre

Le modèle poisson-zèbre est un modèle populaire dans les laboratoires de recherche biomédicale, grâce notamment au taux de conservation très élevé (82%) de gènes impliqués dans les pathologies humaines entre son génome et le génome humain (Howe et al., 2013 ; White and Patton, 2023) et son fort potentiel en tant que plateforme de criblage (Dash and Patnaik, 2023). Pour les recherches focalisées sur la cascade métastatique, c'est au stade d'embryon que le poisson-zèbre est particulièrement attrayant. En effet, à deux jours post-fertilisation, l'embryon de poisson-zèbre est un système physiologique comportant un cœur et un système vasculaire stéréotypé dans lequel des flux tels qu'on en trouve dans de nombreux organes humains sont récapitulés (Follain et al., 2020). De plus, la facilité de maintenir l'embryon de poisson-zèbre transparent à ce stade et l'existence de nombreuses lignées transgéniques, notamment certaines exprimant des protéines fluorescentes dans les cellules endothéliales, le rendant parfaitement compatible avec la microscopie pour visualiser son système vasculaire par exemple. De plus, les étapes intravasculaires (circulation, arrêt/adhésion, extravasation) sont récapitulées en 24 heures après l'injection de cellules tumorales dans la circulation.

Embryon de poisson-zèbre (plexus caudal)

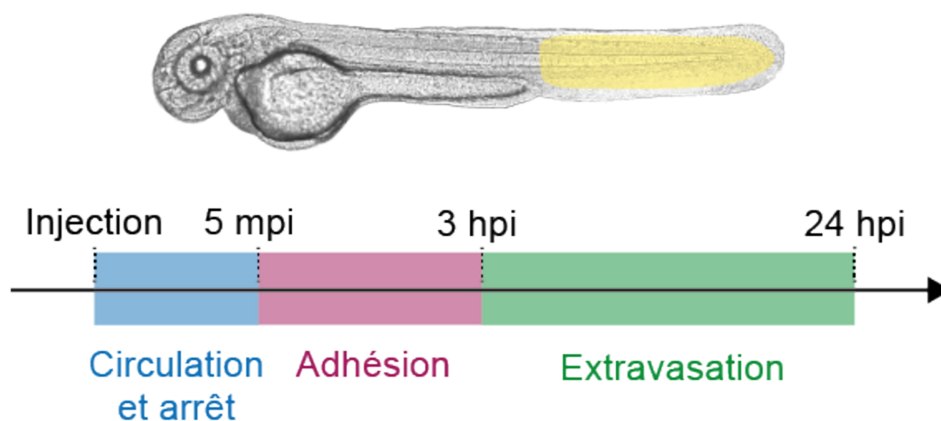


Figure 15 : Fenêtres temporelles pour l'étude des étapes intravasculaires du développement métastatique dans l'embryon de poisson-zèbre. La circulation et l'arrêt se déroulent dans les minutes qui suivent l'injection. Les cellules arrêtées stabilisent leur adhésion jusqu'à 3 heures après l'injection puis le processus d'extravasation se déroule jusqu'à environ 24 heures post-injection.

1) Injection intravasculaire

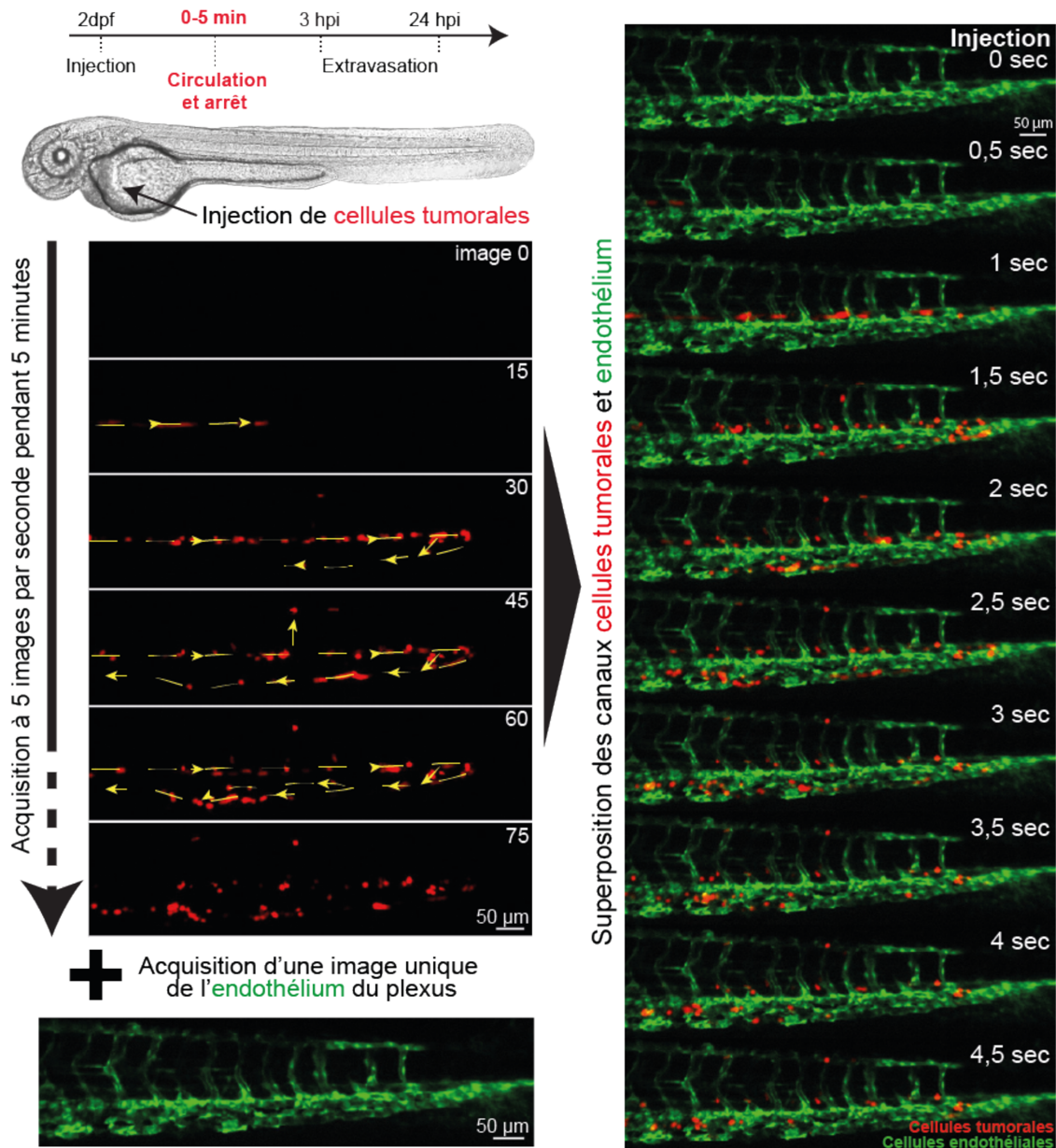
L'injection se fait dans le canal de cuvier à l'aide d'un micro-injecteur sur lequel un capillaire de verre est monté. Les cellules tumorales, préparées à environ $40 \cdot 10^6$ cellules/mL sont d'abord aspirées dans le capillaire en verre. L'injection dans le canal de cuvier se fait ensuite avec des volumes allant de 9 nL à 27 nL, ajustables tout au long de la session d'injection pour obtenir des nombres d'événements de circulation et d'arrêt appropriés.



Figure 16 : Injection intravasculaire dans le canal de cuvier. Les cellules endothéliales des embryons expriment la GFP tandis que les cellules tumorales expriment la tdTomato. (Adapté de Follain et al., *Methods in Molecular Biology*, 2016).

2) Imagerie des événements de circulation et d'arrêt des CTCs

Dans le but d'imager les tous premiers événements de circulation et d'arrêt faisant suite à la mise en circulation de cellules tumorales dans le système circulatoire du poisson-zèbre, les injections sont réalisées sous un stéréomicroscope Leica M205 FA avec lequel sont effectués, pour chaque embryon injecté, des enregistrements de 5 minutes pour capturer le signal des CTCs en vidéo, ainsi que des images arrêtées du signal des vaisseaux. La superposition des deux canaux permet, à l'analyse, de visualiser le mouvement et les arrêts des CTCs dans le plexus caudal de l'embryon de poisson-zèbre.



Localisation des événements sur une carte de référence



Génération de cartes thermiques

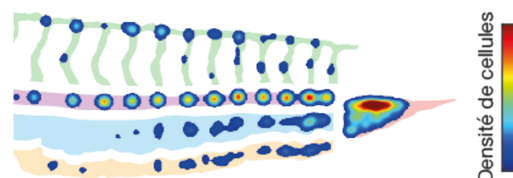


Figure 17 : Imagerie et analyse des événements de circulation et d'arrêt des CTCs. (Adapté de Follain et al., *Methods in Molecular Biology*, 2016).

L'analyse consiste notamment en la quantification de la répartition des événements d'arrêt dans les 5 sous-régions vasculaires constituant le plexus caudal de l'embryon de poisson-zèbre, et présentant des caractéristiques de taille et de topographie différentes.

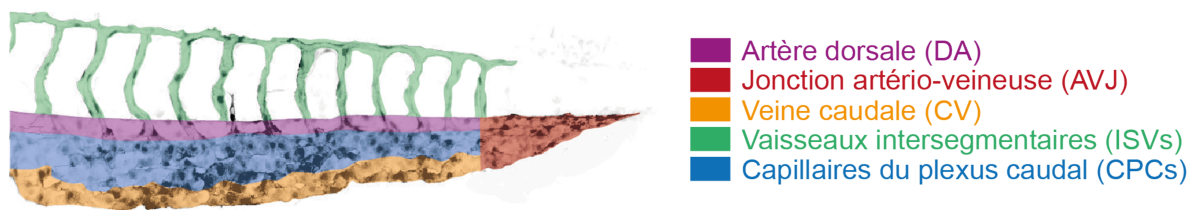


Figure 18 : Les sous-régions vasculaires constituant le plexus caudal de l'embryon de poisson-zèbre.

3) Imagerie de l'extravasation des cellules tumorales

Le processus d'extravasation débutant quelques heures après l'arrêt intravasculaire et étant généralement terminé 24 heures après, l'imagerie des embryons injectés s'effectue 3 heures après injection pour visualiser l'initiation de l'extravasation et 24 heures après pour visualiser les cellules tumorales extravasées, avec un microscope confocal SP5 ou un spinning-disk Olympus.

L'analyse à ces temps de 3 et 24 heures post-injection consiste en la quantification des cellules intravasculaires, des événements de "pocketing" (= initiation de l'extravasation par remodelage endothéliale) et des cellules pleinement extravasées, ainsi qu'en la génération de cartes thermiques rapportant des sites où ces événements ont lieu.

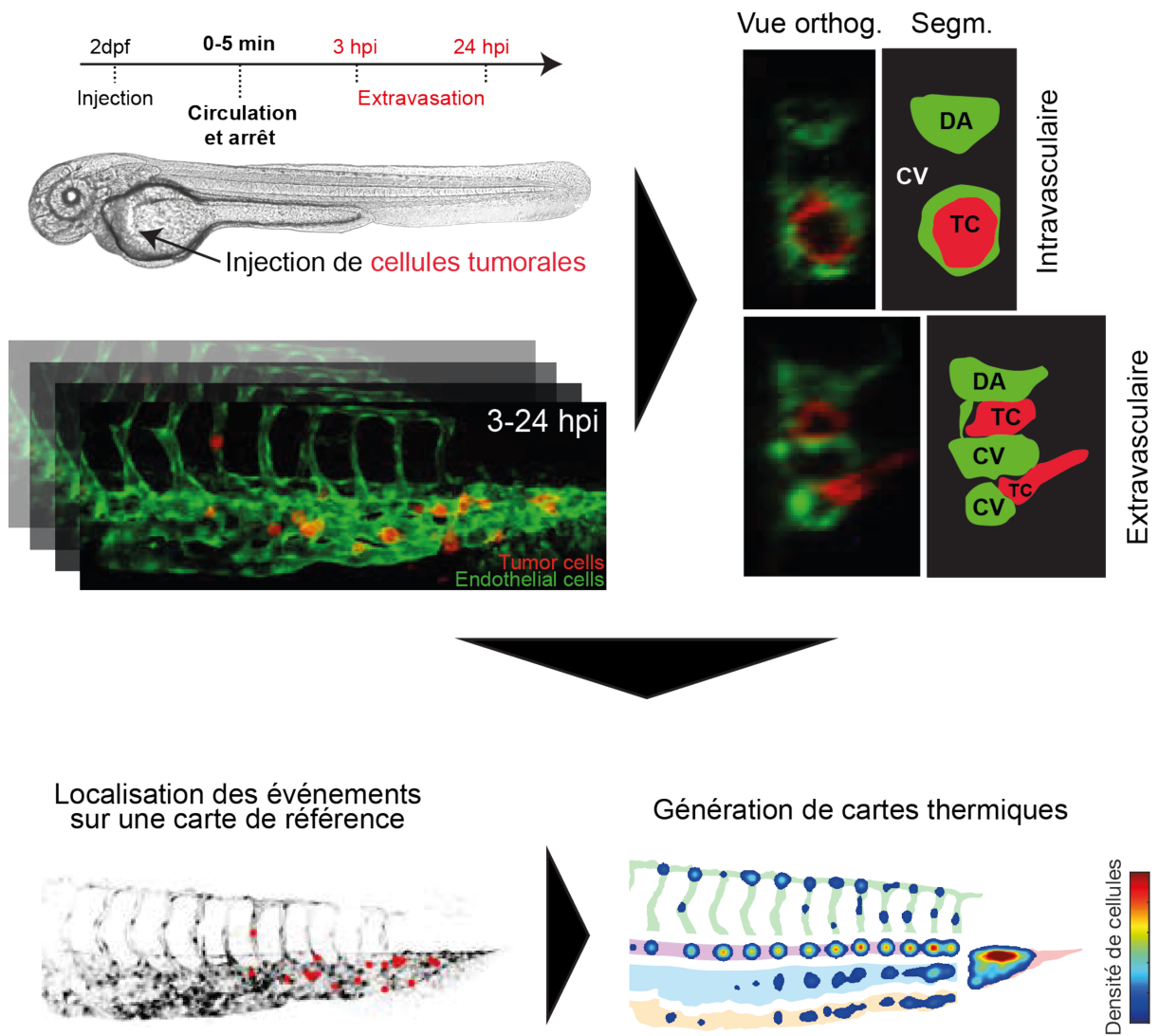


Figure 19 : Imagerie et analyse des événements de remodelage endothélial et d'extravasation de cellules tumorales. (Adapté de Follain et al., *Methods in Molecular Biology*, 2016).

B) Billes élastiques de polyacrylamide

Des billes élastiques en gel de polyacrylamide sont utilisées pour modéliser des CTCs dans le système circulatoire de l'embryon de poisson-zèbre (Girardo et al., 2018). Deux types d'utilisation en sont faites.

1) Étude de la contribution du mécanisme d'occlusion dans l'arrêt intravasculaire

Ces billes de polyacrylamide élastiques étant totalement inertes et dénuées de molécules d'adhésion, elles ne peuvent s'arrêter que par occlusion mécanique dans le système vasculaire de l'embryon de poisson-zèbre. Des populations de billes présentant des propriétés de taille et de rigidité différentes ont ainsi été générées afin de mettre en lumière la contribution et la localisation des événements d'occlusion mécanique dans le plexus caudal de l'embryon. Les injections et l'imagerie sont réalisées telles que décrites précédemment dans A) 1).

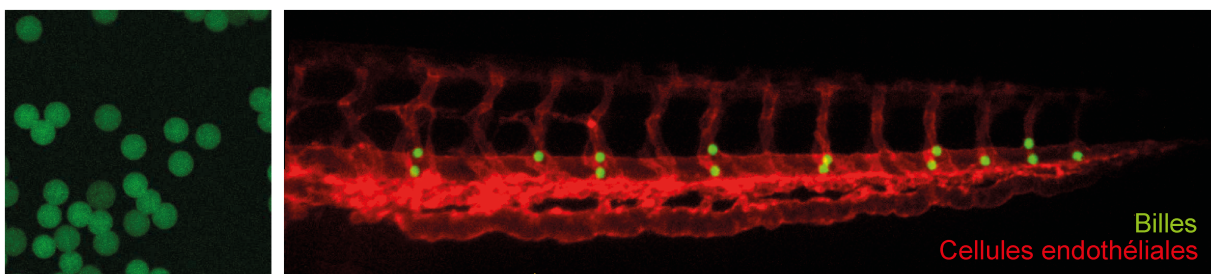


Figure 20 : Injection intravasculaire de billes de polyacrylamide dans l'embryon de poisson-zèbre. Les billes de polyacrylamide fonctionnalisées avec de la GFP (gauche) s'arrêtent par occlusion mécanique dans le système circulatoire de l'embryon de poisson-zèbre (droite).

2) Mesure des forces exercées par l'architecture vasculaire

Les billes de polyacrylamide étaient, à l'origine, imaginées et produites pour être couplées à une analyse numérique permettant d'extraire, à partir de leur déformation, la quantité de pression mécanique subie (Träber et al., 2019). Nous avons voulu en tirer profit pour mesurer la pression mécanique perçue par des billes piégées dans l'architecture du système vasculaire de l'embryon de poisson-zèbre. Après injection des billes, les embryons sont imagés le plus

rapidement possible avec un microscope confocal Leica SP5. Des stacks très zoomés avec un pas de $0.25\ \mu\text{m}$ sont réalisés pour reconstruire le plus précisément possible la géométrie des billes imagées. La géométrie ainsi reconstruite est comparée à la géométrie théorique des billes non-déformées. L'analyse numérique COMPAX, via la méthode des éléments finis, projette les vecteurs de forces sur la géométrie de la bille en conséquent et permet ainsi de déduire la pression volumétrique moyenne subie par la bille.

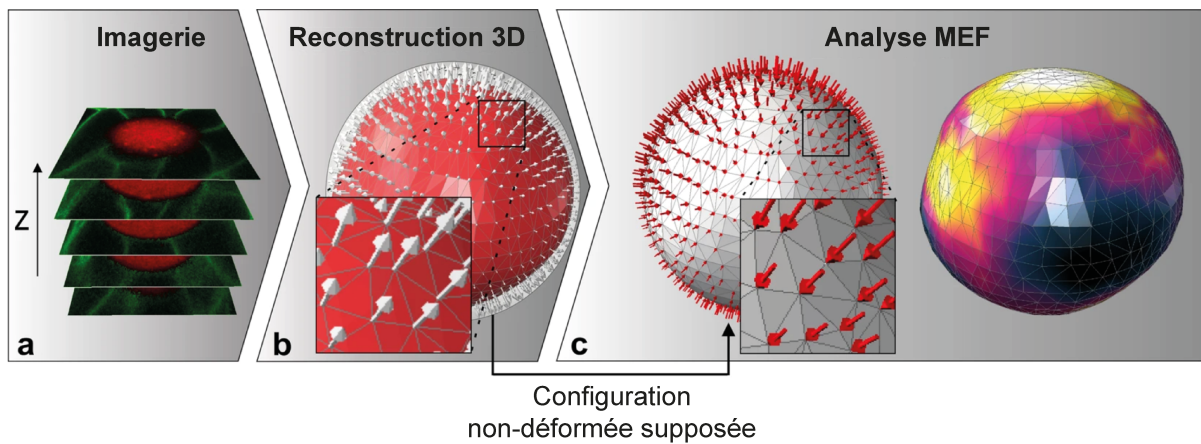


Figure 21 : Analyse numérique de la déformation des billes. (a) Stack de microscopie confocale. (b) Reconstruction de la géométrie de la bille en 3 dimensions. (c) Méthode des éléments finis pour numérisation des forces responsables de la déformation. (Adapté de [Träber et al., Scientific Reports, 2019](#))

C) Génération de populations de cellules tumorales mécaniquement altérées

Les billes de polyacrylamide purement élastique ne récapitulant pas les propriétés viscoélastiques des cellules tumorales, il est nécessaire de générer des populations de cellules tumorales présentant des phénotypes mécaniques différents. Comme pour les études précédentes du laboratoire, nous employons ici aussi la lignée D2A1 (Carcinome malin de la glande mammaire de souris) dont nous savons qu'elles récapitulent efficacement les comportements d'adhésion et d'extravasation dans le modèle poisson-zèbre (Follain et al., 2018 ; Osmani et al., 2019 ; Follain et al., 2021).

1) Déplétion de protéines liées à la mécanique cellulaire

Le cytosquelette étant responsable des propriétés mécaniques des cellules, nous le ciblons dans les cellules D2A1 en 4 niveaux différents via une approche ARN interférant, dans le but d'assouplir les cellules de 4 manières différentes. Les protéines ciblées sont la lamine A/C (enveloppe nucléaire du noyau), la vimentine (filaments intermédiaires), la myosine non-musculaire IIA (cortex d'actomyosine) et la cavéoline-1 (membrane plasmique).

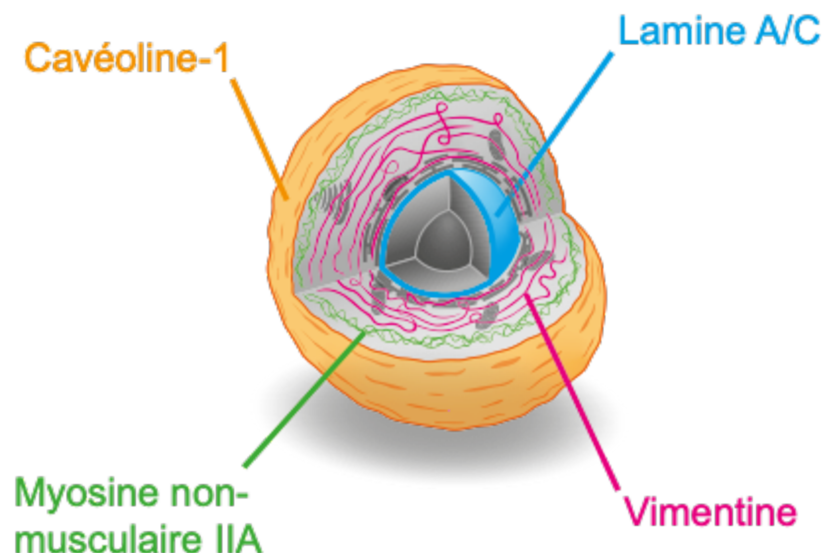


Figure 22 : Protéines ciblées pour l'altération des propriétés mécaniques de cellules tumorales D2A1. L'efficacité des traitements ARN interférant est vérifiée en Western Blot et les cellules sont utilisées 3 jours après transfection, quand la déplétion des protéines ciblées est maximale.

2) Mesure des propriétés viscoélastiques des cellules tumorales

Les aspirations sont réalisées à l'aide d'une installation sur-mesure dans laquelle le déplacement vertical d'une colonne de PBS permet d'aspirer ou d'expulser les cellules dans un capillaire de verre micro-forgé à 3,5 μm d'ouverture. Le système est équipé avec un objectif et une caméra permettant l'enregistrement de vidéos des aspirations de cellules réalisées. Les enregistrements sont traités sur Image J afin de visualiser les courbes représentant l'entrée de cellule aspirée dans le capillaire en fonction du temps et d'en extraire les coordonnées. Les coordonnées sont ensuite importées dans IGOR Pro pour faire de l'ajustement de courbe et extraire les coefficients rhéologiques des cellules aspirées.

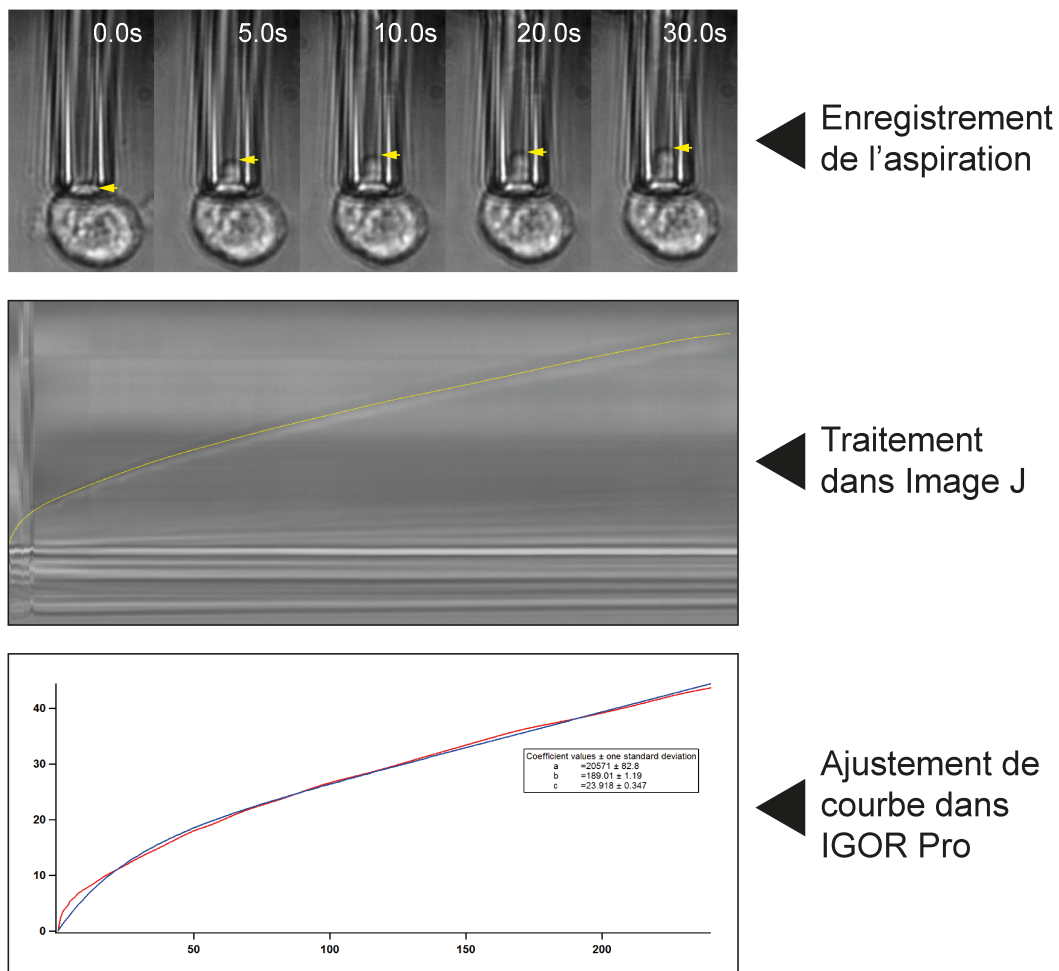


Figure 23 : Déroulé de l'expérience d'aspiration par micropipette. Les films des aspirations sont enregistrés à 5 images/seconde. Le traitement dans FIJI fait intervenir les fonctions « Crop », « Rotate », « Orthogonal views » puis la courbe est tracée à l'aide de l'outil de sélection. Les fonctions « Fit spline », « Interpolate » et « Properties > List coordinates » sont ensuite appliquées pour extraire les coordonnées des courbes, qui peuvent alors être ouvertes sur Igor PRO pour l'ajustement de courbe.

Nous adaptons un modèle rhéologique d'aspiration par micropipette de sphères viscoélastiques précédemment décrit pour nos ajustements de courbe (Guevorkian et al., 2010).

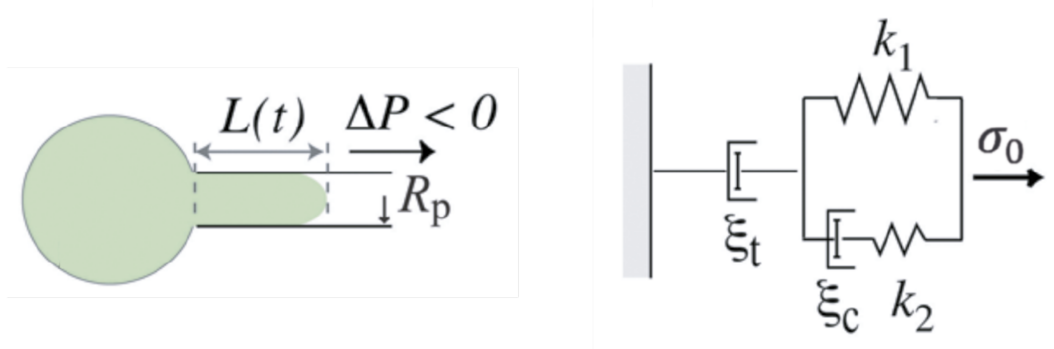


Figure 24 : Modèle rhéologique utilisé pour l'ajustement de courbe. Avec $L(t)$ la longueur de cellule aspirée dans le capillaire, R_p le rayon du capillaire, ΔP la pression négative appliquée pour aspirer la cellule, k_1 la constante de ressort associée à l'élasticité de la cellule aspirée, k_2 la composante associée à l'augmentation brute de $L(t)$ lors de l'initiation de l'aspiration, ξ_c le coefficient de friction associé à la déformation élastique, ξ_t la dissipation visqueuse de la longueur de cellule aspirée et σ_0 la contrainte appliquée à la surface de la cellule prise dans l'aire du capillaire pour déclencher l'aspiration de la cellule, correspondant environ à $2R_p\Delta P/\pi$, avec $\Delta P = \rho g \Delta h$ où ρ est la masse volumique du PBS (1000 g/L), g l'accélération de la pesanteur terrestre et Δh la hauteur du déplacement de la colonne de PBS appliqué pour l'aspiration (0,105 m) (Adapté de Guevorkian et al., *Physical Review Letters*, 2010).

La longueur de cellule aspirée dans le capillaire $L(t)$ se définit ainsi par :

$$L(t) = \frac{\sigma_0}{k_1} \left(1 - \frac{k_2}{k_1 + k_2} e^{(-t/\tau_c)} \right) + \frac{\sigma_0}{\xi_t} t$$

Où le premier terme faisant apparaître le temps de relaxation τ_c caractérise le régime élastique de la cellule, avec $\tau_c = [\xi_c(k_1+k_2)]/(k_1k_2)$, tandis que le deuxième terme caractérise son régime visqueux. k_1 étant directement proportionnel au module élastique E par la relation $k_1 = \pi R_p E$, il est utilisé pour rapporter de l'élasticité de la cellule aspirée tandis que ξ_t est utilisé pour rapporter de sa viscosité.

III) RÉSULTATS

Cell Viscoelasticity Orchestrates Intravascular and Early Steps of Metastasis

Valentin Gensbittel¹⁻⁴, Gautier Follain^{1-4§}, Klemens Uhlmann⁵, Louis Bochler¹⁻⁴, Olivier Lefèbvre¹⁻⁴, Annabel Larnicol¹⁻⁴, Sébastien Harlepp^{1-4\$}, Ruchi Goswami⁶, Salvatore Girardo⁶, Martin Kräter⁶, Daniel Balzani⁵, Jochen Guck^{6#}, Naël Osmani^{1-4#}, Jacky G. Goetz^{1-4#}

1. Tumor Biomechanics, INSERM UMR_S1109, Strasbourg, France.
 2. Université de Strasbourg, Strasbourg, France.
 3. Fédération de Médecine Translationnelle de Strasbourg (FMTS), Strasbourg, France.
 4. Équipe Labellisée Ligue Contre le Cancer
 5. Chair of Continuum Mechanics, Ruhr-Universität Bochum, Universitätsstraße 150, 44801, Bochum, Germany.
 6. Max Planck Institute for the Science of Light & Max-Planck-Zentrum für Physik und Medizin, Erlangen Germany.
- §. Current address: Turku Bioscience Centre, University of Turku and Åbo Akademi University, FI-20520 Turku, Finland.
- \$. Current address: Nanotranslational laboratory, Institut de Cancérologie Strasbourg Europe, Strasbourg, 67000 France.

Résumé en français

Les métastases apparaissent à la fin de la cascade métastatique, un processus complexe de plusieurs étapes au cours duquel les cellules tumorales sont constamment soumises à des forces biomécaniques. Leurs propriétés mécaniques jouent ainsi probablement un rôle décisif dans leur capacité à faire face à ces forces et à compléter la cascade métastatique. La contribution des propriétés mécaniques des CTC au cours de la dissémination hématogène reste à ce jour mal documentée. Dans cette étude, nous utilisons le modèle de l'embryon de poisson zèbre pour étudier la contribution des propriétés mécaniques des CTCs pendant les étapes de circulation, d'arrêt et d'extravasation de la cascade métastatique. Nous utilisons des billes élastiques de polyacrylamide comme outil de comparaison pour établir que les cellules tumorales viscoélastiques en appellent à leur viscosité pour s'adapter aux contraintes mécaniques de l'architecture vasculaire. En ajustant et en mesurant les propriétés viscoélastiques de cellules tumorales, nous démontrons que le niveau de viscosité des CTC est un facteur déterminant pour leur entrée et leur arrêt dans les petits vaisseaux contraignants. Nous montrons enfin qu'un profil de viscosité élevé favorise le déclenchement de l'extravasation des cellules tumorales via remodelage endothélial. Ainsi, nous identifions la viscosité des CTCs comme un paramètre biomécanique clé qui détermine les schémas de circulation et d'arrêt des CTC et joue un rôle inattendu dans leur capacité à réaliser l'extravasation.

Introduction

Metastatic development represents the most dangerous aspect of cancer disease (Steeg, 2016). Life-threatening metastases appear at the end of the metastatic cascade, a complex multi-step process that includes a step of dissemination via body fluids that allows tumor cells to reach distant organs (Follain et al., 2020). Biomechanical forces challenge tumor cells throughout the entirety of the metastatic process. Known examples include increasing compressive stress at the primary tumor site (Stylianopoulos et al., 2012) or the hemodynamic and collision forces that often threaten to destroy circulating tumor cells (CTCs) (Regmi et al., 2017 ; Wirtz et al., 2011). As such, the mechanical properties of tumor cells likely represent a critical parameter in their ability to cope with such mechanical forces throughout the metastatic cascade (Matthews et al., 2020 ; Moose et al., 2020).

While it is commonly accepted that mechanical softness of tumor cells scales with their metastatic potential (Guck et al., 2005 ; Swaminathan et al., 2011 ; Alibert et al., 2017), we recently speculated that the contribution of tumor cell deformability might not be so black-and-white after all and could look very different at different stages of the metastatic process (Gensbittel et al., 2021). In particular, the extent to which mechanical properties of CTCs play a role during hematogenous dissemination remains poorly documented. Evidence suggests that CTC speed decreases in constraining vessels, and that vascular branch points represent highly probable arrest sites for CTCs (Kienast et al., 2010). As such, the ability of CTCs to undergo deformation and accommodate to constraining vessels likely plays an important role in the circulation routes that they take and the vascular sites where they arrest. How their deformability comes into play during the extravasation step also remains elusive as different extravasation mechanisms have been described and might have different mechanical requirements for tumor cells.

The zebrafish embryo represents an ideal model that we already successfully used in the past for investigating the contribution of biomechanical clues during these steps of metastasis. In particular, we found that hemodynamic and adhesion forces play joint and critical roles in the arrest, adhesion and extravasation of CTCs (Follain et al., 2018 ; Osmani et al. 2019 ; Follain et al., 2021). We highlighted and characterized endothelial remodeling-driven extravasation, a flow-sensitive process in which arrested

tumor cells are actively extracted from blood vessels by endothelial cells (Follain et al., 2018 ; Follain et al., 2021).

In this follow-up work, we keep taking advantage of this *in vivo* model to broaden our understanding of biomechanics in metastasis by investigating the contribution of mechanical properties of CTCs during the steps of circulation, arrest and extravasation of the metastatic cascade. We use polyacrylamide elastic beads as a comparison tool to establish that viscoelastic tumor cells heavily rely on their viscosity to accommodate to the constraining vasculature in a time-dependent manner. By tuning and measuring viscoelastic properties of tumor cells, we demonstrate that the viscosity level of CTCs is a critical enabler of their entry and arrest in small constraining vessels. Finally, we show that a high viscosity profile favors the triggering of endothelial remodeling-driven extravasation of tumor cells. Altogether, we identify CTC viscosity as a key biomechanical parameter that drives circulation and arrest patterns of CTCs and plays an unexpected part in their ability to perform extravasation and complete the intravascular steps of metastasis.

Mechanical occlusion drives intravascular arrest of circulating objects.

We first sought to demonstrate the importance of mechanical occlusion in the intravascular steps of metastasis, which can be recapitulated in the zebrafish embryo model (Figure S1A).

Our approach involved injecting polyacrylamide elastic beads designed with different diameters and elasticity levels, record the very first circulation and arrest events and quantify the ratios of arrest in 5 subregions that constitute the caudal plexus of the zebrafish embryo (Figure 1A): Dorsal aorta (DA), arterio-venous junction (AVJ), caudal vein (CV), intersegmental vessels (ISVs) and caudal plexus capillaries (CPCs) (Figures 1B, S1B). The parameters of the beads were set to reflect small, large, soft and stiff cells inside of a population of D2A1 tumor cells (Figures 1C, S1C). Recordings of circulating beads were stopped 5 minutes post-injection for quantification of arrest events (Figure 1D). Heatmapping was performed in order to highlight hotspots of arrest of small, large, soft and stiff circulating beads. We found the highest bead arrest densities to be located in the DA at every vascular branch point that connect it to small ISVs, as well as in the AVJ where the DA gets subdivided into the large CV and the small CPCs (Figures 1E, S1D). These patterns are consistent with occlusion-driven arrest, which could be visualized in 3D reconstructions of arrested beads at these vascular shrinkage sites (Figure 1F). Although the hotspots of arrest were the same in the different bead populations tested, the differences in diameter and elasticity of the beads seemingly led to significant swings in their abilities to enter and arrest in certain vascular regions: small beads displayed significantly lower arrest ratios in the AVJ and the CV, and the opposite trend in the ISVs and CPCs compared to large beads (Figure 1G). The same trend, although not quite significant, could be seen when comparing soft to stiff beads (Figure S1D-E). Combining the ISVs and the CPCs in order to quantify the overall ratios of arrest occurring in small vessels allowed us to highlight that both reduced diameter and reduced elasticity favor entry and arrest in small vessels (Figures 1H-I). Interestingly, these results obtained with non-adherent elastic beads closely recapitulate the patterns that could be seen when analyzing the final arrest sites of multiple tumor cell lines that displayed different cell diameters (Figures S1F-H).

Altogether, these results highlight mechanical occlusion as a major driver of intravascular arrest. We identified the major occlusion sites to be located at DA-ISV

connections and in the AVJ in our zebrafish embryo model and found that properties that would allow circulating objects to escape those major occlusion sites, such as reduced diameter or increased deformability, favor entry and arrest in small blood vessels (Figure 1J).

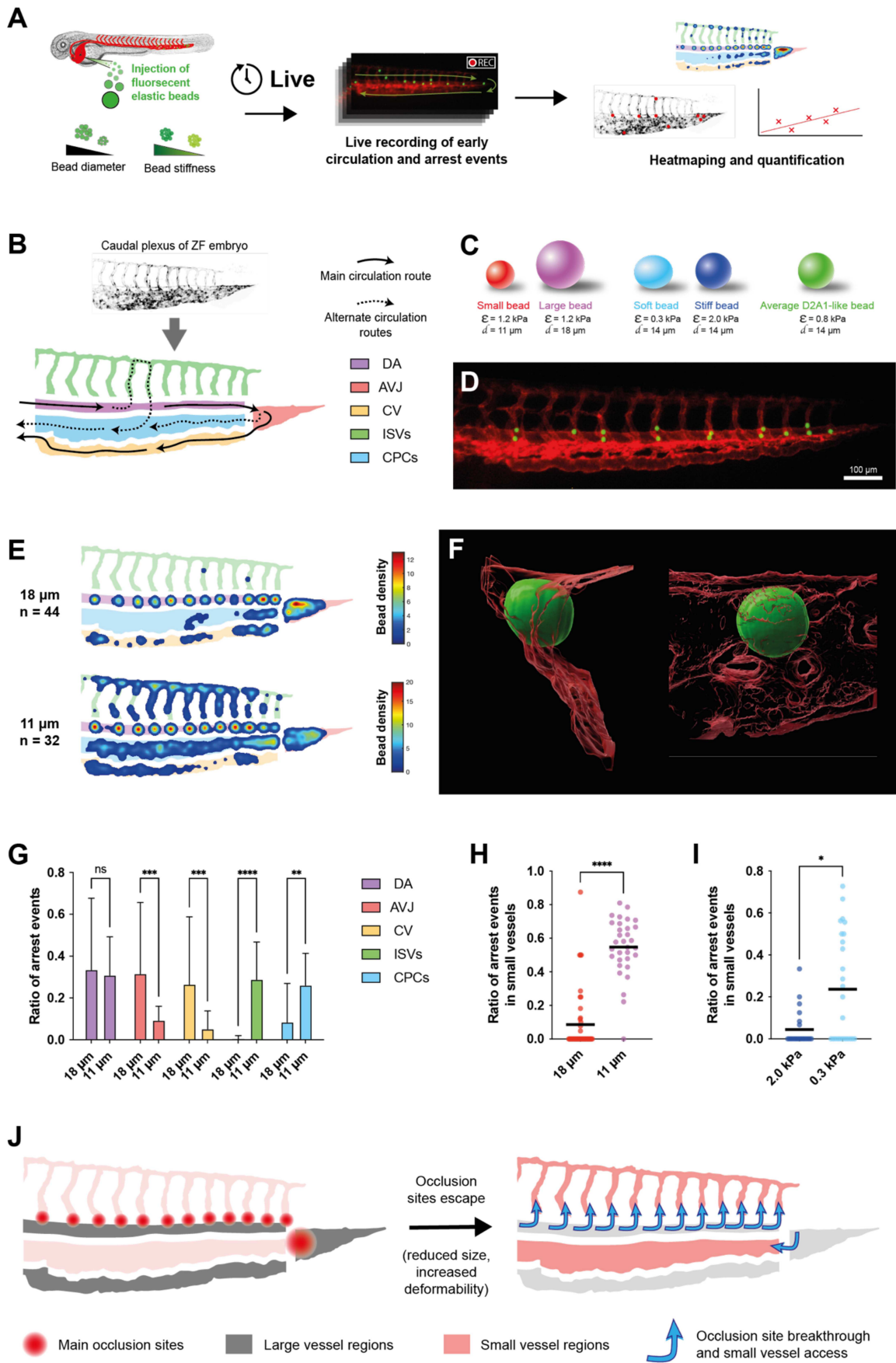


Figure 1: Mechanical occlusion drives intravascular arrest of circulating objects.

- (A) Bead injection workflow for the study of mechanical occlusion patterns in the zebrafish embryo.
- (B) Breakdown of the vascular subregions and the circulation routes in the caudal plexus of the zebrafish embryo.
- (C) Polyacrylamide elastic bead populations and their parameters
- (D) Merged stereomicroscope image of elastic beads (green) in the zebrafish embryo caudal plexus vascular system (red) 5 minutes post-injection.
- (E) Heatmaps displaying hotspots of arrested bead densities at the 5 minutes post-injection time point for large (18 μm) and small (11 μm) beads.
- (F) 3D IMARIS renders of D2A1-like beads (0,8 kPa ; 14 μm) arrested by occlusion at the interface of the DA and an ISV (left) and in the AVJ (right).
- (G) Quantification of the ratios of large (18 μm) and small (11 μm) bead arrest recorded at the 5 minutes post-injection time point in the 5 vascular subregions of the zebrafish embryo's caudal plexus.
- (H) Quantification of the ratios of large (18 μm) and small (11 μm) bead arrest recorded at the 5 minutes post-injection time point in the small vessels (ISVs + CPCs) of the zebrafish embryo's caudal plexus.
- (I) Quantification of the ratios of stiff (2,0 kPa) and soft (0,3 kPa) bead arrest recorded at the 5 minutes post-injection time point in the small vessels (ISVs + CPCs) of the zebrafish embryo's caudal plexus.
- (J) Graphical summary of the contribution of mechanical occlusion in the intravascular arrest of circulating objects in the circulatory system of the zebrafish embryo caudal plexus.

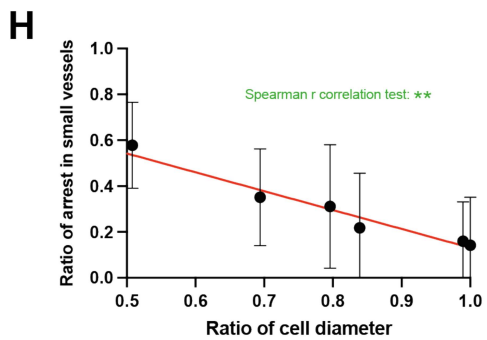
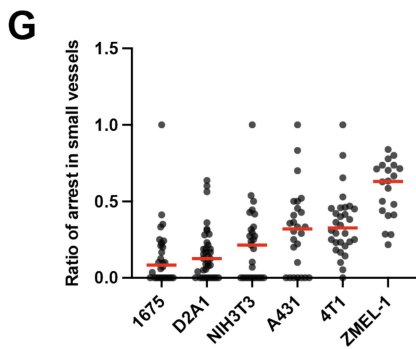
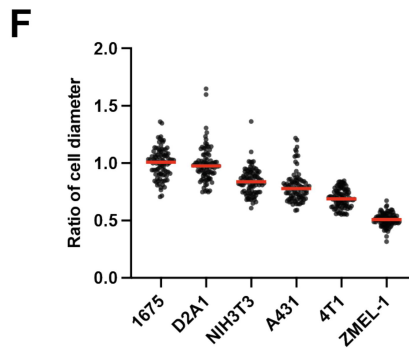
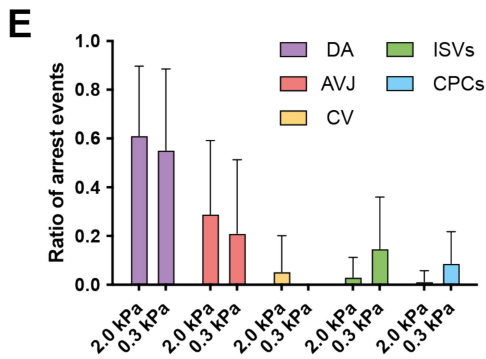
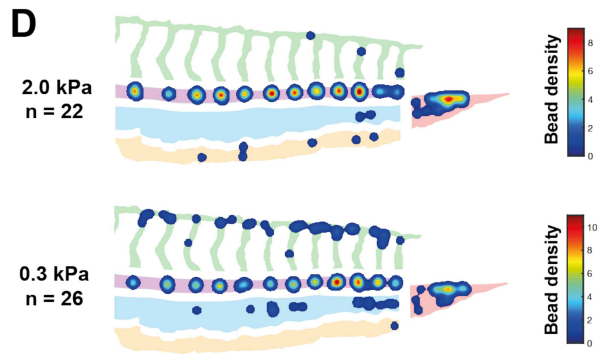
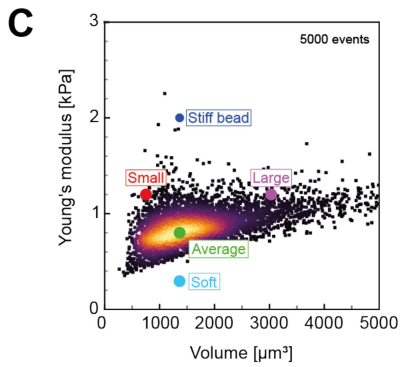
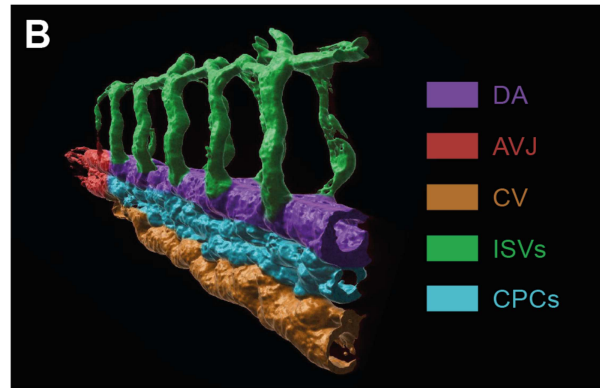
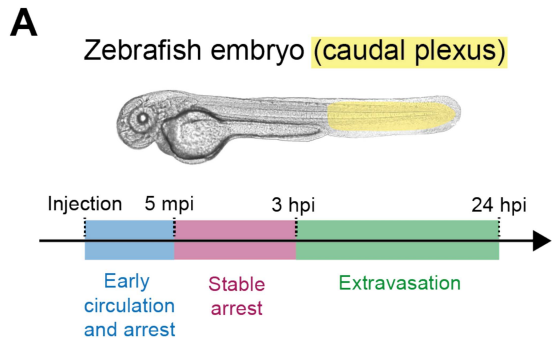


Figure S1 related to Figure 1: Mechanical occlusion drives intravascular arrest of circulating objects.

(A) Time windows for studying circulation, arrest and extravasation following tumor cell injection in the zebrafish embryo.

(B) Color-coded 3D IMARIS render of the caudal plexus of the zebrafish embryo.

(C) Real Time-Deformability Cytometry (RT-DC) plot of D2A1 tumor cells and how injected bead populations compare in size and stiffness.

(D) Heatmaps displaying hotspots of arrested bead densities at the 5 minutes post-injection time point for stiff (2,0 kPa) and soft (0,3 kPa) beads.

(E) Quantification of the ratios of stiff (2,0 kPa) and soft (0,3 kPa) bead arrest recorded at the 5 minutes post-injection time point in the 5 vascular subregions of the zebrafish embryo's caudal plexus.

(F) Ratios of cell diameter of 1675, D2A1, NIH3T3, A431, 4T1 and ZMEL-1 tumor cell lines normalized to the 1675 cell line.

(G) Quantification of the ratios of cell arrest recorded at the 3 hours post-injection time point in the small vessels (ISVs + CPCs) of the zebrafish embryo's caudal plexus.

(H) Correlation of ratio of cell diameter (F) and arrest in small vessels (G).

CTCs tap into their viscosity property to navigate the intravascular environment.

We next wanted to characterize the mechanical efforts made by circulating objects within the intravascular environment. To that end, we injected polyacrylamide elastic beads and D2A1 tumor cells in the zebrafish embryo with the intent to analyze their shapes, and in the case of the beads, use them as force sensors in a computational analysis meant to extract pressure values sustained in the various vascular regions of the zebrafish embryo (Figure 2A). High-resolution confocal imaging was used to image arrested beads (Figure 2B) and reconstruct their geometry in 3D (Figures 2C, S2A). Computational analysis for extracting volumetric mean of pressure values was performed on multiple beads for each vascular subregions of the plexus (Figure S2B). To our surprise, we were unable to highlight any differences in volumetric mean of pressure between beads arrested in the 5 different subregions that constitute the plexus (Figure S2C), between beads arrested in large vs small vessels (Figure 2D) or between beads arrested at main occlusion sites previously identified vs other sites (Figure S2D). Consistently, our shape factor analysis of the bead geometry of these same beads did not highlight any significant differences in bead volume (Figure S2E), in bead elongation (Figure 2E) or in bead flatness (Figure S2F) between beads located in small vs large vessels. These results indicate that over time, it is most likely the vasculature that adapts its geometry to the presence of the beads rather than the beads taping into their elastic deformation potential to cope with the constraining intravascular environment.

D2A1 tumor cells were imaged similarly (Figure 2F) and processed for 3D visualization of their geometry (Figures 2G, S2G). In line with our previous bead circulation and arrest analysis, we found the average cell volume of arrested tumor cells to be significantly smaller for cells arrested in small vessels compared to ones arrested in large vessels (Figure S2H). Both cell elongation (Figure 2H) and cell flatness (Figure S2I) were significantly higher for cells arrested in small vessels, suggesting that contrary to elastic beads, viscoelastic tumor cells do significantly alter their shape to adapt to the constraining vascular architecture (Figures 2I, S2J-K).

In order to analyze the deformation behavior of circulating objects getting past occlusion sites, we went back to our live recordings of 0.3 kPa elastic beads circulating in the zebrafish embryo caudal plexus to track aspect ratio changes as beads manage to enter in small constraining ISVs (Figure 2J). We went on to perform the same

analysis with D2A1 tumor cells (Figure 2K). We found that the aspect ratio of beads stuck at ISV entrances remained very stable over time, while the aspect ratio of tumor cells in the same situation was progressively increasing with time (Figure 2L). Normalizing both the change in aspect ratio and the time spent at ISV entrance allowed to highlight that while tumor cells do indeed progressively change their shape until they reach the deformation state that allows them to get past the occlusion site, beads on the other hand display a sudden burst of deformation in the final instants that they spent at the occlusion site (Figure 2M). Interestingly, despite their supposedly very high elastic compliance resulting from their very low elasticity (0.3 kPa), the sudden burst of deformation of the beads only allowed them to recapitulate a fraction of the shape changes that tumor cells underwent (Figure S2L). As a result of the clearly time-dependent vs more random timing of the process for cells and beads respectively, the average time spent at ISV entrance before completing entry was significantly higher for cells (Figure S2M).

Altogether, these results demonstrate that viscoelastic tumor cells undergo significant shape changes in their intravascular environment, and that they call to their viscosity property during their transient arrests at occlusion sites to overcome these mechanical challenges in a time-dependent manner and further progress in smaller vessels (Figure 2N).

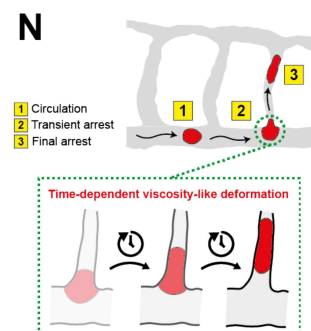
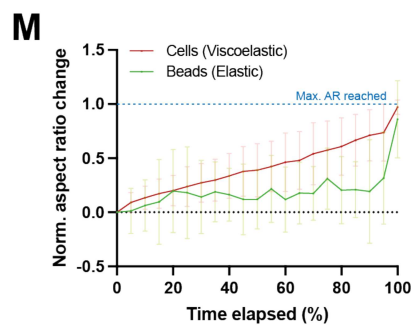
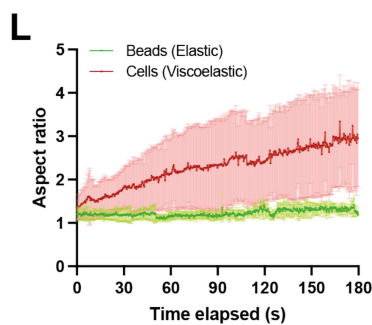
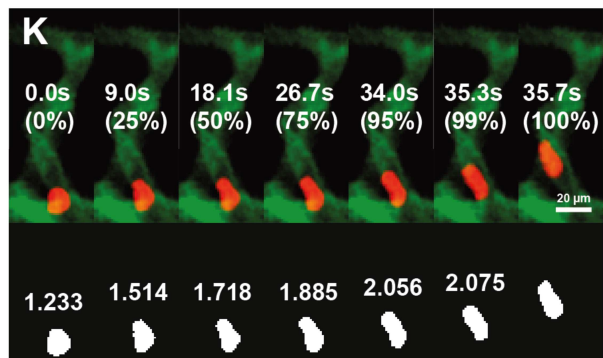
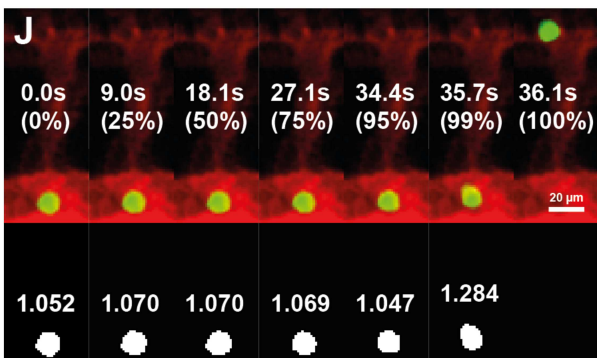
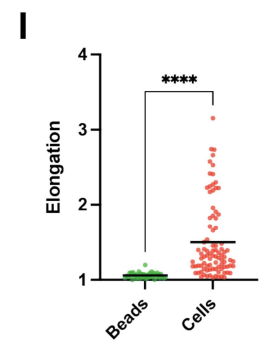
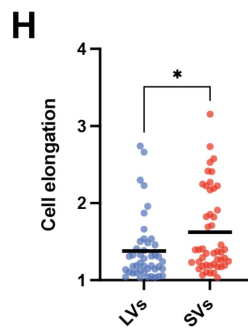
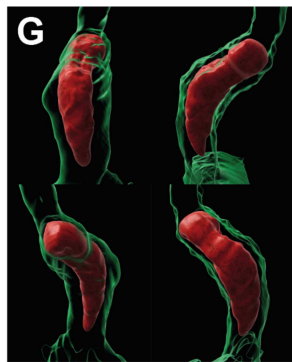
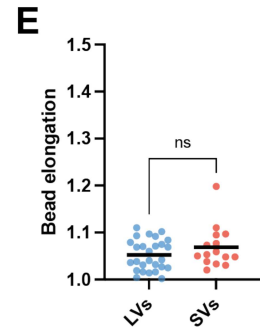
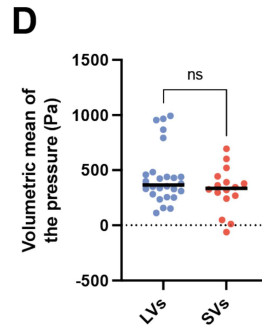
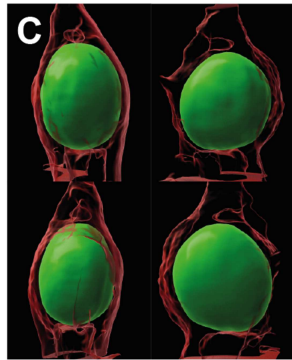
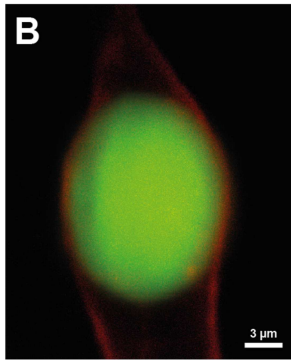
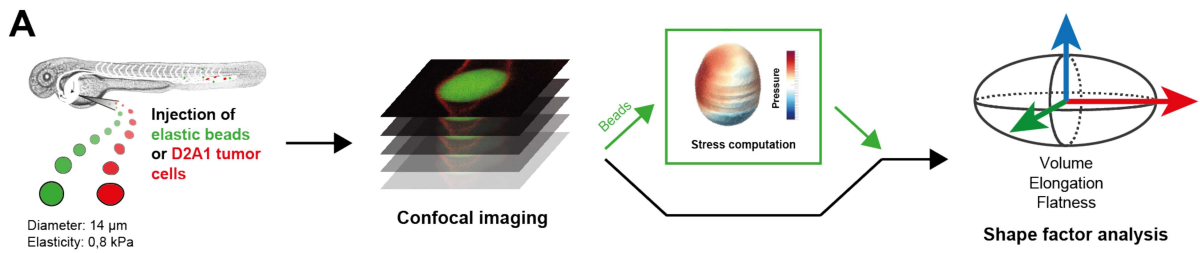


Figure 2: CTCs tap into their viscosity property to navigate the intravascular environment.

(A) Workflow for the analysis of bead deformation and the computation of mechanical stress experienced in the intravascular environment of the zebrafish embryo caudal plexus.

(B) Z-projection of confocal stack of an arrested “D2A1-like” polyacrylamide elastic bead in an ISV.

(C) Multiple views of 3D IMARIS render of (B).

(D) Volumetric mean of pressure sustained by analyzed “D2A1-like” beads in large vs small vessels.

(E) Elongation factor of analyzed “D2A1-like” beads in large vs small vessels.

(F) Z-projection of confocal stack of an arrested D2A1 tumor cell in an ISV.

(G) Multiple views of 3D IMARIS render of (F).

(H) Elongation factor of analyzed D2A1 cells in large vs small vessels.

(I) Elongation factor of “D2A1-like” beads and D2A1 cells, all vascular subregions of the zebrafish embryo caudal plexus considered.

(J) Stereomicroscope time lapse and aspect ratio evolution of a 0,3 kPa polyacrylamide elastic bead stuck at an ISV entrance upon injection in the zebrafish embryo.

(K) Stereomicroscope time lapse and aspect ratio evolution of a D2A1 tumor cell stuck at an ISV entrance upon injection in the zebrafish embryo.

(L) Aspect ratio as a function of time spent at ISV entrance for 0,3 kPa elastic beads and D2A1 tumor cells.

(M) Normalized change of aspect ratio as a function of normalized time spent at ISV entrance for 0,3 kPa elastic beads and D2A1 tumor cells.

(N) Graphical summary of viscosity-dependent deformation of tumor cells during transient arrest at an ISV entrance.

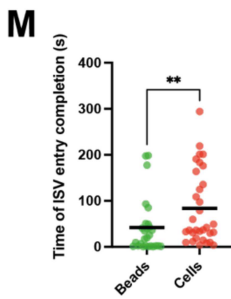
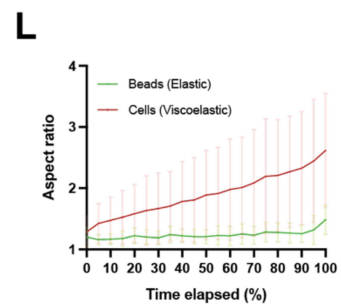
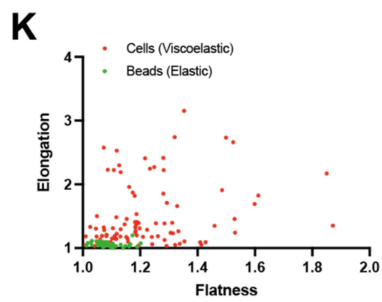
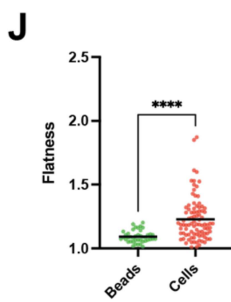
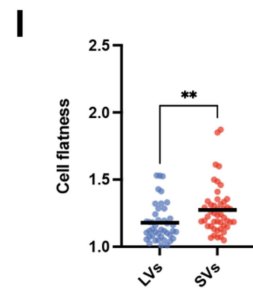
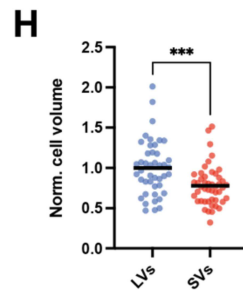
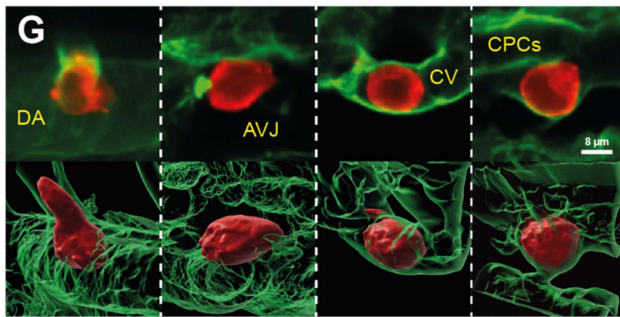
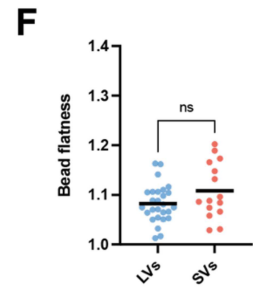
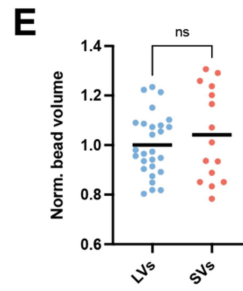
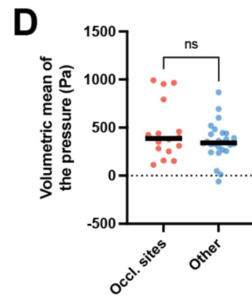
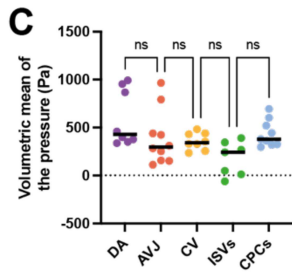
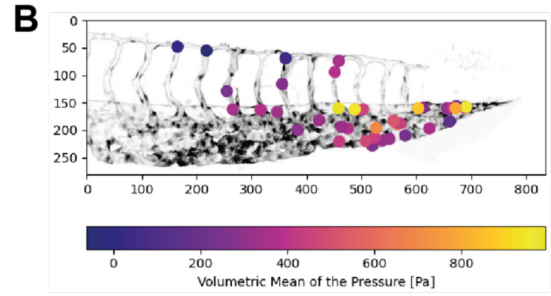
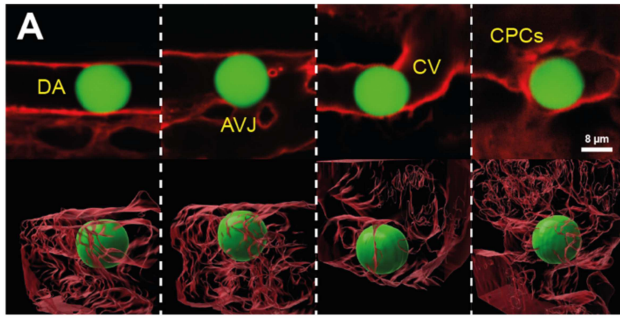


Figure S2 related to Figure 2: CTCs tap into their viscosity property to navigate the intravascular environment.

(A) Z-projections of confocal stacks of arrested “D2A1-like” polyacrylamide elastic beads and corresponding 3D IMARIS renders.

(B) Mapping of all analyzed beads across the caudal plexus of the zebrafish embryo.

(C) Volumetric mean of pressure sustained by analyzed “D2A1-like” beads in the 5 vascular subregions that constitute the zebrafish embryo caudal plexus.

(D) Volumetric mean of pressure sustained by analyzed “D2A1-like” beads at occlusion sites vs other sites.

(E) Normalized volume of analyzed “D2A1-like” beads in large vs small vessels.

(F) Flatness factor of analyzed “D2A1-like” beads in large vs small vessels.

(G) Z-projections of confocal stacks of arrested D2A1 tumor cells and corresponding 3D IMARIS renders.

(H) Normalized volume of arrested D2A1 tumor cells in large vs small vessels.

(I) Flatness factor of arrested D2A1 tumor cells in large vs small vessels.

(J) Flatness factor of “D2A1-like” beads and D2A1 cells, all vascular subregions of the zebrafish embryo caudal plexus considered.

(K) Plot of elongation and flatness factors of all analyzed “D2A1-like” beads and D2A1 tumor cells.

(L) Aspect ratio as a function of normalized time spent at ISV entrance for 0,3 kPa elastic beads and D2A1 tumor cells.

(M) Time spent at ISV entry before completing entry for 0,3 kPa elastic beads and D2A1 tumor cells.

CTC circulation routes and arrest sites are determined by their viscosity levels.

We next wanted to properly quantify the impact of the mechanical properties of circulating tumor cells during their hematogenous dissemination. We used an RNAi silencing strategy on D2A1 tumor cells to knock down expression levels of cytoskeleton-associated genes well-known to be involved in cell mechanics (Figure S3A). We assessed whether RNAi treatments led to changes in cell diameter to be aware of potential biases that could impact entry and arrest in small vessels other than cell deformability (Figure S3B). To probe the mechanical properties of treated cells, we turned to a micropipette aspiration assay as it represents the *in vitro* measuring method that most-closely recapitulates the *in vivo* situations where mechanical properties of CTCs intervene at occlusion sites (Figures 3A, S3C). We found that all RNAi treatments led to significant and very similar decreases of elasticity in tumor cells (Figure 3B). Viscosity was also very significantly reduced in all-but-one RNAi treatments (Figure 3C), leaving us with a control condition where neither elasticity nor viscosity were altered (siCTRL), a condition in which only elasticity was decreased while viscosity remained unaltered (siMYH9) and 3 conditions in which both elasticity and viscosity were significantly decreased (siLMNA, siVIM, siCAV1). These RNAi treatments were next used to generate D2A1 tumor cell populations displaying different mechanical phenotypes to be injected in the zebrafish embryo for *in vivo* analysis and quantification of early circulation and arrest events (Figure 3D). Recordings of cell circulation were stopped 5 minutes post-injection for quantification of arrest events of tumor cells (Figure 3E). Heatmaps were generated to highlight arrested cell densities in small vessels for all RNAi conditions (Figures 3F, S3D). Strikingly, our quantification of ratios of arrest in small vessels showed that low viscosity conditions (siLMNA, siVIM, siCAV1) all displayed significant increases in the CTC's ability to enter and arrest in small vessels, which was not the case for the low elasticity-only condition (siMYH9) as it remained on par with the control (siCTRL) (Figure 3G). We performed a correlation test of viscosity and ratio of arrest in small vessels that further confirmed our impression that viscosity is the key enabler of entry, circulation and arrest in small blood vessels (Figure 3H). In addition, inducing vimentin over-expression in D2A1 cells allowed us to recapitulate these results with opposite and proportional trends (Figures S3E-I) that further increased the significance of the correlation of viscosity and arrest

in small vessels (Figure S3J). We remained unable to highlight a similar correlation of elasticity and entry and arrest in small vessels (Figure S3K).

Altogether, these results provide a quantification and a demonstration of the impactful role played by cellular viscosity on the circulation paths and arrest patterns of CTCs. In line with our previous identification of the involvement of viscosity during passage through occlusion sites, we find that low viscosity-enabled deformability increases chances of CTCs getting past occlusion sites and finding their arrest sites in small vessels (Figure 3J).

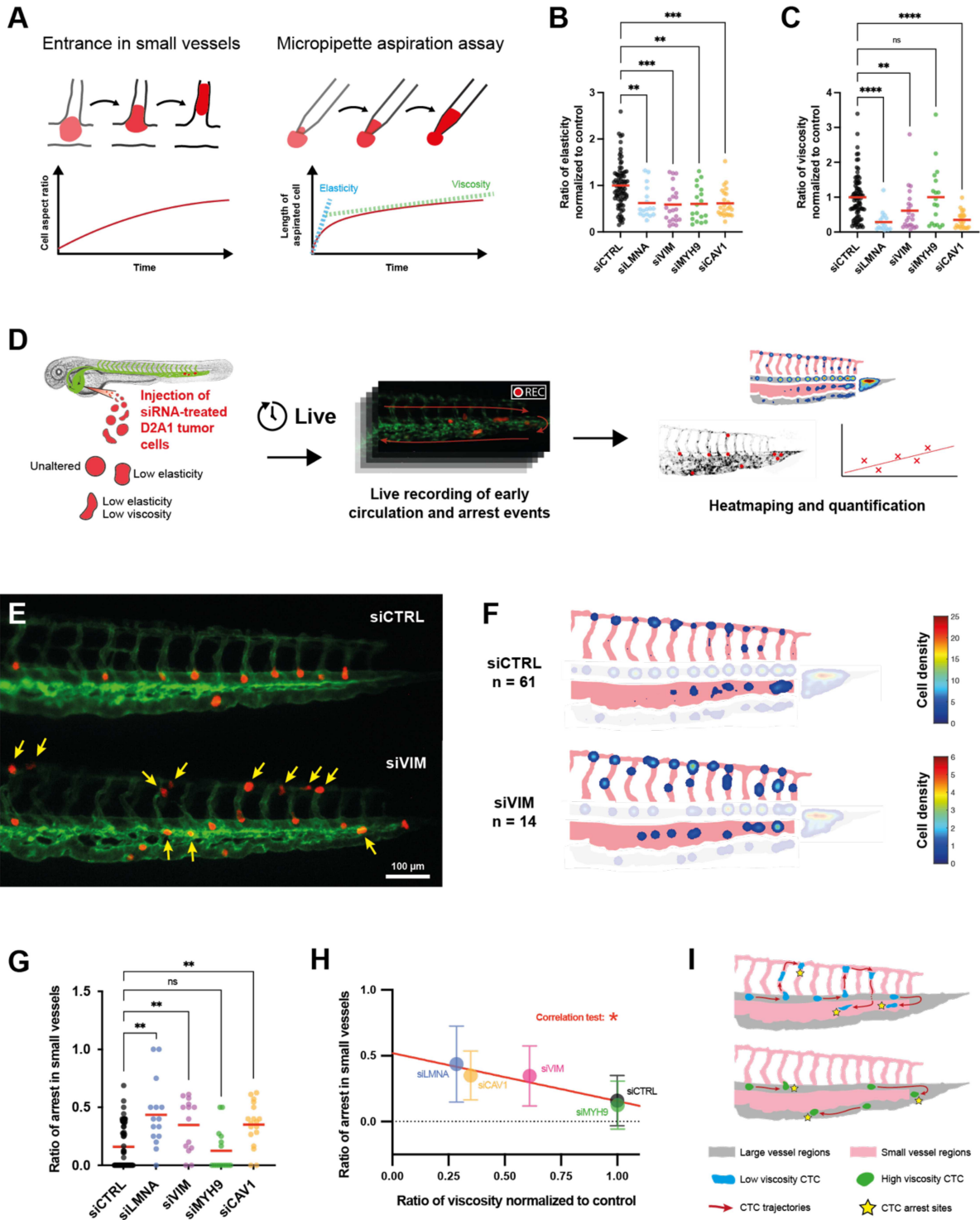


Figure 3: CTC circulation routes and arrest sites are determined by their viscosity levels.

(A) Micropipette aspiration assay as a mechanical property measuring method that recapitulates *in vivo* deformation behavior of tumor cells in the intravascular environment of the zebrafish embryo.

(B) Ratio of elasticity of siRNA-treated D2A1 tumor cells normalized to siCTRL.

(C) Ratio of viscosity of siRNA-treated D2A1 tumor cells normalized to siCTRL.

(D) Mechanically-altered tumor cell injection workflow for analyzing the impact of the mechanical properties of CTCs on their circulation and arrest patterns.

(E) Merged stereomicroscope image of siRNA-treated D2A1 tumor cells (red) in the zebrafish embryo caudal plexus vascular system (green) 5 minutes post-injection. Yellow arrows indicate cells arrested in small vessels (ISVs + CPCs).

(F) Heatmaps displaying hotspots of arrested siRNA-treated D2A1 tumor cells at the 5 minutes post-injection time point. Small vessels (ISVs + CPCs) are highlighted (red).

(G) Quantification of the ratios of arrest of siRNA-treated D2A1 tumor cells at the 5 minutes post-injection time point in the small vessels (ISVs + CPCs) of the zebrafish embryo's caudal plexus.

(H) Correlation of ratio of viscosity (C) and ratio of arrest in small vessels (G) of siRNA-treated D2A1 tumor cells.

(I) Graphical summary of the impact of cellular viscosity on the circulation routes and arrest patterns of circulating tumor cells.

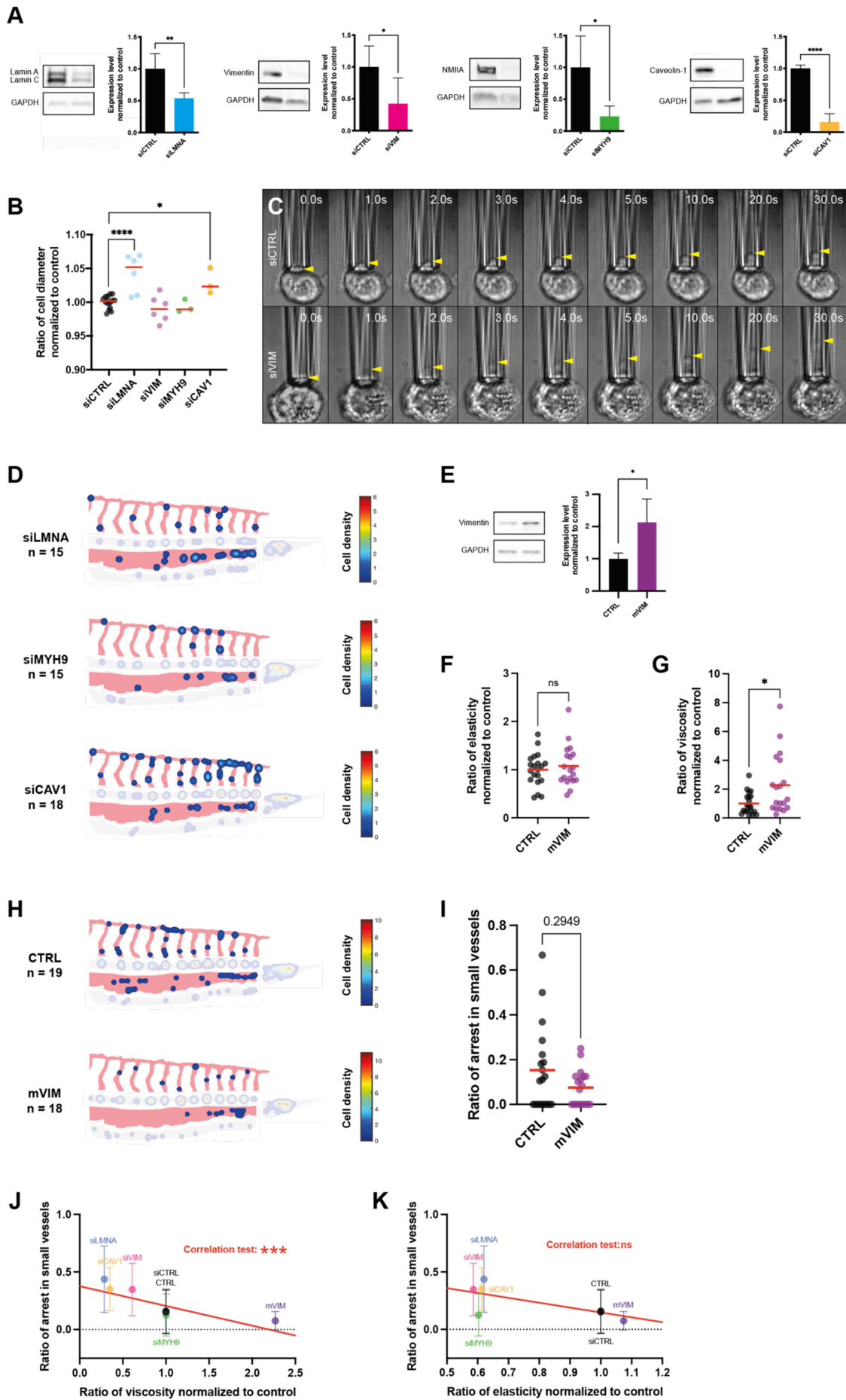


Figure S3 related to Figure 3: CTC circulation routes and arrest sites are determined by their viscosity levels.

- (A) Western Blot quantifications of target-proteins expression levels in D2A1 tumor cells 3 days post-transfection with siRNAs.
- (B) Real Time-Deformability Cytometry (RT-DC) analysis of the diameter of siRNA-treated D2A1 tumor cells.
- (C) Micropipette aspiration assay time lapses of siRNA-treated D2A1 tumor cells.
- (D) Heatmaps displaying hotspots of arrested siRNA-treated D2A1 tumor cells at the 5 minutes post-injection time point. Small vessels (ISVs + CPCs) are highlighted (red).
- (E) Western Blot quantification of vimentin expression level in D2A1 tumor cells transfected with empty (CTRL) or mouse vimentin (mVIM) plasmids.
- (F) Ratio of elasticity of empty or mVIM plasmid-transfected D2A1 tumor cells.
- (G) Ratio of viscosity of empty or mVIM plasmid-transfected D2A1 tumor cells.
- (H) Heatmaps displaying hotspots of arrested empty or mVIM plasmid-transfected D2A1 tumor cells at the 5 minutes post-injection time point. Small vessels (ISVs + CPCs) are highlighted (red).
- (I) Quantification of the ratios of arrest of empty or mVIM plasmid-transfected D2A1 tumor cells at the 5 minutes post-injection time point in the small vessels (ISVs + CPCs) of the zebrafish embryo's caudal plexus.
- (J) Correlation of ratio of viscosity and ratio of arrest in small vessels of mechanically-altered D2A1 tumor cells.
- (K) Correlation of ratio of elasticity and ratio of arrest in small vessels of mechanically-altered D2A1 tumor cells.

Tumor cell viscosity plays an impactful role in the extravasation process.

We next investigated whether mechanical properties of CTCs could also impact the extravasation step that concludes the intravascular stage of metastasis. We kept using our RNAi treatments to alter mechanical properties of D2A1 cells and quantify extravasation 24 hours post-injection (Figure 4A). Confocal imaging was used (Figure 4B) and allowed easy discrimination of intravascular and extravasated tumor cells (Figure 4C). Heatmapping was also performed for intravascular and extravasated cells in every condition (Figure S4A). We quantified the ratios of extravasated cells and found that the RNAi treatments that reduced viscosity also led to significant decreases in ratios of extravasation (Figure 4D).

In an attempt to understand the reason behind this surprising result, we repeated the experiments with a 3 hours post-injection imaging timepoint in order to assess how tumor cells engage with the endothelium when they have been fully arrested for a while and should be starting to engage in the extravasation process (Figure 4E). Confocal imaging revealed that many cells found themselves pocketed by the endothelium at this timepoint, which is characteristic of an endothelial remodeling-driven extravasation process (Figures 4F). Heatmapping was performed to highlight most likely locations of pocketed tumor cells, alongside intravascular and already extravasated cells (Figures 4G, S5A). Quantification of the ratios of pocketed cells showed that low viscosity-conditions displayed significantly reduced ratios of pocketed cells (Figure 4H), which was mirrored by significantly increased ratios of intravascular cells that remained unengaged by the endothelium (Figure S6A). The reduced extravasation trend seen at the 24 hours post-injection timepoint barely started to show at the 3 hours post-injection timepoint as very few cells managed to complete extravasation at this timepoint (Figure S6B). While pocketing events could be seen in all vascular subregions of the caudal plexus (Figures 4I, S6C), completed extravasation events were more sparsely seen and often occurred at the ISVs (Figure 4J) or towards the CV/CPCs region, where it was often impossible to determine precisely from which subregion the extravasation arose as extravasated cells often appeared squished exactly between the large CV and the small CPCs (Figure S6D).

In order to identify whether some vascular subregions of the plexus favor fast extravasation of tumor cells, we quantified the ratios of intravascular, pocketed and extravasated cells in 4 vascular subregions (4 instead of 5 due to the merging of the

CV and the CPCs to which extravasation events cannot assuredly be attributed) within the control condition. We found that the ISVs and the merged CV and CPCs displayed significantly higher ratios of fast extravasation events, with a quarter of tumor cells already extravasated at the early 3 hours post-injection timepoint in these regions compared to 8% in the AVJ and virtually no extravasated cells at all in the DA (< 1%) (Figure 4K). Ratios of pocketed cells were very similar in the AVJ, ISVs and CV/CPCs (40-43%) and much higher than in the DA (12%) (Figure S6E). All-in-all, this analysis highlights the ISVs and the combined CV and CPCs as fast extravasation regions that happen to heavily overlap with the small vessel regions (ISVs and CPCs) previously found to be more easily accessible to low viscosity tumor cells.

In light of the previously discovered involvement of viscosity in the triggering of the endothelial remodeling-driven extravasation mechanism, we brought back our shape factor analysis in order to verify if shape changes could be seen in tumor cells undergoing this process (Figure S6F). We found no differences in volume between intravascular, pocketed and extravasated cells (Figure S6G). Both the elongation (Figure S6H) and the flatness (Figure S6I) factors were similar between unengaged intravascular cells and pocketed cells, and only increased in cells that had fully completed extravasation, likely due to post-extravasation cell spreading. This result points toward this endothelial remodeling-driven process not requiring of the tumor cells that they change their shape, which is compatible with the high viscosity- / low deformability-profile that we found to favor the triggering of this extravasation mechanism.

Altogether, our results demonstrate that tumor cell viscosity plays an impactful role in the extravasation step of metastasis. We found that fast extravasation was more likely to occur in vascular regions that we previously found to be more easily accessible to low-viscosity tumor cells, suggesting that the effect of CTC viscosity during early circulation could have a lasting and indirect impact on extravasation in the zebrafish embryo setting. However, this indirect beneficial effect of low viscosity is not sufficient to compensate the direct and detrimental effect on the triggering of the endothelial remodeling-driven extravasation process that results from lower viscosity levels, with low-viscosity tumor cell populations displaying reduced extravasation completion at later timepoints (Figure 4L).

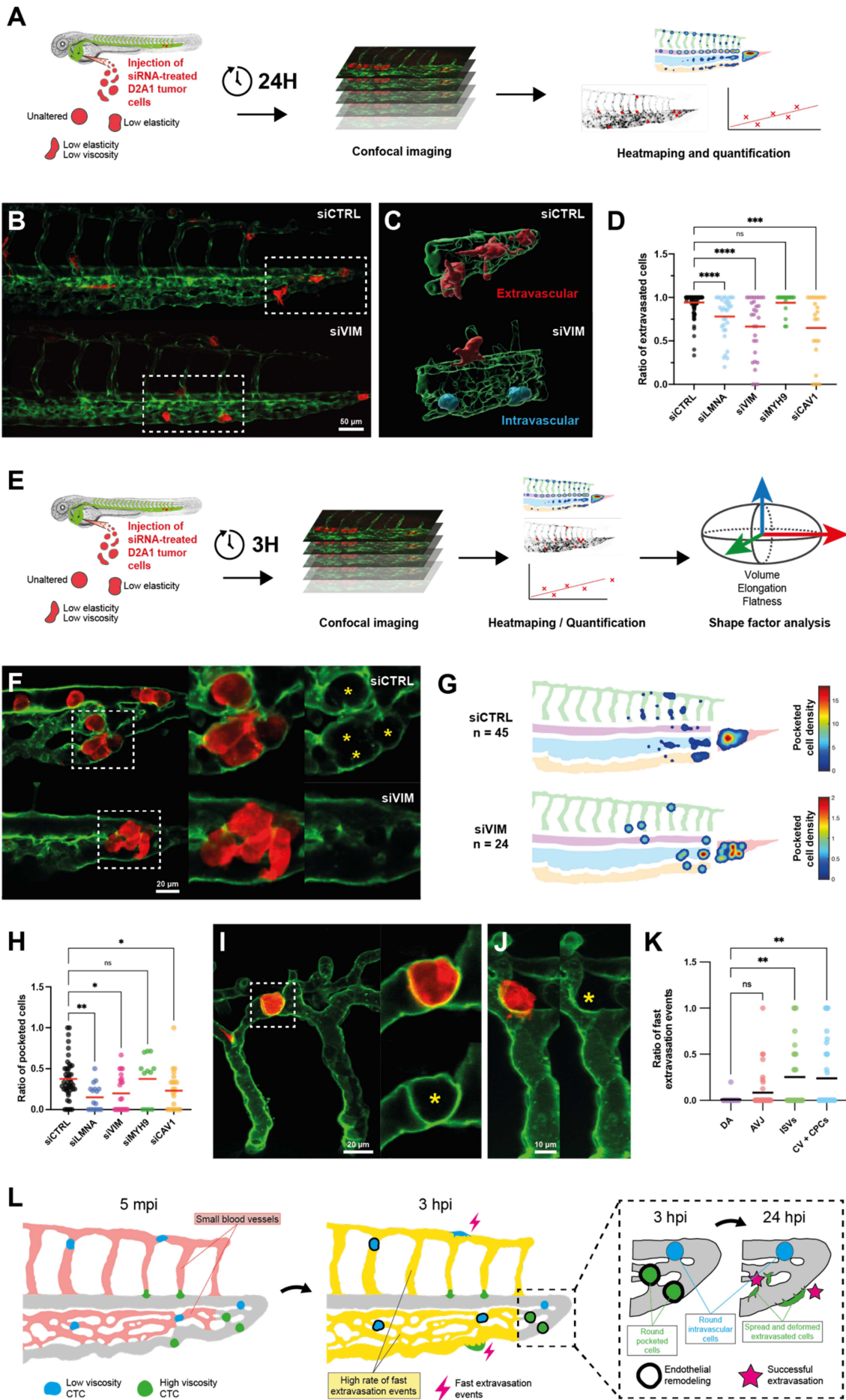


Figure 4: Tumor cell viscosity plays an impactful role in the extravasation process.

- (A) Mechanically-altered tumor cell injection workflow for quantifying the impact of the mechanical properties of CTCs on metastatic extravasation completion.
- (B) Z-projections of confocal stacks of siRNA-treated D2A1 tumor cells in the caudal plexus of the zebrafish embryo at the 24 hours post-injection time point.
- (C) 3D IMARIS renders and color-coding of extravasated (red) and intravascular (blue) tumor cells in ROIs highlighted in (B).
- (D) Quantification of ratios of extravasated siRNA-treated D2A1 tumor cells in the zebrafish embryo caudal plexus at the 24 hours post-injection time point.
- (E) Mechanically-altered tumor cell injection workflow for analyzing the impact of the mechanical properties of CTCs in metastatic extravasation initiation.
- (F) Z-projections of confocal stacks of siRNA-treated D2A1 tumor cells in the caudal plexus of the zebrafish embryo at the 3 hours post-injection time point. Yellow stars indicate endothelial pockets that formed around tumor cells in highlighted ROIs.
- (G) Heatmaps displaying hotspots of pocketing events of siRNA-transfected D2A1 tumor cells at the 3 hours post-injection time point.
- (H) Quantification of ratios of pocketed siRNA-treated D2A1 tumor cells in the zebrafish embryo caudal plexus at the 3 hours post-injection time point.
- (I) Z-projection of confocal stack of a pocketed D2A1 tumor cell in the ISV vascular subregion at the 3 hours post-injection time point. Yellow star indicates the endothelial pocket that formed around the tumor cell in the highlighted ROI.
- (J) Z-projection of confocal stack of an extravasated D2A1 tumor cell in the ISV vascular subregion at the 3 hours post-injection time point. Yellow star indicates the extravascular location of the tumor cell.
- (K) Quantification of ratios of extravasated siCTRL-treated D2A1 tumor cells in the vascular subregions of the zebrafish embryo caudal plexus at the 3 hours post-injection time point.
- (L) Graphical summary of the direct and indirect impacts of cellular viscosity on the extravasation process tumor cells.

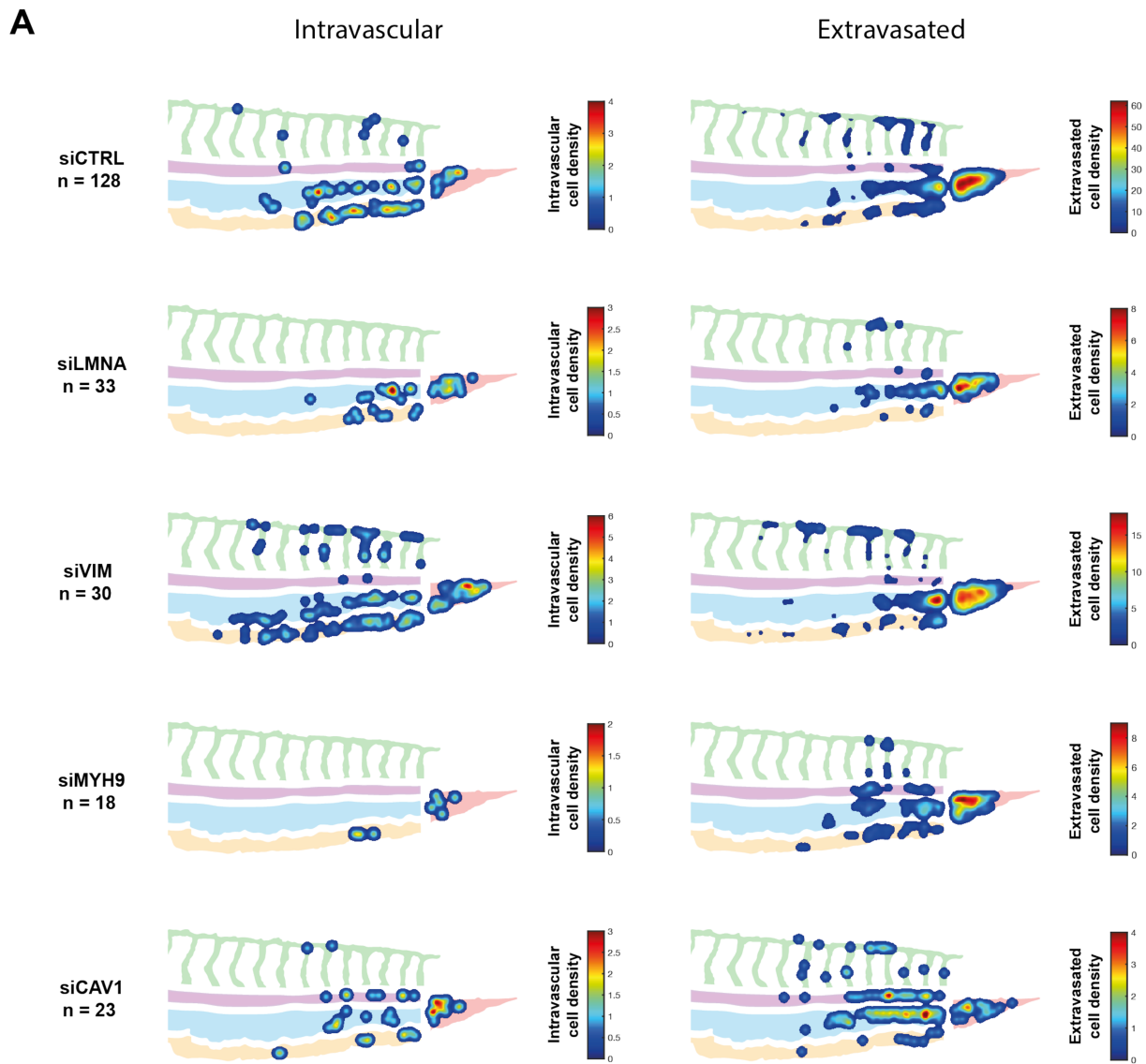


Figure S4 related to Figure 4: Tumor cell viscosity plays an impactful role in the extravasation process.

(A) Heatmaps displaying hotspots of intravascular and extravasated siRNA-transfected D2A1 tumor cells at the 24 hours post-injection time point.

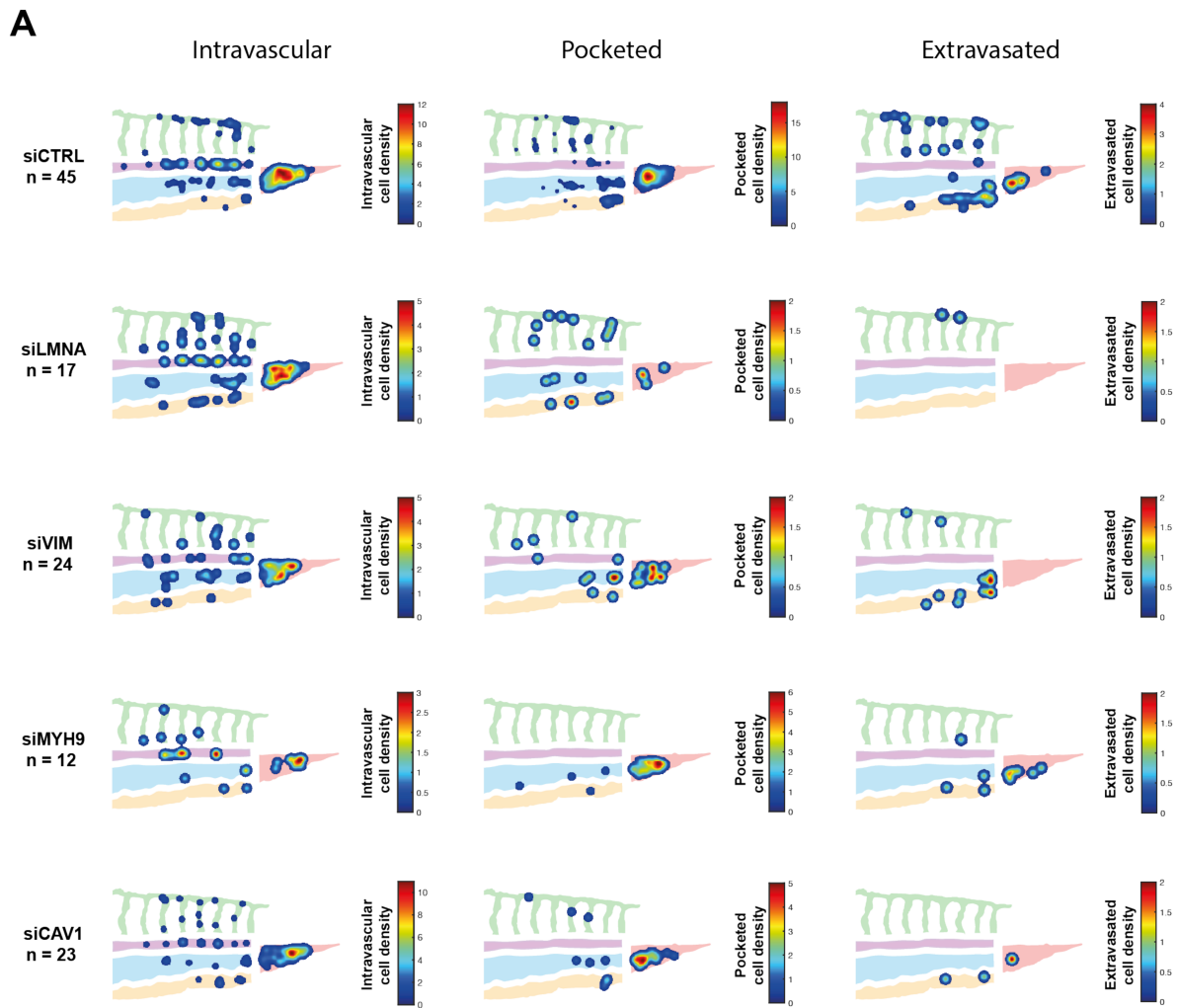


Figure S5 related to Figure 4: Tumor cell viscosity plays an impactful role in the extravasation process.

(A) Heatmaps displaying hotspots of intravascular, pocketed and extravasated siRNA-transfected D2A1 tumor cells at the 3 hours post-injection time point.

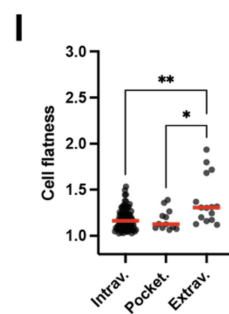
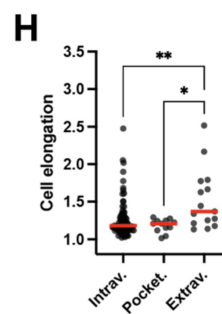
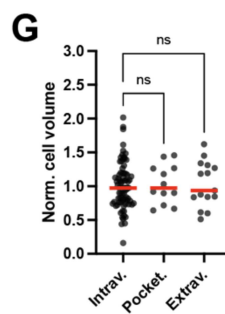
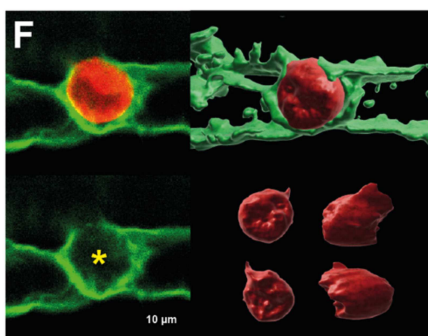
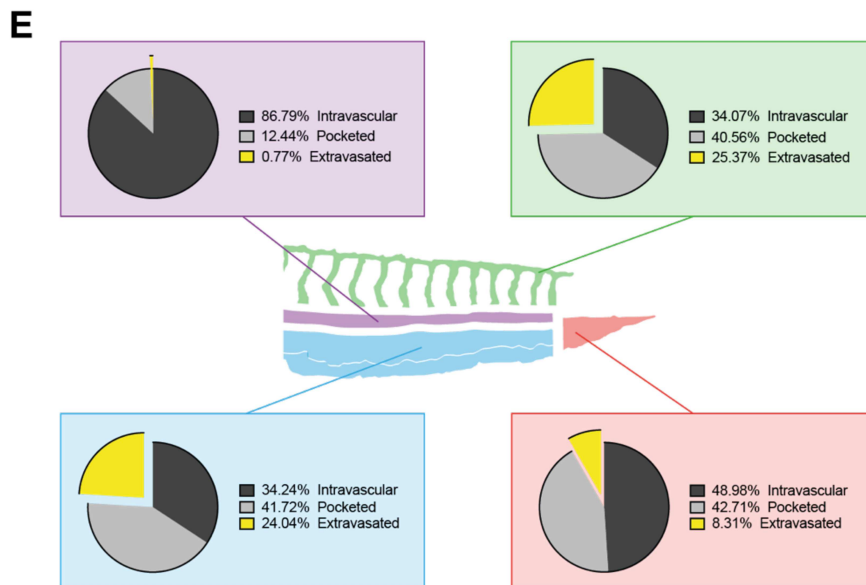
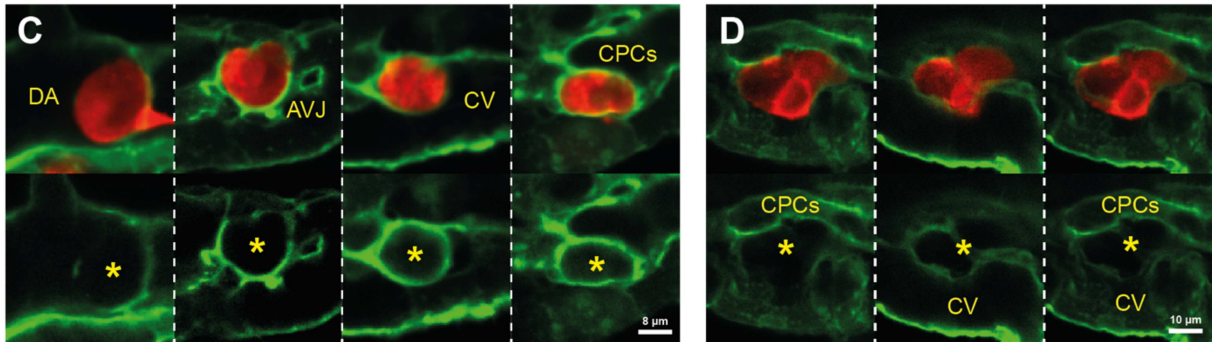
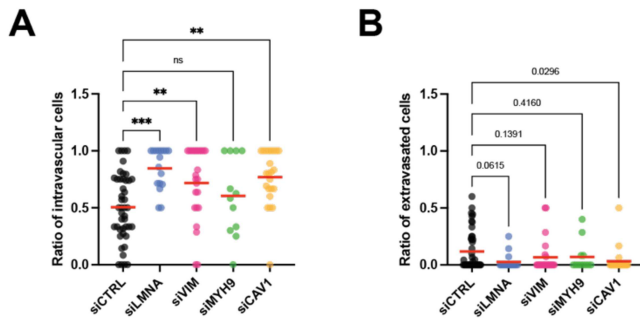


Figure S6 related to figure 4: Tumor cell viscosity plays an impactful role in the extravasation process.

- (A) Quantification of ratios of intravascular siRNA-treated D2A1 tumor cells in the zebrafish embryo caudal plexus at the 3 hours post-injection time point.
- (B) Quantification of ratios of extravasated siRNA-treated D2A1 tumor cells in the zebrafish embryo caudal plexus at the 3 hours post-injection time point.
- (C) Z-projections of confocal stacks of pocketed D2A1 tumor cells in the zebrafish embryo caudal plexus at the 3 hours post-injection time point. Yellow stars indicate the endothelial pockets that formed around the tumor cells.
- (D) Selected confocal z-projections of an extravasated tumor cell cluster. From left to right, z-projections are focused respectively on the CPCs (top of the cluster), between the CPCs and the CV or on the CV (bottom of the cluster). Yellow stars indicate the extravascular location of the cluster between the CPCs and the CV.
- (E) Breakdown of the distribution of intravascular, pocketed and extravasated siCTRL-treated D2A1 tumor cells in 4 vascular subregions of the zebrafish embryo caudal plexus at the 3 hours post-injection time point.
- (F) Confocal z-projections of a pocketed D2A1 tumor cell (left, yellow star indicates the endothelial pocket that formed around the tumor cell) at the 3 hours post-injection time point, and multiple views of corresponding 3D IMARIS render (right).
- (G) Cell volume of intravascular, pocketed and extravasated siCTRL-treated D2A1 tumor cells normalized to intravascular cells at the 3 hours post-injection time point.
- (H) Elongation factor of intravascular, pocketed and extravasated siCTRL-treated D2A1 tumor cells at the 3 hours post-injection time point.
- (I) Flatness factor of intravascular, pocketed and extravasated siCTRL-treated D2A1 tumor cells at the 3 hours post-injection time point.

Discussion

In this work, we combine polyacrylamide elastic beads as a tool to model CTCs, mechanically altered tumor cell populations and intravital imaging to investigate the contribution of cell mechanics in the steps of circulation, arrest and extravasation of the metastatic cascade.

Tuning the properties (size, stiffness) of elastic beads allowed us to pinpoint occlusion hotspots in the zebrafish embryo caudal plexus. These hotspots of occlusion-driven arrest of non-adherent beads at DA-ISV connections and in the AVJ matched the hotspots of arrest of the D2A1 tumor cell line that we used throughout the entirety of this study, reinforcing that mechanical occlusion is a major contributor to intravascular arrest of CTCs. By analyzing circulation patterns of various elastic bead populations, we identified reduced diameter and increased deformability as properties that favor transit through occlusion sites and grant access to small constraining vessels.

We attempted to link the vessel characteristics to the mechanical forces that they exert on trapped polyacrylamide elastic beads designed to act as force sensors. To our surprise, we found that pressure sustained by beads was similar in all vascular subregions of the zebrafish embryo caudal plexus, irrespective of vessel diameter or whether the sites constituted hotspots of occlusion. We attribute this result to the fact that beads were engineered to mimic D2A1 tumor cells as closely as possible, with a Young modulus of 0,8 kPa. This stiffness level turned out to be too high for the intended initial purpose of the experiment as the imaging clearly revealed that it was the vascular architecture that adapted its configuration to the presence of beads at constraining sites, rather than the beads getting deformed by the constraining vessels (Figure 2B-C). Another group recently performed very similar experiments in the lung vasculature of mice using softer beads (0,5 kPa) and was able to link the pressure sustained by beads to the diameter of the vessels in which they were trapped (Zhang et al., 2023). While we remained unable to draw a link between vessel geometry and exerted mechanical forces, a crucial conclusion still arose from our experiments: The elasticity level alone of D2A1 tumor cells (0,8 kPa) is, in theory, sufficiently high for them to resist mechanical pressure within the intravascular environment and induce deformation of vessels around them instead of undergoing deformation themselves, as implied by the behavior of our D2A1-mimicking beads. However, our 3D shape factor analysis revealed arrested D2A1 tumor cells to display significantly more deformation compared

to arrested elastic beads within the intravascular environment. Two parameters could explain this observation: 1) Tumor cells could at some point actively adapt their shape by engaging into migratory behavior and in doing so, release the pressure that their presence would exert on the vasculature and 2) Their viscosity, which is the property that makes them fundamentally different from polyacrylamide elastic beads from a mechanics standpoint, could rapidly take over after elastic behavior and cause them to passively deform to extensive levels when faced with a constraining intravascular environment.

Our confocal imaging pipeline did obviously not offer sufficient time resolution to reach a decisive conclusion on the matter. Turning back to our stereomicroscope video recording pipeline allowed us to dissect the deformation behavior of very soft (0,3 kPa) elastic beads and viscoelastic D2A1 tumor cells in a highly stereotyped manner at the numerous DA-ISV connections found within the caudal plexus of the zebrafish embryo. Our analysis positively identified viscosity as a key property for CTC entry in small constraining vessels as cell deformation during the process of entry was significantly larger and clearly time-dependent compared to that of elastic beads.

Given our observation that viscosity seemed key in the process of tumor cell entry in small vessels and our earlier quantification that highlighted lower elasticity as an enabler of bead entry in such small vessels, we sought to find a way to reliably generate D2A1 tumor cell populations with a variety of mechanical profiles in order to properly dissect the contribution of cell mechanics in early circulation and arrest patterns of CTCs.

Using an empirical approach, we targeted various genes known to be involved in cell mechanics and tested the consequences of their depletion with a micropipette aspiration assay. Knocking-down the nuclear envelope intermediate filament protein lamin A/C (LMNA) resulted in decreased elasticity and viscosity in the cells, which was not surprising given its well-described contribution to whole-cell mechanics via LINC-complexes ([Vahabikashi et al., 2022](#)). Targeting vimentin (VIM) intermediate filaments resulted in the same mechanical phenotype of decreased elasticity and viscosity. This was expected given that vimentin intermediate filaments have long been known to act as security belts protecting cells from large deformations ([Janmey et al., 1991](#)). Targeting caveolin-1 (CAV1) offered yet another alternative for obtaining tumor cells displaying decreases in both elasticity and viscosity. While the distinct mechanisms that allow the CAV1 gene to operate at the level of whole-cell mechanics remain

elusive, it was recently identified as a key cell mechanics regulator commonly at play in various cancer cell types (Urbanska et al., 2023), supporting our results. Opportunely, targeting non-muscle myosin IIA (MYH9) offered some variety in mechanical phenotypes at our disposal as it only decreased elasticity while viscosity remained unaltered. This result is in line with the known role of MYH9 as a regulator of the contractile tension of the actomyosin cortex beneath the plasma membrane (Chugh and Paluch, 2018).

Analysis of the early circulation and arrest patterns of these mechanically altered tumor cell populations highlighted a clear correlation between viscosity and arrest in small constraining vessels, which was consistent with our earlier observation that viscosity comes into play during the process of CTC entry in small vessels at occlusion sites. While the contribution of viscosity was clearly demonstrated, we remained unable to show a similar contribution of elasticity when experimenting with these tumor cell populations. However, given the fact that we previously found low elasticity to facilitate elastic bead entry in small vessels, and the fact that our siRNA treatments all led to very similar elasticity drops, resulting in a very thin range of altered elasticity values tested, we cannot fully exclude that elasticity also plays a role, to a lesser extent, in the process of tumor cells getting past occlusion sites and entering in small constraining vessels.

Identifying the property that allows CTCs to enter and arrest in the small vessels of the zebrafish embryo caudal plexus during our experiments is relevant because such vessels are closest to mimicking capillary beds at metastatic organs where CTCs have often been found to arrest (Kienast et al., 2010 ; Entenberg et al., 2015 ; Headley et al., 2016). In the zebrafish embryo setting specifically, we found these vessels to be fast extravasation sites where a quarter of arrested tumor cells were already extravasated 3 hours after injection and arrest. There is no doubt that performing extravasation quickly would be beneficial to tumor cells as the intravascular environment and its hemodynamic forces are hostile towards them (Follain et al., 2020 ; Moose et al., 2020).

While this would constitute an indirect beneficial effect of low viscosity for tumor cell extravasation, we also presented data that strongly suggests that overall, low viscosity is detrimental to tumor cells in need of performing extravasation. Indeed, we found a surprising link between tumor cell viscosity and endothelial remodeling-driven extravasation. Our results show low viscosity tumor cells to be less likely to have

engaged in this extravasation process 3 hours after intravascular arrest, which translated into significantly lower proportions of extravasation completions at the 24 hours post-injection time point. How tumor cell viscosity comes into play in endothelial remodeling-driven extravasation is unclear at this stage, but one could hypothesize that this process, which we previously found to be mechanosensitive to hemodynamic forces (Follain et al., 2018 ; Follain et al., 2021), could also be sensitive to the mechanical inconvenience that the presence of an arrested tumor cell represents. Compared to low-viscosity tumor cells, high-viscosity cells would be less compliant and closer to recapitulate what we saw with polyacrylamide elastic beads that forced blood vessels to stretch around them. This would also be an explanation as to why small vessels were faster at extravasating trapped tumor cells. Further strengthening this hypothesis, endothelial remodeling-driven extravasation was also described in the mouse brain vasculature (Karreman et al., 2023), where the endothelium is known to deal with persistent emboli by pocketing and extravasating them (Lam et al., 2010). In the end, it seems likely that some tumor cells are capable of hijacking a mechanism meant to recanalize occluded microvessels, and that the most mechanically inconvenient tumor cells (bigger, stiffer) could be more likely to trigger this mechanism.

Overall, our work highlights viscosity as a major property of circulating tumor cells that dictates their circulation possibilities and their arrest patterns, and that affects their extravasation probabilities in an unexpected manner. Ideally, CTCs would first benefit from displaying low viscosity in order to easily access small capillaries and arrest there, and then switch to a stiffer high-viscosity phenotype that would increase their chances of being actively extravasated by the remodeling endothelium. How the mechanical phenotype of tumor cells affects their fate after extravasation remains an open question that needs to be addressed to complement our results and clarify the bigger picture of the contribution of mechanical adaptation abilities of tumor cells in metastasis.

Materials and methods

Cell Lines / Cell culture

D2A1 Cells (CVCL_0190). Mouse Mammary Carcinoma (BALB/c female).

Culture conditions: 37°/5% CO₂. DMEM HG with 5% NBCS, 5% FBS, 1% NEAA-MEM, 1% Penstrep. Authentication: Injection in the nipple of mammary gland of BALB/c mice lead to mammary tumor. Cells do not show contamination to mycoplasma.

JIMT-1 BR3 Cells (CVCL_2077). Human Ductal Breast Carcinoma (Female) Highly Metastatic in the Brain.

Culture condition: 37°/5%CO₂. DMEM HG with 10% FBS, 1% Penstrep. Authentication: Intracardiac injection in nude mice (NU/NU) lead to cerebral metastasis. Cells do not show contamination to mycoplasma.

1675 Cells (WM115, CVCL_0040). Human Melanoma (Female).

Culture condition: 37°/5%CO₂. DMEM HG with 10% FBS, 1% Penstrep. Cells do not show contamination to mycoplasma.

A431 Cells (CRL_1555). Human Skin Epidermoid Carcinoma (Female).

Culture conditions: 37°/5% CO₂. DMEM HG with 10% FBS, 1% Penstrep. Cells do not show contamination to mycoplasma.

4T1 Cells (CVCL_0125). Mouse Mammary Gland Carcinoma (BALB/c Female).

Culture condition: 37°/5%CO₂. RPMI 1640 with 10% FBS, 1% Penstrep. Authentication: Injection in the nipple of mammary gland of BALB/c mice lead to mammary tumor. Cells do not show contamination to mycoplasma.

ZMEL1 Cells (Zebrafish melanoma).

Culture condition: 28°/5% CO₂. DMEM HG, 10% FBS, 1% Penstrep. Cells do not show contamination to mycoplasma.

Cell line engineering

For in vivo imaging in zebrafish embryos, D2A1 cells were engineered to express a Lifeactin-GFP or a Lifeactin-tdTomato fusion protein. Briefly, the Lifeactin-GFP or Lifeactin-tdTomato DNA fragment was inserted in a pLSFFV-Ires-Puromycin lentiviral vector to generate pLSFFV-LifeActin-GFP-Ires-Puro and pLSFFV-LifeActin-tdTomato-Ires-Puro lentiviral vectors used to transduce D2A1 cells. Vimentin-overexpressing

D2A1 cells were obtained similarly with a mouse vimentin DNA fragment kindly provided by Sandrine Etienne-Manneville. Lentivirus particles production and transduction procedures were performed as described previously (Hyenne et al., 2019).

siRNA transfection

D2A1 stably expressing LifeAct-tdT or LifeAct-GFP were grown as previously described (Shibue et al., 2013), in DMEM with 4.5 g/l glucose (Dutscher) supplemented with 5% FBS, 5% NBCS, 1% NEAA and 1% penicillin-streptomycin (Gibco). siRNAs were transfected into D2A1 cells using Lipofectamine RNAiMAX (Invitrogen) following the manufacturer's instructions. Experiments were performed 72 h post-transfection.

The following siRNA sequences were used:

siCTRL: Dharmacon ON-TARGET plus Non-targeting Pool (D-001810-10-20)

siLMNA: Dharmacon ON-TARGETplus Mouse Lmna (16905) siRNA – SMARTpool (L-040758-00-0010)

siVIM: Dharmacon ON-TARGETplus Mouse Vim (22352) siRNA – SMARTpool (L-061596-01-0010)

siMYH9: Sigma-Aldrich custom-made sequences

GACAAAGGUUCGAGAGAAA[dt][dt] and UUUCUCUCGAACCUUUGUC[dt][dt]

siCAV1: Dharmacon ON-TARGETplus Mouse Cav1 (12389) siRNA – SMARTpool (L-058415-00-0010)

Micropipette aspiration assay

Cells were trypsinized and kept in PBS during MPA experiments. Measurements were performed on a custom-made MPA setup equipped with a camera and connected to a computer. Capillaries used for the aspirations were micro-forged to set their opening at 3,5 μm . A vertical water column displacement of 10,5 cm was used to induce suction of the cells in the capillary. Movies of cell aspirations were recorded at 5 frames per second and cropped, rotated and edited to have the entering of the cell in the capillary start precisely at the first frame of the recordings and progress vertically at an angle of 90°. The “orthogonal view” tool was used to generate the curve representing the cell

entering the capillary in function of time. The segmented line tool was used to manually trace the curves and generate the associated coordinates. Obtained coordinates were opened in IGOR Pro7 (WaveMetrics software). Coordinates values were converted from pixels to microns for the Y wave (entering of the cell in the capillary) and from pixels to seconds for the X wave (time elapsed). Minor adjustments to the coordinates were done to make all curves start at the origin of the graph (the coordinates of the first point of the curves were set at (0;0). Finally, curve-fitting was performed to extract elasticity and viscosity coefficients of aspirated cells using a rheological model for micropipette aspiration of biological viscoelastic droplets described previously (Guevorkian et al., 2010).

Real Time-Deformability Cytometry

Measurements were performed in the lab of prof. Jochen Guck as described previously (Rosendahl et al., 2018)

Zebrafish handling

Tg(fli1a:eGFP) and *Tg(kdrl:Hsa.HRAS-mCherry)* Zebrafish (*Danio rerio*) were crossed to obtain the embryos used in the experiments. Embryos were maintained in Danieau 0.3X medium (17,4 mM NaCl, 0,2 mM KCl, 0,1 mM MgSO₄, 0,2 mM Ca(NO₃)₂) buffered with HEPES 0,15 mM (pH = 7.6), supplemented with 200 µM of 1-Phenyl-2-thiourea (Sigma-Aldrich) to inhibit the melanogenesis, as previously described (Goetz et al., 2014).

Polyacrylamide bead production

GFP-labeled polyacrylamide elastic beads were produced in the lab of prof. Jochen Guck as previously described (Girardo et al., 2018).

Atomic Force Microscopy (AFM) and Real Time-Deformability Cytometry (RT-DC) were used for quality control and sorting of properties of interest:

“Large beads”: diameter = 18 µm, elasticity = 1,2 kPa

“Small beads”: diameter = 11 µm, elasticity = 1,2 kPa

“Stiff beads”: diameter = 14 µm, elasticity = 2,0 kPa

“Soft beads”: diameter = 14 μm , elasticity = 0,3 kPa

“D2A1-mimicking beads”: diameter = 14 μm , elasticity = 0,8 kPa

Beads were stored in PBS at 4°C.

Intravascular injections of beads and tumor cells in the zebrafish embryo

48-hour post-fertilization (hpf) *Tg(Fli1a:eGFP)* of *Tg(Kdrl:Hsa.HRAS-mCherry)* embryos were mounted in 0.8% low melting point agarose pad containing 650 μM of tricain (ethyl-3-aminobenzoate-methanesulfonate) to immobilize the embryos. D2A1 LifeAct-RFP or LifeAct-GFP cells were injected with a Nanoject microinjector 2 (Drummond) and micro-forged glass capillaries (25 to 30 μm inner diameter) filled with mineral oil (Sigma). Cell suspensions were prepared at approximately $40 \cdot 10^6$ cells per ml for loading into the injection capillaries. Injection volume was initially set at 18nL but could be adjusted throughout injection sessions anywhere between 9nL and 27nL. Injections were targeted at the duct of Cuvier of the embryos and were performed under a M205 FA stereomicroscope (Leica), as previously described (Stoletov et al., 2010). The same protocol was used when injecting 1675, NIH3T3, A431, 4T1 and ZMEL1 cells. Similarly, injections of fluorescent polyacrylamide elastic beads were performed with similar concentrations of beads.

Live recording of early circulation events in the zebrafish embryo

The earliest bead/cell circulation and arrest events following injection in the zebrafish embryo were captured with the M205 FA stereomicroscope (Leica) under which the injections were performed. The stereomicroscope was connected to a laptop equipped with Leica's LAS AF software, allowing image/video acquisition. Exposure time was set to 200 ms in the appropriate channel for capturing the fluorescent signal of the beads or tumor cells, which resulted in a rate of acquisition of one frame every 0,43 s. Recordings of 5 minutes started right after embryo injection was performed. Once recordings of bead/cell circulation were complete, a single image was acquired in the appropriate channel for capturing the fluorescent signal of the embryo's endothelium.

Confocal imaging of injected zebrafish embryos

Confocal imaging was alternatively performed with an upright Leica TCS SP5 (20X objective, 0.75 NA) or an inverted Olympus Spinning Disk (30X objective, 0.8 NA). The caudal plexus region (around 50 μ m width) was imaged with a z-step of 2 μ m in experiments aiming at locating and/or assessing the extravasation status of arrested tumor cells. The z-step was set at 0.25 μ m in experiments aiming at performing 3D reconstruction and shape/volume analysis of arrested beads or cells.

Image processing and analysis

All image treatments were performed in ImageJ software (<https://imagej.nih.gov/ij/index.html>).

For early circulation and arrest of beads and CTCs, the stereomicroscope still images of the embryos' endothelium were duplicated and stacked to match the frame numbers of their corresponding video recordings of bead / CTC signal. Both channels were merged to visualize bead / CTC circulation and arrest in the blood vessels. Arrest events were manually counted and reported on a stereotyped reference map of the caudal plexus for heatmapping (See "heatmapping" section).

For longitudinal tracking of shape changes of beads / CTCs at ISV entrances, events of bead / CTC arrival at ISV entrance followed by successful entry were cropped and isolated from merged stereomicroscope recordings of bead / CTC circulation and arrest. Thresholding was used to generate binary mask stacks of bead / CTC shape in which aspect ratios were measured.

For quantification of intravascular, pocketed and extravasated cells at 3- or 24-hours post-injection time points, confocal z-stacks were carefully scrolled through to evaluate the extravasation status of arrested cells. Events were manually counted and reported on a stereotyped reference map of the caudal plexus for heatmapping.

For analysis of bead / cell shape factors, z-steps of confocal stacks were first adjusted to account for spherical aberrations using a plugin previously described (Diel et al., 2020), allowing faithful 3D reconstruction of beads / cells. Gaussian blur, thresholding, make binary, and fill holes functions were used to generate clean binary stacks of whole shape of beads / cells. 3D ImageJ Suite plugin (<https://mcib3d.frama.io/3d-suite-imagej/>) was then used to measure 3D ellipsoid shape descriptors of processed stacks.

Bead deformation conversion to mechanical stress

Computational analysis-based cell-scale stress sensing (COMPAX) was performed in the lab of prof. Daniel Balzani as described previously (Träber et al., 2019). Beads used for this purpose went through extensive sorting steps in order to reduce the standard deviation of bead diameter as much as possible (0,15 μm) within the bead population, allowing for more accurate computation based on more accurate assumed non-deformed bead configurations. Simulations were also run multiple times for each bead, with a diameter distribution of assumed non-deformed beads reflecting the actual diameter distribution and standard deviation within the bead population injected and imaged.

Heatmapping

The heatmaps were generated using ImageJ and MATLAB (MathWorks) softwares. Events of interest (arrested / intravascular / pocketed / extravasated cells) were identified in embryos after careful analysis of the stereomicroscope recordings or confocal z-stacks with ImageJ. The positions of these events were manually reported on a reference map of the stereotyped 2.5 days post-fertilization zebrafish embryo caudal plexus vasculature. Then, all the support images representing each embryo for one condition were put together in an image stack using ImageJ. The stack was read layer by layer in MATLAB and the dots representing event locations were automatically detected with the Hough circles function (Yuan-Liang Tang, Department of Information Management, Chaoyang University of Technology, Taichung, Taiwan) (<https://fr.mathworks.com/matlabcentral/fileexchange/22543-detects-multiple-disks--coins--in-an-image-using-hough-transform>) using the Circular Hough Transform based algorithm, giving in output the coordinates of the detected dots. Gaussian spots were then created at these coordinates. The amplitude of each Gaussian spot was equal to 1. The different layers of one condition were added to each other through a sum projection. The gaussian spot amplitudes of all layers were summed to produce the heatmap. The areas of the sum projection where the gaussian spot amplitudes are higher corresponds to high density areas of events. To produce the final heatmap, a custom colormap, inspired by the jet colormap, was applied to the sum projection. The colormap was then added on top of color-coded versions of the reference map initially used to report event locations in order to highlight densities of events in different vascular subregions of the zebrafish embryo caudal plexus.

Western Blot

Protein extractions were performed with homemade RIPA buffer. Protein concentrations of the extracts were first quantified using a Bradford assay, and equal protein quantities were then loaded on 4-20% polyacrylamide gels (Biorad) or 4-20% Tris-Glycine gels (Introvigen) and run under denaturing conditions.

The following primary antibodies were used:

Anti-vimentin (D21H3), Cell Signaling

Anti-lamin A/C (sc-7292 and sc-20681), Santa Cruz

Anti-non-muscle myosin IIA (M8064), Sigma

Anti-caveolin-1 (D46G3), Cell signaling

IV) PERSPECTIVES & DISCUSSION ÉLARGIE

A) Travaux en cours

Si la majeure partie des objectifs (voir [Introduction > D\) Objectifs de mes travaux](#)) de mes travaux de thèse ont déjà pu être atteints dans la version de “Cell Viscoelasticity Orchestrates Intravascular and Early Steps of Metastasis” présentée dans la partie précédente, des expériences sont toujours en cours afin de remplir l’objectif suivant :

« (vi) Resituer, dans le contexte de l’hypothèse de l’adaptabilité mécanique des cellules tumorales, les phénotypes mécaniques identifiés comme importants pour le franchissement des étapes intravasculaires dont il est ici question.

Comparer les propriétés mécaniques avantageuses pour la résistance aux forces de cisaillement, pour la réalisation de l’arrêt intravasculaire, pour l’extravasation ou encore pour la croissance métastatique post-extravasation. »

En particulier, il nous tient à cœur de réconcilier la contribution de la mécanique cellulaire dans les étapes intravasculaires, que nous avons bien démontrée, avec son éventuelle contribution post-extravasation dans l’étape de croissance métastatique. Cette étape de la progression tumorale n’étant pas étudiable dans notre modèle embryon de poisson-zèbre avec les modèles de cellules tumorales mécaniquement altérées que nous avons établis (D2A1 traitées aux ARN interférents), nous avons entrepris de passer au modèle souris dans lequel une combinaison d’expériences ex vivo et in vivo devrait nous permettre de rattacher nos résultats in vivo acquis dans l’embryon de poisson-zèbre au modèle souris, et de prolonger notre étude au-delà de l’étape d’extravasation.

1) Récapitulation de l’étape d’extravasation

Dans le but de nous rapprocher de l’imagerie et des quantifications qui sont possibles dans l’embryon de poisson-zèbre, nous avons imaginé une expérience ex vivo nous permettant de visualiser et quantifier des événements d’extravasation dans les vaisseaux des poumons de la souris. Des injections tail-vein de cellules D2A1 mécaniquement altérées seront réalisées pour les faire circuler et s’arrêter dans les poumons. Les souris seront sacrifiées le lendemain après injection de colorant Evans blue pour marquer les vaisseaux. Les poumons pourront être prélevés et coupés au

vibratome pour imagerie, au microscope confocal, de cellules tumorales dans l'architecture vasculaire de poumons de souris.

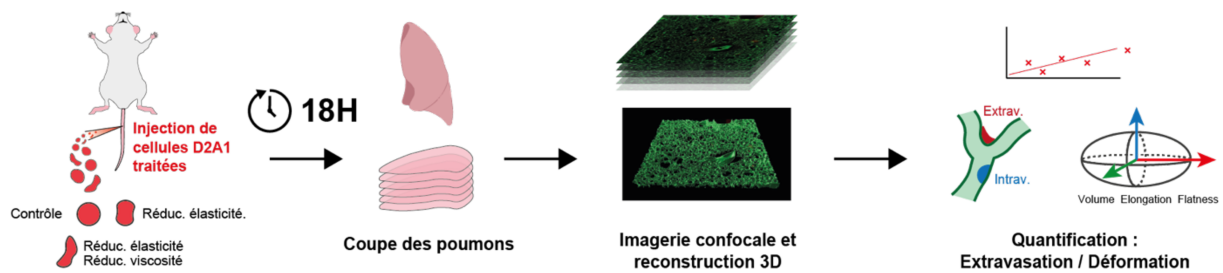


Figure 25 : Approche expérimentale *ex vivo* pour la visualisation et quantification d'événements d'extravasation dans le poumon de souris.

2) Analyse des foyers métastatiques

Dans la continuité de l'expérience *ex vivo* visant à distinguer et quantifier cellules intravasculaires et extravasées, réaliser la même expérience en laissant plus de temps s'écouler entre les injections de cellules et le sacrifice des animaux pour imagerie des poumons nous permettra de visualiser des foyers métastatiques résultant de l'arrivée et de l'établissement de cellules tumorales présentant des phénotypes mécaniques différents. Nous procéderons ainsi à l'imagerie des poumons 10 jours après injections, et quantifierons la taille des foyers, leur nombre et le ratio aire de tissus métastasé / aire de tissus sain.

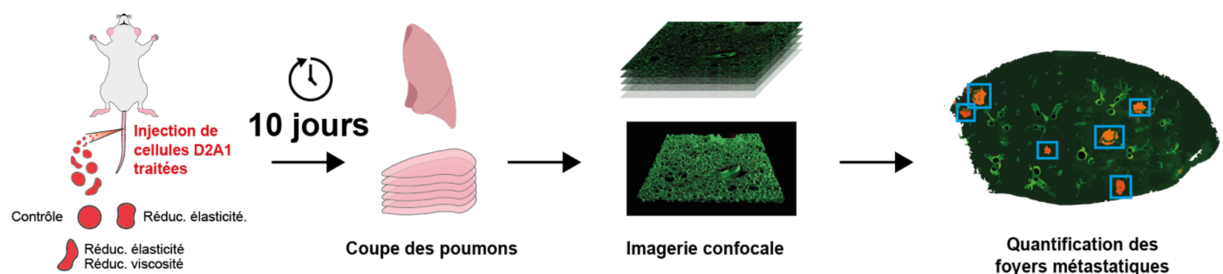


Figure 26 : Approche expérimentale *ex vivo* pour l'imagerie et analyse de foyers métastatiques dans le poumon de souris.

3) Suivi de la croissance métastatique

Enfin, nous pourrions procéder à des expériences de métastases expérimentales *in vivo* plus classiques consistant en l'injection de cellules tumorales bioluminescentes (dans lesquelles nous aurons une fois encore induit des changements de phénotype mécanique) et en le suivi de la bioluminescence dans les souris sur deux semaines. Les injections pourront être faites une fois encore en tail-vein pour s'intéresser spécifiquement à la croissance métastatique dans les poumons, mais aussi en intra-cardiaque afin d'étendre la dissémination à plus d'organes et permettre notamment l'arrivée de plus de cellules tumorales circulantes au cerveau. Réaliser ce type de suivi dans une multitude d'organes permettra peut-être de mettre en lumière des effets organes-spécifiques liés aux phénotypes mécaniques des cellules tumorales injectées.

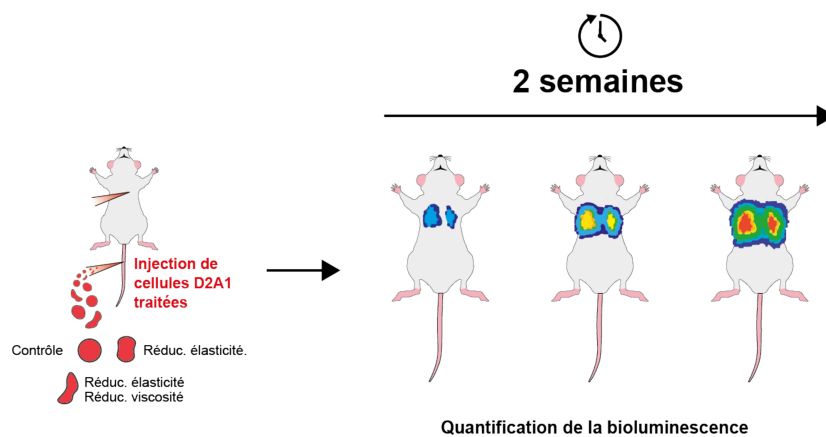


Figure 27 : Approche expérimentale *in vivo* pour la quantification de la croissance métastatique dans le modèle souris.

B) Propriétés mécaniques des cellules tumorales dans la progression tumorale

1) Zones d'ombre subsistantes

Bien que nos travaux contribuent à accroître notre compréhension de la contribution des propriétés mécaniques des cellules tumorales dans la progression tumorale, certaines zones d'ombre subsistent

(i) Intravasation

Il n'y a à l'heure actuelle aucune étude qui s'est intéressée à la déformabilité des cellules tumorales dans le contexte de l'étape d'intravasation de la cascade métastatique. Cela s'explique en grande partie par le fait que cette étape soit très difficile à visualiser et donc à étudier dans une configuration *in vivo* pertinente. On peut néanmoins formuler quelques hypothèses sur la base de certaines données.

Nous citons en introduction une étude rapportant que l'organisation anarchique et dysfonctionnelle des vaisseaux aux sites de tumeurs primaires pouvait comporter des pores et des espaces inter-cellulaires dans les parois endothéliales de dimensions allant de 0,3 à 4,7 μm à peine (Hashizume et al., 2000). Si les cellules tumorales devaient exploiter des ouvertures de telles tailles pour s'intravaser, elles devraient forcément soit se déformer assez drastiquement pour entrer dans ces espaces, soit exercer une activité de dégradation ou contractile pour forcer le passage. D'ailleurs, une étude démontre par de l'expérimentation *in vivo* notamment que les cellules tumorales génèrent des invadopodes (= protrusions capables de dégrader la matrice) qu'elles envoient entre les cellules endothéliales pour faciliter leur intravasation (Roh-Johnson et al., 2014). Ce mécanisme serait initié par une collaboration avec des macrophages et passerait par la voie de signalisation RhoA. Des expériences de microscopie intravital dans le modèle poisson-zèbre (Stoletov et al., 2007) et dans la souris (Harney et al., 2015) montrent par ailleurs que les événements d'intravasation auraient lieu exclusivement en des sites où l'architecture vasculaire est perméable ou en remodelage, confirmant ainsi l'importance de la présence d'ouvertures exploitables par les cellules tumorales dans l'étape d'intravasation.

Néanmoins, le flou persiste quant aux propriétés mécaniques qui seraient avantageuses dans ce processus. Les petits espaces dans lesquels les cellules tumorales doivent s'engouffrer suggéreraient qu'une déformabilité accrue serait avantageuse, mais l'activité RhoA et la génération d'invadopodes semblent nécessaires dans le processus suggéreraient quant à eux qu'une forte activité contractile, et donc peut être une rigidité accrue, serait préférable.

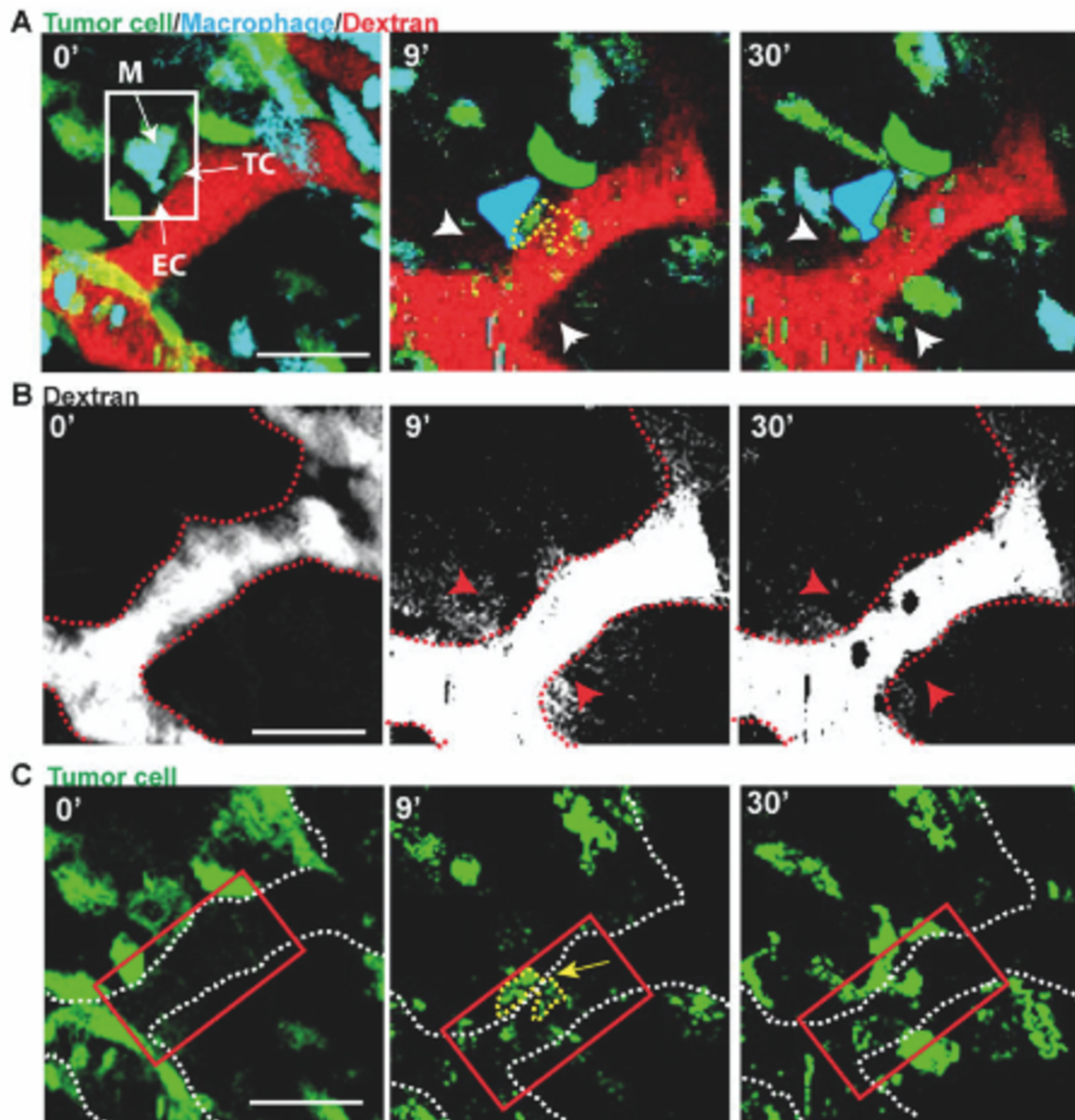


Figure 28 : Intravasation en microscopie intravital. Les cellules tumorales (en vert), au contact de macrophages (en bleu), s'intravasent en passant par des pores (panel B, 30') présent dans la paroi endothéliale. (Extrait de Harney et al., *Cancer Discovery*, 2015)

(ii) Croissance métastatique

Les données donnant des indications quant à l'éventuelle contribution de la mécanique cellulaire dans les étapes finales de croissance / dormance sont à ce jour quasi inexistantes.

On pourra citer une étude dans laquelle il est démontré que les cellules tumorales fraîchement extravasées et rampant sur les capillaires telles des péricytes présentent une activation importante des mécano-transducteurs YAP et MRTF (Er et al., 2018). Bien que l'étude ne présente pas de mesures de propriétés mécaniques de cellules tumorales, il est supposé que l'activation de ces mécano-transducteurs s'accompagne logiquement d'une rigidification des cellules tumorales. Dans l'étude, l'activité de YAP et MRTF (et la supposée rigidification allant avec ?) jouait un rôle critique dans la régulation de la sortie de la phase de latence et l'entrée en phase de croissance métastatique dans de multiples organes.

Une deuxième étude particulièrement intéressante à mettre en perspective par rapport aux résultats de mes travaux mérite d'être mentionnée ici. Il s'agit de travaux récents qui s'intéressent aux effets de l'expression de vimentine aux différents stades de la progression tumorale. Certaines des expériences de l'étude comprennent des injections de cellules tumorales génétiquement modifiées pour diminuer leur expression de vimentine, de manière très similaire à ce que nous avons réalisé dans mes travaux et comptons continuer à faire dans le modèle souris. Les résultats des auteurs de ces travaux suggèrent que pour des cellules de cancer du sein triple-négatif, l'expression de vimentine est requise lors des étapes d'invasion et migration au début de la progression tumorale, mais qu'elle devient plus tard inhibitrice de la croissance métastatique (Grasset et al., 2022). Ainsi, ces résultats pourraient suggérer que dans le cas de cellules tumorales de cancer triple-négatif, la déformabilité accrue associée à une baisse d'expression de vimentine conférerait un avantage pour la croissance métastatique. Il sera intéressant de comparer les résultats que nous obtiendrons en suivant la croissance métastatique de notre modèle D2A1 siVIM dans le modèle souris aux résultats de cette étude.

2) Transition épithélio-mésenchymateuse et mécanique cellulaire

(i) Transition et plasticité épithélio-mésenchymateuses

La transition épithélio-mésenchymateuse (TEM) est un processus morphogénique important au cours duquel les cellules perdent leurs caractéristiques épithéliales au profit de caractéristiques mésenchymateuses. Ce processus, jouant un rôle critique et très bien décrit au cours du développement embryonnaire notamment, était fût un temps également considéré comme important dans la progression tumorale, en permettant supposément à des cellules épithéliales transformées d'adopter un phénotype mésenchymateux associé à des capacités d'invasion et de migration améliorées (Thompson and Newgreen, 2005). Cette vision "binaire" a néanmoins toujours fait l'objet de vives controverses (Tarin et al., 2005), et a depuis été supplanté par le concept de plasticité épithélio-mésenchymateuse (PEM). Le concept de PEM veut que les cellules tumorales puissent continuellement adapter leurs expressions de marqueurs et évoluer sur l'ensemble d'un spectre de phénotypes épithéliaux, intermédiaires et mésenchymateux (Nieto et al., 2016).

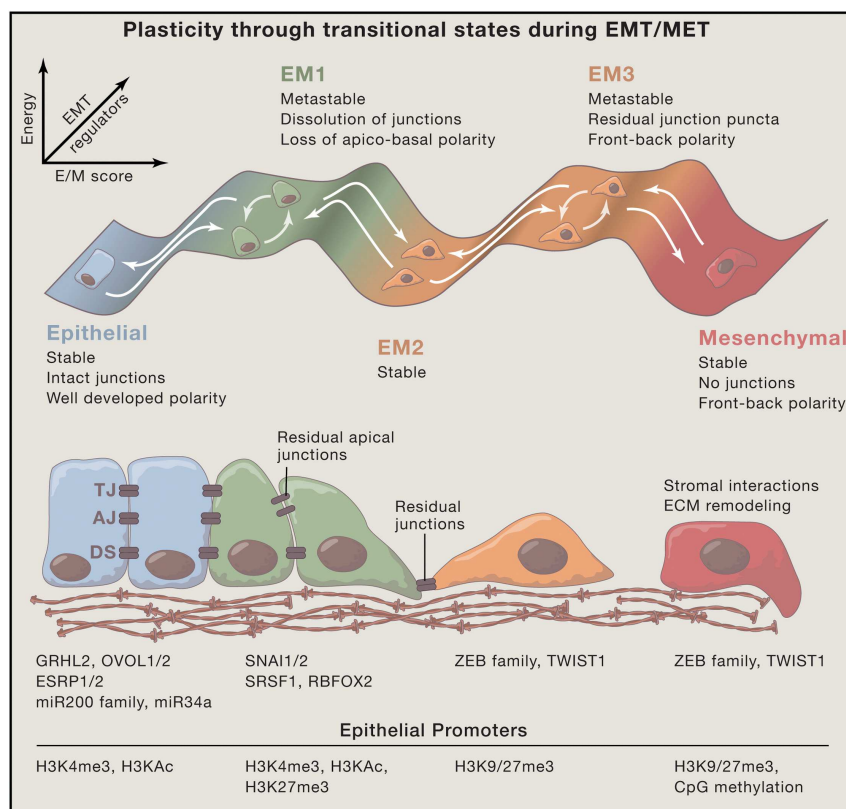


Figure 29 : Plasticité épithélio-mésenchymateuse. La TEM peut être considérée comme un continuum, dans lequel les cellules présentent des phénotypes épithéliaux (E), intermédiaires (EM) et mésenchymateux (M). Lorsque les cellules passent de la gauche à la droite, elles perdent séquentiellement la polarité apico-basale et les adhésions cellule-cellule et acquièrent une polarité avant-arrière et des interactions cellule-matrice renforcées. (Extrait de [Nieto et al., Cell, 2016](#))

(ii) Changements de propriétés mécaniques dans la plasticité épithélio-mésenchymateuse

Il est difficile de ne pas faire de parallèle entre ce concept de plasticité épithélio-mésenchymateuse, qui a supplanté la vision simpliste et binaire de la TEM brute, et le concept d'adaptabilité mécanique des cellules tumorales qui supprime maintenant la vision simpliste stipulant qu'un phénotype mécanique souple correspond nécessairement à un potentiel métastatique amélioré. D'autant plus que des données suggèrent que les transitions sur le spectre de la PEM s'accompagnent de changements de propriétés mécaniques.

En effet, les cellules tumorales, lorsqu'elles s'éloignent de leur phénotype épithélial initial, expriment la vimentine au détriment de la N-cadhérine, mais également au détriment de la kératine. Il y a ainsi un remplacement des filaments intermédiaires de kératine par des filaments intermédiaires de vimentine dans le cytosquelette des cellules tumorales. Or ces deux types de filaments intermédiaires répondent très différemment lorsqu'ils sont mécaniquement sollicités. En effet, à l'échelle des filaments uniques, les filaments de kératine s'étirent mais maintiennent leur rigidité lorsqu'ils sont soumis à une répétition de cycles d'étirement et de relaxation, tandis que les filaments de vimentine, à l'inverse, maintiennent leur longueur initiale mais s'assouplissent en réponse à de tels cycles ([Lorenz et al., 2023](#)). Il a ainsi pu être suggéré que les cellules pourraient directement adapter leurs propriétés mécaniques en alternant entre ces deux types de filaments intermédiaires ([Lorenz et al., 2019](#)). Cette hypothèse est appuyée par une étude dans laquelle figurent des mesures de propriétés mécaniques de cellules tumorales à plusieurs stades de la TEM ([Chen et al., 2018](#)), et d'autres travaux récents corrélant l'expression de gènes associés à la TEM, et notamment la vimentine, à un phénotype mécanique plus déformable dans les cellules tumorales ([Young et al., 2023](#)).

3) Métastases collectives et mécanique cellulaire

Les résultats de mes travaux sont à nuancer et à recontextualiser avec les mécanismes bien connus de métastases collectives qui pourraient être à l'origine de la majorité des métastases.

(i) Exemples de mécanismes de métastases collectives

Dès les années 60, des pathologistes constatèrent que des « nids » de cellules tumorales étaient présents dans l'environnement tumoral, suggérant qu'elles se déplaçaient en groupe (Leighton et al., 1960). Aujourd'hui, il est communément admis que l'invasion et la migration de cellules tumorales se font principalement de manière collective dans la plupart des tumeurs solides (Friedl et al., 2012). Les outils de microscopie et de traçage de lignées ont permis de disséquer certains de ces mécanismes. Dans un modèle de métastases pulmonaires spontanées dans la souris, des données montrent que des clusters de cellules tumorales exprimant de la kératine 14 sont très efficaces pour envahir les tissus et seraient à l'origine de 90% des métastases finissant par se former (Cheung et al., 2016). D'autres travaux ont pu montrer que l'environnement hypoxique de l'environnement tumoral pouvait favoriser l'intravasation de clusters de cellules tumorales, contribuant ainsi à la génération de clusters de CTCs (Donato et al., 2020). Les clusters de CTCs ont justement fait l'objet de plusieurs études leur ayant décerné plusieurs caractéristiques avantageuses. Ils présenteraient par exemple un potentiel métastatique 23 à 50 fois plus élevé comparé aux cellules tumorales circulant seules (Aceto et al., 2014), pourraient via une association avec des neutrophiles voire leur expression de gènes associés à une accélération du cycle cellulaire augmenter pour plus tard favoriser l'établissement de métastases (Szczerba et al., 2019) et bénéficieraient, par rapport à des CTCs seules, de marques épigénétiques leurs conférant des caractéristiques de cellules souches (Gkountela et al., 2019). Enfin, concernant l'ensemble de la cascade métastatique, la configuration en cluster donne aux cellules tumorales un moyen unique de réguler leur comportement. En effet, des cavités « nanoluminales » présentes entre les cellules composant les clusters sont utilisées comme réservoirs de facteurs de croissance et permettent aux clusters de cellules tumorales d'alterner entre activités migratoire et proliférative (Wrenn et al., 2020 ; Gensbittel et al., 2020) (Annexe 4).

single cell metastasis

collective metastasis

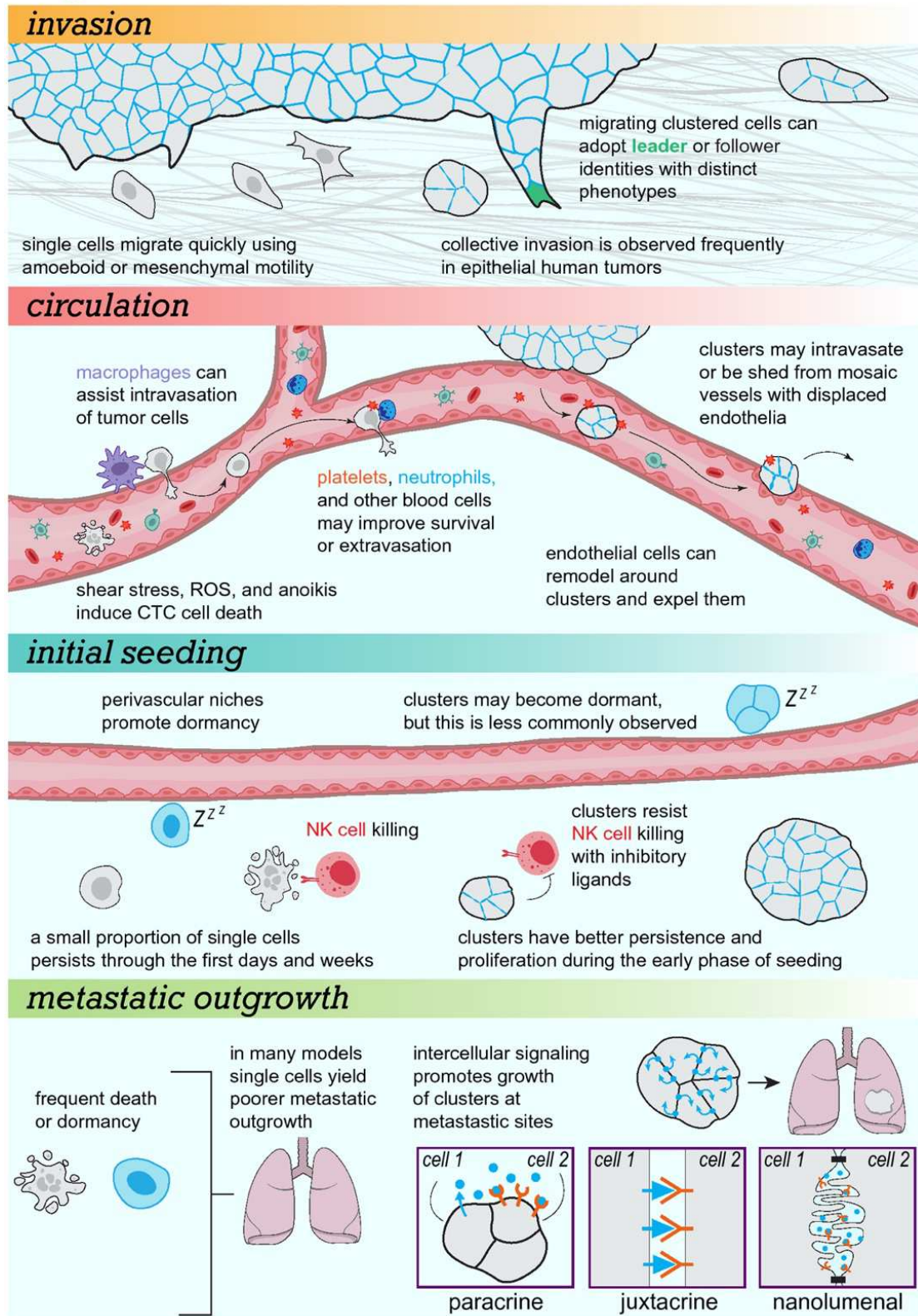


Figure 30 : Mécanismes collectifs vs mécanismes cellule unique. (Extrait de Wrenn et al., *Clinical & Experimental Metastasis*, 2021)

(ii) Implications biomécaniques dans l'environnement intravasculaire

Forces de cisaillement, forces d'adhésion, contribution de la déformabilité des cellules : la quasi-totalité de nos connaissances au sujet de ces paramètres biomécaniques considèrent exclusivement la configuration dans laquelle les cellules tumorales circulent individuellement et non en configuration de clusters. Ces nombreuses données sont donc à nuancer, d'autant plus que plusieurs études laissent entendre que le passage à la configuration cluster pourrait changer la donne et modifier les sensibilités des CTCs à plusieurs paramètres de l'environnement intravasculaire.

Tout d'abord concernant les forces de cisaillement, la circulation en configuration de clusters présenterait l'avantage considérable de réduire la sensibilité des CTCs à ces forces, augmentant ainsi leurs chances de survie (Aceto et al., 2014). Pour l'arrêt intravasculaire, des modèles numériques prédisent que les clusters circuleraient plus lentement comparés à des CTCs individuelles, résultant en de meilleures probabilités de former des interactions d'adhésions avec l'endothélium et de s'arrêter stablement (Anderson et al., 2017). La taille significativement plus importante d'un cluster par rapport à une cellule unique doit évidemment également favoriser l'arrêt via occlusion dans des capillaires, qui restent accessibles aux clusters de CTCs car ces dernières seraient capables d'alterner dynamiquement entre configurations sphériques et configuration en file pour s'adapter à une architecture vasculaire contraignante (Au et al., 2016). On peut alors supposer que les propriétés mécaniques et peut-être en particulier la viscosité de la CTC en tête de file entrent en jeu de manière similaire à ce qui a été vu dans mes travaux lors de ce processus. Dans tous les cas les dispositions avantageuses pour l'arrêt liées à la vitesse de circulation réduite et à la taille plus conséquente des clusters se vérifient dans des expériences conduites dans la souris mesurant la demi-vie de clusters et de CTCs individuelles dans la circulation, montrant que les clusters circuleraient significativement moins longtemps (Aceto et al., 2014). Aucune étude ne s'est à ce jour focalisée sur d'éventuelles contributions de paramètres biomécaniques au cours du processus d'extravasation de clusters de CTCs. On peut néanmoins supposer, sur la base de mes travaux, que des clusters de CTCs arrêtés seraient particulièrement encombrant dans la circulation et qu'ils seraient ainsi particulièrement disposés à déclencher le mécanisme d'extravasation

par remodelage endothélial, plus indépendamment du niveau de rigidité des cellules composant les clusters.

Ainsi, en leur conférant une résistance aux forces de cisaillement accrue, en accélérant leur arrêt par occlusion sans nécessairement les empêcher de circuler par des capillaires contraignants et en favorisant peut-être leur extravasation, on peut peut-être voir derrière la configuration en cluster un moyen pour les CTCs de s'affranchir des exigences d'adaptabilité mécanique qui seraient imposées à des CTCs se disséminant individuellement.

C) Implications en « mécano-immunologie »

Les nombreux aspects mécaniques de la progression tumorale ont évidemment également des implications dans la réponse immunitaire. En lien avec les propriétés mécaniques des cellules tumorales, qui étaient l'objet de mes travaux, des études récentes ont établi un lien entre la rigidité des cellules tumorales et leur sensibilité à l'activité cytotoxique de cellules immunitaires. Pour finir cette discussion, je présente un article de type review qui paraîtra très prochainement dans Nature Nanotechnology et qui fait un état des lieux des connaissances et des perspectives thérapeutiques liées aux nombreux aspects biomécaniques de la surveillance immunitaire, détaillant notamment l'importance des propriétés mécaniques des cellules tumorales dans ce contexte (Publication imminente, proofs ci-dessous).

Evidence and therapeutic implications of biomechanically regulated immunosurveillance in cancer and other diseases

Vincent Mittelheisser^{1-4#}, Valentin Gensbittel^{1-4#}, Lucia Bonati^{5#}, Weilin Li^{5#}, Li Tang^{5,6*}, Jacky G. Goetz^{1-4*}

1. Tumor Biomechanics, INSERM UMR_S1109, Strasbourg, France.
2. Université de Strasbourg, Strasbourg, France.
3. Fédération de Médecine Translationnelle de Strasbourg (FMTS), Strasbourg, France.
4. Equipe Labellisée Ligue Contre le Cancer
5. Institute of Bioengineering, École Polytechnique Fédérale de Lausanne (EPFL), Lausanne, CH-1015, Switzerland
6. Institute of Materials Science & Engineering, EPFL, Lausanne, CH-1015, Switzerland

These authors have contributed equally

* co-corresponding authors: li.tang@epfl.ch, jacky.goetz@inserm.fr

One-sentence summary (for website)

This Review highlights the mechanisms underlying the mechanical changes occurring in diseased and immune cells and discusses new approaches to target and exploit biomechanical cues for therapeutic applications.

Evidence and therapeutic implications of biomechanically regulated immunosurveillance in cancer and other diseases

Received: 31 January 2023

Accepted: 26 September 2023



Check for updates

Vincent Mittelheisser^{1,2,3,4,7}, Valentin Gensbittel^{1,2,3,4,7}, Lucia Bonati^{5,7},
Weilin Li^{5,7}, Li Tang^{5,6} & Jacky G. Goetz^{1,2,3,4}

Disease progression is usually accompanied by changes in the biochemical composition of cells and tissues and their biophysical properties. For instance, hallmarks of cancer include the stiffening of tissues caused by extracellular matrix remodelling and the softening of individual cancer cells. In this context, accumulating evidence has shown that immune cells sense and respond to mechanical signals from the environment. However, the mechanisms regulating these mechanical aspects of immune surveillance remain partially understood. The growing appreciation for the ‘mechano-immunology’ field has urged researchers to investigate how immune cells sense and respond to mechanical cues in various disease settings, paving the way for the development of novel engineering strategies that aim at mechanically modulating and potentiating immune cells for enhanced immunotherapies. Recent pioneer developments in this direction have laid the foundations for leveraging ‘mechanical immunoengineering’ strategies to treat various diseases. This Review first outlines the mechanical changes occurring during pathological progression in several diseases, including cancer, fibrosis and infection. We next highlight the mechanosensitive nature of immune cells and how mechanical forces govern the immune responses in different diseases. Finally, we discuss how targeting the biomechanical features of the disease milieu and immune cells is a promising strategy for manipulating therapeutic outcomes.

Disease progression is often associated with dynamic changes in mechanical properties at cellular and tissue levels. Such mechanical aspects of disease progression have been extensively studied in various pathological conditions, including cystic fibrosis¹, viral² and bacterial³ infections, inflammation⁴ and cancer⁵. Evidence shows that immune

cells experience and respond to passive and active mechanical forces throughout their lifecycles. These mechanical forces have important roles in regulating the development, activation, migration, differentiation and effector functions of immune cells⁶. In particular, growing evidence has shown that T cells are mechanosensitive⁷. Upon cognate

¹Tumor Biomechanics, INSERM UMR_S1109, Strasbourg, France. ²Université de Strasbourg, Strasbourg, France. ³Fédération de Médecine Translationnelle de Strasbourg (FMTS), Strasbourg, France. ⁴Equipe Labellisée Ligue Contre le Cancer, Strasbourg, France. ⁵Institute of Bioengineering, École Polytechnique Fédérale de Lausanne (EPFL), Lausanne, Switzerland. ⁶Institute of Materials Science and Engineering, EPFL, Lausanne, Switzerland.

⁷These authors contributed equally: Vincent Mittelheisser, Valentin Gensbittel, Lucia Bonati, Weilin Li. ✉e-mail: li.tang@epfl.ch; jacky.goetz@inserm.fr

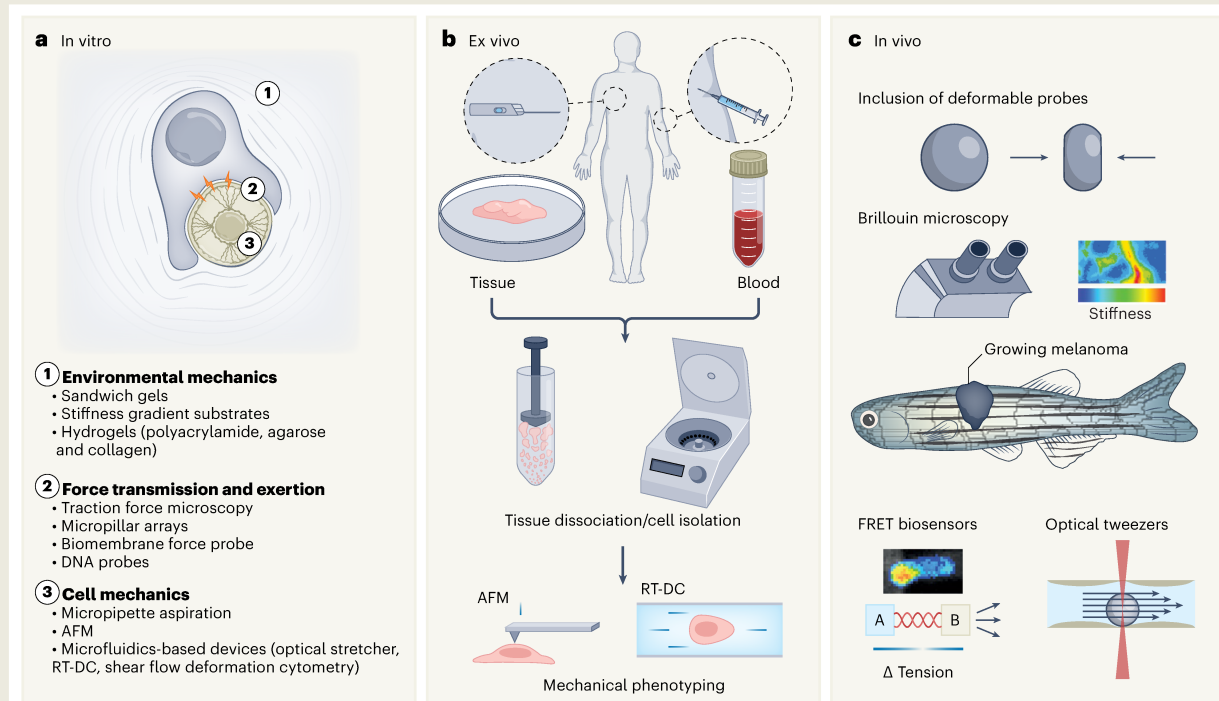
BOX 1

Relevant technologies for mechanical immunoengineering

Full dissection of the mechano-surveillance mechanisms inevitably relies on accurate methods for measuring forces. A plethora of *in vitro* techniques, such as micropipette aspiration, atomic force microscopy (AFM) and biomembrane force probe, have been available for measuring the mechanical properties of single cells, tissues and interaction forces between cells²²¹. Although extensively used to highlight differences in mechanical properties between healthy and diseased cells and tissues, these techniques suffer from low throughput. More recently, microfluidic approaches have been developed to address this issue and allow high-throughput mechanical single-cell measurements. The development of real-time deformability cytometry (RT-DC) now allows to probe instant deformation and elasticity of cells at high throughput²¹² and should soon expand its potential to allow fast measurements of viscoelastic properties²¹³. The techniques mentioned above are all perfectly compatible with *ex vivo* measurements of patient-derived samples.

While certainly more challenging, probing forces and mechanical properties *in vivo* has a bright future ahead owing to recent technological breakthroughs. Brillouin microscopy has emerged to allow extraction of elastic and viscous properties of living tissues²¹⁴ and has been applied for mapping mechanical properties of cancer nodules in three dimensions²¹⁵. Particle-tracking microrheology has been used to compare how mechanical properties of normal versus carcinoma cells evolve in living mice²¹⁶. Hydrostatic pressure of fluid-filled cavities can be directly measured via the insertion of pressure-measuring micropipettes. Such methods were initially designed to measure pressure inside blood vessels²¹⁷ and can now be applied to measure cytoplasmic pressure in single cells²¹⁸.

Optical tweezers have been used to quantify haemodynamic and adhesion forces in the zebrafish embryo model²¹⁹. Slightly invasive methods based on inclusion of deformable probes such as microdroplets/microbeads can quantify the mechanical stress acting on cells within living tissues^{220,221}. Likewise, a recently developed microparticle-based platform was injected into tissues, allowing the characterization of the force profile of individual T cells *in vivo*²²². FRET tension sensors provide mechanical stress quantification when coupled with intravital imaging. These molecular springs can be genetically encoded in living cells/tissues, which then emit fluorescence that reports the local mechanical tension^{223,224}. Such sensors have notably been used to quantify intercellular tension within endothelial cell monolayers exposed to fluid shear stress²²⁵. Similarly, viscosity can be followed *in vivo* by using molecular rotors that will adjust their conformational states upon viscosity changes^{226,227}. Finally, breakthroughs in *in vivo* mechanical measurements have benefited researchers and found applications in the clinic. Novel diagnostic tools such as acoustic radiation force impulse²²⁸ or magnetic resonance elastography²²⁸ have allowed the probing of mechanical properties of patient-derived tissues in the clinic. In addition, recent progress in tissue mechanical dissociation coupled with RT-DC approaches will allow rapid probing of mechanical properties of surgically removed cells. This will help clinical decision-making during extemporaneous histological analysis²²⁹. Fine-tuning, spreading and combining these novel techniques will allow researchers to measure and investigate mechanical forces in the context of immune surveillance at all relevant scales, from whole tissues to single force-bearing receptors at immune synapses.



Relevant technologies for mechanical immunoengineering. a–c. A wide range of techniques are available to researchers for investigating environment mechanics, interaction forces and cell properties *in vitro* (a), *ex vivo* (b) and *in vivo* (c).

antigen recognition, T cells form a well-defined nanostructure at their interface with antigen-presenting cells, called the immunological synapse (IS). T cells and their target cells are known to engage in extensive mechanical exchanges at the IS, which have been possible to investigate through the development of multiple nanotechnologies (see Box 1 on techniques). Both murine and human CD4⁺ T cells are activated to higher extents and secrete more effector cytokines when seeded on stiff substrates^{8–11}. T cells exert mechanical forces to potentiate the killing of cancer cells¹². In addition, T-cell-mediated lysis of tumour cells is enhanced when cancer cells are stiffened and decreased when they are softened^{13–15}. These results provide solid evidence that mechanical aspects of pathologies do indeed impact immune responses.

Currently, most immunotherapies target biochemical cues of diseased tissues and immune cells. However, the growing appreciation of the mechanobiology of immune cells offers a good foundation for developing new engineering strategies aiming at mechanically modulating immune cells or target cells for enhanced therapies against various diseases. For example, emerging studies have been aiming at stiffening cancer cells to sensitize them to immune surveillance^{14,15}. Expanding this concept to engineering strategies focusing on the mechanical modification of immunity–disease interactions shows enormous promise for developing next-generation immunotherapies. Here we first review the mechanical changes during pathological progression in several diseases, including cancer, fibrosis and infection. We then highlight the mechanosensing abilities of immune cells and the mechanosensitive nature of the immune response in various pathologies. Finally, we discuss how targeting the mechanical features of the disease milieu and immune cells is a viable strategy to enhance current immunotherapies. We also highlight several challenges yet to be addressed in this emerging field of ‘mechanical immunoengineering’.

Altered mechanics in disease initiation and progression

Cancer

Mechanical changes in tissues constitute a signature trait of solid tumour pathologies that has long been exploited for diagnosing diseases, notably in breast cancer cases where mechanical probing of the tissues is routinely performed (palpation, mammography or elastography) (Fig. 1a). The mechanisms underlying the stiffening of tumour tissues and their metastatic secondary foci are well understood and have been expertly reviewed in the past⁵. Increases in the synthesis of matrix proteins, collagen crosslinking, integrin clustering and focal adhesion are the main contributors to extracellular matrix (ECM) remodelling. This is caused mainly by the concerted action of stromal cells and tumour growth-mediated solid stress, which leads to the stiffening of cancer tissues^{16–18}. The pro-inflammatory environment of the initial malignant progression also sustains ECM stiffening. More specifically, cytokines and chemokines released by innate immune cells act in a paracrine way on stromal cells, driving their differentiation into ‘activated fibroblasts’ bearing a myofibroblast-like phenotype¹⁹. These ‘activated fibroblasts’, collectively named cancer-associated fibroblasts (CAFs), express higher levels of α -smooth muscle actin and collagen, and acquire greater contractile and proliferating capacities. Deposition of a stiff and non-elastic ECM in cancer results in impeded diffusion of chemotherapeutic molecules^{20,21} and hinders infiltration of immune cells²², which are key features of malignant progression. Other noteworthy changes during this desmoplastic reaction include disorganized and leaky vascularization. This results in a subsequent imbalance of interstitial fluid pressure, further preventing efficient delivery of chemotherapeutic molecules to the tumour²³.

Surprisingly, the stiffening at the scale of cancer (or metastatic) tissues can hardly be a representation or a consequence of the stiffness level of individual tumour cells. Although tumour tissues are stiffer than healthy tissues, it is so far widely accepted that tumour cells are softer than their healthy counterparts²⁴. Consistently, nanomechanical

profiling of tumour tissues has shown intratumoural stiffness to be highly heterogeneous compared with healthy tissues, with tumour cells constituting the softest spots of the probed cancer tissues²⁵. As such, two very distinct scales must be considered when discussing mechanical changes in cancer diseases: (1) the whole-tissue scale, where solid cancer tissues, in general, are known to be stiffer than healthy tissues, and (2) the single-cell scale, where individual tumour cells are often thought to be softer than healthy cells. However, whether the consensus on the softer mechanical phenotype of single cancer cells is truly relevant remains debatable, as proper *in vivo* demonstrations have been lacking. As such, the potential link between the mechanical properties of tumour cells and disease progression remains unclear, despite some evidence hinting that both parameters probably affect each other. In addition, stromal components of tumours (fibroblast and immune cells mostly) are active elements from a mechanical standpoint and contribute to physical aspects of tumour progression, whose targeting offers a promising future for cancer therapy²⁶.

We recently speculated that cancer cells are not simply ‘softer’ but rather mechanically ‘dynamic and adaptable’, a feature that would undoubtedly grant them a significant advantage for completing the metastatic cascade²⁷. Accumulating evidence suggests that the mechanical properties of tumour cells confer a selective advantage in almost all the steps of cancer progression. A study investigating the link between mechanical phenotype and tumourigenicity of cancer stem cells found that only soft cancer stem cells could lead to primary tumour initiation²⁸. This suggests that the mechanical properties of tumour cells are critical at the earliest stage of cancer progression. Tumour cells that later find themselves inside a growing primary tumour are subjected to increasing compressive stress levels and proliferate more efficiently by becoming spherical and stiffening their cell cortex²⁹. Cancer cells that subsequently become invasive and escape the primary tumour site are softer and are subjected to gene expression changes associated with the epithelial–mesenchymal transition³⁰. Such a softer mechanical phenotype facilitates migration through the ECM, as this process often requires extensive cell and nucleus deformation³¹. During intravasation, circulating tumour cells (CTCs) face drastic environmental changes. As their diameter is generally significantly larger than that of normal circulating cells, such as leukocytes, CTCs are more prone to shear-stress-induced destruction in mechanically hostile blood flow³². To cope with haemodynamic forces, CTCs have been shown to undergo stiffening and improve their chances of survival³³. Tumour cells might again get softer once they have stably arrested and require performing extravasation through diapedesis³⁴. Such an example of a dynamic adaptation mechanism to perform extravasation has recently been observed for primordial germ cells in avian embryos³⁵. How mechanical properties of tumour cells evolve after extravasation remains largely unknown at this stage. However, one study suggested that freshly extravasated pericyte-like tumour cells might stiffen in a YAP- and myocardin-related transcription factor (MRTF)-dependent manner to facilitate colonization of perivascular niches³⁶. Such post-extravasation mechanical adaptation may impact or be impacted by the state that tumour cells might enter next: dormant or proliferative. In conclusion, the mechanical plasticity of tumour cells is an additional hallmark of metastatic progression.

Viral and bacterial infections

Similarly to cancer, two scales must be considered when discussing mechanical changes associated with viral and bacterial infections (Fig. 1b). Indeed, at the intracellular scale, bacteria and viruses can hijack the cytoskeleton of host cells to enhance transportation to the cytoplasm where they will replicate and assemble. In addition, bacteria and viruses can promote local actin polymerization to generate a mechanical force facilitating their progression. This phenomenon applies to several viruses, such as coronavirus³⁷ and respiratory syncytial virus³⁸. Cytoskeleton changes do not occur exclusively in the

Q1

Q2

Q3

Q4

Q5

Q6

Q9

Q10

Q11

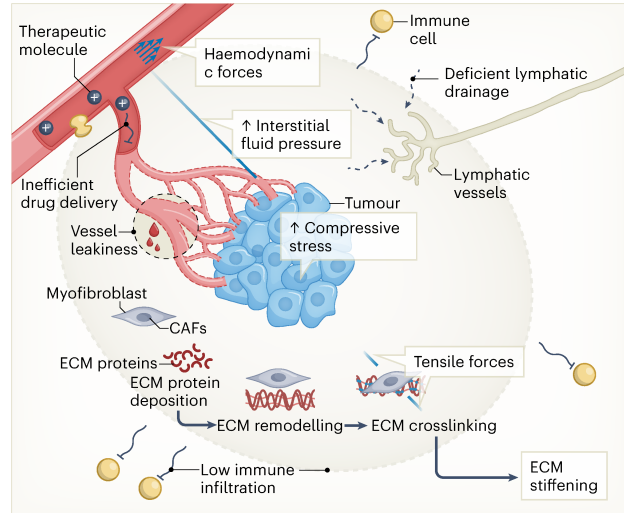
host cells infected by viruses (that is, ACE2⁺ cells in the case of severe acute respiratory syndrome coronavirus 2), but also in the immune cells at the infection site. Indeed, a recent study showed lymphocyte stiffening due to the clinical syndrome of coronavirus disease 2019³⁹. Like cancer cells, pathogens, and more specifically bacteria, can also be affected by fluid shear stress^{40,41} and develop strategies to resist it⁴².

At the whole-tissue scale, bacteria and viruses can alter the biophysical properties of the infected tissue by changing the ECM structure and/or composition. Upon viral infection by rhinovirus, stromal cells markedly increase their production and deposition of fibronectin, perlecan and collagen IV in response to activation of Toll-like receptor (TLR)-3 and -7/8⁴³. In parallel, TLR activation in stromal and epithelial cells triggers the secretion of high-molecular-weight hyaluronic acid⁴⁴, which traps fluid arriving through permeable endothelium and swells tissue, causing oedema and increased stiffness⁴⁴. Oedema formation can be further fostered by secreted matrix metalloproteinases that degrade the endothelial barrier, resulting in abnormal Starling forces and fluid diffusion⁴⁵. Upon acute inflammation, the lymph node architecture may undergo a late remodelling process, resulting in increased collagen deposition and ECM remodelling, which can profoundly impact tissue stiffness, such as scarring and eventually fibrosis⁴⁶. Mechanical changes are actively experienced by immune cells as they travel through different tissue environments and contribute to the early recognition of danger and the induction of immune responses.

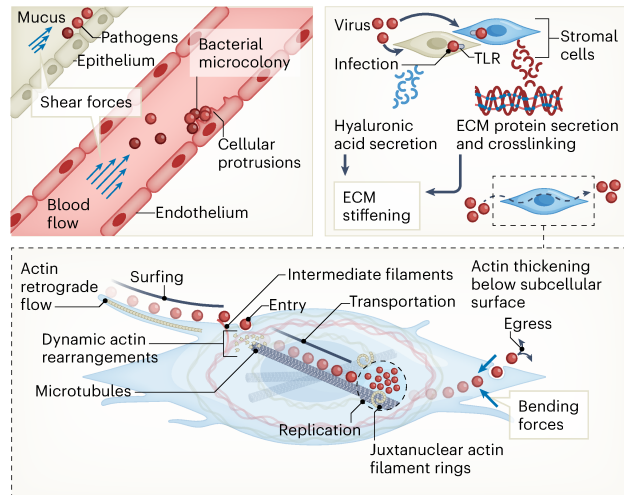
Fibrosis

Fibrotic diseases, such as idiopathic pulmonary fibrosis or scleroderma, are accompanied by numerous mechanical alterations (Fig. 1c). Fibrosis is the wound-healing response following iterative injuries of chemical (asbestos, alcohol and so on), mechanical or microbiological (hepatitis viruses, *Mycobacterium tuberculosis* and so on) origins^{47,48}. Regardless of the underlying cause, chronic injury causes parenchymal cell death associated with a positive feedback loop between inflammatory damages, fibroblast proliferation and matrix deposition⁴⁹. In some cases of acute stress, such as myocardial infarction, the emergence of fibrotic scars is crucial to replace the necrotic tissue and avoid cardiac rupture⁵⁰. Increases in collagen and glycosaminoglycan depositions in the ECM promote the development of non-contractile fibrotic areas, leading to

a Cancer



b Infection



c Fibrosis

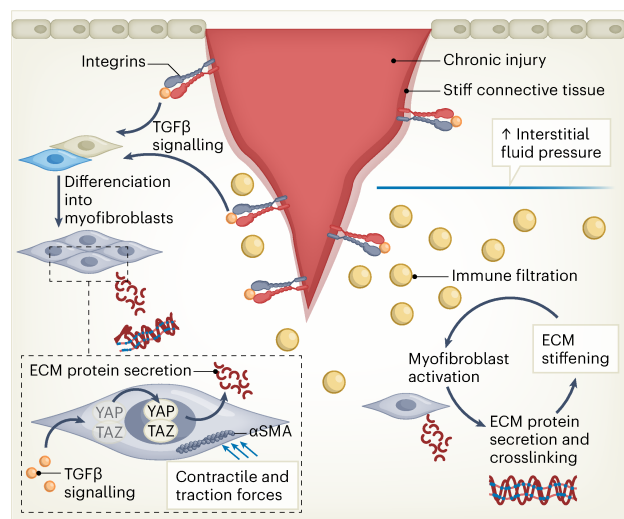


Fig. 1 | Different disease settings share common mechanical cues. a, Solid cancer diseases come with a variety of mechanical features that lead to the characteristic stiffness of tumour tissues. Compressive stress arises as the tumour volume expands and interstitial fluid pressure increases because of vessel leakiness and inefficient lymphatic drainage. Activated CAFs exert tensile forces on ECM fibres that they also secrete, remodel and crosslink. As a result of these changes, immune infiltration and delivery of therapeutic molecules to the tumour site are compromised. **b**, Mechanical forces are also at play in infectious diseases. Pathogens are sensitive to shear forces they encounter in mucus as they attempt to cross an epithelium or in the blood flow. Bacteria form microcolonies to deal with such forces. Stromal cells infected by viruses drive ECM stiffening by secreting hyaluronic acid and ECM proteins upon TLR activation. At the intracellular level, viruses hijack the cytoskeleton of their host cell to complete their replication and thrive. Viruses take advantage of actin retrograde flow in protrusions to ‘surf’ to their entry point. Entry is allowed by actin rearrangements and intermediate filaments acting as co-receptors at the cell surface. Microtubules are exploited for transportation to the replication site where acid filament rings come into play. Finally, actin thickening below the cell surface generate the bending forces necessary for freshly replicated virus particles to exit. **c**, Fibrotic diseases share very similar traits to cancer. Integrin-mediated TGFβ signalling originating from stiff connective tissue causes stromal cells to differentiate into activated myfibroblasts that secrete and crosslink ECM fibres and also exert high α -smooth actin-driven contractile and traction forces. The resulting ECM stiffening further activates myfibroblasts, thus creating a feedback loop that endlessly drives cellular activation and fibrosis. In addition, the chronic inflammation state of fibrotic tissues also leads to immune and fluid infiltrations that increase local hydrostatic pressure and further contribute to the stiffening of fibrotic tissues.

Q8

progressive tissue stiffening, which is a hallmark of fibrotic diseases. Indeed, various studies have shown that the elastic modulus of lung⁵¹, liver⁵² and kidney⁵³ tissues increased upon fibrosis when compared with healthy tissues. Several diseases, such as myocardial infarction, inflammatory cardiomyopathy or non-alcoholic fatty liver disease, can evolve into fibrosis^{48,54}. A chronic inflammatory state can also occur with ageing. Indeed, unresolved systemic inflammation is a hallmark of immune ageing⁵⁵. This persistent low-grade inflammation can lead to arteriosclerosis characterized by a stiff and thickened artery wall, resulting in the decline of cardiac function⁵⁶.

Although more work is needed to understand how matrix stiffness regulates tissue fibrosis comprehensively, accumulating evidence indicates that stiffening of connective tissue directly contributes to the progression of the fibrosis by promoting three fundamental profibrotic mechanisms: (1) mechano-activation of myofibroblasts through mechanotransduction pathways, (2) integrin-mediated activation of latent transforming growth factor β 1 (TGF β 1), and (3) activation of non-canonical TGF β 1 signalling pathways. Mechanically induced activation triggers myofibroblast secretion of multiple types of ECM protein as well as matrix-crosslinking enzymes, resulting in a more stable and stiffer ECM⁵⁷. This effect results in a positive feedback loop, leading to persistent cellular activation and fibrosis⁵⁸. Moreover, reinforced activation of myofibroblasts also leads to upregulation of α -smooth muscle actin, further increasing their contractility⁵⁹. As a result of this hypercontractile state, myofibroblasts exert higher traction forces on the stiff fibrotic ECM, which leads to more matrix remodelling and stiffening and integrin-mediated latent TGF β 1 activation (integrin α v β 6, α v β 5 and α v β 1), thus completing the fibrosis amplification loop⁶⁰. Consequently, matrix stiffening in fibrosis should not simply be viewed as a by-product but as a key initiator and regulator of profibrotic fibrogenesis⁶¹.

Mechanosensing and mechanotransduction of the immune system

Immune cells respond to various biochemical signals arising from pathogen-associated molecular patterns or specific activating ligands expressed at the surface of infected or transformed cells⁶². These signals are first detected by sentinel cells of the innate immune system, such as macrophages, dendritic cells (DCs) and natural killer (NK) cells. The innate immune system recognizes biochemical signals quickly through germ-line-encoded pattern-recognition receptors (PRRs) and other cell surface molecules, orchestrating inflammatory responses⁶³. The effector functions of innate immune cells further drive adaptive immune responses by recruiting and activating T and B cells⁶³. Professional antigen-presenting cells (APCs) expressing co-stimulatory molecules (CD80, CD86 and so on) prime T cells by presenting them cognate antigens as peptides bound to major histocompatibility complex (MHC) molecules⁶⁴.

In addition to their biochemical activation, immune cells encounter numerous forces as they circulate throughout the body to perform immunosurveillance and effector functions. Accumulating evidence shows that immune cells are sensitive to mechanical stimuli, such as shear stress, hydrostatic pressure and tension of their surrounding environment. Such forces are sensed and converted from mechanical cues to biochemical signals, thus activating cellular pathways and influencing their function. Current understanding of the mechanosensing of immune cells has been enabled largely by *in vitro* models of ligand-coated artificial substrates (for example, polydimethylsiloxane (PDMS), polyacrylamide gels, beads) that allow the decoupling of biophysical cues and biochemical signals involved in the interactions of immune cells with their environment and target cells^{65,66}. As the physical properties of their surrounding microenvironment are essential to immune cell function, PDMS hydrogels offer an ideal model to manipulate and test the impact of stiffness⁶⁷. Yet, the stiffness of PDMS gels typically spans from 100 kPa to 10 MPa (ref. 68), whereas the

physiological stiffness normally ranges from 100 Pa (brain) to 100 kPa (carcinoma), except bones⁶⁹. Therefore, polyacrylamide gels (typical stiffness ranging from 10 kPa to 10 kPa) might be more suitable to recapitulate the physiological stiffness of tissues⁷⁰. Nevertheless, efforts are needed to generate models that better mimic the dynamic mechanical environment and cellular stiffness to model cell–cell interactions.

Monocytes and macrophages

Monocytes and macrophages are important innate immune cells that have a pivotal role in the initial recognition and elimination of pathogens through phagocytosis and/or cytokine secretion. Monocytes circulate in the peripheral blood for approximately one to three days and then migrate into tissues throughout the body where they differentiate into macrophages and DCs⁷¹. As these cells scout the body using body fluids, they are subjected to hostile fluid forces. For example, patrolling monocytes can sense haemodynamic forces, such as fluid shear stress, through mechano-gated ion channels^{72,73}. The responses of circulating monocytes to high shear stress include enhanced adhesion, activation of CD11b integrin, phagocytosis and pro-inflammatory cytokine secretion⁷⁴.

Macrophages are terminally differentiated monocytes that reside in tissues, actively sensing their surroundings and launch effector responses accordingly. Macrophages are markedly affected by the wide range of phagocytic targets (pathogens, cancer cells, apoptotic bodies and so on) and their mechanical parameters^{75–77}. Macrophages sense opsonized target stiffness through the Fc γ receptor, triggering integrin localization into the phagocytic cup. This further allows macrophages to close the phagocytic cup and complete phagocytosis⁷⁸. Furthermore, target stiffness can overpower the SIRP α -CD47 ‘don’t eat me’ signal⁷⁶. In addition to phagocytosis, substrate stiffness is instrumental in tuning macrophage migration⁷⁷ and differentiation into anti-inflammatory (‘M2 like’) and pro-inflammatory (‘M1 like’) phenotypes⁷⁷. Multiple research groups have shown that macrophages cultured on soft substrates have reduced inflammatory activation compared with those cultured on stiff surfaces⁷⁷. Macrophages can sense their substrate’s mechanical properties through integrins⁷⁹ and ion channels, such as PIEZO1 and transient receptor potential vanilloid 4 (TRPV4). The stiffness of the substrate favours the influx of Ca²⁺ ions through PIEZO1, a mechano-gated ion channel, and subsequent nuclear factor kappa B (NF- κ B) activation and secretion of inflammatory cytokines leading to a more prominent ‘M1 like’ inflammatory phenotype⁷⁹.

Furthermore, the concerted action of PIEZO1 and TLR-4 is necessary to achieve innate responses against pathogens, including phagocytosis, reactive-oxygen-species production and bacterial clearance⁸⁰. In addition to ion-channel-mediated mechanosensing, YAP/TAZ signalling orchestrates the response of macrophages to biophysical cues. Indeed, the translocation of YAP/TAZ to the nucleus, which allows the regulatory activity of downstream gene expression, is impacted by ECM stiffness⁸¹. When modelled *in vitro*, the stiffness of the culture substrate regulates the nuclear translocation of YAP and its downstream functions in various cell types^{82–84}. In particular, macrophages cultured on hydrogels with a stiffness of 20 kPa or more have increased nuclear YAP, enhancing their response to the inflammatory agonist lipopolysaccharide⁸⁴.

Dendritic cells

DCs are the dominant population of professional APCs that present antigens to naive T cells and B cells⁸⁵. Activation of DCs by their endogenous PRR or other inflammatory mediators leads to the overexpression of specific activation markers, such as CD80, CD83, CD86, and MHC class I and class II. In addition to biochemical stimuli^{86–88}, DCs sense mechanical cues through ion channels, integrins and the YAP/TAZ pathway, influencing DC biology (migration, antigen uptake, IS formation)^{88–90}. Shear stress activates mechano-gated ion channels of circulating DCs, inducing high expression of activation markers MHC

Q12

Q13

Q14

Q15

Q16

class I and CD86⁹¹ and forming podosomes, which improve their adhesion and migration abilities^{91,92}. Once infiltrated in the inflamed stiff tissue, DCs adjust their activation levels and cytokine secretion. DCs cultured on stiff substrates show high YAP/TAZ nuclear translocation, leading to enhanced expression of downstream genes regulating DC activation, co-stimulatory molecule (that is, CD80/CD86) expression, proliferation and metabolism⁹³. In addition, DCs modulate their antigen internalization and presentation capacities according to substrate stiffness^{93,94}. A partial explanation can be found in the recent description of substrate stiffness responsiveness of the C-type lectin receptors, which are essential for antigen internalization by DCs^{94,95}. Other studies show that DC activation through antigen uptake increases their cortical stiffness without necessarily increasing the expression of their maturation markers⁹⁶. Thus, increased DC cortical stiffness is an additional feature of maturation that further lowers the antigen concentration threshold needed for efficient T-cell activation¹¹. Indeed, actin cytoskeleton changes in mature DCs restrain ICAM lateral mobility, which promotes T-cell priming via affinity regulation of LFA-1 expressed by interacting T cells⁹⁷. Finally, stiffness of the environment impacts mechano-gated ion channels that regulate the secretion of polarizing cytokine interleukin-12 (IL-12) by DCs, resulting in T helper cell 1 (T_H1) differentiation, inhibition of regulatory-T-cell lineage commitment and tumour growth inhibition⁹⁸.

Q17

Lymphocytes (T cells, NK cells and B cells)

Upon scouting throughout the body, lymphocytes recognize characteristic biochemical features that lead to their activation. Lymphoid cells also encounter different environments in which they can sense mechanical cues through mechanosensitive receptors, including integrins^{99,100}, ion channels (for example, TRPV4, PIEZO)¹⁰¹, the T-cell receptor (TCR)^{102,103} and cytoskeletal components^{104,105}, and convert these biomechanical stimuli to biochemical signals (migration, scanning, activation and so on). Emerging evidence shows mechanical cues govern CD4⁺ and CD8⁺ T-cell activation and effector functions. When seeded on stiff artificial substrates presenting CD3 and CD28 antibodies, mouse and human naive CD4⁺ T cells show higher proliferation, metabolism and cytokine production^{8,10,106}. TCR-related ZAP70 and Src kinases are phosphorylated in response to mechanosensing^{8,107}. The stiffening of professional APCs also seems to enhance CD4⁺ and CD8⁺ T-cell activation¹¹. Upon activation, the TCR not only senses mechanical cues of its environment but also exerts active pulling forces against their antigen^{102,108,109}. DNA-based tension sensors (see Box 1 on techniques) revealed that T cells harness cytoskeletal coupling to transmit 12–19 pN forces per TCR, initiating strong T-cell activation^{103,110}. Co-stimulation by CD28 further increases cellular force generation on TCR adhesions¹⁰⁸. Moreover, TCR activation induces the inside-out upregulation of integrins, providing synergistic adhesive strength and mediating force transmission at the IS^{111–113}. Other mechanoreceptors, such as PIEZO1, also synergize with TCR mechano-activation¹¹⁴. Mechano-activation of lymphocytes by TCR signalling also triggers cytoskeleton changes, inducing cytotoxic granule polarization and IS formation^{111,112,115,116}. Besides, cytoskeleton disruption by pharmacological small molecule inhibitors (for example, latrunculin A, blebbistatin, nocodazole) completely abolishes immune cell stiffness-dependent activation and cytokine secretion^{14,15,117}. In that way, cytoskeleton changes act as a second layer of mechanosensing by T cells. While naive T cells have a stiff cortical cytoskeleton, effector T cells are typically softer, resulting in the formation of larger IS with APCs¹⁰⁴. This observation suggests that in addition to TCR mechanosensing and force exertion, the baseline cytoskeletal state controls T-cell responsiveness.

Similarly, NK cells sense the mechanical features of their environment that synergize with biochemical signals to modulate their activation and inhibition^{11,66,118,119}. Stiff substrates coated with antibodies directed against LFA-1 or the natural cytotoxicity receptor Nkp30 stimulate NK-cell degranulation by recruiting phosphorylated ZAP70

to the NK IS^{120,121}. Stiff substrates also induce strong clustering of DNAX-protein 10, whose hexameric complex with NKG2D activates signalling in NK cells^{66,122}. On the contrary, softer substrates impair microtubule organizing centre polarization, lytic granule polarization and F-actin accumulation at NK IS, leading to the formation of unstable asymmetrical synapses and decreased degranulation¹²³. How NK cells sense the mechanical features of their environment is still unclear, but a recent study leans towards mechano-gated ion channels¹²⁴.

Like T and NK cells, B-cell activation is also modulated by the mechanical properties of their environment and partners, notably by the stiffness of the APCs¹²⁵. Antigens presented on stiff substrates induce higher B-cell receptor microcluster formation compared with antigens tethered to soft substrates, leading to increased B-cell activation¹²⁵. In addition, B cells are also able to differentiate high-affinity antigens from low-affinity antigens tethered on the APC by using diacylglycerol kinase ζ and myosin IIa to pull-out and invaginate the APC membranes presenting high-affinity antigens^{126,127}. Therefore, substrate stiffness has a crucial role in B-cell activation, affinity maturation, class switch and antibody responses^{128,129}. Although stiff substrates have been reported to induce better B-cell receptor clustering, high-affinity antigen extraction and affinity maturation, soft substrates, on the other hand, appear to be preferable for class switch and T-cell-independent antibody responses¹²⁸. Altogether, the physical extraction of environmental signals by B cells accelerates their adaptation but may also cause the extinction of unfitted cell populations¹³⁰.

Evidence and mechanisms of mechano-immune surveillance

Anti-infection mechano-immunology

Viruses and bacteria can modify the host mechanobiology at the single cell or the tissue levels to evade immunosurveillance. At the host-cell level, the mechanical evasion from immunosurveillance is often mediated by a remodelling of the actin cytoskeleton. For example, upon infection, the human cytomegalovirus expresses the pUL135 protein, inducing remodelling of the actin cytoskeleton. Such a process is characterized by actin stress fibre loss, which markedly reduces the efficiency of IS formation upon recognition by immune cells¹³¹. This trait is exploited by human cytomegalovirus to protect the host cell against cytotoxic immune effector cells and to promote viral proliferation. Likewise, bacteria can also impair IS assembly by either reducing antigen presentation by APCs in *M. tuberculosis* infections¹³² or by increasing T-cell actin polymerization, thereby impairing the ability of T cells to scan APCs in *Shigella*-mediated diarrhoeal diseases¹³³.

Nevertheless, actin cytoskeleton modifications can eventually serve as damage-associated molecular patterns to activate the immune system. For instance, F-actin is recognized by DNGR-1 specifically expressed in DCs, leading to cross-priming of cytotoxic T lymphocytes (CTLs) in virus-infected mice¹³⁴. Actin polymerization is also required to induce NLRC4 inflammasome and to secrete antimicrobial molecules by bone-marrow-derived macrophages¹³⁵.

While altered biophysical properties of infected cells lead to immune evasion at the single-cell scale, pathogen-infected tissues with altered mechanical properties at the tissue level induce potent immune activation. Early activation of PRRs in Langerhans cells and stromal cells activated by virus- and bacteria-derived danger signals triggers the secretion of copious amounts of hyaluronic acid to promote oedema and attract immune cells to the infection site⁴⁴. Mechanical forces applied on immune cells when they squeeze through the endothelium and dense ECM drive chromatin changes that promote inflammation and chemotaxis-related transcripts¹³⁶. At the same time, oedema-induced tensile stress and hydrostatic pressure encountered by innate immune cells activate their mechanosensitive ion channels (PIEZO1, TRP and so on), priming them for bioenergetic demands of activation and reducing the threshold required for optimal PRR

Q18

Q19

Q20

stimulation^{80,93,137}. These ion channels play an important role in the early immune response against infections as their depletion abrogates the inflammatory response that clears pathogens^{137,138}.

Upon immune-response progression, T cells migrate and proliferate in the lymph node, which causes local stiffening and swelling¹³⁹. Lymph node tissue mechanics can be sensed by T cells, which further promotes their proliferation, activation and metabolism while lowering the antigen dose needed to elicit effector responses¹³⁹. Stiffness of the environment can be sufficient to prime T cells, as reported in a recent study. Indeed, T cells that crawl through stiff 40 kPa matrices show enhanced activation, regardless of the stiffness level of the APC that interacts with them¹⁰⁶. Activated T cells will eventually migrate to an infection site where they will experience multiple mechanical stimuli. Notably, migrating T cells interact with secreted hyaluronic acid through CD44, a key mechanosensitive receptor involved in T-cell extravasation¹⁴⁰. Additional studies will be necessary to decipher whether this interaction promotes or suppresses T-cell activation. Finally, mechanical changes in tissues are reverted during infection resolution, with dissolution of hyaluronic acid, reduced oedema and impaired immunity to danger signals. However, chronic inflammation can sometimes arise from a positive association of mechanical stimulation, T-cell-dependent T_H2 cytokine (IL-4 and IL-13) and chemokine (MCP-1) signalling, leaving a lasting mechanical imprint at the inflammatory response site¹⁴¹.

Q21

Anticancer mechano-immune surveillance

Anticancer immune surveillance kicks in early after malignancy and the immune system patrols throughout the body to identify and destroy nascent tumours¹⁴². NK cells and CTLs recognize transformation-associated molecules and tumour-associated antigens expressed on the surface of tumour cells¹⁴³. Upon formation of the IS between cancer cells and lymphocytes, lymphocytes secrete the pore-forming protein perforin, which allows entry of death-inducing toxic granzymes and lysis of target cancer cells¹⁴⁴. Although tumour cell killing had been mostly linked to canonical signalling pathways involving receptor–ligand recognition, recent evidence demonstrates that lymphocytes also sense tumour-dependent mechanical cues (see Section 2) and respond accordingly towards target cells. Upon tumour infiltration and IS formation, NK cells and CTLs exert up to nanonewton-scale cellular forces towards target cells^{102,108,109}. The force exerted at the IS regulates the cytotoxic responses in several ways. Mechanical cues are transduced inside lymphocytes from the plasma membrane into the nucleus through the linker of the nucleoskeleton and cytoskeleton complex. This leads to the expression of target genes (for example, *CD69*, *IL2*, *IFNG*), lymphocyte activation and the formation of a mature IS¹⁴⁵. Forces exerted at the IS also directly influence lymphocyte-mediated cytotoxicity by increasing membrane tension and potentiating lysis of target cells^{12,15}. During this process, surface receptors (for example, TCR, $\alpha_1\beta_2$ integrin LFA-1, NKG2D) at the IS change their conformation to form catch bonds with their respective ligands. Such catch bonds were found to rely on forces to achieve high affinity for their ligands^{103,146,147}. The forces exerted at the IS heavily depend on the target cell's mechanical profile and compliance. Hence, it is important to note that the biophysical properties of the targeted tumour cells profoundly regulate the killing processes¹². We and others recently found that the softness of cancer cells, independently of other biochemical features, acts as an 'immune checkpoint' of mechanical nature (or termed 'mechanical immune checkpoint'), which induces immune evasion of lymphocyte-mediated cytotoxicity^{13–15}. The immune system is consequently more sensitive to stiff(er) tumour cells, yet the mechanisms must be fully unravelled (Fig. 2). First, stiff cancer cells may allow higher synaptic force exertion by lymphocytes, which potentiates cytotoxicity by enhancing target cell membrane tension to facilitate pore formation mediated by perforin^{12,15}. Second, the mechanics of target cells probably impact

Q22

the strength and morphology of the IS. Lymphocytes spatiotemporally coordinate the force exertion and perforin secretion within the synapse by forming Wiskott–Aldrich-syndrome-dependent interfacial actin-based protrusions^{112,148,149}, which could be enhanced when encountering stiffer target cells. Third, stronger activating signalling through lymphocyte's mechanosensitive receptors exerted by stiffer target cells could also increase the degranulation and cytokine production, leading to enhanced cytotoxicity^{14,15}. Once cancer cell killing is achieved, immune cells sense the cytoskeletal contraction of apoptotic targets and respond to this mechanosensory feedback by dissolving the IS. Such IS turnout is critical for serial killing by CTLs and apoptotic body clearance by patrolling phagocytes¹⁵⁰. Altogether, immune cells, particularly CTL and NK cells, modulate their activation and cytotoxic functions according to the biophysical status of the cancer cells that they probe. This biophysical angle of immunosurveillance has led to the emergence of a new unique field of 'mechano-immune surveillance'.

Several strategies have been reported to stiffen cancer cells for therapeutic purposes. Cholesterol enrichment in the plasma membrane reduces the cortical (plasma membrane and the underlying dense actin network) stiffness of cancer cells^{151,152} in many types of cancer. One can thus envision that stiffening tumour cells by depleting membrane cholesterol with methyl- β -cyclodextrin (Me β CD), a cholesterol scavenger, could be a promising therapeutic intervention¹⁵. Treatment with Me β CD efficiently decreased the cholesterol levels at the plasma membrane of mouse and human cancer cells. It further increased the target cell stiffness, and sensitized the cancer cells towards T-cell-mediated killing in vitro and in vivo. Impressively, the combination therapy of Me β CD and adoptive transfer of tumour-specific T cells adjuvanted with an IL-15 super-agonist (IL-15SA) increased the rate of complete tumour eradication to 41.7% compared with 0% in the case of immunotherapy alone. In another elegant study, a subset of metastatic cancer cells was found to overexpress MRTFs, a cytoskeletal-associated transcriptional factor known to promote cancer migration and metastasis³⁶.

Interestingly, MRTF overexpression also enhances F-actin polymerization and, thereby, the stiffness of cancer cells. By inducing MRTF overexpression, the cancer cells increase their membrane tension, becoming more susceptible to T-cell and NK-cell-mediated cytotoxicity due to increased degranulation and cytokine production¹⁴. Of note, the selective depletion of F-actin in cancer cells completely abolishes the immune sensitization induced by MRTF overexpression, confirming the biophysical basis of these observations. Similarly, treating cancer cells with jasplakinolide, an actin polymerization promotor, also increased the stiffness of tumour-repopulating cells, a specific population among tumour cells that show features of self-renewal, low differentiation, high tumourigenicity and, in particular, softness and resistance towards T-cell-mediated killing¹³. Therefore, the combination of jasplakinolide, adoptive T-cell transfer therapy and PD-1 antibody improved the therapeutic efficacy in a mouse melanoma model.

Q23

Q24

Current and future strategies towards mechanical immunoengineering to improve immunotherapies

Targeting mechanical adaptability of tumour cells

As discussed above, antitumour mechanical immune checkpoints can be targeted therapeutically. Indeed, soft cancer cells can be stiffened and sensitized towards current immunotherapies, including immune checkpoint blockade antibodies and adoptive T-cell transfer^{13–15} (Fig. 3). Such discovery is also clinically relevant as soft human cancer cells also show resistance to perforin-mediated killing¹³. Moreover, patients with melanoma exhibiting constitutive actin cytoskeleton-mediated stiffening are found to present enhanced responsiveness to immune checkpoint blockade therapy¹⁴. Yet, tumour cell mechanics cannot be

Q25

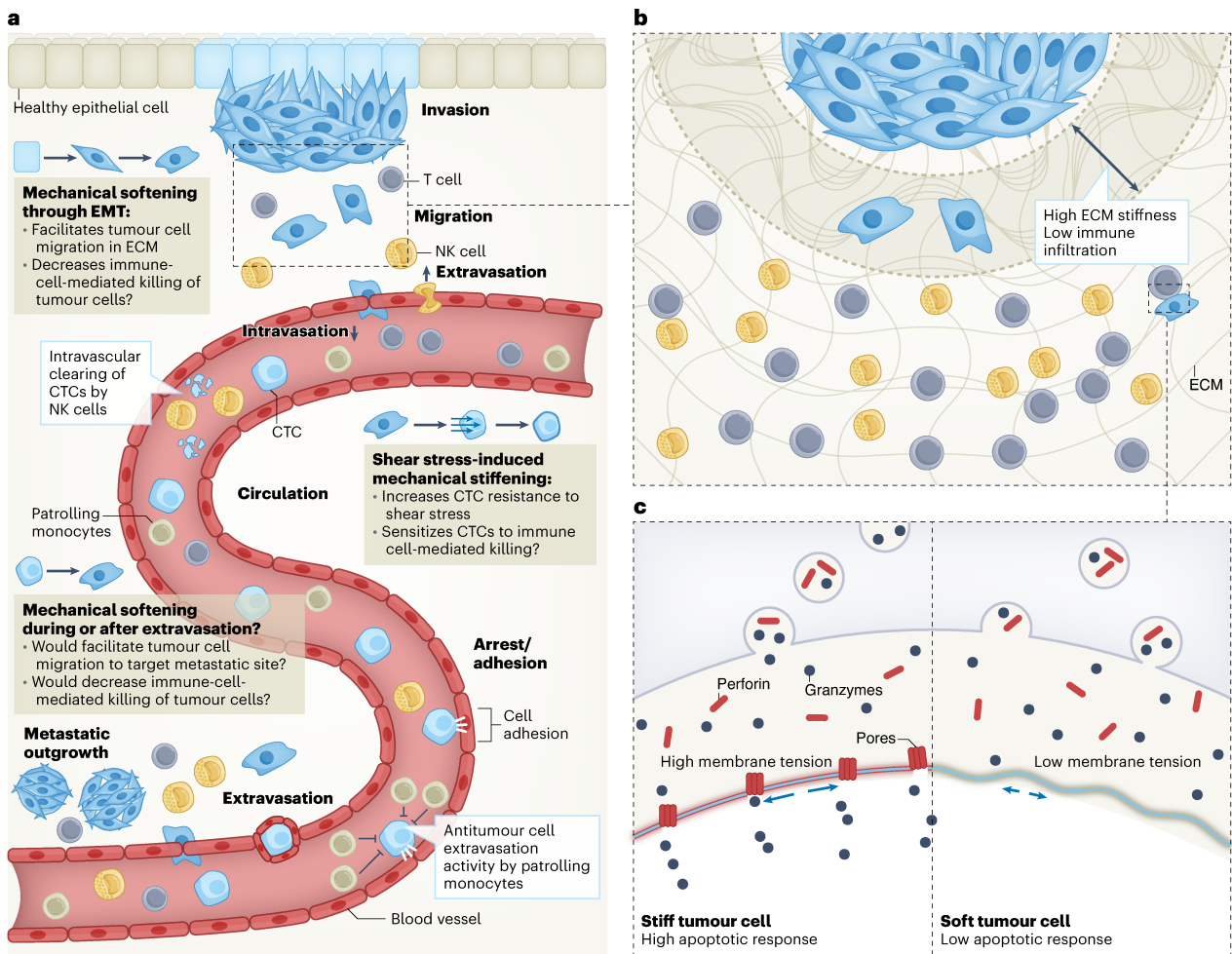


Fig. 2 | Spatiotemporal windows for optimal mechanical antitumour activity of immune cells. a, Tumour cells are probably adjusting their mechanical properties as they progress through the metastatic cascade. Following transformation of healthy epithelial cells and rise of a primary tumour, a select number of cancer cells will get softer as they go through the epithelial–mesenchymal transition (EMT) and perform invasion and migration. They later undergo stiffening as they enter the blood flow and become CTCs. As such, taking advantage of the optimal time windows when interactions between immune cells and stiffened tumour cells are most likely to occur might be key when establishing therapeutic strategies. Examples include NK cells performing

intravascular clearing of CTCs and patrolling monocytes exerting antitumour cell extravasation activity. **b**, Alternatively, windows in which immune cells show shortcomings could be identified to leverage mechanical immunoengineering and help them overcome them. The primary tumour site with its stiffened ECM and softened tumour cells represents a good example of such windows, with suboptimal mechanical features for NK- and T-cell antitumour activity. **c**, The aim should be to get immune cells in contact with tumour cells as stiff as possible as increased target cell stiffness favours IS formation and potentiates perforin and granzyme-dependent cytotoxic activity of immune cells.

Q26

a binary process where softness would fully explain and correlate with malignancy and metastatic progression. On the contrary, we believe that cancer cells are ‘dynamic and adaptable’ to perform and survive through the multiple mechanical and biochemical constraints they face along their path to metastasis²⁷ (as discussed in Section 1A). Their mechanical plasticity is an additional hallmark of metastatic progression that is likely to impact mechano-immune surveillance with, in theory, spatiotemporal windows in which immune cells can most efficiently recognize and kill tumour cells. As CTCs may get stiffened in response to the hostile haemodynamic forces in the circulation, we expect them to be, at this moment, the most vulnerable to T- and NK-cell-mediated killing, whose efficiency is likely also impacted by shear forces¹⁰¹.

Recent studies have reported that CTCs could indeed be sensitive to immune cell-mediated killing, which contributes in part to the

inefficiency of the metastatic process^{153–155}. One of them showed that NK cells could clear tumour cells in the intravascular environment around the liver site and limit tumour cell seeding at a distant site in the lung. That same study highlighted an efficient synergy between NK cells and T cells, with the NK cells killing tumour cells in circulation and promoting T-cell recruitment, which would then restrict metastatic foci growth *in situ*¹⁵⁴. In addition, patrolling monocytes might also contribute to antitumour activity in the circulation by directly scavenging tumour materials, secreting cytokines¹⁵⁶ and recruiting NK cells^{153,157}. While evidence of intravascular antitumour activity of immune cells exist, this metastasis stage appears challenging to exploit because of the highly dynamic movement and low frequency of tumour antigen-specific T cells in the circulation¹⁵⁸.

Instead, stiffening tumour cells during the invasion and migration processes, at which stage they typically display soft mechanical phenotypes, may be a promising strategy to sensitize them to T- and

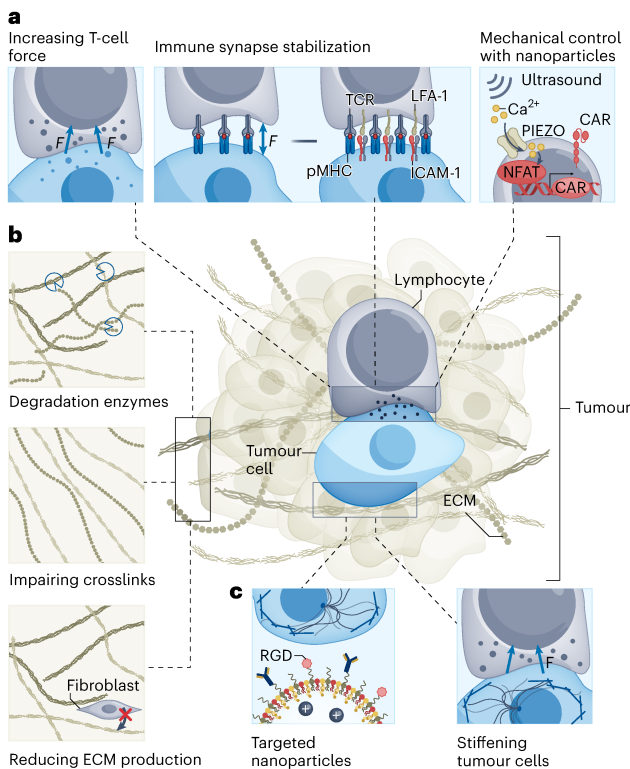


Fig. 3 | Improving therapies through mechanical immunoeengineering of tumours and immune cells. Immune cells, tumour cells or the ECM of the tumour environment can be targeted using different strategies aiming at modulating the mechanical features of the immune response. **a**, Potentiating the mechanical activity of T cells (grey) can be achieved by enhancing their force exertion abilities, increasing the stability of immune synapses composed of the TCR (blue) recognizing tumour-associated antigens presented by MHC class I (dark grey) and integrins, or controlling spatiotemporal activation of key genes through novel tools (for example, microbubbles and ultrasounds). **b**, Inducing ECM remodelling through release of degradation enzymes, impairing ECM crosslinking with inhibitors, or decreasing ECM protein production in fibroblasts can improve immune cell infiltration to target disease sites. **c**, Altering the mechanical properties of tumour cells (pink) to increase force transmission at the IS and potentiate antitumour activity of immune cells can be achieved by using stiffening agents such as Me β CD, or nanoparticles loaded with anticancer drug or gene therapy.

NK-cell-mediated killing. Enhancing cancer cell stiffness could also favour macrophage engulfment as the target stiffness could partially override the SIRP α -CD47 'don't eat me' immune checkpoint⁷⁶. Previous studies have shown that depleting membrane cholesterol using Me β CD¹⁵, activating myosin with 4-HAP¹⁵⁹ or inducing actin crosslinking with jasplakinolide^{13,28} can stiffen cancer cells. However, none of these pharmacological approaches are specific. A challenging aspect of such strategies is to find ways to specifically stiffen the tumour cells without stiffening the ECM, which would hinder immune cell infiltration, possibly trigger pro-metastatic mechanotransduction in tumour cells and all-in-all be counterproductive. Tumour-targeted-nanoparticles might be a promising tool for achieving specific stiffening of tumour cells¹⁶⁰. Moreover, their own mechanical properties can be tuned to foster their internalization in tumour cells. Soft nanomaterials and microparticles tend to better accumulate in tumour tissues and be preferentially taken up by cancer cells^{161,162}. In a recent example, anticancer drug-loaded nanoparticles were developed to target soft cancer stem cells, allowing their specific

elimination *in vitro* and *in vivo* with minimal side effects¹⁶³. Besides, recent studies have also demonstrated that cancer cells can be transiently stiffened through increased F-actin polymerization upon internalization of iron oxide nanoparticles¹⁶⁴. Cytoskeleton alterations and cell stiffening upon nanoparticle internalization have been described in macrophages¹⁶⁵ and such an approach might also be applied to tumour cells. As an alternative mechanical intervention approach, gene therapies for overexpression of MRTF and acyl-CoA:cholesterol acyltransferase 1 might be promising to facilitate specific stiffening of cancer cells^{14,15}.

Targeting tumour ECM mechanics for enhanced immunotherapy

The tumour microenvironment (TME) is known to impair anticancer immune responses. In addition to the highly immunosuppressive biochemical signals in the TME¹⁶⁶, its biophysical properties play a crucial role in immune cell migration and activation. During malignant progression, increased ECM stiffness together with other biochemical changes (for example, integrin clustering, altered chemokine profile) alter infiltration of T cells and other anticancer immune cells, and restricts them away from tumour cell nests, which reduces their antitumoural capacities^{22,167,168}. Factors including TGF β , matrix components and integrins are known to control the mechanical properties of the tumour ECM and its sensing by cancer cells. In addition, recent studies have shed light on how ECM mechanical properties might impact tumour cell dormancy^{169,170}. Therefore, targeting actors of ECM stiffness and improving the diffusion of chemotherapeutic drugs and/or immune cells is a therapeutic approach with clinical potential¹⁷¹ (Fig. 3). Inhibiting the production of matrix components by fibroblasts can be achieved by blocking the TGF β profibrotic pathway. The use of neutralizing antibodies or the repurposing of angiotensin inhibitors, such as Losartan, has been shown to efficiently reduce collagen and hyaluronic acid production^{172,173}. Collagen fibre alignment can also be reduced by targeting the discoidin domain receptor 1 (DDR1) ectodomain with monoclonal antibodies¹⁶⁹. This strategy restores T-cell invasion into the tumour bed, resulting in remission in 56% of treated mice bearing triple-negative breast cancer. Conversely, DDR1 has been described to sustain tumour cell dormancy by maintaining type III collagen fibre at a low degree of alignment¹⁷⁰. Hence, DDR1 depletion and subsequent realignment of collagen fibres was found to be a key trait of the dormancy-to-reactivation transition¹⁷⁰. Of note, this study also indicates that enriching the TME with collagen III could promote or even induce a dormant state, thus preventing the formation of metastases¹⁷⁰.

Hyaluronic acid can also be reduced in the tumour ECM by using degradative enzymes, such as the pegvorhyaluronidase alfa investigated in a phase III clinical trial in association with gemcitabine for patients presenting hyaluronan-high metastatic pancreatic adenocarcinoma (NCT02715804)¹⁷⁴. However, the use of hyaluronidase might also degrade avascular cartilage. A hyaluronidase nanoformulation showed no accumulation at these sites¹⁷⁵. When combined with gemcitabine to treat a pancreatic ductal adenocarcinoma mouse model, the hyaluronidase nanoformulation resulted in a near doubling of overall survival¹⁷⁵. The safety of use can be further improved by developing TME-responsive nanoparticles. Reactive-oxygen-species-activatable collagenase is selectively activated in the TME, significantly relieving ECM stress and increasing paclitaxel penetration¹⁷⁶. Degradative enzymes of ECM components can be used to enhance adoptive cell transfer immunotherapies. One strategy relies on engineered chimeric antigen receptor (CAR)-T cells secreting heparanase, which degrades heparan sulfate proteoglycans, one of the main components of the ECM¹⁷⁷. These heparanase-secreting CAR-T cells showed improved ECM degradation capacity, which promoted immune cell infiltration in tumour xenografts, resulting in increased survival of treated mice¹⁷⁷. Recently, new strategies based on the bioorthogonal modification of the surface of immune cells to avoid viral transfection have been

developed^{178,179}. CAR-T cells cultured with azide-containing saccharides allowed for metabolic incorporation and membrane expression of azide groups for further conjugation with dibenzocyclooctyne-modified hyaluronidase through click chemistry¹⁸⁰. These hyaluronidase-modified CAR-T cells presented better infiltration in the tumour, which correlated with improved tumour regression and survival.

As an alternative strategy, ECM stiffness can be reduced by preventing matrix crosslinking. Lysyl oxidase (LOX) is an enzyme responsible for the reticulation of collagen fibres¹⁷. Its inhibition by β -aminopropionitrile allowed to overcome chemoresistance and increase intratumoural T-cell migration, thus improving response to anti-PD-1 therapy^{181,182}. The co-encapsulation of LOX inhibitors and epirubicin resulted in better biocompatibility and prolonged survival, providing an all-in-one nanoparticle-based ECM-targeting chemotherapy for cancer treatment¹⁸³. Nanoparticle-based approaches can also be used to assess LOX activity in the tumour ECM and allow selection of patients that may benefit from LOX inhibitor treatments in addition to their chemotherapy¹⁸⁴. Other studies have shown that LOX antibodies functionalized on polymeric PLGA nanoparticles efficiently decrease the expansion of breast cancer¹⁸⁵.

Finally, inhibiting fibroblast contractility may help to reduce global ECM integrity. Among the different targets, the use of fasudil to inhibit the Rho-associated protein kinase leads to loss of stress fibres and focal adhesion complexes¹⁸⁶. Fasudil treatment, hence, alters cytoskeleton-based contractility of fibroblasts, disrupting ECM integrity and improving chemotherapy effectiveness¹⁸⁶. Other studies have shown that focal adhesion kinases can be directly inhibited, reducing ECM force transmission to the actomyosin complex, and thus reducing cellular response to matrix mechanical cues. A focal-adhesion-kinase inhibitor (AMP945) improved response to gemcitabine in a pancreatic adenocarcinoma model and is now being investigated in a phase II clinical trial for this indication (NCT05355298)¹⁸⁷. However, these molecules can lead to life-threatening adverse events, such as hypotension, hepatotoxicity and excessive bleeding. Efforts to develop targeted formulations of these molecules are still required to improve their safety in clinics. CAFs expressing the fibroblast activation protein (FAP) are found in nearly all solid tumours and can be depleted by using anti-FAP CAR-T cells. Several studies have evaluated the use of anti-FAP CAR-T cells, and it has been shown that depletion of FAP⁺ stromal cells results in decreased tumour growth in an immune-dependent fashion^{188,189}. Of interest, this strategy is also investigated to treat post-cardiac infarction fibrosis and to restore cardiac function¹⁹⁰. While killing fibroblasts at the primary tumour site could reduce global ECM stiffness, their destruction in target organs of dissemination could help to maintain tumour cell dormancy¹⁹¹. Indeed, hepatic stellate cell activation upon chronic liver injury induces a myofibroblast-like phenotype that further disrupts NK-cell-sustained breast cancer dormancy¹⁹¹. As FAP is also expressed by skeletal muscle, adipose tissue and pancreas, depleting FAP⁺ stromal cells can lead to muscle atrophy, bone marrow hypoplasia and rapid weight loss¹⁹².

Strategies to soften the ECM have been extensively studied to enhance the diffusion of chemotherapeutic drugs into the tumour bed and could favour tumour targeting of other therapeutics, such as antibodies or CAR-T cells, whose access is also hindered by the stiff ECM^{22,193}. Yet, only a few studies have investigated the perspective of ECM stiffness disruption to increase intratumoural T-cell migration and response to PD-1 blockade^{169,177,180,182}. As ECM proteins cover a large part of the physical barrier hindering immune cell migration, strategies involving engineered CAR-T cells capable of degrading ECM proteins are elegant due to their abilities to degrade ECM while migrating and performing tumour cell killing. The therapeutic advantage of ECM softening in immune checkpoint blockade and cellular immunotherapies remains to be evaluated. Yet, due to the potential opposite functions of some targeted molecules, any therapeutic strategy aimed at influencing the ECM architecture will require careful planning and timing.

Finally, combining these approaches with methods to control cell mechanics in an all-mechanics strategy, could synergistically enhance antitumour immune surveillance.

Mechanical immunoengineering for enhanced T- and NK-cell-based immunotherapy

Most immunotherapies currently aim at targeting biochemical cues of tumours and immune cells to enhance the immune response. The emergence of the ‘mechano-immune surveillance’ concept paves the way for developing next-generation therapeutic strategies targeting biophysical features of immune cells to boost their functions against various diseases. Selective delivery to immune cells could be achieved by targeting selective immune markers with antibody–nanoparticle conjugates¹⁶⁰. One such approach of mechanical immunoengineering could aim at enhancing the tumour infiltration of T cells. As described previously, tumour ECM presents a mechanical hurdle for antitumour immune cells to access the tumour bed^{22,167,168}. One could circumvent that by further favouring the through-matrix migration potential of immune cells. For example, pharmacological or genetic manipulation of microtubules of T cells increases Rho-pathway-dependent cortical contractility, which favoured infiltration in a three-dimensional environment *in vitro* by shifting CD4⁺ T cells towards an amoeboid phenotype¹⁹⁴. In stark contrast, microtubule stabilization with a commonly used drug, taxol, induced a marked reduction in T-cell infiltration abilities.

Another strategy is to enhance the mechanosensitivity of immune cells. Mechanical force exertion and underlying actin remodeling are essential for IS formation and stabilization^{109,112,115,116}. Indeed, treatment of T cells with the actin polymerization inhibitor latrunculin A resulted in complete abrogation of force exertion by T cells and consequent loss of activation and effector functions¹². In contrast, modulation of actin polymerization-stimulating proteins at the lymphocyte/APC interface could provide a strategy for enhancing T-cell force exertion and thereby, possibly enhancing effector function and cytotoxicity. A series of studies showed that CTLs with phosphatase and tensin homologue (PTEN) knockdown show increased force exertion and significantly enhanced tumour cell killing *in vitro*¹². While CTL granule polarization and release were unaffected by PTEN knockdown, this strategy led to limited improvement of tumour growth control *in vivo*¹⁹⁵. Nevertheless, the involvement of PTEN in numerous cellular processes makes it challenging for systemic inhibition of PTEN using pharmacological or genetic therapies, representing a key limitation in this strategy.

As an alternative approach, one may engineer T cells capable of developing a stable IS (Fig. 3). The canonical IS is characterized by a concentric architecture in which a central cluster of antigen-presenting receptors is surrounded by concentric, annular accumulations of integrins and F-actin¹⁴⁰. In contrast to the IS of the TCR:peptide–MHC complex, the non-classical CAR IS shows less-organized structures with diffusive CAR:antigen clustering and reduced actin distribution¹⁹⁶. As the IS structure and morphology influence the effector functions, CAR-NK cells have recently been engineered with a novel receptor that modulates and tunes the IS to a more ordered state¹⁹⁷. Fusing a second-generation CAR with the post-synaptic density protein 95, *Drosophila* disc large tumour suppressor and zonula occludens-1 protein (PDZ) domain of a molecule implicated in IS formation, the cytotoxic and regulatory-T-cell-associated molecule, resulted in increased synaptic area and accumulation of pZAP70, a key kinase in T-cell signalling¹⁹⁷. Moreover, the PDZ domain enabled additional scaffolding crosslinks between the CAR and the cytoskeleton via mediators such as ezrin. Anchoring the receptor to cytoskeletal components enhanced the avidity and binding strength of IS thus succeeding in higher antitumour activity. CAR-T and CAR-NK cells were elegantly developed with synthetic Notch receptor (SynNotch) or apelin-based synthetic Notch receptor to increase their safety and expand the set of targetable antigens¹⁹⁸. Activation of these receptors by their cognate ligand caused

Q30

Q31

Q32

the proteolytic cleavage of their intramembrane domain, releasing a transcriptional factor that could activate a specific transcriptional programme (expression of a CAR, cytokines and so on)¹⁹⁹. Structure-guided mutagenesis was also used to develop new cutting-edge designs of SynNotch receptors capable of increasing mechanical sensitivity to the piconewton range²⁰⁰. In response to varying tensile forces, these receptors are expected to enact tailored transcriptional programmes. These studies provide evidence that tuning the IS via anchoring domains or by repurposing SynNotch receptors to increase mechanosensitivity might offer an orthogonal and complementary dimension to biochemical engineering for CAR-based immunotherapies.

In addition, nanoparticles can be leveraged to improve immune cell activation. Several types of artificial APC composed of nanoparticles coated with anti-CD3, anti-CD28 or peptide–MHC complex have been developed²⁰¹ and can be used to trigger T-cell activation and expansion in vitro by TCR clustering under a magnetic field^{202,203}. After adoptive cell transfer, these ex vivo-activated T cells showed better tumour control. Some ultrasmall silica nanoparticles can directly ligate the TCR:CD3 complex and activate the T cells²⁰⁴. As ultrasmall nanoparticles avoid liver accumulation and are quickly eliminated by renal clearance, they present very promising clinical translation prospects. A similar strategy has been evaluated for NK-cell activation. Magneto-activated NK cells show increased secretion of lytic granules correlating with therapeutic efficacies against hepatocellular carcinoma^{205,206}. Other optomechanical actuators can be used to trigger immune cell activation such as optical systems²⁰⁷ or ultrasounds²⁰⁸. However, these optical systems are poorly transferable in vivo due to the low light penetration through tissues (micrometres to millimetres)²⁰⁹. On the other hand, ultrasounds can penetrate tissues up to several centimetres. A sonic stimulus of integrin-bound microbubbles was used to induce calcium influx²¹⁰ through PIEZO1 channels in T cells in vitro. This was followed by the nuclear factor of activated T cells transcription factor translocation to the nucleus, which drove expression of T-cell activation genes. Despite the originality of this approach, in vivo translation is limited as shear forces will probably damage or burst the microbubbles coupled to T cells during their migration and extravasation.

Outlook

This Review has outlined the changes in cellular and tissular biomechanical properties arising in several pathological processes such as infectious diseases, fibrosis and, most importantly, cancer. We highlighted how immune cells sense these biomechanical changes and tune their response accordingly. The recent advances in the understanding of disease mechanobiology impact on immune surveillance mechanisms gave birth to a promising mechanical immunoengineering field where additional in vivo studies in preclinical models will be instrumental to develop efficient therapies. Preliminary studies have shown that different approaches can leverage immune cell mechano-activation. Nevertheless, each target should be thoroughly analysed and evaluated for its potential for desired therapeutic applications. In the context of cancer in particular, a further and closer inspection of tumour cell mechanics and how it evolves and adapts throughout disease progression is warranted to optimize the inhibitory tools. Although many challenges arise, mechanical modulation of effectors and/or targets, through genetic, pharmacogenetic or nanomedicine approaches is expected to evolve and gain precision in the future. We envision that mechanical immunoengineering will lead to a paradigm shift in the design of next-generation immunotherapy by combining approaches targeting biochemical and biophysical disease–immune interactions.

References

- Klotter, V. et al. Assessment of pathologic increase in liver stiffness enables earlier diagnosis of CFLD: results from a prospective longitudinal cohort study. *PLoS ONE* **12**, e0178784 (2017).
- Medrano, L. M. et al. Elevated liver stiffness is linked to increased biomarkers of inflammation and immune activation in HIV/hepatitis C virus-coinfected patients. *AIDS* **32**, 1095–1105 (2018).
- Tomlin, H. & Piccinini, A. M. A complex interplay between the extracellular matrix and the innate immune response to microbial pathogens. *Immunology* **155**, 186–201 (2018).
- Martinez-Vidal, L. et al. Causal contributors to tissue stiffness and clinical relevance in urology. *Commun. Biol.* **4**, 1011 (2021).
- Mohammadi, H. & Sahai, E. Mechanisms and impact of altered tumour mechanics. *Nat. Cell Biol.* **20**, 766–774 (2018).
- Du, H. et al. Tuning immunity through tissue mechanotransduction. *Nat. Rev. Immunol.* <https://doi.org/10.1038/s41577-022-00761-w> (2022).
- Zhu, C., Chen, W., Lou, J., Rittase, W. & Li, K. Mechanosensing through immunoreceptors. *Nat. Immunol.* **20**, 1269–1278 (2019).
- Judokusumo, E., Tabdanov, E., Kumari, S., Dustin, M. L. & Kam, L. C. Mechanosensing in T lymphocyte activation. *Biophys. J.* **102**, L5–L7 (2012).
- O'Connor, R. S. et al. Substrate rigidity regulates human T cell activation and proliferation. *J. Immunol.* **189**, 1330–1339 (2012).
- Saitakis, M. et al. Different TCR-induced T lymphocyte responses are potentiated by stiffness with variable sensitivity. *eLife* **6**, e23190 (2017).
- Blumenthal, D., Chandra, V., Avery, L. & Burkhardt, J. K. Mouse T cell priming is enhanced by maturation-dependent stiffening of the dendritic cell cortex. *eLife* **9**, e55995 (2020).
- Important work that sheds light on the mechanical aspect of dendritic cell-mediated activation of T cells.**
- Basu, R. et al. Cytotoxic T cells use mechanical force to potentiate target cell killing. *Cell* **165**, 100–110 (2016).
- Seminal study that highlights the critical role of mechanical forces in cytotoxic activity of T cells.**
- Liu, Y. et al. Cell softness prevents cytolytic T-cell killing of tumor-repopulating cells. *Cancer Res.* **81**, 476–488 (2021).
- Tello-Lafoz, M. et al. Cytotoxic lymphocytes target characteristic biophysical vulnerabilities in cancer. *Immunity* **54**, 1037–1054.e7 (2021).
- Lei, K. et al. Cancer-cell stiffening via cholesterol depletion enhances adoptive T-cell immunotherapy. *Nat. Biomed. Eng.* **5**, 1411–1425 (2021).
- Influential studies (refs. 14,15) that show that stiffening tumour cells through genetic manipulation targeting MRTF or by depleting cholesterol of the cell membrane results in higher vulnerability to T-cell-mediated killing.**
- Provenzano, P. P. et al. Collagen reorganization at the tumor-stromal interface facilitates local invasion. *BMC Med.* **4**, 38 (2006).
- Levental, K. R. et al. Matrix crosslinking forces tumor progression by enhancing integrin signaling. *Cell* **139**, 891–906 (2009).
- Goetz, J. G. et al. Biomechanical remodeling of the microenvironment by stromal caveolin-1 favors tumor invasion and metastasis. *Cell* **146**, 148–163 (2011).
- Massagué, J. TGFβ in cancer. *Cell* **134**, 215–230 (2008).
- Insua-Rodríguez, J. et al. Stress signaling in breast cancer cells induces matrix components that promote chemoresistant metastasis. *EMBO Mol. Med.* **10**, e9003 (2018).
- He, X. et al. Extracellular matrix physical properties govern the diffusion of nanoparticles in tumor microenvironment. *Proc. Natl Acad. Sci. USA* **120**, e2209260120 (2023).
- Salmon, H. et al. Matrix architecture defines the preferential localization and migration of T cells into the stroma of human lung tumors. *J. Clin. Invest.* **122**, 899–910 (2012).
- Salnikov, A. V. et al. Lowering of tumor interstitial fluid pressure specifically augments efficacy of chemotherapy. *FASEB J.* **17**, 1756–1758 (2003).

24. Guck, J. et al. Optical deformability as an inherent cell marker for testing malignant transformation and metastatic competence. *Biophys. J.* **88**, 3689–3698 (2005).
25. Plodinec, M. et al. The nanomechanical signature of breast cancer. *Nat. Nanotechnol.* **7**, 757–765 (2012).
26. Chen, Y., McAndrews, K. M. & Kalluri, R. Clinical and therapeutic relevance of cancer-associated fibroblasts. *Nat. Rev. Clin. Oncol.* **18**, 792–804 (2021).
27. Gensbittel, V. et al. Mechanical adaptability of tumor cells in metastasis. *Dev. Cell* **56**, 164–179 (2021).
- This review presents the hypothesis that tumour cells adjust their mechanical properties throughout their metastatic journey.**
28. Lv, J. et al. Cell softness regulates tumorigenicity and stemness of cancer cells. *EMBO J.* **40**, e106123 (2021).
29. Matthews, H. K. et al. Oncogenic signaling alters cell shape and mechanics to facilitate cell division under confinement. *Dev. Cell* **52**, 563–573.e3 (2020).
30. Young, K. M. et al. Correlating mechanical and gene expression data on the single cell level to investigate metastatic phenotypes. *iScience* **26**, 106393 (2023).
31. Rianna, C., Radmacher, M. & Kumar, S. Direct evidence that tumor cells soften when navigating confined spaces. *Mol. Biol. Cell* **31**, 1726–1734 (2020).
32. Regmi, S., Fu, A. & Luo, K. Q. High shear stresses under exercise condition destroy circulating tumor cells in a microfluidic system. *Sci. Rep.* **7**, 39975 (2017).
33. Moose, D. L. et al. Cancer cells resist mechanical destruction in circulation via rhoa/actomyosin-dependent mechano-adaptation. *Cell Rep.* **30**, 3864–3874.e6 (2020).
34. Chen, J. et al. Efficient extravasation of tumor-repopulating cells depends on cell deformability. *Sci. Rep.* **6**, 19304 (2016).
35. Saito, D. et al. Stiffness of primordial germ cells is required for their extravasation in avian embryos. *iScience* **25**, 105629 (2022).
36. Er, E. E. et al. Pericyte-like spreading by disseminated cancer cells activates YAP and MRTF for metastatic colonization. *Nat. Cell Biol.* **20**, 966–978 (2018).
37. Wen, Z., Zhang, Y., Lin, Z., Shi, K. & Jiu, Y. Cytoskeleton—a crucial key in host cell for coronavirus infection. *J. Mol. Cell. Biol.* **12**, 968–979 (2021).
38. Paluck, A. et al. Role of ARP2/3 complex-driven actin polymerization in RSV infection. *Pathogens* **11**, 26 (2021).
39. Kubánková, M. et al. Physical phenotype of blood cells is altered in COVID-19. *Biophys. J.* **120**, 2838–2847 (2021).
40. Yang, J., Barrila, J., Roland, K. L., Ott, C. M. & Nickerson, C. A. Physiological fluid shear alters the virulence potential of invasive multidrug-resistant non-typhoidal *Salmonella typhimurium* D23580. *npj Microgravity* **2**, 16021 (2016).
41. Padron, G. C. et al. Shear rate sensitizes bacterial pathogens to H₂O₂ stress. *Proc. Natl Acad. Sci. USA* **120**, e2216774120 (2023).
42. Mikáty, G. et al. Extracellular bacterial pathogen induces host cell surface reorganization to resist shear stress. *PLoS Pathog.* **5**, e1000314 (2009).
43. Kuo, C. et al. Rhinovirus infection induces extracellular matrix protein deposition in asthmatic and nonasthmatic airway smooth muscle cells. *Am. J. Physiol. Lung Cell. Mol. Physiol.* **300**, L951–L957 (2011).
44. Nagy, N. et al. Hyaluronan in immune dysregulation and autoimmune diseases. *Matrix Biol.* **78–79**, 292–313 (2019).
45. Fingleton, B. Matrix metalloproteinases as regulators of inflammatory processes. *Biochim. Biophys. Acta Mol. Cell Res.* **1864**, 2036–2042 (2017).
46. Krishnamurthy, A. T. & Turley, S. J. Lymph node stromal cells: cartographers of the immune system. *Nat. Immunol.* **21**, 369–380 (2020).
47. Wynn, T. A. Integrating mechanisms of pulmonary fibrosis. *J. Exp. Med.* **208**, 1339–1350 (2011).
48. Tschöpe, C. et al. Myocarditis and inflammatory cardiomyopathy: current evidence and future directions. *Nat. Rev. Cardiol.* **18**, 169–193 (2021).
49. Fabre, T. et al. Identification of a broadly fibrogenic macrophage subset induced by type 3 inflammation. *Sci. Immunol.* **8**, eadd8945 (2023).
50. de Boer, R. A. et al. Towards better definition, quantification and treatment of fibrosis in heart failure. A scientific roadmap by the Committee of Translational Research of the Heart Failure Association (HFA) of the European Society of Cardiology. *Eur. J. Heart Fail.* **21**, 272–285 (2019).
51. Liu, F. et al. Feedback amplification of fibrosis through matrix stiffening and COX-2 suppression. *J. Cell Biol.* **190**, 693–706 (2010).
52. Georges, P. C. et al. Increased stiffness of the rat liver precedes matrix deposition: implications for fibrosis. *Am. J. Physiol. Gastrointest. Liver Physiol.* **293**, G1147–G1154 (2007).
53. Stock, K. F. et al. ARFI-based tissue elasticity quantification in comparison to histology for the diagnosis of renal transplant fibrosis. *Clin. Hemorheol. Microcirc.* **46**, 139–148 (2010).
54. Gadd, V. L. et al. The portal inflammatory infiltrate and ductular reaction in human nonalcoholic fatty liver disease. *Hepatology* **59**, 1393–1405 (2014).
55. Mogilenko, D. A., Shchukina, I. & Artyomov, M. N. Immune ageing at single-cell resolution. *Nat. Rev. Immunol.* **22**, 484–498 (2022).
56. Roman, M. J. et al. Arterial stiffness in chronic inflammatory diseases. *Hypertension* **46**, 194–199 (2005).
57. Klingberg, F., Hinz, B. & White, E. S. The myofibroblast matrix: implications for tissue repair and fibrosis: the myofibroblast matrix. *J. Pathol.* **229**, 298–309 (2013).
58. Liu, F. et al. Mechanosignaling through YAP and TAZ drives fibroblast activation and fibrosis. *Am. J. Physiol. Lung Cell. Mol. Physiol.* **308**, L344–L357 (2015).
59. Tomasek, J. J., Gabbiani, G., Hinz, B., Chaponnier, C. & Brown, R. A. Myofibroblasts and mechano-regulation of connective tissue remodelling. *Nat. Rev. Mol. Cell Biol.* **3**, 349–363 (2002).
60. Munger, J. S. et al. A mechanism for regulating pulmonary inflammation and fibrosis: the integrin $\alpha\beta6$ binds and activates latent TGF $\beta1$. *Cell* **96**, 319–328 (1999).
61. Santos, A. & Lagares, D. Matrix stiffness: the conductor of organ fibrosis. *Curr. Rheumatol. Rep.* **20**, 2 (2018).
62. Morvan, M. G. & Lanier, L. L. NK cells and cancer: you can teach innate cells new tricks. *Nat. Rev. Cancer* **16**, 7–19 (2016).
63. Janeway, C. A. How the immune system works to protect the host from infection: a personal view. *Proc. Natl Acad. Sci. USA* **98**, 7461–7468 (2001).
64. Dustin, M. L. T-cell activation through immunological synapses and kinapses. *Immunol. Rev.* **221**, 77–89 (2008).
65. Feng, Y., Zhao, X., White, A. K., Garcia, K. C. & Fordyce, P. M. A bead-based method for high-throughput mapping of the sequence- and force-dependence of T cell activation. *Nat. Methods* **19**, 1295–1305 (2022).
66. Mordechay, L. et al. Mechanical regulation of the cytotoxic activity of natural killer cells. *ACS Biomater. Sci. Eng.* **7**, 122–132 (2021).
67. Lei, K., Kurum, A. & Tang, L. Mechanical immunoengineering of T cells for therapeutic applications. *Acc. Chem. Res.* **53**, 2777–2790 (2020).
- Comprehensive review on recent advances in mechanical immunoengineering and their potential therapeutic applications.**
68. Seghir, R. & Arscott, S. Extended PDMS stiffness range for flexible systems. *Sens. Actuators Phys.* **230**, 33–39 (2015).

69. Guimarães, C. F., Gasperini, L., Marques, A. P. & Reis, R. L. The stiffness of living tissues and its implications for tissue engineering. *Nat. Rev. Mater.* **5**, 351–370 (2020).
 70. Denisin, A. K. & Pruitt, B. L. Tuning the range of polyacrylamide gel stiffness for mechanobiology applications. *ACS Appl. Mater. Interfaces* **8**, 21893–21902 (2016).
 71. Geissmann, F. et al. Development of monocytes, macrophages, and dendritic cells. *Science* **327**, 656–661 (2010).
 72. Follain, G. et al. Fluids and their mechanics in tumour transit: shaping metastasis. *Nat. Rev. Cancer* **20**, 107–124 (2020).
 73. Baratchi, S. et al. Transcatheter aortic valve implantation represents an anti-inflammatory therapy via reduction of shear stress-induced, piezo-1-mediated monocyte activation. *Circulation* **142**, 1092–1105 (2020).
 74. Serafini, N. et al. The TRPM4 channel controls monocyte and macrophage, but not neutrophil, function for survival in sepsis. *J. Immunol.* **189**, 3689–3699 (2012).
 75. Beningo, K. A. & Wang, Y. Fc-receptor-mediated phagocytosis is regulated by mechanical properties of the target. *J. Cell Sci.* **115**, 849–856 (2002).
 76. Sosale, N. G. et al. Cell rigidity and shape override CD47's 'self'-signaling in phagocytosis by hyperactivating myosin-II. *Blood* **125**, 542–552 (2015).
 77. Sridharan, R., Cavanagh, B., Cameron, A. R., Kelly, D. J. & O'Brien, F. J. Material stiffness influences the polarization state, function and migration mode of macrophages. *Acta Biomater.* **89**, 47–59 (2019).
 78. Hu, Y. et al. Molecular force imaging reveals that integrin-dependent mechanical checkpoint regulates Fcγ-receptor-mediated phagocytosis in macrophages. *Nano Lett.* **23**, 5562–5572 (2023).
 79. Atcha, H. et al. Mechanically activated ion channel Piezo1 modulates macrophage polarization and stiffness sensing. *Nat. Commun.* **12**, 3256 (2021).
 80. Geng, J. et al. TLR4 signalling via Piezo1 engages and enhances the macrophage mediated host response during bacterial infection. *Nat. Commun.* **12**, 3519 (2021).
 81. Dupont, S. et al. Role of YAP/TAZ in mechanotransduction. *Nature* **474**, 179–183 (2011).
 82. Rice, A. J. et al. Matrix stiffness induces epithelial–mesenchymal transition and promotes chemoresistance in pancreatic cancer cells. *Oncogenesis* **6**, e352 (2017).
 83. Oliver-De La Cruz, J. et al. Substrate mechanics controls adipogenesis through YAP phosphorylation by dictating cell spreading. *Biomaterials* **205**, 64–80 (2019).
 84. Meli, V. S. et al. YAP-mediated mechanotransduction tunes the macrophage inflammatory response. *Sci. Adv.* **6**, eabb8471 (2020).
 85. Steinman, R. M. Decisions about dendritic cells: past, present, and future. *Annu. Rev. Immunol.* **30**, 1–22 (2012).
 86. Moreau, H. D. et al. Macropinocytosis overcomes directional bias in dendritic cells due to hydraulic resistance and facilitates space exploration. *Dev. Cell* **49**, 171–188.e5 (2019).
 87. Laplaud, V. et al. Pinching the cortex of live cells reveals thickness instabilities caused by myosin II motors. *Sci. Adv.* **7**, eabe3640 (2021).
 88. Barbier, L. et al. Myosin II activity is selectively needed for migration in highly confined microenvironments in mature dendritic cells. *Front. Immunol.* **10**, 747 (2019).
 89. Chabaud, M. et al. Cell migration and antigen capture are antagonistic processes coupled by myosin II in dendritic cells. *Nat. Commun.* **6**, 7526 (2015).
 90. Leithner, A. et al. Dendritic cell actin dynamics control contact duration and priming efficiency at the immunological synapse. *J. Cell Biol.* **220**, e202006081 (2021).
 91. Kang, J.-H. et al. Biomechanical forces enhance directed migration and activation of bone marrow-derived dendritic cells. *Sci. Rep.* **11**, 12106 (2021).
 92. van den Dries, K. et al. Geometry sensing by dendritic cells dictates spatial organization and PGE2-induced dissolution of podosomes. *Cell. Mol. Life Sci.* **69**, 1889–1901 (2012).
 93. Chakraborty, M. et al. Mechanical stiffness controls dendritic cell metabolism and function. *Cell Rep.* **34**, 108609 (2021).
 94. Mennens, S. F. B. et al. Substrate stiffness influences phenotype and function of human antigen-presenting dendritic cells. *Sci. Rep.* **7**, 17511 (2017).
 95. Figdor, C. G., van Kooyk, Y. & Adema, G. J. C-type lectin receptors on dendritic cells and langerhans cells. *Nat. Rev. Immunol.* **2**, 77–84 (2002).
 96. Bufi, N. et al. Human primary immune cells exhibit distinct mechanical properties that are modified by inflammation. *Biophys. J.* **108**, 2181–2190 (2015).
 97. Comrie, W. A., Babich, A. & Burkhardt, J. K. F-actin flow drives affinity maturation and spatial organization of LFA-1 at the immunological synapse. *J. Cell Biol.* **208**, 475–491 (2015).
 98. Wang, Y. et al. Dendritic cell Piezo1 directs the differentiation of T_H1 and T_{reg} cells in cancer. *eLife* **11**, e79957 (2022).
 99. Valignat, M.-P. et al. Lymphocytes can self-steer passively with wind vane uropods. *Nat. Commun.* **5**, 5213 (2014).
 100. Roy, N. H., MacKay, J. L., Robertson, T. F., Hammer, D. A. & Burkhardt, J. K. Crk adaptor proteins mediate actin-dependent T cell migration and mechanosensing induced by the integrin LFA-1. *Sci. Signal.* **11**, eaat3178 (2018).
 101. Hope, J. M. et al. Fluid shear stress enhances T cell activation through Piezo1. *BMC Biol.* **20**, 61 (2022).
 102. Husson, J., Chemin, K., Bohineust, A., Hivroz, C. & Henry, N. Force generation upon T cell receptor engagement. *PLoS ONE* **6**, e19680 (2011).
- An elegant use of a biomembrane force probe technique for measuring forces exerted by T cells upon engagement with antigen-presenting cells.**
103. Liu, B., Chen, W., Evavold, B. D. & Zhu, C. Accumulation of dynamic catch bonds between TCR and agonist peptide–MHC triggers T cell signaling. *Cell* **157**, 357–368 (2014).
 104. Thauland, T. J., Hu, K. H., Bruce, M. A. & Butte, M. J. Cytoskeletal adaptivity regulates T cell receptor signaling. *Sci. Signal.* **10**, eaah3737 (2017).
 105. Gaertner, F. et al. WASp triggers mechanosensitive actin patches to facilitate immune cell migration in dense tissues. *Dev. Cell* **57**, 47–62.e9 (2022).
 106. Majedi, F. S. et al. T-cell activation is modulated by the 3D mechanical microenvironment. *Biomaterials* **252**, 120058 (2020).
 107. Wang, H. et al. ZAP-70: an essential kinase in T-cell signaling. *Cold Spring Harb. Perspect. Biol.* **2**, a002279 (2010).
 108. Bashour, K. T. et al. CD28 and CD3 have complementary roles in T-cell traction forces. *Proc. Natl Acad. Sci. USA* **111**, 2241–2246 (2014).
 109. Hu, K. H. & Butte, M. J. T cell activation requires force generation. *J. Cell Biol.* **213**, 535–542 (2016).
 110. Liu, Y. et al. DNA-based nanoparticle tension sensors reveal that T-cell receptors transmit defined pN forces to their antigens for enhanced fidelity. *Proc. Natl Acad. Sci. USA* **113**, 5610–5615 (2016).
 111. Tabdanov, E. et al. Micropatterning of TCR and LFA-1 ligands reveals complementary effects on cytoskeleton mechanics in T cells. *Integr. Biol.* **7**, 1272–1284 (2015).
 112. Govendir, M. A. et al. T cell cytoskeletal forces shape synapse topography for targeted lysis via membrane curvature bias of perforin. *Dev. Cell* **57**, 2237–2247.e8 (2022).

113. Wang, M. S. et al. Mechanically active integrins target lytic secretion at the immune synapse to facilitate cellular cytotoxicity. *Nat. Commun.* **13**, 3222 (2022).
114. Liu, C. S. C. et al. Cutting edge: Piezo1 mechanosensors optimize human T cell activation. *J. Immunol.* **200**, 1255–1260 (2018).
115. Jin, W. et al. T cell activation and immune synapse organization respond to the microscale mechanics of structured surfaces. *Proc. Natl Acad. Sci. USA* **116**, 19835–19840 (2019).
116. Kumari, S. et al. Cytoskeletal tension actively sustains the migratory T-cell synaptic contact. *EMBO J.* **39**, e102783 (2020).
117. Huby, R. D. J., Weiss, A. & Ley, S. C. Nocodazole inhibits signal transduction by the T cell antigen receptor. *J. Biol. Chem.* **273**, 12024–12031 (1998).
118. Le Saux, G. et al. Nanoscale mechanosensing of natural killer cells is revealed by antigen-functionalized nanowires. *Adv. Mater.* **31**, 1805954 (2019).
119. Bhingardive, V. et al. Nanowire based mechanostimulating platform for tunable activation of natural killer cells. *Adv. Funct. Mater.* **31**, 2103063 (2021).
120. Brumbaugh, K. M. et al. Functional role for Syk tyrosine kinase in natural killer cell-mediated natural cytotoxicity. *J. Exp. Med.* **186**, 1965–1974 (1997).
121. Matalon, O. et al. Actin retrograde flow controls natural killer cell response by regulating the conformation state of SHP-1. *EMBO J.* **37**, e96264 (2018).
122. Garrity, D., Call, M. E., Feng, J. & Wucherpfennig, K. W. The activating NKG2D receptor assembles in the membrane with two signaling dimers into a hexameric structure. *Proc. Natl Acad. Sci. USA* **102**, 7641–7646 (2005).
123. Friedman, D. et al. Natural killer cell immune synapse formation and cytotoxicity are controlled by tension of the target interface. *J. Cell Sci.* **134**, jcs258570 (2021).
124. Yanamandra, A. K. et al. PIEZO1-mediated mechanosensing governs NK cell killing efficiency in 3D. Preprint at *bioRxiv* <https://doi.org/10.1101/2023.03.27.534435> (2023).
125. Wan, Z. et al. B cell activation is regulated by the stiffness properties of the substrate presenting the antigens. *J. Immunol.* **190**, 4661–4675 (2013).
126. Natkanski, E. et al. B cells use mechanical energy to discriminate antigen affinities. *Science* **340**, 1587–1590 (2013).
127. Merino-Cortés, S. V. et al. Diacylglycerol kinase ζ promotes actin cytoskeleton remodeling and mechanical forces at the B cell immune synapse. *Sci. Signal.* **13**, eaaw8214 (2020).
128. Zeng, Y. et al. Substrate stiffness regulates B-cell activation, proliferation, class switch, and T-cell-independent antibody responses in vivo: Cellular immune response. *Eur. J. Immunol.* **45**, 1621–1634 (2015).
129. Nowosad, C. R., Spillane, K. M. & Tolar, P. Germinal center B cells recognize antigen through a specialized immune synapse architecture. *Nat. Immunol.* **17**, 870–877 (2016).
130. Jiang, H. & Wang, S. Immune cells use active tugging forces to distinguish affinity and accelerate evolution. *Proc. Natl Acad. Sci. USA* **120**, e2213067120 (2023).
131. Stanton, R. J. et al. HCMV pUL135 remodels the actin cytoskeleton to impair immune recognition of infected cells. *Cell Host Microbe* **16**, 201–214 (2014).
132. Pai, R. K., Convery, M., Hamilton, T. A., Boom, W. H. & Harding, C. V. Inhibition of IFN- γ -induced class II transactivator expression by a 19-kDa lipoprotein from *Mycobacterium tuberculosis*: a potential mechanism for immune evasion. *J. Immunol.* **171**, 175–184 (2003).
133. Samassa, F. et al. *Shigella* impairs human T lymphocyte responsiveness by hijacking actin cytoskeleton dynamics and T cell receptor vesicular trafficking. *Cell. Microbiol.* **22**, e13166 (2020).
134. Hanč, P. et al. Structure of the complex of F-actin and DNGR-1, a C-type lectin receptor involved in dendritic cell cross-presentation of dead cell-associated antigens. *Immunity* **42**, 839–849 (2015).
135. Man, S. M. et al. Actin polymerization as a key innate immune effector mechanism to control *Salmonella* infection. *Proc. Natl Acad. Sci. USA* **111**, 17588–17593 (2014).
136. Jacobson, E. C. et al. Migration through a small pore disrupts inactive chromatin organization in neutrophil-like cells. *BMC Biol.* **16**, 142 (2018).
137. Solis, A. G. et al. Mechanosensation of cyclical force by PIEZO1 is essential for innate immunity. *Nature* **573**, 69–74 (2019).
138. Robledo-Avila, F. H., Ruiz-Rosado, J., de, D., Brockman, K. L. & Partida-Sánchez, S. The TRPM2 ion channel regulates inflammatory functions of neutrophils during *Listeria monocytogenes* infection. *Front. Immunol.* **11**, 97 (2020).
139. Meng, K. P., Majedi, F. S., Thauland, T. J. & Butte, M. J. Mechanosensing through YAP controls T cell activation and metabolism. *J. Exp. Med.* **217**, e20200053 (2020).
- This study sheds light on T cells sensing the mechanical signals of their environment and tuning their response accordingly.**
140. Al-Aghbar, M. A., Jainarayanan, A. K., Dustin, M. L. & Roffler, S. R. The interplay between membrane topology and mechanical forces in regulating T cell receptor activity. *Commun. Biol.* **5**, 40 (2022).
141. Wong, V. W. et al. Mechanical force prolongs acute inflammation via T-cell-dependent pathways during scar formation. *FASEB J.* **25**, 4498–4510 (2011).
142. Chen, D. S. & Mellman, I. Oncology meets immunology: the cancer-immunity cycle. *Immunity* **39**, 1–10 (2013).
143. O'Donnell, J. S., Teng, M. W. L. & Smyth, M. J. Cancer immunoeediting and resistance to T cell-based immunotherapy. *Nat. Rev. Clin. Oncol.* **16**, 151–167 (2019).
144. Dustin, M. L. & Long, E. O. Cytotoxic immunological synapses: NK and CTL synapses. *Immunol. Rev.* **235**, 24–34 (2010).
145. González-Granado, J. M. et al. Nuclear envelope lamin-A couples actin dynamics with immunological synapse architecture and T cell activation. *Sci. Signal.* **7**, ra37 (2014).
146. González, C. et al. Nanobody-CD16 catch bond reveals NK cell mechanosensitivity. *Biophys. J.* **116**, 1516–1526 (2019).
147. Fan, J. et al. NKG2D discriminates diverse ligands through selectively mechano-regulated ligand conformational changes. *EMBO J.* **41**, e107739 (2022).
148. Tsopoulidis, N. et al. T cell receptor-triggered nuclear actin network formation drives CD4⁺ T cell effector functions. *Sci. Immunol.* **4**, eaav1987 (2019).
149. Tamzalit, F. et al. Interfacial actin protrusions mechanically enhance killing by cytotoxic T cells. *Sci. Immunol.* **4**, eaav5445 (2019).
150. Sanchez, E. E. et al. Apoptotic contraction drives target cell release by cytotoxic T cells. *Nat. Immunol.* <https://doi.org/10.1038/s41590-023-01572-4> (2023).
151. Händel, C. et al. Cell membrane softening in human breast and cervical cancer cells. *N. J. Phys.* **17**, 083008 (2015).
152. Huang, B., Song, B. & Xu, C. Cholesterol metabolism in cancer: mechanisms and therapeutic opportunities. *Nat. Metab.* **2**, 132–141 (2020).
153. Hanna, R. N. et al. Patrolling monocytes control tumor metastasis to the lung. *Science* **350**, 985–990 (2015).
154. Vyas, M. et al. Natural killer cells suppress cancer metastasis by eliminating circulating cancer cells. *Front. Immunol.* **13**, 1098445 (2023).
155. Hu, B., Xin, Y., Hu, G., Li, K. & Tan, Y. Fluid shear stress enhances natural killer cell's cytotoxicity toward circulating tumor cells through NKG2D-mediated mechanosensing. *APL Bioeng.* **7**, 036108 (2023).

156. Boussommier-Calleja, A. et al. The effects of monocytes on tumor cell extravasation in a 3D vascularized microfluidic model. *Biomaterials* **198**, 180–193 (2019).
157. Soderquest, K. et al. Monocytes control natural killer cell differentiation to effector phenotypes. *Blood* **117**, 4511–4518 (2011).
158. Kumar, B. V., Connors, T. J. & Farber, D. L. Human T cell development, localization, and function throughout life. *Immunity* **48**, 202–213 (2018).
159. Surcel, A. et al. Pharmacological activation of myosin II paralogs to correct cell mechanics defects. *Proc. Natl Acad. Sci. USA* **112**, 1428–1433 (2015).
160. Mittelheisser, V. et al. Optimal physicochemical properties of antibody–nanoparticle conjugates for improved tumor targeting. *Adv. Mater.* **34**, 2110305 (2022).
161. Guo, P. et al. Nanoparticle elasticity directs tumor uptake. *Nat. Commun.* **9**, 130 (2018).
162. Liang, Q. et al. The softness of tumour-cell-derived microparticles regulates their drug-delivery efficiency. *Nat. Biomed. Eng.* **3**, 729–740 (2019).
163. Chen, X. et al. Nanoparticle-mediated specific elimination of soft cancer stem cells by targeting low cell stiffness. *Acta Biomater.* **135**, 493–505 (2021).
164. Perez, J. E. et al. Transient cell stiffening triggered by magnetic nanoparticle exposure. *J. Nanobiotechnol.* **19**, 117 (2021).
165. Liu, Y. X. et al. Single-cell mechanics provides an effective means to probe in vivo interactions between alveolar macrophages and silver nanoparticles. *J. Phys. Chem. B* **119**, 15118–15129 (2015).
166. Binnewies, M. et al. Understanding the tumor immune microenvironment (TIME) for effective therapy. *Nat. Med.* **24**, 541–550 (2018).
167. Hartmann, N. et al. Prevailing role of contact guidance in intrastromal T-cell trapping in human pancreatic cancer. *Clin. Cancer Res.* **20**, 3422–3433 (2014).
168. Kuczek, D. E. et al. Collagen density regulates the activity of tumor-infiltrating T cells. *J. Immunother. Cancer* **7**, 68 (2019).
169. Sun, X. et al. Tumour DDR1 promotes collagen fibre alignment to instigate immune exclusion. *Nature* **599**, 673–678 (2021).
170. Di Martino, J. S. et al. A tumor-derived type III collagen-rich ECM niche regulates tumor cell dormancy. *Nat. Cancer* **3**, 90–107 (2021).
171. Lampi, M. C. & Reinhart-King, C. A. Targeting extracellular matrix stiffness to attenuate disease: from molecular mechanisms to clinical trials. *Sci. Transl. Med.* **10**, eaao0475 (2018).
172. Diop-Frimpong, B., Chauhan, V. P., Krane, S., Boucher, Y. & Jain, R. K. Losartan inhibits collagen I synthesis and improves the distribution and efficacy of nanotherapeutics in tumors. *Proc. Natl Acad. Sci. USA* **108**, 2909–2914 (2011).
173. Liu, J. et al. TGF- β blockade improves the distribution and efficacy of therapeutics in breast carcinoma by normalizing the tumor stroma. *Proc. Natl Acad. Sci. USA* **109**, 16618–16623 (2012).
174. Van Cutsem, E. et al. Randomized phase III trial of pegvorhyaluronidase alfa with nab-paclitaxel plus gemcitabine for patients with hyaluronan-high metastatic pancreatic adenocarcinoma. *J. Clin. Oncol.* **38**, 3185–3194 (2020).
175. Provenzano, P. P. et al. Enzymatic targeting of the stroma ablates physical barriers to treatment of pancreatic ductal adenocarcinoma. *Cancer Cell* **21**, 418–429 (2012).
176. Zhong, Y. et al. Tumor microenvironment-activatable nanoenzymes for mechanical remodeling of extracellular matrix and enhanced tumor chemotherapy. *Adv. Funct. Mater.* **31**, 2007544 (2021).
177. Caruana, I. et al. Heparanase promotes tumor infiltration and antitumor activity of CAR-redirected T lymphocytes. *Nat. Med.* **21**, 524–529 (2015).
178. Prescher, J. A., Dube, D. H. & Bertozzi, C. R. Chemical remodeling of cell surfaces in living animals. *Nature* **430**, 873–877 (2004).
179. Meng, D. et al. In situ activated NK cell as bio-orthogonal targeted live-cell nanocarrier augmented solid tumor immunotherapy. *Adv. Funct. Mater.* **32**, 2202603 (2022).
180. Zhao, Y. et al. Bioorthogonal equipping CAR-T cells with hyaluronidase and checkpoint blocking antibody for enhanced solid tumor immunotherapy. *ACS Cent. Sci.* **8**, 603–614 (2022).
181. Saatci, O. et al. Targeting lysyl oxidase (LOX) overcomes chemotherapy resistance in triple negative breast cancer. *Nat. Commun.* **11**, 2416 (2020).
182. Nicolas-Boluda, A. et al. Tumor stiffening reversion through collagen crosslinking inhibition improves T cell migration and anti-PD-1 treatment. *eLife* **10**, e58688 (2021).
183. De Vita, A. et al. Lysyl oxidase engineered lipid nanovesicles for the treatment of triple negative breast cancer. *Sci. Rep.* **11**, 5107 (2021).
184. Kim, H. Y. et al. Detection of lysyl oxidase activity in tumor extracellular matrix using peptide-functionalized gold nanoproboscopes. *Cancers* **13**, 4523 (2021).
185. Kanapathipillai, M. et al. Inhibition of mammary tumor growth using lysyl oxidase-targeting nanoparticles to modify extracellular matrix. *Nano Lett.* **12**, 3213–3217 (2012).
186. Vennin, C. et al. Transient tissue priming via ROCK inhibition uncouples pancreatic cancer progression, sensitivity to chemotherapy, and metastasis. *Sci. Transl. Med.* **9**, eaai8504 (2017).
- A compelling demonstration that altering the mechanical features of the tumour environment holds great potential for improving therapies.**
187. Murphy, K. J. et al. Intravital imaging technology guides FAK-mediated priming in pancreatic cancer precision medicine according to Merlin status. *Sci. Adv.* **7**, eabh0363 (2021).
188. Tran, E. et al. Immune targeting of fibroblast activation protein triggers recognition of multipotent bone marrow stromal cells and cachexia. *J. Exp. Med.* **210**, 1125–1135 (2013).
189. Wang, L.-C. S. et al. Targeting fibroblast activation protein in tumor stroma with chimeric antigen receptor T cells can inhibit tumor growth and augment host immunity without severe toxicity. *Cancer Immunol. Res.* **2**, 154–166 (2014).
190. Rurik, J. G. et al. CAR T cells produced in vivo to treat cardiac injury. *Science* **375**, 91–96 (2022).
191. Correia, A. L. et al. Hepatic stellate cells suppress NK cell-sustained breast cancer dormancy. *Nature* **594**, 566–571 (2021).
192. Roberts, E. W. et al. Depletion of stromal cells expressing fibroblast activation protein- α from skeletal muscle and bone marrow results in cachexia and anemia. *J. Exp. Med.* **210**, 1137–1151 (2013).
193. Fujimori, K., Covell, D. G., Fletcher, J. E. & Weinstein, J. N. Modeling analysis of the global and microscopic distribution of immunoglobulin G, F(ab')₂, and Fab in tumors. *Cancer Res.* **49**, 5656–5663 (1989).
194. Tabdanov, E. D. et al. Engineering T cells to enhance 3D migration through structurally and mechanically complex tumor microenvironments. *Nat. Commun.* **12**, 2815 (2021).
195. Whitlock, B. *Enhancing Cytotoxic T Cell Killing by PTEN Depletion* (Weill Cornell Medicine, 2018).
196. Li, R., Ma, C., Cai, H. & Chen, W. The CAR T-cell mechanoimmunology at a glance. *Adv. Sci.* **7**, 2002628 (2020).
197. Chockley, P. J., Ibanez-Vega, J., Krenციute, G., Talbot, L. J. & Gottschalk, S. Synapse-tuned CARs enhance immune cell anti-tumor activity. *Nat. Biotechnol.* <https://doi.org/10.1038/s41587-022-01650-2> (2023).
- This study shows that improving the immunological synapse architecture of CAR-NK cells leads to superior therapeutic efficacy.**

198. Roybal, K. T. et al. Precision tumor recognition by T cells with combinatorial antigen-sensing circuits. *Cell* **164**, 770–779 (2016).
199. Gordon, W. R. et al. Mechanical allostery: evidence for a force requirement in the proteolytic activation of notch. *Dev. Cell* **33**, 729–736 (2015).
200. Sloas, D. C., Tran, J. C., Marzilli, A. M. & Ngo, J. T. Tension-tuned receptors for synthetic mechanotransduction and intercellular force detection. *Nat. Biotechnol.* <https://doi.org/10.1038/s41587-022-01638-y> (2023).
201. Mittelheisser, V. et al. Leveraging immunotherapy with nanomedicine. *Adv. Ther.* **3**, 2000134 (2020).
202. Perica, K. et al. Magnetic field-induced T cell receptor clustering by nanoparticles enhances T cell activation and stimulates antitumor activity. *ACS Nano* **8**, 2252–2260 (2014).
203. Majedi, F. S. et al. Augmentation of T-cell activation by oscillatory forces and engineered antigen-presenting cells. *Nano Lett.* **19**, 6945–6954 (2019).
204. Vis, B. et al. Ultrasmall silica nanoparticles directly ligate the T cell receptor complex. *Proc. Natl Acad. Sci. USA* **117**, 285–291 (2020).
205. Kim, K.-S. et al. Cationic nanoparticle-mediated activation of natural killer cells for effective cancer immunotherapy. *ACS Appl. Mater. Interfaces* **12**, 56731–56740 (2020).
206. Sim, T. et al. Magneto-activation and magnetic resonance imaging of natural killer cells labeled with magnetic nanocomplexes for the treatment of solid tumors. *ACS Nano* **15**, 12780–12793 (2021).
207. Liu, Z. et al. Nanoscale optomechanical actuators for controlling mechanotransduction in living cells. *Nat. Methods* **13**, 143–146 (2016).
208. Farhadi, A., Ho, G. H., Sawyer, D. P., Bourdeau, R. W. & Shapiro, M. G. Ultrasound imaging of gene expression in mammalian cells. *Science* **365**, 1469–1475 (2019).
209. Wang, X., Chen, X. & Yang, Y. Spatiotemporal control of gene expression by a light-switchable transgene system. *Nat. Methods* **9**, 266–269 (2012).
210. Pan, Y. et al. Mechanogenetics for the remote and noninvasive control of cancer immunotherapy. *Proc. Natl Acad. Sci. USA* **115**, 992–997 (2018).
211. González-Bermúdez, B., Guinea, G. V. & Plaza, G. R. Advances in micropipette aspiration: applications in cell biomechanics, models, and extended studies. *Biophys. J.* **116**, 587–594 (2019).
212. Otto, O. et al. Real-time deformability cytometry: on-the-fly cell mechanical phenotyping. *Nat. Methods* **12**, 199–202 (2015).
Introduction of the state-of-the-art and high-throughput RT-DC technology for measuring the mechanical properties of cells.
213. Gerum, R. et al. Viscoelastic properties of suspended cells measured with shear flow deformation cytometry. *eLife* **11**, e78823 (2022).
214. Sánchez-Iranzo, H., Bevilacqua, C., Diz-Muñoz, A. & Prevedel, R. A 3D Brillouin microscopy dataset of the in-vivo zebrafish eye. *Data Brief* **30**, 105427 (2020).
215. Conrad, C., Gray, K. M., Stroka, K. M., Rizvi, I. & Scarcelli, G. Mechanical characterization of 3D ovarian cancer nodules using Brillouin confocal microscopy. *Cell. Mol. Bioeng.* **12**, 215–226 (2019).
216. Wu, P.-H. et al. Particle tracking microrheology of cancer cells in living subjects. *Mater. Today* **39**, 98–109 (2020).
217. Falchuk, K. & Berliner, R. Hydrostatic pressures in peritubular capillaries and tubules in the rat kidney. *Am. J. Physiol.* **220**, 1422–1426 (1971).
218. Petrie, R. J. & Koo, H. Direct measurement of intracellular pressure. *Curr. Protoc. Cell Biol.* **63**, (2014).
219. Harlepp, S., Thalmann, F., Follain, G. & Goetz, J. G. Hemodynamic forces can be accurately measured in vivo with optical tweezers. *Mol. Biol. Cell* **28**, 3252–3260 (2017).
220. Mongera, A. et al. A fluid-to-solid jamming transition underlies vertebrate body axis elongation. *Nature* **561**, 401–405 (2018).
221. Mongera, A. et al. Mechanics of the cellular microenvironment as probed by cells in vivo during zebrafish presomitic mesoderm differentiation. *Nat. Mater.* **22**, 135–143 (2023).
222. Vorselen, D. et al. Microparticle traction force microscopy reveals subcellular force exertion patterns in immune cell–target interactions. *Nat. Commun.* **11**, 20 (2020).
223. Meng, F., Suchyna, T. M. & Sachs, F. A fluorescence energy transfer-based mechanical stress sensor for specific proteins in situ: mechanical stress sensor. *FEBS J.* **275**, 3072–3087 (2008).
224. Grashoff, C. et al. Measuring mechanical tension across vinculin reveals regulation of focal adhesion dynamics. *Nature* **466**, 263–266 (2010).
225. Conway, D. E. et al. Fluid shear stress on endothelial cells modulates mechanical tension across VE-cadherin and PECAM-1. *Curr. Biol.* **23**, 1024–1030 (2013).
226. Pan, X. et al. Assessment of cancer cell migration using a viscosity-sensitive fluorescent probe. *Chem. Commun.* **58**, 4663–4666 (2022).
227. Shimolina, L. E. et al. Imaging tumor microscopic viscosity in vivo using molecular rotors. *Sci. Rep.* **7**, 41097 (2017).
228. Sack, I. Magnetic resonance elastography from fundamental soft-tissue mechanics to diagnostic imaging. *Nat. Rev. Phys.* **5**, 25–42 (2022).
229. Soteriou, D. et al. Rapid single-cell physical phenotyping of mechanically dissociated tissue biopsies. *Nat. Biomed. Eng.* <https://doi.org/10.1038/s41551-023-01015-3> (2023).

Acknowledgements

L.T. acknowledges the grant support from Swiss National Science Foundation (315230_204202, IZLCZO_206035, CRSII5_205930), European Research Council under the ERC grant agreement MechanoMM (805337), Swiss Cancer Research Foundation (KFS-4600-08-2018), Kristian Gerhard Jebsen Foundation, Anna Fuller Fund, Xtalpi Inc., and EPFL. J.G.G. acknowledges support from INSERM, University of Strasbourg and charities (Ligue contre le Cancer, Fondation ARC pour la recherche sur le cancer), which also support fellowships to V.M. and V.G. This work was also supported by grants from Plan Cancer to J.G.G. We apologize to the authors whose work could not be cited due to size constraints.

Author contributions

V.M., V.G., L.B., W.L., L.T. and J.G.G. researched data for the paper. All authors made substantial contributions to the discussion of content, wrote the paper and reviewed and/or edited the paper before submission.

Competing interests

L.T. is a co-founder, shareholder and advisor for Leman Biotech. The interests of L.T. were reviewed and managed by EPFL. The other authors declare no competing interests.

Additional information

Correspondence and requests for materials should be addressed to Li Tang or Jacky G. Goetz.

Peer review information *Nature Nanotechnology* thanks Claire Hivroz and the other, anonymous, reviewer(s) for their contribution to the peer review of this work.

Reprints and permissions information is available at www.nature.com/reprints.

Q34

Publisher's note Springer Nature remains neutral with regard to jurisdictional claims in published maps and institutional affiliations.

Springer Nature or its licensor (e.g. a society or other partner) holds exclusive rights to this article under a publishing agreement with

the author(s) or other rightsholder(s); author self-archiving of the accepted manuscript version of this article is solely governed by the terms of such publishing agreement and applicable law.

© The Author(s), under exclusive licence to Springer Nature Limited 2023

RÉFÉRENCES

- Acerbi, I. *et al.* (2015) Human breast cancer invasion and aggression correlates with ECM stiffening and immune cell infiltration. *Integr Biol (Camb)* 7, 1120–1134
- Aceto, N. *et al.* (2014) Circulating tumor cell clusters are oligoclonal precursors of breast cancer metastasis. *Cell* 158, 1110–1122
- Aigner, S. *et al.* (1998) CD24 mediates rolling of breast carcinoma cells on P-selectin. *FASEB J* 12, 1241–1251
- Alibert, C. *et al.* (2017) Are cancer cells really softer than normal cells? *Biol Cell* 109, 167–189
- Allen, T.A. *et al.* (2017) Angiopeliosis as an Alternative Mechanism of Cell Extravasation. *Stem Cells* 35, 170–180
- Anderson, K.J. *et al.* (2017) Effect of circulating tumor cell aggregate configuration on hemodynamic transport and wall contact. *Math Biosci* 294, 181–194
- Ashikawa, K. *et al.* (1986) Phasic blood flow velocity pattern in epimyocardial microvessels in the beating canine left ventricle. *Circ Res* 59, 704–711
- Au, S.H. *et al.* (2016) Clusters of circulating tumor cells traverse capillary-sized vessels. *Proc Natl Acad Sci U S A* 113, 4947–4952
- Baxter, L.T. and Jain, R.K. (1989) Transport of fluid and macromolecules in tumors. I. Role of interstitial pressure and convection. *Microvascular Research* 37, 77–104
- Bell, G.I. *et al.* (1984) Cell adhesion. Competition between nonspecific repulsion and specific bonding. *Biophys J* 45, 1051–1064
- Bell, G.I. (1978) Models for the specific adhesion of cells to cells. *Science* 200, 618–627
- Bera, K. *et al.* (2022) Extracellular fluid viscosity enhances cell migration and cancer dissemination. *Nature* 611, 365–373
- Bordeleau, F. *et al.* (2017) Matrix stiffening promotes a tumor vasculature phenotype. *Proc Natl Acad Sci U S A* 114, 492–497
- Boyd, N.F. *et al.* (2014) Evidence That Breast Tissue Stiffness Is Associated with Risk of Breast Cancer. *PLoS One* 9, e100937
- Brown, M. *et al.* (2018) Lymph node blood vessels provide exit routes for metastatic tumor cell dissemination in mice. *Science* 359, 1408–1411
- Calvo, F. *et al.* (2013) Mechanotransduction and YAP-dependent matrix remodelling is required for the generation and maintenance of cancer-associated fibroblasts. *Nat Cell Biol* 15, 637–646

- Cameron, M.D. *et al.* (2000) Temporal progression of metastasis in lung: cell survival, dormancy, and location dependence of metastatic inefficiency. *Cancer Res* 60, 2541–2546
- Carrara, S. *et al.* (2018) EUS elastography (strain ratio) and fractal-based quantitative analysis for the diagnosis of solid pancreatic lesions. *Gastrointest Endosc* 87, 1464–1473
- Chang, S.-F. *et al.* (2008) Tumor cell cycle arrest induced by shear stress: Roles of integrins and Smad. *Proc Natl Acad Sci U S A* 105, 3927–3932
- Chauhan, V.P. *et al.* (2013) Angiotensin inhibition enhances drug delivery and potentiates chemotherapy by decompressing tumour blood vessels. *Nat Commun* 4, 2516
- Chen, Y.-Q. *et al.* (2018) Epithelial-mesenchymal transition softens head and neck cancer cells to facilitate migration in 3D environments. *J Cell Mol Med* 22, 3837–3846
- Cheng, G. *et al.* (2009) Micro-Environmental Mechanical Stress Controls Tumor Spheroid Size and Morphology by Suppressing Proliferation and Inducing Apoptosis in Cancer Cells. *PLOS ONE* 4, e4632
- Cheung, K.J. *et al.* (2016) Polyclonal breast cancer metastases arise from collective dissemination of keratin 14-expressing tumor cell clusters. *Proc Natl Acad Sci U S A* 113, E854-863
- Choi, H.Y. *et al.* (2019) Hydrodynamic shear stress promotes epithelial-mesenchymal transition by downregulating ERK and GSK3 β activities. *Breast Cancer Res* 21, 6
- Choquet, D. *et al.* (1997) Extracellular matrix rigidity causes strengthening of integrin-cytoskeleton linkages. *Cell* 88, 39–48
- Chugh, P. and Paluch, E.K. (2018) The actin cortex at a glance. *Journal of Cell Science* 131, jcs186254
- Cochlin, D.L. *et al.* (2002) Elastography in the detection of prostatic cancer. *Clin Radiol* 57, 1014–1020
- Coffman, J.D. and Lempert, J.A. (1975) Venous flow velocity, venous volume and arterial blood flow. *Circulation* 52, 141–145
- Colin, F. *et al.* (2021) Biomechanics: a driving force behind metastatic progression. *Comptes Rendus. Biologies* 344, 249–262
- Cui, J. *et al.* (2021) Numerical study on the adhesion of a circulating tumor cell in a curved microvessel. *Biomech Model Mechanobiol* 20, 243–254
- Dash, S.N. and Patnaik, L. (2023) Flight for fish in drug discovery: a review of zebrafish-based screening of molecules. *Biol Lett* 19, 20220541
- Delarue, M. *et al.* (2014) Compressive Stress Inhibits Proliferation in Tumor Spheroids through a Volume Limitation. *Biophys J* 107, 1821–1828

- Demou, Z.N. (2010) Gene Expression Profiles in 3D Tumor Analogs Indicate Compressive Strain Differentially Enhances Metastatic Potential. *Ann Biomed Eng* 38, 3509–3520
- Denais, C.M. *et al.* (2016) Nuclear envelope rupture and repair during cancer cell migration. *Science* 352, 353–358
- Diel, E.E. *et al.* (2020) Tutorial: avoiding and correcting sample-induced spherical aberration artifacts in 3D fluorescence microscopy. *Nat Protoc* 15, 2773–2784
- Dillekås, H. *et al.* (2019) Are 90% of deaths from cancer caused by metastases? *Cancer Med* 8, 5574–5576
- Dixon, J.B. *et al.* (2006) Lymph flow, shear stress, and lymphocyte velocity in rat mesenteric prenodal lymphatics. *Microcirculation* 13, 597–610
- Donato, C. *et al.* (2020) Hypoxia Triggers the Intravasation of Clustered Circulating Tumor Cells. *Cell Rep* 32, 108105
- Dupont, S. *et al.* (2011) Role of YAP/TAZ in mechanotransduction. *Nature* 474, 179–183
- Entenberg, D. *et al.* (2015) In vivo subcellular resolution optical imaging in the lung reveals early metastatic proliferation and motility. *Intravital* 4, 1–11
- Er, E.E. *et al.* (2018) Pericyte-like spreading by disseminated cancer cells activates YAP and MRTF for metastatic colonization. *Nat Cell Biol* 20, 966–978
- Evans, A. *et al.* (2012) Differentiating benign from malignant solid breast masses: value of shear wave elastography according to lesion stiffness combined with greyscale ultrasound according to BI-RADS classification. *Br J Cancer* 107, 224–229
- Ewing, J. (1928) Neoplastic Diseases: A Treatise on Tumours. By James Ewing, A.M., M.D., Sc.D., Professor of Pathology at Cornell University Medical College, N.Y.; Pathologist to the Memorial Hospital. Third edition. Royal 8vo. Pp. 1127, with 546 illustrations. 1928. Philadelphia and London: W. B. Saunders Co. Ltd. 63s. net. *BJS (British Journal of Surgery)* 16, 174–175
- Fares, J. *et al.* (2020) Molecular principles of metastasis: a hallmark of cancer revisited. *Signal Transduct Target Ther* 5, 28
- Follain, G. *et al.* (2020) Fluids and their mechanics in tumour transit: shaping metastasis. *Nat Rev Cancer* 20, 107–124
- Follain, G. *et al.* (2018) Hemodynamic Forces Tune the Arrest, Adhesion, and Extravasation of Circulating Tumor Cells. *Developmental Cell* 45, 33–52.e12
- Follain, G. *et al.* (2018) Using the Zebrafish Embryo to Dissect the Early Steps of the Metastasis Cascade. *Methods Mol Biol* 1749, 195–211
- Follain, G. *et al.* (2021) Impairing flow-mediated endothelial remodeling reduces extravasation of tumor cells. *Sci Rep* 11, 13144

- Friedl, P. *et al.* (2012) Classifying collective cancer cell invasion. *Nat Cell Biol* 14, 777–783
- Furlow, P.W. *et al.* (2015) Mechanosensitive pannexin-1 channels mediate microvascular metastatic cell survival. *Nat Cell Biol* 17, 943–952
- Gao, Y. *et al.* (2019) Metastasis Organotropism: Redefining the Congenial Soil. *Developmental Cell* 49, 375–391
- Gassmann, P. *et al.* (2009) Metastatic tumor cell arrest in the liver-lumen occlusion and specific adhesion are not exclusive. *Int J Colorectal Dis* 24, 851–858
- Gensbittel, V. *et al.* (2021) Nanoluminal Signaling Shapes Collective Metastasis. *Trends Cancer* 7, 9–11
- Gensbittel, V. *et al.* (2021) Mechanical Adaptability of Tumor Cells in Metastasis. *Dev Cell* 56, 164–179
- Gerum, R. *et al.* (2022) Viscoelastic properties of suspended cells measured with shear flow deformation cytometry. *eLife* 11, e78823
- Girardo, S. *et al.* (2018) Standardized microgel beads as elastic cell mechanical probes. *J. Mater. Chem. B* 6, 6245–6261
- Gkountela, S. *et al.* (2019) Circulating Tumor Cell Clustering Shapes DNA Methylation to Enable Metastasis Seeding. *Cell* 176, 98–112.e14
- Goetz, J.G. *et al.* (2011) Biomechanical remodeling of the microenvironment by stromal caveolin-1 favors tumor invasion and metastasis. *Cell* 146, 148–163
- Goetz, J.G. *et al.* (2014) Endothelial cilia mediate low flow sensing during zebrafish vascular development. *Cell Rep* 6, 799–808
- Grasset, E.M. *et al.* (2022) Triple-negative breast cancer metastasis involves complex epithelial-mesenchymal transition dynamics and requires vimentin. *Sci Transl Med* 14, eabn7571
- Griffon-Etienne, G. *et al.* (1999) Taxane-induced apoptosis decompresses blood vessels and lowers interstitial fluid pressure in solid tumors: clinical implications. *Cancer Res* 59, 3776–3782
- Guck, J. *et al.* (2005) Optical deformability as an inherent cell marker for testing malignant transformation and metastatic competence. *Biophys J* 88, 3689–3698
- Guevorkian, K. *et al.* (2010) Aspiration of biological viscoelastic drops. *Phys Rev Lett* 104, 218101
- Gürbüz, A. *et al.* (2023) Effects of membrane viscoelasticity on the red blood cell dynamics in a microcapillary. *Biophysical Journal* 122, 2230–2241

- Gutmann, R. *et al.* (1992) Interstitial hypertension in head and neck tumors in patients: correlation with tumor size. *Cancer Res* 52, 1993–1995
- Han, Y.L. *et al.* (2018) Cell contraction induces long-ranged stress stiffening in the extracellular matrix. *Proceedings of the National Academy of Sciences* 115, 4075–4080
- Han, Y. *et al.* (2023) CX43 down-regulation promotes cell aggressiveness and 5-fluorouracil-resistance by attenuating cell stiffness in colorectal carcinoma. *Cancer Biol Ther* 24, 2221879
- Harney, A.S. *et al.* (2015) Real-Time Imaging Reveals Local, Transient Vascular Permeability, and Tumor Cell Intravasation Stimulated by TIE2hi Macrophage-Derived VEGFA. *Cancer Discov* 5, 932–943
- Hashizume, H. *et al.* (2000) Openings between Defective Endothelial Cells Explain Tumor Vessel Leakiness. *Am J Pathol* 156, 1363–1380
- Headley, M.B. *et al.* (2016) Visualization of immediate immune responses to pioneer metastatic cells in the lung. *Nature* 531, 513–517
- Heldin, C.-H. *et al.* (2004) High interstitial fluid pressure — an obstacle in cancer therapy. *Nat Rev Cancer* 4, 806–813
- Hiratsuka, S. *et al.* (2011) Endothelial focal adhesion kinase mediates cancer cell homing to discrete regions of the lungs via E-selectin up-regulation. *Proc Natl Acad Sci U S A* 108, 3725–3730
- Hosseini, H. *et al.* (2016) Early dissemination seeds metastasis in breast cancer. *Nature* 540, 552–558
- Howe, K. *et al.* (2013) The zebrafish reference genome sequence and its relationship to the human genome. *Nature* 496, 498–503
- Huang, C.-H. *et al.* (2023) Investigation of Stem Cell-Like Characteristics and Immune Cell Interaction of Tumor Cells Survived from Continuous Shear Flow Environment. *Advanced Biology* n/a, 2300332
- Huang, X. *et al.* (2018) RhoA-stimulated intra-capillary morphology switch facilitates the arrest of individual circulating tumor cells. *Int J Cancer* 142, 2094–2105
- Hyenne, V. *et al.* (2019) Studying the Fate of Tumor Extracellular Vesicles at High Spatiotemporal Resolution Using the Zebrafish Embryo. *Developmental Cell* 48, 554-572.e7
- Janmey, P.A. *et al.* (1991) Viscoelastic properties of vimentin compared with other filamentous biopolymer networks. *J Cell Biol* 113, 155–160
- Jiang, K. *et al.* (2023) Deleterious Mechanical Deformation Selects Mechanoresilient Cancer Cells with Enhanced Proliferation and Chemoresistance. *Adv Sci (Weinh)* 10, e2201663
- Karreman, M.A. *et al.* (2023) Active Remodeling of Capillary Endothelium via Cancer Cell-Derived MMP9 Promotes Metastatic Brain Colonization. *Cancer Res* 83, 1299–1314

- Khismatullin, D.B. and Truskey, G.A. (2012) Leukocyte Rolling on P-Selectin: A Three-Dimensional Numerical Study of the Effect of Cytoplasmic Viscosity. *Biophys J* 102, 1757–1766
- Kienast, Y. *et al.* (2010) Real-time imaging reveals the single steps of brain metastasis formation. *Nat Med* 16, 116–122
- Lam, C.K. *et al.* (2010) Embolus extravasation is an alternative mechanism for cerebral microvascular recanalization. *Nature* 465, 478–482
- Lang, N.R. *et al.* (2015) Biphasic response of cell invasion to matrix stiffness in three-dimensional biopolymer networks. *Acta Biomater* 13, 61–67
- Langley, R.R. and Fidler, I.J. (2011) The seed and soil hypothesis revisited—The role of tumor-stroma interactions in metastasis to different organs. *International Journal of Cancer* 128, 2527–2535
- Lee, H.J. *et al.* (2017) Fluid shear stress activates YAP1 to promote cancer cell motility. *Nat Commun* 8, 14122
- Leighton, J. *et al.* (1960) Pathogenesis of Tumor Invasion: II. Aggregate Replication* †. *Cancer Research* 20, 575–586
- Leiter, A. *et al.* (2023) The global burden of lung cancer: current status and future trends. *Nat Rev Clin Oncol* 20, 624–639
- Less, J.R. *et al.* (1992) Interstitial hypertension in human breast and colorectal tumors. *Cancer Res* 52, 6371–6374
- Leu, A.J. *et al.* (2000) Absence of functional lymphatics within a murine sarcoma: a molecular and functional evaluation. *Cancer Res* 60, 4324–4327
- Levental, K.R. *et al.* (2009) Matrix crosslinking forces tumor progression by enhancing integrin signaling. *Cell* 139, 891–906
- Li, Y. *et al.* (2023) Compressive forces stabilize microtubules in living cells. *Nat. Mater.* 22, 913–924
- Lien, S.-C. *et al.* (2013) Mechanical regulation of cancer cell apoptosis and autophagy: roles of bone morphogenetic protein receptor, Smad1/5, and p38 MAPK. *Biochim Biophys Acta* 1833, 3124–3133
- Lorenz, C. *et al.* (2019) Lateral Subunit Coupling Determines Intermediate Filament Mechanics. *Phys Rev Lett* 123, 188102
- Lorenz, C. *et al.* (2023) Keratin filament mechanics and energy dissipation are determined by metal-like plasticity. *Matter* 6, 2019–2033

- Lu, X. *et al.* (2011) VCAM-1 Promotes Osteolytic Expansion of Indolent Bone Micrometastasis of Breast Cancer by Engaging $\alpha 4\beta 1$ -Positive Osteoclast Progenitors. *Cancer Cell* 20, 701–714
- Lu, Y. *et al.* (2019) Circulation patterns and seed-soil compatibility factors cooperate to cause cancer organ-specific metastasis. *Experimental Cell Research* 375, 62–72
- Luzzi, K.J. *et al.* (1998) Multistep Nature of Metastatic Inefficiency. *Am J Pathol* 153, 865–873
- Massagué, J. (2008) TGFbeta in Cancer. *Cell* 134, 215–230
- Matthews, H.K. *et al.* (2020) Oncogenic Signaling Alters Cell Shape and Mechanics to Facilitate Cell Division under Confinement. *Dev Cell* 52, 563-573.e3
- Miller, B.W. *et al.* (2015) Targeting the LOX/hypoxia axis reverses many of the features that make pancreatic cancer deadly: inhibition of LOX abrogates metastasis and enhances drug efficacy. *EMBO Mol Med* 7, 1063–1076
- Milosevic, M. *et al.* (2023) Modeling critical interaction for metastasis between circulating tumor cells (CTCs) and platelets adhered to the capillary wall. *Comput Methods Programs Biomed* 242, 107810
- Mohammadi, H. and Sahai, E. (2018) Mechanisms and impact of altered tumour mechanics. *Nat Cell Biol* 20, 766–774
- Moose, D.L. *et al.* (2020) Cancer Cells Resist Mechanical Destruction in Circulation via RhoA/Actomyosin-Dependent Mechano-Adaptation. *Cell Rep* 30, 3864-3874.e6
- Muz, B. *et al.* (2015) The role of hypoxia in cancer progression, angiogenesis, metastasis, and resistance to therapy. *Hypoxia (Auckl)* 3, 83–92
- Nathanson, S.D. and Nelson, L. (1994) Interstitial fluid pressure in breast cancer, benign breast conditions, and breast parenchyma. *Ann Surg Oncol* 1, 333–338
- Naxerova, K. *et al.* (2017) Origins of lymphatic and distant metastases in human colorectal cancer. *Science* 357, 55–60
- Nguyen, D.X. *et al.* (2009) Metastasis: from dissemination to organ-specific colonization. *Nat Rev Cancer* 9, 274–284
- Nia, H.T. *et al.* (2016) Solid stress and elastic energy as measures of tumour mechanopathology. *Nat Biomed Eng* 1, 1–11
- Nia, H.T. *et al.* (2020) Physical traits of cancer. *Science* 370, eaaz0868
- Nieto, M.A. *et al.* (2016) EMT: 2016. *Cell* 166, 21–45
- Offeddu, G.S. *et al.* (2021) The cancer glycocalyx mediates intravascular adhesion and extravasation during metastatic dissemination. *Commun Biol* 4, 1–10

- Oh, M. *et al.* (2023) High extracellular glucose promotes cell motility by modulating cell deformability and contractility via the cAMP-RhoA-ROCK axis in human breast cancer cells. *Mol Biol Cell* 34, ar79
- Olive, K.P. *et al.* (2009) Inhibition of Hedgehog signaling enhances delivery of chemotherapy in a mouse model of pancreatic cancer. *Science* 324, 1457–1461
- Osmani, N. *et al.* (2019) Metastatic Tumor Cells Exploit Their Adhesion Repertoire to Counteract Shear Forces during Intravascular Arrest. *Cell Rep* 28, 2491-2500.e5
- Padera, T.P. *et al.* (2002) Lymphatic metastasis in the absence of functional intratumor lymphatics. *Science* 296, 1883–1886
- Padera, T.P. *et al.* (2004) Cancer cells compress intratumour vessels. *Nature* 427, 695–695
- Paget, S. (1889) THE DISTRIBUTION OF SECONDARY GROWTHS IN CANCER OF THE BREAST. *The Lancet* 133, 571–573
- Pathak, A. and Kumar, S. (2012) Independent regulation of tumor cell migration by matrix stiffness and confinement. *Proc Natl Acad Sci U S A* 109, 10334–10339
- Paul, C.D. *et al.* (2019) Tissue Architectural Cues Drive Organ Targeting of Tumor Cells in Zebrafish. *cells* 9, 187-206.e16
- Peinado, H. *et al.* (2017) Pre-metastatic niches: organ-specific homes for metastases. *Nat Rev Cancer* 17, 302–317
- Pereira, E.R. *et al.* (2018) Lymph node metastases can invade local blood vessels, exit the node, and colonize distant organs in mice. *Science* 359, 1403–1407
- Provenzano, P.P. *et al.* (2006) Collagen reorganization at the tumor-stromal interface facilitates local invasion. *BMC Med* 4, 38
- Qi, J. *et al.* (2005) Transendothelial Migration of Melanoma Cells Involves N-Cadherin-mediated Adhesion and Activation of the β -Catenin Signaling Pathway. *Mol Biol Cell* 16, 4386–4397
- Regmi, S. *et al.* (2017) High Shear Stresses under Exercise Condition Destroy Circulating Tumor Cells in a Microfluidic System. *Sci Rep* 7, 39975
- Roberts, A.B. *et al.* (2021) Tumor cell nuclei soften during transendothelial migration. *J Biomech* 121, 110400
- Roh-Johnson, M. *et al.* (2014) Macrophage contact induces RhoA GTPase signaling to trigger tumor cell intravasation. *Oncogene* 33, 4203–4212
- Rosendahl, P. *et al.* (2018) Real-time fluorescence and deformability cytometry. *Nat Methods* 15, 355–358

- Rouvière, O. *et al.* (2017) Stiffness of benign and malignant prostate tissue measured by shear-wave elastography: a preliminary study. *Eur Radiol* 27, 1858–1866
- Shahryari, M. *et al.* (2019) Tomoelastography Distinguishes Noninvasively between Benign and Malignant Liver Lesions. *Cancer Res* 79, 5704–5710
- Soerjomataram, I. and Bray, F. (2021) Planning for tomorrow: global cancer incidence and the role of prevention 2020–2070. *Nat Rev Clin Oncol* 18, 663–672
- Steeg, P.S. (2016) Targeting metastasis. *Nat Rev Cancer* 16, 201–218
- Steele, N.G. *et al.* (2021) Inhibition of Hedgehog Signaling Alters Fibroblast Composition in Pancreatic Cancer. *Clin Cancer Res* 27, 2023–2037
- Stoletov, K. *et al.* (2010) Visualizing extravasation dynamics of metastatic tumor cells. *J Cell Sci* 123, 2332–2341
- Stoletov, K. *et al.* (2007) High-resolution imaging of the dynamic tumor cell vascular interface in transparent zebrafish. *Proc Natl Acad Sci U S A* 104, 17406–17411
- Stotsky, J.A. and Othmer, H.G. (2022) The effects of internal forces and membrane heterogeneity on three-dimensional cell shapes. *J Math Biol* 86, 1
- Strell, C. and Entschladen, F. (2008) Extravasation of leukocytes in comparison to tumor cells. *Cell Commun Signal* 6, 10
- Stylianopoulos, T. *et al.* (2012) Causes, consequences, and remedies for growth-induced solid stress in murine and human tumors. *Proceedings of the National Academy of Sciences* 109, 15101–15108
- Swaminathan, V. *et al.* (2011) Mechanical stiffness grades metastatic potential in patient tumor cells and in cancer cell lines. *Cancer Res* 71, 5075–5080
- Szczerba, B.M. *et al.* (2019) Neutrophils escort circulating tumour cells to enable cell cycle progression. *Nature* 566, 553–557
- Tarin, D. *et al.* (2005) The fallacy of epithelial mesenchymal transition in neoplasia. *Cancer Res* 65, 5996–6000; discussion 6000–6001
- Taubenberger, A.V. *et al.* (2019) 3D Microenvironment Stiffness Regulates Tumor Spheroid Growth and Mechanics via p21 and ROCK. *Adv Biosyst* 3, e1900128
- Thompson, E.W. *et al.* (2005) Carcinoma invasion and metastasis: a role for epithelial-mesenchymal transition? *Cancer Res* 65, 5991–5995; discussion 5995
- Tong, R.T. *et al.* (2004) Vascular normalization by vascular endothelial growth factor receptor 2 blockade induces a pressure gradient across the vasculature and improves drug penetration in tumors. *Cancer Res* 64, 3731–3736

- Träber, N. *et al.* (2019) Polyacrylamide Bead Sensors for in vivo Quantification of Cell-Scale Stress in Zebrafish Development. *Sci Rep* 9, 17031
- Tse, J.M. *et al.* (2012) Mechanical compression drives cancer cells toward invasive phenotype. *Proceedings of the National Academy of Sciences* 109, 911–916
- Ugai, T. *et al.* (2022) Is early-onset cancer an emerging global epidemic? Current evidence and future implications. *Nat Rev Clin Oncol* 19, 656–673
- Urbanska, M. *et al.* (2023) De novo identification of universal cell mechanics gene signatures. *eLife* 12
- Urbanska, M. *et al.* (2020) A comparison of microfluidic methods for high-throughput cell deformability measurements. *Nat Methods* 17, 587–593
- Vahabikashi, A. *et al.* (2022) Nuclear lamin isoforms differentially contribute to LINC complex-dependent nucleocytoskeletal coupling and whole-cell mechanics. *Proc Natl Acad Sci U S A* 119, e2121816119
- Van Bodegraven *et al.* (2023) Intermediate filaments promote glioblastoma cell invasion by controlling cell deformability and mechanosensitive gene expression, *In Review*, doi: 10.21203/rs.3.rs-2828066/v1
- Vestweber, D. (2015) How leukocytes cross the vascular endothelium. *Nat Rev Immunol* 15, 692–704
- Weiss, F. *et al.* (2022) Towards targeting of shared mechanisms of cancer metastasis and therapy resistance. *Nat Rev Cancer* 22, 157–173
- Weiss, L. *et al.* (1992) Lethal deformation of cancer cells in the microcirculation: a potential rate regulator of hematogenous metastasis. *Int J Cancer* 50, 103–107
- White, R.M. and Patton, E.E. (2023) Adult zebrafish as advanced models of human disease. *Dis Model Mech* 16, dmm050351
- Wirtz, D. *et al.* (2011) The physics of cancer: the role of physical interactions and mechanical forces in metastasis. *Nat Rev Cancer* 11, 512–522
- Wrenn, E.D. *et al.* (2020) Regulation of Collective Metastasis by Nanolumenal Signaling. *Cell* 183, 395-410.e19
- Xing, F. *et al.* (2013) Reactive astrocytes promote the metastatic growth of breast cancer stem-like cells by activating Notch signalling in brain. *EMBO Molecular Medicine* 5, 384–396
- Yamauchi, K. *et al.* (2005) Real-time in vivo dual-color imaging of intracapillary cancer cell and nucleus deformation and migration. *Cancer Res* 65, 4246–4252

Yang, L. *et al.* (2022) Pin1/YAP pathway mediates matrix stiffness-induced epithelial–mesenchymal transition driving cervical cancer metastasis via a non-Hippo mechanism. *Bioeng Transl Med* 8, e10375

Young, K.M. *et al.* (2023) Correlating mechanical and gene expression data on the single cell level to investigate metastatic phenotypes. *iScience* 26, 106393

Zeng, Y. *et al.* (2023) Normalizing Tumor Blood Vessels to Improve Chemotherapy and Inhibit Breast Cancer Metastasis by Multifunctional Nanoparticles. *Mol Pharm* 20, 5078–5089

Zhang, S. *et al.* (2023) Intravital measurements of solid stresses in tumours reveal length-scale and microenvironmentally dependent force transmission. *Nat. Biomed. Eng* DOI: [10.1038/s41551-023-01080-8](https://doi.org/10.1038/s41551-023-01080-8)

Zulueta-Coarasa, T. *et al.* (2022) Physical confinement promotes mesenchymal trans-differentiation of invading transformed cells in vivo. *iScience* 25, 105330

ANNEXES

ANNEXE 1



OPEN

Impairing flow-mediated endothelial remodeling reduces extravasation of tumor cells

Gautier Follain^{1,2,3,4,5,7}, Naël Osmani^{1,2,3,4,7}, Valentin Gensbittel^{1,2,3,4}, Nandini Asokan^{1,2,3,4}, Annabel Larnicol^{1,2,3,4}, Luc Mercier^{1,2,3,4,6}, Maria Jesus Garcia-Leon^{1,2,3,4}, Ignacio Busnelli^{1,2,3,4}, Angelique Pichot^{1,2,3}, Nicodème Paul^{1,2,3}, Raphaël Carapito^{1,2,3}, Seiamak Bahram^{1,2,3}, Olivier Lefebvre^{1,2,3,4}✉ & Jacky G. Goetz^{1,2,3,4}✉

Tumor progression and metastatic dissemination are driven by cell-intrinsic and biomechanical cues that favor the growth of life-threatening secondary tumors. We recently identified pro-metastatic vascular regions with blood flow profiles that are permissive for the arrest of circulating tumor cells. We have further established that such flow profiles also control endothelial remodeling, which favors extravasation of arrested CTCs. Yet, how shear forces control endothelial remodeling is unknown. In the present work, we aimed at dissecting the cellular and molecular mechanisms driving blood flow-dependent endothelial remodeling. Transcriptomic analysis of endothelial cells revealed that blood flow enhanced VEGFR signaling, among others. Using a combination of in vitro microfluidics and intravital imaging in zebrafish embryos, we now demonstrate that the early flow-driven endothelial response can be prevented upon specific inhibition of VEGFR tyrosine kinase and subsequent signaling. Inhibitory targeting of VEGFRs reduced endothelial remodeling and subsequent metastatic extravasation. These results confirm the importance of VEGFR-dependent endothelial remodeling as a driving force of CTC extravasation and metastatic dissemination. Furthermore, the present work suggests that therapies targeting endothelial remodeling might be a relevant clinical strategy in order to impede metastatic progression.

Metastatic colonization occurring during advanced tumorigenic progression is the main reason for cancer-related death¹. It is currently well admitted that their development relies on biological and biophysical cues that influence their location and development². Indeed, adhesion molecule repertoire^{3,4}, vascular architecture⁵⁻⁷ and hemodynamics^{2,8,9} impact the early steps of tumor cells dissemination. Several biochemical and physical parameters found in colonized organs such as growth factors, chemokines, stromal cell composition¹⁰⁻¹³ and matrix stiffness¹⁴⁻¹⁶ will permit the growth of secondary tumors.

In order to reach distant organs, tumor cells need to go through several rate-limiting steps including intravasation, blood-borne transport and extravasation¹⁷. Thus, a comprehensive understanding of these steps is necessary in order to design relevant pharmacological therapeutic strategies. Recently, using zebrafish embryo and mouse experimental metastasis models, we and others have demonstrated that blood flow-induced endothelial remodeling acts as a driving force to cell extravasation and subsequent micro-metastasis formation^{9,18-20}. Specifically, we have shown that the endothelium wall actively remodels around arrested tumor cells in order to maintain vessel perfusion and thus actively promotes tumor cell extravasation. Such phenomenon relies on the ability of endothelial cells to protrude apically, migrate intravascularly and enwrap arrested CTCs, excluding them from the inner vasculature. Careful intravital imaging of mouse brain metastasis by triple negative breast cancer cells also revealed the presence of intraluminal endothelial plugs, which isolated invading cells from the circulation^{9,20}. It was suggested that MMP enzymatic activity is required to resolve blood clot and maintain vessel perfusion through similar endothelial remodeling in mouse brain²¹ suggesting that tumor cells potentially hijack

¹Tumor Biomechanics, INSERM UMR_S1109, CRBS, 67000 Strasbourg, France. ²Université de Strasbourg, 67000 Strasbourg, France. ³Fédération de Médecine Translationnelle de Strasbourg (FMTS), 67000 Strasbourg, France. ⁴Equipe Labellisée Ligue Contre le Cancer, Paris, France. ⁵Present address: Turku Bioscience Center,, University of Turku, Åbo Akademi University, 20520 Turku, Finland. ⁶Present address: UMR 5297, Interdisciplinary Institute for Neurosciences, CNRS Université de Bordeaux, 33076 Bordeaux, France. ⁷These authors contributed equally: Gautier Follain and Naël Osmani. ✉email: lefebvre@unistra.fr; jacky.goetz@inserm.fr

a physiological mechanism. However, the molecular mechanisms driving endothelial remodeling downstream of blood flow biomechanical cues remain elusive.

In the following report, we aimed at identifying the molecular programs that are transcriptionally activated downstream of flow forces, at values that are permissive to metastatic extravasation. Among others, activation of VEGFR signaling emerged as a potential major molecular signature of endothelial remodeling and thus an attractive target. Using two potent tyrosine-kinase and VEGFR inhibitor, one of them approved for clinical use to treat specific tumors such as renal cell carcinoma, gastro-intestinal stromal tumors or pancreatic neuroendocrine tumors²², we further demonstrate that VEGFR inhibition impairs extravasation of circulating tumor cells by blocking the endothelial remodeling. Thus, our findings confirm that endothelial remodeling is an essential step in metastatic extravasation and can be controlled at the molecular level using existing pharmacological tools²³.

Results

Flow upregulates VEGF signaling pathway. In order to identify signaling pathways that drive endothelial remodeling in dependence of permissive flow forces, we applied RNA sequencing on cultured primary endothelial cells (HUVEC) to identify transcriptional programs activated by previously identified flow profiles. We used previously described methods based on Human Umbilical Venous Endothelial Cells (HUVEC) culture in microfluidic channels⁹. The HUVEC monolayer was cultured for 16 h in static conditions or with medium perfusion at a flow rate of 400 $\mu\text{m/s}$ (Fig. 1A). Such flow velocity was selected for two reasons: similar flow regime favors extravasation of tumor cells in zebrafish embryos, and it matches the flow rate measured in capillary-like vessels that we and others reported^{9,24–27}. Total RNAs were then extracted, quantitative RNA sequencing was carried out and flow-responsive genes were clustered and functionally annotated using Gene Ontology (GO) databases.

Strikingly, endothelial cells switched their transcriptional programs from cell division and mitosis to cell migration/angiogenesis when exposed to flow (Fig. 1B and Fig S1A), as previously suggested²⁸. Interestingly, a significant fraction of genes upregulated in response to flow is involved in vascular development, angiogenesis, and response to oxidative stress (Fig. 1B, Fig S1A and S4). This is in accordance with previously described endothelial transcriptional response to shear stress²⁹. Shear stress is indeed an essential biomechanical cue that controls the sprouting and migration of endothelial cells as well as vessel remodeling during angiogenesis^{30–32}. Interestingly, intraluminal sprouting and migration of endothelial cells is initiated quickly upon CTC arrest in our models, the zebrafish embryo and the mouse brain⁹. We thus hypothesized that angiogenesis related genes might be elemental in driving endothelial remodeling during CTC extravasation. We thus focused on the GO class “Angiogenesis” (Fig. 1C) and applied a stringent threshold to our list of significantly impacted gene (with fold changes > 1.5 and $p\text{-value} < 0.05$). Among others, we identified FLT1 (VEGFR1) and KDR (VEGFR2), two VEGF receptors (VEGFR) that were strongly upregulated in endothelial cells subjected to our reference flow velocity (400 $\mu\text{m/s}$). Using RT-qPCR, we confirmed a specific two-fold increase in gene expression of FLT1 and KDR upon flow stimulation while non-VEGFR endothelial genes (Notch and LAMA4) were unaffected (Fig S1B,C). Using similar conditions, we assessed the protein levels of all three VEGFRs (FLT1, KDR and FLT4 (VEGFR3)) using western-blot and immunofluorescence (Fig. 1D–F, S5). Expression levels of KDR are significantly and consistently increased in response to flow. Expression levels of FLT1 and FLT4 also increase in response to flow, yet they display a heterogeneous response (Fig. 1D–F, S5). We sought out to confirm these results in vivo using the zebrafish embryo endothelium as a model. *Tg(fli1a:EGFP)* zebrafish embryos at 48 h post-fertilization (hpf) expressing EGFP in the endothelium were treated for 14 h with lidocaine or vehicle to decrease the heart pacemaker activity and thus blood flow as we previously described⁹. Embryos were dissociated and GFP+ endothelial cells were FACS sorted. Total RNAs of the endothelium were extracted and the expression levels of KDR and KDRL, the 2 zebrafish orthologs of VEGFR2, in vehicle and lidocaine-treated embryos was assessed by RT-qPCR. We observed that decreasing blood flow led to a decrease in both KDR and KDRL expression (Fig S1D). Altogether, these data suggest that permissive flow profiles for endothelial remodeling and subsequent extravasation of CTCs drive expression of VEGFRs, both at the RNA and protein levels. This prompted us to test the role of VEGFR pathways on the flow-dependent endothelial remodeling leading to extravasation of tumor cells.

Inhibition of the VEGF pathway in vitro suppresses endothelial remodeling. Based on our previous results, we hypothesized that VEGFR signaling could trigger flow-dependent endothelial remodeling, and subsequent metastasis, and decided to pharmacologically impair it. Here, we decided to employ pharmacological inhibition using a clinically approved drug, sunitinib (Sutent or SU11248), for its known anti-angiogenic properties through VEGFRs, among others, as we further confirmed that several of its known targets were upregulated in response to flow in HUVEC cells (Fig S1C). Our goal, at this stage, was to demonstrate that molecular inhibition of VEGFR, using treatment regimes that do not cause major vascular remodeling effects but rather target flow-mediated intraluminal endothelial remodeling⁹, is a possible avenue for impairing metastatic extravasation. We first relied on our previously published microfluidic-based experimental model⁹. This system allows to recapitulate major features of the metastatic cascade such as arrest, adhesion and extravasation³³. In brief, D2A1 cancer cells (mouse mammary carcinoma) are loaded into a microfluidic channel containing a monolayer of endothelial (HUVEC) cells and left to adhere for 10 min. Using a peristaltic pump, cells were then submitted to flow with a speed of 400 $\mu\text{m/s}$ (i.e. permissive for CTC adhesion and activating endothelial response)⁹. With this approach, we confirmed that VEGFR2, a VEGFR isoform we found consistently overexpressed at the RNA and protein level, is recruited at the plasma membrane of endothelial cells undergoing remodeling during CTC extravasation in vitro (Fig. 2A). Using similar microfluidics where endothelial cells were subjected to VEGFR inhibition using sunitinib prior to CTC perfusion, we next assessed whether such treatment would

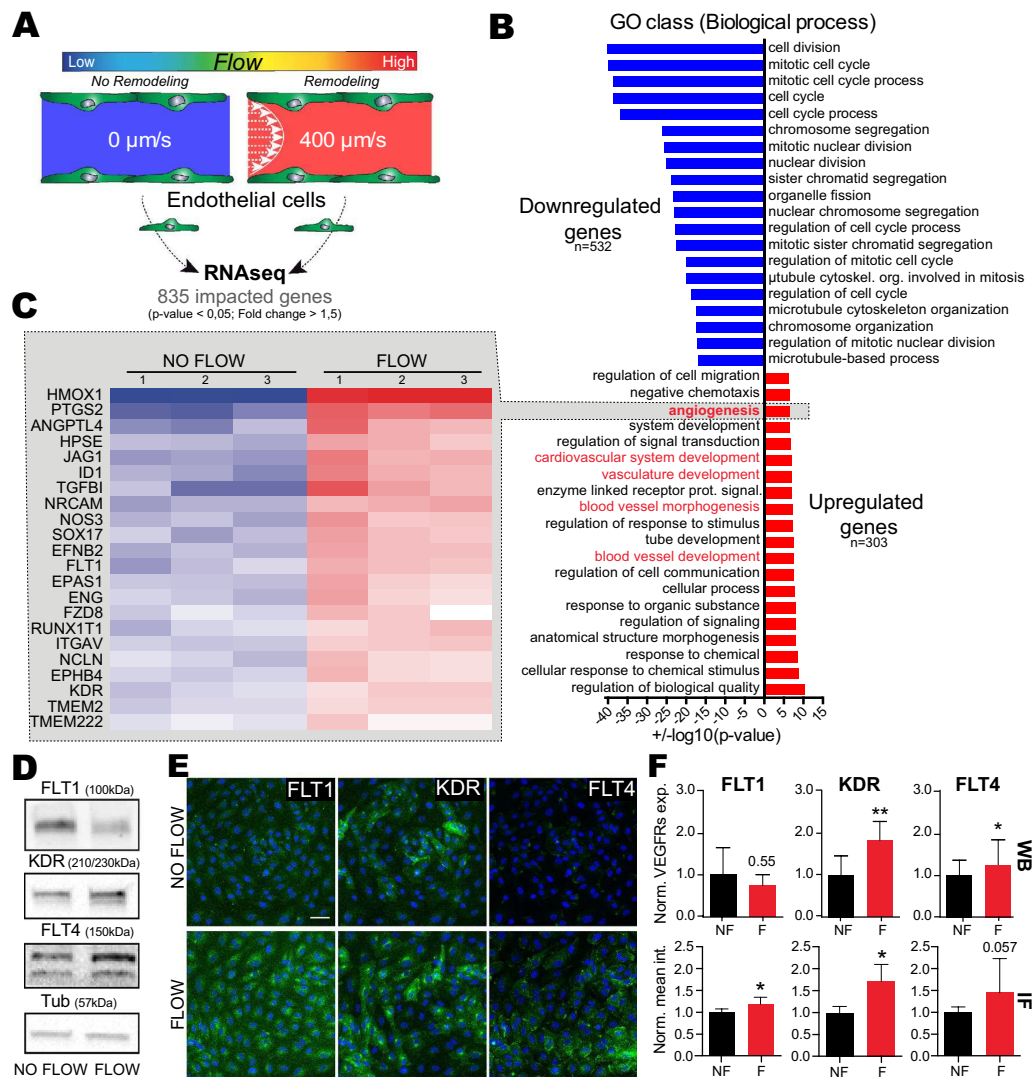


Figure 1. Flow favors expression of gene program driving vasculature remodeling, including VEGFRs. (A) Experimental setup: microfluidic experiment for RNA sequencing. (B) Results from global Gene Ontology (GO) analysis on 'biological process', showing most significantly impacted GO class. (C) Fold changes heatmap, based on GO class: Angiogenesis, showing significantly upregulated genes in flow condition compared to no flow. (D) Western blot quantification validating some of VEGFR RNAseq data. (E) Representative image of flow vs no flow immunofluorescence labelling of FLT1, KDR and FLT4 (green) with DAPI (blue). (F) Quantification associated with D and E, showing increased expression and signal intensity of VEGFRs. WB: N = 5, Mann Whitney test, IF: N = 4 with min 5 fields/exp, Mann Whitney test.

impact endothelial remodeling and CTC transmigration (Fig. 2B). The microfluidic channels were perfused with tumor cells (CTCs) that adhered to endothelial cells and further flow-stimulated for 16 h in the presence of vehicle or sunitinib. As previously described⁹, flow stimulation favored transmigration through the endothelial cells monolayer of ~95% of the cancer cells. Among these, the vast majority (~80%) of the cells that had crossed the endothelial wall did so through endothelial remodeling (Fig. 2C,D). VEGFR inhibition through mild sunitinib treatment significantly decreased the number of tumor cells that could cross the endothelial barrier and suppressed the endothelial remodeling activity (Fig. 2C,D). In conclusion, flow stimulates VEGFR-dependent endothelial remodeling and subsequent metastatic extravasation in microfluidic artificial environments in vitro.

Inhibition of the VEGFR pathway blocks early endothelial remodeling in zebrafish embryos. We next wondered whether such mechanism would occur in realistic hemodynamic situations. Zebrafish is an easy-to-use experimental metastasis model which is fully compatible with intravital imaging and

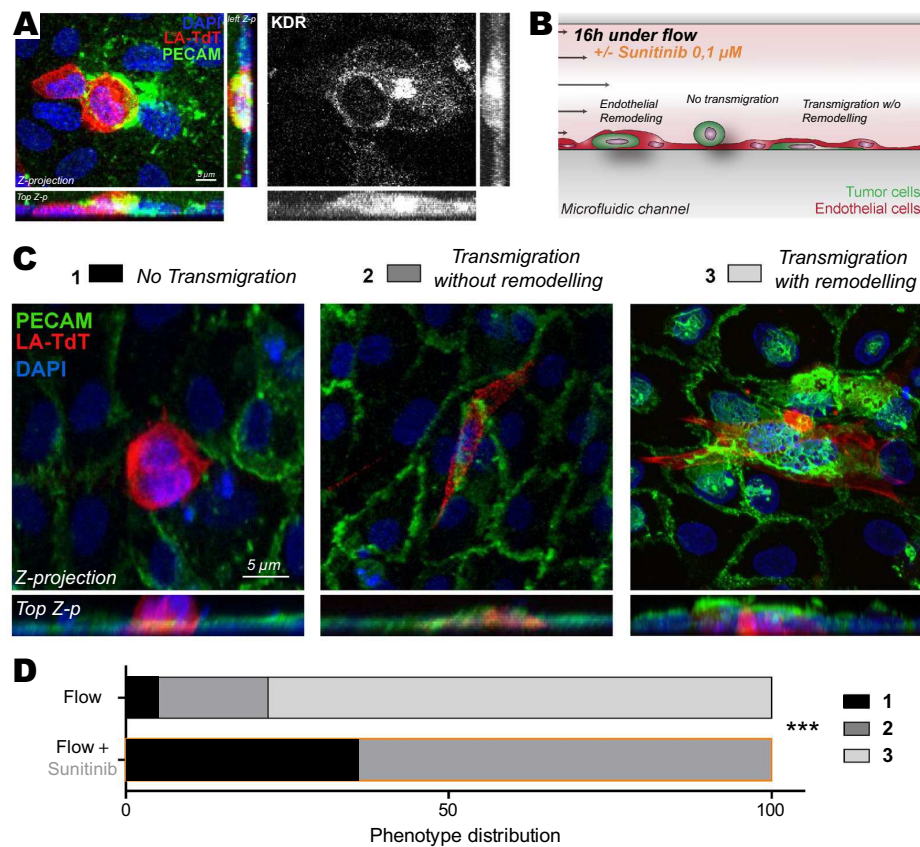


Figure 2. Inhibition of VEGFRs with sunitinib impairs endothelial remodeling in vitro. (A) Immuno-labelling pictures showing the presence of KDR (white) at the site of endothelial remodeling (Assessed with PECAM enrichment (green) around tumor cell (red)). Z-projections and two z-projection from side and top view are shown. (B) Experimental setup: microfluidic channel for endothelial remodeling assay. (C) Representative images of all steps: 1-No transmigration, 2-Transmigration without remodeling evidence, 3-Transmigration with remodeling. Quantification of the normalized number of transmigrating cells and remodeling activity. (D) Phenotypic distribution of CTCs attached to endothelial layers exposed to flow and treated with vehicle or sunitinib. N: flow/vehicle = 88, flow/sunitinib = 150, Fischer test.

chemical compound screening which can be directly added into the water^{34,35}. In addition, we and others have shown that tumor cells engage in intraluminal vascular remodeling during metastatic extravasation^{9,18,19}. We thus set out to test the involvement of VEGFR signaling, and its potential inhibition, in endothelial remodeling in vivo, using intravital imaging of intravascularly arrested tumor cells in zebrafish embryos.

Using our intravital imaging-based experimental metastasis model in zebrafish, we next injected tumor cells directly in the circulation through the duct of Cuvier of 48hpf embryos³⁶ and quantitatively addressed the effect of sunitinib on extravasation in vivo (Fig. 3A). We classified the behavior of injected tumor cells into three populations at different stages of this process, whose dynamics has been characterized in our previous work: “intravascular”, “pocketing” (i.e. in the process of extravasation through endothelial remodeling) and “extravasated”. After only 3 h post-injection (hpi), tumor cells are stably adhered to the endothelium, which starts to remodel in order to restore blood flow and favor metastatic extravasation (Fig. 3B,C). Quantification performed over a large number of embryos shows that short sunitinib treatment significantly impairs endothelial remodeling in a dose-dependent manner. Indeed, VEGFR inhibition increases the ratio of intravascular cells and decreases the number of pocketing events (Fig. 3B,C).

Interestingly, we carefully documented that such treatment regime, i.e. short and potent, has no effect on the overall vasculature and hemodynamics properties.

To rule out side-effects, we first controlled whether a short (3 h) sunitinib treatment (5 μ M) would impair the vascular system and hemodynamics of *Tg(fli1a:EGFP; gata1:DsRed)* zebrafish embryos at 48 h post-fertilization (hpf) expressing EGFP in the endothelium and RFP in red blood cells (Fig. 3D). Pharmacological treatments of the embryos had mostly no impact on the vascular architecture of embryos, with only the most caudal inter-somitic vessels (ISVs) failing to lumenize in a few embryos (Fig. 3D). Anatomical analysis and quantification of the vascular system revealed that the vascular architecture was mostly unperturbed upon sunitinib treatment

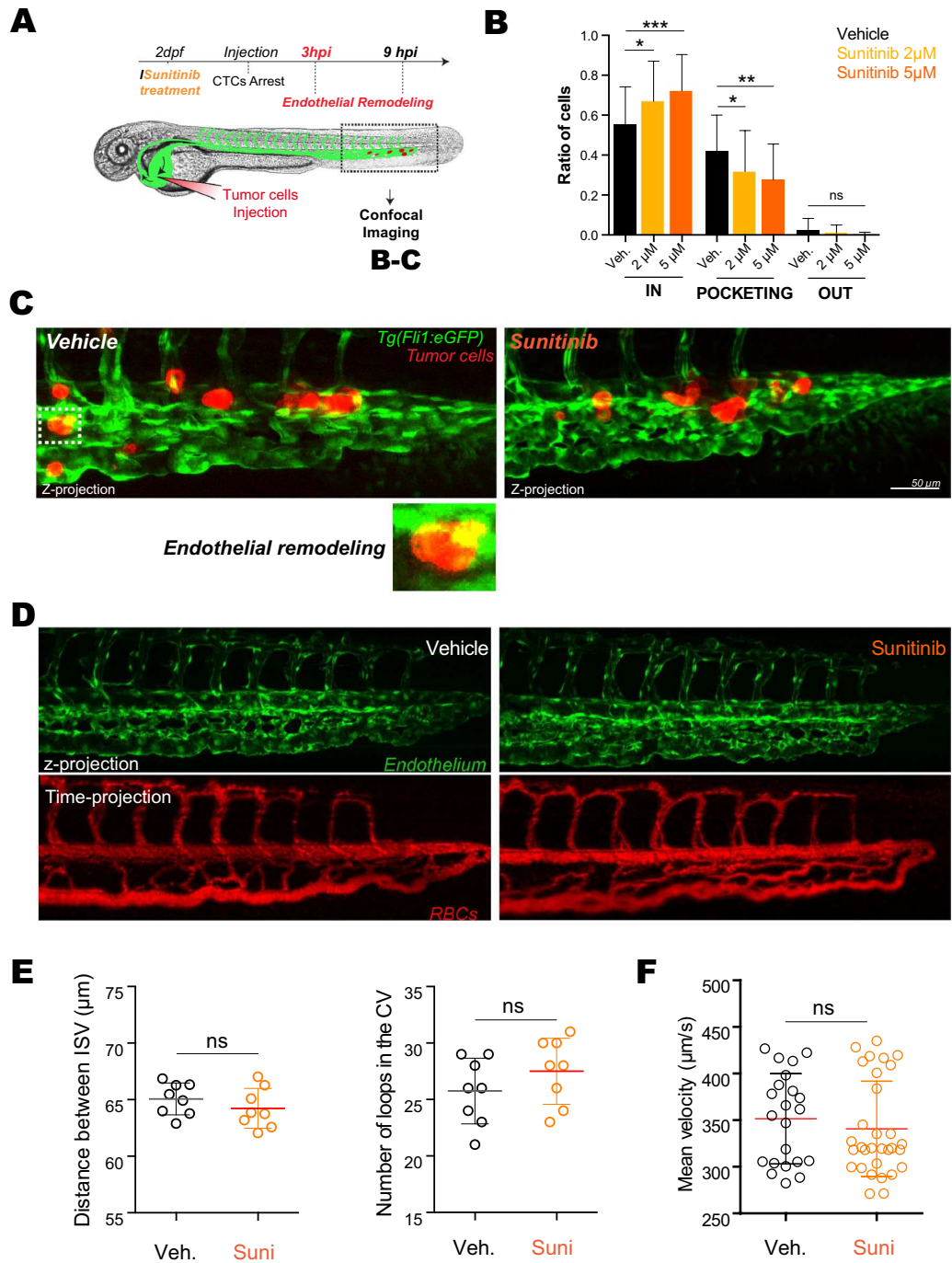


Figure 3. Inhibition of VEGFRs with sunitinib reduces endothelial remodeling in zebrafish embryos. **(A)** Experimental setup used: zebrafish are imaged at 3 hpi (hours post-injection). **(B)** Quantification of intravascular, remodeling and extravasated cells 3hpi. N cells: vehicle = 622, sunitinib 2 μM = 375, sunitinib 5 μM = 254. N embryos : vehicle = 62, sunitinib 2 μM = 34, sunitinib 5 μM = 27, Kruskal–Wallis test followed by Dunn’s multiple Comparison test. **(C)** Representative image of arrested D2A1 cells in the caudal plexus of vehicle or sunitinib treated embryos. Vehicle: DMSO. **(D)** Representative confocal image of the caudal plexus architecture (upper panel) and blood flow (lower panel, RBC = red blood cells) 3 h post-treatment with sunitinib vs vehicle in *Tg(fli1a:EGFP;gata1:DsRed)*. **(E)** Quantification of the effect of sunitinib on vessel architecture after 3 h of treatment with vehicle or 5 μM of sunitinib, N = 8, Student t test. **(F)** Blood flow perfusion profiles of the same embryos (from **D**) and quantification of the blood flow velocity in the caudal plexus of embryos in both conditions after 3 h of treatment with vehicle or 5 μM of sunitinib. N embryos: vehicle = 8, sunitinib 5 μM = 10. Mann Whitney test.

Figure 4. Inhibition of VEGFRs with sunitinib impacts extravasation by endothelial remodeling. (A) Experimental setup used: zebrafish are imaged at 9 hpi & 24 hpi. (B) Quantification of intravascular, remodeling and extravasated cells 9 hpi. N cells: vehicle = 134, sunitinib = 155. N embryos: vehicle = 23, sunitinib = 25, Kruskal–Wallis test followed by Dunn’s multiple Comparison test. (C,D) Representative image of the caudal plexus by confocal intravital imaging (upper panel), corresponding correlative light and electron microscopy imaging (middle panel) and reconstructed segmented images (lower panel). In vehicle treated embryos, tumor cells of interest are *a* and *b* (white squares on (C)). In sunitinib treated embryos, tumor cells of interest are *c* and *d* (white squares on (D)). *TC* tumor cell, *EC* endothelial cell, *L* lumen. (E) The heatmaps show the quantification and location of extravascular CTCs at 24 hpi in the caudal plexus treated with vehicle or 2 μ M of sunitinib. (F) Representative images and orthoslice at 24 hpi. (G) Quantification of extravasated cells ratio at 24 hpi treated with vehicle or 2 μ M of sunitinib. N cells: vehicle = 588, sunitinib = 441. N embryos: vehicle = 27, sunitinib = 27, Mann Whitney test. (H) Quantification of extravasated cells ratio at 24 hpi treated with vehicle or 0.1 μ M of cediranib. N cells: vehicle = 134, cediranib = 143. N embryos: vehicle = 13, cediranib = 17, Mann Whitney test.

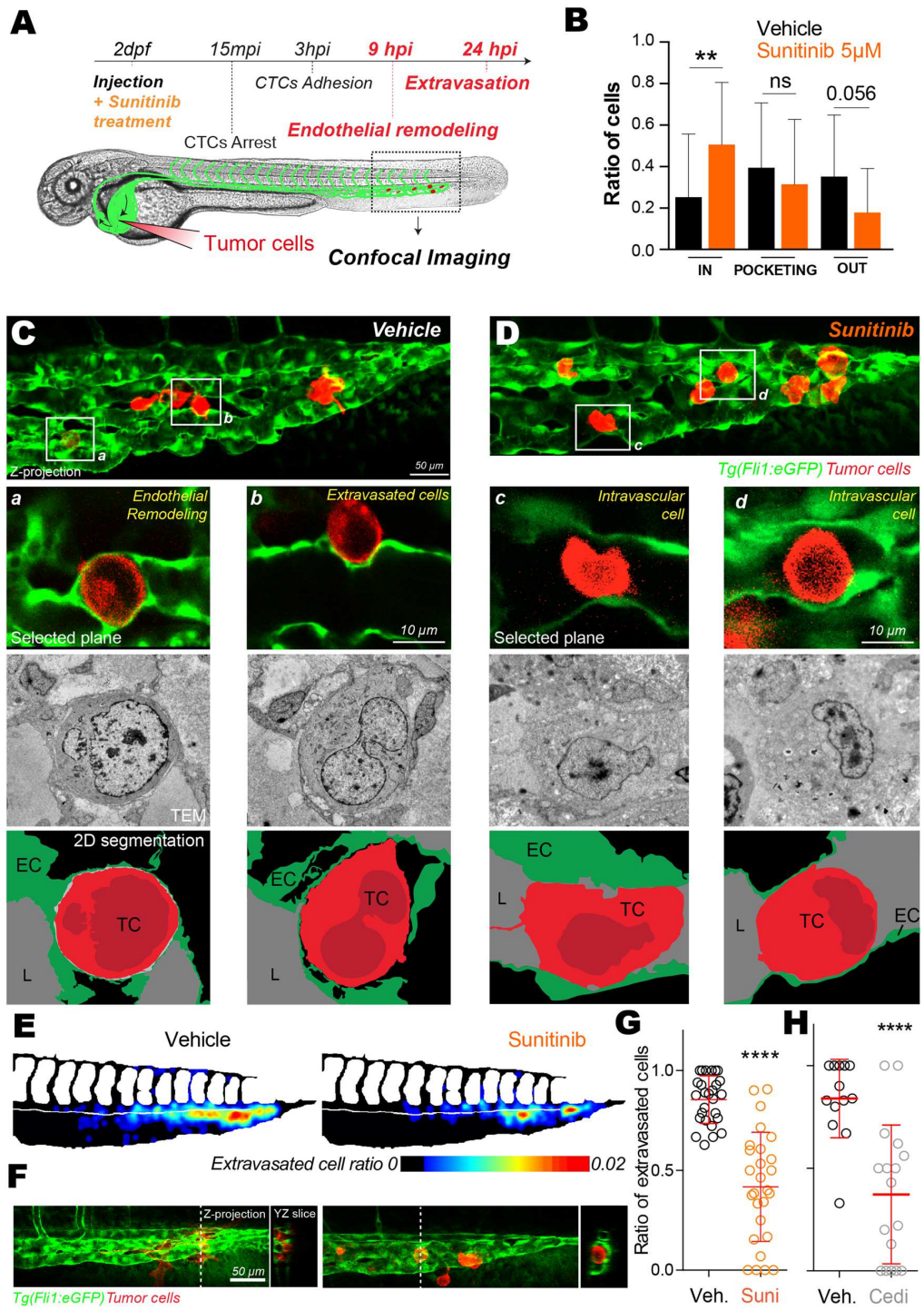
(Fig. 3E). Furthermore, using automated tracking analysis of the red blood cells (DsRed-positive) that allows to extract and quantify the mean velocity of the blood flow, we could not detect any major effect of VEGFR inhibition of overall hemodynamics (Fig. 3F). Altogether, this set of control experiments demonstrates that short sunitinib treatment does not impact the pre-established vascular system, allowing us to investigate whether it would perturb endothelial remodeling and subsequent metastasis.

Taken together, these *in vivo* experiments demonstrate that short inhibition of VEGFR, at regimes that target intraluminal remodeling and do not cause major vascular defects, is capable of impairing local endothelial remodeling upon CTC arrest without major deleterious effects on hemodynamics and vascular architecture. Thus, VEGFR signaling pathway is involved in the early steps of endothelial remodeling.

Inhibition of the VEGF pathway impairs extravasation of metastatic cells in zebrafish embryos.

We next investigated the role of VEGFR signaling during the latter steps of endothelial remodeling (Fig. 4A). We thus performed 3D confocal intravital imaging at 9 hpi where we previously demonstrated that most of extravasating cells are enwrapped by the endothelium, and thus engaged in the pro-extravasation endothelial remodeling process, or extravasated⁹. Inhibition of VEGFRs significantly impairs extravasation of tumor cells at 9hpi (Fig. 4B–D). More specifically, while a majority of the tumor cells remained intravascular or in the process of being pocketed upon VEGFR inhibition, ~80% of cells were either fully pocketed or extravasated in control embryos (Fig. 4B). To confirm these quantitative results and further investigate endothelial remodeling at high-resolution, we set out a correlative light and electron microscopy (CLEM) experiment on representative embryos in both conditions (Fig. 4C,D). CLEM analysis of embryos treated with vehicle immediately after cells injection into the vasculature allowed us to highlight cells that are either in the process of extravasation, through endothelial remodeling, or already fully extravasated and seemingly in contact with the perivascular environment (Fig. 4C). Cells undergoing active endothelial remodeling were fully enwrapped with a layer of endothelium observed all around the extravasating CTC (Fig. 4Ca). We also observed that extravasated cells were present in the perivascular niche and still in close contact with endothelial cells (Fig. 4Cb). When tracking tumor cells in sunitinib-treated embryos, we observed that they remained intravascular with no obvious ultrastructural protrusions that would suggest endothelial remodeling initiation (Fig. 4D). Although these cells were in close contact with the endothelium, we could not observe any protrusions from endothelial cells in close proximity suggesting that endothelial remodeling was either impaired or endothelial migration around the arrested CTCs was delayed (Fig. 4D).

We next investigated the effect of sunitinib treatment on the efficiency of extravasation and the formation of micrometastases. We previously demonstrated that the majority of tumor cells were extravasated at 24 hpi⁹. We thus quantified the ratio of extravasated tumor cells at 24 hpi in embryos that had been treated with vehicle or sunitinib over the whole course of the experiment. We confirmed that treating embryos for 24 h with 5 μ M of sunitinib led to severe defects on the vasculature confirming sunitinib efficiency (data not shown). To rule out any deleterious effects on the vascular architecture that could result from high-dose sunitinib, we thus employed sunitinib at low dose (2 μ M) where only mild perturbations to vascular anatomy could be observed after 24 h of treatment. We observed a 8–9% increase in ISV spacing which we considered as a mild effect compared to a 24 h treatment with 5 μ M of sunitinib which fully abolishes ISVs (data not shown). We previously demonstrated that endothelial remodeling does not occur in ISVs, and most of the tumor cells will stop in the arterio-venous junction⁹. Thus this mild effect does not affect endothelial remodeling since the hotspot for extravasation is not affected. We did not measure any significant difference in blood flow speed nor in red blood cells counts (Fig. S2A,B). Interestingly, in these conditions, the number of extravascular tumor cells was significantly decreased in the caudal plexus region upon VEGFR inhibition (Fig. 4E,F, S2C). In details, we measured a ~ twofold decrease in extravasation efficiency in sunitinib-treated embryos (Fig. 4G) with more CTC staying intravascular compared to vehicle-treated embryos (Fig. 4F). While this phenotype and drug effect raise very exciting avenues in the treatment of metastasis, sunitinib is known to affect other tyrosine kinase receptors in addition to VEGFR (PDGFRs, c-Kit, RET, G-CSF-R, M-CSF-R, FLT3...)³⁷. We thus sought to demonstrate the specific involvement of VEGFR using cediranib, a tyrosine kinase inhibitor with higher specificity for VEGFRs and more specifically toward KDR/VEGFR2³⁸. Cediranib was previously used in zebrafish to inhibit angiogenesis of syngeneic ERMS tumors³⁹. Using a similar experimental strategy, we treated embryos with 0.1 μ M of cediranib following tumor cells injection. We observed that extravasation was reduced in cediranib-treated embryos to the same extent as sunitinib-treated embryos (Fig. 4H). To rule out any side effect of cediranib on the vasculature, we confirmed



that cediranib did not alter the vascular architecture nor blood flow velocity at working concentration (Fig S3A,B). Interestingly again, the treatment regime that we used was potent in inhibiting CTC extravasation by targeting VEGFR-dependent intraluminal remodeling without causing major vascular defects. Taken together, these *in vivo* experiments in a validated experimental metastasis assay demonstrate that blood flow dependent indoctrination of endothelial cells requires VEGFR2 and the VEGFR signaling pathway to favor extravasation of tumor cells in zebrafish embryos.

Discussion

CTC extravasation is an essential step preceding the rate-limiting organ colonization and the foundation of secondary tumor foci¹⁷. Yet, the cellular dynamics and molecular mechanisms of CTC extravasation remain incompletely understood. Extravasation of tumor cells is a rare event at the scale of an entire organism and full understanding requires resolute imaging technologies applied to relevant experimental metastasis models. Based on this, we previously discovered that extravasation occurs mainly through an active endothelial-dependent process that we named endothelial remodeling⁹. Our findings were recently extended to human melanoma and cervix cancer lines¹⁹, suggesting that it is not a cell line specific mechanism. Incidentally, a similar process had also been linked to extravasation of stem cells⁴⁰ and is at play during the important step of blood clot removal, through angiophagy^{21,41}. While recent work demonstrated that endothelial cell death through necroptosis is important for tumor cell extravasation⁴², earlier work had also suggested endothelialization of tumor cells during metastasis^{43,44}. In addition, while such extravasation of tumor cells using endothelial remodeling remains to be documented and functionally tested in classical metastatic organs (lungs, liver, etc...), we and others had shown that it is very likely an important process in the context of mouse brain metastasis^{9,20}. Altogether, this demonstrates that the endothelial wall is a key determinant of the metastatic success. Yet, the underlying molecular triggers and mechanisms favoring plasticity of the endothelium during extravasation remain, at this stage, poorly understood.

Using a flow-tuning approach in the zebrafish embryo and *in vitro* microfluidics, we demonstrated that endothelial remodeling is driven and tuned by hemodynamic cues from the blood flow⁹. Here, using a combination of *in vitro* microfluidics and transcriptomics, but also of intravital imaging and ultrastructural analysis in the zebrafish embryo, we demonstrate that endothelial remodeling around arrested tumor cell is driven, in part, by VEGFR signaling downstream of hemodynamic cues. This is further supported by the observation that endothelial remodeling can be impaired using VEGFR inhibitors initially developed to prevent tumor neo-angiogenesis and used as adjuvant to chemotherapies. We thus demonstrate that intravascular cues that are at play during metastasis are capable of indoctrinating the endothelial wall through a classical VEGFR pathway to stimulate metastatic extravasation of CTCs.

Using transcriptomic analysis, we first demonstrate that permissive flow profiles favor the activation of molecular programs that are linked to angiogenesis, as previously described during developmental angiogenesis^{30,45–47}. Within this molecular program, VEGF receptors, and more specifically KDR (VEGFR2), appear significantly upregulated in response to flow. Endothelial cells have developed several strategies to sense flow which include the cilium, the glycocalyx, mechano-sensitive ions channels, G protein coupled receptors, caveolae, adhesion receptors and VEGFRs^{48,49}. Thus, mechanisms that are relevant for developmental angiogenesis are also likely to be essential for pathological vessel remodeling, including during metastatic extravasation.

With the idea to further validate a molecular node that controls extravasation of tumor cells through endothelial remodeling, we decided to employ sunitinib and cediranib, as potent endothelial remodeling inhibitors. These anti-VEGFR treatments successfully inhibit the extravasation of tumor cells both in an *in vitro* microfluidic setup and in the zebrafish embryos. Our data argue that the VEGFR2 pathway is a major actor of the flow-dependent endothelial remodeling, driving extravasation as we described previously⁹. Whether VEGFR, and more specifically the mechanosensory VEGFR2 and 3, are direct flow mechano-transducers, are acting together with other mechanosensory complexes or are activated downstream of other flow sensors remains to be elucidated⁴⁸. The VEGFR canonical activation is complex, due to partial ligand specificity and crosstalk between VEGF A, B, C, D or PlGF ligands and VEGFR1, R2 or R3 receptors and the heterodimerization between the VEGFRs^{29,50}. Interestingly, non-canonical (ligand-independent) VEGFR activation has been described in the context of mechano-transduction^{31,51–53}. Blood flow changes that occur at the apical side of the endothelial cell, when CTC arrest, might be sufficient to activate VEGFR kinase cascade and transduce the signal into the endothelial cells^{54,55}. Alternatively, indirect forces that result from shear forces on the arrested CTC and that could be transmitted to the endothelial cell which is directly engaged through CTC-endothelium cell-cell adhesions on the luminal side are likely to favor certain transcriptional programs^{32,56}. Such a hypothesis is exciting and further work is needed to determine whether indirect flow forces on arrested tumor cells are likely to impact neighboring endothelial cells. Combination of biophysical tools (such as optical tweezing technologies to manipulate CTC and/or endothelial cells) with microfluidic approaches could be helpful in that regard^{4,9,57}. In addition, there are obviously additional molecular programs that are likely to be involved during this endothelium-dependent process. Interestingly, the process of angiophagy is driven by MMP2/9 activity²¹ and could be involved in driving endothelial remodeling that highly depends on endothelial cell protrusions. In our case, however, expression levels of MMP 2 and 9 are only mildly affected (data not shown). Furthermore, more work is needed to demonstrate whether endothelial remodeling is a universal process used by CTCs to extravasate, or this is limited to certain vascular and hemodynamic conditions or to specific organs. Indeed, the latter likely depends on the organ of metastasis. Although the vasculature of the early zebrafish embryo differs from mature vessels of other relevant models such as mice, we had shown that endothelial remodeling is also initiated during metastatic extravasation of tumor cells in the mouse brain⁹. In that case, VEGFR or other signaling pathways could control endothelial remodeling and metastatic extravasation. More work is required to determine whether endothelial remodeling

occurs in distinct vascular environments, within distinct metastatic organs, and whether they use common or alternative signaling pathways.

Sunitinib is a tyrosine-kinase receptor inhibitor, mainly targeting VEGFR, PDGFR and c-KIT receptors that was first identified in 1999⁵⁸. It is currently clinically used for several cancer treatments including renal or gastrointestinal cancer⁵⁹. Several clinical trials are being conducted to block vascular development around well-established tumors aiming at comparing the effects of sunitinib and cediranib with similar drugs such as pazopanib, another VEGFR/PDGFR/cKit Inhibitor^{60,61}. Being with bevacizumab and to a lesser extent imatinib, the only anti-VEGF therapies clinically approved and despite positive results in its ability to impair tumor growth and cancer progression⁶², the clinical impact of sunitinib is currently questioned as contradictory results have been obtained in the context of tumor metastasis. At this stage, although sunitinib displays detrimental properties that impair its usage in this context, we believe that its powerful inhibition of the VEGFR pathway demonstrates that metastatic extravasation of tumor cells is likely to occur through VEGFR-dependent endothelial remodeling. These results are further strengthened by the observation that cediranib, a VEGFR-specific tyrosine kinase inhibitor phenocopies sunitinib effects on CTC extravasation. In line with our results, a recent study used zebrafish model to predict the clinical efficiency of bevacizumab, another anti-angiogenic therapeutic agent, in anti-metastatic response⁶³. Inhibition of vascular endothelial growth factor-A (VEGF-A) also induced long-term dormancy of lung cancer micrometastases by preventing angiogenic growth to macrometastases in a mouse model of brain metastasis⁶. Flow-independent biomechanical cues might also be elemental to the endothelial response during metastatic progression. It was recently demonstrated that stiffness reduction in liver metastasis induced a higher therapeutic response to bevacizumab⁶⁴, similarly to our observations pointing at a crosstalk between VEGFR-mediated endothelial response and external biomechanical cues. More work is needed to identify additional signaling pathways, and more specific molecules, to efficiently counteract this new mechanism of metastatic extravasation.

Altogether, our data argue that the endothelial remodeling leading to extravasation of metastatic cells can be chemically inhibited *in vivo*. Sunitinib appears as a promising drug to specifically target tumor cells extravasation whose efficiency should be carefully assessed in mouse experimental metastasis models.

Material and methods

Cell lines. D2A1 were provided by Robert A. Weinberg (MIT). Cells stably expressing LifeAct-TdTomato were obtained using lentiviral transfection. Cells were grown as previously described⁶⁵, in DMEM with 4.5 g/l glucose (Dutscher) supplemented with 5% FBS, 5% NBCS, 1% NEAA and 1% penicillin–streptomycin (Gibco). Human Umbilical Vein Endothelial Cells (HUVEC) (PromoCell) were grown in ECGM (PromoCell) supplemented with supplemental mix (PromoCell C-39215) and 1% penicillin–streptomycin (Gibco). To maximize the reproducibility of our experiments, we always used these cells at 4th passage in the microfluidic channels.

Zebrafish handling and sunitinib/cediranib treatment. We used the following zebrafish (*Danio rerio*) lines *Tg(fli1a:EGFP)*⁶⁶, *Tg(kdr:EGFP; gata1:DsRed)*⁶⁷. We generated the following lines by crossing and selecting double positive embryos: *Tg(fli1a:EGFP; gata1:DsRed)*^{66,68} and *Tg(CD41:EGFP; gata1:DsRed)*^{68,69}. Embryos were maintained in Danieau 0.3X medium (17.4 mM NaCl, 0.2 mM KCl, 0.1 mM MgSO₄, 0.2 mM Ca(NO₃)₂) buffered with HEPES 0.15 mM (pH 7.6), supplemented with 200 μM of 1-Phenyl-2-thiourea (Sigma-Aldrich) to inhibit the melanogenesis, as previously described⁷⁰. Sunitinib (Sigma-Aldrich) was added in the breeding water of the embryos directly after injection of tumor cells at the concentration of 2 μM or 5 μM vs vehicle (DMSO). Cediranib (BioVision) was added in the breeding water of the embryos directly after injection of tumor cells at the concentration of 0.1 μM vs vehicle (DMSO).

Control experiments for sunitinib & cediranib effect on zebrafish embryos. Sunitinib and cediranib treatment were tested for their potential impact on vascular architecture and/or on blood flow pattern in the caudal region. After 3 or 24 h of treatment (sunitinib, cediranib or vehicle), we performed confocal microscopy using an inverted TCS SP5 confocal microscope with a 20× /0.75 (Leica) and manually analyzed the architectures of landmark vessels. In the plexus, the conservation of the distance between intersegmental vessels and the number of vascular branching in the caudal veins was quantified using ImageJ software. Also, we performed fast recording using the resonant scanner at a speed of 27 fps in *Tg(kdr:EGFP; gata1:DsRed)* or *Tg(CD41:EGFP; gata1:DsRed)* embryos. We measured the mean flow velocity using the TrackMate plugin⁷¹ in Fiji 1.52n (<https://fiji.sc/>).

To measure red blood cells counts, the number of red blood cells in individual movies was counted in the dorsal aorta of embryos and normalized to the length of the region of interest which had been considered.

Intravascular injection and imaging of CTCs in the zebrafish embryo. 48 h post-fertilization (hpf) *Tg(fli1a:EGFP)* embryos were mounted in 0.8% low melting point agarose pad containing 650 μM of tricain (ethyl-3-aminobenzoate-methanesulfonate) to immobilize the embryos. D2A1 LifeAct-TdTomato cells were injected with a Nanoject microinjector 2 (Drummond) and microforged glass capillaries (25 to 30 μm inner diameter) filled with mineral oil (Sigma). 18 nL of a cell suspension at 100.10⁶ cells per ml were injected in the duct of Cuvier of the embryos under the M205 FA stereomicroscope (Leica).

For caudal plexus, confocal imaging was performed with an inverted TCS SP5 confocal microscope with a 20× /0.75 (Leica). The caudal plexus region (around 50 μm width) was imaged with a z-step of less than 1.5 μm for at least 20 embryos per conditions from 3 independent experiments. Cell number and situations was manually characterized (Intravascular, ongoing endothelial remodeling/pocketing, extravascular) using z-projections and orthogonal views in ImageJ.

Correlative Light and Electron Microscopy was performed to describe ultrastructural characteristics of CTCs and the endothelium in the zebrafish embryo. Chosen embryos of both condition (Vehicle and Sunitinib treated) were imaged using confocal microscopy between 3 to 4 hpi. Just after imaging, they were chemically fixed and processed for EM (see dedicated section “EM preparation”).

EM preparation and correlation between light and electron microscopy. The samples (fish tails after confocal microscopy) have been post fixed in a solution of 2,5% glutaraldehyde and 2% paraformaldehyde in 0.1 M Cacodylate buffer at 4 °C overnight. Samples were rinsed in 0.1 M Cacodylate buffer for 2 × 5 min and post-fixed using 1% OsO₄ in 0.1 M Cacodylate buffer, for 1 h at room temperature. Then, samples were rinsed for 3 × 5 min in 0.1 M Cacodylate buffer, followed by washing 2 × 5 min in pure water. Samples were secondary post-fixed with 4% water solution of uranyl acetate for 1 h at room temperature. Followed by 5 min wash in pure water, the samples were stepwise dehydrated in Ethanol (50% 3 × 5 min, 70% 3 × 10 min, 90% 3 × 10 min and 100% 3 × 10 min) and infiltrated in a graded series of Epon (Ethanol abs/Epon 3/1, 1/1, 1/3, each 30 min). Samples were left in absolute Epon (EmBed812—EMS) overnight. Then, samples were placed in a fresh absolute Epon for 1 h and polymerized (flat embedded) at 60 °C for 24–48 h. Once polymerized, most surrounding Epon was cut off using razorblade and samples were mounted on empty Epon blocks (samples flat at the surface of the blocks) and left at 60 °C for 24 h–48 h.

To do the correlation in 3d, semi thin sections (500 nm) were obtained using glass knife in ultramicrotome LEICA UCT. Sections were placed on slide, stained with 1% borax Toluidine blue solution and checked out in the optical microscope. Anatomical landmarks were used to retrieve the ROI (dorsal aorta, tumor cells...).

Ultrathin sections (100 nm) were serially sectioned using ultramicrotome (Leica Ultracut UCT), collected on formvar-coated slot grids and stained with 4% water solution of uranyl acetate for 5 min and lead citrate for 3 min. Ultra-thin sections were imaged with a CM120 transmission electron microscope (Philips Biotwin) operating at 120 kV. Images were recorded with Veleta 2 k × 2 k (Olympus-SIS) camera using iTEM 5.0 software. The ROI was approached by progressive serial sectioning of the samples. Multiple sections were further processed and acquired.

Zebrafish heatmaps. The heatmaps were generated as previously described³⁶ using ImageJ 1.52n (<https://imagej.nih.gov/ij/index.html>) and MATLAB R2016b (MathWorks, <https://www.mathworks.com/>) softwares.

Microfluidic experiments. For endothelial remodeling experiments in vitro, two μ-slides I⁰₄ Luer (IBIDI) coated with fibronectin from bovine plasma at 10 μg/ml (Sigma F-1141) were used in parallel for each experiment. HUVEC cells were seeded at 100 000 cells per channel. Medium was changed twice a day for 2 or 3 days, before perfusing the channels under a flow of 400 μm/s using REGLO Digital MS-2/12 peristaltic pump (Ismatec) and Tygon tubing (IDEX). Sunitinib treatment was added at a concentration of 0.1 μM in flow. At confluence, D2A1 LifeAct-TdTomato cells were added at a concentration of 200,000 cells/ml for 10 min. Then, floating tumor cells were washed using fresh medium and the channels were incubated for 16 h with flow. Position of the tumor cells and presence of endothelial remodeling around tumor cells relative to the HUVEC monolayer were determined using the piezo stage of the confocal microscope after fixation and Immunofluorescent staining (see next section).

Antibodies. Mouse anti-human CD31 (PECAM) monoclonal antibody (MEM-5) was purchased from Thermo, mouse anti-human FLT1 (ab9540) and rat anti-mouse FLT4 (ab51874) monoclonal antibodies were purchased from AbCam, rabbit anti-KDR monoclonal antibody (D5B1) was purchased from Cell Signaling and α-tubulin (DM1A) was purchased from Millipore. Fluorescently labelled secondary antibodies were purchased from Invitrogen: goat anti-mouse/rat/rabbit coupled with Alexa Fluor 488, Cy3, Alexa 555, Cy5 or Alexa 647. HRP-conjugated secondary antibodies were purchased from Jackson Immunoresearch.

Immunofluorescent staining in the microfluidic channels. Cells were fixed using 4% PFA (Electronic Microscopy Sciences), permeabilized with 0.2% Triton-X100 (Sigma) and quenched with 2 mg/ml NaBH₄ (Sigma) 10 min at room temperature before using the following primary antibodies. Cells were incubated 1 h at room temperature on a tilting stage and washed with PBS. Cells were incubated with secondary antibodies 30 min at room temperature on a tilting stage and protected from light. Cells were mounted using Vectashield (Vector Laboratories).

Western blotting. Channels were seeded simultaneously with 100,000 cells 4 days prior to experiment. Extracts corresponding to similar cell numbers were loaded on 4–20% polyacrylamide gels (Biorad) and run under denaturing conditions. Primary antibodies were incubated 2 h at room temperature. HRP-conjugated secondary antibodies were incubated 1 h at room temperature. Data were acquired using with ECL (GE Healthcare) and the ChemiDoc XRS (Biorad). Intensities were normalized over α-tubulin levels.

RNA sequencing. 3 independent couples (flow and no flow) of HUVEC samples were isolated from μ-slides I⁰₄ Luer (ibidi) using Tri-reagent (MRC) 100 μl of Tri-reagent was added directly in one side of the channel and aspire in the other side 5 times. This was followed by chloroform extraction and alcohol washing. Total cDNA was obtained using Thermo Fisher kit (SuperScript VILO Master mix).

RNA integrity was assessed with the Agilent total RNA Pico Kit on a 2100 Bioanalyzer instrument (Agilent Technologies, Palo Alto, USA). The construction of libraries was done with the “SMARTer Stranded Total

RNA-Seq Kit v2—Pico Input Mammalian" (TaKaRa Bio USA) with a final multiplexing of 12 libraries according to the manufacturer's instructions. The library pool was denatured according to the Illumina protocol "Denature and Dilute Libraries Guide" and then deposited at a concentration of 1.3 pM to be sequenced on the NextSeq 500 (Illumina).

The transcriptome data set, composed of sequencing reads, was generated by an Illumina NextSeq instrument. The objective is to identify genes that are differentially expressed between two experimental conditions: *flow* and *no flow*. First, the data were mapped to the human genome/transcriptome (hg19) using the HISAT2 software v2.1.0 (<http://daehwankimlab.github.io/hisat2/>)^{72,73}, a fast and sensitive alignment program. The total reads mapped were finally available in BAM format for raw read counts extraction. Next, read counts were found by the htseq-count tool of the Python package HTSeq⁷⁴ with default parameters to generate an abundant matrix. Then, differential analyses were performed by the DESEQ2⁷⁵ package of the Bioconductor framework. Up-regulated and down-regulated genes were selected based on the adjusted p-value cutoff 10%. Finally, Gene Ontology Consortium (<http://www.geneontology.org/>) platform was used for data analysis and heatmaps creation. The heatmaps were formatted using IGOR pro 8 software (<https://www.wavemetrics.com/>).

qPCR validation. 3 to 7 independent couples (flow and no flow) of HUVEC samples total RNAs were isolated from μ -slides I^{0.4} Luer (ibidi) using Tri-reagent (MRC) followed by chloroform extraction and alcohol precipitation. Total cDNA was obtained using ThermoFisher kit (SuperScript VILO Master mix). RT qPCR reactions were made using either TaqMan master mix (ThermoFisher—4444557) or SYBR green master mix (Thermo Fisher—A25742) in an Applied Biosystem qPCR machine (QuantStudio 3—Thermo Fisher). See next table of qPCR primer sequences for Flt1, Kdr, Flt4, Notch1, Lama4 (lab designed). For human GAPDH, a commercial TaqMan probe was used (Thermo Fisher—4333764F). Amplification results were normalized using GAPDH level and double Δ Ct method⁷⁶.

Targets	Primer sequences
h Flt1 fwd	CCA GCA GCG AAA GCT TTG CG
h Flt1 rev	CTC CTT GTA GAA ACC GTC AG
h Kdr fwd	ATG ACA TTT TGA TCA TGG AGC
h Kdr rev	CCC AGA TGC CGT GCA TGA G
h Flt4 fwd	TGC AAG AGG AAG AGG AGG TCT
h Flt4 rev	CAG GCT TGG CGG GCT GTC C
h Notch1 fwd	CAG GAC GGC TGC GGC TCC TAC
h Notch1 rev	CCG CCG TTC TTG CAG GGC GAG
h Lama4 fwd	ACC TCC TCA ATC AAG CCA GA
h Lama4 rev	TCA GCC ACT GCT TCA TCA CT

RT-qPCR in FACS-sorted zebrafish endothelium. Embryos were euthanized using tricaine overdose collected in 1.5 ml Eppendorf tubes (30 embryos per tube). Embryos are washed twice with 1 ml of 1× PBS and 500 μ l of the dissociation mix (collagenase 4 mg/ml in 0.25% trypsin-EDTA pre-heated at 30 °C) was added and each tube was incubated at 30 °C. Embryos were mechanically dissociated and homogenized using harsh pipetting until tissues were no longer visible. 800 μ l of DMEM-10% FBS was added to the tubes to stop the dissociation. Tubes were mixed and centrifuged at 700g for 5 min. Pellets were resuspended in 1 ml of 1× PBS and centrifuged at 700g for 5 min. The pellet was resuspended in 500 μ l of cell-sorting buffer (5 mM EDTA, 25 mM HEPES, 2% FCS in 1× PBS). Samples were sorted through 70 μ m nylon-mesh and collected in a new Eppendorf tube for FACS sorting. GFP+ cells were sorted using an Aria II SORP FACS cell sorter (BD Bioscience). Total RNAs were isolated from 200,000 GFP+ FACS-sorted cell population using Tri-reagent (MRC) followed by chloroform extraction and alcohol precipitation. Total cDNA was obtained using High-Capacity cDNA Reverse Transcription Kit (Thermo Fischer—4368814). RT-qPCR reactions were made using either TaqMan master mix (Thermo Fisher—4444557) or SYBR green master mix (Thermo Fisher—A25742) in an Applied Biosystem qPCR machine (QuantStudio 3—Thermo Fisher). Commercial TaqMan probes were used KDR (Thermo Fisher—Dr03116261_m1) and KDRL (Thermo Fisher—Dr03432904_m1). Zebrafish GAPDH primers forward: tcagtcactcaccaagt, reverse: cgaccgaatccgtaatacc. Amplification results were normalized using GAPDH level and double Δ Ct method⁷⁶.

Statistical analysis. Statistical analysis was performed using the GraphPad Prism program version 5.04 (<https://www.graphpad.com/>). The Shapiro-Wilk normality test was used to confirm the normality of the data. For data following a Gaussian distribution, a Student unpaired two-tailed t test, with Welch's correction in case of unequal variances was used. For data not following a Gaussian distribution, the Mann-Whitney test was used. When more than 3 groups are compared, a Kruskal-Wallis test followed by Dunn's multiple comparison test was used. For qualitative data, the Fisher test was used. Illustrations of these statistical analyses are displayed as the mean \pm standard deviation (SD). p-values smaller than 0.05 were considered as significant. *, p < 0.05, **, p < 0.01, ***, p < 0.001, ****, p < 0.0001, ns = not significant.

Received: 17 September 2020; Accepted: 31 May 2021
Published online: 23 June 2021

References

1. Massagué, J. & Obenauf, A. C. Metastatic colonization by circulating tumour cells. *Nature* **529**, 298–306 (2016).
2. Follain, G. *et al.* Fluids and their mechanics in tumour transit: Shaping metastasis. *Nat. Rev. Cancer* **20**, 107–124 (2020).
3. Reymond, N., d'Agua, B. B. & Ridley, A. J. Crossing the endothelial barrier during metastasis. *Nat. Rev. Cancer* **13**, 858–870 (2013).
4. Osmani, N. *et al.* Metastatic tumor cells exploit their adhesion repertoire to counteract shear forces during intravascular arrest. *Cell Rep.* **28**, 2491–2500.e5 (2019).
5. Chambers, A. F., Groom, A. C. & MacDonald, I. C. Metastasis: Dissemination and growth of cancer cells in metastatic sites. *Nat. Rev. Cancer* **2**, 563–572 (2002).
6. Kienast, Y. *et al.* Real-time imaging reveals the single steps of brain metastasis formation. *Nat. Med.* **16**, 116–122 (2010).
7. Headley, M. B. *et al.* Visualization of immediate immune responses to pioneer metastatic cells in the lung. *Nature* **531**, 513–517 (2016).
8. Wirtz, D., Konstantopoulos, K. & Searson, P. C. The physics of cancer: The role of physical interactions and mechanical forces in metastasis. *Nat. Rev. Cancer* **11**, 512–522 (2011).
9. Follain, G. *et al.* Hemodynamic forces tune the arrest, adhesion, and extravasation of circulating tumor cells. *Dev. Cell* **45**, 33–52.e12 (2018).
10. Paget, S. The distribution of secondary growths in cancer of the breast. *Lancet* **133**, 571–573 (1889).
11. Obenauf, A. C. & Massagué, J. Surviving at a distance: Organ-specific metastasis. *Trends Cancer* **1**, 76–91 (2015).
12. DeNardo, D. G., Andreu, P. & Coussens, L. M. Interactions between lymphocytes and myeloid cells regulate pro- versus anti-tumor immunity. *Cancer Metastasis Rev.* **29**, 309–316 (2010).
13. Nagarsheth, N., Wicha, M. S. & Zou, W. Chemokines in the cancer microenvironment and their relevance in cancer immunotherapy. *Nat. Rev. Immunol.* **17**, 559–572 (2017).
14. Paszek, M. J. *et al.* Tensional homeostasis and the malignant phenotype. *Cancer Cell* **8**, 241–254 (2005).
15. Levental, K. R. *et al.* Matrix crosslinking forces tumor progression by enhancing integrin signaling. *Cell* **139**, 891–906 (2009).
16. Mouw, J. K. *et al.* Tissue mechanics modulate microRNA-dependent PTEN expression to regulate malignant progression. *Nat. Med.* **20**, 360–367 (2014).
17. Valastyan, S. & Weinberg, R. A. Tumor metastasis: Molecular insights and evolving paradigms. *Cell* **147**, 275–292 (2011).
18. Stoletov, K. *et al.* Visualizing extravasation dynamics of metastatic tumor cells. *J. Cell Sci.* **123**, 2332–2341 (2010).
19. Allen, T. A. *et al.* Circulating tumor cells exit circulation while maintaining multicellularity, augmenting metastatic potential. *J. Cell Sci.* **132**, jcs231563 (2019).
20. Haskó, J. *et al.* Response of the neurovascular unit to brain metastatic breast cancer cells. *Acta Neuropathol. Commun.* **7**, 133 (2019).
21. Lam, C. K., Yoo, T., Hiner, B., Liu, Z. & Grutzendler, J. Embolus extravasation is an alternative mechanism for cerebral microvascular recanalization. *Nature* **465**, 478 (2010).
22. Carmeliet, P. & Jain, R. K. Molecular mechanisms and clinical applications of angiogenesis. *Nature* **473**, 298–307 (2011).
23. Meadows, K. L. & Hurwitz, H. I. Anti-VEGF therapies in the clinic. *Cold Spring Harb. Perspect. Med.* **2** (2012).
24. Ivanov, K. P., Kalinina, M. K. & Levkovich, Yu. I. Microcirculation velocity changes under hypoxia in brain, muscles, liver, and their physiological significance. 10–18 (1985).
25. Anton, H. *et al.* Pulse propagation by a capacitive mechanism drives embryonic blood flow. *Development* **140**, 4426–4434 (2013).
26. Hill, R. A. *et al.* Regional blood flow in the normal and ischemic brain is controlled by arteriolar smooth muscle cell contractility and not by capillary pericytes. *Neuron* **87**, 95–110 (2015).
27. Sugden, W. W. *et al.* Endoglin controls blood vessel diameter through endothelial cell shape changes in response to haemodynamic cues. *Nat. Cell Biol.* **19**, 653–665 (2017).
28. Fang, J. S. *et al.* Shear-induced Notch-Cx37-p27 axis arrests endothelial cell cycle to enable arterial specification. *Nat. Commun.* **8** (2017).
29. Simons, M., Gordon, E. & Claesson-Welsh, L. Mechanisms and regulation of endothelial VEGF receptor signalling. *Nat. Rev. Mol. Cell Biol.* **17**, 611–625 (2016).
30. Galie, P. A. *et al.* Fluid shear stress threshold regulates angiogenic sprouting. *PNAS* **111**, 7968–7973 (2014).
31. Baeyens, N. *et al.* Vascular remodeling is governed by a VEGFR3-dependent fluid shear stress set point. *eLife* **4**, e04645 (2015).
32. Baeyens, N. & Schwartz, M. A. Biomechanics of vascular mechanosensation and remodeling. *Mol. Biol. Cell* **27**, 7–11 (2016).
33. Osmani, N. *et al.* Probing intravascular adhesion and extravasation of tumor cells with microfluidics. In *Metastasis: Methods and Protocols* (ed. Stein, U. S.) 111–132 (Springer, New York, NY, 2021).
34. Cagan, R. L., Zon, L. I. & White, R. M. Modeling cancer with flies and fish. *Dev. Cell* **49**, 317–324 (2019).
35. Osmani, N. & Goetz, J. G. multiscale imaging of metastasis in zebrafish. *Trends Cancer* **5**, 766–778 (2019).
36. Follain, G. *et al.* Using the zebrafish embryo to dissect the early steps of the metastasis cascade. In *Cell Migration* 195–211. https://doi.org/10.1007/978-1-4939-7701-7_15 (Humana Press, 2018).
37. Mendel, D. B. *et al.* In vivo antitumor activity of SU11248, a novel tyrosine kinase inhibitor targeting vascular endothelial growth factor and platelet-derived growth factor receptors: Determination of a pharmacokinetic/pharmacodynamic relationship. *Clin. Cancer Res.* **9**, 327–337 (2003).
38. Wedge, S. R. *et al.* AZD2171: A highly potent, orally bioavailable, vascular endothelial growth factor receptor-2 tyrosine kinase inhibitor for the treatment of cancer. *Cancer Res.* **65**, 4389–4400 (2005).
39. Chen, E. Y. *et al.* Cross-species array comparative genomic hybridization identifies novel oncogenic events in zebrafish and human embryonal rhabdomyosarcoma. *PLOS Genet.* **9**, e1003727 (2013).
40. Allen, T. A. *et al.* Angiopoiesis as an alternative mechanism of cell extravasation. *Stem Cells* **35**, 170–180 (2017).
41. Grutzendler, J. *et al.* Angiophagy prevents early embolus washout but recanalizes microvessels through embolus extravasation. *Sci. Transl. Med.* **6**, 226ra31–226ra31 (2014).
42. Strilic, B. *et al.* Tumour-cell-induced endothelial cell necroptosis via death receptor 6 promotes metastasis. *Nature* **536**, 215–218 (2016).
43. Lapis, K., Paku, S. & Liotta, L. A. Endothelialization of embolized tumor cells during metastasis formation. *Clin. Exp. Metast.* **6**, 73–89 (1988).
44. Paku, S., Döme, B., Tóth, R. & Timár, J. Organ-specificity of the extravasation process: An ultrastructural study. *Clin. Exp. Metastasis* **18**, 481–492 (2000).
45. García-Cardena, G., Comander, J., Anderson, K. R., Blackman, B. R. & Gimbrone, M. A. Biomechanical activation of vascular endothelium as a determinant of its functional phenotype. *PNAS* **98**, 4478–4485 (2001).
46. Nakajima, H. *et al.* Flow-dependent endothelial YAP regulation contributes to vessel maintenance. *Dev. Cell* **40**, 523–536.e6 (2017).

47. Nicoli, S. *et al.* MicroRNA-mediated integration of haemodynamics and Vegf signalling during angiogenesis. *Nature* **464**, 1196–1200 (2010).
48. Freund, J. B., Goetz, J. G., Hill, K. L. & Vermot, J. Fluid flows and forces in development: Functions, features and biophysical principles. *Development* **139**, 1229–1245 (2012).
49. Baratchi, S. *et al.* molecular sensors of blood flow in endothelial cells. *Trends Mol. Med.* **23**, 850–868 (2017).
50. Domigan, C. K., Ziyad, S. & Iruela-Arispe, M. L. Canonical and non-canonical VEGF pathways: New developments in biology and signal transduction. *Arterioscler. Thromb. Vasc. Biol.* **35**, 30–39 (2015).
51. Tzima, E. *et al.* A mechanosensory complex that mediates the endothelial cell response to fluid shear stress. *Nature* **437**, 426–431 (2005).
52. Conway, D. E. *et al.* Fluid shear stress on endothelial cells modulates mechanical tension across VE-cadherin and PECAM-1. *Curr. Biol.* **23**, 1024–1030 (2013).
53. Coon, B. G. *et al.* Intramembrane binding of VE-cadherin to VEGFR2 and VEGFR3 assembles the endothelial mechanosensory complex. *J. Cell Biol.* **208**, 975–986 (2015).
54. dela Paz, N. G., Walshe, T. E., Leach, L. L., Saint-Geniez, M. & D'Amore, P. A. Role of shear-stress-induced VEGF expression in endothelial cell survival. *J. Cell Sci.* **125**, 831–843 (2012).
55. Koch, S., Tugues, S., Li, X., Gualandi, L. & Claesson-Welsh, L. Signal transduction by vascular endothelial growth factor receptors. *Biochem. J.* **437**, 169–183 (2011).
56. Schaefer, A. & Hordijk, P. L. Cell-stiffness-induced mechanosignaling—A key driver of leukocyte transendothelial migration. *J. Cell Sci.* **128**, 2221–2230 (2015).
57. Harlepp, S., Thalmann, F., Follain, G. & Goetz, J. G. Hemodynamic forces can be accurately measured in vivo with optical tweezers. *Mol. Biol. Cell* **28**, 3252–3260 (2017).
58. Fong, T. A. T. *et al.* SU5416 is a potent and selective inhibitor of the vascular endothelial growth factor receptor (Flk-1/KDR) that inhibits tyrosine kinase catalysis, tumor vascularization, and growth of multiple tumor types. *Cancer Res.* **59**, 99–106 (1999).
59. Younus, J., Verma, S., Franek, J. & Coakley, N. Sunitinib malate for gastrointestinal stromal tumour in imatinib mesylate-resistant patients: Recommendations and evidence. *Curr. Oncol.* **17**, 4 (2010).
60. Chellappan, D. K. *et al.* The role of pazopanib on tumour angiogenesis and in the management of cancers: A review. *Biomed. Pharmacother.* **96**, 768–781 (2017).
61. Rodriguez-Vida, A., Hutson, T. E., Bellmunt, J. & Strijbos, M. H. New treatment options for metastatic renal cell carcinoma. *ESMO Open* **2**, e000185 (2017).
62. Young, E. *et al.* SU11248, A selective tyrosine kinases inhibitor suppresses breast tumor angiogenesis and growth via targeting both tumor vasculature and breast cancer cells. *Cancer Biol. Ther.* **10**, 703–711 (2010).
63. Rebelo de Almeida, C. *et al.* Zebrafish xenografts as a fast screening platform for bevacizumab cancer therapy. *Commun. Biol.* **3**, 1–13 (2020).
64. Shen, Y. *et al.* Reduction of liver metastasis stiffness improves response to bevacizumab in metastatic colorectal cancer. *Cancer Cell* **37**, 800–817.e7 (2020).
65. Shibue, T., Brooks, M. W., Inan, M. F., Reinhardt, F. & Weinberg, R. A. The outgrowth of micrometastases is enabled by the formation of filopodium-like protrusions. *Cancer Discov.* **2**, 706–721 (2012).
66. Lawson, N. D. & Weinstein, B. M. In vivo imaging of embryonic vascular development using transgenic zebrafish. *Dev. Biol.* **248**, 307–318 (2002).
67. Daetwyler, S., Günther, U., Modes, C. D., Harrington, K. & Huisken, J. Multi-sample SPIM image acquisition, processing and analysis of vascular growth in zebrafish. *Development* **146** (2019).
68. Traver, D. *et al.* Transplantation and in vivo imaging of multilineage engraftment in zebrafish bloodless mutants. *Nat. Immunol.* **4**, 1238–1246 (2003).
69. Lin, H.-F. *et al.* Analysis of thrombocyte development in CD41-GFP transgenic zebrafish. *Blood* **106**, 3803–3810 (2005).
70. Goetz, J. G. *et al.* Endothelial cilia mediate low flow sensing during zebrafish vascular development. *Cell Rep.* **6**, 799–808 (2014).
71. Tinevez, J.-Y. *et al.* TrackMate: An open and extensible platform for single-particle tracking. *Methods* **115**, 80–90 (2017).
72. Kim, D., Langmead, B. & Salzberg, S. L. HISAT: A fast spliced aligner with low memory requirements. *Nat. Methods* **12**, 357–360 (2015).
73. Kim, D., Paggi, J. M., Park, C., Bennett, C. & Salzberg, S. L. Graph-based genome alignment and genotyping with HISAT2 and HISAT-genotype. *Nat. Biotechnol.* **37**, 907–915 (2019).
74. Anders, S., Pyl, P. T. & Huber, W. HTSeq—A Python framework to work with high-throughput sequencing data. *Bioinformatics* **31**, 166–169 (2015).
75. Love, M. I., Huber, W. & Anders, S. Moderated estimation of fold change and dispersion for RNA-seq data with DESeq2. *Genome Biol.* **15** (2014).
76. Livak, K. J. & Schmittgen, T. D. Analysis of relative gene expression data using real-time quantitative PCR and the 2⁻ $\Delta\Delta$ CT method. *Methods* **25**, 402–408 (2001).

Acknowledgements

This work is dedicated to the memory of Karin KONRADT. We thank all members of the GOETZ Lab for helpful discussions and Sébastien HARLEPP for assistance throughout the study. We are very grateful to Paul TIMPSON, David HERMANN and Cecilia CHAMBERS (Garvan Institute, Sydney) for help throughout the study, and to Francesca PERI and Kerstin RICHTER (EMBL, Heidelberg) for providing zebrafish embryos at the early stage of the project. We thank Frank WINKLER and Matthia KARREMAN for discussions at early stages of the manuscript. We thank the imaging facility members from EFS (INSERM U949, Strasbourg), IGBMC (CNRS UMR 7104, INSERM U 1258) and INCI (CNRS UPR 3212) for access to light and electron microscopes and FACS sorting facility members of the IGBMC for their assistance.

Author contributions

G.F. and N.O. performed most of the experiments and analysis. V.G. helped with zebrafish experiments. N.A. performed zebrafish embryo FACS sorting. A.L. helped with RT-qPCR and western blot experiments. I.B. performed the CLEM procedures with input from G.F. and L.M. L.M. and M.J.G.L. helped with data analysis. A.P., N.P., R.C. and S.B. performed the RNAseq experiment and sequence alignment. O.L. set up transcriptomics analysis, performed RNA purification and RT-qPCR analysis, generated stable cell lines and supervised the study. J.G.G. conceived the project, acquired funding and supervised the study. G.F. and N.O. wrote the manuscript with input from O.L. and J.G.G.

Funding

This work has been funded by Plan Cancer (OptoMetaTrap to JG) and CNRS IMAG'IN (to JG) and INCa (to JG, PLBIO-2014-151, PLBIO 2015-140 and PLBIO 2016-164) and by institutional funds from INSERM and University of Strasbourg. NO is supported by Plan Cancer 2014-2019 (OptoMetaTrap) and the Association pour la Recherche contre le Cancer. GF was supported by La Ligue Contre le Cancer and University of Strasbourg. MJGL is funded by University of Strasbourg and LM was supported by Region Alsace and INSERM. Current work is funded by ITMO Cancer of AVIESAN (Alliance Nationale pour les Sciences de la Vie et de la Santé, National Alliance for Life Sciences & Health) within the framework of the Cancer Plan Cancer (Nanotumor, to JG), la Ligue Contre le Cancer ("Equipe Labellisée" to JG) and IdEx Attractivité program (University of Strasbourg to NO).

Competing interests

The authors declare no competing interests.

Additional information

Supplementary Information The online version contains supplementary material available at <https://doi.org/10.1038/s41598-021-92515-2>.

Correspondence and requests for materials should be addressed to O.L. or J.G.G.

Reprints and permissions information is available at www.nature.com/reprints.

Publisher's note Springer Nature remains neutral with regard to jurisdictional claims in published maps and institutional affiliations.



Open Access This article is licensed under a Creative Commons Attribution 4.0 International License, which permits use, sharing, adaptation, distribution and reproduction in any medium or format, as long as you give appropriate credit to the original author(s) and the source, provide a link to the Creative Commons licence, and indicate if changes were made. The images or other third party material in this article are included in the article's Creative Commons licence, unless indicated otherwise in a credit line to the material. If material is not included in the article's Creative Commons licence and your intended use is not permitted by statutory regulation or exceeds the permitted use, you will need to obtain permission directly from the copyright holder. To view a copy of this licence, visit <http://creativecommons.org/licenses/by/4.0/>.

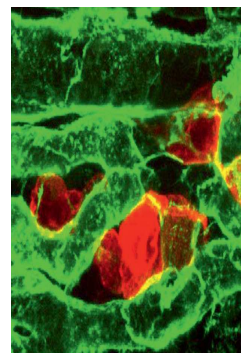
© The Author(s) 2021, corrected publication 2021

ANNEXE 2

> La suite d'évènements menant à l'apparition de métastases est appelée « cascade métastatique ». L'étude récente de la composante biomécanique de cette cascade a révélé le rôle central des liquides biologiques dans la dissémination métastatique. Tout en participant au transport des cellules tumorales circulantes et des facteurs qu'elles sécrètent, ces liquides circulants influencent cette cascade par les forces mécaniques qu'ils génèrent. Les propriétés hémodynamiques et les contraintes topologiques de l'architecture vasculaire contrôlent la formation de niches métastatiques et le potentiel métastatique des cellules tumorales. <

Influence de la mécanique des fluides sur la formation des métastases

Gautier Follain^{1-3,5*}, Valentin Gensbittel^{1-3*}, Benjamin Mary^{1-3*}, Olivier Lefebvre¹⁻³, Sébastien Harlepp¹⁻³, Vincent Hyenne¹⁻⁴, Jacky G. Goetz¹⁻³



¹Inserm UMR_S1109, 1 place de l'Hôpital, F-67000 Strasbourg, France.

²Université de Strasbourg, F-67000 Strasbourg, France.

³Fédération de médecine translationnelle de Strasbourg (FMTS), F-67000 Strasbourg, France.

⁴CNRS, SNC 5055.

*Contribution égale pour ces auteurs

⁵Adresse actuelle : Turku Bioscience Center, University of Turku and Åbo Akademi University, FI-20520, Turku, Finlande. jacky.goetz@inserm.fr

Les métastases sont responsables de la grande majorité des décès liés au cancer. Leur formation fait suite à un processus complexe comportant plusieurs étapes [1, 2]. À partir du développement d'une tumeur primaire, certaines cellules cancéreuses, devenues invasives, s'échapperont et se propageront à travers l'organisme en utilisant différents systèmes circulatoires – notamment sanguins et lymphatiques – pour finalement atteindre des organes éloignés du site primitif. Cette colonisation à distance, dans des organes possédant à la fois un réseau vasculaire et un microenvironnement adapté, conduit à la formation de tumeurs secondaires : les métastases. Celles-ci se développent préférentiellement au niveau de niches pré-métastatiques, des sites dont la formation dépend de facteurs solubles ou vésiculaires sécrétés par la tumeur primaire, qui suivent des voies identiques à celles empruntées par les cellules métastatiques. De nombreuses données suggèrent que l'apparition de lésions métastatiques n'est pas un processus aléatoire, mais qu'elle est gouvernée par des caractéristiques intrinsèques aux cellules tumorales (dont

leur site d'origine) ainsi que par des facteurs environnementaux spécifiques de chaque organe [51] (→).

Cet organotropisme¹, initialement expliqué par l'hypothèse du *seed and soil*² par S. Paget il y a plus d'un siècle [3], est une loi fondamentale de la progression métastatique. Il est très étudié médicalement, sur la base d'analyses et de corrélations cliniques, complétées par de nombreuses études biologiques et chimiques fondamentales afin d'en comprendre les mécanismes. Jusqu'ici, ces travaux ont majoritairement identifié les composantes génétiques, immunitaires et biochimiques de ce processus, ne prenant que très rarement en compte la contribution de facteurs biomécaniques, et notamment hémodynamiques. Depuis, l'émergence d'un nouveau champ d'étude, la *mécanobiologie*, et le développement concomitant important d'une communauté scientifique, ont démontré la pertinence de prendre en compte ces facteurs biomécaniques dont le champ d'action, sur les plans développemental, physiologique et pathologique, est large.

À titre d'exemple, il est maintenant clairement établi que l'augmentation de la pression interstitielle³ dans les tumeurs solides primaires,

(→) Voir la Nouvelle de C. Marceaux et M.L. Asselin-Labat, m/s n° 2, février 2020, page 109

Vignette (Photo © Jacky G. Goetz).

¹ Processus par lequel les cellules tumorales circulantes ciblent préférentiellement un organe plutôt qu'un autre.

² Seed and soil : analogie à la graine (*seed*) qui ne germe que sur un terrain fertile (*soil*).

³ Pression due à la présence de liquide interstitiel au sein de la tumeur.

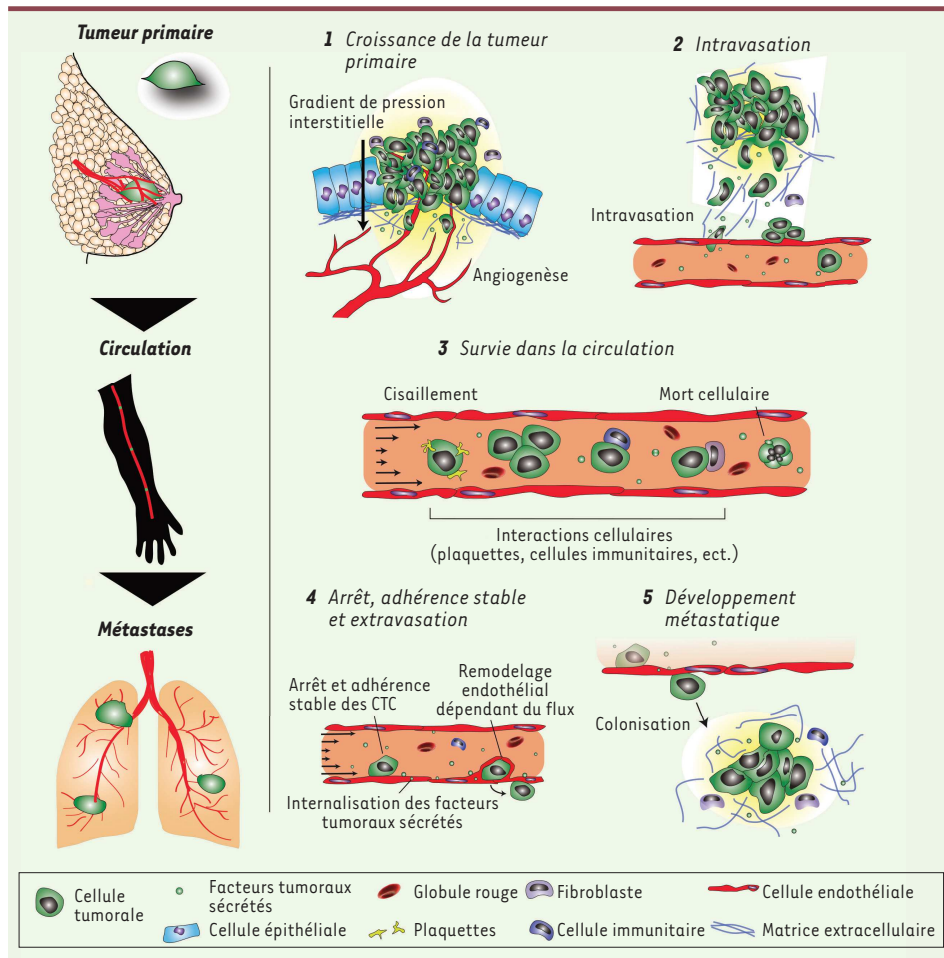


Figure 1. Schéma récapitulatif décrivant le rôle central des liquides corporels dans la dissémination des cellules tumorales.



stimule l'invasion des cellules tumorales [4] et freine l'accès de molécules chimiothérapeutiques au cœur des tumeurs, diminuant ainsi leur efficacité [5] (Figure 1). La rigidification du microenvironnement d'une tumeur solide, notamment pour les tumeurs mammaires et pancréatiques, est, par ailleurs, un facteur déterminant de leur progression et de leur agressivité [6]. Ces modifications mécaniques du tissu tumoral, détectables par des techniques d'élastographie⁴ [7], sont d'ailleurs des témoins fidèles de l'état d'avancement de la tumeur. Ces exemples illustrent bien l'impact de facteurs mécaniques sur la progression tumorale et métastatique. Soulignons qu'une grande partie de la cascade d'événements menant à la formation des métastases a lieu dans le système circulatoire et lymphatique, où les conditions physico-chimiques, mécaniques et hémodynamiques sont à même d'impacter le devenir des cellules tumorales, mais également les facteurs pro-métastatiques sécrétés par la tumeur, et leur propension à former des foyers métastatiques (Figure 1). Il y a quelques années, nous avons, avec d'autres chercheurs [8, 9], fait le

constat que nos connaissances actuelles sur ces phénomènes restaient parcellaires. Nous avons alors décidé d'élaborer des stratégies expérimentales permettant d'interroger directement la contribution de facteurs mécaniques et hémodynamiques à la cascade métastatique. L'architecture du système circulatoire permet ainsi, systématiquement et majoritairement, aux facteurs pro-métastatiques (qu'ils soient solubles ou vésiculaires) et aux cellules tumorales circulantes (CTC) d'une tumeur de rejoindre les premiers lits capillaires (et organes correspondants) irrigués consécutivement à l'organe dont est issue la tumeur. Par ce processus strictement dépendant de la direction de notre système circulatoire et du site tumoral d'origine, les organes qui sont irrigués en priorité seront les organes fortement métastatiques (par exemple les poumons dans les cancers du sein, ou le foie pour les cancers colorectaux) [10]. Comme le relevaient certains chercheurs [8], les capillaires sanguins, qui sont les voies de transport

⁴ Technique d'imagerie médicale pour mesurer l'élasticité d'un tissu.

Fluide corporel	Contenu cellulaire	Vitesses d'écoulement et forces associées	Type d'écoulement	Modélisation biophysique
Fluide interstitiel	Dépend de l'organe considéré	0,001-4 mm/sec 0,1-1 Dyn/cm ²	Laminaire, dirigé par le gradient de pression interstitielle	Convection et diffusion (modèle de Darcy) [45, 46]
Lymphhe	Cellules immunitaires	0,2-1 mm/sec 0,6-12 Dyn/cm ²	Laminaire, faiblement pulsatile	Modèle de Navier-Stokes [47]
Sang	Artères	100-500 mm/sec 4-30 Dyn/cm ²	Laminaire à turbulent, fortement pulsatile	Modèle de Navier-Stokes en ajoutant les interactions fluide-structure [48, 49]
	Veines	Hématies, plaquettes, cellules immunitaires 1-200 mm/sec 1-4 Dyn/cm ²	Laminaire, pulsatile (faible amplitude, fréquence moyenne)	
	Capillaires	0,1-1,5 mm/sec 10-20 Dyn/cm ²	Laminaire, pulsatile (faible amplitude)	

Tableau 1. Principales caractéristiques des liquides corporels.

majoritaires de cellules au destin métastatique, possèdent un environnement hémodynamique et topologique (ramifications, diamètre interne réduit, etc.) qui influence naturellement, par les contraintes mécaniques qu'il impose, les sites préférentiels d'arrêt des cellules tumorales. Alors que ces interrogations avaient été soulevées très tôt au sein de la communauté, un nombre limité d'études, notamment *in vivo*, permettait de tester expérimentalement l'impact de ces facteurs biomécaniques sur la progression métastatique. Aujourd'hui, les études portant sur l'influence directe (*via* les contraintes mécaniques) ou indirecte (*via* le transport) de la mécanique des fluides sur la progression tumorale se multiplient. Dans cette revue, nous discutons les caractéristiques biomécaniques (et leurs conséquences) des fluides corporels liés au microenvironnement tumoral. Nous détaillons également les découvertes récentes démontrant l'influence des liquides circulants⁵ sur la cascade métastatique. Cette discussion portera sur l'impact des fluides biologiques sur la dissémination des signaux tumoraux qui préparent la niche pré-métastatique, et sur celle des cellules tumorales métastatiques.

Propriétés mécaniques des fluides corporels impliqués dans le microenvironnement tumoral

Il est essentiel de prendre en compte les caractéristiques mécaniques et biochimiques des 3 principaux fluides corporels irrigant le microenvironnement tumoral – le sang, la lymphhe et le fluide interstitiel⁶ – pour mesurer leur impact sur la dispersion des cellules tumorales. Au regard de la composition de ces fluides et de l'architecture des systèmes circulatoires, il est possible d'estimer les forces mécaniques qu'ils exercent sur les cellules tumorales et sur les facteurs qu'elles sécrètent (molécules solubles et vésicules extracellulaires). Ainsi, les mouvements

du fluide interstitiel sont déterminés par les gradients de pression exercés sur ce fluide. Physiologiquement, le fluide interstitiel est ainsi dirigé des vaisseaux sanguins vers les vaisseaux lymphatiques [11]. La présence d'une tumeur en croissance, composée de cellules et de matrice extracellulaire très dense et en constante rigidification, modifie ces gradients de pression et perturbe l'écoulement du fluide interstitiel (Figure 1). En général, le fluide interstitiel s'écoule de façon laminaire⁷ et se caractérise par une densité élevée et une vitesse faible, ce qui induit des forces de cisaillement⁸ de faible amplitude (Tableau 1). L'écoulement lymphatique, lui, est laminaire et caractérisé par une pulsatilité faible, une vitesse d'écoulement faible à moyenne, et des contraintes de cisaillement qui varient en fonction de la taille des vaisseaux. La lymphhe est un liquide peu dense en particules et cellules (Tableau 1), contrairement au milieu sanguin qui possède une haute densité de cellules circulantes et donc une forte probabilité que ces cellules entrent en collision. Enfin, les écoulements sanguins ont des caractéristiques différentes selon le type de vaisseau (artères, capillaires ou veines) (Tableau 1). Dans les artères, une forte pulsatilité et un flux très élevé entraînent des forces de cisaillement fortes et un écoulement parfois turbulent. Dans les capillaires, un flux pulsatile de faible vitesse dans des vaisseaux de faibles diamètres entraîne des contraintes de cisaillement moyennes (Tableau 1). Dans les veines, un flux légèrement pulsatile et de faible vitesse entraîne de faibles forces de cisaillement (Figure 1).

⁵ Fait ici référence au fluide interstitiel, au sang et à la lymphhe.

⁶ Liquide remplissant l'espace entre capillaires sanguins et cellules, qualifié de « lymphhe » une fois drainé dans le système lymphatique.

⁷ Mode d'écoulement d'un fluide où l'on peut considérer que les couches de fluides glissent les unes sur les autres sans contradiction (par opposition à l'écoulement turbulent).

⁸ Contrainte appliquée de manière parallèle à la paroi (Pa).



Si ces trois types de fluides corporels peuvent paraître différents de par leurs propriétés hémodynamiques, tous contribuent à l'invasion des cellules tumorales au niveau de la tumeur primaire. Les mouvements de fluides interstitiels, allant du centre vers la périphérie de la tumeur, entraînent avec eux les facteurs sécrétés par les cellules et les cellules tumorales, les plaçant ainsi en position favorable pour quitter la tumeur primaire. Les vaisseaux sanguins tortueux, créés par la néo-angiogenèse tumorale (Figure 1) et présentant des fuites vasculaires, constituent alors une échappatoire facilement accessible, notamment parce que la pression y est plus élevée [12]. Moins directement, le système lymphatique, chargé de drainer les liquides interstitiels, permet également aux cellules tumorales et aux facteurs sécrétés d'accéder au système circulatoire sanguin après un détour par les ganglions lymphatiques [13] (→).

Ce mécanisme est facilité par la lymphangiogenèse⁹. Ces événements précoces sont par ailleurs accompagnés d'une libération constante de facteurs pro-métastatiques, véritables éclaireurs de la formation de métastases, qui emprunteront les mêmes voies et seront soumis aux mêmes forces mécaniques.

(→) Voir la Synthèse de D. Leclers et al., m/s n° 10, octobre 2005, page 839

Influence des liquides circulants sur la dissémination des facteurs sécrétés par les cellules tumorales

La formation de métastases est sous la dépendance de niches pré-métastatiques dont la formation est régie par des signaux tumoraux qui sont libérés au cours des phases précoces de la croissance tumorale. La diffusion à l'échelle de l'organisme de ces facteurs sécrétés par les cellules tumorales est facilitée par l'apparition de nouveaux vaisseaux sanguins et lymphatiques à l'organisation anarchique accompagnant la croissance de la tumeur primaire. Ces facteurs peuvent alors modifier le phénotype de cellules réceptrices à distance de la tumeur primaire, et créer un microenvironnement favorable au développement de métastases dans des organes distants. Ainsi, la lymphe et le sang permettent la dissémination de molécules solubles telles que des chimiokines, des cytokines, des métalloprotéases, voire des acides nucléiques [14], ainsi que des vésicules extracellulaires tumorales. Ces vésicules extracellulaires (VE) sont hétérogènes en taille (de quelques nanomètres à plusieurs microns), en contenu (protéines, récepteurs membranaires, acides nucléiques et lipides) et éventuellement en fonction [15]. Les VE tumorales se retrouvent en grande quantité dans le sang des patients atteints de cancer, sans doute guidées par les gradients de pression interstitielle précédemment décrits. Une fois dans la circulation, ces VE sont passivement emportées par le flux sanguin ou lymphatique jusqu'à atteindre un site distant, qui peut être un ganglion lymphatique dans le contexte de la circulation lymphatique, ou un organe à distance dans celui du système sanguin. Elles déclencheront alors une cascade d'événements aboutissant à une modification du microenvironnement et à l'établissement d'une niche propice au développement de futures métastases, la niche pré-métastatique [16, 17].

⁹ Formation de nouveaux vaisseaux lymphatique à partir de vaisseaux existants.

Des études récentes, menées *in vivo* chez la souris et l'embryon de poisson zèbre, ont montré que le temps de demi-vie des VE dans la circulation ne dépasse pas 10 minutes [18, 19] : elles sont rapidement internalisées par les monocytes présents dans la circulation et par les cellules endothéliales [18, 20]. L'impact des forces hémodynamiques sur ces vésicules reste mal connu. L'étude, par microscopie ultra-rapide, de vésicules circulantes dans les vaisseaux sanguins de poisson zèbre indique qu'elles répondent à la loi de Poiseuille : les vésicules proches des parois de l'endothélium ont une vitesse quasi nulle tandis que celles au centre du vaisseau sont les plus rapides. On observe ainsi, dans les régions où le flux sanguin est le plus faible, une augmentation de l'arrêt des VE dans le vaisseau et de leur internalisation par les cellules endothéliales [18]. La fonction de ces vésicules, qui portent de nombreux messages de signalisation, serait donc en partie contrôlée par les paramètres hémodynamiques du système circulatoire qui les transporte, avec l'existence d'une fenêtre précise de vitesse de flux – sanguin ou lymphatique [18, 21] – qui favoriserait les interactions moléculaires entre ces VE et les cellules avec lesquelles elles interagissent (Figure 1).

Des études suggèrent également que le répertoire de molécules de surface des VE tumorales est responsable de leur organotropisme (à l'instar des CTC). Chez la souris, il a été montré que des VE exprimant les intégrines $\alpha 6 \beta 4$ favorisent le développement de métastases dans le poumon, tandis que des VE exprimant les intégrines $\alpha V \beta 5$ favorisent des métastases dans le foie [22]. Ainsi, le site d'arrêt des VE tumorales circulantes (et donc le site de formation d'une niche pré-métastatique) pourrait dépendre de facteurs physiques (*via* les forces hémodynamiques) mais aussi biochimiques (le répertoire de molécules de surface des VE tumorales qui varie selon le type de cancer). Les forces hémodynamiques pourraient également influencer la distribution des facteurs tumoraux sécrétés de manière indirecte, par exemple en stimulant leur internalisation par les cellules endothéliales. Lors des phases précoces de la croissance et de l'invasion tumorales, les forces hémodynamiques sont donc importantes pour la dissémination des facteurs sécrétés par la tumeur primaire, à la fois car elles transportent ces facteurs, mais également parce qu'elles déterminent des sites favorables à leurs interactions avec leurs cibles à distance de la tumeur primaire.

Impact des liquides circulants sur la dissémination des cellules tumorales

En parallèle des éléments permettant l'établissement de niches pré-métastatiques, les cellules tumorales

répondent à de nombreux facteurs. Certains d'entre eux sont mécaniques, comme la pression interstitielle, et confèrent aux cellules tumorales un potentiel invasif les rendant capables de migrer activement dans le stroma, au sein et autour de la tumeur primaire. Elles profitent alors de l'angiogenèse et la lymphangiogenèse pour atteindre les systèmes circulatoires et y entrer par un processus d'intravasation [23]. Une fois en circulation, ces cellules tumorales deviennent circulantes (CTC) et sont emportées par les fluides corporels à distance de la tumeur primaire. Leur détection dans le sang représente alors un outil intéressant à la fois pour le diagnostic et pour la mise au point de traitements individualisés de la maladie [24, 50] (→).

L'importance de ces fluides circulants, en particulier du flux sanguin, dans la dissémination des cellules tumorales fut initialement soulevée par J. Ewing [25], puis fortement appuyée par les travaux de L. Weiss portant sur des centaines d'autopsies de patients atteints de cancer [26]. Dans ses études, Weiss corrèle la fréquence d'apparition de métastases à (1) l'architecture vasculaire ou (2) la nature capillaire des vaisseaux dans les organes cibles fortement touchés [26,27]. Il démontre ainsi qu'indépendamment du *seed and soil*, l'architecture vasculaire, le flux sanguin et l'approvisionnement en cellules tumorales qu'ils permettent, sont des contributeurs majeurs au développement de métastases. En plus de l'importance des paramètres hémodynamiques, des paramètres physiques simples, tels que la taille des cellules et l'étréitesse des vaisseaux, ont aussi générés des discussions [8]. Sur un plan biomécanique et morphologique, des expériences de microscopie intravitale montrent que les cellules tumorales possèdent des diamètres supérieurs à celui des capillaires sanguins les plus fins et irriguant des organes vitaux, tels que les reins, les poumons et le cerveau. Ce paramètre peut, par conséquent, suffire à entraîner leur séquestration par occlusion, comme cela avait été suggéré il y a quelques années [28]. La contribution d'un tel mécanisme reste néanmoins à démontrer. Un autre paramètre mécanique influence la dissémination des CTC : les forces de cisaillements auxquelles elles sont soumises lorsqu'elles circulent et s'arrêtent. Ainsi, *in vitro*, les forces de cisaillement physiologiques, que l'on retrouve *in vivo* chez l'homme (Tableau 1), détruisent une grande partie des cellules tumorales circulantes [29, 30] (Figure 1). À ce stade, il est intéressant de spéculer que ce processus aboutit probablement à une sélection de CTC aux propriétés mécaniques plus adaptées à leur survie [31], et qui pourraient être autant de nouvelles cibles thérapeutiques. Les CTC sont également capables d'interagir avec d'autres cellules (tumorales ou sanguines) afin d'augmenter leur résistance au stress mécanique (Figure 1). Par exemple, leur capacité d'agrégation augmente leur résistance au stress et leur potentiel métastatique [32]. De la même manière, d'autres types cellulaires, sanguins ou issus du microenvironnement tumoral, interagissent avec les CTC et les protègent des forces de cisaillement, favorisant ainsi la progression métastatique. C'est le cas des fibroblastes [33], des neutrophiles [34] et des plaquettes sanguines [35], ce qui démontre l'importance du contexte intravasculaire, et des forces qui en découlent, dans le potentiel métastatique d'une cellule tumorale (Figure 1).

(→) Voir la Synthèse de A.R. Thierry et R. Tanos, m/s n° 10, octobre 2018, page 824

Au-delà de l'impact sur leur survie, les forces de cisaillement influencent de nombreuses caractéristiques intrinsèques des CTC. Le cycle cellulaire peut en effet être inhibé dans le cas d'une exposition à des forces de cisaillement importantes (> 10 Dynes/cm²) [36], ou activé *via* le co-activateur de transcription TAZ (*transcriptional coactivator with PDZ-binding motif*)¹⁰, dans le cas d'expositions à des forces très faibles ($< 0,1$ Dynes/cm²) [37]. Des forces de cisaillement élevées, comme celles trouvées dans certains capillaires et les artères (> 5 Dynes/cm²), forcent également les CTC à adopter des profils plus mésenchymateux, *via* la transition épithelio-mésenchymateuse¹¹ [38], et augmentent ainsi leur agressivité métastatique [39,40].

Les flux sanguins et lymphatiques, par leurs propriétés hémodynamiques intrinsèques, jouent un rôle déterminant dans la destination finale des CTC. Ainsi, les cellules qui ont survécu aux évènements de collision, aux forces de cisaillement et échappé au système immunitaire, exploiteront leur potentiel adhésif et les propriétés hémodynamiques des vaisseaux qui les transportent, pour coloniser des régions vasculaires précises. En effet, les CTC s'arrêtent préférentiellement dans des vaisseaux sanguins dont les caractéristiques hémodynamiques (vélocité du flux sanguin notamment) sont permissives [21]. Ces propriétés leur permettent de s'arrêter et d'adhérer, de manière stable, aux cellules endothéliales par le biais de leur répertoire de molécules d'adhérence [41] (Figure 1). L'adhérence entre CTC et la paroi endothéliale n'est possible que si les forces d'interaction entre cellules tumorales et cellules endothéliales, résultant de la liaison entre ligand porté par l'une et récepteur présenté par l'autre, sont supérieures aux forces exercées par le flux [41]. Cette étape d'arrêt intravasculaire est essentielle au processus métastatique et peut également être influencée par les propriétés mécaniques de la paroi vasculaire et les propriétés visco-élastiques des cellules tumorales. Cependant, alors qu'une réduction de la perfusion sanguine favorise l'émergence de foyers métastatiques dans des régions vasculaires définies, l'étape essentielle d'extravasation des cellules tumorales requiert l'activation de la paroi endothéliale par des forces hémodynamiques. En effet, nous avons démontré que les CTC n'utilisent pas uniquement le mécanisme de diapédèse (largement décrit pour l'extravasation des

¹⁰ YAP1/TAZ : protéines mécano-sensibles participant à la régulation de l'expression de gènes en réponse à un étirement du cytosquelette.

¹¹ Processus au cours duquel une cellule perd ses caractéristiques épithéliales au profit de propriétés mésenchymateuses, synonymes de capacités de motilité et d'invasion.



leucocytes [42]) pour quitter la circulation sanguine et former des foyers tumoraux secondaires. L'extravasation des cellules tumorales fait aussi intervenir les cellules endothéliales constituant la paroi vasculaire, qui sont extrêmement sensibles au flux sanguin (Figure 1). Sous l'influence de signaux extracellulaires et du flux sanguin, cet endothélium est capable de se réorganiser autour des cellules tumorales intravasculaires, en formant des protrusions aboutissant à la création de nouvelles lumières vasculaires, et *in fine* à l'exclusion des CTC du milieu intravasculaire. Ce processus de remodelage endothélial [43] est sous le contrôle, entre autres, de forces de cisaillement et conduit à une extravasation « passive » des cellules tumorales (c'est-à-dire sans déformation cellulaire, contrairement à la diapédèse des leucocytes) [21]. Il est intéressant de noter qu'un tel processus est aussi observé dans le cas de caillots obstruant des micro-vaisseaux du cerveau qui sont expulsés par remodelage endothélial, ce qui conduit au rétablissement de la circulation sanguine normale [44].

Ces observations démontrent donc l'importance des propriétés mécaniques et hémodynamiques de l'environnement intravasculaire dans le potentiel métastatique des cellules tumorales circulantes.

Conclusion

De nombreuses recherches se concentrent sur l'étude de l'impact du microenvironnement tumoral, notamment de celui de propriétés mécaniques, sur la progression tumorale. Nous avons résumé ici les résultats récents qui démontrent que les fluides corporels, par les molécules qu'ils transportent et les forces qu'ils imposent sur les cellules stromales et tumorales, s'ajoutent à la liste des facteurs micro-environnementaux influençant le développement des cancers. Ils sont responsables de la dissémination de facteurs tumoraux sécrétés et des cellules tumorales circulantes, participent à la modification phénotypique des cellules tumorales, et jouent un rôle central dans la sélection (1) des sites préférentiels de formation des métastases et (2) des cellules tumorales qui parviennent à survivre au cours du processus métastatique. Aussi, la nature universelle (*a minima* commune à tous les cancers solides) de ce facteur rend pertinente la démarche de compréhension des mécanismes d'interactions et de résistances à ces fluides. En conclusion, nous espérons qu'une approche fondamentale de l'impact biophysique de la mécanique des fluides corporels sur la progression tumorale nourrira la recherche dans l'avenir et aboutira *in fine* à la découverte de nouvelles thérapies anti-cancéreuses. ♦

SUMMARY

Influence of fluid mechanics on metastasis formation

Metastases are the main cause of cancer-related deaths. The chain of events leading to their development is called "the metastatic cascade". The biological and biochemical aspects of this process have been well studied but the importance of biomechanical parameters only recently became a focus in the field. Studies have shown the biological fluids (blood, lymph and interstitial fluid) to play a key role in the metastatic cascade. These fluids participate in the transport of circulating tumor cells (CTCs) as well as the factors that they secrete, while at the same

time influencing the events of the metastatic cascade through the forces that they generate. The hemodynamic properties and topological constraints of the vascular architecture control the formation of metastatic niches and the metastatic potential of tumor cells. In this review, we discuss the importance of these mechanical forces and highlight the novel questions and research avenues that they open. ♦

LIENS D'INTÉRÊT

Les auteurs déclarent n'avoir aucun lien d'intérêt concernant les données publiées dans cet article.

RÉFÉRENCES

1. Gupta GP, Massagué J. Cancer metastasis: building a framework. *Cell* 2006 ; 127 : 679-95.
2. Valastyan S, Weinberg RA. Tumor metastasis: molecular insights and evolving paradigms. *Cell* 2011 ; 147 : 275-92.
3. Paget S. The distribution of secondary growths in cancer of the breast. *Lancet* 1889 ; 133 : 571-3.
4. Swartz MA, Lund AW. Lymphatic and interstitial flow in the tumour microenvironment: linking mechanobiology with immunity. *Nat Rev Cancer* 2012 ; 12 : 210-9.
5. Stylianopoulos T, Munn LL, Jain RK. Reengineering the physical microenvironment of tumors to improve drug delivery and efficacy: from mathematical modeling to bench to bedside. *Trends Cancer* 2018 ; 4 : 292-319.
6. Goetz JG, Minguet S, Navarro-Lérida I, et al. Biomechanical remodeling of the microenvironment by stromal caveolin-1 favors tumor invasion and metastasis. *Cell* 2011 ; 146 : 148-63.
7. Sigrist RMS, Liu J, Kaffas AE, et al. Ultrasound elastography: review of techniques and clinical applications. *Theranostics* 2017 ; 7 : 1303-29.
8. Wirtz D, Konstantopoulos K, Searson PC. The physics of cancer: the role of physical interactions and mechanical forces in metastasis. *Nat Rev Cancer* 2011 ; 11 : 512-22.
9. Azevedo AS, Follain G, Patthabhiraman S, et al. Metastasis of circulating tumor cells: Favorable soil or suitable biomechanics, or both? *Cell Adh Migr* 2015 ; 9 : 345-56.
10. Chambers AF, Groom AC, MacDonald IC. Dissemination and growth of cancer cells in metastatic sites. *Nat Rev Cancer* 2002 ; 2 : 563-72.
11. Wagner M, Wiig H. Tumor interstitial fluid formation, characterization, and clinical implications. *Front Oncol* 2015 ; 5 .
12. Piotrowski-Daspit AS, Tien J, Nelson CM. Interstitial fluid pressure regulates collective invasion in engineered human breast tumors via Snail, vimentin, and E-cadherin. *Integr Biol (Camb)* 2016 ; 8 : 319-31.
13. Leclers D, Durand K, Dutour A, et al. Vaisseaux lymphatiques et cancer. *Med Sci (Paris)* 2005 ; 21 : 839-48.
14. Broggi MAS, Maillat L, Clement CC, et al. Tumor-associated factors are enriched in lymphatic exudate compared to plasma in metastatic melanoma patients. *J Exp Med* 2019 ; 216 : 1091-107.
15. Kowal J, Arras G, Colombo M, et al. Proteomic comparison defines novel markers to characterize heterogeneous populations of extracellular vesicle subtypes. *Proc Natl Acad Sci USA* 2016 ; 113 : E968-77.
16. Peinado H, Alečković M, Lavotshkin S, et al. Melanoma exosomes educate bone marrow progenitor cells toward a pro-metastatic phenotype through MET. *Nat Med* 2012 ; 18 : 883-91.
17. Costa-Silva B, Aiello NM, Ocean AJ, et al. Pancreatic cancer exosomes initiate pre-metastatic niche formation in the liver. *Nat Cell Biol* 2015 ; 17 : 816-26.
18. Hyenne V, Ghoroghi S, Collot M, et al. Studying the fate of tumor extracellular vesicles at high spatiotemporal resolution using the zebrafish embryo. *Dev Cell* 2019 ; 48 : 554-72.e7.
19. Matsumoto A, Takahashi Y, Chang H-Y, et al. Blood concentrations of small extracellular vesicles are determined by a balance between abundant secretion and rapid clearance. *J Extracell Vesicles* 2019 ; 9.
20. Verweij FJ, Revenu C, Arras G, et al. Live tracking of inter-organ communication by endogenous exosomes in vivo. *Dev Cell* 2019 ; 48 : 573-89.e4.



RÉFÉRENCES

21. Follain G, Osmani N, Azevedo AS, *et al.* Hemodynamic forces tune the arrest, adhesion, and extravasation of circulating tumor cells. *Dev Cell* 2018 ; 45 : 33-52.e12.
22. Hoshino A, Costa-Silva B, Shen T-L, *et al.* Tumour exosome integrins determine organotropic metastasis. *Nature* 2015 ; 527 : 329-35.
23. Chiang SPH, Cabrera RM, Segall JE. Tumor cell intravasation. *Am J Physiol Cell Physiol* 2016 ; 311 : C1-14.
24. Cristofanilli M, Budd GT, Ellis MJ, *et al.* Circulating tumor cells, disease progression, and survival in metastatic breast cancer. *N Engl J Med* 2004 ; 351 : 781-91.
25. Ewing J. Neoplastic diseases: a treatise on tumours. *Br J Surg* 1928 ; 16 : 174-5.
26. Weiss L. Comments on hematogenous metastatic patterns in humans as revealed by autopsy. *Clin Exp Metastasis* 1992 ; 10 : 191-9.
27. Weiss L, Haydock K, Pickren JW, *et al.* Organ vascularity and metastatic frequency. *Am J Pathol* 1980 ; 101 : 101-13.
28. Kienast Y, Baumgarten L von, Fuhrmann M, *et al.* Real-time imaging reveals the single steps of brain metastasis formation. *Nat Med* 2010 ; 16 : 116-22.
29. Headley MB, Bins A, Nip A, *et al.* Visualization of immediate immune responses to pioneer metastatic cells in the lung. *Nature* 2016 ; 531 : 513-7.
30. Regmi S, Fu A, Luo KQ. High shear stresses under exercise condition destroy circulating tumor cells in a microfluidic system. *Sci Rep* 2017 ; 7 : 39975.
31. Moose DL, Krog BL, Kim TH, *et al.* Cancer cells resist mechanical destruction in circulation via RhoA/actomyosin-dependent mechano-adaptation. *Cell Rep* 2020 ; 30 : 3864-74.e6.
32. Aceto N, Bardia A, Miyamoto DT, *et al.* Circulating tumor cell clusters are oligoclonal precursors of breast cancer metastasis. *Cell* 2014 ; 158 : 1110-22.
33. Ao Z, Shah SH, Machlin LM, *et al.* Identification of cancer-associated fibroblasts in circulating blood from patients with metastatic breast cancer. *Cancer Res* 2015 ; 75 : 4681-7.
34. Szczerba BM, Castro-Giner F, Vetter M, *et al.* Neutrophils escort circulating tumour cells to enable cell cycle progression. *Nature* 2019 ; 566 : 553-7.
35. Labelle M, Begum S, Hynes RO. Platelets guide the formation of early metastatic niches. *Proc Natl Acad Sci USA* 2014 ; 111 : E3053-61.
36. Chang SF, Chang CA, Lee DY, *et al.* Tumor cell cycle arrest induced by shear stress: roles of integrins and Smad. *Proc Natl Acad Sci USA* 2008 ; 105 : 3927-32.
37. Lee HJ, Ewere A, Diaz MF, *et al.* TAZ responds to fluid shear stress to regulate the cell cycle. *Cell Cycle* 2018 ; 17 : 147-53.
38. Lamouille S, Xu J, Derynck R. Molecular mechanisms of epithelial-mesenchymal transition. *Nat Rev Mol Cell Biol* 2014 ; 15 : 178-96.
39. Rizvi I, Gurkan UA, Tasoglu S, *et al.* Flow induces epithelial-mesenchymal transition, cellular heterogeneity and biomarker modulation in 3D ovarian cancer nodules. *Proc Natl Acad Sci USA* 2013 ; 110 : E1974-83.
40. Choi HY, Yang GM, Dayem AA, *et al.* Hydrodynamic shear stress promotes epithelial-mesenchymal transition by downregulating ERK and GSK3 β activities. *Breast Cancer Res* 2019 ; 21 : 6.
41. Osmani N, Follain G, García León MJ, *et al.* Metastatic tumor cells exploit their adhesion repertoire to counteract shear forces during intravascular arrest. *Cell Rep* 2019 ; 28 : 2491-500.e5.
42. Muller WA. Mechanisms of leukocyte transendothelial migration. *Annu Rev Pathol* 2011 ; 6 : 323-44.
43. Lapis K, Paku S, Liotta LA. Endothelialization of embolized tumor cells during metastasis formation. *Clin Exp Metastasis* 1988 ; 6 : 73-89.
44. Lam CK, Yoo T, Hiner B, *et al.* Embolus extravasation is an alternative mechanism for cerebral microvascular recanalization. *Nature* 2010 ; 465 : 478-82.
45. Darcy H. *Les fontaines publiques de la ville de Dijon : exposition et application des principes à suivre et des formules à employer dans les questions de distribution d'eau.* Paris : V. Dalmont, 1856 : 668 p. <https://gallica.bnf.fr/ark:/12148/bpt6k624312/f1n657.pdf>
46. Chary SR, Jain RK. Direct measurement of interstitial convection and diffusion of albumin in normal and neoplastic tissues by fluorescence photobleaching. *Proc Natl Acad Sci USA* 1989 ; 86 : 5385-9.
47. Dixon JB, Greiner ST, Gashev AA, *et al.* Lymph flow, shear stress, and lymphocyte velocity in rat mesenteric prenodal lymphatics. *Microcirculation* 2006 ; 13 : 597-610.
48. Peng SL, Shih CT, Huang CW, *et al.* Optimized analysis of blood flow and wall shear stress in the common carotid artery of rat model by phase-contrast MRI. *Sci Rep* 2017 ; 7 : 1-9.
49. Freund JB, Goetz JG, Hill KL, *et al.* Fluid flows and forces in development: functions, features and biophysical principles. *Development* 2012 ; 139 : 1229-45.
50. Thierry AR, Tanos R. La biopsie liquide : une voie possible pour le dépistage du cancer. *Med Sci (Paris)* 2018 ; 34 : 824-32.
51. Marceaux C, Asselin-Labat ML. Étude des premiers événements contribuant à l'implantation des cellules cancéreuses dans une niche métastatique. *Med Sci (Paris)* 2020 ; 36 : 109-12.

TIRÉS À PART

J.G. Goetz



Avec *m/s*, vivez en direct
les progrès et débats
de la biologie et de la médecine

CHAQUE MOIS / AVEC LES ARTICLES DE RÉFÉRENCE DE M/S
CHAQUE JOUR / SUR WWW.MEDECINESCIENCES.ORG

Abonnez-vous sur

www.medecinesciences.org

ANNEXE 3



INSTITUT DE FRANCE
Académie des sciences

Comptes Rendus

Biologies


Florent Colin, Valentin Gensbittel and Jacky G. Goetz

Biomechanics: a driving force behind metastatic progression

Volume 344, issue 3 (2021), p. 249-262

Published online: 15 November 2021

<https://doi.org/10.5802/crbio1.62>

 This article is licensed under the
CREATIVE COMMONS ATTRIBUTION 4.0 INTERNATIONAL LICENSE.
<http://creativecommons.org/licenses/by/4.0/>



*Les Comptes Rendus. Biologies sont membres du
Centre Mersenne pour l'édition scientifique ouverte*
www.centre-mersenne.org
e-ISSN : 1768-3238



Articles / Reviews / *Articles / Revues*

Biomechanics: a driving force behind metastatic progression

La biomécanique : un élément moteur de la progression métastatique

Florent Colin^{*, #, a}, Valentin Gensbittel^{*, #, a} and Jacky G. Goetz^{*, a}

^aInserm UMR_S1109, Tumor Biomechanics Lab, Université de Strasbourg, Fédération de Médecine Translationnelle de Strasbourg (FMTS), Equipe Labellisée Ligue Contre le Cancer, Strasbourg, France

Current address: CRBS, 1 rue Eugène Boeckel, 67000 Strasbourg, France (F. Colin, J. G. Goetz)

E-mails: florent.colin@inserm.fr (F. Colin), valentin.gensbittel@etu.unistra.fr (V. Gensbittel), jacky.goetz@inserm.fr (J. G. Goetz)

Jacky Goetz is the 2020 recipient of the Prix de Cancérologie/Fondation Simone et Cino Del Duca/Fondation de l'Institut de France / Jacky Goetz est lauréat 2020 du Prix de Cancérologie/Fondation Simone et Cino Del Duca/Fondation de l'Institut de France

Abstract. Metastatic progression, which begins with the invasion and migration of tumor cells from a primary tumor, marks a major turning point in the evolution of cancer. Indeed, it eventually leads to the formation of secondary tumors, the metastases, which are very often responsible for the patient's death. Understanding the mechanisms controlling the different steps of this process, as well as those explaining the fundamental phenomenon of organotropism (i.e. the distribution of metastases in distant organs by a non-random and tumor-specific process), is essential to define new innovative therapeutic solutions. In this review paper, we will present how biomechanics is an essential element to this understanding, and will emphasize the importance of this orthogonal and promising angle of study as well as our laboratory's focus on the late stages of dissemination, arrest and extravasation of circulating cancer cells and factors secreted by the primary tumor such as extracellular vesicles.

Résumé. La progression métastatique, qui débute par l'invasion et la migration de cellules tumorales depuis une tumeur primaire, marque un tournant majeur dans l'évolution du cancer. En effet, elle conduit à terme à la formation des tumeurs secondaires, les métastases, responsables très souvent de la mort du patient. Comprendre les mécanismes contrôlant les différentes étapes de ce processus, ainsi que ceux expliquant le phénomène fondamental d'organotropisme (c'est-à-dire la distribution

* Corresponding authors.

Contributed equally.

des métastases dans les organes distants par un processus non aléatoire et tumeur-spécifique), est essentiel pour définir de nouvelles solutions thérapeutiques innovantes. Dans ce document de synthèse, nous présenterons comment la biomécanique est un élément essentiel à cette compréhension, et insisterons sur l'importance de cet angle d'étude orthogonal et prometteur ainsi que la focalisation de notre laboratoire sur les étapes tardives de dissémination, d'arrêt et d'extravasation des cellules cancéreuses circulantes et des facteurs sécrétés par la tumeur primaire comme les vésicules extracellulaires.

Keywords. Biomechanics, Metastasis, Intravasation, Adhesion, Extravasation, Circulating tumor cells.

Mots-clés. Biomécanique, Métastases, Intravasation, Adhésion, Extravasation, Cellules tumorales circulantes.

Manuscript received 27th September 2021, accepted 4th October 2021.

1. Introduction

Metastatic progression—the last step of the multi-stage carcinogenesis process—is ultimately leading to the development of metastases that are usually responsible for the death of cancer patients [1, 2]. It begins when malignant cancer cells escape from the primary tumor and its microenvironment, invade the patient's body through the lymphatic and/or the vascular systems, and finally reach distant organs. The colonization of these organs, an inefficient process requiring the conjunction of multiple helping factors, leads to the formation of secondary tumors called metastases. In support of Steven Paget's "seed and soil" concept [3] there are considerable evidences to suggest that the development of metastasis is induced by intrinsic characteristics of tumor cells—notably their genetic and epigenetic alterations—as well as organ-specific environmental factors [4]. This so-called "organotropism" has been extensively studied from a medical, biological and chemical perspective in order to understand and anticipate tumor and metastatic progression in patients. Insofar as the metastases are largely incurable and currently very difficult to detect early enough during the natural history of the pathology, the exploration of the molecular and cellular pathways leading to the establishment of site-specific metastasis are thus in the forefront of cancer research. Other factors promote metastasis, among which the formation of permissive microenvironments, the so-called pre-metastatic niche priming. This mechanism occurs when factors secreted and released by the primary tumor create, in organs distant to the primary tumor, an environment where extravasation and growth of disseminating cancer cells are facilitated [5]. The discovery of the role of extracellular vesicles (EVs) in intercellular communication, and in our case of their

role (in particular that of exosomes) in the promotion of the formation of the pre-metastatic niche (PMN) is the subject of intense research, including in our laboratory.

In recent years, we have seen the emergence of biomechanical studies—in addition to our own—aimed at understanding the contribution of fundamental driving forces and their involvement in each stage of the metastatic progression (Figure 1—highlighted in yellow). During growth of solid tumors for instance, the increased interstitial pressure has been shown to promote invasion and concomitantly limit access to chemotherapeutic molecules [6]. Later during the metastatic cascade—after invasion through complex extracellular matrix environments and intravasation through blood vessels of cancer cells evading from the primary tumor—the vascular tree will mechanically disseminate and guide circulating tumor cells to a first capillary bed, often a highly metastatic organ (i.e. the lungs in breast cancer, the liver in colorectal cancer). At the level of blood capillaries, hemodynamic parameters and the topography of the vessels themselves influence the sites of tumor cell arrest [7]. This is also probably true for soluble pro-metastatic factors—including EVs—secreted by the primary tumor, suggesting that the locations of the pre-metastatic niches must themselves respond to this set of physical constraints. Although these aspects are well described, their real biological impacts remain only poorly described *in vivo*, particularly in the later steps that occur in and off the bloodstream. Our laboratory primary objective is to continue to further elucidate the central role of biomechanics on the entire metastatic cascade, from the tumor progression to the metastasis itself (Figure 1—red star references). To this end, we combine state-of-the-art sophisticated tools (notably microfluidics-based),

in vitro and *in vivo* models (mouse and zebrafish) with high-resolution imaging—such as correlated light and electron microscopy [8]—and biophysical approaches to mimic pathological situations highly relevant to cancer research. In doing so, we aim to ultimately identify innovative therapeutic alternatives.

2. Forces that shape tumors and its microenvironment (TME)

A primary tumor and its highly-plastic microenvironment (TME) form an intricate non-homogeneous structure composed of different elements: the cancer cells themselves, a broad spectrum of stromal cells that can be activated including notably cancer-associated fibroblasts (CAFs), immune cells, and the lymphatic and blood vessels. It also includes the extracellular matrix (ECM) which contains, in addition to fiber-like molecules such as collagen and fibronectin, cell-secreted products (i.e. cytokine, chemokines, extracellular vesicles), various metabolites, and present hypoxic and acidic properties [4]. The growth of the primary tumor (Figure 1—1. Growth) results from uncontrolled proliferation in a healthy tissue and creates solid stress, which in turn induces various forces and tensile stress around and within the tumor itself [9]. This, in conjunction with the activation of neighboring stromal cells with high contractibility potential, results in the extracellular matrix becoming significantly stiffer and anisotropic, a feature correlated with a malignant tumor phenotype. We, and others, have previously demonstrated that the contractility of these stromal cells is a key factor in metastatic progression. In particular, we observed that Caveolin-1—a multifunctional scaffolding protein associated with cell-surface caveolae [10]—is a major regulator of tumor cell invasion and subsequent metastasis (Figure 1—2. Invasion) through the control of focal adhesion dynamics within tumor cells [11] and the biomechanical remodeling of the tumor-associated microenvironment by stromal cells [12]. The microenvironment of the tumor, influenced by the increased forces and abnormal fluids flows, will gradually transition from an anti-malignancy to a pro-malignancy behavior [13], promote the migration of cancer cells through the extracellular matrix (Figure 1—3. Migration), their

intravasation in the body circulatory systems (Figure 1—4. Intravasation) and/or by lymphatic diffusion, and ultimately trigger circulating cancer cells (CTCs) dissemination (Figure 1—5. Dissemination). On a side note, while angiogenesis and lymphangiogenesis of the primary tumor play a potentiating role [14], tumor dissemination is an event that can also be observed in early lesions [7]. In conclusion, identifying and characterizing the flow-based mechanical constraints inherent to the tumor progression and metastasis cascade is of the utmost importance [15] and at the heart of our laboratory's efforts [7].

To understand the mechanical forces at work, it is necessary to consider the primary tumor and TME irrigating fluids, namely the interstitial fluid, the lymph and the blood circulation. Each has its own biochemical characteristics, cellular content and flow patterns. The interstitial fluid, originating from blood capillaries' leakiness and surrounding the cells, has a laminar flow heading towards the lymphatic draining sites. In a primary tumor, such flow is driven by the decreasing interstitial pressure gradient directed outward from its center (schematically its highest-pressure point). Lymphatic vessels exhibit a weakly pulsatile laminar flow, draining material from the primary tumor outward to the lymph nodes. Finally, the blood system, which presents different types of vessels (capillaries, veins and arteries), irrigates the primary tumor and delivers oxygen but also connects the growing tumor to distant parts of the organism. While capillaries and veins present a laminar flow of low to medium intensity, and a rather reduced pulsativity, they are supply and dissemination routes of the primary tumor (as illustrated in Figure 1), a phenomenon reinforced by their neo-formations following the release of pro-angiogenic factors from the tumor and its TME. The arteries present a laminar or turbulent flow of high intensity as well as a strong pulsativity and also participate to this process. Arterial circulation is a particularly hostile environment for the propagation of CTCs, since they exhibit the highest shear stresses [7]. Altogether, lymph and blood circulation offer optimal platforms to tumor cells for colonizing distant lands. Remarkably, CTCs are not the only ones to disseminate through these fluids and vasculatures: other tumor-secreted factors such as extracellular vesicles, some

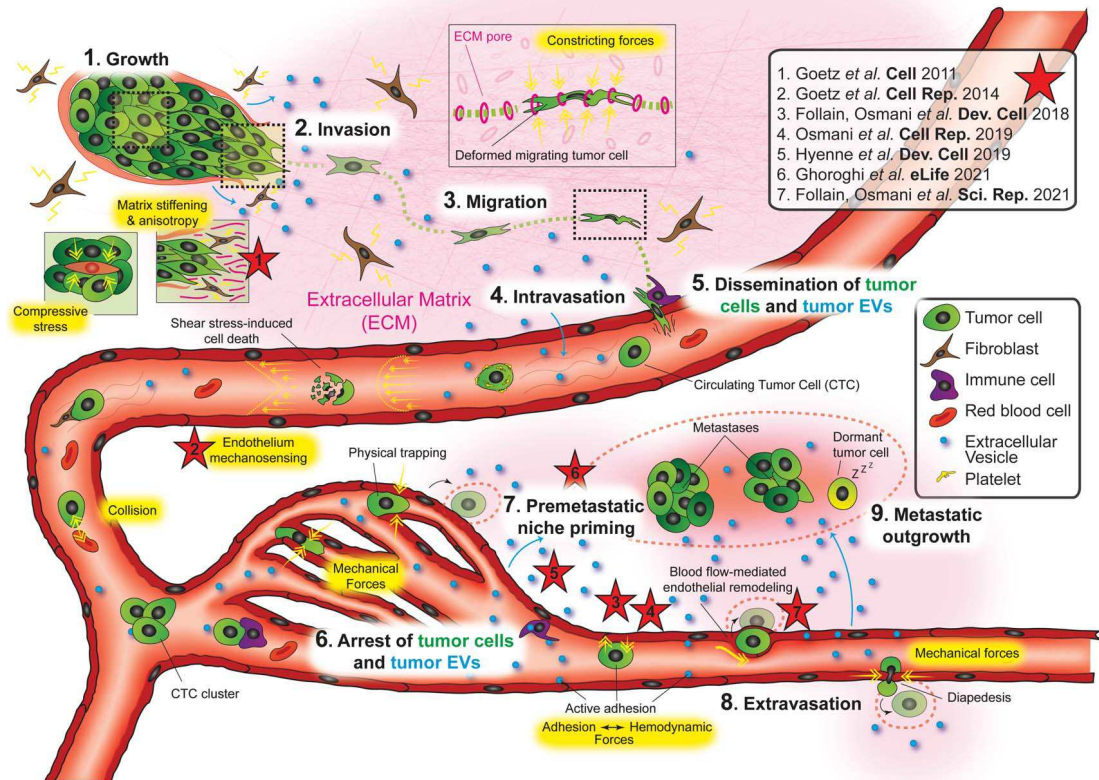


Figure 1. Biomechanics of the metastatic cascade: a schematic representation of the path of cancer cells and extracellular vesicles during the cascade of events leading to the formation of metastases. The nine major steps are indicated in black on a white background, large font, and are referenced in the text. The biomechanical forces involved are highlighted in yellow. There are two legends on the right: the first one on top gives the references of the laboratory studies (red stars, numbered). A second one on the bottom references the types of cells and factors.

of which have pro-metastatic properties, use similar strategies to the benefit of metastatic fitness of CTCs.

3. The pre-metastatic niche (PMN) priming

Lymphatic and blood vessels allow the dissemination of various tumor-secreted factors such as cytokines, chemokines, growth factors, matrix metalloproteinases, circulating tumor DNA, antigens and extracellular vesicles (Figure 1—EVs, in blue) [16, 17]. Given their abundance in the body fluids of patients and their short half-life, it is likely that the primary tumor and its TME release them consistently and regularly. Yet, this remains poorly understood and should

provide fertile grounds for future research. These tumor-secreted factors are subjected to hemodynamic constraints [18]—similarly to CTCs—and may arrest in various metastasis-free organs where they can locally modify the microenvironment and create so-called “pre-metastatic niches” (PMNs), which are ideal sites for CTC targeting and metastases formation (Figure 1—7. Premetastatic niche priming). Extracellular vesicles (EVs) in particular—small lipid bilayer particles that serve as signaling cargoes and which can be quickly cleared from the blood by intravascular macrophages/monocytes [18] and endothelial cells of the PMNs—have been demonstrated to exhibit specific organotropism depending

on their primary tumor of origin, a feature made possible by the exposure of a variable repertoire of surface adhesion molecules [19]. Because they are transported by the blood flow, these non-inert circulating objects may “stop” in specific vascular regions as a function of their adhesive potential and the hemodynamic forces at play [18]. In relation to this mechanism, we have recently demonstrated that the Ral GTPases control the biogenesis, the secretion and the content of tumor extracellular vesicles [20] that favor tumor metastasis in mouse syngeneic models of breast cancer [21]. It appears thus likely that the formation of the PMNs depends not only on physical factors such as the architecture, permeability, leakiness, local flux and hemodynamic forces existing in the vasculature system, but also on biological factors such as cell-adhesion molecules or intravesicular cargoes (i.e. proteins or nucleic acids) that make these extracellular vesicles important actors of the metastatic cascade. It is interesting to note at this point that EVs and CTCs might share similar targeting strategies for colonizing distant organs. Subsequently to the PMN priming process, cancer cells that have completed their migration and intravasation steps will be able to begin their intravascular journey as “circulating tumor cells” (CTC) until reaching their final destination.

4. Intravascular journey of a CTCs: flow forces, adhesion and extravasation

Steven Paget’s concept of “seed and soil” [3]—while remaining a central principle—was somewhat challenged by James Ewing (as early as 1928) and Dale Coman [22] by the introduction of the concept that the mechanics of the bloodstream were responsible for the dissemination of tumors to secondary organs followed by the demonstration that the frequency of occurrence of metastases and the vascular architecture as well as the capillary nature of the vessels in the heavily affected target organs were correlated [23]. Hematogenous circulation mechanics appeared thus responsible for the distribution of tumor cells in target organs. These two models, which may appear to be independent or even contradictory, actually represent two aspects of a single combinatorial “bio-mechanical” phenomenon. Indeed, although the non-specific and mechanical arrest of CTCs is an existing mechanism, the fate of

these depends also on the organ in which they are located [24]. Numerous works, including our own, have since demonstrated that the metastatic process results from multifactorial physical and biochemical selective events where fluid biomechanics is an essential element [4,7]. As soon as a cancer cell escapes from the primary tumor, intravasates in the blood circulation and becomes a CTC, an essential parameter for its survival and intravascular arrest is the shear stress, which depends on the fluid viscosity and the velocity gradient. Concretely, the more a CTC moves away from the center of the vessel—which it does naturally thanks to its margination properties—the more it will be deformed by the shearing phenomenon (this is especially true in blood due to its high viscosity) (Figure 1—5. Dissemination, shear stress-induced cell death). When entering the lymphatic or venous system, the shear stress remains low and the friction with the membrane of the vascular endothelium presumably harmless. Some CTCs will succeed in reaching the arteries, where the shear stress is high and where the risks of collision are statistically important: there, cells might undergo deformation, fragmentation and ultimately death [25]. This bottleneck results in the selection of CTCs with the most suitable properties for their survival—both physico-chemically and physiologically with reported modification of genes expression [26]—, and promotes their patterning into more resistant cell clusters, either among themselves as CTC clusters [27] or in association with other cell types (fibroblasts, neutrophils or blood platelets) [7] (Figure 1—5. Dissemination, illustrated). CTCs that have survived collision events, shear stress, and escape the immune system during their migration will exploit their adhesive potential and the hemodynamic properties of the vessels that carry them to colonize specific and permissive regions [28,29], presumably PMNs *in vivo*. However, it is not so much when the CTCs are free within the circulation that they undergo the greatest stress, but when they attach and try to extravasate: one indication is that upon injection of tumor cells into the afferent vessel of metastatic organs, although 80% of the cells are thought to stably arrest one day after injection, less than 4% of injected cells efficiently form metastatic foci [30]. Although the intravascular arrest process of CTCs can occur passively by physical occlusion of small capillaries [31] (Figure 1—6. Arrest, physical trapping), which is currently a subject of re-

search of our laboratory, the active adhesion to the vessel wall has been also reported to participate—at least in part—to further extravasation [28]. Adhesion between CTCs and the endothelium of the blood vasculature is only possible if the binding forces (i.e. ligand–receptor interaction) between them is greater than the forces exerted by the flow and shear stress [29] (Figure 1—8. Extravasation, active adhesion). This essential step can be influenced by the physicochemical characteristics of the vascular wall, the viscoelastic properties of the CTCs, but also by the homogenous or polarized distribution of the ligands and receptors. Different mechanisms/models—though not necessarily exclusive—have been proposed to describe the arrest and extravasation steps of CTCs. They could follow strategies similar to those of leukocytes, namely a rolling along the endothelial wall and then a (paracellular or transcellular) diapedesis step (Figure 1—8. Extravasation, diapedesis). The formation of “low adhesive strength—rapid activation” followed by “higher adhesive strength—slow activation” ligand–receptor bonds through a tug-of-war with blood flow has been documented [28, 29], and could explain both the rolling and arrest. However, our own observations tend to suggest that CTCs arrest intravascularly rather abruptly, with a risk of detachment: more work is thus needed to clarify this behavior. Furthermore, we demonstrated that CTCs do not only use diapedesis to leave the bloodstream and form secondary tumor foci: they can also use a flow-dependent endothelial remodeling mechanism [28] (Figure 1—8. Extravasation, endothelial remodeling), which is characterized by the formation of protrusions leading to the creation of new vascular lumens (pocketing), and the passive exclusion of CTCs from the vascular environment. Indeed, the vascular endothelium displays considerable mechano-sensing abilities that make it likely to sense, react and adapt to any conditions [32]. In the context of intravascular CTC dissemination, we recently observed that the VEGFR2-dependent pathway as a signaling node sensitive to flow forces and driver of tumor metastasis through endothelial remodeling [33]. Doing so, we identified a potential therapeutic target in the fight against tumor metastases. Finally,—although dormancy phenomena (ranging from a few hours to years) have been reported [34]—the CTC will eventually initiate extravascular proliferation to form a secondary tu-

mor called metastases (Figure 1—9. Metastatic outgrowth). The proliferation efficiency will arguably depend on the metastatic microenvironment characteristics, and presumably on its further remodeling by pro-tumor factors such as EVs. Then, the new-formed metastases will, in turn, potentially initiate their own process of tumor progression and metastasis in the manner of the primary tumor, and dramatically accelerate the worsening of the cancer patient's health condition.

5. Conclusion and perspectives

Our ability to effectively treat cancer depends in large part on our ability to decipher, correctly diagnose and prevent cancer progression and metastasis. In this regard, research on the role played by mechanical forces in these processes is fundamental and complementary to other approaches. The different body fluids, due to the types of flows that animate them and their resulting constraints (notably shear stress in blood circulation), are responsible for the dissemination of secreted tumor factors and CTCs. They play a central role in the selection and preparation of pre-metastatic niche for the formation of metastases, thus preparing an ideal soil. They are also key elements in selecting CTCs capable of surviving during the metastatic process, whether during their migration, adhesion, arrest or extravasation—each of them requiring biomechanical and physiological adaptations—thus carrying the metastatic seed. We recently demonstrated that fluid forces are also key in activating flow sensing receptors (in our models, but presumably in cancer patients PMN as well) and promote extravasation processes and thus metastasis. The pervasiveness of biomechanics in solid cancers (some elements of which also apply to blood cancers) makes research efforts in this area relevant. Although many studies have focused in the past decade on understanding forces within the primary tumor, more work is needed to understand, for example, how these can tune the secretion and nature of tumor-promoting factors such as extracellular vesicles. To understand how shear stress and flow forces impact the secretion, dissemination and uptake of factors secreted by the primary tumor and its TME, and to what extent they are involved in their cancer-dependent organotropism, are major challenges. Furthermore,

how mechanical properties of CTCs themselves impact their metastatic fitness is conceptually appealing and thus studied in our laboratory. A detailed understanding of the forces at play could allow the development of innovative therapeutics taking advantage of biomechanical constraints to specifically target pre-metastatic niches—in the manner of factors secreted by tumors, i.e. engineered drug delivery EVs—and block or delay their establishment and subsequent endothelial remodeling and metastasis. The fragility of CTCs to shear stress must also be considered: if the use of drugs targeting blood pressure does not appear to be in the best interest of a cancer patient, tools allowing their continuous removal from the blood are already being developed [35] and more work is needed to understand whether their mechanical profiles are involved in such behavior. Understanding the biomechanics at work in a patient will also require considering the parameters acting on them. The physical/physiological characteristics of a patient—in particular age [36]—the potential effects of the treatments followed, and finally their evolution during the natural history of the pathology are all elements that could enable more efficient and personalized therapies. Another axis is the study of the effect of factors secreted by tumor and non-tumor

cells, of their possible pro- vs. anti-tumor competition during the metastatic cascade, as well as their potential involvement in a biomechanical modification of the PMN.

Acknowledgments

We thank particularly Vincent Hyenne, Naël Osmani and Sébastien Harlepp, but also all members of Jacky G. Goetz's team for their discussions, explanations and ideas to improve the manuscript. Florent Colin is funded by the NANOTUMOR Consortium (PFA), a program from ITMO Cancer of AVIESAN (Alliance Nationale pour les Sciences de la Vie et de la Santé, National Alliance for Life Sciences and Health) within the framework of the Cancer Plan (France). Valentin Gensbittel is funded by Région Alsace—Inserm. Jacky G. Goetz is a Research Director at Inserm and 2020 Grand Prize of Cancerology of the “Fondation Del Duca” (Académie de Sciences, France). Work in the lab of Jacky G. Goetz is mostly supported by the INCa (Institut National Du Cancer), La Ligue contre le Cancer, the ARC Foundation, the FRM (Fondation pour la Recherche Médicale), Le Plan Cancer, the Region Est, the INSERM and the University of Strasbourg.

French version

1. Introduction

La progression métastatique — la dernière des étapes du processus de carcinogénèse — conduit finalement au développement de métastases qui sont généralement responsables de la mort des patients atteints de cancer [1, 2]. Le processus commence lorsque des cellules cancéreuses malignes s'échappent de la tumeur primaire et de son microenvironnement, envahissent le corps du patient par les systèmes lymphatique et/ou vasculaire, et atteignent finalement des organes distants. La colonisation de ces organes, un processus inefficace nécessitant la conjonction de multiples facteurs facilitateurs, conduit à la formation de tumeurs secondaires appelées métastases. À l'appui du concept de « graine et sol » de Steven Paget [3], de nombreuses preuves suggèrent que le développement des métastases est induit par les caractéristiques intrinsèques des cellules tumorales — notamment leurs altérations géné-

tiques et épigénétiques — ainsi que par des facteurs environnementaux spécifiques aux organes [4]. Cet « organotropisme » a été largement étudié d'un point de vue médical, biologique et chimique afin de comprendre et d'anticiper la progression des tumeurs et des métastases chez les patients. Dans la mesure où les métastases sont en grande partie incurables et encore actuellement difficiles à détecter suffisamment tôt au cours de l'histoire naturelle de la pathologie, l'exploration des voies moléculaires et cellulaires conduisant à l'établissement de métastases dans des organes / sites spécifiques est donc au premier plan de la recherche sur le cancer. D'autres facteurs favorisent les métastases parmi lesquels le mécanisme de formation de microenvironnements permissifs appelés niches pré-métastatiques. Ce mécanisme se produit lorsque des facteurs sécrétés et libérés par la tumeur primaire créent, dans des organes distants de la tumeur primaire, un environnement où l'ex-travasation et la croissance des cellules cancéreuses

disséminées sont facilitées [5]. La découverte du rôle des vésicules extracellulaires (VEs) dans la communication intercellulaire, et dans notre cas de leur rôle (en particulier celui des exosomes) dans la promotion de la formation de la niche pré-métastatique (PMN) fait l'objet d'intenses recherches, y compris dans notre laboratoire.

Ces dernières années, nous avons assisté à l'émergence d'études biomécaniques — en plus des nôtres — visant à comprendre la contribution des forces mécaniques fondamentales et leur implication dans chaque étape de la progression métastatique (Figure 1 — surligné en jaune). Pendant la croissance des tumeurs solides, par exemple, il a été démontré que l'augmentation de la pression interstitielle favorise l'invasion et limite simultanément l'accès aux molécules chimiothérapeutiques [6]. Plus tard, au cours de la cascade métastatique — après l'invasion à travers des environnements complexes de la matrice extracellulaire et l'intravasation à travers les vaisseaux sanguins des cellules cancéreuses qui ont échappé à la tumeur primaire — le réseau vasculaire va disséminer mécaniquement et guider les cellules tumorales circulantes vers un premier lit capillaire, souvent un organe hautement métastatique (par exemple les poumons dans le cancer du sein, le foie dans le cancer colorectal). Au niveau des capillaires sanguins, les paramètres hémodynamiques et la topographie des vaisseaux eux-mêmes influencent les sites d'arrêt des cellules tumorales [7]. Ceci est probablement aussi vrai pour les facteurs solubles pro-métastatiques — y compris les VEs — sécrétés par la tumeur primaire, ce qui suggère que les emplacements des niches pré-métastatiques doivent eux-mêmes répondre à cet ensemble de contraintes physiques. Bien que ces aspects soient bien décrits, leurs impacts biologiques réels ne sont que peu décrits *in vivo*, en particulier dans les étapes ultérieures qui se produisent dans et hors de la circulation sanguine. L'objectif principal de notre laboratoire est de continuer à élucider le rôle central de la biomécanique sur l'ensemble de la cascade métastatique, de la progression de la tumeur à la métastase elle-même (Figure 1 — références en étoile rouge). À cette fin, nous combinons des outils sophistiqués de pointe (notamment basés sur la microfluidique), des modèles *in vitro* et *in vivo* (souris et poisson-zèbre) avec une imagerie à haute résolution — comme la microscopie optique et électronique corrélée ou microscopie

corrélative [8] — et des approches biophysiques pour imiter des situations pathologiques très pertinentes pour la recherche sur le cancer. Ce faisant, nous visons à identifier des alternatives thérapeutiques innovantes.

2. Les forces qui façonnent les tumeurs et leur microenvironnement (TME)

Une tumeur primaire et son microenvironnement (TME) hautement plastique forment une structure complexe et non homogène composée de différents éléments : les cellules cancéreuses elles-mêmes, un large éventail de cellules stromales qui peuvent être activées, notamment les fibroblastes associés au cancer (CAFs), les cellules immunitaires et les vaisseaux lymphatiques et sanguins. Elle comprend également la matrice extracellulaire (MEC) qui contient, outre des molécules fibreuses telles que le collagène et la fibronectine, des produits sécrétés par les cellules (c'est-à-dire des cytokines, des chimiokines, des vésicules extracellulaires), divers métabolites, et présente des propriétés hypoxiques et acides [4]. La croissance de la tumeur primaire (Figure 1 — 1. Growth) résulte d'une prolifération incontrôlée dans un tissu sain et crée un stress solide, qui à son tour induit diverses forces et tensions autour et à l'intérieur de la tumeur elle-même [9]. Ce phénomène, associé à l'activation des cellules stromales voisines à fort potentiel de contractilité, a pour conséquence de rendre la matrice extracellulaire nettement plus rigide et anisotrope, une caractéristique corrélée à un phénotype tumoral malin. Nous et d'autres avons précédemment démontré que la contractilité de ces cellules stromales, les CAFs, est un facteur clé dans la progression métastatique. Nous avons notamment observé que la cavéoline-1 — une protéine d'échafaudage multifonctionnelle associée aux cavéoles de la surface cellulaire [10] — est un régulateur majeur de l'invasion des cellules tumorales et des métastases qui s'ensuivent (Figure 1 — 2. Invasion) par le biais du contrôle de la dynamique des adhésions focales au sein des cellules tumorales [11] et du remodelage biomécanique du microenvironnement associé à la tumeur par les cellules stromales ou CAFs [12]. Le microenvironnement de la tumeur, influencé par les forces accrues et les flux de

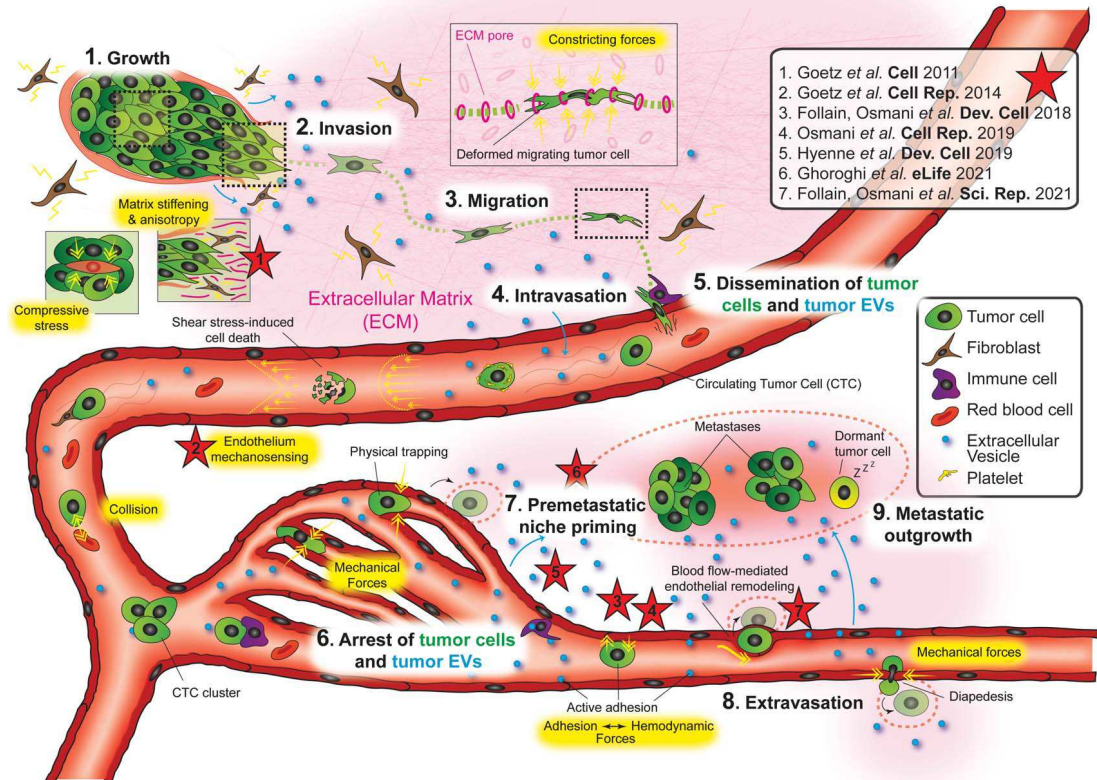


FIGURE 1. Biomécanique de la cascade métastatique : représentation schématique du parcours des cellules cancéreuses et des vésicules extracellulaires au cours de la cascade d'événements conduisant à la formation de métastases. Les neuf étapes majeures sont indiquées en noir sur fond blanc, en gros caractères, et sont référencées dans le texte. Les forces biomécaniques impliquées sont mises en évidence en jaune. Il y a deux légendes sur la droite : la première en haut donne les références des études de laboratoire (étoiles rouges, numérotées). Une deuxième légende, en bas, donne les références des types de cellules et de facteurs.

fluides anormaux, passe progressivement d'un comportement anti-maligne à un comportement pro-maligne [13], favorise la migration des cellules cancéreuses à travers la matrice extracellulaire (Figure 1 — 3. Migration), leur intravasation dans les systèmes circulatoires du corps (Figure 1 — 4. Intravasation) et/ou par diffusion lymphatique, et déclenche finalement la dissémination des cellules cancéreuses circulantes (CTCs) (Figure 1 — 5. Dissémination). Par ailleurs, alors que l'angiogenèse et la lymphangiogenèse de la tumeur primaire jouent un rôle de potentialisation [14], la dissémination tumorale est un événement qui peut également être observé dans les lésions précoces [7]. En conclusion, l'identification et

la caractérisation des contraintes mécaniques liées à l'écoulement, inhérentes à la cascade de progression tumorale et de métastases sont de la plus haute importance [15] et sont au cœur des efforts de notre laboratoire [7].

Pour comprendre les forces mécaniques à l'œuvre, il est nécessaire de considérer les fluides d'irrigation de la tumeur primaire et de la TME, à savoir le fluide interstitiel, la lymphe et la circulation sanguine. Chacun d'entre eux possède ses propres caractéristiques biochimiques, son contenu cellulaire et ses schémas d'écoulement. Le fluide interstitiel, provenant de la fuite des capillaires sanguins et entourant les cellules, a un flux laminaire se dirigeant vers les sites de

drainage lymphatique. Dans une tumeur primaire, ce flux est entraîné par le gradient de pression interstitielle décroissant dirigé vers l'extérieur à partir de son centre (schématiquement, son point de pression le plus élevé). Les vaisseaux lymphatiques présentent un flux laminaire faiblement pulsatile, drainant la matière de la tumeur primaire vers les ganglions lymphatiques. Enfin, le système sanguin, qui présente différents types de vaisseaux (capillaires, veines et artères), irrigue la tumeur primaire et fournit de l'oxygène mais relie également la tumeur en croissance à des parties distantes de l'organisme. Alors que les capillaires et les veines présentent un flux laminaire d'intensité faible à moyenne, et une pulsativité plutôt réduite, ils sont des voies d'approvisionnement et de dissémination de la tumeur primaire (comme illustré dans la Figure 1), un phénomène renforcé par leurs néo-formations suite à la libération de facteurs pro-angiogéniques de la tumeur et de sa TME. Les artères présentent un flux laminaire ou turbulent de haute intensité ainsi qu'une forte pulsativité et participent également à ce processus. La circulation artérielle est un environnement particulièrement hostile à la propagation des CTCs, car elle présente les contraintes de cisaillement les plus élevées [7]. Dans l'ensemble, les circulations lymphatique et sanguine offrent aux cellules tumorales des plateformes optimales pour coloniser des terres lointaines. Il est remarquable que les CTCs ne soient pas les seules à se disséminer par ces fluides et ces vaisseaux : d'autres facteurs sécrétés par les tumeurs, comme les vésicules extracellulaires, dont certains ont des propriétés pro-métastatiques, utilisent des stratégies similaires au profit de la capacité métastatique des CTCs.

3. La formation de la niche pré-métastatique (PMN)

Les vaisseaux lymphatiques et sanguins permettent la dissémination de divers facteurs sécrétés par la tumeur tels que les cytokines, les chimiokines, les facteurs de croissance, les métalloprotéinases matricielles, l'ADN tumoral circulant, les antigènes et les vésicules extracellulaires (Figure 1 — EVs, en bleu) [16, 17]. Étant donné leur abondance dans les fluides corporels des patients et leur courte demi-vie, il est probable que la tumeur primaire et sa TME les libèrent de manière constante et régulière. Pourtant, cela reste mal compris et devrait fournir un terrain

fertile pour de futures recherches. Ces facteurs sécrétés par la tumeur sont soumis à des contraintes hémodynamiques [18] — tout comme les CTCs — et peuvent s'arrêter dans divers organes exempts alors de métastases où ils peuvent modifier localement le microenvironnement et créer des « niches pré-métastatiques » (PMNs), qui sont des sites idéaux pour le ciblage des CTCs et la formation de métastases (Figure 1 — 7. Premitastatic niche priming). Il a été démontré que les vésicules extracellulaires (VEs) en particulier — de petites particules entourées d'une bicouche lipidique qui servent de transporteurs et qui peuvent être rapidement éliminées du sang par les macrophages/monocytes intravasculaires [18] ou captées par les cellules endothéliales des PMNs — présentent un organotropisme spécifique en fonction de leur tumeur d'origine primaire, une caractéristique rendue possible par l'exposition d'un répertoire variable de molécules d'adhésion de surface [19]. Parce qu'ils sont transportés par le flux sanguin, ces objets circulants non inertes peuvent « s'arrêter » dans des régions vasculaires spécifiques en fonction de leur potentiel adhésif et des forces hémodynamiques en jeu [18]. En relation avec ce mécanisme, nous avons récemment démontré que les GTPases de la famille Ral contrôlent la biogenèse, la sécrétion et le contenu des vésicules extracellulaires tumorales [20] qui favorisent les métastases tumorales dans des modèles murins syngéniques de cancer du sein [21]. Il semble donc probable que la formation des PMNs dépend non seulement de facteurs physiques tels que l'architecture, la perméabilité, les fuites, les flux locaux et les forces hémodynamiques existant dans le système vasculaire, mais aussi de facteurs biologiques tels que les molécules d'adhésion cellulaire ou les cargaisons vésiculaires (c'est-à-dire les protéines ou les acides nucléiques) qui font de ces vésicules extracellulaires des acteurs importants de la cascade métastatique. Il est intéressant de noter à ce stade que les VEs et les CTCs pourraient partager des stratégies de ciblage similaires pour coloniser des organes distants. Après le processus d'amorçage des PMN, les cellules cancéreuses qui ont terminé leurs étapes de migration et d'intravasation pourront commencer leur voyage intravasculaire en tant que « cellules tumorales circulantes » (CTC) jusqu'à atteindre leur destination finale.

4. Voyage intravasculaire d'une CTC : forces d'écoulement, adhésion et extravasation

Le concept de Steven Paget de « graine et sol » [3] — tout en restant un principe central — a été quelque peu remis en question par James Ewing (dès 1928) et Dale Coman [22] par l'introduction du concept selon lequel la mécanique de la circulation sanguine était responsable de la dissémination des tumeurs dans les organes secondaires, suivie de la démonstration de la corrélation entre la fréquence d'apparition des métastases et l'architecture vasculaire ainsi que la nature capillaire des vaisseaux dans les organes cibles fortement touchés [23]. La mécanique de la circulation hématogène semblait donc responsable de la distribution des cellules tumorales dans les organes cibles. Ces deux modèles, qui peuvent sembler indépendants, voire contradictoires, représentent en fait deux aspects d'un même phénomène « bio-mécanique » combinatoire. En effet, bien que l'arrêt mécanique et non spécifique des CTCs soit un mécanisme existant, le destin de ces dernières dépend également de l'organe dans lequel elles se trouvent [24]. De nombreux travaux, dont les nôtres, ont depuis démontré que le processus métastatique résulte d'événements sélectifs physiques et biochimiques multifactoriels où la biomécanique des fluides est un élément essentiel [4, 7]. Dès qu'une cellule cancéreuse s'échappe de la tumeur primaire, s'infiltré dans la circulation sanguine et devient une CTC, un paramètre essentiel pour sa survie et son arrêt intravasculaire est la contrainte de cisaillement, qui dépend de la viscosité du fluide et du gradient de vitesse. Concrètement, plus une CTC s'éloigne du centre du vaisseau — ce qu'il fait naturellement de par ses propriétés de margination — plus elle sera déformée par le phénomène de cisaillement (ceci est particulièrement vrai dans le sang en raison de sa forte viscosité) (Figure 1 — 5. Dissémination, mort cellulaire induite par la contrainte de cisaillement). Lors de la pénétration dans le système lymphatique ou veineux, la contrainte de cisaillement reste faible et la friction avec la membrane de l'endothélium vasculaire vraisemblablement inoffensive. Certaines CTCs parviendront à atteindre les artères, où la contrainte de cisaillement est élevée et où les risques de collision sont statistiquement importants : là, les cellules peuvent subir une déformation, une fragmentation et finalement la mort [25].

Ce goulot d'étranglement entraîne la sélection des CTCs ayant les propriétés les plus favorables à leur survie — tant sur le plan physico-chimique que physiologique, avec une modification de l'expression des gènes [26] — et favorise leur structuration en groupes cellulaires plus résistants, soit entre elles en tant que groupes de CTCs [27], soit en association avec d'autres types de cellules (fibroblastes, neutrophiles ou plaquettes sanguines) [7] (Figure 1 — 5. Dissémination, illustrée). Les CTCs qui ont survécu aux événements de collision, aux contraintes de cisaillement et qui échappent au système immunitaire au cours de leur migration vont exploiter leur potentiel adhésif et les propriétés hémodynamiques des vaisseaux qui les transportent pour coloniser des régions spécifiques et permissives [28, 29], vraisemblablement les PMNs *in vivo*. Cependant, ce n'est pas tant lorsque les CTCs sont libres dans la circulation qu'elles subissent le plus grand stress, mais lorsqu'elles se fixent et tentent de quitter la circulation par le processus d'extravasation : une indication est que lors de l'injection de cellules tumorales dans le vaisseau afférent d'organes métastatiques, bien que 80% des cellules soient censées s'arrêter de manière stable un jour après l'injection, moins de 4% des cellules injectées forment efficacement des foyers métastatiques [30]. Bien que le processus d'arrêt intravasculaire des CTCs puisse se produire de manière passive par l'occlusion physique dans des petits capillaires [31] (Figure 1 — 6. Arrest, physical trapping), dont l'impact est actuellement un sujet de recherche de notre laboratoire, l'adhésion active à la paroi du vaisseau a également été signalée comme favorisant — au moins en partie — l'extravasation [28]. L'adhésion entre les CTCs et l'endothélium du système vasculaire sanguin n'est possible que si les forces de liaison (c'est-à-dire l'interaction ligand-récepteur) entre eux sont supérieures aux forces exercées par le flux et la contrainte de cisaillement [29] (Figure 1 — 8. Extravasation, adhésion active). Cette étape essentielle peut être influencée par les caractéristiques physicochimiques de la paroi vasculaire, les propriétés viscoélastiques des CTCs, mais aussi par la distribution homogène ou polarisée des ligands et des récepteurs. Différents mécanismes/modèles — mais pas nécessairement exclusifs — ont été proposés pour décrire les étapes d'arrêt et d'extravasation des CTCs. Ils pourraient suivre des stratégies similaires à celles des leucocytes, à sa-

voir un roulement le long de la paroi endothéliale puis une étape de diapédèse (paracellulaire ou transcellulaire) (Figure 1 — 8. Extravasation, diapedesis). La formation de liaisons ligand–récepteur de « faible force adhésive — activation rapide » suivie de « force adhésive plus élevée — activation lente » par un tiraillement avec le flux sanguin a été documentée [28, 29], et pourrait expliquer à la fois le roulement et l'arrêt. Cependant, nos propres observations tendent à suggérer que les CTCs s'arrêtent de manière intravasculaire plutôt abrupte, avec un risque de détachement : des travaux supplémentaires sont donc nécessaires pour clarifier ce comportement. De plus, nous avons démontré que les CTC n'utilisent pas seulement la diapédèse pour quitter la circulation sanguine et former des foyers tumoraux secondaires : ils peuvent également utiliser un mécanisme de remodelage endothélial dépendant du flux [28] (Figure 1 — 8. Extravasation, endothelial remodeling), qui se caractérise par la formation de protrusions conduisant à la création de nouvelles lumières vasculaires (pocketing), et l'exclusion passive des CTCs de l'environnement vasculaire. En effet, l'endothélium vasculaire présente des capacités de mécanosensibilité considérables qui lui permettent de détecter, de réagir et de s'adapter à toutes les conditions [32]. Dans le contexte de la dissémination intravasculaire des CTCs, nous avons récemment observé que la voie dépendante du VEGFR2 est un nœud de signalisation sensible aux forces d'écoulement et un moteur des métastases tumorales par le biais du remodelage endothélial [33]. Nous avons ainsi identifié une cible thérapeutique potentielle dans la lutte contre les métastases tumorales. Enfin, bien que des phénomènes de dormance (allant de quelques heures à plusieurs années) aient été rapportés [34], les CTCs vont finalement initier une prolifération extravasculaire pour former une tumeur secondaire appelée métastase (Figure 1 — 9. Croissance métastatique). L'efficacité de la prolifération dépendra sans doute des caractéristiques du microenvironnement métastatique, et vraisemblablement de son remodelage ultérieur par des facteurs pro-tumoraux tels que les VEs. Ensuite, les métastases nouvellement formées pourront, à leur tour, initier leur propre processus de progression tumorale et de métastase à la manière de la tumeur primaire, et accélérer considérablement l'aggravation de l'état de santé du patient cancéreux.

5. Conclusion et perspectives

Notre capacité à traiter efficacement le cancer dépend en grande partie de notre capacité à décrypter, diagnostiquer correctement et prévenir la progression du cancer et des métastases. A cet égard, la recherche sur le rôle joué par les forces mécaniques dans ces processus est fondamentale et complémentaire à d'autres approches. Les différents fluides corporels, de par les types d'écoulements qui les animent et les contraintes qui en résultent (notamment la contrainte de cisaillement dans la circulation sanguine), sont responsables de la dissémination des facteurs tumoraux sécrétés et des CTCs. Ils jouent un rôle central dans la sélection et la préparation de la niche pré-métastatique pour la formation des métastases, préparant ainsi un terrain idéal. Elles sont également des éléments clés dans la sélection des CTCs capables de survivre au cours du processus métastatique, que ce soit lors de leur migration, de leur adhésion, de leur arrêt ou de leur extravasation — chacune d'entre elles nécessitant des adaptations biomécaniques et physiologiques — portant ainsi la graine métastatique. Nous avons récemment démontré que les différentes forces présentes au sein des divers fluides corporels sont également essentielles à l'activation des récepteurs de détection du flux (dans nos modèles, mais probablement aussi dans les PMNs des patients cancéreux) et favorisent les processus d'extravasation et donc les métastases. L'omniprésence de la biomécanique dans les cancers solides (dont certains éléments s'appliquent également aux cancers du sang) rend les efforts de recherche dans ce domaine pertinents. Bien que de nombreuses études se soient concentrées au cours de la dernière décennie sur la compréhension des forces à l'intérieur de la tumeur primaire, des travaux supplémentaires sont nécessaires pour comprendre, par exemple, comment ces forces peuvent influencer la sécrétion et la nature des facteurs favorisant la tumeur, tels que les vésicules extracellulaires. Comprendre comment la contrainte de cisaillement et les forces d'écoulement ont un impact sur la sécrétion, la dissémination et l'absorption des facteurs sécrétés par la tumeur primaire et sa TME, et dans quelle mesure ils sont impliqués dans leur organotropisme (lui-même variable en fonction du cancer), sont des défis majeurs. En outre, la manière dont les propriétés mécaniques des CTCs elles-mêmes

influent sur leur aptitude métastatique est conceptuellement intéressante et donc étudiée dans notre laboratoire. Une compréhension détaillée des forces en jeu pourrait permettre le développement de thérapies innovantes tirant parti des contraintes biomécaniques pour cibler spécifiquement les niches pré-métastatiques — en s’inspirant des facteurs sécrétés par les tumeurs et en désignant, par exemple, des VEs porteuses de médicaments — et bloquer ou retarder leur établissement, puis le remodelage endothélial et les métastases. La fragilité des CTCs à la contrainte de cisaillement doit également être prise en compte : si l’utilisation de médicaments ciblant la pression sanguine ne semble pas être dans le meilleur intérêt d’un patient cancéreux, des outils permettant leur élimination continue du sang sont déjà en cours de développement [35] et des travaux supplémentaires sont nécessaires pour comprendre si leurs profils mécaniques sont impliqués dans un tel comportement. Comprendre la biomécanique à l’œuvre chez un patient nécessitera également de considérer les paramètres qui agissent sur eux. Les caractéristiques physiques/physiologiques d’un patient — notamment l’âge [36] — les effets potentiels des traitements suivis, et enfin leur évolution au cours de l’histoire naturelle de la pathologie sont autant d’éléments qui pourraient permettre des thérapies plus efficaces et personnalisées. Un autre axe est l’étude de l’effet des facteurs sécrétés par les cellules tumorales et non tumorales, de leur éventuelle compétition pro- vs anti-tumorale au cours de la cascade métastatique, ainsi que de leur implication potentielle dans une modification biomécanique des PMNs.

Remerciements

Nous remercions particulièrement Vincent Hyenne, Naël Osmani et Sébastien Harlepp, mais aussi tous les membres de l’équipe de Jacky G. Goetz pour leurs discussions, explications et idées pour améliorer le manuscrit. Florent Colin est financé par le Consortium NANOTUMOR (PFA), un programme de l’ITMO Cancer d’AVIESAN (Alliance Nationale pour les Sciences de la Vie et de la Santé) dans le cadre du Plan Cancer (France). Valentin Gensbittel est financé par la Région Alsace — Inserm. Jacky G. Goetz est Directeur de Recherche à l’Inserm et Grand Prix

2020 de Cancérologie de la Fondation Del Duca (Académie de Sciences, France). Les travaux du laboratoire de Jacky G. Goetz sont principalement soutenus par l’INCa (Institut National Du Cancer), la Ligue contre le Cancer, la Fondation ARC, la FRM (Fondation pour la Recherche Médicale), Le Plan Cancer, la Région Est, l’Inserm et l’Université de Strasbourg.

References

- [1] S. Valastyan, R. A. Weinberg, “Tumor metastasis: molecular insights and evolving paradigms”, *Cell* **147** (2011), no. 2, p. 275-292.
- [2] G. P. Gupta, J. Massagué, “Cancer metastasis: building a framework”, *Cell* **127** (2006), no. 4, p. 679-695.
- [3] S. Paget, “The distribution of secondary growths in cancer of the breast. 1889”, *Cancer Metastasis Rev.* **8** (1889), no. 2, p. 98-101.
- [4] S. Maman, I. P. Witz, “A history of exploring cancer in context”, *Nat. Rev. Cancer* **18** (2018), no. 6, p. 359-376.
- [5] R. N. Kaplan, B. Psaila, D. Lyden, “Niche-to-niche migration of bone-marrow-derived cells”, *Trends Mol. Med.* **13** (2007), no. 2, p. 72-81.
- [6] H. T. Nia, L. L. Munn, R. K. Jain, “Physical traits of cancer”, *Science* **370** (2020), no. 6516, article no. eaaz0868.
- [7] G. Follain *et al.*, “Fluids and their mechanics in tumour transit: shaping metastasis”, *Nat. Rev. Cancer* **20** (2020), no. 2, p. 107-124.
- [8] M. A. Karreman, V. Hyenne, Y. Schwab, J. G. Goetz, “Intravital correlative microscopy: imaging life at the nanoscale”, *Trends Cell Biol.* **26** (2016), no. 11, p. 848-863.
- [9] T. Stylianopoulos *et al.*, “Causes, consequences, and remedies for growth-induced solid stress in murine and human tumors”, *Proc. Natl. Acad. Sci. USA* **109** (2012), no. 38, p. 15101-15108.
- [10] J. G. Goetz, P. Lajoie, S. M. Wiseman, I. R. Nabi, “Caveolin-1 in tumor progression: the good, the bad and the ugly”, *Cancer Metastasis Rev.* **27** (2008), no. 4, p. 715-735.
- [11] J. G. Goetz *et al.*, “Concerted regulation of focal adhesion dynamics by galectin-3 and tyrosine-phosphorylated caveolin-1”, *J. Cell Biol.* **180** (2008), no. 6, p. 1261-1275.
- [12] J. G. Goetz *et al.*, “Biomechanical remodeling of the microenvironment by stromal caveolin-1 favors tumor invasion and metastasis”, *Cell* **146** (2011), no. 1, p. 148-163.
- [13] A. Klein-Goldberg, S. Maman, I. P. Witz, “The role played by the microenvironment in site-specific metastasis”, *Cancer Lett.* **352** (2014), no. 1, p. 54-58.
- [14] S. P. H. Chiang, R. M. Cabrera, J. E. Segall, “Tumor cell intravasation”, *Am. J. Physiol. Cell Physiol.* **311** (2016), no. 1, p. C1-C14.
- [15] A. S. Azevedo, G. Follain, P. Shankaranarayanan, S. Harlepp, J. G. Goetz, “Metastasis of circulating tumor cells: Favorable soil or suitable biomechanics, or both?”, *Cell Adhes. Migr.* **9** (2015), no. 5, p. 345-356.
- [16] S. García-Silva *et al.*, “Use of extracellular vesicles from lymphatic drainage as surrogate markers of melanoma progres-

- sion and BRAF V600E mutation”, *J. Exp. Med.* **216** (2019), no. 5, p. 1061-1070.
- [17] M. A. S. Broggi *et al.*, “Tumor-associated factors are enriched in lymphatic exudate compared to plasma in metastatic melanoma patients”, *J. Exp. Med.* **216** (2019), no. 5, p. 1091-1107.
- [18] V. Hyenne *et al.*, “Studying the fate of tumor extracellular vesicles at high spatiotemporal resolution using the zebrafish embryo”, *Dev. Cell* **48** (2019), no. 4, p. 554-572.e7.
- [19] A. Hoshino *et al.*, “Tumour exosome integrins determine organotropic metastasis”, *Nature* **527** (2015), no. 7578, p. 329-335.
- [20] V. Hyenne *et al.*, “RAL-1 controls multivesicular body biogenesis and exosome secretion”, *J. Cell Biol.* **211** (2015), no. 1, p. 27-37.
- [21] S. Ghoroghi *et al.*, “Ral GTPases promote breast cancer metastasis by controlling biogenesis and organ targeting of exosomes”, *Elife* **10** (2021), p. 1-29.
- [22] D. R. Coman, “Mechanisms responsible for the origin and distribution of blood-borne tumor metastases: a review”, *Cancer Res.* **13** (1953), no. 6, p. 397-404.
- [23] L. Weiss, J. Bronk, J. W. Pickren, W. W. Lane, “Metastatic patterns and target organ arterial blood flow”, *Invasion Metastasis* **1** (1981), no. 2, p. 126-135.
- [24] I. Fidler, G. Nicolson, “Organ selectivity for implantation survival and growth of B16 melanoma variant tumor lines”, *J. Natl. Cancer Inst.* **57** (1976), no. 5, p. 1199-1202.
- [25] M. B. Headley *et al.*, “Visualization of immediate immune responses to pioneer metastatic cells in the lung”, *Nature* **531** (2016), no. 7595, p. 513-517.
- [26] S. Lamouille, J. Xu, R. Derynck, “Molecular mechanisms of epithelial-mesenchymal transition”, *Nat. Rev. Mol. Cell Biol.* **15** (2014), no. 3, p. 178-196.
- [27] N. Aceto *et al.*, “Circulating tumor cell clusters are oligoclonal precursors of breast cancer metastasis”, *Cell* **158** (2014), no. 5, p. 1110-1122.
- [28] G. Follain *et al.*, “Hemodynamic forces tune the arrest, adhesion, and extravasation of circulating tumor cells”, *Dev. Cell* **45** (2018), no. 1, p. 33-52.e12.
- [29] N. Osmani *et al.*, “Metastatic tumor cells exploit their adhesion repertoire to counteract shear forces during intravascular arrest”, *Cell Rep.* **28** (2019), no. 10, p. 2491-2500.e5.
- [30] M. D. Cameron *et al.*, “Temporal progression of metastasis in lung: cell survival, dormancy, and location dependence of metastatic inefficiency”, *Cancer Res.* **60** (2000), no. 9, p. 2541-2546.
- [31] Y. Kienast *et al.*, “Real-time imaging reveals the single steps of brain metastasis formation”, *Nat. Med.* **16** (2010), no. 1, p. 116-122.
- [32] J. G. Goetz *et al.*, “Endothelial cilia mediate low flow sensing during zebrafish vascular development”, *Cell Rep.* **6** (2014), no. 5, p. 799-808.
- [33] G. Follain *et al.*, “Impairing flow-mediated endothelial remodeling reduces extravasation of tumor cells”, *Sci. Rep.* **11** (2021), no. 1, article no. 13144.
- [34] C. M. Neophytou, T.-C. Kyriakou, P. Papageorgis, “Mechanisms of metastatic tumor dormancy and implications for cancer therapy”, *Int. J. Mol. Sci.* **20** (2019), no. 24, article no. 6158.
- [35] A. Weth *et al.*, “A novel device for elimination of cancer cells from blood specimens”, *Sci. Rep.* **10** (2020), no. 1, article no. 10181.
- [36] M. Fane, A. T. Weeraratna, “How the ageing microenvironment influences tumour progression”, *Nat. Rev. Cancer* **20** (2020), no. 2, p. 89-106.

ANNEXE 4

Spotlight

Nanoluminal Signaling
Shapes Collective
Metastasis

Valentin Gensbittel,^{1,2,3}
Ignacio Busnelli,^{1,2,3}
Naël Osmani,^{1,2,3,5,*} and
Jacky G. Goetz^{1,2,3,4,5,@}

Clustering of tumor cells is known to grant superior metastatic efficiency compared with single cells. However, the mechanisms involved remain elusive. Reporting in *Cell*, Wrenn *et al.* describe how sealed intercellular compartments, nanolumina, are used as growth factor reservoirs within tumor cell clusters to regulate tumor cell proliferation.

Metastases culminate at the end of a complex metastatic cascade where tumor cells need to overcome several obstacles. Recent evidence suggests that, when acting as a collective, tumor cells significantly increase their chances of success in forming life-threatening metastases. While this concept is gaining momentum, how tumor cells exacerbate their metastatic potential when clustered remains to be fully solved and could put the spotlight on new therapeutic targets. The process of tumor cell aggregation depends on cell–cell adhesion interactions, such as plakoglobin, CD44, and E-cadherin [1–3], and offers up to a 50-fold boost in metastatic potential to tumor cell clusters [1]. Consequently, tumor cell clusters end up being at the origin of most of the metastases that arise in cancer [1,4]. They are present at every step of the metastatic process (invasion [5], intravasation [6], circulation [7], extravasation [8], and stemness [9]) and, as such, are likely capable of completing, as clusters, the metastatic journey in its entirety [3]. While some of the benefits that come with clustering have already been identified

(Figure 1A), our understanding remains sparse and many implications and mechanisms of tumor cell clustering remain to be identified. In a recent article in *Cell*, Wrenn *et al.* report a mechanism that grants plasticity to tumor cell clusters to regulate their behavior during their metastatic journey [10]. Tumor cell clusters adapt to their needs by switching between proliferative and migratory states based on the concentration of the growth factor epigen in nanoscale intercellular compartments (nanolumina) formed within the clusters (Figure 1).

When investigating the genetic programs that link clustering and metastasis using RNA-seq on tumor cells of different aggregation conditions, the authors identified several genes of which the expression levels scaled with tumor cell clustering. Among them, the gene encoding the growth factor epigen (Epgn) was the most induced gene upon tumor cell clustering. Upon Epgn depletion, using lentiviral-mediated RNAi, the authors found that: (i) Epgn is not required for clustering (thus likely acting downstream of clustering); and (ii) Epgn strongly supports metastatic outgrowth because metastatic outgrowth was reduced by 94% in a lung metastasis assay with Epgn-kd clusters.

A parallel observation that emerged from the RNA-seq analysis revealed that Epgn-kd clusters repressed expression of cell-cycle genes and favored the expression of migration-associated ones. To test the effects of Epgn depletion on proliferation and migration, the authors embedded Epgn-kd and control tumor cell clusters in 3D gels and monitored their behavior with time-lapse microscopy. Concomitantly with the RNA-seq results, the Epgn-kd clusters displayed reduced proliferation but increased migration. To determine the range of action of Epgn, the authors either cocultured control clusters and Epgn-kd clusters together, or mixed Epgn-expressing cells with Epgn-kd clusters before assessing

their migration and outgrowth. They found that Epgn, the expression of which is restricted locally, acts noncell-autonomously as a shared growth signal.

To further unravel how Epgn enrichment is locally restricted, the authors used nanoresolution electron and optical microscopy to precisely track epigen location. Remarkably, the authors discovered that Epgn was highly concentrated in intercellular nanoscale cavities permeably sealed by cell–cell junctions referred to as ‘nanolumina’. While Epgn accumulated specifically in the cavities, it was excluded from cell–cell junctions. When probing junctional permeability of the clusters, the authors found that hermetic cell–cell junctions prevented ligand diffusion, in turn allowing Epgn accumulation in nanolumina.

To interrogate these mechanisms *in vivo*, tumor cell clusters were transplanted into mammary fat pads of mice and both primary tumor outgrowth and development of metastases were monitored. Epgn is highly expressed in primary tumors and was frequently expressed in disseminated tumor cell clusters but absent or weakly expressed in disseminated single tumor cells. Interestingly, while protrusive clusters displayed low Epgn expression, nonprotrusive and proliferative clusters had high Epgn expression, mirroring *in vitro* observations. Again, nanoluminal permeability and Epgn accumulation correlated with outgrowth, both in primary tumors and metastases. Transplantation of control and Epgn-kd clusters showed Epgn to be critical for primary tumor and metastatic outgrowth but not for initial metastatic seeding. While additional work is required to determine how universal these findings are across various cancer types (and origins), the authors demonstrated that these mechanisms operate in the context of a particular breast cancer subtype, the aggressive basal-like 2 triple-negative breast cancer. They further showed that treatment with IFN γ , a

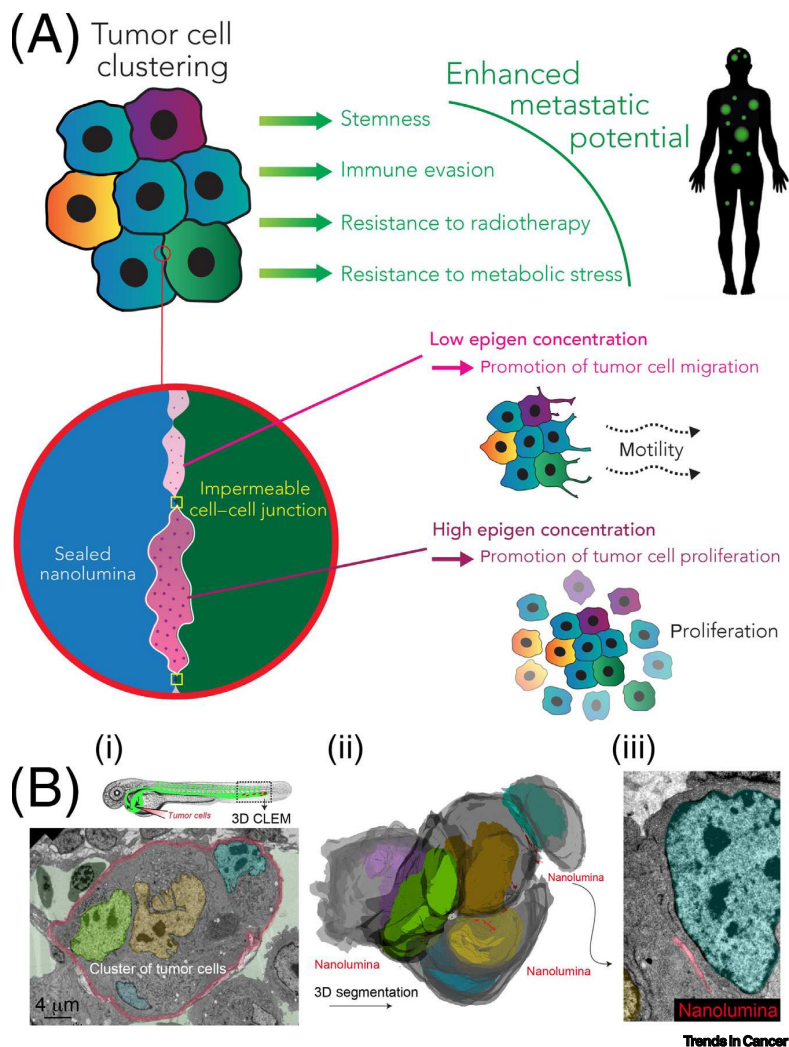


Figure 1. Epigen (Epgn) Signaling upon Tumor Cell Clustering. (A) A high Epgn concentration in nanolumina promotes tumor cell proliferation, whereas a low concentration promotes cluster migration. This signaling mechanism, driven by junctional permeability, enables tumor cell clusters to adapt their behavior, increasing our understanding of the advantages granted by clustering in metastasis. (B) Intravital correlative microscopy allows 3D visualization of nanolumina in clusters of tumor cells undergoing extravasation. Circulating tumor cells (CTCs) were injected intravascularly in 2-day-post fertilization embryos, fixed 9 h post injection, and imaged by serial sectioning transmission electron microscopy (i). Individual CTCs were manually segmented to create a 3D volume (ii). EM micrograph showing nanolumina at high resolution (iii). Adapted from [8]. Abbreviation: CLEM, correlative light and electron microscopy.

cytokine that favors paracellular diffusion, could reduce the accumulation of Epgn and subsequent metastatic outgrowth by forcing the permeability of tumor cell clusters. Thus, in addition to offering new insights into why collective metastasis

benefits from a boost in metastatic potential, the study provides the first therapeutic strategy to impair collective metastasis.

This work by Wrenn *et al.* [10] also raises the important question as to whether this

nanoluminal signaling is a general mechanism shared by different cancer types in which metastatic potential is enhanced by clusters of tumor cells. Conceptually, while providing a new paradigm for cancer cells, which mimic a previously shown developmental process aiming at concentrating growth factors within lumens [11], more work is needed to identify the molecular mechanisms of lumen formation and regulation over the course of the metastatic process. Whether cancer cells are hijacking a developmental program similar to epithelial-mesenchymal transition and whether it can be found in differentiated cells remain to be elucidated. Furthermore, it will be of interest to demonstrate which mechanism controls transcriptional regulation of Epgn, and at which stage, and whether Epgn enrichment depends both on the formation of impermeable nanolumens and enhanced transcription. Long-term intravital imaging and longitudinal analysis of mouse models expressing a tagged Epgn could address this issue. Alternatively, transcriptional regulation of Epgn (and associated transcriptional programs) throughout the metastatic cascade could be interrogated via single-cell (sc)RNA-seq in matched primary tumors, circulating tumor cells (CTCs), and developing metastatic foci. Documenting whether epigen nanolumina signaling is at play at each step of the metastatic cascade and, in particular, when clusters of tumor cells disseminate in the blood circulation, would allow an understanding of the overall impact of these structures on not only growth, but also survival, stemness, and extravasation of metastatic cancer cells. In addition to tracking these features in patient-derived CTC clusters, animal models that combine intravital imaging and high-resolution 3D electron microscopy, such as the zebrafish embryo [12], could be instrumental. Volume electron microscopy would allow one to appreciate how these lumens are topologically organized (Figure 1B). Finally, although additional work is required to validate therapeutic

strategies to effectively target CTC clusters, Wrenn *et al.* [10] have provided an exciting observation that improves our understanding of collective metastasis.

¹INSERM UMR_S1109, Tumor Biomechanics, Strasbourg, France

²Université de Strasbourg, Strasbourg, France

³Fédération de Médecine Translationnelle de Strasbourg (FMTS), Strasbourg, France

⁴Website: www.goetzlab.com

⁵Lead authors

*Correspondence:

osmani@unistra.fr (N. Osmani) and

jacky.goetz@inserm.fr (J.G. Goetz).

⁶Twitter: @GoetzJacky (J.G. Goetz).

<https://doi.org/10.1016/j.trecan.2020.11.003>

© 2020 Elsevier Inc. All rights reserved.

References

1. Aceto, N. *et al.* (2014) Circulating tumor cell clusters are oligoclonal precursors of breast cancer metastasis. *Cell* 158, 1110–1122
2. Liu, X. *et al.* (2019) Homophilic CD44 interactions mediate tumor cell aggregation and polyclonal metastasis in patient-derived breast cancer models. *Cancer Discov.* 9, 96–113
3. Padmanaban, V. *et al.* (2019) E-cadherin is required for metastasis in multiple models of breast cancer. *Nature* 573, 439–444
4. Cheung, K.J. *et al.* (2016) Polyclonal breast cancer metastases arise from collective dissemination of keratin 14-expressing tumor cell clusters. *Proc. Natl. Acad. Sci. U. S. A.* 113, E854–E863
5. Cheung, K.J. *et al.* (2013) Collective invasion in breast cancer requires a conserved basal epithelial program. *Cell* 155, 1639–1651
6. Donato, C. *et al.* (2020) Hypoxia triggers the intravasation of clustered circulating tumor cells. *Cell Rep.* 32, 108105
7. Au, S.H. *et al.* (2016) Clusters of circulating tumor cells traverse capillary-sized vessels. *Proc. Natl. Acad. Sci. U. S. A.* 113, 4947–4952
8. Follain, G. *et al.* (2018) Hemodynamic forces tune the arrest, adhesion, and extravasation of circulating tumor cells. *Dev. Cell* 45, 33–52
9. Gkoutela, S. *et al.* (2019) Circulating tumor cell clustering shapes DNA methylation to enable metastasis seeding. *Cell* 176, 98–112
10. Wrenn, E.D. *et al.* (2020) Regulation of collective metastasis by nanoluminal signaling. *Cell* 183, 395–410
11. Durdu, S. *et al.* (2014) Luminal signaling links cell communication to tissue architecture during organogenesis. *Nature* 515, 120–124
12. Osmani, N. and Goetz, J.G. (2019) Multiscale imaging of metastasis in zebrafish. *Trends Cancer* 5, 766–778

ANNEXE 5



Probing Intravascular Adhesion and Extravasation of Tumor Cells with Microfluidics

Naël Osmani, Gautier Follain, Valentin Gensbittel,
María Jesús García-León, Sébastien Harlepp, and Jacky G. Goetz

Abstract

Cancer metastasis is a multistep process during which tumor cells leave the primary tumor mass and form distant secondary colonies that are lethal. Circulating tumor cells (CTCs) are transported by body fluids to reach distant organs, where they will extravasate and either remain dormant or form new tumor foci. Development of methods to study the behavior of CTCs at the late stages of the intravascular journey is thus required to dissect the molecular mechanisms at play. Using recently developed microfluidics approaches, we have demonstrated that CTCs arrest intravascularly, through a two-step process: (a) CTCs stop using low energy and rapidly activated adhesion receptors to form transient metastable adhesions and (b) CTCs stabilize their adhesions to the endothelial layer with high energy and slowly activated adhesion receptors. In this methods chapter, we describe these easy-to-implement quantitative methods using commercially available microfluidic channels. We detail the use of fast live imaging combined to fine-tuned perfusion to measure the adhesion potential of CTC depending on flow velocities. We document how rapidly engaged early metastable adhesion can be discriminated from slower activated stable adhesion using microfluidics. Finally, CTC extravasation potential can be assessed within this setup using long-term cell culture under flow. Altogether, this experimental pipeline can be adapted to probe the adhesion (to the endothelial layer) and extravasation potential of any circulating cell.

Key words Microfluidics, Circulating tumor cells (CTCs), Adhesion, Extravasation, Metastasis, Live imaging

1 Introduction

Metastasis is the leading cause of cancer death in patient [1]. Metastatic progression is a multistep process whereby tumor cells disseminate using body fluids and colonize distant organs to ultimately develop life-threatening secondary tumors [2, 3]. As they develop into an in situ tumor, cancer cells will eventually acquire an invasive potential and breach through the extracellular

Naël Osmani and Gautier Follain contributed equally to this work.

Ulrike S. Stein (ed.), *Metastasis: Methods and Protocols*, Methods in Molecular Biology, vol. 2294, https://doi.org/10.1007/978-1-0716-1350-4_8, © Springer Science+Business Media, LLC, part of Springer Nature 2021

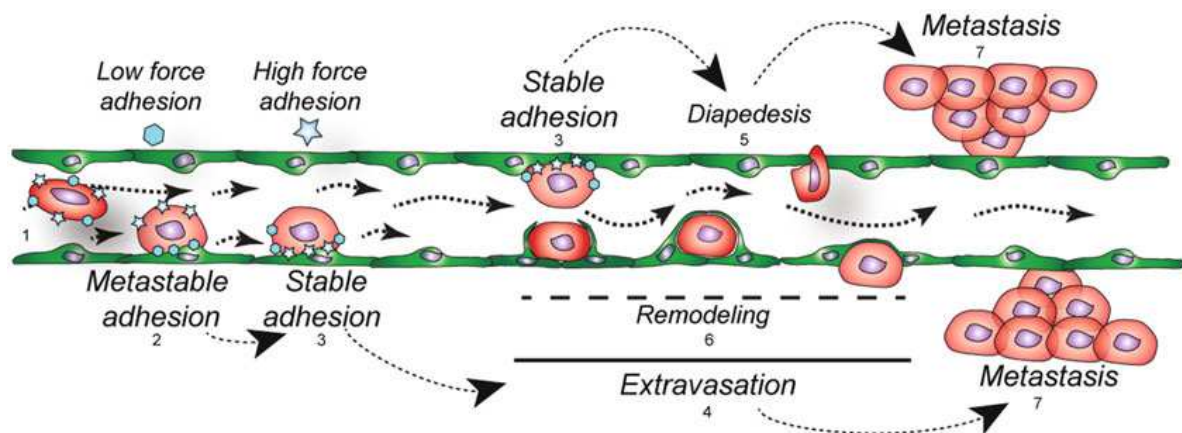


Fig. 1 The metastatic cascade during hematogenous dissemination. Schematic representation of the metastatic cascade. (1) Circulating tumor cells (CTCs) are disseminated through blood circulation. (2) As CTCs reach vessels with lower and adhesion permissive flow velocities, they form metastable adhesions with low energy and fast to engage adhesion receptors which allow their transient arrest. (3) Once arrested, CTCs strengthen their adhesion to the luminal side of endothelial cells by clustering high energy and slow to engage adhesion receptors. This is essential for CTCs to resist to the shear-ripping forces of the blood flow. (4) CTCs' stable adhesions further permit cells to engage different strategies to escape circulation. (5) CTCs can extravasate by actively migrating through the endothelial layer using diapedesis. (6) The endothelium can also favor CTC passive extravasation by remodeling in order to restore blood flow after CTC arrest. (7) Once extravasated, CTCs will colonize the perivascular niche and ultimately form secondary colonies in distant organs

matrix of their organ of origin. (a) These escaping tumor cells will invade the surrounding stroma and reach neighboring vessels. (b) Cancer cells will then enter blood circulation by crossing the endothelial barrier (intravasation). (c) As they become circulating tumor cells (CTCs), they are transported to distant organs by blood circulation. (d) CTCs will stop into the capillary beds of distant organs in regions of adhesion-permissive flows and exit blood stream by crossing the endothelial layer (extravasation) either through active transendothelial migration or through flow-dependent endothelial remodeling [3]. (e) Finally, they will invade the organs and settle to secondary metastatic sites into metastatic niches where they either enter dormancy or form secondary colonies [4, 5] (Fig. 1).

Adhesion receptors at the surface of CTCs have been involved in the ability of CTC to roll or to arrest on the surface of endothelial cells using receptors of different binding energies [6] in a mechanism that is highly reminiscent of leukocytes rolling, arrest, and adhesion steps preceding their extravasation [7, 8] (Fig. 1). Among those, glycoproteins involved in leukocytes rolling at the surface of the endothelium, such as selectins, are required for the adhesion of CTCs to endothelial cells [9, 10]. CD24, CD44, PODXL, and mucins are involved in CTC adhesion to the endothelium [9, 11–15]. Finally, ECM adhesion receptors of the integrin family such as

integrins $\alpha\beta3$, $\beta1$, and $\beta4$ are also involved in adhesion of CTCs to endothelial cells [15–20]. These experimental approaches probed the role of specific adhesion receptors in CTC arrest or extravasation by various means. They used either parallel plate chambers with ligand-coated dish or Boyden chamber covered with a HUVEC monolayer, respectively, which unfortunately does not fully recapitulate the complex interaction between CTCs and endothelial cells in flow during arrest and extravasation. Thus, the respective contributions of these different receptors in early intravascular arrest versus stable adhesions have rarely been probed simultaneously. Hence, the correlation between the adhesive and the metastatic potentials of CTCs remains elusive. Furthermore, the important function of the biomechanical cues from blood flow during CTC arrest and extravasation has also been understudied [15, 21].

Microfluidics have long been used as a tool to study cells in flow from leukocyte to cancer biology and to probe their biological and mechanical properties [6, 8]. Recent developments in microfluidic tools now allow both biomechanical and biochemical characterization of CTCs [22–27]. Our recent work as demonstrated that the use of in vitro microfluidics in parallel with intravital imaging in the zebrafish embryo is a fast, efficient, and cost effective experimental metastasis framework that can be ultimately validated in mouse experimental metastasis models and patients [15, 21, 28, 29].

In this chapter, we propose an original framework using microfluidic microchannels as an in vitro experimental metastasis model to study the different steps of hematogenous dissemination. These methods are based on commercially available systems that require little/no expertise in microfluidics microfabrication or PDMS (polydimethylsiloxane) handling and are thus easy to implement in any cell biology laboratory. These methods enable to probe the potential of hematogenous dissemination of CTCs in physiological conditions where the vascular wall (endothelial cells) and the underlying hemodynamics (with some limitations) can be easily reproduced.

2 Materials

2.1 Cell

Classical cancer cell lines from human and mouse origin can be used. These can be easily genetically modified using CRISPR/Cas9, stably transfected or virally transduced with gene expression vectors or shRNA expression vectors, or transiently transfected with gene expression vectors or siRNA. We are using the metastatic mouse mammary carcinoma cell line D2A1 as shown in our recent reports [15, 21], which we fluorescently label at will when fluorescence analysis is required. Endothelial cells of primary origin either commercially available or from homemade purification should be

used. In the methods we present here, we are using human umbilical vein endothelial cells (HUVEC) from a single donor as they are easy to culture.

2.2 Cell Culture

1. Endothelial cell culture medium containing fetal calf serum 0.02 ml/ml, endothelial cell growth supplement 0.004 ml/ml, epidermal growth factor (recombinant human) 0.1 ng/ml, basic fibroblast growth factor (recombinant human) 1 ng/ml, heparin 90 µg/ml, hydrocortisone 1 µg/ml, penicillin-streptomycin 100 U–0.1 mg/ml.
2. Fibronectin from bovine plasma.
3. PBS–EDTA: 0.2 g/l.
4. Trypsin–EDTA: 0.05% for HUVEC and trypsin adapted to the cancer cell line of interest.
5. Cancer cell line medium: The appropriate medium for the cell line of interest, supplemented with all additives.
6. HEPES 1 M sterile.

2.3 Microfluidic Equipment (Fig. 2a–d)

1. Peristaltic pump. In the methods we present here, we use the Reglo Digital with 2 or 4 channels and 12 rollers (ISMATEC) (*see Note 1*).
2. Tygon[®] LMT-55 3-Stop Tubing 0.38 mm, 12-pack, Wall Thickness = ~0.86 mm (IDEX Corporation) to drive medium and cell perfusion.
3. 23G × 1" (0.6 × 25 mm) hypodermic needles extracted from their Luer adaptors are used to connect the 3-stop tubing to normal tubing (*see Note 2*).
4. Silicon tubing 0.5 mm (*ibidi*).
5. Fitting reducer 0.5–1.6 mm (*ibidi*).
6. Silicon tubing 1.6 mm (*ibidi*).
7. Elbow Luer connector (*ibidi*).

2.4 Microchannels (Fig. 2e)

1. µSlide I 0.4 Luer *ibiTreat*: #1.5 polymer coverslip (*ibidi*).
2. µSlide VI 0.4 *ibiTreat*: #1.5 polymer coverslip (*ibidi*).
3. sticky-Slide I Luer (*ibidi*).
4. Dow Corning[®] high-vacuum silicone grease is used to seal sticky-Slide I to rectangular glass coverslips (*see Note 3*).

2.5 Live Microscopy (Fig. 2f)

1. Any inverted live imaging compatible microscope can be used.
2. A heating system (we use a thermo-controlled heating box OKO Lab Cage from Okolab).
3. A dry 10× objective (we use a UPLFLN-P 10×/0.3 objective from Olympus).

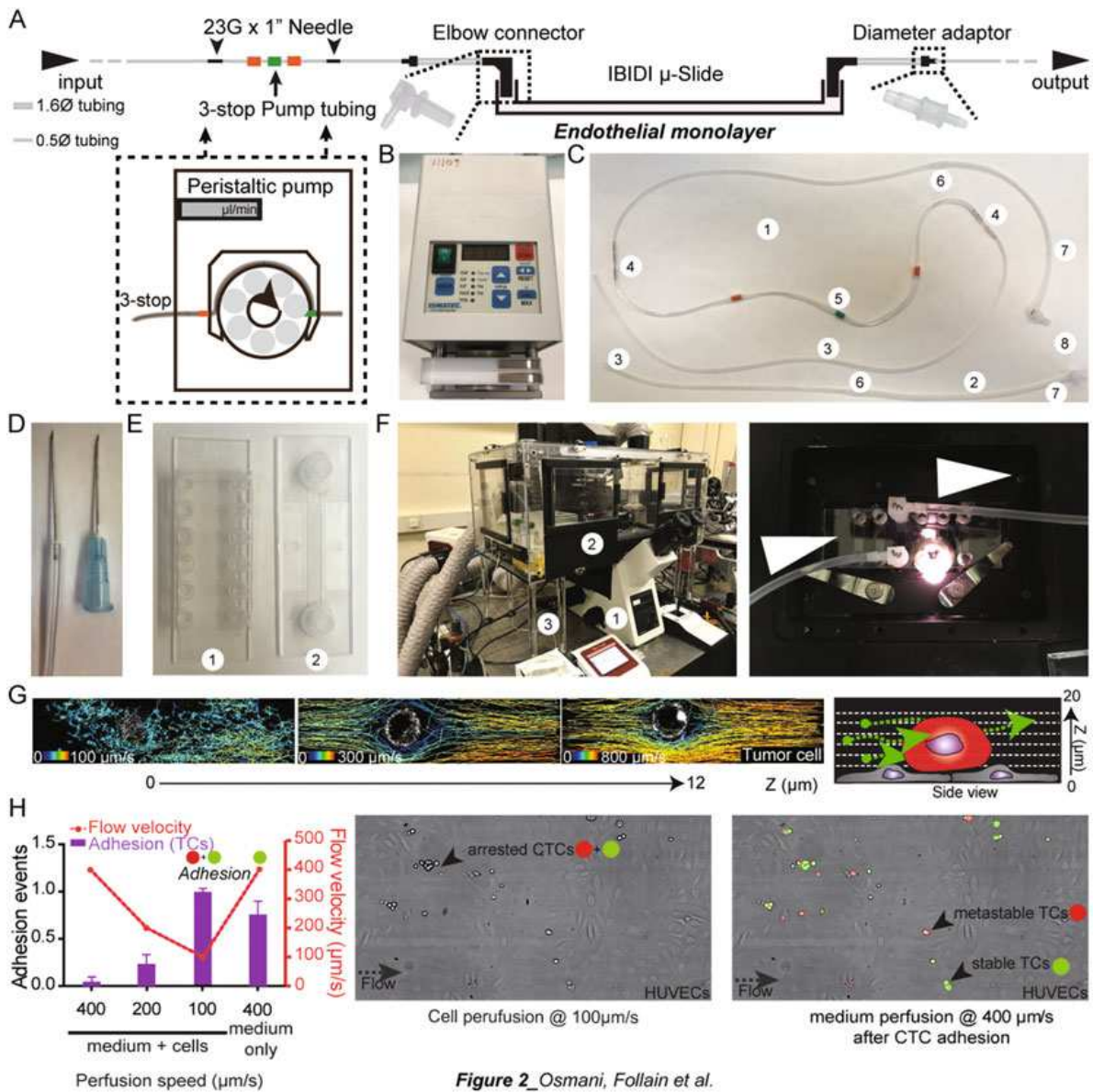


Figure 2_Osmani, Follain et al.

Fig. 2 Live adhesion assay. (a) Scheme of the microfluidic setup. (b) Peristaltic pump (here Ismatec Reglo Digital MS/2). (c) Tubing used for all microfluidic experiments: (1) 3-stop containing tubing. (2) Tubing without 3-stop. (3) 0.5 mm tubing. (4) Needle junction. (5) 3-stop tubing. (6) 0.5 to 1.6 filter. (7) 1.6 mm tubing. (8) Elbow Luer. (d) 23G × 1" hypodermic needle without Luer inserted into the 3-stop tubing next 23G × 1" hypodermic needle with luer. (e) Commercially available µSlide I (1) and IV (2) 0.4. (f) (Left) Live microscopy setup: (1) Inverted microscope (Olympus). (2) Thermo-controlled heating box with 5% CO₂ atmosphere (Okolab). (3) CCD fast camera (Thorlabs). (Right) µSlide inserted into the stage. White arrows highlight medium flow direction. (g) (left) Examples of flow pattern analysis and flow velocities quantification using fast confocal imaging and automated tracking. CTCs are shown in gray. (right) Scheme of the sequential fast confocal acquisition performed along the z axis. (Adapted from [21]). (h) Data analysis: (left) chart showing increased evaluation inversely correlated to flow speed. The final washing step allows to assess the stability of CTC adhesions engaged with endothelial cells. Pictures showing (center) arresting CTC at 100 µm/s and (right) CTC discriminated during the washing step as stably adhered (stable) and transiently adhered (metastable). (Adapted from [15])

4. A camera able to image at 24 frame per second (we use a CMOS fast camera DCC3240M from Thorlabs).
5. A 5% CO₂ atmosphere is also recommended but can be replaced by supplementing medium with 20 mM of sterile Hepes.

2.6 Confocal Microscopy

Any inverted confocal microscope of choice would be appropriate. We are using a TCS SP5 inverted confocal microscope systems (Leica) with an immersion oil 63× objective (HCX PL APO 63×/1.4 OIL).

2.7 Fluorescent Beads for Flow Calibration

FluoSpheres™ Carboxylate-Modified Microspheres, 0.1 μm, yellow-green fluorescent (505/515), 2% solids (Thermo Fischer).

2.8 Scanning Electron Microscopy Reagents

1. 1,1,1,3,3,3-hexamethyldisilazane (HDMS).
2. 25, 4 mm EM Aluminum Mounts for AMRAY (EMS, Hatfield).
3. Leit-C conductive carbon cement (CCC, Plano GmbH, Germany).
4. Cressington Sputter Coater 208HR coupled to a Pfeiffer Vacuum (Germany).

2.9 Scanning Electron Microscopy Reagents

Image acquisition can be performed with any desktop SEM microscope. We use a Phenom-World SEM desktop microscope (Phenom-World B.V, The Netherlands) (collaboration with EFS, Strasbourg, INSERM U1255).

3 Methods

3.1 Endothelial Cell Seeding in Microchannels

1. A single P0 vial is expended for 4 passages in 100 cm petri dishes. The P4 vials are then stored in liquid nitrogen. A single vial will be used for each experiment.
2. μSlide microchannels are coated with fibronectin to favor HUVEC seeding. Fibronectin is diluted at 10 μg/ml in PBS. 100 μl or 30 μl of this solution are added in μSlide I or VI, respectively. Microchannels are incubated 1 h at 37 °C (alternatively, μSlide can be incubated O/N at 4 °C). Microchannels are then washed three times with sterile PBS (*see Note 4*).
3. Freshly thawed HUVEC are lifted and resuspended in pre-heated ECGM. Cells are centrifuged 5 min at 100 × *g* and room temperature. The supernatant is discarded. The cell pellet is resuspended in ECGM at a concentration of 10⁶ cells/ml. 100 μl or 30 μl of this solution are added in μSlide I or VI, respectively (*see Note 4*).

4. Medium should be changed twice a day in the microchannels as long as it is not perfused. Each change of medium consists of two steps of wash with preheated medium to ensure that the used one is washed away and a final step of adding fresh medium to fill the microchannels and both wells. The gap time between two change of medium should not exceed 15–16 h (*see Note 4*).

3.2 Tubing Setup (Fig. 2a, c)

To ensure sterility, this step should be performed under a sterile cell culture hood.

1. For the 3-stop tubing, insert 23G \times 1" hypodermic needles extracted from their Luer in each side of the 3-stop tubing. Connect the 0.5 mm tubing to the 3-stop tubing using the needles on each side. We recommend adapting the tubing length to the specificity of your microscope and keep the tubing as short as possible. Connect a 0.5 to 1.6 fitting reducer on one side of the 3-stop tube. Connect 1.6 mm tube to the fitting reducer. We advise to reduce the length of this part as much as possible (5–10 cm maximum).
2. For the short tubing, cut a piece of 0.5 mm tubing adapted to the specificity of your microscope setup. We advise to use a tubing as short as possible. Connect a 0.5 to 1.6 fitting reducer on one side of the 3-stop tube. Connect 1.6 mm tube to the fitting reducer. We advise to reduce the length of this part as much as possible (5–10 cm maximum).

3.3 Calibrating the Microfluidic Perfusion and Probing Flow Profiles

100 nm fluorescent beads can be used to assess flow speed within the channel at each given flowrate. We advise to measure the flow speed from the bottom to the middle of the channel at several z heights (using a piezoelectrical caliper) to characterize the Poiseuille flow (*see Note 5*).

1. Prepare the live imaging microscope. Heat the setup at 37 °C and 5% CO₂ (if available).
2. Prepare cells for perfusion. Wash cells with PBS–EDTA. Trypsinize cells and resuspend them in ECGM. Centrifuge cells to remove trypsin and resuspend them in ECGM at a concentration of 10⁶ cells/ml (*see Note 6*).
3. Inject a volume of cells equivalent to the microchannel volume (*see Note 4*). Tilt the channel along its length to homogenize. Incubate 5 min at 37 °C to favor CTC stable adhesion.
4. Prepare the μ Slide for perfusion. Perfuse ECGM-containing fluorescent beads at 0.02% in the 3-stop containing tubing using “pushing perfusion” (Fig. 3c). Connect the elbow Luer to the microfluidic channel, once the medium starts to drip. *This is essential to avoid bubbles as it would eventually destroy*

endothelial cells. Connect then the elbow Luer of the outlet tubing (without the 3-stop tubing) and put the outlet tubing into a liquid bin (*see Note 6*).

5. Microchannels are imaged at high speed (50 ~ 100 fps) using a Leica SP5 confocal microscope equipped with resonant scanner at different height from the bottom of the microchannel, where cells are sitting (0 μm) up to +20 μm . Each movie contains at least 1000 frames.

The tubing should not be reused for other experiments besides calibration as they will be filled with fluorescent beads.

6. To analyze data, we advise using the TrackMate plugin available in ImageJ (<https://imagej.net/TrackMate>). Use the metadata from the confocal to calibrate pixel size (x , y — z will not be considered as acquisition is performed on single planes) as well as the time between each frame.
7. Use the LoG detector and indicate the size of the beads.
8. Adjust spot detection using the thresholding from the plugin. We suggest using the autodetection as a first step and to manually filter aberrant detection.
9. Use Hyperstack displayer.
10. We do not use filters on spot.
11. We use the simple LAP tracker. We advise using parameters adapted to your experiments. You should measure the average distance traveled by the beads during each frame, and use this average value for linking max distance and gap-closing max distance. We advise using 1 as gap-closing max frame gap. This will be the most stringent and unbiased detection methods which, while it results in the loss of many events, is compensated by increasing their number.
12. On the “Set filter on tracks” page, use “Set color by mean velocity.” Extra filters can be applied to manually filter out biased trajectories.
13. On the “Display” page, check “Display tracks” and select “Set color by mean velocity.”
14. Spots and tracks can be manually modified to remove artifacts using “TrackScheme.”
Data can be recovered using “Analysis” for further quantification (*see Note 7*).
15. Select “Capture overlay” to create the movie containing tracks and click on “Execute.”
16. Flow profiles and speeds can be analyzed using the rendered view of TrackMate (Fig. 2g).
17. Pump perfusion speed corresponding to flow velocities within the channel can be estimated for pump calibration. We provide

Table 1
Chart showing the flow rates for the setup using Ismatec Reglo Digital MS 2 or 4/12 pumps, μ Slide I 0.4 or VI 0.4 and the tubing described in 3.2

Mean flow velocity ($\mu\text{m/s}$)	μ Slide I 0,4 Flow rate ($\mu\text{l/min}$)	μ Slide VI 0,4 Flow rate ($\mu\text{l/min}$)
100	12	9
200	24	18
300	36	27
400	48	36
500	60	45
600	72	54
700	84	63
800	96	72
900	108	81
1000	120	90
1100	132	99
1200	144	108
1300	156	117
1400	168	126
1500	180	135

the flow rates for the Ismatec Reglo Digital MS 2 or 4/12 and μ Slide I 0.4 or VI 0.4 and the tubing described in Subheading 3.2 in Table 1.

3.4 Microfluidic Shear Stress Resistance Assay

Prior to adhering and extravasating, CTCs transit in the blood circulation, which represents a key step of the metastatic cascade [3]. Their survival is threatened by mechanical stresses such as cell–cell collisions and most importantly fluid shear stress. Multiple parameters are critical to CTCs surviving these threats during their transit in the blood flow: cell–cell collision probability, shear stress level, exposition duration [30], and mechanical properties of CTCs [31]. Microfluidics, in the form of closed tubing circuits, offer simple approaches to recapitulate and probe the effects of all those parameters on CTC survival. Here, we propose a simple protocol that allows exposing tumor cells to various levels of shear stress (*see* Notes 8 and 9). Our setup allows probing physiologically relevant shear stress levels ranging from 0.1 Dynes/cm² (level found in interstitial flow *in vivo*) to 16 Dynes/cm² (found in capillaries and some small arteries) for relatively short but physiologically relevant durations (<10 h).

1. To prepare the specific tubing, *see* steps in Subheading 3.2.1. We recommend adapting the tubing length to the volume of medium that is intended to be put in circulation (*see* **Note 10**). Connect a 0.5 to 1.6 fitting reducer on both 0.5 mm tubing ends. Use a short piece of 1.6 mm tubing to connect both fitting reducers and close the circuit.
2. Prepare a large volume (roughly 2.5 times the volume that is intended to be put in circulation) of cells in medium supplemented with HEPES, at desired concentration. Split it into two different tubes.
3. Turn on the pump and open the circuit by disconnecting one of the 0.5 mm tubing ends from its fitting reducer.
4. Perfuse the content of one of the two tubes containing cells. Reconnect the 0.5 mm tubing end to its fitting reducer once liquid starts dripping at the other end to close the circuit.
5. Put the other tube containing cells on a shaker to keep the cells in suspension.
6. Leave the cells in circulation and under agitation for the duration of shear stress exposure of interest (*see* **Note 11**).
7. Disconnect one of the 0.5 mm tubing ends from its fitting reducer to open the circuit and collect the cells that have been circulating in a tube. Retrieve the tube of cells that have been kept in suspension.
8. Assess cell viability in both tubes. This can be done using the classical Trypan blue exclusion test. We provide as an example the shear stress values for the setup using Ismatec Reglo Digital MS 2 or 4/12 pumps and 0.5 mm or 1.6 mm diameter ibidi silicon tubing in Table 2.

3.5 Live Cell Adhesion Assay

The aim of this approach is to quantify both the arrest potential of perfused cancer cells through specific receptors and to assess the stability of these adhesions. It is essential to perform the experiment when the endothelial monolayer is fully confluent as CTCs adhere with high affinity to the underlying fibronectin and can thus potentially bias the results. The monolayer should be carefully checked using a standard cell culture microscope, and HUVEC should be confluent before starting the experiment. Given that the microfluidic channel cannot be customized and also the peristaltic pump and the tubing presented in this protocol have a limited perfusion capacity, CTC perfusion can only be performed at flow speeds that are typically found in capillary vessels (0–1000 $\mu\text{m}/\text{s}$).

1. Prepare the live imaging microscope. Heat the setup at 37 °C and 5% CO₂ (if available).
2. Fix the $\mu\text{Slide VI}$ on the microscope stage and the $\mu\text{Slide VI}$ containing confluent HUVEC for perfusion. Perfuse ECGM in

Table 2
Chart showing the shear stress values for the setup using Ismatec Reglo Digital MS 2 or 4/12 pumps and 0.5 mm or 1.6 mm diameter ibidi silicon tubing

Flow rate setting ($\mu\text{l}/\text{min}$)	Tubing 1.6 mm Shear stress (Dynes/cm^2)	Tubing 0.5 mm Shear stress (Dynes/cm^2)
4	0.016	0.511
9	0.035	1.149
18	0.070	2.298
27	0.105	3.447
36	0.140	4.596
45	0.175	5.745
54	0.210	6.894
63	0.245	8.043
72	0.281	9.192
81	0.316	10.341
90	0.351	11.490
99	0.386	12.639
108	0.421	13.788
117	0.456	14.937
126	0.490893942	16.086

the 3-stop containing tubing using “pushing perfusion” (Fig. 3c). Connect the elbow Luer to the microfluidic channel once medium starts to drip (*see Note 12*). *This is essential to avoid bubbles as it would eventually destroy endothelial cells.* Connect the elbow Luer of the outlet tubing (without the 3-stop tubing) and put the outlet tubing into a liquid bin. Perfuse medium while preparing cells for perfusion.

3. Prepare cells for perfusion. Wash cells with PBS–EDTA. Trypsinize cells and resuspend them in ECGM. Centrifuge cells to remove trypsin and resuspend them in ECGM at a concentration of 10^6 cells/ml (*see Note 6*).
4. Put the inlet from the 3-stop containing tubing into medium. Perfuse using “pushing perfusion” (Fig. 2a, c, f). This step should be adapted to the cells of interest.

We use D2A1 mouse mammary carcinoma cells. In our experiments, we perform three steps of perfusion at physiologically relevant speeds with decreasing values to favor cancer cell adhesion to the endothelial monolayer.

- 400 $\mu\text{m/s}$ for 2 min.
- 200 $\mu\text{m/s}$ for 2 min.
- 100 $\mu\text{m/s}$ for 2 min.

We perform a final wash step of ECGM medium at 400 $\mu\text{m/s}$ for 2 min. This final step is essential to probe the stability of CTC adhesion (*see* **Note 6**).

5. The tubing can be reused for cell perfusion in series by connecting to new channels for each new set of cell perfusion. We recommend washing the tubing with PBS–EDTA to remove cells that might adhere to the tubing. Once done repeat **steps 2–4**. for each set of cell perfusion.

The tubing can be reused for following experiments. We advise cleaning the tubing using the pump by performing a wash with Milli-Q grade Ultrapure water for at least 2 min, a wash with absolute ethanol for at least 2 min, a wash with Milli-Q grade Ultrapure water for at least 2 min to remove ethanol. Dry the tubing by aspirating air through the tubing using the pump.

6. This method can be adapted to probe the adhesion properties of specific cell surface receptors either by transient siRNA or stable shRNA knockdown, using antagonist antibodies or chemical compounds directly within the perfusion medium.
7. To analyze data, we count the number of cells adhering at each step of perfusion (400 $\mu\text{m/s}$, 200 $\mu\text{m/s}$, and 100 $\mu\text{m/s}$) to quantify the flow dependence of cell adhesion. The number of cells remaining adhered after the washing step should also be quantified in order to assess the stability of cancer cell adhesion to the endothelial layer. In order to compare different conditions (i.e., the role of adhesion receptors as in [15] or comparing cell types), we advise normalizing all values to the mean value of control cells adhesion after perfusion at 100 $\mu\text{m/s}$ (Fig. 2h).

3.6 Microfluidic Extravasation Assay

Once endothelial cells have been seeded in microchannels as described in Subheading 3.1, this method allows to study extravasation of CTCs either through active transendothelial migration or the active role of the endothelium in extravasating cancer cells. The flow-dependence of cancer cell extravasation can be studied by culturing endothelial cells with various flow conditions. Specific drugs can be added to the medium to assess the biological function of specific cellular pathways during CTC extravasation. This method is compatible with live imaging, chemical fixation and fluorescent immunostaining, or chemical fixation and scanning electron microscopy.

1. For the “no-flow” condition, keep changing medium twice a day as described in Subheading 3.1 **step 4** until performing experiments.
2. For the “flow” condition, 1 ~ 1.5 day after seeding, microchannels containing endothelial cells can be connected to the microfluidics setup. We advise to perform this step under a cell culture hood to maintain sterility (*see Note 13*).
3. Preheat ECGM medium (without Hepes) at 37 °C in a Falcon tube. Cover it with parafilm under the cell culture hood. Open a hole with a hypodermic needle (Fig. 3a) and insert the inlet from the 3-stop containing tubing into medium through parafilm (Fig. 3b) (*see Note 13*).
4. Perfuse ECGM in the 3-stop containing tubing using “pushing perfusion” (Fig. 3c). Connect the elbow Luer to the microfluidic channel once medium starts to drip. *This is essential to avoid bubbles as it would eventually destroy endothelial cells.* Connect then the elbow Luer of the outlet tubing (without the 3-stop tubing) and put the outlet tubing into a liquid bin until it starts to drip (*see Note 12*).
5. Stop medium perfusion. Open a second hole with a hypodermic needle into the parafilm and insert the outlet tubing with medium through the parafilm. Seal and maintain tubing using tape (*see Note 14*).
6. Resume perfusion using “pushing perfusion” until no bubbles are seen coming out of the outlet (Fig. 3d). *This is essential to avoid bubbles.*
7. Reverse the rotation direction of the peristaltic pump and switch to “aspiration perfusion” (Fig. 3d). *This is essential to avoid bubbles during long-term culture under flow (see Note 15).*
8. Endothelial cells should be flow-activated for 24 h.
9. Proceed with the experimental workflows described in Subheadings 3.7–3.9.

3.7 Live Imaging

1. Prepare the live imaging microscope. Heat the setup at 37 °C and 5% CO₂ (if available).
2. Stain endothelial cells using lipidic dyes following the manufacturer’s protocol.
3. Prepare cancer cells for perfusion at a concentration of 10⁶ cells/ml in ECGM as described in Subheading 3.5 **step 3** (*see Notes 6 and 16*).
4. Disconnect the “flow” condition microchannel from the tubing.

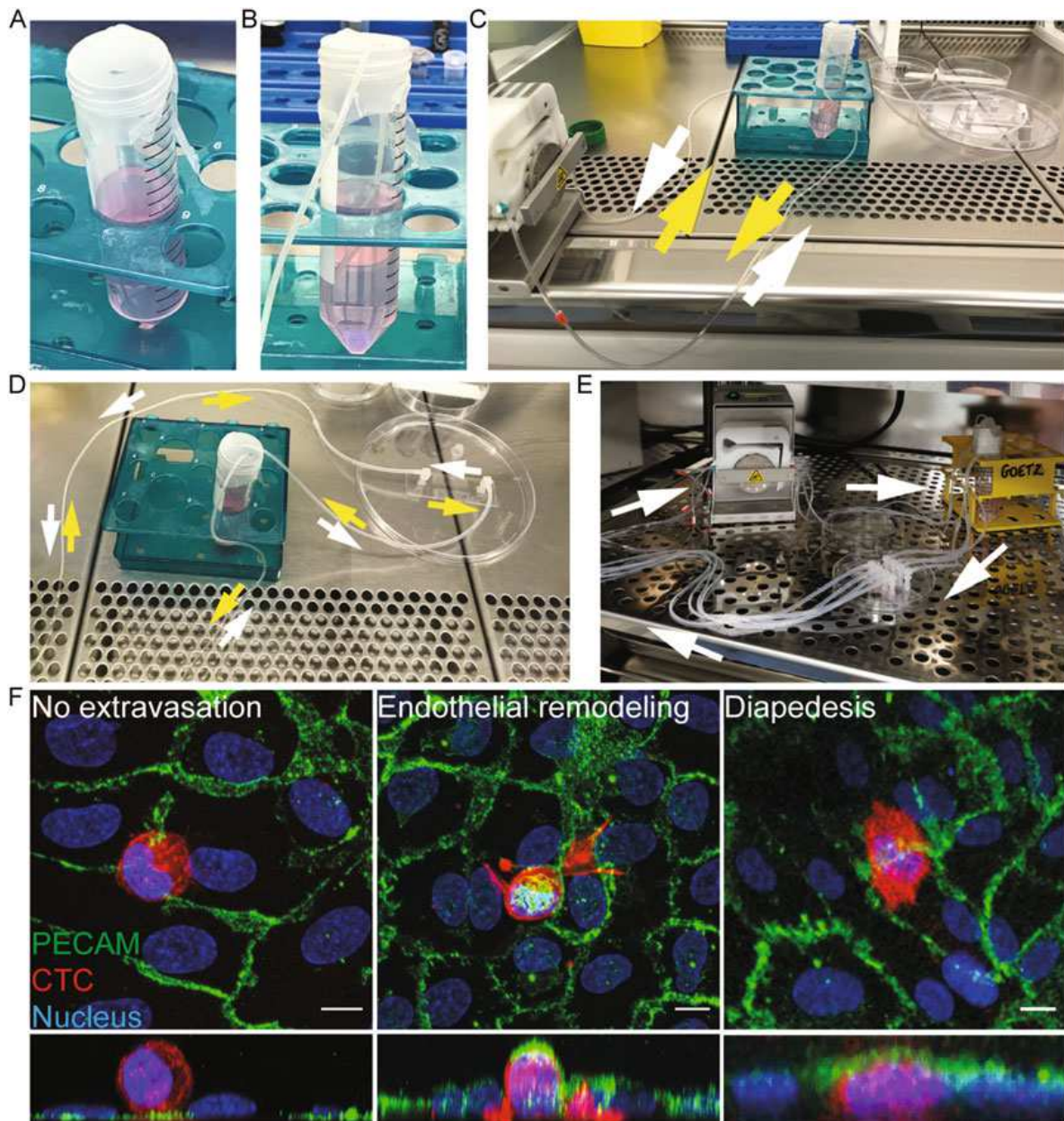


Fig. 3 Extravasation assay. (a) Picture showing a 50 ml tube containing ECGM covered with parafilm with a hole pierced. (b) a 50 ml tube containing ECGM covered with parafilm with tubing going through. (c) Picture showing the microfluidic setup associated to the pump. Yellow arrows show “pushing” perfusion. White arrows show “aspiration” perfusion. (d) Picture showing a larger view of the microfluidic setup. Yellow arrows show “pushing” perfusion. White arrows show “aspiration” perfusion. (e) Picture showing the microfluidic setup associated to the pump within the cell culture incubator. White arrows show “aspiration” perfusion. (f) 3D confocal pictures showing cell staying intravascular or that underwent extravasation through endothelial remodeling or diapedesis. Endothelial cells are stained for PECAM (green), CTCs (D2A1 cell line) express Td-Tomato-LifeAct, nuclei are stained with DAPI. Scale bar = 10 μm

5. Add 100 μl of cancer cells at 10^6 cells/ml in “flow” and “no flow” conditions. Homogenize them by tilting left-right from one well to the other.

6. Let cancer cells adhere for the required time to engage stable adhesions with the endothelial layer (in our case, with D2A1 cells, at least 5 min).
7. Resume perfusion in “flow” conditions as described in Subheading 3.6 steps 4–7.
8. Fix the μ Slide I on the microscope stage. Resume medium “pushing perfusion.”
9. Perform confocal 3D imaging. We suggest using an immersion objective with high magnification ($63\times$ or $100\times$) and large numerical aperture ($NA > 1.3 \sim 1.4$). Excitation/integration parameters are adjusted depending on the samples and a $0.5 \mu\text{m}$ Z -step is used to maximize 3D resolution. Acquisition parameters should be fixed throughout experimental dataset for statistical analysis (*see Note 17*).

3.8 Immunostaining and 3D Confocal Imaging

1. Prepare cancer cells for perfusion at a concentration of 10^6 cells/ml in ECGM as described in Subheading 3.5 step 3 (*see Note 15*).
2. Disconnect the “flow” condition microchannel from the tubing.
3. Add $100 \mu\text{l}$ of cancer cells at 10^6 cells/ml in “flow” and “no flow” conditions. Homogenize them by tilting left-right from one well to the other.
4. Let cancer cells adhere for the required time to engage stable adhesions with the endothelial layer (in our case, with D2A1 cells, at least 5 min).
5. Change medium in all microchannels as described in Subheading 3.1 step 4.
6. Resume perfusion in “flow” conditions as described in Subheading 3.6 steps 4–7.
7. Incubate the required amount of time depending on your cell line of interest (in our case, with D2A1 cells, 16 h). If the required time exceeds overnight incubation, the medium should be changed in “no flow” conditions as described in Subheading 3.1 step 4. (Fig. 3e).
8. Fix cells using PFA 4% at room temperature for 10 min (*see Note 18*). Wash three times with PBS $1\times$.
9. Permeabilize cells using PBS-0.2% Triton X-100 at room temperature for 10 min (*see Note 18*). Wash three times with PBS $1\times$.
10. Quench PFA cells using PBS- NaBH_4 2 mg/ml or NH_4Cl 50 mM at room temperature for 10 min (*see Note 18*). Wash three times with PBS $1\times$.

11. Add primary antibody against a specific endothelial marker (we recommend using anti-PECAM/CD31 or anti-VE-cadherin) diluted in PBS at the manufacturers' recommended dilution. Incubate 1 h at room temperature on a tilting shaker (*see* **Notes 18** and **19**). Wash three times with PBS 1×.
12. Add secondary antibody against the primary antibody and DAPI diluted in PBS at the manufacturers' recommended dilution. Incubate 30 min at room temperature on a tilting shaker (*see* **Notes 18–20**). Wash three times with PBS 1×.
13. Add non-polymerizing mounting medium with antifading properties (we use VectaShield, Vectorlabs) (*see* **Note 18**).
14. We suggest using 3D confocal imaging with an immersion objective with high magnification (63× or 100×) and a large numerical aperture (NA > 1.3 ~ 1.4). Excitation/integration parameters are adjusted depending on the samples and a 0.5 μm Z-step is used. Acquisition parameters should be fixed throughout the experimental dataset for statistical analysis.
15. To analyze data, we count the number of intravascular-like cells (i.e., still adhering over the endothelial monolayer) and the total number of extravascular-like cells (i.e., present between the endothelial monolayer and the bottom of the microchannel). Within this last population, we discriminate between diapedesis-extravasation with no obvious endothelial remodeling and endothelial remodeling as observed with specific markers such as PECAM or VE-cadherin (Fig. 3f).

3.9 Scanning Electron Microscopy (Fig. 4)

Use sticky-Slide. We advise to preferentially manipulate chambers under sterile conditions.

1. Gently remove the glue from the bottom part of the chamber by 5 min immersion on pure acetone (Fig. 4a).
2. Remove acetone-soaked glue by using sterile gauze. If not all the glue is removed by these means, do a second 5 min acetone immersion (*see* **Note 21**).
3. Stick the μSlide I on a sterile rectangular glass coverslip using vacuum grease by gently pressing the coverslip around the chamber to ensure proper vacuum (Fig. 4a) (*see* **Note 22**).
4. Seed HUVEC as described in Subheading 3.1.
5. Prepare the experiment as described in Subheading 3.6 **steps 1–8**.
6. Run experiment as described in Subheading 3.8 **steps 1–7**.
7. Fix with glutaraldehyde 2.5% in 0.1 M sodium cacodylate buffer (pH 7.4) for 15 min at room temperature or overnight at 4 °C.

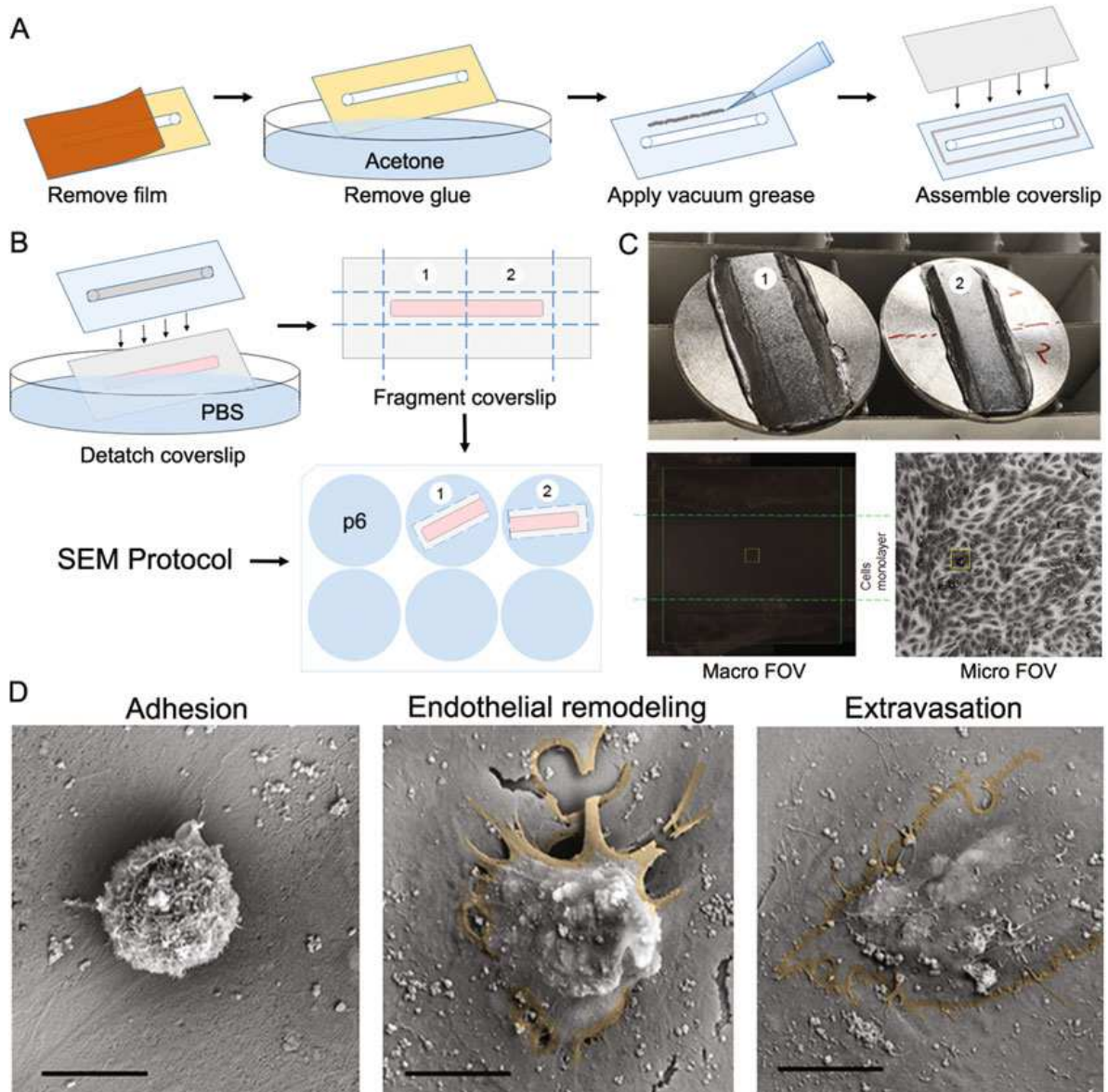


Fig. 4 Scanning electron microscopy analysis of extravasation using microfluidics. **(a)** Scheme showing the procedure for microchannel setup. **(b)** Scheme showing the procedure for microchannel unmounting prior to EM processing. **(c)** **(top)** Picture showing the samples mounting before acquisition. Picture showing the field of view (FOV) observed with desktop SEM **(bottom left)** at small and **(bottom right)** larger magnification. **(d)** Pictures of scanning electron microscopy at larger magnification showing adhered “intravascular-like” CTC **(left)**, endothelial remodeling **(center)**, and fully extravasated cell **(right)**. Scale bar = 10 μm

8. Wash the channel with Milli-Q grade Ultrapure water for 5 min.
9. Immerse the whole chamber on a 10 cm petri dish filled with Milli-Q grade Ultrapure water and proceed to carefully remove the glass coverslip with precision tweezers. Keep glass coverslip always immersed in water.

10. Once detached, place the glass coverslip in a clean 10 cm petri dish containing Milli-Q grade Ultrapure water containing. Carefully cut the cell-containing portion of the coverslip with a diamond knife in two pieces (Fig. 4b) (*see Note 23*).
11. Place the two cell-containing glass fragments into two wells of a 6-well plate filled with Milli-Q grade Ultrapure water. Wash at least of three times.
12. Dehydrate samples by sequential washes on ethanol-graded series (3×5 min on 70%, 1×5 min on 80% and 90%, and 2×30 min on 100%).
13. Irreversibly dehydrate samples with 5–10 min baths on 1,1,1,3,3,3-hexamethyldisilazane (HMDS)/ethanol-graded series (1:2, 2:1, 100% HDMS).
14. Mount samples onto EM Aluminum Mounts using carbon sticky tabs or cement (Fig. 4c).
15. Dry overnight at room temperature.
16. Metalize samples by platinum vaporization under vacuum up to 12 nm.
17. Acquire images on a SEM desktop microscope (Fig. 4c, d).

4 Notes

1. The number of rollers is essential for controlling and fine-tuning the flow. We advise using a peristaltic pump with at least 12 rollers. Each roller will induce a small pulsation. Thus, the more roller, the smoother the flow will be. Also, using a digital pump is a plus for fine control of flow perfusion. Pulsatile flows can also be performed, but this should be carefully assessed as it can be perturbed by the rollers (especially fast pulsatility).
2. The 23G \times 1" hypodermic needle should be removed from their Luer using ethanol-sterilized needle-nose pliers. First, remove the white glue sticking the needle to the Luer by scratching it with the plier. Second, pull the needle out of the Luer. During this step, it is essential to avoid bending the needle as this might clog it.
3. We advise using μ Slide with a height of 0.4 mm to maximize the efficiency of HUVEC growth. We observed that HUVEC do not grow efficiently at lower height. We also advise not to use larger heights as this would reduce shear stress on HUVEC.
4. To avoid bubbles within microchannels, it is essential to avoid making bubbles when pipetting and removing bubbles. We advise to add at least 10% of volume to any required pipetting volume when loading microchannels. Preheated medium will also prevent bubble formation.

5. The Poiseuille law states that flow speed is maximal in the center of the channel and decreases linearly as it gets closer to the border, where the flow is null.
6. For live imaging experiment, we advise using a 5% CO₂ atmosphere. This can be replaced by using ECGM supplemented with 20 mM of Hepes. In that situation, ECGM supplemented to Hepes should be added to the channel prior to starting experiments, and cells for perfusion should be prepared in ECGM supplemented with Hepes.
7. Tracking can be performed in regions of interest using the Mosaic plugin in ImageJ (<https://imagej.net/MOSAICSuite>).
8. The two most interesting parameters that can be tuned in this setup are the exposure time to shear stress and the strength of the shear stress.
9. The level of shear stress depends on multiple parameters such as viscosity of the medium, radius of the tubing, and the fluid flow that is set on the pump. Poiseuilles' equation linking these parameters is as follows:

$$SS = 4\mu Q / \pi r^3$$

with:

SS the shear stress in Pa.

μ the viscosity of the medium in Pa.s (In our case, 0.0094 with DMEM).

Q the fluid flow in m³.s⁻¹.

r the radius of the tubing in m (in our case, 0.0025).

10. The formula linking the tubing length to the volume of cells that can be perfused is $v = \pi r^2 L$, with v the volume in m³, r and L , respectively the radius and the length of the tubing in m. Convert v from m³ to μ L for easy assessment of pipetting volumes needed.
11. Hepes is a reliable buffer that can replace CO₂ input for maximum 10 h. For studying longer shear stress exposure durations, a reservoir allowing O₂/CO₂ entry in the system while preventing medium evaporation is required.
12. When connecting the microfluidics tubing to the microchannel, we advise to let medium drip into a bin to rinse the tubing with medium.
13. When connecting the tubing to the microchannel for long-term cell culture under the cell culture hood, we advise letting the pump outside.

14. For a single channel and overnight flow cell culture, 20 ~ 25 ml of medium is enough. For more channels or longer flow cell culture, 40 ~ 50 ml of medium should be used. For long-term flow culture, medium should be checked on a daily basis and changed if required.
15. We advise using “aspiration”-based medium perfusion (i.e., the pump is located after the microchannel and aspire medium from the medium container through the channel). This maintains elbow Luer in position by creating a depression and avoid air entry and bubbles formation.
16. We advise using a cell line stably expressing a genetically encoded fluorescent marker or alternatively stain cells with stable lipid markers such as DiI/DiO or MemBright [32].
17. For live imaging, we advise using a heating chamber with 5% CO₂ for long-term experiment (more than 9–10 h).
18. Each loading of reagent consists of three steps of wash with medium to ensure that the former liquid is washed away and a final step of adding the reagent to fill the microchannels and both wells.
19. During antibody incubation, the channel should be constantly tilted. Use a tilting stage and attach channels to it using tape. We advise putting the channel into the same direction as the tilt of the stage if bidirectional to maximize antibody homogenization.
20. Fluorescent secondary antibody should be incubated while the microchannels are protected from light (using aluminum foil, for instance).
21. Complete glue removal without chamber surface damage is capital for assuring further grease vacuum and avoid leakiness during perfusion.
22. Avoid grease entering into the channel.
23. It is very important to remove all vacuum grease present on the glass before starting EM procedure.

Acknowledgments

We thank all members of the Goetz Lab for helpful discussions throughout the development of this technology, and to Florent Colin for careful proofreading. We are grateful to INSERM U1255 (EFS, Strasbourg) for providing access to the SEM microscope. This work has been funded by Plan Cancer (OptoMetaTrap and Nanotumor) and CNRS IMAG'IN to S.H. and J.G., by INCa (National Cancer Institute, PLBIO 2015-140) to J.G and by institutional funds from INSERM and University of Strasbourg to

J.G. N.O was supported by Plan Cancer 2014-2019 (OptoMeta-Trap) and the Association pour la Recherche contre le Cancer. G.F. was supported by La Ligue Contre le Cancer and University of Strasbourg. V.G. is supported by INSERM and Region Alsace. M.J.G.L. is funded by INCa and University of Strasbourg.

References

1. Valastyan S, Weinberg RA (2011) Tumor metastasis: molecular insights and evolving paradigms. *Cell* 147:275–292
2. Massagué J, Obenauf AC (2016) Metastatic colonization by circulating tumour cells. *Nature* 529:298–306. <https://doi.org/10.1038/nature17038>
3. Follain G, Herrmann D, Harlepp S et al (2020) Fluids and their mechanics in tumour transit: shaping metastasis. *Nat Rev Cancer* 20:107–124. <https://doi.org/10.1038/s41568-019-0221-x>
4. Nguyen DX, Bos PD, Massagué J (2009) Metastasis: from dissemination to organ-specific colonization. *Nat Rev Cancer* 9:274–284. <https://doi.org/10.1038/nrc2622>
5. Obenauf AC, Massagué J (2015) Surviving at a distance: organ-specific metastasis. *Trends Cancer* 1:76–91. <https://doi.org/10.1016/j.trecan.2015.07.009>
6. Reymond N, d'Água BB, Ridley AJ (2013) Crossing the endothelial barrier during metastasis. *Nat Rev Cancer* 13:858–870. <https://doi.org/10.1038/nrc3628>
7. Eibl C, Grigoriu S, Hessenberger M et al (2012) Structural and functional analysis of the NLRP4 pyrin domain. *Biochemistry* 51:7330–7341. <https://doi.org/10.1021/bi3007059>
8. McEver RP, Zhu C (2010) Rolling cell adhesion. *Annu Rev Cell Dev Biol* 26:363–396. <https://doi.org/10.1146/annurev.cellbio.042308.113238>
9. Aigner S, Ramos CL, Hafezi-moghadam A et al (1998) CD24 mediates rolling of breast carcinoma cells on P-selectin. *FASEB J* 12:1241–1251
10. Laferrière J, Houle F, Taher MM et al (2001) Transendothelial migration of colon carcinoma cells requires expression of E-selectin by endothelial cells and activation of stress-activated protein kinase-2 (SAPK2/p38) in the tumor cells. *J Biol Chem* 276:33762–33772. <https://doi.org/10.1074/jbc.M008564200>
11. Dallas MR, Liu G, Chen W-C et al (2012) Divergent roles of CD44 and carcinoembryonic antigen in colon cancer metastasis. *FASEB J* 26:2648–2656. <https://doi.org/10.1096/fj.12-203786>
12. Hanley WD, Napier SL, Burdick MM et al (2006) Variant isoforms of CD44 are P- and L-selectin ligands on colon carcinoma cells. *FASEB J* 20:337–339. <https://doi.org/10.1096/fj.05-4574fje>
13. Rahn JJ, Chow JW, Horne GJ et al (2005) MUC1 mediates transendothelial migration in vitro by ligating endothelial cell ICAM-1. *Clin Exp Metastasis* 22:475–483. <https://doi.org/10.1007/s10585-005-3098-x>
14. Shea DJ, Wirtz D, Stebe KJ, Konstantopoulos K (2015) Distinct kinetic and mechanical properties govern mucin 16- and podocalyxin-mediated tumor cell adhesion to E- and L-selectin in shear flow. *Oncotarget* 6:24842–24855. <https://doi.org/10.18632/oncotarget.4704>
15. Osmani N, Follain G, García León MJ et al (2019) Metastatic tumor cells exploit their adhesion repertoire to counteract shear forces during intravascular arrest. *Cell Rep* 28:2491–2500.e5. <https://doi.org/10.1016/j.celrep.2019.07.102>
16. Felding-Habermann B, O'Toole TE, Smith JW et al (2001) Integrin activation controls metastasis in human breast cancer. *Proc Natl Acad Sci* 98:1853–1858. <https://doi.org/10.1073/pnas.98.4.1853>
17. Laferrière J, Houle F, Huot J (2004) Adhesion of HT-29 colon carcinoma cells to endothelial cells requires sequential events involving E-selectin and integrin beta4. *Clin Exp Metastasis* 21:257–264
18. Klemke M, Weschenfelder T, Konstantin MH, Samstag Y (2007) High affinity interaction of integrin alpha4beta1 (VLA-4) and vascular cell adhesion molecule 1 (VCAM-1) enhances migration of human melanoma cells across activated endothelial cell layers. *J Cell Physiol* 212:368–374. <https://doi.org/10.1002/jcp.21029>
19. Reymond N, Im JH, Garg R et al (2012) Cdc42 promotes transendothelial migration of cancer cells through β 1 integrin. *J Cell Biol*

- 199:653–668. <https://doi.org/10.1083/jcb.201205169>
20. Barthel SR, Hays DL, Yazawa EM et al (2013) Definition of molecular determinants of prostate cancer cell bone extravasation. *Cancer Res* 73:942–952. <https://doi.org/10.1158/0008-5472.CAN-12-3264>
 21. Follain G, Osmani N, Azevedo AS et al (2018) Hemodynamic forces tune the arrest, adhesion, and extravasation of circulating tumor cells. *Dev Cell* 45:33–52.e12. <https://doi.org/10.1016/j.devcel.2018.02.015>
 22. Nagrath S, Sequist LV, Maheswaran S et al (2007) Isolation of rare circulating tumour cells in cancer patients by microchip technology. *Nature* 450:1235–1239. <https://doi.org/10.1038/nature06385>
 23. Stott SL, Hsu C-H, Tsukrov DI et al (2010) Isolation of circulating tumor cells using a microvortex-generating herringbone-chip. *PNAS* 107:18392–18397. <https://doi.org/10.1073/pnas.1012539107>
 24. Yu M, Bardia A, Wittner BS et al (2013) Circulating breast tumor cells exhibit dynamic changes in epithelial and mesenchymal composition. *Science* 339:580–584. <https://doi.org/10.1126/science.1228522>
 25. Aceto N, Bardia A, Miyamoto DT et al (2014) Circulating tumor cell clusters are oligoclonal precursors of breast cancer metastasis. *Cell* 158:1110–1122. <https://doi.org/10.1016/j.cell.2014.07.013>
 26. Bagnall JS, Byun S, Begum S et al (2015) Deformability of tumor cells versus blood cells. *Sci Rep* 5:18542. <https://doi.org/10.1038/srep18542>
 27. Au SH, Storey BD, Moore JC et al (2016) Clusters of circulating tumor cells traverse capillary-sized vessels. *Proc Natl Acad Sci U S A* 113:4947–4952. <https://doi.org/10.1073/pnas.1524448113>
 28. Follain G, Osmani N, Fuchs C et al (2018) Using the zebrafish embryo to dissect the early steps of the metastasis cascade. In: *Cell migration*. Humana Press, New York, NY, pp 195–211
 29. Osmani N, Goetz JG (2019) Multiscale imaging of metastasis in zebrafish. *Trends Cancer* 5:766–778. <https://doi.org/10.1016/j.trecan.2019.10.003>
 30. Regmi S, Fu A, Luo KQ (2017) High shear stresses under exercise condition destroy circulating tumor cells in a microfluidic system. *Sci Rep* 7:39975. <https://doi.org/10.1038/srep39975>
 31. Xin Y, Chen X, Tang X et al (2019) Mechanics and actomyosin-dependent survival/chemoresistance of suspended tumor cells in shear flow. *Biophys J* 116:1803–1814. <https://doi.org/10.1016/j.bpj.2019.04.011>
 32. Hyenne V, Ghoroghi S, Collot M et al (2019) Studying the fate of tumor extracellular vesicles at high spatiotemporal resolution using the zebrafish embryo. *Dev Cell* 48:554–572.e7. <https://doi.org/10.1016/j.devcel.2019.01.014>

ANNEXE 6

Near Infra-Red Light Responsive Carbon Nanotubes@Mesoporous Silica for Photothermia and Drug Delivery to Cancer Cells

Bing Li^{1,2}, Sébastien Harlepp³⁻⁵, Valentin Gensbittel³⁻⁵, Connor J. R. Wells¹, Ophélie Bringel², Jacky G. Goetz³⁻⁵, Sylvie Begin-Colin¹, Mariana Tasso⁶, Dominique Begin², Damien Mertz^{1*}

¹Institut de Physique et Chimie des Matériaux de Strasbourg (IPCMS), UMR-7504 CNRS-Université de Strasbourg, 23 rue du Lœss, BP 34 67034, Strasbourg Cedex 2, France, §

²Institut de Chimie et Procédés pour l'Energie, l'Environnement et la Santé (ICPEES), UMR-7515 CNRS-Université de Strasbourg, 25 rue Becquerel, 67087 Strasbourg, Cedex 2, France

³Tumor Biomechanics, INSERM UMR_S1109, Strasbourg, France,

⁴Université de Strasbourg, Strasbourg, France.

⁵Fédération de Médecine Translationnelle de Strasbourg (FMTS), Strasbourg, France.

⁶Instituto de Investigaciones Fisicoquímicas Teóricas y Aplicadas (INIFTA), Departamento de Química, Facultad de Ciencias Exactas, Universidad Nacional de La Plata - CONICET, Diagonal 113 y 64, 1900 La Plata, Argentina.

E-mail : damien.mertz@ipcms.unistra.fr

Keywords : Phototherapy ; NIR-Light Induced Drug Delivery; Carbon Nanotubes; Mesoporous Silica Coatings , Nanocomposite Hydrogels, Cancer Cells.

ABSTRACT. Among smart activable nanomaterials used for nanomedicine applications, carbon-based nanocomposites are well known to ensure phototherapy while their use for controlled drug delivery is still rarely investigated. In this work, original hybrid mesoporous silica (MS)-coated carbon nanotubes (CNTs) nanoplateforms have been designed to provide phototherapy combined with drug release mediated by NIR laser excitation. The responsive CNT@MS are chemically modified with original isobutyramide (IBAM) grafts acting as non-covalent binders, which ensure a very high drug loading capacity (≥ 80 wt%) of the antitumor drug doxorubicin (DOX) as well as the final adsorption of a human serum albumin (HSA) shell as biocompatible interface and drug gate-keeping. The drug is demonstrated to unbind from the nanocomposite only upon photothermal excitation and to release in the solution. Such smart platforms are further shown to deliver drug upon several pulsatile NIR excitations with controlled temperature profiles. Regarding antitumor action, we demonstrate here that the NIR light induced photothermic effect from the nanocomposites is the main effect accounting for cancer cell toxicity and that DOX delivery mediated by the NIR light brings an additional toxicity allowing a synergistic effect to efficiently kill tumor cells. Finally, when our nanocomposites are embedded within a hydrogel mimicking extracellular matrix, the resulting smart responsive scaffolds efficiently release DOX upon NIR light to the cells localized above the composite hydrogel. These results demonstrate that such nanocomposites are highly promising as new

components of implantable antitumor scaffolds that are able to respond to external stimuli in time and location for a better disease management.

INTRODUCTION

The development of smart multi-functional nanocomposites capable of releasing therapeutic molecules under various external stimuli has become a major challenge in recent years in the biomedical field. These nanocomposites are designed to be either injected as circulating objects [1–6] or implanted *in situ* in a polymer support matrix [7–12] for the treatment of different types of tumors. Another challenge now is the design of multifunctional nanoplateforms (NPFs) able to combine, in one formulation, two or more functionalities, e.g. simultaneous therapy and diagnostic (theranostic) for real-time therapy monitoring, and synergic action of two or more therapeutic approaches.

In the field of tissue engineering, the incorporation of activable inorganic materials (e.g. iron oxide, gold or carbon materials) into polymer scaffolds (e.g. hydrogels or electrospun fibers) is a way to formulate new composite materials that would be used as smart implants or integrated devices in the body.[13–15] The advantages to add remote responsive NPs into such polymer matrix are: i) improved mechanical properties; ii) the response to external stimuli (near infrared light, mechanical force, electric or magnetic field, etc.); iii) the eventual clinical imaging property (MRI, X rays, etc), and iv) encapsulation of the activable material into a biocompatible scaffold, thus preventing material-related toxicity issues. In this work, we report on the design and use of drug-loaded carbon-based composites incorporated in a biocompatible hydrogel mimicking the extracellular matrix (ECM).

Among the different materials needed to produce such activable nanocomposites, carbon-based materials are promising materials.[16–18] Besides their exceptional mechanical and electrical conductive properties, they are able to release heat under near-infrared radiation by vibrational relaxation of graphite structures in the near infrared (NIR) range (750-1400 nm). Given the relative transparency of biological tissues in the NIR optical window, this property is of huge interest for combining both phototherapy and remotely activable drug delivery under such external stimuli.[19–23] Indeed, the use of infrared light to trigger the release of an active ingredient locally could be of great interest in the treatment of tumors because of its easier implementation than other sources of radiation (X-ray scanner, gamma radiation, magnetic waves, etc.). However, the design of carbon-based composites for biomedical applications endowed with phototherapy and remote drug delivery faces important challenges as follows. Main issues with CNTs are their asbestos form factor (very long length-to-diameter ratio) and the inherent hydrophobicity of carbon leading to self-aggregation in biological medium.[24–26] To solve these problems, newly processed CNTs with a better form factor were developed.

Several fractionation and split treatments decrease the form factor of these carbon nanotubes, such as mechanical grinding (length of about less than 500 nm), or CNT compression induced by ultrasonic effects [27] or by harsh acidic treatment of CNTs [28].

Besides, CNTs can be rendered hydrophilic by the cutting treatment which introduces hydroxyl groups or by a post-functionalization.[19,20,29] A capping layer playing the role of drug reservoirs may also be obtained by the surface modification with various polymers[30–33] or chemical groups[20] or by the deposition of a uniform layer of porous silica [34–36]. Among current coating layers for drug loading, mesoporous silica (MS) shells are particularly attractive materials as they are robust, biocompatible, hydrophilic, easily chemically modified and have a high drug delivery capability thanks to their important pore volume and after a suitable surface functionalization.[37]

Recently, we and coworkers developed various functionalized MS NPs having well-controlled pore sizes (from 2 to 15 nm) [38,39] and translated these approaches to coat CNTs but also iron oxide NPs with various MS shell nanostructures [40–43]. Especially small pore MS around CNTs allowed loading of such nanocomposites with doxorubicin, (DOX, an antitumor anthracycline molecule with antimitotic action by DNA intercalation) with increased rates (up to several times the mass of the carrier) when compared to past work [42]. However, different issues were raised in this previous work: i) the loading of DOX was initially performed at an aminosiloxane surface which is not optimal for biomedical applications given its high surface charge and marked fouling, ii) the drug release was activated with a quite high laser power (6 W/cm²) which may lead to overheating in a biological medium; iii) these nano-composites were also shown to release a moderate proportion of immobilized DOX under near IR radiation (1064 nm) and iv) no functional study on cells was done with these systems.

Herein, to address these issues, we designed a new class of functional CNT@MS nanocomposites (**Figure 1**). First, the CNTs are processed in acidic conditions to afford sliced CNTs with a more suitable size distribution adapted for medical applications. Their coating by a MS shell having small pore size (*ca.* 3 nm) is performed with a precise control over silica shell thickness. Then, we used here the grafting of IBAM groups to ensure high drug loading and a final protein capping. Indeed, IBAM groups grafted at silica surfaces were reported previously to be versatile non-covalent surface binders of a range of proteins through a single step adsorption. [44–46]. Here, IBAM grafts at silica surface are assessed for the first time to load DOX through non-covalent interactions followed by HSA coating to ensure a good integrity of the nanocomposites. We assumed here that IBAM grafts play the role of a thermoresponsive interface that unbind the loaded drugs from the surface upon the photo-induced local heating generated from the underneath CNTs. Hence, we address here the full characterization of CNTs@MS nanocomposites and of DOX loading and subsequent HSA wrapping on

CNTs@MS@IBAM and we investigated the efficiency of drug release upon NIR light application. Various drug profiles as a function of time, concentration, and laser power are provided demonstrating the possibility for NIR light remote release.

In the last step of this design, with the aim to create a drug releasing scaffold upon NIR light exposure, the drug loaded nanocomposites CNTs@MS@IBAM-DOX@HSA are formulated within a hydrogel made of various extracellular matrix biopolymers (Matrigel, ECM-like hydrogel) often used in biomaterials field.[47–49] The development of such hydrogel nanocomposites is very attractive for antitumor and tissue engineering applications. Indeed, the scaffold can display some advantages over circulating NPs, such as limiting macrophage uptake, or decreasing the drug loss (or the non-targeted drug delivery) by injecting the scaffold in the diseased site and thus avoiding sides effects.

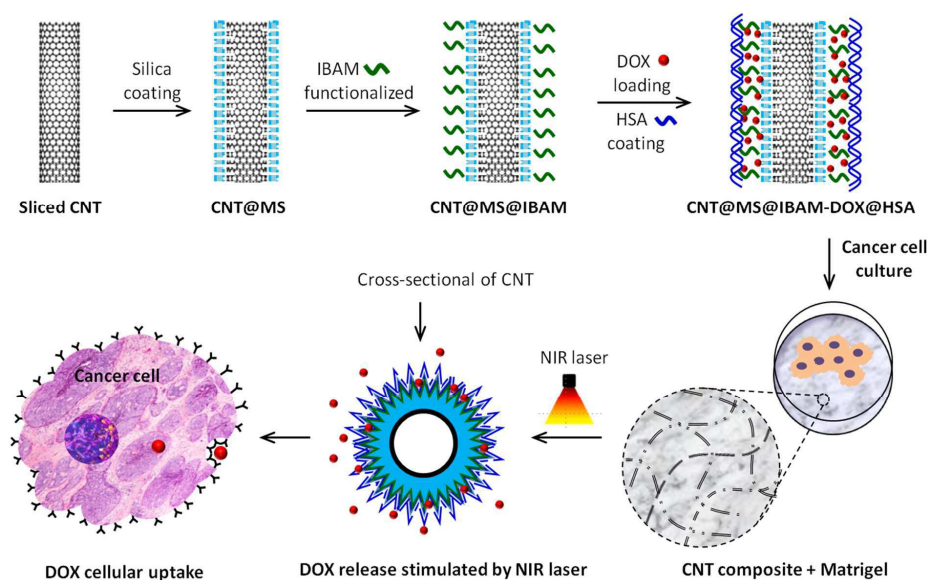


Figure 1. Scheme describing the formation of the CNT@MS@IBAM-DOX@HSA nanoconstructs and their formulation into a hydrogel assessed with breast cancer cells.

Materials and Methods

Chemicals.

Carbon nanotubes PR-24-XT-PS (CNTs) were supplied by Pyrograf-III. Cetyltrimethylammonium bromide (CTAB) was obtained from Roth (France). Nitric acid (HNO₃), sulfuric acid (H₂SO₄), ethanol (EtOH), tetraethyl orthosilicate (TEOS), sodium hydroxide (NaOH), ammonium nitrate

(NH_4NO_3 , >99%), 3-aminopropyltriethoxysilane (APTS), isobutyl chloride (IBC), triethylamine (Et_3N), dimethylformamide (DMF), dimethylsulfoxide (DMSO), sodium bicarbonate (NaHCO_3), human serum albumin (HSA, >97%) and fluorescein isothiocyanate (FITC) were obtained from Sigma-Aldrich (France). Doxorubicin hydrochloride (DOX, purity 99%) was purchased from OChem Incorporation (France). Ammonium hydroxide solution (25% in H_2O) was obtained from Fluka. The MTS reagents CellTiter 96[®] AQueous were obtained from Promega. The D2A1 cells were seeded and grown up at 37°C at 5% CO_2 , using DMEM high glucose medium supplemented with 5% NBCS, 5% FBS, 1% NEAA-MEM, 1% Penstrep (Sigma Aldrich). For 2D or 3D growth the cells were seeded into either an opaque-walled 96 well plate (Fisher scientific) or a 15 well plate suited for 3D cell culture (Ibidi). The Membrane Matrix used to built the 3D scaffold was obtained from Thermo Fisher Scientific.

Procedures.

Synthesis of cleaved CNTs. The acid treatment was performed by adding 0.75 g of CNTs into a mixture of $\text{H}_2\text{SO}_4/\text{HNO}_3$ (3:1, 108 mL) and then bath sonicated (Bandelin SONOREX RK 255 S) for 24 h under at 0 °C. After this time, 100 mL of NaOH aqueous solution (10 M) was added dropwise into the acidic black suspension for neutralization, and finally the mixture was adjusted to neutral by the dropwise addition of NaOH (1 M). The CNTs were then centrifuged (13000 g, 13 min, Eppendorf Centrifuge 5804 R) and washed with distilled water (twice with 25 mL each). After washing, the CNTs were reduced at 900°C for 2 h with a heating ramp of 10 °C/min under argon. The resulting material was used as the initial material for the following functionalization procedures.

Synthesis of mesoporous silica coated CNTs. In a typical procedure, 372 mg of CTAB was added into a mixture of H_2O (90 mL) and EtOH (60 mL) with stirring at 60 °C for 2 h. 72 mg of CNTs were dispersed in the CTAB solution by ultrasonication (2 x 20 min, power = 750 W, amplitude = 40%, temperature = 30 °C, runs: 50" ON, 50" OFF, Vibracell 75043 from Bioblock Scientific), yielding a black suspension. The sol gel process was initiated after addition of TEOS (180 μL) and NaOH (180 μL , 1M) into the above mixture. The mixture was stirred for 16 h at room temperature. Finally, the composite was centrifuged and washed with EtOH (2 x 25 mL, 12000 g, 12 min) and re-dispersed in EtOH. The process resulted in the formation of a uniform layer of silica on every individual CNT.

CTAB extraction from CNT@MS composite. The removal of mesostructural templating agent CTAB from the silica pores was done by mixing the CNT@MS composite with 25 mL NH_4NO_3 (20 mg mL^{-1} in EtOH) under 60 °C with stirring for 1 h. The surface charge of CNT@MS was

measured by Zeta potential after each washing, in order to make sure that the majority of CTAB was removed. This process was repeated approximately 5 times.

CNT@MS surface modification with aminopropyltriethoxysilane APTS. 50 mg of CNT@MS were dispersed in 27 mL of EtOH. Then, 1.2 mL of NH_4OH (25 % in water) and 5 mL of APTS were added respectively and the mixture was agitated on a mechanical wheel (40 rpm) at room temperature for 2 h. After that, the amino-modified composite was centrifuged and washed with EtOH (2 x 20 mL, 13000 g, 14 min). The composite after APTS modification was denoted as CNT@MS@APTS.

CNT@MS surface functionalization with IBAM moieties. In a typical procedure, the resulting CNT@MS@APTS composite was washed and centrifuged with 20 mL DMF (13000 g, 13 min). Once the supernatant had been removed, a mixture of 1.2 mL Et_3N and 1.5 mL DMF was added. The mixture was vortexed for 10 s before the addition of 1.65 mL of IBC pre-mixed with 1.5 mL of DMF. The reaction was left on the mechanical wheel for 1 h 30 min. After this time, a small volume of water (*ca.* 1-2 mL) was added to dissolve the precipitate formed by the reaction. This was followed with centrifugation and washing at 13000 g for 14 min (1 x 20 mL wash in DMF, 1 x 20 mL wash in H_2O). The composite at this point was denoted as CNT@MS@IBAM.

Impregnation of doxorubicin. Typically, 2.5 mg of CNT@MS@IBAM after surface functionalization were dispersed in 1 mL of DOX aqueous solution at a given concentration and agitated on a mechanical wheel (40 rpm) for 16 h. After impregnation, the mixture was centrifuged (13000 g, 10 min) and 400 μL of the supernatant were mixed with 3.6 mL of H_2O to obtain a solution diluted 10 times. The composite was denoted as CNT@MS@IBAM-DOX. The DOX loading capacities were calculated by measuring the UV/Vis spectra (Lambda 950 UV/VIS Spectrometer by Perkin Elmer) of the diluted supernatant. A series of additional washes with water (3 x 1 mL) were implemented to remove loosely-bound impregnated DOX prior HSA modification (as follows).

FITC labeling of HSA. 531 μL of fluorescein isothiocyanate (10 mg mL^{-1} in DMSO) were mixed with 30 mL of HSA (10 mg mL^{-1}) in sodium bicarbonate buffer (NaHCO_3 0.1 M, pH 8.5). The mixture was stirred overnight and then dialyzed (membrane pore size: 10 kDa) in MilliQ water to remove free FITC. Finally, the concentration of HSA^{FITC} was adjusted to 10 mg mL^{-1} in water for further use.

HSA coating. 6.4 mg of CNT@MS@IBAM-DOX composite after surface functionalization and DOX impregnation were dispersed in 3 mL HSA at a concentration of 0.21 mg mL^{-1} , then the mixture was stirred on a mechanical wheel for 1 h. Afterwards, the solution was centrifuged and washed with H_2O (2 x 2 mL, 13000 g, 13 min). The composite was denoted as CNT@MS@IBAM-

DOX@HSA. The supernatant was measured with UV/vis spectroscopy to detect the mass loss of DOX during this step.

DOX release stimulated by NIR laser. To study the release of DOX under NIR irradiation, 1 mL of a given concentration of CNT@MS@IBAM-DOX@HSA solution (DLC ca 58%) was placed in a 1 mL plastic cuvette and then irradiated with the 1064 nm laser with power densities at either 1 or 2.5 W.cm⁻². For every trial, the sample was exposed to NIR light for 15 min, followed by a break lasting 3 days at 4°C. The mixture was centrifuged after this period and the released DOX in the supernatant was removed and measured by UV/vis spectrometry to determine the amount of DOX released. Then 1 mL of fresh water was added and the composite was dispersed by 10 s of sonication and stored in a 4 °C refrigerator. Regarding pulsatile assay, the same procedure was applied: the samples were passed for the next NIR exposure and rest period and so on for four times. The cumulative DOX release is the sum of each trial of DOX release.

Cell culture and NIR exposure setup for in vitro experiments.

D2A1 cells (CVCL_0190). Mouse mammary carcinoma (BALB/c female). Major information on the D2A1 cell line can be found following this link: https://web.expasy.org/cellosaurus/CVCL_0190. Culture conditions: 37°C/5% CO₂. DMEM HG with 5% NBCS, 5% FBS, 1% NEAA-MEM, 1% Penstrep.

Bidimensional cell proliferation and viability assays. D2A1 cells were seeded (8000 cells per well in 50µl of DMEM) in each of the wells of the opaque 96 well plate and incubated at 37 °C in 5% CO₂ for 45minutes to an hour to allow the cells to adhere [50,51]. Then, DMEM medium (150 uL) supplemented with the final concentration of CNT@MS@IBAM@HSA or CNT@MS@IBAM-DOX@HSA suspensions were introduced and incubated at 37°C, 5% of CO₂ for 24h. NIR irradiation (at 1W.cm⁻² for 15 minutes) was applied and the cells were further incubated at 37 °C in 5% CO₂ for 24 h. NIR irradiation was performed with a homemade setup. The illumination was performed from the top cover towards the well. Cell Titer Glo (Promega) reagent was then added to each well (20 uL) followed by one-hour incubation at room temperature, allowing cell lysis to be completed and luciferin to be oxidized by the cellular ATP. The 96 well plate was introduced into a plate cell reader (SpectraMaxID5 from MolecularDevices) and luminescence was collected. The intensity of control wells (cells without CNTs called Luminescence Control) were used to normalize the luminescence values (all values are between 0 and 1, value of the control wells). We checked the luminescence values from wells filled with medium and the values were at the noise level, therefore we decided to not correct with these values. Nevertheless, CNTs have a black aspect and therefore have the ability to absorb part of the emitted light from the viability experiments such as for Optical density

filters. We, thus, characterized the part of absorbed light. We cultured different wells with 8000 cells per well for 48h in normal cell growth conditions. Before running the Cell Titer Glo experiment, we first added the 4 studied concentrations of CNT@MS@IBAM@HSA in different wells. This short time where the CNTs were in contact with the cells is assumed to only affect the emitted light. As shown on figure S6B, we observe that only $\approx 23\%$ of the luminescence is collected. Therefore, we used the average values of what we introduce as Absorption for the different concentrations of CNTs to correct all the signals measured in presence of CNTs. Using the mathematical formulation we can write:

$$Relative\ Viability = \frac{Measured\ luminescence}{Luminescence\ Control} \times \frac{1}{Absorption}$$

Short time 3D cell culture and DOX cellular uptake after NIR irradiation. To study the cellular uptake of DOX upon NIR irradiation, a 50 μ l total volume of Matrigel with a given concentration of CNT@MS@IBAM-DOX@HSA or CNT@MS@IBAM@HSA composite were mixed and coated before subsequent cell seeding. D2A1 cells were incubated for 24 h and subjected to laser irradiation of $1W.cm^{-2}$ for 15 minutes. NIR-illuminated cells were cultivated for an additional 24 h before assessing DOX release. NIR irradiation was performed for 15 minutes at power density of $1W.cm^{-2}$. DOX release/delivery was characterized using a Leica SP5 confocal microscopy. To follow intracellular DOX fluorescence, we excited the sample at 488 nm (argon laser) and collected the fluorescence on a broad range in emission from 520 to 650 nm on stacks of images with steps in z of about 400nm. Each image from the stack was then analyzed with Image J and the average intensity from the cell with respect to its area in each plane was computed. Thus we could address the intensity distribution or the average signal from a single cell or cluster of cells.

Longer time 3D cell culture in presence of CNT@MS. To study the toxicity linked to the presence of CNTs embedded in a 3D scaffold close to the tumor cells, a 50 μ l total volume of Matrigel with a given concentration of CNT@MS@IBAM-DOX@HSA or CNT@MS@IBAM@HSA composite were mixed and coated before subsequent cell seeding. murine breast carcinoma cells labelled with Nuclear Localization Signal fused with Green Fluorescent Protein (D2A1, n=8000) were added on top of the gel and again incubated for 5 days allowing the growth of tumor spheroids[52]. The cells were grown in 3 different conditions. In the first condition, cells were seeded on just Matrigel without any CNT@MS. In the second condition 2.5 mg mL⁻¹ CNT@MS@IBAM@HSA-Fitc complemented the Matrigel composition, whereas in the last condition 2.5 mg mL⁻¹ CNT@MS@IBAM-DOX@HSA was added. Upon 5 days of culture, tumor spheroids were imaged under the confocal microscope.

Statistical analysis. Statistical analysis of the results obtained were performed using the GraphPad Prism program version 5.04. The Shapiro-Wilk normality test was used to confirm the normality of the data. For data not following a Gaussian distribution, the Mann-Whitney test was used.

Characterization Methods

TEM microscopy. Morphologies of the different nanocomposites were characterized by transmission electron microscopy (TEM) with a JEOL 2100 ultra-high-resolution microscope operating at 200 kV. The sample was first dispersed in EtOH and then we deposited 2 drops of the nanocomposite solution on a carbon-coated copper grid. The thickness of the silica shell was determined using Image J software on the TEM pictures. Results are indicated as mean layer thickness (nm) \pm standard deviation (nm).

Zeta potential. Zeta potential measurements at different synthesis stages were measured by using a Zetasizer nano ZS by Malvern Instruments. The measurements were performed by diluting 10 μ L of a nanoparticles' suspension in 1 mL water using a DTS1070 folded capillary cell. The pH of the measured solution was adjusted with HCl (100mM) and NaOH (100mM) aqueous solution.

Nitrogen adsorption / desorption analysis. Specific surface area of the silica coated CNTs was characterized by N₂ adsorption/desorption analysis and was calculated by the Brunauer-Emmett-Teller (BET) method. The pore size and pore volume were calculated by the Barrett-Joyner-Halenda (BJH) method. All the measurements were done on a Tristar 3000 Gas Adsorption Analyzer by Micromeritics Instruments. Before the tests, the samples were outgassed under vacuum at 150°C for about 4h.

Thermal gravimetric analysis (TGA). TGA was performed with a Q5000 Automatic Sample Processor by TA Instruments. The sample was dried in an oven at 150 °C for 24 h to remove the solvent and water before the TGA analysis. The runs were started from room temperature to 800 °C at a heating rate of 10 °C/min under air with a flow rate of 25 mL/min.

UV/Vis spectroscopy. UV-vis spectroscopy was used to determine the amount of drug loaded and released. The UV-vis spectra were recorded with a Lambda 950 UV/vis Spectrometer by Perkin Elmer. The solutions and the quartz cell were always protected from light using aluminum foil until the measurements were done.

Confocal microscopy. Microscopy of tumor cells was performed on a Leica SP5 confocal microscope. Samples were imaged with a 40X oil immersion objective. DOX was excited with a single 488 nm wavelength, and the emission was collected between 520 and 650nm. All the

image intensities were further analyzed and processed with the Image J software. For instance, the procedure to obtain figure 9B and C is described in figure S8.

Results and Discussion

1. Synthesis of mesoporous silica coated carbon nanotubes

In a first step, the commercial CNTs were sliced from the microscale to the nanoscale using a solution of sulphuric and nitric acids. This acidic treatment increased the number of oxidative functional groups on the surface of the CNTs, resulting in break points which led to mechanical cleavage. NaOH was then used to neutralize the CNTs, followed by washings to subtract the salts produced. Then the CNTs oxygenated groups on the outer surface were reduced under a flow of argon in an oven at 900°C for 2 hours. The average length of the nanotubes was found in a range of 100 – 1000 nm, using transmission electron microscopy (TEM) whereas the initial CNTs had lengths of several tens of microns (in the range of 50-200 microns) (**Figure 2.A and B** before and after reduction).

Then a MS shell was coated around the CNTs using a modified procedure from Bian et al.[36]. A solution of cetyltrimethylammonium bromide (CTAB), water and ethanol was heated to 60 °C for 2 h. CTAB is a well-known surfactant that forms positively charged micelles in solution. When CNTs are dispersed in this mixture and given the hydrophobicity of heat-treated CNTs, the micelles arrange around the carbon nanotubes. The sol gel process begins upon addition of tetraethyl orthosilicate (TEOS) and NaOH. NaOH catalyzes the hydrolysis of TEOS, which condenses into silicate polyanions, leading to further condensation reactions, forming a network of Si-O-Si bonds. Once this MS structure is obtained, surfactant extractions are necessary to remove the CTAB from the pores of the silica. This was achieved with NH_4NO_3 ; Zeta potential (ZP) measurements allowed to monitor the surface charge change from positive to negative. Five extractions were required to reach a stable negative zeta potential value indicating the completion of the process. The composites from this point onwards will be referred to as CNT@MS. TEM images showed homogenous coverage of the CNT@MS (**Figure 2.C**) on almost all the CNTs and a zoomed image (**Figure 2.D**) indicated the well-organized mesoporous structure of the MS shell around the CNTs. TEM images were used to establish the thickness of the MS shell, which was of 30 ± 4 nm.

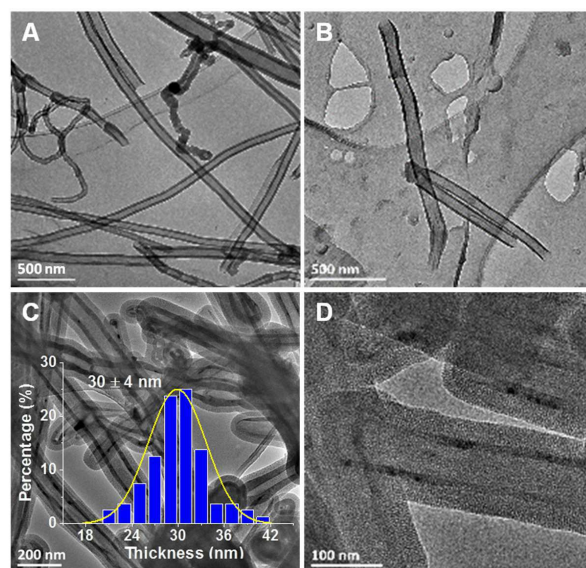


Figure 2. Representative TEM images of A) uncleaved CNTs. B) Acid-treated sliced CNTs. C) CNT@MS in a large area associated with the silica layer thickness distribution and D) CNT@MS in a zoomed image showing the mesoporous structures.

The porosity was investigated by nitrogen adsorption-desorption isotherms. **Figure S1** shows the nitrogen adsorption-desorption isotherm curves which exhibit a type IV isotherm, characteristic of mesoporous materials and which was used to calculate the surface area, pore size and pore volume. The Brunauer-Emmett-Teller (BET) surface area was thus calculated as $594 \pm 14 \text{ m}^2 \text{ g}^{-1}$ and the pore size was found to be of *ca.* 3.4 nm with a pore volume of $0.53 \text{ cm}^3 \text{ g}^{-1}$. These data are consistent with the results obtained by Bian *et al.*[36], and in our previous studies [41,42]. Thermogravimetric analysis (TGA) was used to determine the C/SiO₂ composition of CNT@MS (**Figure 3. A**). The analysis of the curve indicated that CNTs started to decompose into CO₂ from 400 to 600 °C. This allowed us estimating a C/SiO₂ mass ratio of 63/37 for the CNT@MS composite system.

2. Surface functionalization with APTS and IBAM moieties

Next, after CTAB extraction from the pores, the surface of the MS was modified with APTS according to a standard process of multilayered siloxane condensation adapted from Wang *et al.* [53] and thereafter reacted with isobutrylchloride (IBC) molecules to form grafted isobutyramide (IBAM) moieties[54] (**Figure 3.A**). For that, the CNT@MS were first dispersed in ethanol, and then a catalytic amount of NH₄OH was added followed by 3-

aminopropyltriethoxysilane (APTS). The presence of NH_4OH allowed the APTS to condense on the silica surface over a 2 h period. The amine-functionalized silica surface was then further modified with isobutrylchloride (IBC) resulting in IBAM functional groups on the outer surface of the silica shell. In previous works, IBAM moieties were, in particular, proved to non-covalently bind human serum albumin (HSA) and other proteins at the surface of MS carriers, leading to a tight biomacromolecular shell [41,43–45]. The APTS and IBAM grafting steps were characterized by TGA (**Figure 3.B**). TGA on the bare CNT@MS was used as a baseline and the TGA of CNT@MS@APTS and CNT@MS@IBAM allowed estimating by subtraction the amount of grafted aminosilane and then of the IBAM moieties. As can be seen, decomposition of APTS is achieved in the T range 300-450 °C and the weight loss was estimated at 10.4% of CNT@MS. Similarly, the IBAM grafts decomposition was overlapped with the APTS one and, by subtraction, the mass of IBAM decomposition was estimated at 7.0% of CNT@MS. TGA results of these hybrids enabled us to evaluate the grafting density: the number of APTS and IBAM molecules grafted on the silica surface was calculated to be of ca. 3.0 and 2.0 molecules per nm^2 , respectively.

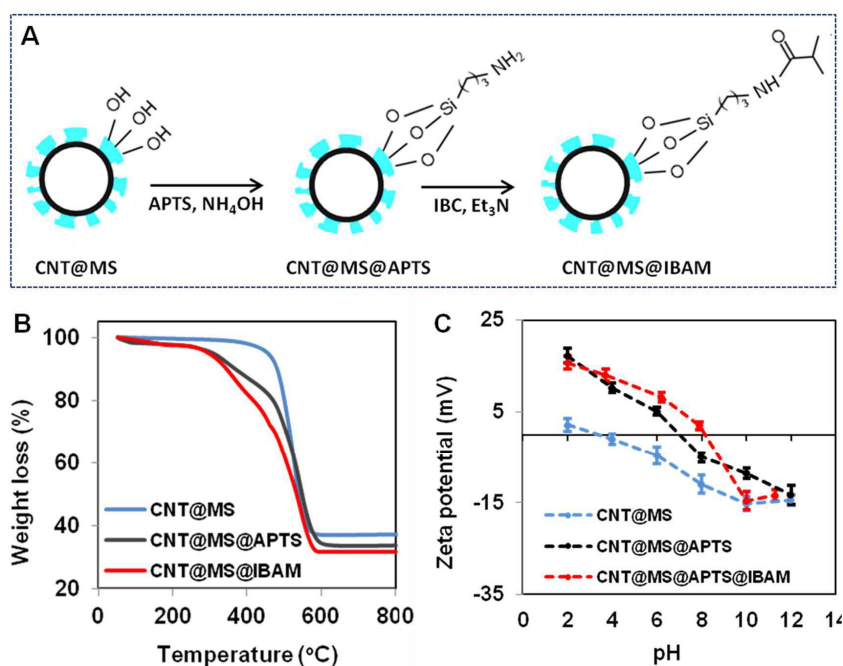


Figure 3. A) The process of reactions for CNT@MS@APTS and CNT@MS@IBAM composite. B) TGA curves of CNT@MS, CNT@MS@APTS and CNT@MS@IBAM. C) Zeta potential measurements of CNT@MS, CNT@MS@APTS and CNT@MS@IBAM as a function of pH value.

The surface functionalization steps of the MS layer were also investigated by zeta potential (ZP) measurements in water (**Figure 3.C**). The ZP curves as a function of pH value for bare CNT@MS and CNT@MS modified with APTS and IBAM moieties were thus traced. The ZP being the electrical potential at the slipping plane of the double ionic layer of the coated surface, gives in a first approximation indication of the surface charge changes. An iso-electric point (IEP) of ca. 2-3 was found on bare CNT@MS, consistent with the IEP value of bare silica surface chemistry as reported in the literature. After APTS modification, the ZP curve shifted towards higher pHs inducing a shift of the IEPs from ca. 3 for bare CNT@MS to a ca. 7 for the APTS-modified CNT@MS. This is consistent with the APTS presence on the silica surface providing a positive ammonium charge. After IBAM modification, CNT@MS@IBAM, the ZP curve was again shifted to higher pH and displayed an IEP of around 8, which indicate that a fraction of APTS moieties still remain after the reaction. Hence, overall, the TGA and ZP results evidenced that the surface of CNT@MS was effectively chemically modified with APTS and IBAM.

3. Drug loading and HSA coating

As we aimed at loading the CNT@MS@IBAM with an antitumoral agent (DOX) and then wrapping them with a serum albumin capping to ensure a biocompatible surface, our strategy was to adsorb DOX directly onto IBAM followed by the HSA coating. Firstly, this required investigating the loading in water of the hydrophilic DOX within the porous structure modified with IBAM groups. DOX displays strong absorption characteristics at 480 nm that allows its suitable detection and to quantify its adsorption. A UV/vis calibration curve of DOX in water measuring the absorbance at 480 nm at different DOX concentrations was plotted (**Figure S2**). For different [DOX] concentrations in water, an impregnation (during 16 hours) of the drug within CNT@MS@IBAM was carried out to load the composite. The suspensions were then centrifuged, and the resulting supernatants were dosed by UV/Vis spectroscopy to determine the mass of DOX that stayed outside of the composite. From that, the mass of DOX that entered the composite could be calculated. The drug loading capacity (DLC) and the drug loading efficacy (DLE) were used as loading parameters to establish the amount of drug within the composites. Their expressions are given below.

$$\text{DLC}\% = \frac{\text{weight of DOX loaded}}{\text{weight of CNT@MS}} \times 100\%$$

$$\text{DLE}\% = \frac{\text{weight of DOX loaded}}{\text{weight of DOX initial}} \times 100\%$$

Evolutions of these both parameters were plotted along with [DOX] (see DLC and DLE curves respectively in **Figure 4.A** and **4.B**). As can be seen in **Figure 4.A**, the DOX DLC increased

with the increasing concentration of DOX from 0.25 to 8 mg mL⁻¹. At a concentration of 8 mg mL⁻¹ DOX_(aq) solution, the DLC reached 68%, equivalent to 0.68 mg DOX per mg of CNT@MS. Interestingly, looking at the efficiency of the drug impregnation process, the DLE remained constant with the various concentrations, maintaining around DLE=23% regardless of the DOX concentration (**Figure 4. B**). This composite seems to behave as a loading matrix which ensures a concentration independent partition between DOX molecules in and outside of the composites. For the subsequent adsorption of a human serum albumin (HSA) shell, three times washes and centrifugation was required to completely remove the free DOX from the supernatant, which also resulted in the spontaneous leaking of the loosely-bound loaded DOX decreasing the DLC from 68% (impregnation by UV vis) to 58% (after washing steps by UV vis).

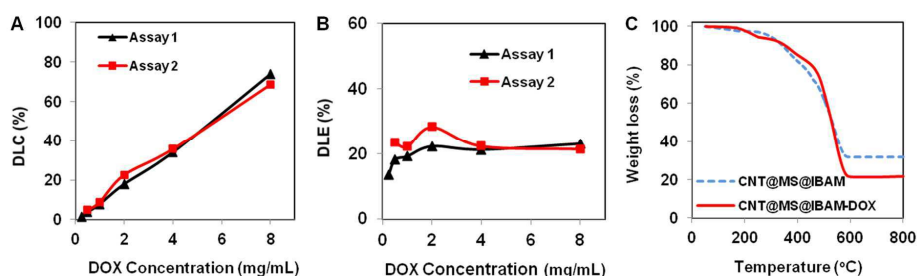


Figure 4. A) DLC and B) DLE curves as a function of DOX concentration in water. C) TGA curves of CNT@MS@IBAM and CNT@MS@IBAM-DOX (DLC= 56% after washing steps)

The DOX loading amount was also evaluated by TGA analysis performed directly on the nanocomposite after the three washing steps. TGA measurements of CNT@MS@IBAM-DOX were performed in the temperature range of 50-800°C and the result is presented in **Figure 4.C**. With CNT@MS@IBAM as the baseline, the amount of DOX loaded could be calculated; the TGA curve revealed a weight loss correlated to the DOX decomposition of ca. 56% of CNT@MS (see **Figure S3** for the TGA of DOX decomposition itself and **Table S1** for explanations about the calculations by TGA). This value is consistent with the DOX content calculated from UV/vis, considering that ca. loosely bound DOX was lost during washing steps. These DLC values are particularly high in the field of MS nanosystems as a usual range of 10-40% is reported, depending on the drug loading conditions [55–58]. We expect that in the case of IBAM grafts, a mechanism of drug-sponge effect similar to the one encountered with APTS in our previous work [42] may be the reason for such high drug loading.

Then, once the composite was suitably loaded with DOX, an HSA coating was directly added just after removing the impregnation supernatant. The adsorption of HSA in aqueous solution at a concentration of ca. 0.21 mg mL⁻¹ was performed on two CNT@MS@IBAM-DOX

nanocomposites with initial DOX loading measured at DLC = 18% and 34%. The quantification of the amount of HSA coated on the CNT@MS@IBAM-DOX composites was achieved and followed by spectrofluorimetry analysis of the supernatant. For that, HSA was labeled with the fluorophore FITC and a spectrofluorimetry calibration curve of HSA^{FITC} (Exc/Em : 480/520 nm) in water measuring the fluorescence intensity emission at 520 nm at different HSA^{FITC} concentrations was traced (**Figure S4**). Fluorescence spectra in **Figure 5.A** showed the complete disappearance in fluorescence at 520 nm of the supernatants after the HSA adsorption on both systems, which is compared to an HSA-FITC solution at 0.21 mg mL⁻¹. This data showed that in the conditions of HSA adsorption, almost all the HSA brought in contact with the CNT@MS@IBAM-DOX composites was coated onto their surfaces, which was attributed to the non-covalent bonds between HSA and isobutyramide (IBAM) functional groups. This allowed us estimating that ca. 98 µg HSA was adsorbed per mg of CNT@MS composite. As observed above, some slight natural DOX leakage arose in both samples as DOX is highly soluble in water (cf slight signals at ca. 560 and 590 nm). After evaluation of the DOX amount loss by using the absorbance calibration curve, the final DLC of the drug tightly retained in the system after HSA coating and washing were found of 16 and 31% as compared to initial DOX loadings during DOX impregnation (DLC = 18% and 34%).

Regarding the surface charge, Zeta potential measurements as a function of the pH were performed on CNT@MS@IBAM@HSA and CNT@MS@IBAM-DOX@HSA systems (**Figure 5. B**) and very similar trends with and without DOX loading were found. The isoelectric point values for CNT@MS@IBAM@HSA and CNT@MS@IBAM-DOX@HSA (DLC = 56 %) composites were found at pH ca. 6 and 5, respectively. These data indicated that despite of the very high amount of DOX introduced, the surface charge is probably the same without and with DOX, which/and is mainly determined by the HSA coating. This confirms the good coverage of composites by HSA and its efficiency as gate-keeper.

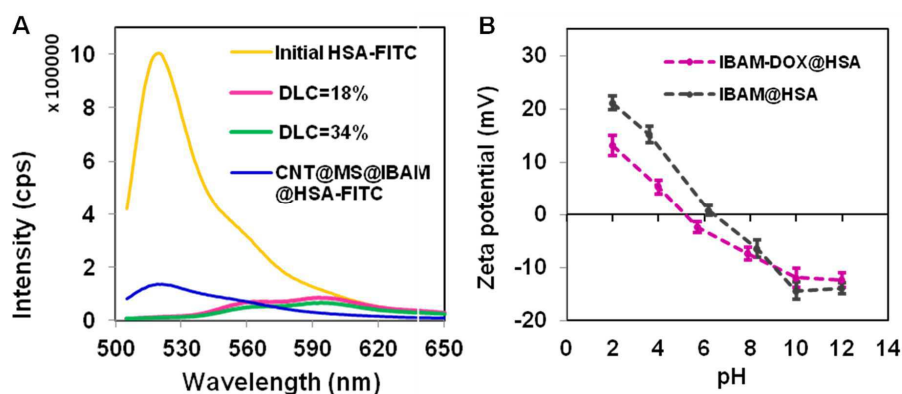


Figure 5. A) Fluorescence spectra of supernatant of CNT@MS@IBAM-DOX@HSA^{FITC} (DLC = 18% and 34%), CTRL (CNT@MS@IBAM@HSA^{FITC}) and HSA-FITC solution at 0.21 mg mL⁻¹. B) Zeta potential curves as a function of pH for CNT@MS@IBAM-DOX@HSA and CNT@MS@IBAM@HSA.

4. DOX Release

CNTs have strong absorbance in NIR region (in the range 750-1400 nm) and can convert the NIR light into local heat. By adding to their surface a thermally responsive coating, they become suitable photo-responsive nanostructures for the remote release of drugs. In this paragraph, we investigated the possibility to deliver DOX upon NIR photothermal effect. We assumed the generated heat would disturb intermolecular interactions between DOX and IBAM facilitating the DOX release.

To evaluate the photothermal properties, aqueous solutions (1 mL) of various concentrations of CNT@MS@IBAM-DOX@HSA (DLC ca. 58%) ranging from 0.32 to 2.5 mg mL⁻¹ (0.32; 0.63; 1.25 and 2.5 mg mL⁻¹) were exposed to a 1064 nm NIR laser with power densities at 2.5 and 1 W cm⁻². The temperature changes were then recorded as a function of time during the 15 min irradiation time of NIR light, as shown in **Figure 6.A** (2.5 W cm⁻²) and **6.B** (1 W cm⁻²). As expected, obvious photothermal heating of the suspensions were observed but with differences in terms of temperature profiles between the two powers used. At the highest NIR power density of 2.5 W cm⁻² (**Figure 6. A**), the temperature profiles of the suspensions were shown not to depend on the nanocomposite concentration and increased rapidly from ca. 31 to 68 °C at the early stage (over the first 5 minutes) and then remained substantially constant with extending exposure time. The effect of the NIR light in water (without CNTs composites) showed a slight increase of the T from 22 to 30 °C when exposure to the 2.5 W cm⁻² NIR laser, confirming a temperature effect of the composites. Oppositely, the temperature of the solution under 1 W cm⁻² NIR irradiation (**Figure 6. B**) increased slowly throughout the run and was found to be finely tunable with concentrations and irradiation times so that temperature could be raised in a

controlled manner from 28 to 41°C. The power effect is important when applied to cells to avoid their necrosis which is expected above 45 °C[59–61]. In contrast, by looking at the effect of the NIR light in the solution without composites, the temperature of pure water showed almost no changes under the same power condition. The excellent photothermal performances of CNTs whatever the power make them thusly an effective photothermal agent and we have now to demonstrate that it is efficient for drug delivery.

Then, the NIR-light controlled drug release properties of CNT@MS@IBAM-DOX@HSA were investigated by measuring the DOX amount released from the exposed suspensions (DLC = 58%) at various concentrations of (0.32 - 2.5 mg ml⁻¹) under NIR laser for 15 min (followed by three days at rest at 4°C) at power densities of 1 and 2.5 W.cm⁻². For each concentration, a control sample (CTRL) not exposed to NIR light at room temperature was also considered. The supernatants of the centrifuged suspensions after NIR treatment (and rest time) were monitored by UV/Vis absorption spectroscopy at 480 nm to determine the amount of DOX released during this period. As shown in **Figure 6.C**, the increased sample concentration resulted in an increased DOX release under NIR light stimulation at both power densities, 1 and 2.5 W cm⁻², with very similar DOX release trends for both power densities. Hence after the first 15 min NIR irradiation trail, respectively ca. 21 and 22 µg of DOX were released at the concentration of 2.5 mg mL⁻¹ under NIR power densities of 2.5 and 1 W cm⁻², respectively, which correspond to almost three times that of the control sample (natural leakage) of 8 µg. This natural release is attributed to a spontaneous desorption of DOX that occurs with time which remains however lower than that of the photo-induced one. A photograph of the supernatants (**Figure 6. D**) illustrated the differences in contrast of DOX between the samples submitted to NIR light and the control. Finally, regarding the results obtained in Figures 6.A and B for the T profiles and the results obtained in drug release in **Figures 6.C** and **D**, we can conclude that the NIR exposure at 1W.cm⁻² condition is optimal as it ensures a better T control and efficient drug release.

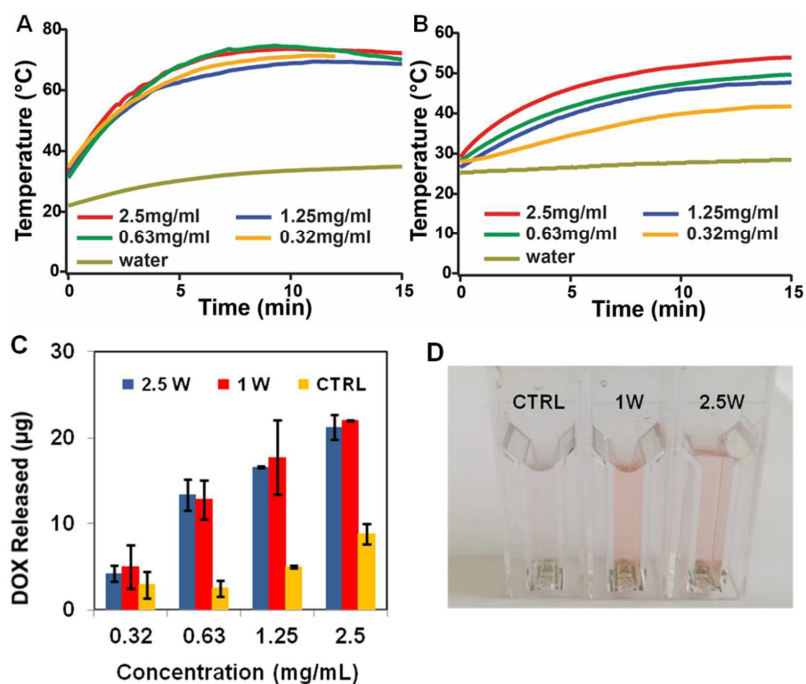


Figure 6. Changes in temperature of 1 mL of CNT@MS@IBAM-DOX@HSA (DLC = 58%) at various concentrations upon irradiation by the 1064 nm NIR laser at a power density of A) 2.5 W cm⁻² and B) 1 W cm⁻². C) Mass of DOX released from various concentrations of CNT@MS@IBAM-DOX@HSA (DLC = 58%) upon NIR laser irradiation at power densities of 2.5 and 1 W cm⁻², and ambient T (CTRL). D) Photograph of the DOX released from the composite concentration of 2.5 mg mL⁻¹ (DLC = 58%) after NIR exposure at the two power densities (1W and 2.5W) or when exposed to room T (CTRL)

We also investigated the effect of pulsatile release by performing four cycles of NIR laser irradiation to the four batches at various concentrations (0.32; 0.63; 1.25 and 2.5 mg ml⁻¹). Pulsatile release is a very attractive approach because triggering the drug release in several pulses with chosen periods could be beneficial for a treatment needing dosing in several sequential steps of the drug administration.[62–65] As observed above, this system is supposed to have a continuous, rather slow release of DOX in the absence of NIR light, and the pulsatile release would ensure bursts of DOX released upon NIR irradiations. As shown in **Figure 7.A**, for nanocomposites at a concentration of 2.5 mg mL⁻¹ (DLC = 58%), along four consecutive NIR treatment cycles, the DOX release enhancement was found to be lower than for the first pulse reaching nevertheless a rate ca. 5 µg DOX/pulse. This can be explained by the observed

agglomeration of the CNT@MS@IBAM-DOX@HSA composite induced by NIR irradiation at the power density of 2.5 W cm^{-2} . Finally, the cumulative amount of DOX released was found to be of *ca.* 37 and $34 \mu\text{g}$ upon NIR laser application at 2.5 and 1 W cm^{-2} , respectively. For 1.25, 0.63 and 0.32 mg mL^{-1} (**Figures 7.B-C-D**), the cumulative DOX release showed also a moderate though progressive increase after each cycle of NIR irradiation with the following slopes after the first pulse: *ca.* 4, 3, 2 $\mu\text{g DOX/NIR pulse}$. Percentages of the cumulative release of DOX as compared to the initial loading of DOX in the CNT@MS@IBAM-DOX@HSA nanocomposites for all of these graphs are provided in **Figure S5**. Even if the DOX loading (58% *i.e.* $580 \mu\text{g.mg}^{-1}$ CNTS@MS) is very high as compared to the literature and the amount released in **Figure 7** are suitable for cancer cell toxicity, the % DOX amount released indicate that only less than 10% of the total DOX loaded amount is released. Nevertheless, this lets envisioning using these systems for long term and sustained pulsatile release. Altogether, these results showed that the amount of DOX released upon NIR is proportional to the composite concentration (at equal DLC). Moreover, since power of NIR had no substantial benefit on the amount of DOX that is released (see **Figure S5.A and B**), using low power (1W) allows to preserve a better temperature control below the inflammation/necrotic temperature of 45°C [59–61].

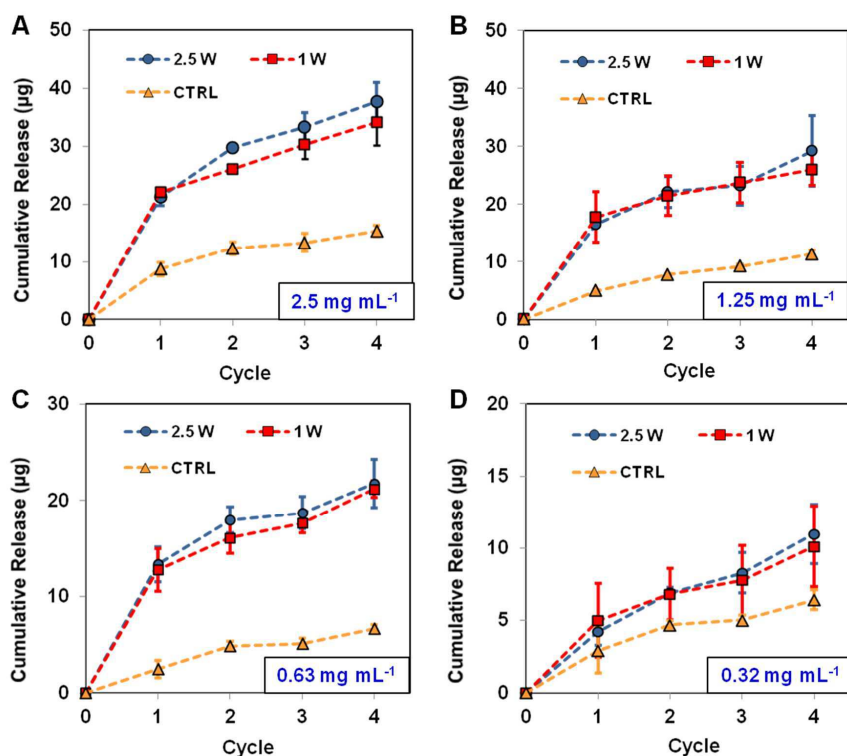


Figure 7. Cumulative DOX release from various concentrations of CNT@MS@IBAM-DOX@HSA: A) 2.5 mg mL⁻¹, B) 1.25 mg mL⁻¹, C) 0.63 mg mL⁻¹ and D) 0.32 mg mL⁻¹ (DLC = 58%) upon four consecutive NIR laser irradiation cycles at power densities of 2.5 and 1 W cm⁻² (15 min ON, 3 days OFF), and at ambient T (CTRL).

5. Uptake of DOX and cytotoxicity upon NIR excitation

Here, we aimed at testing the cytotoxic potential of our functionalized nanocomposites using a classical breast carcinoma tumor cell line. We tested its cytotoxic effect using either (i) classical cell culture where CNTs are supplemented to the cell culture medium, or (ii) a hydrogel-composite formulation where the nanocomposites are dispersed in the hydrogel (Matrigel) on top of which cells are seeded.

Cytotoxicity of CNT@MS@IBAM@HSA (without DOX) and CNT@MS@IBAM-DOX@HSA-loaded cells without and with NIR irradiation was estimated at various concentrations (**Figure 8.A-C**). First, we observe a very little cytotoxicity of CNT@MS@IBAM@HSA on tumor cells when no NIR is applied (**Figure 8.A**, yellow curve), independently of the nanocomposite concentration. Indeed, without any irradiation, D2A1 cells treated with CNT@MS@IBAM@HSA are only poorly affected with an average viability that remains for the 4 concentration conditions over 90%. Interestingly, a dose-dependent cytotoxicity was observed when tumor cells were subjected to CNT@MS@IBAM-DOX@HSA (**Figure 8.A**, blue curve), that could arise from previously observed DOX leaking from the nanocomposites.

Upon NIR light, cytotoxicities of CNT@MS@IBAM@HSA and of CNT@MS@IBAMDOX@HSA were significantly increased suggesting that T increase is sufficient to promote a cytotoxic effect of the CNTs (**Figure 8.A** green and red curves). Indeed, if we compare nanocomposites loaded with DOX, CNT@MS@IBAM-DOX@HSA, under NIR irradiation with the one without DOX, the release of DOX appears to moderately enhance cellular death (, DOX vs NO DOX under NIR light). However it can be observed that, we reached a very efficient cytotoxic effect when both NIR and CNT@MS@IBAMDOX@HSA are applied, demonstrating the synergistic effects of photothermia and DOX release. (**Figure 8.C**)

Noteworthy, as a control, we investigated also the NIR irradiation effect onto cells without the composites. NIR irradiation showed no significant cytotoxicity further indicating that the locally increase heat from the nanocomposites is required to induce subsequent cell death (**Figure S7.A**). In conclusion, cytotoxicity is predominantly mediated by CNTs-dependent local T° increase and it can be enhanced with DOX release.

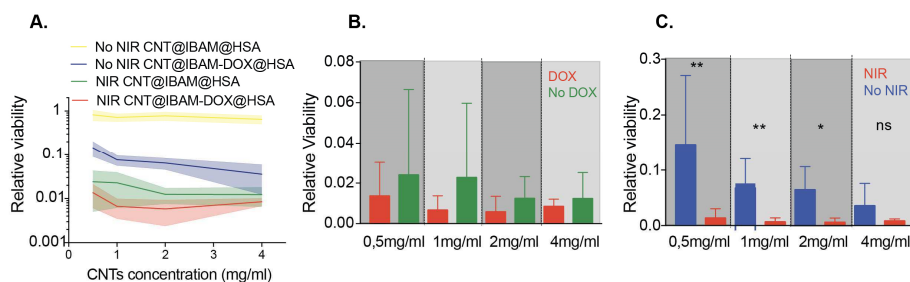


Figure 8. Viability assay results. A) The relative emission values in semi logarithmic scale as compared to the control (cells grown without nanocomposites) after 24 h of incubation with the nanocomposites followed by 15 min NIR irradiation. CNT@MS@IBAM@HSA (no DOX) and CNT@MS@IBAM-DOX@HSA (DOX) composites at concentrations 0.5, 1, 2, and 4 mg ml⁻¹ were considered. Represented on the graph are the average values and the SEM. B) Relative cellular viability extracted from graph A with and without DOX, upon 15 minutes of NIR exposure for CNT@MS@IBAM@HSA (no DOX) and CNT@MS@IBAM-DOX@HSA (DOX) at concentrations of 0.5, 1, 2, and 4 mg ml⁻¹. C) Relative cellular viability with and without 15 minutes of NIR light exposure on CNT@MS@IBAM-DOX@HSA at the concentrations of 0.5, 1, 2 and 4mg ml⁻¹,

With the aim to evidence that the DOX loaded in the CNT@MS@IBAM-DOX@HSA nanocomposites can be efficiently delivered to the cancer cells following NIR light application, thereby enhancing cytotoxic activity, we decided to incorporate the composites inside a 3D hydrogel scaffold. Additionally, this allows to shield cells from the unwanted non-specific adsorption of heat-inducing composite particles. Hence, the CNT@MS@IBAM-DOX@HSA nanocomposites were formulated within a commercially-available biocompatible protein-based hydrogel (Matrigel) that mimicks a biocompatible implantable scaffold. Indeed, the development of activable nanocomposite scaffolds has become an emerging field in nanomedicine and biomaterials which allows to solve issues associated with the use of injectable scaffolds (such as local injection, controlled release, limited loss of therapeutics). To build such nanocomposite scaffolds, CNT@MS@IBAM-DOX@HSA suspensions at 2 and 4 mg ml⁻¹ were mixed with Matrigel as substrates for the growth of the tumor cells and CNT@MS@IBAM@HSA were mixed to Matrigels to be used as controls. DOX release and uptake upon NIR was followed by confocal microscopy and the results showed significantly increased red fluorescence signals when cells were treated with CNT@MS@IBAM-DOX@HSA (**Figure 9.A, B and C**). The procedure allowing to visualize the cellular DOX uptake (red color) and the CNTs@MS@IBAM-DOX-HSA nanocomposites (white color) distribution is detailed in **Figure S8**. While absence of NIR led to backgrounds levels of DOX we observed a dose-dependent NIR-stimulated DOX release in tumor

cells (**Figure 9.A**). Overall, this confirms that DOX is released from the CNT@MS@IBAM-DOX@HSA nanocomposites upon NIR light application and that it contributes to synergistic effect of photothermia and DOX release observed in the 2C cell culture in the previous paragraph.

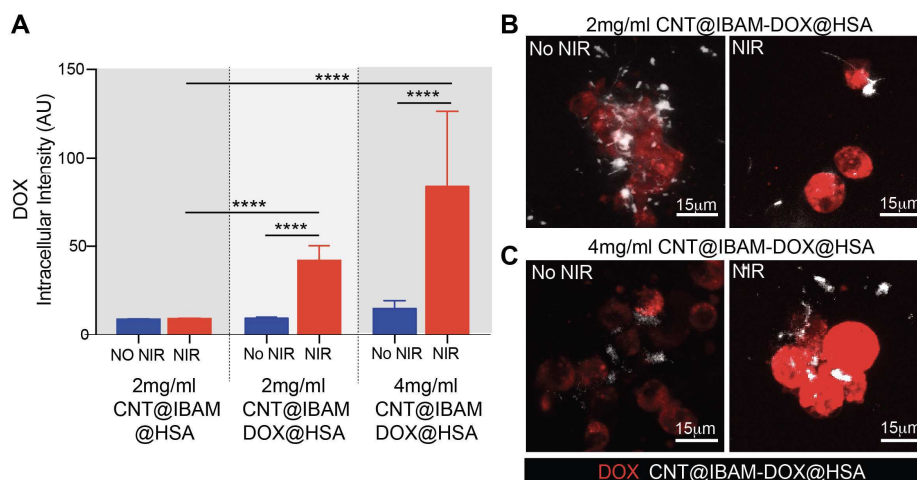


Figure 9. A) Intracellular DOX intensity. Average and standard deviation from the red DOX fluorescence signal in the different scaffold conditions. *P* values were calculated by the Mann Whitney test (**** $p < 0.0001$). Z-projection of a fluorescent stack of images taken on D2A1 cells grown in CNT@IBAM-DOX@HSA composite at concentrations of B) 2 mg mL⁻¹ and C) 4 mg mL⁻¹ without and with NIR irradiation, respectively.

At last, to assess whether this hydrogel nanocomposite loaded with CNTs@MS@IBAM-DOX@HSA displays cytotoxicity towards murine breast cancer cells in 3D conditions, we assessed cellular growth in presence of different nanocomposites (**Figure 10**). The cells were grown over 5 days in either Matrigel (control without nanocomposites) or in a mixture of Matrigel added with the nanocomposites at 2.5 mg mL⁻¹. While CNT@MS@IBAM@HSA had no effect on cellular growth as compared to the control without nanocomposites (**Fig.10A-B**), CNT@IBAM-DOX@HSA significantly lead to cell death in these conditions (**Fig.10C**). Thus, when incorporated into a matrix, CNTs@IBAM@HSA are not cytotoxic. When functionalized with DOX, its release would favor cytotoxicity (as expected upon NIR light). Such property could be beneficial for antitumor applications where drug release could be potentiated with an external stimulus such as NIR light.

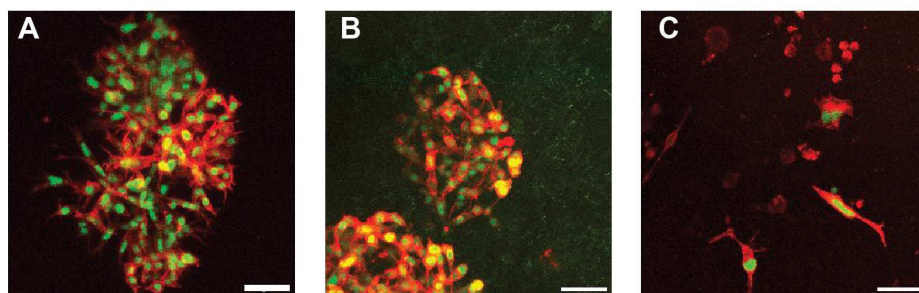


Figure 10. Confocal microscopy imaging of 3D tumoral D2A1 cancer cell growth in Matrigel over 5 days in the absence or in the presence of the nanocomposites. D2A1 grown in Matrigel (A) in the absence of nanocomposites (B) treated with 2.5 mg mL^{-1} CNT@MS@IBAM@HSA and (C) treated with 2.5 mg mL^{-1} CNT@MS@IBAM-DOX@HSA. (scale bars $50 \mu\text{m}$). (C) In green : the nuclear localization signal and in red : the actin filaments.

Conclusion

In this work, we have designed new NIR light-responsive nanocomposites made of MS shell coated CNTs, loaded with the antitumor drug doxorubicin (DOX), and capped with plasma protein human serum albumin (HSA) as a biocompatible interface and gate keeper. We have developed here a novel way to immobilize DOX with a DLC up to 80%, (a very high amount as compared to the literature), via the powerful strategy based on IBAM versatile non-covalent binders grafted on CNT@MS shells which additionally allow the tight anchoring of HSA.

The photothermal properties of these composites were investigated as a function of their concentration and of the laser power. We found that adjusting the power at 1 W.cm^2 is well suited to control the temperature under the necrosis temperature (45°C). These drug loaded CNTs@MS@IBAM-DOX-HSA nanocomposites were shown to release DOX in response to NIR light applied. We demonstrated that this release occurs first by a burst that depends on the concentration of the composites but can also be controlled on a pulsatile fashion as a regular increase of DOX occurs after each NIR light application. We demonstrated that a NIR power of 1 W.cm^{-2} is efficient to control the release of DOX dose on time.

We further demonstrated the cytotoxic potential of DOX-loaded nanocomposites and highlighted a potentially interesting feature of our nanocomposites: even if photothermic effect from the CNTs composites allows an important cancer cell cytotoxicity, the DOX-mediated release ensure an additional cytotoxicity allowing synergy of both effect to kill cancer cells. Finally, another originality of this work is the integration of such nanocomposites into a hydrogel mimicking the extracellular matrix which can have potential applications in the field of antitumoral scaffolds or polymer matrices for tissue engineering (if DOX is replaced by another

molecule). We showed here that the application of NIR light on such nanocomposite hydrogel scaffold covered with D2A1 murine breast cancer cells allows triggering the release of DOX to the cellular media, which results in cell toxicity over time.

Hence, such nanosystems may be of huge interest as components of implantable scaffolds for antitumor or tissue engineering applications. This approach would make it possible the development of new (nano) medical devices for the medicine of tomorrow.

Data availability.

The raw/processed data required to produce these findings can be shared on demand.

Author contributions.

The manuscript was written with contributions of all authors. All authors have given approval to the final version of the manuscript.

Acknowledgements

D.M. acknowledges the Materials Institute Carnot Alsace (project ProtRemote) and the Canceropôle Est (project VIVIRMAG) for the financial supports. Bing LI would like to thank the Chinese Scholarship Council (CSC) for the grant during her PhD at the University of Strasbourg. M.T. acknowledges CONICET for funding and support for researchers' exchange, as well as the EU project Hygraphen for researchers' mobility allowances. Work in the Goetz lab (VG, SH, JGG) is supported by institutional funds from INSERM and University of Strasbourg as well as by Canceropôle Est (project VIVIRMAG). V.G. funded by an INSERM/RegionEst *Ph.D.* fellowship.

Bibliography

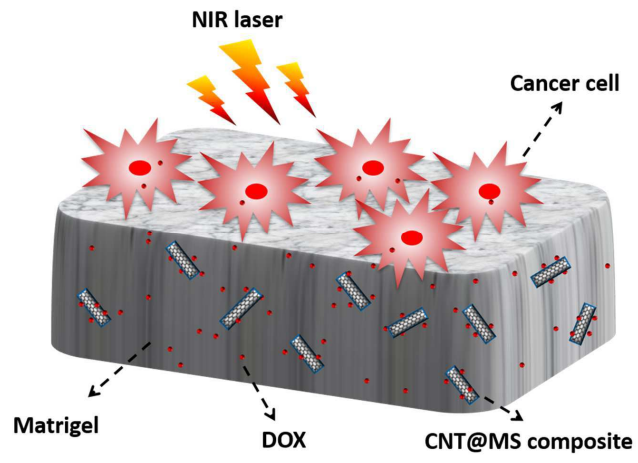
- [1] S. Augustine, J. Singh, M. Srivastava, M. Sharma, A. Das, B.D. Malhotra, Recent advances in carbon based nanosystems for cancer theranostics, *Biomater. Sci.* 5 (2017) 901–952. <https://doi.org/10.1039/C7BM00008A>.
- [2] E. Cazares-Cortes, S. Cabana-Montenegro, C. Boitard, E. Nehling, N. Griffete, J. Fresnais, C. Wilhelm, A. Abou-Hassan, C. Ménager, Recent insights in magnetic hyperthermia: From the “hot-spot” effect for local delivery to combined magneto-photo-thermia using magneto-plasmonic hybrids, *Adv. Drug Deliv. Rev.* (2018).
- [3] S. Kralj, T. Potrc, P. Kocbek, S. Marchesan, D. Makovec, Design and fabrication of magnetically responsive nanocarriers for drug delivery, *Curr. Med. Chem.* 24 (2017) 454–469.
- [4] D. Mertz, O. Sandre, S. Bégin-Colin, Drug releasing nanoplatforms activated by alternating magnetic fields, *Biochim. Biophys. Acta BBA - Gen. Subj.* 1861 (2017) 1617–1641. <https://doi.org/10.1016/j.bbagen.2017.02.025>.
- [5] S. Mura, J. Nicolas, P. Couvreur, Stimuli-responsive nanocarriers for drug delivery, *Nat. Mater.* 12 (2013) 991–1003. <https://doi.org/10.1038/nmat3776>.
- [6] M.A.C. Stuart, W.T.S. Huck, J. Genzer, M. Müller, C. Ober, M. Stamm, G.B. Sukhorukov, I. Szeleifer, V.V. Tsukruk, M. Urban, F. Winnik, S. Zauscher, I. Luzinov, S. Minko, *Emerging*

- applications of stimuli-responsive polymer materials, *Nat. Mater.* 9 (2010) 101–113. <https://doi.org/10.1038/nmat2614>.
- [7] A.K. Gaharwar, N.A. Peppas, A. Khademhosseini, Nanocomposite hydrogels for biomedical applications, *Biotechnol. Bioeng.* 111 (2014) 441–453. <https://doi.org/10.1002/bit.25160>.
- [8] L. Gao, L. Xia, R. Zhang, D. Duan, X. Liu, J. Xu, L. Luo, Enhanced antitumor efficacy of poly (D, L-lactide-co-glycolide)-based methotrexate-loaded implants on sarcoma 180 tumor-bearing mice, *Drug Des. Devel. Ther.* 11 (2017) 3065.
- [9] N.S. Satarkar, D. Biswal, J.Z. Hilt, Hydrogel nanocomposites: a review of applications as remote controlled biomaterials, *Soft Matter.* 6 (2010) 2364–2371.
- [10] S. Talebian, J. Foroughi, S.J. Wade, K.L. Vine, A. Dolatshahi-Pirouz, M. Mehrali, J. Conde, G.G. Wallace, Biopolymers for Antitumor Implantable Drug Delivery Systems: Recent Advances and Future Outlook, *Adv. Mater.* 30 (2018) 1706665. <https://doi.org/10.1002/adma.201706665>.
- [11] B.D. Weinberg, E. Blanco, J. Gao, Polymer implants for intratumoral drug delivery and cancer therapy, *J. Pharm. Sci.* 97 (2008) 1681–1702.
- [12] Y. Zhang, J. Yu, H.N. Bomba, Y. Zhu, Z. Gu, Mechanical Force-Triggered Drug Delivery, *Chem. Rev.* 116 (2016) 12536–12563. <https://doi.org/10.1021/acs.chemrev.6b00369>.
- [13] D. Mertz, S. Harlepp, J. Goetz, D. Bégin, G. Schlatter, S. Bégin-Colin, A. Hébraud, Nanocomposite Polymer Scaffolds Responding under External Stimuli for Drug Delivery and Tissue Engineering Applications, *Adv. Ther.* n/a (n.d.) 1900143. <https://doi.org/10.1002/adtp.201900143>.
- [14] S. Merino, C. Martín, K. Kostarelos, M. Prato, E. Vázquez, Nanocomposite Hydrogels: 3D Polymer–Nanoparticle Synergies for On-Demand Drug Delivery, *ACS Nano.* 9 (2015) 4686–4697. <https://doi.org/10.1021/acs.nano.5b01433>.
- [15] A.A. Adedoyin, A.K. Ekenseair, Biomedical applications of magneto-responsive scaffolds, *Nano Res.* 11 (2018) 5049–5064. <https://doi.org/10.1007/s12274-018-2198-2>.
- [16] A. Battigelli, C. Ménard-Moyon, T. Da Ros, M. Prato, A. Bianco, Endowing carbon nanotubes with biological and biomedical properties by chemical modifications, *Adv. Drug Deliv. Rev.* 65 (2013) 1899–1920.
- [17] H. Gong, R. Peng, Z. Liu, Carbon nanotubes for biomedical imaging: the recent advances, *Adv. Drug Deliv. Rev.* 65 (2013) 1951–1963.
- [18] H. Dai, Carbon nanotubes: synthesis, integration, and properties, *Acc. Chem. Res.* 35 (2002) 1035–1044.
- [19] A. Bianco, K. Kostarelos, C.D. Partidos, M. Prato, Biomedical applications of functionalised carbon nanotubes, *Chem. Commun.* (2005) 571–577.
- [20] K. Kostarelos, A. Bianco, M. Prato, Promises and challenges for carbon nanotubes in imaging and therapeutics, *Nat. Nanotechnol.* 4 (2009) 627–633.
- [21] Z. Liu, J.T. Robinson, S.M. Tabakman, K. Yang, H. Dai, Carbon materials for drug delivery & cancer therapy, *Mater. Today.* 14 (2011) 316–323.
- [22] R. Singh, S.V. Torti, Carbon nanotubes in hyperthermia therapy, *Adv. Drug Deliv. Rev.* 65 (2013) 2045–2060.
- [23] B.S. Wong, S.L. Yoong, A. Jagusiak, T. Panczyk, H.K. Ho, W.H. Ang, G. Pastorin, Carbon nanotubes for delivery of small molecule drugs, *Adv. Drug Deliv. Rev.* 65 (2013) 1964–2015.
- [24] C. Ge, J. Du, L. Zhao, L. Wang, Y. Liu, D. Li, Y. Yang, R. Zhou, Y. Zhao, Z. Chai, Binding of blood proteins to carbon nanotubes reduces cytotoxicity, *Proc. Natl. Acad. Sci.* 108 (2011) 16968–16973.
- [25] B. Koh, W. Cheng, Mechanisms of Carbon Nanotube Aggregation and the Reversion of Carbon Nanotube Aggregates in Aqueous Medium, *Langmuir.* 30 (2014) 10899–10909. <https://doi.org/10.1021/la5014279>.
- [26] X. Wang, T. Xia, S.A. Ntim, Z. Ji, S. George, H. Meng, H. Zhang, V. Castranova, S. Mitra, A.E. Nel, Quantitative Techniques for Assessing and Controlling the Dispersion and Biological Effects of Multiwalled Carbon Nanotubes in Mammalian Tissue Culture Cells, *ACS Nano.* 4 (2010) 7241–7252. <https://doi.org/10.1021/nn102112b>.

- [27] H.B. Chew, M.-W. Moon, K.R. Lee, K.-S. Kim, Compressive dynamic scission of carbon nanotubes under sonication: fracture by atomic ejection, in: *Proc. R. Soc. Lond. Math. Phys. Eng. Sci., The Royal Society*, 2011: pp. 1270–1289.
- [28] J. Liu, A.G. Rinzler, H. Dai, J.H. Hafner, R.K. Bradley, P.J. Boul, A. Lu, T. Iverson, K. Shelimov, C.B. Huffman, Fullerene pipes, *Science*. 280 (1998) 1253–1256.
- [29] X. Liu, R.H. Hurt, A.B. Kane, Biodurability of single-walled carbon nanotubes depends on surface functionalization, *Carbon*. 48 (2010) 1961–1969. <https://doi.org/10.1016/j.carbon.2010.02.002>.
- [30] Z. Liu, X. Sun, N. Nakayama-Ratchford, H. Dai, Supramolecular chemistry on water-soluble carbon nanotubes for drug loading and delivery, *ACS Nano*. 1 (2007) 50–56.
- [31] Z. Liu, K. Chen, C. Davis, S. Sherlock, Q. Cao, X. Chen, H. Dai, Drug delivery with carbon nanotubes for in vivo cancer treatment, *Cancer Res*. 68 (2008) 6652–6660.
- [32] Z. Liu, A.C. Fan, K. Rakhra, S. Sherlock, A. Goodwin, X. Chen, Q. Yang, D.W. Felsher, H. Dai, Supramolecular stacking of doxorubicin on carbon nanotubes for in vivo cancer therapy, *Angew. Chem. Int. Ed.* 48 (2009) 7668–7672.
- [33] M. Zheng, A. Jagota, E.D. Semke, B.A. Diner, R.S. Mclean, S.R. Lustig, R.E. Richardson, N.G. Tassi, DNA-assisted dispersion and separation of carbon nanotubes, *Nat. Mater.* 2 (2003) 338–342. <https://doi.org/10.1038/nmat877>.
- [34] M. Zhang, X. Zhang, X. He, L. Chen, Y. Zhang, A facile method to coat mesoporous silica layer on carbon nanotubes by anionic surfactant, *Mater. Lett.* 64 (2010) 1383–1386.
- [35] K. Ding, B. Hu, Y. Xie, G. An, R. Tao, H. Zhang, Z. Liu, A simple route to coat mesoporous SiO₂ layer on carbon nanotubes, *J. Mater. Chem.* 19 (2009) 3725–3731.
- [36] S.-W. Bian, Z. Ma, L.-S. Zhang, F. Niu, W.-G. Song, Silica nanotubes with mesoporous walls and various internal morphologies using hard/soft dual templates, *Chem. Commun.* (2009) 1261–1263.
- [37] P. Yang, S. Gai, J. Lin, Functionalized mesoporous silica materials for controlled drug delivery, *Chem. Soc. Rev.* 41 (2012) 3679–3698.
- [38] M. Ménard, F. Meyer, K. Parkhomenko, C. Leuvrey, G. Francius, S. Bégin-Colin, D. Mertz, Mesoporous silica templated-albumin nanoparticles with high doxorubicin payload for drug delivery assessed with a 3-D tumor cell model, *Biochim. Biophys. Acta BBA - Gen. Subj.* 1863 (2019) 332–341. <https://doi.org/10.1016/j.bbagen.2018.10.020>.
- [39] F. Perton, S. Harlepp, G. Follain, K. Parkhomenko, J.G. Goetz, S. Bégin-Colin, D. Mertz, Wrapped stellate silica nanocomposites as biocompatible luminescent nanoplatforms assessed in vivo, *J. Colloid Interface Sci.* 542 (2019) 469–482. <https://doi.org/10.1016/j.jcis.2019.01.098>.
- [40] M. Ménard, F. Meyer, C. Affolter-Zbaraszczuk, M. Rabineau, A. Adam, P.D. Ramirez, S. Bégin-Colin, D. Mertz, Design of hybrid protein-coated magnetic core-mesoporous silica shell nanocomposites for MRI and drug release assessed in a 3D tumor cell model, *Nanotechnology*. 30 (2019) 174001. <https://doi.org/10.1088/1361-6528/aafe1c>.
- [41] V. Fiegel, S. Harlepp, S. Begin-Colin, D. Begin, D. Mertz, Design of Protein-Coated Carbon Nanotubes Loaded with Hydrophobic Drugs through Sacrificial Templating of Mesoporous Silica Shells, *Chem. – Eur. J.* 24 (2018) 4662–4670. <https://doi.org/10.1002/chem.201705845>.
- [42] C. Wells, O. Vollin-Bringel, V. Fiegel, S. Harlepp, B.V. der Schueren, S. Bégin-Colin, D. Bégin, D. Mertz, Engineering of Mesoporous Silica Coated Carbon-Based Materials Optimized for an Ultrahigh Doxorubicin Payload and a Drug Release Activated by pH, T, and NIR-light, *Adv. Funct. Mater.* 28 (2018) 1706996. <https://doi.org/10.1002/adfm.201706996>.
- [43] F. Perton, M. Tasso, G.A. Muñoz Medina, M. Ménard, C. Blanco-Andujar, E. Portiansky, M.B.F. van Raap, D. Bégin, F. Meyer, S. Begin-Colin, D. Mertz, Fluorescent and magnetic stellate mesoporous silica for bimodal imaging and magnetic hyperthermia, *Appl. Mater. Today*. 16 (2019) 301–314. <https://doi.org/10.1016/j.apmt.2019.06.006>.
- [44] D. Mertz, P. Tan, Y. Wang, T.K. Goh, A. Blencowe, F. Caruso, Bromoisobutyramide as an Intermolecular Surface Binder for the Preparation of Free-standing Biopolymer Assemblies, *Adv. Mater.* 23 (2011) 5668–5673. <https://doi.org/10.1002/adma.201102890>.

- [45] D. Mertz, J. Cui, Y. Yan, G. Devlin, C. Chaubaroux, A. Dochter, R. Alles, P. Lavalle, J.C. Voegel, A. Blencowe, Protein capsules assembled via isobutyramide grafts: sequential growth, biofunctionalization, and cellular uptake, *ACS Nano*. 6 (2012) 7584–7594.
- [46] D. Mertz, H. Wu, J.S. Wong, J. Cui, P. Tan, R. Alles, F. Caruso, Ultrathin, bioresponsive and drug-functionalized protein capsules, *J. Mater. Chem.* 22 (2012) 21434–21442.
- [47] S.H. Lü, Q. Lin, Y.N. Liu, Q. Gao, T. Hao, Y. Wang, J. Zhou, H. Wang, Z. Du, J. Wu, C.Y. Wang, Self-assembly of renal cells into engineered renal tissues in collagen/Matrigel scaffold in vitro, *J. Tissue Eng. Regen. Med.* 6 (2012) 786–792. <https://doi.org/10.1002/term.484>.
- [48] Y. Kimura, M. Ozeki, T. Inamoto, Y. Tabata, Time Course of de Novo Adipogenesis in Matrigel by Gelatin Microspheres Incorporating Basic Fibroblast Growth Factor, *Tissue Eng.* 8 (2002) 603–613. <https://doi.org/10.1089/107632702760240526>.
- [49] M.W. Laschke, M. Rücker, G. Jensen, C. Carvalho, R. Mülhaupt, N.-C. Gellrich, M.D. Menger, Incorporation of growth factor containing Matrigel promotes vascularization of porous PLGA scaffolds, *J. Biomed. Mater. Res. A*. 85A (2008) 397–407. <https://doi.org/10.1002/jbm.a.31503>.
- [50] G. Follain, N. Osmani, A.S. Azevedo, G. Allio, L. Mercier, M.A. Karreman, G. Solecki, M.J. Garcia León, O. Lefebvre, N. Fekonja, C. Hille, V. Chabannes, G. Dollé, T. Metivet, F.D. Hovsepian, C. Prudhomme, A. Pichot, N. Paul, R. Carapito, S. Bahram, B. Ruthensteiner, A. Kemmling, S. Siemonsen, T. Schneider, J. Fiehler, M. Glatzel, F. Winkler, Y. Schwab, K. Pantel, S. Harlepp, J.G. Goetz, Hemodynamic Forces Tune the Arrest, Adhesion, and Extravasation of Circulating Tumor Cells, *Dev. Cell*. 45 (2018) 33–52.e12. <https://doi.org/10.1016/j.devcel.2018.02.015>.
- [51] N. Osmani, G. Follain, M.J. García León, O. Lefebvre, I. Busnelli, A. Larnicol, S. Harlepp, J.G. Goetz, Metastatic Tumor Cells Exploit Their Adhesion Repertoire to Counteract Shear Forces during Intravascular Arrest, *Cell Rep.* 28 (2019) 2491–2500.e5. <https://doi.org/10.1016/j.celrep.2019.07.102>.
- [52] M. Vinci, S. Gowan, F. Boxall, L. Patterson, M. Zimmermann, W. Court, C. Lomas, M. Mendiola, D. Hardisson, S.A. Eccles, Advances in establishment and analysis of three-dimensional tumor spheroid-based functional assays for target validation and drug evaluation, *BMC Biol.* 10 (2012) 29. <https://doi.org/10.1186/1741-7007-10-29>.
- [53] X.-Y. Wang, D. Mertz, C. Blanco-Andujar, A. Bora, M. Ménard, F. Meyer, C. Giraudeau, S. Bégin-Colin, Optimizing the silanization of thermally-decomposed iron oxide nanoparticles for efficient aqueous phase transfer and MRI applications, *RSC Adv.* 6 (2016) 93784–93793.
- [54] D. Mertz, C. Affolter-Zbaraszcuk, J. Barthès, J. Cui, F. Caruso, T.F. Baumert, J.-C. Voegel, J. Ogier, F. Meyer, Templated assembly of albumin-based nanoparticles for simultaneous gene silencing and magnetic resonance imaging, *Nanoscale*. 6 (2014) 11676–11680.
- [55] N.Ž. Knežević, I.I. Slowing, V.S.-Y. Lin, Tuning the release of anticancer drugs from magnetic iron oxide/mesoporous silica core/shell nanoparticles, *ChemPlusChem*. 77 (2012) 48–55.
- [56] L. Yuan, Q. Tang, D. Yang, J.Z. Zhang, F. Zhang, J. Hu, Preparation of pH-responsive mesoporous silica nanoparticles and their application in controlled drug delivery, *J. Phys. Chem. C*. 115 (2011) 9926–9932.
- [57] J. Shen, Q. He, Y. Gao, J. Shi, Y. Li, Mesoporous silica nanoparticles loading doxorubicin reverse multidrug resistance: performance and mechanism, *Nanoscale*. 3 (2011) 4314–4322.
- [58] J. Liu, C. Detrembleur, M.-C. De Pauw-Gillet, S. Mornet, L. Vander Elst, S. Laurent, C. Jérôme, E. Duguet, Heat-triggered drug release systems based on mesoporous silica nanoparticles filled with a maghemite core and phase-change molecules as gatekeepers, *J. Mater. Chem. B*. 2 (2014) 59–70.
- [59] B.V. Harmon, A.M. Corder, R.J. Collins, G.C. Gobé, J. Allen, D.J. Allan, J.F.R. Kerr, Cell Death Induced in a Murine Mastocytoma by 42–47°C Heating in Vitro: Evidence that the Form of Death Changes from Apoptosis to Necrosis Above a Critical Heat Load, *Int. J. Radiat. Biol.* 58 (1990) 845–858. <https://doi.org/10.1080/09553009014552221>.
- [60] S. Li, S. Chien, P.-I. Brånemark, Heat shock-induced necrosis and apoptosis in osteoblasts, *J. Orthop. Res.* 17 (1999) 891–899. <https://doi.org/10.1002/jor.1100170614>.

- [61] S.S. Mambula, D. >Stuart K. Calderwood, Heat induced release of Hsp70 from prostate carcinoma cells involves both active secretion and passive release from necrotic cells, *Int. J. Hyperthermia*. 22 (2006) 575–585. <https://doi.org/10.1080/02656730600976042>.
- [62] J. Wu, A. Chen, M. Qin, R. Huang, G. Zhang, B. Xue, J. Wei, Y. Li, Y. Cao, W. Wang, Hierarchical construction of a mechanically stable peptide–graphene oxide hybrid hydrogel for drug delivery and pulsatile triggered release in vivo, *Nanoscale*. 7 (2015) 1655–1660. <https://doi.org/10.1039/C4NR05798H>.
- [63] J. Liu, C. Wang, X. Wang, X. Wang, L. Cheng, Y. Li, Z. Liu, Mesoporous Silica Coated Single-Walled Carbon Nanotubes as a Multifunctional Light-Responsive Platform for Cancer Combination Therapy, *Adv. Funct. Mater.* 25 (2015) 384–392.
- [64] W.-L. Chiang, C.-J. Ke, Z.-X. Liao, S.-Y. Chen, F.-R. Chen, C.-Y. Tsai, Y. Xia, H.-W. Sung, Pulsatile drug release from PLGA hollow microspheres by controlling the permeability of their walls with a magnetic field, *Small*. 8 (2012) 3584–3588.
- [65] Magnetoresponse Smart Capsules Formed with Polyelectrolytes, Lipid Bilayers and Magnetic Nanoparticles | *ACS Applied Materials & Interfaces*, (n.d.). <https://pubs.acs.org/doi/abs/10.1021/am900784a> (accessed January 29, 2020).



Valentin GENSBITTEL
**Importance des propriétés mécaniques des cellules
tumoraales circulantes au cours du développement
métastatique**

Résumé

Les métastases apparaissent à la fin de la cascade métastatique, un processus complexe dans lequel plusieurs paramètres biomécaniques jouent un rôle important. La contribution de la déformabilité des cellules tumorales circulantes (CTCs) lors de la dissémination hématogène reste mal comprise. Mes travaux identifient la propriété de viscosité comme composante clé de la mécanique cellulaire impactant le comportement des CTCs dans les étapes intravasculaires de la cascade métastatique. Cette propriété intervient au cours de la déformation permettant aux CTCs de surmonter les contraintes aux sites d'occlusion, leur donnant ainsi accès à des itinéraires de circulation alternatifs dans des vaisseaux à petits diamètres où elles pourront se loger. La propriété de viscosité intervient encore au cours de l'étape d'extravasation en impactant le déclenchement du mécanisme de remodelage endothélial extirpant les cellules tumorales des vaisseaux où elles se trouvent arrêtées.

Cancer, Métastase, Mécanique cellulaire, Déformabilité, Viscosité

Résumé en anglais

Metastasis occurs at the end of the metastatic cascade, a complex process in which several biomechanical parameters play an important role. The contribution of the deformability of circulating tumor cells (CTCs) during hematogenous dissemination remains poorly understood. My work identifies the property of viscosity as a key component of cell mechanics impacting the behavior of CTCs in the intravascular stages of the metastatic cascade. This property comes into play during deformation, enabling CTCs to overcome constraints at sites of occlusion, giving them access to alternative circulation routes in small-diameter vessels where they can lodge. The property of viscosity also comes into play during the extravasation stage as it impacts the triggering of the endothelial remodeling mechanism that extirpates arrested tumor cells from the circulation.

Cancer, Metastasis, Cell mechanics, Deformability, Viscosity